

Paleomagnetism, structure and magnetic fabrics in a  
traverse of the Quetico Subprovince between Atikokan and  
Kashabowie, NW Ontario.

by

**Tomasz Werner**

Submitted in partial fulfilment of  
the requirements for the degree of

**Master of Science**

Supervisor: Dr Graham J. Borradaile

Geology Department  
Lakehead University  
Thunder Bay, Ontario  
Canada

June 1993

LAKEHEAD UNIVERSITY  
SENATE GRADUATE STUDIES COMMITTEE

TITLE OF THESIS: Paleomagnetism, structure and magnetic fabrics in a traverse of the Quetico Subprovince between Atikokan and Kashabowie, NW Ontario

NAME OF STUDENT: Tomasz Werner

DEGREE AWARDED: M.Sc.

\* \* \* \* \*

This thesis has been prepared under my supervision and the candidate has complied with the Master's regulations.



\_\_\_\_\_  
Signature of Supervisor

September 30, 1993

Date

### Abstract.

The metasedimentary rocks along the traverse reveal low to high grade metamorphism from chlorite schist near Atikokan, through biotite schist to migmatites in the west within the centre of the Quetico Belt. Continuing towards the ESE, near Huronian Lake, the metamorphic grade decreases symmetrically but with somewhat less steep gradients to Kashabowie. The metamorphism was syn- to late- tectonic.

Only one pervasive tectonic fabric was observed in the interior of the belt, with NE-SW striking  $S_1$  foliations (mean direction:  $256/85^\circ$  NW,  $n=121$ ) and extension lineations  $L_1$  plunging shallowly to the NE (mean direction:  $70-20^\circ$ ,  $n=52$ ). In migmatite and pegmatite zones foliation was often less steep. It was probably deflected due to the intrusion of pegmatite or granitoid bodies.

Minerals contributing to ferromagnetic properties are mostly monoclinic ferrimagnetic pyrrhotite within the belt with some magnetite in medium grade amphibolite - rich outcrops in metavolcanics of Shebandowan Belt.

Anisotropy of magnetic susceptibility fabric (AMS) is mainly controlled by paramagnetic biotite or chlorite and subordinate ferromagnetic pyrrhotite in metasediments of the Quetico Belt. In some outcrops of mafic metavolcanics near Kashabowie, the high magnetite content controls bulk susceptibility more than its anisotropy. Variations in AMS fabric are largely due to variations in relative composition of magnetite, pyrrhotite and paramagnetic sheet silicates, not due to changes in strain along the traverse.

AMS foliations and lineations within the belt and on its south-east margin are generally coaxial with tectonic fabric, with AMS foliation less steep (dip of  $70^\circ$ ) in the interior of the belt. However a slight ( $2-5^\circ$ ) anticlockwise offset of the mean AMS foliation from  $S_1$  can be postulated in the centre of the belt and at the southern margin. When fabric data is studied separately for each sample, such offsets are not significant. In the Atikokan area, AMS fabric is partly of sedimentary origin. The offset of mean AMS lineations with respect to  $L_1$  was confirmed for the Kashabowie - Huronian Lake area (also reported by Borradaile and Spark, 1990) but it is not prominent in the centre of the belt.

Anisotropy of remanence based on acquisition of anhysteretic remanence (AARM) is controlled by preferred crystallographic orientation of pyrrhotite in metasediments and partly by preferred dimensional orientation of magnetite in metavolcanics. It is substantially higher than AMS fabric (mean  $P'$  of order 3 to 5). AARM foliation is usually oriented closer to the tectonic fabric than AMS foliation; it is vertical at the margins and less steep in the centre of the Belt. AARM lineations usually plunge more gently than tectonic and AMS lineations in the centre of the Belt and at the southern margin

in the Kashabowie - Huronian Lake area. At the northern margin, AARM fabric is highly oblate, so that fabric lineations are difficult to define.

At the belt margins, a slight anticlockwise offset of AARM foliations with respect to the tectonic fabric exists, when fabrics for individual samples are examined.

However, the relative orientation of tectonic and magnetic fabric (AMS and AARM) are not a region - wide consistent kinematic indicator of dextral transpression.

Correlation studies between magnetic susceptibility and ARM intensity indicate that a monotonic correlation between ARM and MS exists only in the Calm Lake - Perch Lake area, in which pyrrhotite controls ARM. In other areas a higher content of magnetite increases magnetic susceptibility in several samples, but not ARM.

Both magnetic fabric (AMS and ARM) are usually oblate in low grade metasedimentary rock (at the Belt margins), but in metavolcanic rocks magnetite can produce prolate ARM, whereas AMS is oblate. In the interior of the Belt, 50% of samples have prolate AARM, but most of them are pyrrhotite-bearing.

The AARM fabric is believed to have arisen by the growth of ferromagnetic grains (at least in case of pyrrhotite) in the later stages of transpressive penetrative deformation with a dominant dextral shear component of deformation along an ENE - SWS, vertical plane. The preferred orientation of pyrrhotite grains was probably controlled by the older biotite - chlorite matrix fabric. This would explain the lack of a more significant deflection of the youngest ARM fabric from the oldest tectonic fabric. However, the accuracy of determinations of ARM axes (at least 5-10°) limits the validity of these conclusions.

Characteristic directions of magnetic remanence obtained during thermal or AF step-wise demagnetization form a weakly developed girdle along the basal plane of ARM anisotropy. Therefore natural remanent magnetization is probably entirely of chemical origin and controlled mostly by high anisotropy of pyrrhotite and its preferred crystallographic orientation.

The orientation of NRM toward basal plane of ARM is believed to be mostly an effect of deflection from the true Earth's magnetic field direction due to anisotropy of pyrrhotite ( $P'$  of values of 3-5, Fuller, 1963), and not the effect of grain rotation. Stress control of post - metamorphic remagnetization of primary ChRM is also a possibility. Therefore, it is suggested that NRM was acquired in the same late stage of deformation as AARM, when sizes of individual ferromagnetic grains were suitable to carry a stable remanence. Any primary magnetization acquired at the time of rock formation was not preserved.

The model of different ages of development of paramagnetic and ferromagnetic fabric is consistent with the dextral transpression model of the deformation for both margins and the interior of the Quetico Belt. The latest ferromagnetic sub-fabric formed along the shear plane when the paramagnetic matrix was already oriented subparallel to this plane and mimetically

controlled the orientation of crystallization of ferromagnetic phase. The ferromagnetic fabric is not therefore useful as a kinematic indicator of shear component in those areas.

### Acknowledgements

This project was funded by the operating expenses and a research assistantship from NSERC research grant No A6861 to Dr. G.J. Borradaile. Additional support came from a Lakehead University entrance scholarship and graduate teaching assistantship. The research was performed with the use of facilities of Rock Magnetism laboratory in Geology Department at Lakehead University established by grants to Dr G. J. Borradaile from NSERC, BILD (Ontario), Bickell Foundation, Noranda, American Barrick Resources, and the Canadian Shield Foundation. Some rock magnetic studies were also performed in the Paleomagnetic Laboratory of Institute of Geophysics, Polish Academy of Science, Warsaw, Poland.

I would like to thank Dr. Graham Borradaile for his continuous support and advice, Dr. M. M. Kehlenbeck for interesting comments about Archean plate tectonics, doc. Magdalena Kądziałko-Hofmokr and friends in the Institute of Geophysics for their help with thermomagnetic studies and helpful comments, Anne Hammond and Reino Vittala for preparing superior thin-sections, cutting cylindrical cores and making mineral separations. Sam Spivak helped with printing, drawing and drafting facilities, Alex Stewart helped during sample collection, and John Dehls provided some references.

I also appreciate the support of my neighbours and friends, (dziękuję Wam bardzo), Tadeusz Nowak and Mrs and Mr Arct.

## Table of contents:

Chapter 1. Introduction. . . . .	1
Chapter 2. The metamorphic history and probable deformation mechanisms in the Quetico Subprovince and adjacent rocks of the Canadian Shield. . . . .	3
2.1. The Superior Province setting and subdivisions. . . . .	3
2.2. The Quetico Belt and its surrounding - lithology and metamorphic grade. . . . .	19
2.3. The deformation and metamorphic events within the Quetico belt and belt boundaries with Wawa and Wabigoon Subprovinces. . . . .	26
Chapter 3. Previous studies of the area. . . . .	37
3.1. General geology & geological mapping, metamorphism & structural studies of the area. . . . .	37
3.2. Paleomagnetism of Archean rock units within the Wabigoon, Shebandowan and Quetico Belts. . . . .	43
Chapter 4. Present project. . . . .	51
4.1. The scope of this study. . . . .	51
4.2. Field areas under investigation. . . . .	56
4.3. Field and laboratory methods of study - collection of material for laboratory studies. . . . .	63

Chapter 5. Lithology and structure of studied areas. . .	73
5.1. Review of lithology and structural observations on the Quetico Belt boundaries. . . . .	73
5.1.1. Shebandowan - Quetico belts boundary. .	73
5.1.2. Wabigoon - Quetico Belt boundary. . . .	76
5.2. Studies of the interior of Quetico Belt. . . .	80
5.2.1. Lithology and sampling. . . . .	80
5.2.2. Structural observations in the Atikokan Huronian Lake area. . . . .	93
5.2.3. Relationships between tectonic fabric along the traverse. . . . .	102
Chapter 6. Review of magnetic properties of minerals and rocks. . . . .	119
Chapter 7. Magnetic mineralogy of studied collections. .	141
7.1. Magnetic mineralogy of the belt boundaries. . .	141
7.2. Magnetic properties of magnetite and pyrrhotite in the area. . . . .	147
Chapter 8. Determinations of the directions of natural remanent magnetization (NRM). . . . .	169
8.1. The record of natural remanence in metamorphic rocks. . . . .	169
8.2. The initial natural remanence for the study area. . . . .	178
8.3. Demagnetization of remanence - procedures. . .	182
8.4. Distribution of characteristic magnetic remanences. . . . .	195



8.5. Interpretation of the distribution of ChRM directions. . . . .	207
Chapter 9. Anisotropy of magnetic susceptibility - overview. . . . .	213
9.1. The method of the AMS determination and the contribution of different minerals into anisotropy of magnetic susceptibility - terms and definitions. . . . .	215
Chapter 10. Results of AMS studies in the area. . . . .	229
10.1. Earlier contributions to MS and AMS studies in the area. . . . .	229
10.2. Sampling and selection of results in this study. . . . .	233
10.3. The bulk magnetic susceptibility results. . . . .	235
10.4. Distribution of AMS anisotropy axes. . . . .	240
10.5. The anisotropy ratios and shapes of AMS ellipsoids. . . . .	261
Chapter 11. Anisotropy of ARM method. . . . .	271
11.1. Anisotropy of remanence. . . . .	271
11.2. The determination of the anisotropy of ARM (AARM). . . . .	276
Chapter 12. ARM and its anisotropy (AARM) in the area. . . . .	287
12.1. Intensity of ARM in the area. . . . .	287
12.2. The distribution of directions of AARM foliations and lineations. . . . .	290

12.3. Shape of AARM fabrics and anisotropy parameters. . . . .	316
Chapter 13. Tectonic and magnetic fabrics - discussion. .	323
13.1. The differences between fabrics in 3 separate suites. . . . .	323
13.2. Detailed correlations of orientations of planar and linear fabrics. . . . .	328
13.3. The correlations between ARM and MS intensities and their anisotropy parameters. . . . .	342
13.4. The timing of development of the ferromagnetic phase and AARM fabric. . . . .	350
13.5. The distribution of ChRM mean planes. . . . .	353
Chapter 14. Conclusions. . . . .	357
14.1. Metamorphism, deformation and fabric in the area. . . . .	357
14.2. The mechanisms of generation of ferromagnetic phase and relations between natural remanence and tectonic and metamorphic history of the area. .	366
References. . . . .	373
Appendix A. Sampling and structural data for Atikokan - Kashabowie Lake.	
Appendix B. Magnetic fabric AMS and ARM data.	
Appendix C. Petrographic data and magnetic mineralogy data.	
Appendix D. Natural remanent magnetization (NRM) studies data.	
Appendix E. Computer programs and algorithm review.	

## Chapter 1.

### Introduction.

The rocks of metasedimentary Quetico Belt have been recently the subject of intensive studies with emphasis on structural geology, metamorphism and general mapping. This part of the Archean craton is comparably less investigated than the adjacent rocks of green-stone - granitic Wabigoon and Wawa Subprovinces. The lack of deposits of economic value and difficulties with access are the reasons that large areas have been mapped only at a reconnaissance scale. The absence of strain indicators within highly metamorphosed interior of the belt create problems with the models of deformation of this area in the late Archean "Kenoran orogeny". The area under investigation in this study (total distance about 120 km along the Highway 11 from 20 km west of Atikokan to Kashabowie Lake) has been chosen because of easy access and created the opportunity for a large area comparison of tectonic and magnetic fabrics across both margins and the interior of the belt.

The magnetic fabrics (anisotropy of magnetic susceptibility, AMS and anisotropy of anhysteretic magnetic remanence AARM) reflect the overall orientation of para- and ferromagnetic minerals within the rock. They can be quite quickly and easily determined for a substantially large collection and therefore their correlations with mesoscopic,

visually identified tectonic fabric (such as schistosity and extension lineations) can be helpful to verify the existing models of deformation of the area, especially in the view of the application of plate tectonic models to the Archean crust.

The actual state of discussion about the development and the deformation of the Superior Province as well as Quetico Belt and adjacent subprovinces is outlined in the next chapter.

## Chapter 2

The metamorphic history and probable deformation mechanisms in the Quetico Subprovince and adjacent rocks of the Canadian Shield.

### 2.1. The Superior Province setting and subdivisions.

The Superior Province within Canadian Shield is defined as an Archean craton 3.0 to 2.7 Ga old which underwent little or no deformation or metamorphism in the Proterozoic and Phanerozoic Periods. It is surrounded by the following Phanerozoic orogenic belts (Hoffman, 1989):

- a) the mainly volcanic Trans-Hudson Orogeny belt (1.9-1.8 Ga) with passive margin sedimentary sequences on the north and west;
- b) the Penokean orogenic belt (2.4 - 2.2 Ga) on the south;
- c) the Grenville orogens (1.6 - 1.0 Ga): gneissic and igneous Central Gneiss Belt and Central Metasedimentary Belt with numerous intruded plutons on the south - east;
- d) the Mesoproterozoic Midcontinental Rift filled with up to 30 km thick plateau basalts and clastic sediments passing through the Lake Superior area (Fig. 2.1.).

The existing subdivision of the Superior Province into subprovinces is based mainly on lithological and structural diversity of constituent rock units. The individual subprovinces are formed as west - east trending linear features bounded

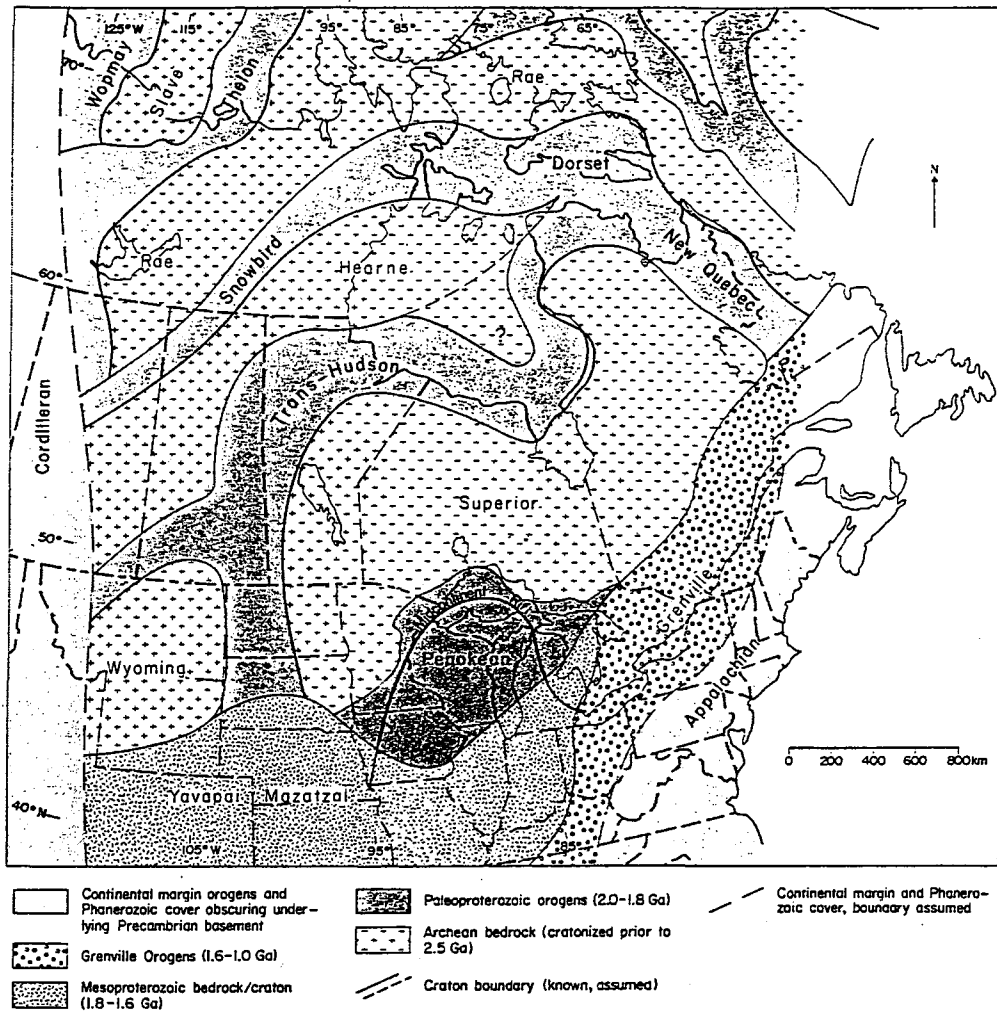


Fig. 2.1. The position of Archean Superior Province craton with respect to Proterozoic belts (from Thurston, 1991).

mainly by major faults of dominant dextral strike - slip motion (Percival, 1989). The vertical displacement of the faults is under investigation and recognized in some areas as varying although some consistent north-over south thrusting components have been proposed (Williams, 1989).

Lithologically, 4 major types of subprovinces have been defined (Card and Ciesielski, 1986):

1. "Volcanic - plutonic" (Card and Ciesielski, 1986) or "granitic - greenstone" (Williams, 1990) subprovinces with low metamorphic grade (low greenschist to low amphibolite facies) greenstone belts cut or embedded by later granitic intrusions with a dome pattern. The rock units within subprovince dated by U-Pb or Ar-Ar methods have been lately found of different ages (3.1 Ma up to 2.7 Ma).

2. Metasedimentary subprovinces consisting of mainly clastic sedimentary rocks of different metamorphic grade from low greenschist facies on subprovinces margins up to paragneisses, migmatites and pegmatites (or locally granulite facies) in the interior. Occasionally late, post - metamorphic plutons intrude. The origin of sedimentary material with respect to surrounding volcanic - plutonic subprovinces is under discussion (Williams, 1990).

3. "Gneissic" or plutonic subprovinces built of tonalite gneisses, with some smaller more mafic units and larger massive earlier sodium and later potassium - rich granitoids (Beakhouse, 1985).

4. High - grade gneissic subprovinces (by Card and Ciesielski, 1986) containing high metamorphic grade (upper amphibolite to granulite) facies meta-igneous gneisses and later cross-cutting intrusions of tonalitic, syenitic or granodioritic composition. These features are also identified within granitic - greenstone subprovinces (e.g. Kapuskasing Structural Zone within Wawa Subprovince, Thurston, 1990).

The major geographic delimitation of subprovinces boundaries offered by Card and Ciesielski (1986) as shown on Fig. 2.2., is now widely accepted (Percival, 1989, Williams, 1990, Bauer et al., 1992).

The pattern of parallel subprovinces delimited by shear zones or strike-slip faults with interleaving sequences of greenstone- granitic subprovinces (such as Wabigoon and Wawa) and meta- sedimentary belts such as Quetico Belt or English River Subprovince is unique amongst Archean terranes (e.g. Card, 1991). The most unusual feature for Superior Province is the existence of metasedimentary belts with highly metamorphosed central axes consisting of clastic material.

In the last decade, precise absolute dating of single zircon or sphene grains by U-Pb method or the use of Ar-Ar method has yielded brackets of minimum ages for the formation of rock units within belts. Occasionally, quite large differences of the age of formation are recorded between adjacent rock units (up to 200 Ma in Uchi Subprovince, Williams et al., 1992).

Major and trace elements geochemical analysis revealed also



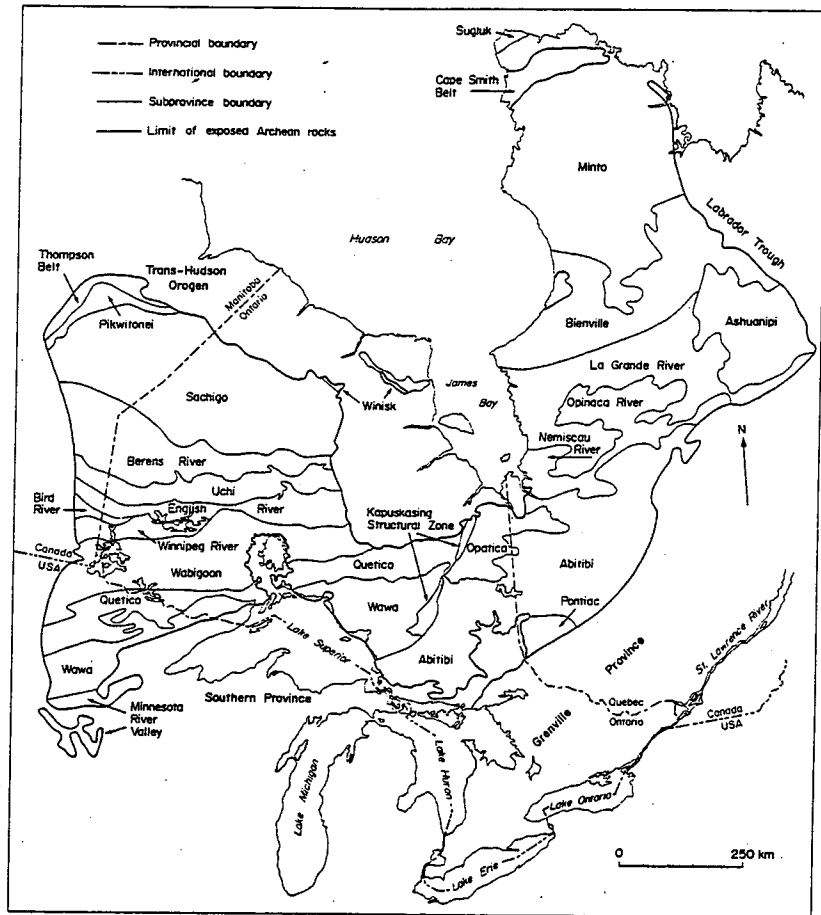


Fig. 2.2. Subdivision of the Superior Province into Subprovinces. (from Thurston, 1991, after Card and Ciesielski, 1986).

various compositions of volcanic units within greenstone belts, leading to the discrimination of different tectono - depositional environments for volcanism in the Archean (Williams et al., 1992). They are only valid if Phanerozoic models of these environments are transferable to the Archean.

In the model of Williams et al. (1992), greenstone - granitic belts are considered as sets of "tectonic assemblages" representing different tectono- depositional environments. These assemblages are believed to be grouped subsequently into larger terranes by plate tectonics: arc - arc accretion onto already earlier stabilized cratonic cores. Such a model was proposed for Wabigoon - Quetico - Wawa Subprovinces, with Wabigoon as a source of sedimentary material for Quetico Belt forming an accretionary prism, and a stable core as well (Williams, 1990, Percival, 1989). Other mobilist models were formulated for the northwestern Superior Province (Thurston and Davis, 1991, with undetermined direction of accretion) and Wabigoon River Subprovince acting as an old crustal nucleus for late Archean accretion (Dickin et al., 1991). However cratonization models (not assuming regional subduction and accretion mechanisms) are also proposed for other subprovinces (e.g. Island Lake belt of Sachigo Subprovince by Stevenson and Turek, see Card and King, 1991).

Williams et al. (1992) assumed that Archean tectono - depositional environments of greenstone belts are similar to those responsible for the evolution of modern island arc

complexes (e.g. Japan). He applied the mechanism of modern plate tectonics to explain several assemblages types in their "assemblages" model of greenstone belts. Listed types include:

- continental platforms;
- mafic plain assemblages;
- syn- to post - accretionary sedimentary sequences, such as conglomerates, wackes, siltstones and iron formations in basins;
- late unconformable basins (historically referred to as "Timiskaming type" or "Shebandowan Group").

The model of accretion is also used to interpret the overall transpressive deformation pattern within Wawa, Quetico and Wabigoon Subprovinces. Observed strike - slip fault displacements along the Quetico Fault are up to 100 km (Percival, 1989) and the shear strain component of late Kenoran deformation as well as locally ductile or brittle - ductile shear zones are recorded belt contact zones (Hudleston et al., 1988, Percival, 1989, Borradaile et al., 1988, Borradaile and Spark, 1991) and within the interior of Quetico Belt (Bauer et al., 1992; D<sub>2</sub> and D<sub>3</sub> deformation, Sawyer, 1983 - D<sub>3</sub> folding).

Some authors (Bauer et al., 1992, Williams, 1990) favour northward accretion of the Wawa Subprovince toward the Wabigoon Subprovince as being responsible for transpressive deformation of the area. Williams (1990) proposes the oblique subduction of Wawa plate beneath Quetico accretionary prism as well as an earlier regional (for the entire eastern part of the Superior Province) dip-slip underthrusting component of accreted units

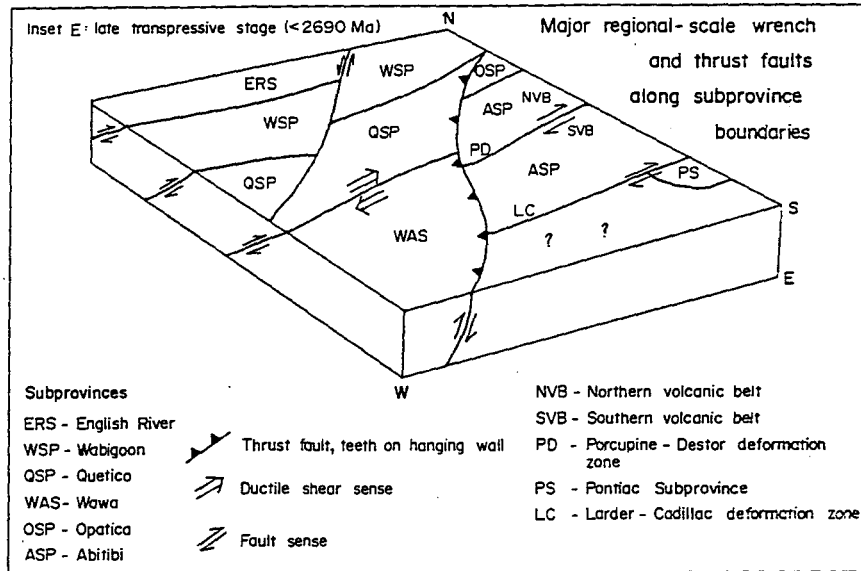


Fig. 2.3. The model (Williams et al., 1992) of a subprovince-wide (?) transpressive deformation stage in the Superior Province resulting in province-wide shortening with regional scale wrench and thrust faulting (?) along subprovince boundaries (from Williams et al., 1992).

with respect to the northern stabilized core (Fig. 2.3.). This is based on his controversial observation of early dip-slip underthrusting of Quetico sediments beneath the Wabigoon Belt in Beardmore - Geraldton Belt prior to strike-slip dextral deformation (Fig. 2.4.). However, this postulated dip - slip south side down thrusting is not reported in other areas of belt contacts.

Another structural study in the Beardmore - Geraldton area (Kehlenbeck, 1986) shows more complex pattern of structural facing and recognizes large variations in plunges of fold with EW vertical axial planes whose vergence is compatible with heterogeneous dextral shear in the area (Fig. 2.5).

The attempts to construct a more uniform accretion model of thin - to thick - skin thrusting in northern Superior Province lead to the suggestion of a southward accretion model (Williams et al., 1992- Woman arcs complex). However, a northward accretion could be also possible (Thurston and Davis, 1991).

The question of whether plate tectonics principles can be applied to the Superior Province (and Archean terranes in general) has also been discussed. Sleep (1991) indicates that Archean plates must have been rigid to produce long, consistent strike - slip faults, with size and velocities similar to modern ones.

However, the toroidal motion of crust is more energetically favoured than oblique convergent subduction to produce strike - slip motion along pre-existing subvertical planes of weakness

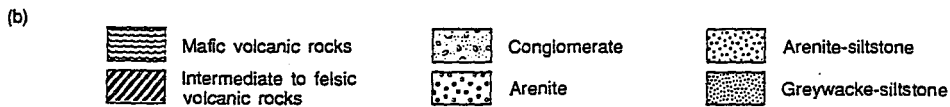
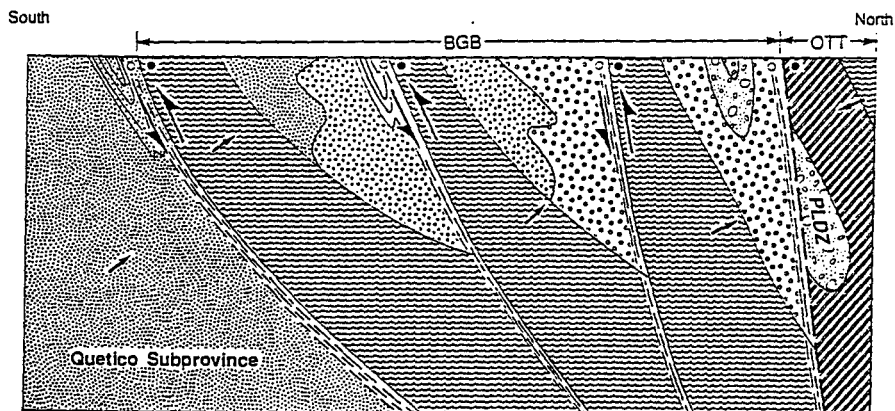
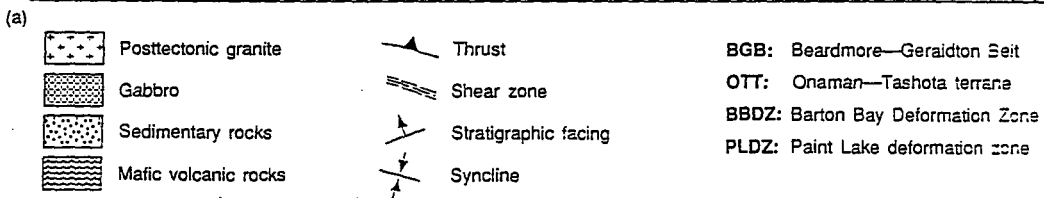
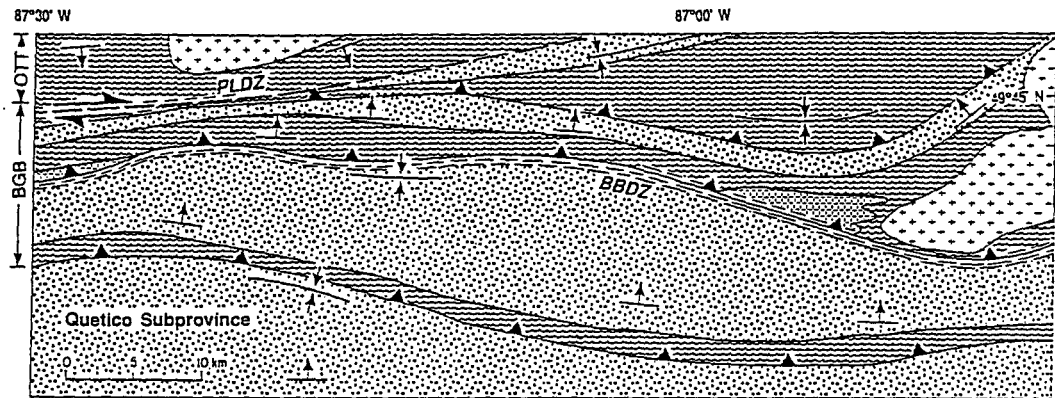


Fig. 2.4. Tectonic model for Beardmore - Geraldton Belt, showing the sequence of dip - slip faults, preceding the dextral transpression (Williams, 1991).

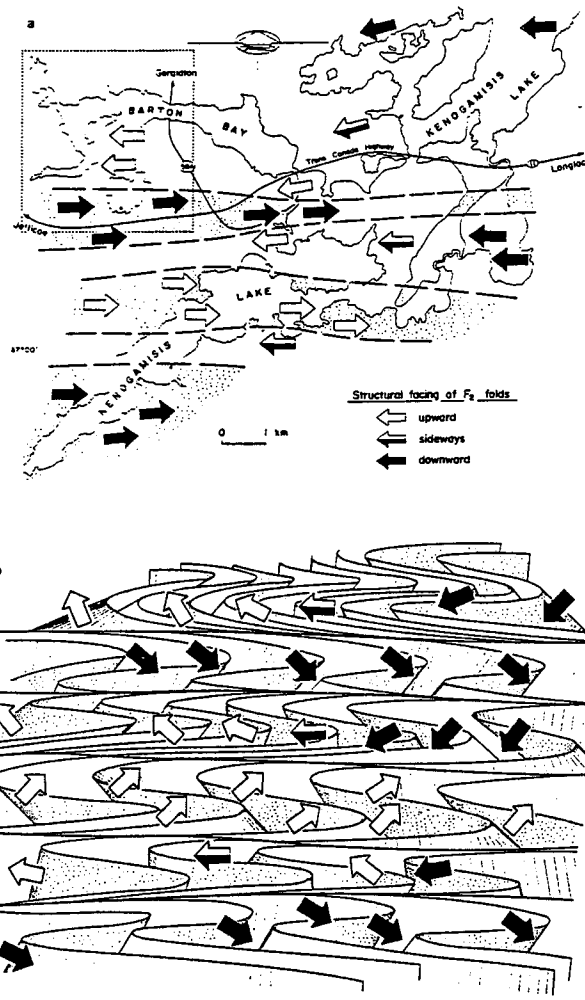


Fig. 2.5. Structural facing of  $F_2$  folds in the vicinity of Geraldton (Beardmore - Geraldton fold belt).  
 (a) Two distinct types of panels defined by sets of folds with a consistent structural facing direction.  
 (b) a schematic diagram based on data of (a), showing variations in orientation of  $F_2$  folds.  
 The zone between panels is a zone of intense shearing and transportation. (from Kehlenbeck, 1986).

such as the vertical orientations of  $S_0$  and schistosity throughout Northern Ontario. Toroidal motion also permits strike-slip movement partitioned along a set of parallel fault planes resulting in overall large boundary displacements along stable vertical faults (more than 1000 km - for a time-scale of 10 Ma).

In the progressive accretion model, the tectonic history of the Superior Province consists of the following steps (Williams et al., 1992, Table 2.6):

1. Probable fragmentation of older (>3 Ga) sialic crust - some old fragments are preserved in many greenstone belts.
2. Progressive accretion of greenstone and plutonic (Winnipeg River) terranes lasting up to 300 Ma (3.0 -2.7 Ga, Williams et al., 1992. They docked with the preexisting North Caribou terrane (Hoffman, 1989) with accompanying early calc-alkalic plutonism (pre- Kenoran "orogeny") - Fig. 2.7.
3. 2.70-2.69 Ga - erosion of older or newly extruded volcanic material and re-distribution of it into sedimentary basins, although sources of some deposited material can be exotic.
4. 2.69 Ga - progressive deformation and tectonic thickening of sedimentary prism and magmatic thickening of greenstone - granitic subprovinces with accompanying tonalitic magmatism in sedimentary prisms. Disputable northwards underthrusting of newly accreted units beneath the existing stabilized core due to the convergent component of plate motion (Williams, 1990).



Event	Time (Ma)	Criteria/Comment
Cratonization, continued thermal relaxation, brittle shearing, mylonite formation, mafic diking	post 2630?	Argon-argon blocking ages for hornblende 2.6 Ga and biotite 2.5 Ga; Matachewan diabase dike swarm 2.454 Ga; ages of mylonite and pseudotachylite 2.3 Ga
Hydrothermal alteration, associated alteration, brittle-ductile shearing and horizontal extension, retrogressive metamorphism, lamprophyre intrusion	2630?-2670	Ages of hydrous alteration in Hemlo
Late unconformable basins and alkalic magmatism, strike- and dip-slip faulting	2660-2670	Ages of Timiskaming volcanic rocks, and of clasts within coarse-grained sedimentary rocks
High-grade metamorphism, migmatization, genesis of granitic rocks, Kenoran deformation	2670-2690	Ages of syn- to posttectonic granitoids in greenstone subprovinces, pegmatites, S-type granites, metamorphic zircon grains in Ryan Migmatite and Kapuskasing Structural Zone
Calc-alkalic tonalitic magmatism in prisms, structural thickening in prism and at subprovince margins	2688-2698	Ages of plutons in Quetico Subprovince, ages of youngest volcanic rocks involved in subprovince accretion
Deposition of sediment in accretionary prisms, arc-coalescence	2690-2698	Zircon ages from Quetico and Pontiac sediments, upper limit
Final stage of calc-alkalic subaerial volcanic centres	2698-2710	
Episodic accretion of komatiitic, tholeiitic and diverse volcanic sequences; pre-Kenoran plutonism, deformation and metamorphism	2700-28??	
Mafic plain komatiitic and minor felsic volcanism, calc-alkalic plutonism	2880-2889	Age of Hawk assemblage
Calc-alkalic plutonism preserved in plutonic subprovinces and at margins of central part of Wabigoon Subprovince	2830-3170	Cedar Lake pluton $3003 \pm 5$ Ma Marmion Lake batholith $2688 \pm 3$ Ma

Fig. 2.6. A simplified table of major tectonic event in the Superior Province (from Williams et al., 1992).

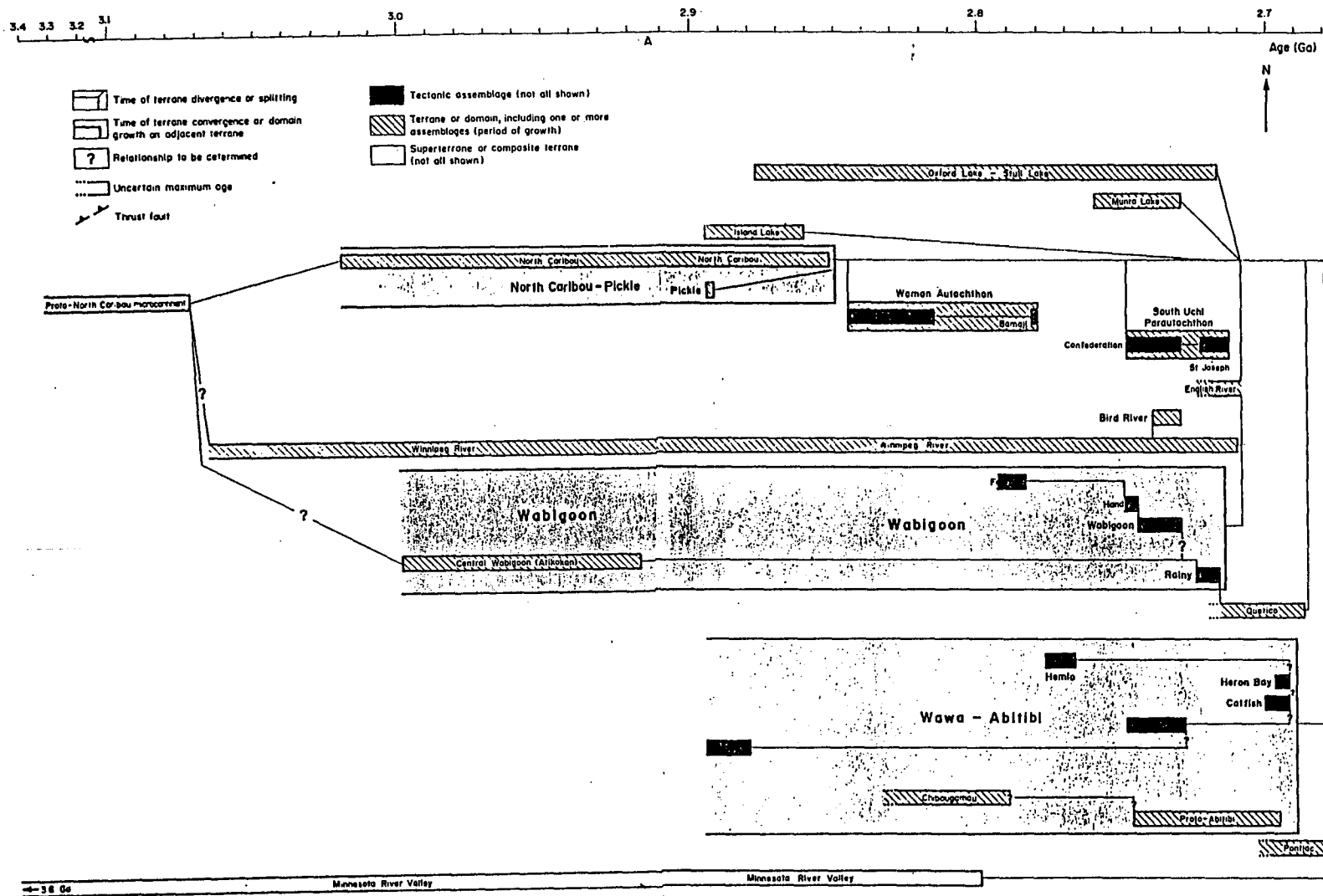


Fig. 2.7. A cladogram (Hoffman, 1986) showing known and inferred spatial and temporal relationships of tectonic units within the Superior Province and sequence of accretionary events in Williams et al. (1992) model of accretion of Superior Province.

5. 2.69 - 2.67 Ga - Kenoran deformation: N-S shortening of Superior Province and synchronous high grade metamorphism within sedimentary belts. Large scale thickening leads to partial melting and migmatization; a regionally penetrative planar fabric is developed ( $S_2$  in Bauer et al, 1991, Williams et al., 1992 terminology, in the area studied here it is  $S_1$ ). Early N - S shortening with a later dextral component (Percival, 1989, Hudleston et al., 1988, Borradaile et al., 1988) occurred during penetrative deformation within the Quetico Belt or/and adjacent rock units within Wabigoon and Wawa Subprovinces. Williams (1992) suggests that this progressive deformation can be described as 4 different stages, but these stages did not produced noticeable cross-cutting separate tectonic fabric in most areas.
6. 2.67 - 2.66 Ga - decrease in felsic magmatism, extensive strike - slip and some smaller scale late dip - slip faulting occur due to stress relaxation in NE - SW directions.
7. 2.63 -2.67 Ga - further retrogressive metamorphism, ductile and brittle - ductile shearing mainly subparallel to pre-existing fabric occur (Hudleston et al., 1988, Borradaile et al., 1988); mylonitic zones begin to form, hydrothermal alteration and late-deformation lamprophyre intrusions (Williams, 1992) take place.

8. post 2.63? Ga - strike - slip brittle shearing continues, mylonite zones are formed (Thurston et al., 1991), intrusion of mafic dykes taking place (e.g. mylonites ages are dated at about 2.3 Ga, Matachewan diabase dykes about 2454 Ma, Osmani, 1991).

Some brittle major strike - slip faulting continued to develop during the Proterozoic (late diabase dyke structures are dated up to 1.1 Ga).

## 2.2. The Quetico Belt and its surrounding - lithology and metamorphic grade.

The metasedimentary Quetico Belt is formed mainly of greywacke, siltstone and sandstones metamorphosed to schist and paragneisses with common intrusions of I - type granitic plutons, pegmatites and leucogranites. In the interior there are S - type granites of metasedimentary origin of the belt (Fig. 2.8.). Iron formations, ultramafic conglomerates and metasediments are rarely met. The sedimentary rocks show features of unstructured turbidite fans, with the rapid deposition and little segregation. Some authors claim the source of detritus from the north (Wabigoon green-stone belts?), especially in the northern part of Quetico belt. However, sedimentary material can be transported from much larger distances (Williams, 1991). The basement rocks on which the sediment was deposited have not been recorded. Dating of detrital zircons shows the ages of clastic sources ranging from 3.1 to 2.702 Ga; the time of sedimentation is bracketed by intrusive diorite plutons and granodioritic dikes as prior to 2.688 Ga (Percival, 1989).

The belt trends SW - NE from northern Minnesota to the Kapuskasing Structural Zone (KSZ) on the east on the distance of 1200 km with varying width from 100 km, down to 10 km near to Kashabowie (as a result of late faulting).

The contact against the Wabigoon Subprovince is delimited

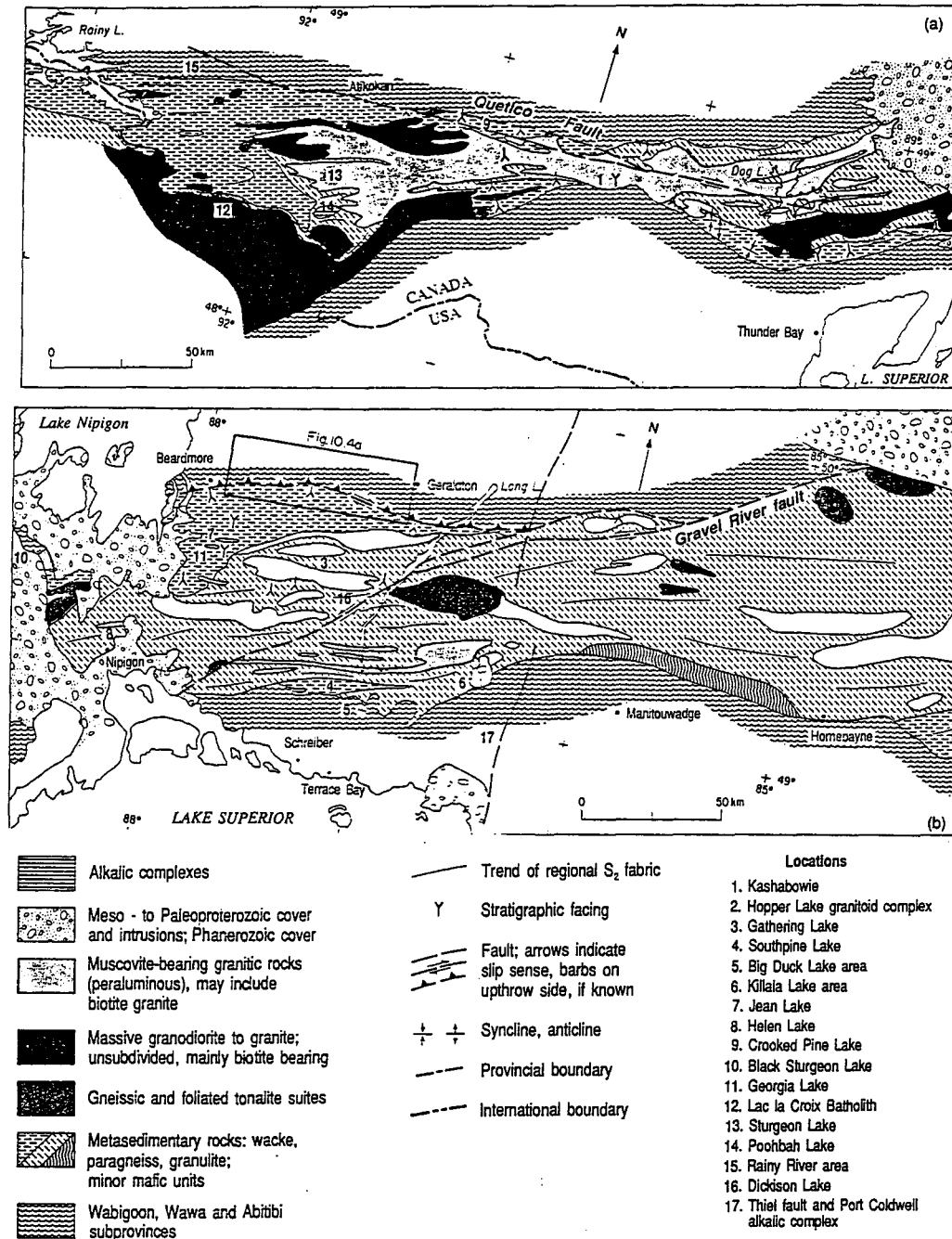


Fig. 2.8. A simplified geological and tectonic map of the Quetico Subprovince (from Williams, 1991).

on the west by the late-formed strike - slip, steeply dipping Rainy Lake - Seine River Fault separating amphibolite facies metamorphic grade volcanic - tonalite plutonic Wabigoon Belt and amphibolite facies metasediments of the Quetico belt. Going east the belt boundary is marked by the late Quetico Fault with mylonitic and cataclastic zones along it. Metamorphic isograds showing a transition from greenschist to amphibolite facies are observed parallel to the fault. A broad ductile dextral shear zone in the stratigraphic volcanic - sedimentary sequence in the Beardmore - Geraldton area is present (Kehlenbeck, 1986) in the east. Williams (1987) claimed also evidence of earlier dip - slip movement (with Quetico Belt rocks underthrusting the Wabigoon Subprovince rock units).

In Minnesota (where the Quetico Belt is named the Vermilion Granitic Complex) the belt boundary with Wawa Subprovince is marked by a set of dip - slip and strike - slip faults, with metamorphic grade facies contrasted across the boundary (amphibolite facies in Quetico belt versus greenschist facies in Wawa), but with common syn-metamorphic penetrative tectonic  $D_2$  fabric (Hudleston et al., 1988), accompanying dextral transpression. This fabric is  $D_1$  fabric of the area described in this thesis.

In the Quetico Park area mylonitic zones separate biotite-rich granites and schists of the Quetico belt from hornblende bearing plutons of Wawa; further east both sinistral and dextral strike -slip faults are present on the subprovinces boundary

(Percival, 1989). In the Huronian Lake area the boundary is only lithological with both sides of the boundary sharing a common penetrative tectonic planar fabric, common younging direction to the north, upward structural facing (Spark, 1990, Borradaile and Spark, 1991), and low metamorphic grade increasing laterally through the contact toward the centre of the Quetico Belt (Pirie and Mackasey, 1978). Further east in the Shebandowan area, faults bound the outliers of "Timiskaming like" conglomerates and volcanics in Wawa Subprovince (Borradaile and Brown, 1987) and penetrative tectonic fabric there (locally  $D_1$ ) is correlated with the  $D_2$  (Percival, 1989) deformation (2689 - 2684 Ma) in both subprovinces. The most eastern part of the belt contact is very heterogeneous with common north dipping mylonite zones (Williams, 1987).

The grade of metamorphism within the Quetico belt increases symmetrically toward the central axis of the belt (Percival, 1989). In Minnesota in the Rainy Lake - Seine River area, biotite schist of high greenschist facies is observed. The belt margin assemblages of garnet - sillimanite - staurolite - biotite (Tabor, 1988) and assemblages with kyanite instead of sillimanite locally along the faulted northern margin of the subprovince are gradationally replaced by higher grade assemblages up to garnet - sillimanite - cordierite, muscovite + K-feldspar and K-feldspar without muscovite migmatites toward the centre of the belt (Bauer et al., 1991). The helitic trails in porphyroblasts as well as relations between fabric and growing



porphyroblasts indicate that metamorphism is syntectonic with transpression events during Kenoran "orogeny". In more plutonic areas, contact metamorphism locally overprints earlier regional metamorphic textures. In the Vermilion granitic complex only few diagnostic assemblages can be found in Lac La Croix granites and migmatites (Percival, 1989).

In the Wawa belt (Vermilion district greenstone belt in Minnesota) the metamorphic conditions were those of lower greenschist facies with local increase to amphibolite facies. In the margins of the belt with prolonged deformation conditions, the observed greenschist facies assemblages are considered as retrograde (Bauer, 1986, Tabor, 1988).

Further north - east along the Quetico Belt in meta-sedimentary schist south of the Quetico Park the metamorphic grade increases slowly toward the centre of the belt from chlorite - muscovite zone through well defined and widely spaced isograds of biotite, sillimanite and garnet sillimanite assemblages toward migmatite zone in the centre of the belt. Pelitic rocks north of Poohbah complex show the presence of cordierite - andalusite - garnet and staurolite bracketing maximum temperature conditions close to 500° C.

The metamorphism of margins of the Quetico belt from Atikokan area to the east was studied by Pirie and Mackasey (1978). The Wabigoon - Quetico north boundary in the Crooked Pine Lake area, Atikokan - Sapawe area and Perch Lake - Calm Lake area (Borradaile et al., 1988, Sarvas, 1988) is

characterized by narrow 4- 5 km lateral transition in metamorphic grade from muscovite - chlorite zone just south of the Quetico Fault through biotite, garnet - andalusite, locally staurolite isograds into garnet - sillimanite, garnet - sillimanite - cordierite and migmatite zones. In the migmatites the paleosome schist of lower grade is still preserved. An analogous, mirror symmetry transition is reported for Planet - Huronian, Shebandowan - Drift Lake (Pirie and Mackasey, 1978) and in the Huronian area (Sawyer, 1983). Numerous leucogranite intrusions of more than 5 km in diameter within the interior of the belt may be responsible for sharp thermal gradients in their surroundings and local contact metamorphism.

The migmatites in the western Quetico Belts have the granitoid component produced by metamorphic differentiation, whereas east of Kashabowie *in situ* melt is present also (Percival, 1989). Kyanite is found only locally at Raith (Percival, 1989) and cordierite is present east of Raith in leucosomes and white granites.

Further east, steep lateral metamorphic gradients in the belt margin areas are recorded, in the Lappe and Geraldton - Long Lake areas. The very high grade granulites are found locally in the Flanders Lake area and regionally at the contact with Kapuskasing Structural Zone in migmatites (Percival, 1989), where Lower Crustal rocks are thrust to the surface.

The geothermobarometry methods applied by Percival (1989) deliver the estimated values of metamorphic pressure from 250

MPa (Lac La Croix - Poohbah Lake area) up to 540 - 610 MPa in the granulite zone. It is suggested that the pressure along the strike of the belt varies from 550 MPa in the Minnesota through 250 MPa (Poohbah Lake) and 330 MPa (Raith) to even 610 MPa in the east near the Lower Crustal rocks of Kapuskasing (granulites). Percival (1989) favours different rates of post-metamorphic uplift and erosion along the belt. The eastern part of the belt achieved also higher temperatures of peak metamorphism as concluded from the existence of cordierite above anatexic reaction, in situ granitic melts and granulites (up to 700° - 780° C) as opposed to 500° C peak temperature at Poohbah Lake - Lac La Croix area).

2.3. The deformation and metamorphic events within the Quetico belt and belt boundaries with Wawa and Wabigoon Subprovinces.

Structural studies at the belt margins as well as in the interior of the Quetico belt have revealed up to four different penetrative fabrics in the some areas (Vermilion Granitic Complex, Bauer et al., 1992, Beardmore - Geraldton area, Williams, 1991). However, the belt margins as well as some areas within the belt possess only one or two penetrative schistosity or a single set of complex- geometry folds (Borradaile et al., 1988, Borradaile and Spark, 1991, Sawyer, 1983, Kehlenbeck, 1986). Therefore the problem of correlation of the fabric throughout the region is crucial for an interpretation of the sequence of events (Bauer et al., 1992).

A local notation of observed fabric ( $D_1, S_1; D_2, S_2$  and so on) is usually for each of different area and this fact should be also taken under consideration (e.g. in Table 2.9).

Rocks of adjacent Wawa and Wabigoon belt prior or in early stage of deposition of Quetico sediments underwent episodes of volcanism and associated plutonism. The early stage of volcanism was recorded in Mormion - Lumby lakes volcanics and tonalites; 2992 -2999 Ma old (Davis and Jackson, 1988) and in Wawa in 2888 Ma old volcanics; "Keewatin" volcanism in both subprovinces was dated at 2755 - 2702 Ma in Wabigoon and about 2733 Ma in Wawa (Percival, 1989, Blackburn et al., 1991).

Table 2.9. A classification of tectonic events and tectonic fabrics for various areas of the Quetico Belt.

Bauer et al., (1992)	Percival (1989)	Borradaile et al. (1988)	Quetico Belt interior	Borradaile & Spark, (1991)	Kehlenbeck (1986)	Williams (OGS) (1992)
Vermillion Granitic Complex, Rainy Lake wrench zone Rainy L. - Seine L. fault zone Quetico - Wawa margin	Quetico belt - overview	Atikokan area Quetico - Wabigoon margin	Interior of Quetico Belt - east of Atikokan - west of Kashabowie	Kashabowie-Huronian area Quetico-Wawa margin	Beardmore - Geraldton area Quetico - Wabigoon margin	Quetico belt overview
<p><b>D<sub>4</sub></b> N-S shortening; kink bands and folds N- NE striking, ductile shear zones &amp; fault zones</p> <p><b>D<sub>3</sub></b> shear deformation; open F3 folds, NW - striking; crenulation cleav. S3; S-C-C' fabrics; steep shear zone (Rainy Lake - Seine River fault zone)</p> <p><b>D<sub>2</sub></b> transpressive deform. - upright F2 folds plunging E or W; penetrative axial planar S2, some brittle-ductile E-striking dextral shear zones.</p> <p><b>D<sub>1</sub></b> major F1 recumbent folds - nappe structures; sheath folds, S1 parallel to S1 at belt margins;</p>	<p><b>D<sub>3</sub></b> small scale F3 folds in migmatitic rocks (?)</p> <p><b>D<sub>2</sub></b> - transpressive deformation - steep regional S2 fabric, upright F2 folds</p> <p><b>D<sub>1</sub></b> N-S compression in Vermillion granitic complex, S1 schistosity locally parallel to primary bedding F1 folds of varying geometry, often nappe-like</p>	<p><b>D<sub>1</sub></b> dextral transpressive deformation; penetrative S1 fabric sub-parallel to bedding; anticlock-wisely asymmetric folds and sheath folds</p>	<p>(?) <b>D<sub>2</sub></b> locally minor folds (?) In migmatites (Kashabowie area, Sawyer, 1983)</p> <p><b>D<sub>1</sub></b> dextral transpression; NE-SW trending S1 penetrative foliation; no fabric in felsic units; less steep dips of S1 than at belt margins shallow plunges of L1; (this thesis)</p>	<p><b>D<sub>1</sub></b> transpressive deformation - only one penetrative schistosity S1 steep, NE-SW trending; fabric is correlated through the contact of Wawa &amp; Quetico Subprovinces</p>	<p>locally S3 -N-S trending axial surfaces of conjugate kinks and chevron folds.</p> <p><b>D<sub>2</sub></b> S2 - E-W striking cleavage coplanar with F2 folds; F2 folds are displaced along shear E-W surfaces.</p> <p><b>D<sub>1</sub></b> S1 fabric parallel to bedding; locally asymmetrical to recumbent F1 folds later refolded.</p>	<p><b>D<sub>4</sub></b> shear zones, boundary dextral shears and N-E faults</p> <p><b>D<sub>3</sub></b> upright folds, shallow plunges of lineations</p> <p><b>D<sub>2</sub></b> isoclinal folding, regionally wide S2 planar fabric, variable plunges</p> <p><b>D<sub>1</sub></b> isoclinal folding; locally observed S1 fabric parallel to bedding, N over S dip - slip faults (Geraldton - Beardmore area (?)).</p>

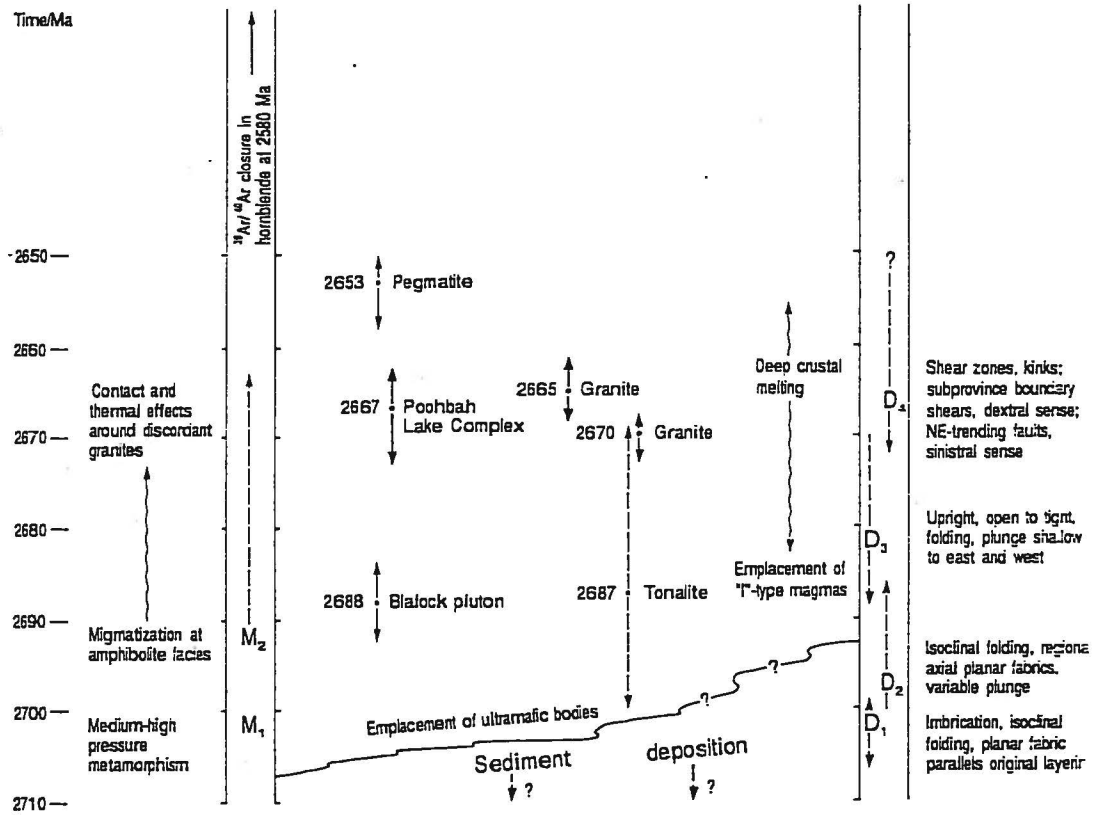
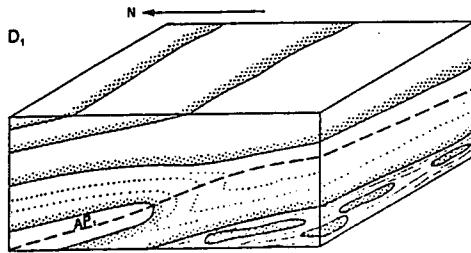


Fig. 2.10. The chronologic sequence of events in the Quetico Belt (from Williams, 1991).



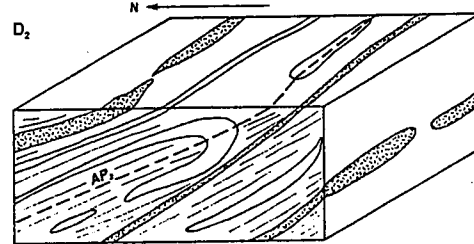
**D<sub>1</sub>**  
 Soft-sediment deformation: sediment dewatering, submarine sliding, breccia formation and quartz veining.

Strain: inhomogeneous, focussed on pelitic layers and bedding-parallel shears.

Stratigraphic facing: predominantly north.

Folding: isoclinal, bedding-parallel planar fabric, axial planes (AP) bedding-parallel, variably oriented axes.

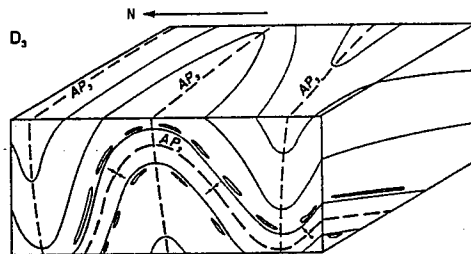
Metamorphism: medium to high pressure, emplacement of ultramafic bodies.



**D<sub>2</sub>**  
 Folding: isoclinal, pervasive, regionally east-trending L-S fabric, axes with curvilinear plunge in schistosity. Layer-parallel shearing, progressive obliteration of bedding and way-up indicators.

Intrusion: emplacement of tonalite and leucogranite.

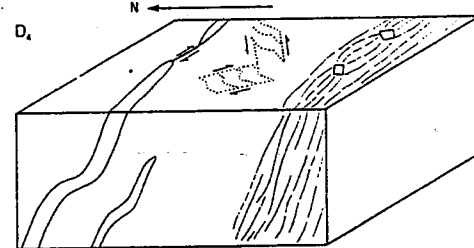
Metamorphism: total recrystallization of primary minerals during amphibolite-facies metamorphism. Migmatization in central and southern parts of Quetico. Folding and boudinage of leucosomes.



**D<sub>3</sub>**  
 Folding: upright, with shallow east- or west-plunging axes. Steepening of tectono-stratigraphic units.

Intrusion: continued development and emplacement of granitic rocks.

Metamorphism: continued production of differentiated layering, migmatitic leucosomes at amphibolite and granulite facies.



**D<sub>4</sub>**  
 Boudinage of veins and intrusive sheets during regional extension along length of subprovince. Formation of sigmoidal veins and extensional shears within shear zones.

Fig. 2.11. A schematic model of 4 stages of deformation within the Quetico Belt (from Williams, 1991).

The early stage of the region-wide deformation  $D_1$  (2695 - 2685 Ma in Wabigoon, 2696- 2689 Ma in Wawa, Williams et al., 1991) was postulated at belt margins (Beardmore - Geraldton area, Williams, 1990) as well as in Vermilion Granitic complex (Bauer et al., 1992, Jirsa et al., 1992). The authors (Bauer et al., 1992) find an evidence for this episode in the existence of  $S_1$  foliation parallel to bedding,  $F_1$  isoclinal, recumbent and nappe folding and sheath folding in the west - southern Quetico and in downward facing of upright  $F_2$  folds in the Wawa - Quetico boundary in Minnesota (Table 2.9). Williams (1990) correlates this episode with the existence of down-dip fold axes and mineral and stretching lineations observed by him in Beardmore - Geraldton area. The dip-slip south-down shearing with shortening across the belts would be responsible for these structures. However no evidence for  $D_1$  deformation was found in other areas (Bauer et al., 1992). Williams (1991) suggests also the existence of regionally wide medium - high pressure, low temperature metamorphic  $M_1$  event correlated with his  $D_1$  (Fig. 2.10. 2.11), based on metamorphic minerals chemistry studies of rocks north of Vermilion Granitic Complex by Tabor et al. (1989). Nevertheless no high pressure metamorphism mineral assemblages were recorded.

The deposition of Seine conglomerate in the northern margin of the Quetico belt, intrusion of granodioritic sills (Percival, 1989) within the Quetico belt and "Timiskaming like" volcanism in Wawa are dated as post-  $D_1$  (Seine conglomerate



deposition: 2686 - 2695 Ma; "Timiskaming like" volcanism, 2689 Ma, Williams et al. , 1991).

The regional transpressive deformation  $D_2$  with dextral shear component (2689 - 2684 Ma, Williams et al., 1991) produced penetrative cleavage  $S_2$  striking WNW to west in all studied areas along the belt margins as well as in the interior. It implies a common history of metamorphism and deformation for all three belts at least pre -  $D_2$ , and maybe also during  $D_1$  deformation (Percival, 1989). But note that Percival uses  $D_1$ ,  $D_2$  etc. to denote major tectonic/plutonic events, not microfabrics.

The  $D_2$  deformation is supposed to rotate existing  $F_1$  folds into vertical plane (Bauer et al, 1992), to produce new upright  $F_2$  folds trending parallel to  $S_2$  and with various plunge (east or west), both planar  $S_2$  and linear  $L_2$  tectonic fabrics, and concentrated brittle - ductile shear zones (Hudleston et al., 1986, Borradaile et al., 1988, Borradaile and Spark, 1991, Kehlenbeck, 1986). The extensive  $F_2$  folding could occur in the areas where the shortening component across the area was dominant. However, in the central region of Quetico belt, where the shear component was parallel to preexisting  $S_0 - S_1?$  fabric no substantial polyphase deformation was recorded (Borradaile et al, 1988, Borradaile and Spark, 1991).

This tectonic episode caused also progressive obliteration of existing bedding and way - up indicators, obscuring determination of younging direction and structural facing in most high grade metamorphosed areas (Borradaile and Spark,

1991).

Williams et al. (1991) correlate this deformation with the emplacement of plutons within greenstone belts (e.g. Burchell Lake pluton in Wawa, Ottertail Lake pluton in Wabigoon) and the beginning of amphibolite facies metamorphism in the Quetico Belt.

Percival (1989) indicates that intrusion of tonalites and leucogranites within the Quetico Belt was much later than adjacent processes in the neighbouring greenstone subprovinces. The differentiated layering and migmatization, the generation of ptygmatic folds and boudins correlated with peak metamorphism (anatexis) in the centre of the belt is also syn- to late -  $D_1$  (Williams, 1991). Some inconsistency in the timing of metamorphism can be noticed as Tabor (1988) interpreted sillimanite as pre - to syn-  $D_2$  and Sawyer (1983) considered staurolite and andalusite post-  $D_2$ . This is most probably a problem of correlation and identification of deformation fabrics, not a genuine difference in age of deformation.

Bauer et al., (1992) correlate more open folds (named as  $F_3$ ), observed in south - western Quetico belt and in the migmatitic core of the belt near Kashabowie (Sawyer, 1983) and a new  $S_3$ -  $L_3$  tectonic fabric in the south - west part of the belt with a new stage of deformation ( $D_3$ ), which follows the same transpressive regime as  $D_2$ . The continuing transpression is responsible for the reorientation of  $F_2$  folds with more shallow plunges of fold axis and  $L_2$  fabric and a steepening of the

tectonic planar fabrics (fig. 2.9) (Williams, 1991).

In the other areas no distinct  $D_3$  structures were generated by the separate event. Bauer et al. (1992) suggest that the lack of an  $S_3$  tectonic fabric in most of the region is due to the contrast in the ductility of the migmatitic core units.

According to Williams (1991), the increase in grade of metamorphism during  $D_3$  of higher grade produced high temperature in situ leucosomes and granulites already during the  $D_3$  episode.

The felsic magmatism within the Quetico Belt and the emplacement of granitic rocks is dated as late  $D_3$  by Williams, (1991). These events are produced due to thermal relaxation and deep crustal melting following the proposed accretion mechanism (Percival, 1989, Williams et al., 1992).

Conjugate ductile shear zones and later, more brittle faults zones (mainly on subprovince boundaries) are associated with  $D_4$  deformation of mainly dextral shear component (Bauer et al. 1992).

In the migmatitic core of the belt no regionally consistent simple shear kinematic structures are recorded due to high local heterogeneity of strain and ductility contrast (Percival, 1989).

The intrusion of pegmatite granites is dated as 2653 Ma (Percival, 1989, Williams, 1991), and therefore late- to post- $D_4$ . These late- intruded units of white, pink and pegmatite granites (2671 - 2653 Ma) should be only weakly deformed by the dominant shear component of strain. These stocks produced also

contact metamorphism aureoles around themselves and locally mechanically tilted the surrounding schist and paragneiss layers.

Distinct  $D_2$  -  $D_4$  deformation phases are not recognized widely on the belt boundaries in central and eastern part of the belt, as the subsequent dextral shear deformation obscured eventual earlier fabrics (Borradaile and Spark, 1991). Instead, rather one long lasting transpressive deformation model is more applicable there.

Variation in plunge of mineral and extension lineations (east or west shallow plunges) as well as the variations in the structural facing (e.g. Kehlenbeck, 1986, Borradaile, 1982, Borradaile et al., 1988) indicate that strain pattern can be very heterogenous locally. The region-wide models of deformation (e.g. Williams et al., 1992, fig. 2.5) cannot be easily confirmed locally (e.g. the sense of shear or dip - slip changes along the Quetico - Wawa margin).

Percival (1989) indicates also the conflict between the metamorphic grade varying along the belt strike and gently east plunging fold axes and extension lineations. Neither post-tectonic passive tilting nor (Williams et al., 1992) south - side down dip-slip  $D_1$  motion can explain these discrepancies. However variations in metamorphic grade of exposed units might be explained by the mechanism of isostatic adjustment of thickened accretionary prism after tectonic deformation (Percival, 1989).

Borradaile and Spark (1991) explained variations in the steep thermal gradients locally in the Kashabowie - Huronian area as a function of thermal conductivity anisotropy (after Borradaile and Hermes, 1980).

It would appear that the regional models of uniform accretionary mechanism similar to modern plate tectonics models (Williams et al., 1992) seem to be too simplified for the Quetico Belt tectonic and metamorphic history.

## Chapter 3.

### Previous studies of the area.

#### 3.1. General geology & geological mapping, metamorphism & structural studies of the area.

The first stratigraphic and lithological studies of the area were performed by Lawson (1888) in the Rainy Lake area (20 km west of Perch Lake). He recognized "Couchiching metasediments" and "Keewatin metavolcanics", but could not determine the reversed sequence of these rocks due to overturned folding (Poulsen et al., 1980). Gradational metamorphism from low grade schists to gneisses and migmatites in the interior of the Quetico belt were first noted in the 1920's by Grout (1925) and Tanton (1926).

More extensive studies of regional metamorphism through the belt were reviewed by Pirie and Mackasey, (1978). They indicated a steep metamorphic gradient toward the axis of the belt in Crooked Pine Lake area (Pirie, 1977), Sapawe - Atikokan area (mapped by McIlwaine and Hillary, 1974 and Shklanka, 1972), Planet - Huronian Lake area (mapped by Giblin, 1964 and Harris, 1970) and Shebandowan - Drift Lake area (mapped by Morin, 1973 and locally by Birk, 1971). The pattern of metamorphic isograds across the Quetico Belt was also studied along Highway 17 by Kennedy (1980).

Studies of chemical composition of igneous intrusive bodies

(from hornblende and nepheline syenite to tonalites, monzonites and leucogranites), within the interior of the belt were summarized by Pirie and Mackasey (1978) and Percival (1989). The variety in their composition together with radiometric dating led to the correlation of the time of their emplacement with the regional tectonic models for the Quetico belt (Williams, 1991).

Systematic regional mapping was mainly performed in areas with economic mineral deposits, such as the Kashabowie - Shebandowan or Atikokan - Steep Rock Lake areas. These areas were mapped at a scale of 1:31,680 by OGS or GSC, presenting lithology, structure, metamorphism and mineralization. The other areas, especially the interior of the belt, were mapped only at a reconnaissance scale. The compilation maps of the area were prepared by Thurston (Atikokan - Lakehead 1:253,440 compilation map, 1985) and Percival (the interior of Quetico, 1:250,000, 1988).

Radiometric dating was performed for metasedimentary greywackes with use of U-Pb method on detrital zircon grains (2702, 2880 and 3100 Ma) as well as for intrusive granites and pegmatites and granodioritic sills (2687 Ma) within metagreywackes (Percival and Sullivan, 1988). "Timiskaming-like" volcanics and later Keewatin volcanic sequences were also dated in the Shebandowan area (Corfu and Stott, 1986, 2689-2696 Ma for Timiskaming). Some intrusive bodies within Quetico belt and in Shebandowan belt near the area were also dated: Shelley Lake granite (Berger and York, 1979, 2580 ± 20 Ma), Poohbah alkaline

complex (Mitchell, 1976,  $2700 \pm 25$  Ma), granites around Burchell Lake pluton (Dunlop, 1984, 2550-2600 Ma). They bracketed the timing for deformation and metamorphic events in the area (Percival, 1989) as well as gave age references for late Archean (2750-2500 Ma) paleopole path for the Superior Province (see Vandall and Symons, 1990 for review).

Structural geology of the area was investigated in detail only recently. Earlier studies were focused on the boundary of Quetico belt with Wabigoon belt. Prior to Hawley's (1929) studies, the structural interpretations are not consistent. They varied from south dipping monoclines (Lawson, 1913) to regional synclines or

anticlines with fold axes along the central axis of the Quetico Belt. Consistent regionally younging to the north with some local reversals in younging directions was first listed by Tanton (1926). Tight folds forming of en-echelon structure were interpreted by Hawley (1929) as contemporary to the formation of the Quetico Fault during horizontal shearing event.

Recent structural studies along the Wabigoon- Quetico belt boundary delimited the set of tight to isoclinal sheath - fold structure showing dextral asymmetry and varying plunges and structural facing. Borradaile's (1982) studies followed by Dutka, (1982), Stubley, (1983) and Stewart, (1984) indicated the locally curvilinear nature of  $F_1$  fold axes and axial planes parallel to the belt boundary. Some primary asymmetrical minor folds show the dextral shear component of deformation



(Borradaile et al., 1988).

A single penetrative subvertical  $S_1$  tectonic fabric parallel to the belt boundary was recorded by Sarvas (1988). Intersection lineations  $S_0/S_1$  plunge gently to east near Atikokan (Borradaile et al., 1988) but they are scattered along the  $S_1$  plane to the west, where the fabrics are more oblate (Calm Lake - Perch Lake area, Sarvas, 1988).

The more detailed studies of the contact of Wawa and Quetico Subprovince near Shebandowan lakes begun in 1960's. Minor faults were delineated during systematic mapping, therefore the fault contact between the belts was postulated (Hodgkinson, 1968). The model of isoclinal folding based on the variations of younging directions in deformed pillow lavas within the Shebandowan belt metavolcanics was also proposed.

Sawyer (1983) mapped fold structures and described the cases of reversed symmetry of minor folds on limbs of major folds. Therefore he introduced a model of multiphase penetrative deformation in the area. The granitic diapirism was proposed as the mechanism responsible for deformation as well as a production of nappe folds. This was not confirmed by studies of Spark (1991) and Borradaile and Spark (1991), who found only a single penetrative deformation fabric  $S_1$  in each studied outcrop (see the last paper for discussion). Along the transect through belt boundary from Kashabowie Lake toward Huronian Lake they recorded consistently oriented E-W vertical  $S_1$  fabrics and younging to the north (where preserved).

Variations in strain pattern ( $L>S$  versus  $S>L$  tectonites) and the plunge direction of the  $L_1$  tectonic fabric component were also observed within the Shebandowan greenstone belt (Stott 1985). Scott associated them with two-phase deformation. However, the pattern of different strain domains did not correlate with a single penetrative foliation for an anisotropy of magnetic susceptibility (AMS) fabric (Borradaile and Brown, 1987) within the Shebandowan belt. Stott appears to have classified lineations as  $L_1$  or  $L_2$  according to the directions of their plunge (E or W). However, Borradaile et al. interpret this as one fabric lineation which varies in plunge. Stott nowhere describes one fabric cutting the other.

Within the interior of Quetico Belt Sawyer (1983) and Stott and Schnieders (1983) mapped penetrative fabrics. Folding correlated to deformation producing regionally penetrative single fabric was observed. Sawyer suggested that the presence of shallow plunges of these folds is due to next deformation event.

In the traverse from Huronian Lake to Atikokan through high grade migmatites no detailed structural study has been performed. The magnetic fabric studies (anisotropy of magnetic susceptibility) method was used on both belt boundaries for correlation with tectonic fabric studies in the area (Spark, 1991, Sarvas, 1988).

Kennedy (1984) used this method along the Quetico Fault and obtained oblate AMS ellipsoid coaxial with strain. Borradaile

and Brown (1987) determined single penetrative AMS foliation in metavolcanics of the Shebandowan belt, contrary to the results of Stott and Schnieders, 1983).

Sarvas (1988) used AMS studies to examine the correlation between AMS magnetic lineations and foliations and tectonic fabric:  $S_1$  cleavage and  $S_0/S_1$  intersection lineations in the Calm Lake - Perch Lake area in low grade metasediments south of the Wabigoon - Quetico Belt boundary. He obtained a single penetrative oblate AMS fabric regionally coaxial to the fold axial planes (Borradaile et al., 1988).

Spark (1991) used this method for the traverse across the Shebandowan - Quetico Belt contact from Kashabowie Lake toward Huronian Lake along steep metamorphic gradient. A single penetrative magnetic lineation is here significantly deflected from the  $L_1$  petrofabric lineation consistently with dextral shear. The shape of the AMS ellipsoid was oblate for all but few outcrops. No significant correlation was found between magnitudes of strain and magnetic fabric.

### 3.2. Paleomagnetism of Archean rock units within the Wabigoon, Shebandowan and Quetico Belts.

The main interest of paleomagnetic studies lies in the determination of the characteristic remanent magnetization (ChRM). It is usually crucial to find whether ChRM is a primary component of the NRM that can be correlated with a specific tectonic event or a chronological event. If the direction of the ancient magnetic field is to be determined the direction of NRM should not have been reoriented due to subsequent tectonic deformations unless the amount of such reorientation can be estimated. Such corrections are not trivial and involve considerable complications. Thus paleomagnetic studies have not been widely performed within metamorphic Archean belts in the Superior Province of Canadian Shield in north-western Ontario.

The only extensive studies of late Archean paleomagnetism in the region were done by Dunlop both in reconnaissance and as more detailed project in several separate late Archean rock units within Wabigoon, Quetico and Shebandowan belts (Dunlop 1979, 1983, 1984a, 1984b, 1985). However, he deliberately chose massive, weakly strained bodies and avoided the sheared metamorphic rocks examined in this study.

Together more than 450 samples from about 120 sites in 12 locations were collected by Dunlop for NRM determinations (see Table 3.2 and map of locations - Fig 3.1). The areas studied were mainly late to syn - tectonic igneous intrusions or weakly

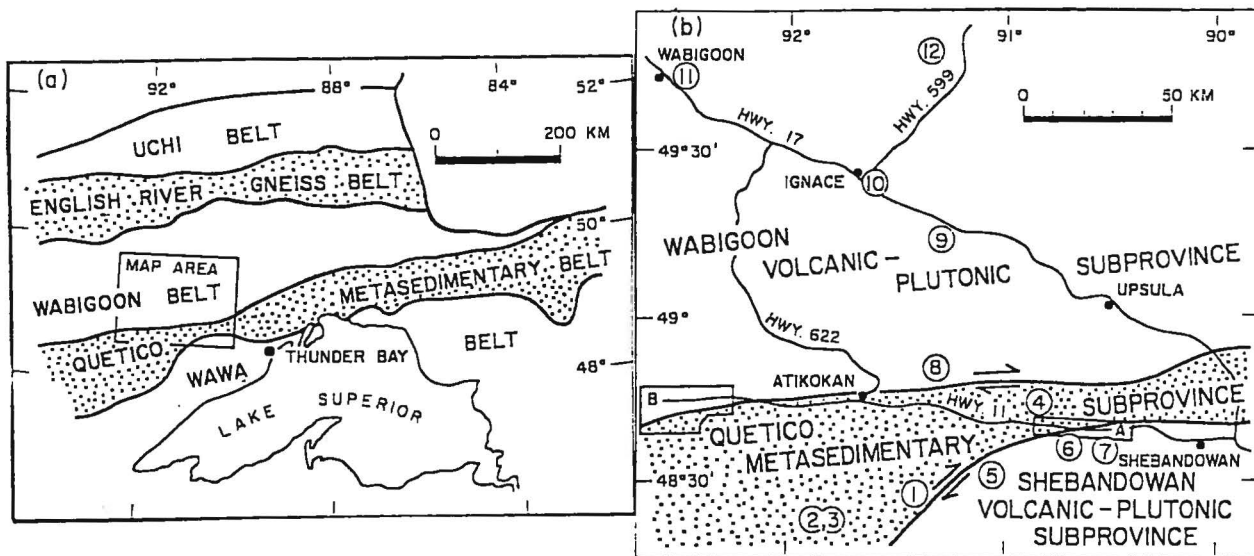


Fig. 3.1. The map of the NW Ontario region showing localities of rock units with found mean NRM directions for Archean. (after Borradaile et al., 1993)

Site numbers are as follows:

- 1 - Shelley Lake granite, 2580 Ma (Dunlop, 1984a);
- 2 - Poohbah Lake alkaline complex, R remanence 2650 Ma (Dunlop 1985);
- 3 - Poohbah Lake alkaline complex, N remanence - 2550 Ma? (Dunlop 1985);
- 4 - Huronian granite, paragneiss, (2.6 Ga?) (Dunlop, 1979);
- 5 - McKenzie Lake diorite (2.6 Ga?) (Dunlop, 1979);
- 6 - Burchell Lake granite, 2550 - 2600 Ma? (Dunlop, 1984b);
- 7 - Shebandowan gabbros, 2.8 Ga (Dunlop 1979);
- 8 - Sapawe iron formation, 2.6 Ga (Dunlop 1979);
- 9 - Gulliver greenstone, 2.8 Ga (Dunlop, 1979);
- 10 - Ignace, Martin gneisses, unknown age (2.8 Ga?) (Dunlop, 1979);
- 11 - Wabigoon gabbro, 2.8 Ga? (Dunlop, 1983);
- 12 - Watcomb granite, 2.6 Ga (Dunlop, 1979);

Note: Disregard the A and B areas.

strained, massive metamorphosed igneous bodies within the interior of the belts (Percival 1989). In these units the ChRM should not have been significantly reoriented due to strain.

**Table 3.2.** Mean remanence directions for Archean formations in NW Ontario (after Dunlop 1979,1983,1984a,1984b,1985).

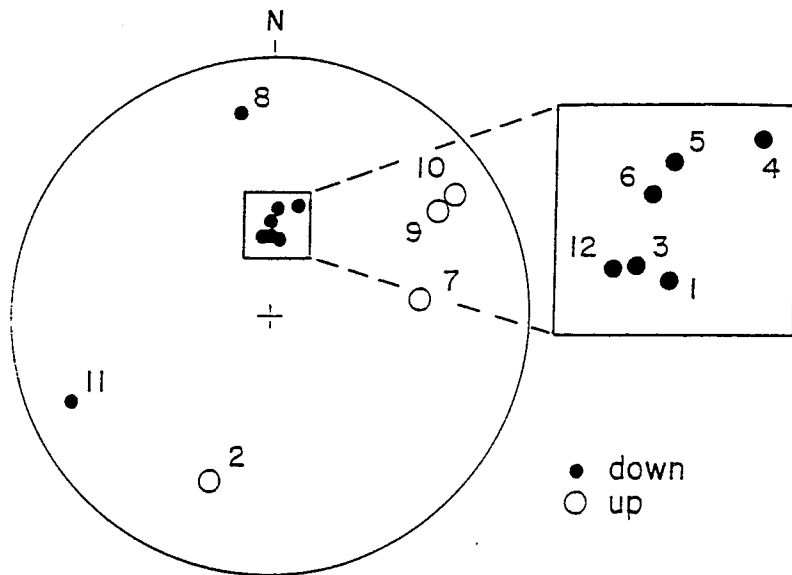
No	Formation	N	D(°)	I(°)	k	$\alpha_{95}$ (°)	References
Quetico gneiss belt							
1	Shelley Lake granite	12/43*	5.9	56.4	95.4	4.4	Dunlop 1984a SL1
2	Poohbah Lake alkaline complex	13/39	198,0	-22.5	62	5.3	Dunlop 1985 R
3	Poohbah Lake alkaline complex	13/35	359.5	55.5	28	8.3	Dunlop 1985 N
4	Huronian granite	?/14	14.7	42.3	25.8	7.9	Dunlop 1979
Shebandowan volcanic - plutonic belt							
5	McKenzie Lake granite	?/6	4.6	45.5	24.1	13.9	Dunlop 1979
6	Burchell Lake granite	10/36	2.3	48.9	23.9	10.0	Dunlop 1984b BL1
7	Shebandowan gabbros	?/8	82.9	-28.6	13.7	15.4	Dunlop 1979
Wabigoon volcanic - plutonic belt							
8	Sapawe iron formation	?/11	351.5	13.4	6.1	20.0	Dunlop 1979
9	Gulliver greenstone	?/9	57.3	-14.6	8.6	18.5	Dunlop 1979
10	Ignace, Martin gneisses	?/5	55.9	-8.7	10.0	25.3	Dunlop 1979
11	Wabigoon gabbro	11/29	246	12	19.5	10.5	Dunlop 1983
12	Watcomb granite	?/11	356.7	55.6	16.3	11.6	Dunlop 1979

Note: \*No of sites/ No of samples, ? - unknown.

Remanence studies for the Huronian Lake granite, McKenzie Lake granite and Shebandowan gabbros as well as for the most of Wabigoon Belt localities should be regarded as of reconnaissance value (only a few samples collected for each unit - see Table 3.2). Later paleomagnetic studies for Poohbah Lake alkaline complex, Burchell Lake granite, and Wabigoon gabbro were based on larger collections of samples and can be expected to give more reliable characteristic remanence directions. These directions which were interpreted by Dunlop as primary remanences are listed in the Table 3.2 (after Borradaile et al., 1993).

It has been assumed that a stable primary component of NRM was acquired by a given rock unit during cooling after post volcanic plutonism (as in the case of igneous bodies such as the Burchell Lake granite) or after low grade metamorphism. The determined characteristic remanence directions were then correlated with tectonic events affecting the investigated rock units. Dunlop interpreted them as locally pre-deformational (pre-tectonic - localities No 7,9,11 in the Table 3.2) or post-tectonic (rock units No 1,2,6,8,12).

Late Archean tectonic events were dated for these units as ranging from 2700 Ma - 2650 Ma (Percival 1989) till 2580 Ma (Shelley Lake granite - Berger and York 1979). These correlate closely with the ending of tectonic activity in all three belts (Wabigoon B. - 2702 Ma, Shebandowan B. - 2692 Ma), detrital deposition in the Quetico sedimentary basin up to 2702 Ma and



NRM primary directions (Dunlop 1979, 1983, 1984 a, b, 1985)

Fig. 3.3. Stereographic plot of the NRM directions obtained by Dunlop for a total of 246 samples, in NW Ontario (see Fig. 3.1 for sites).



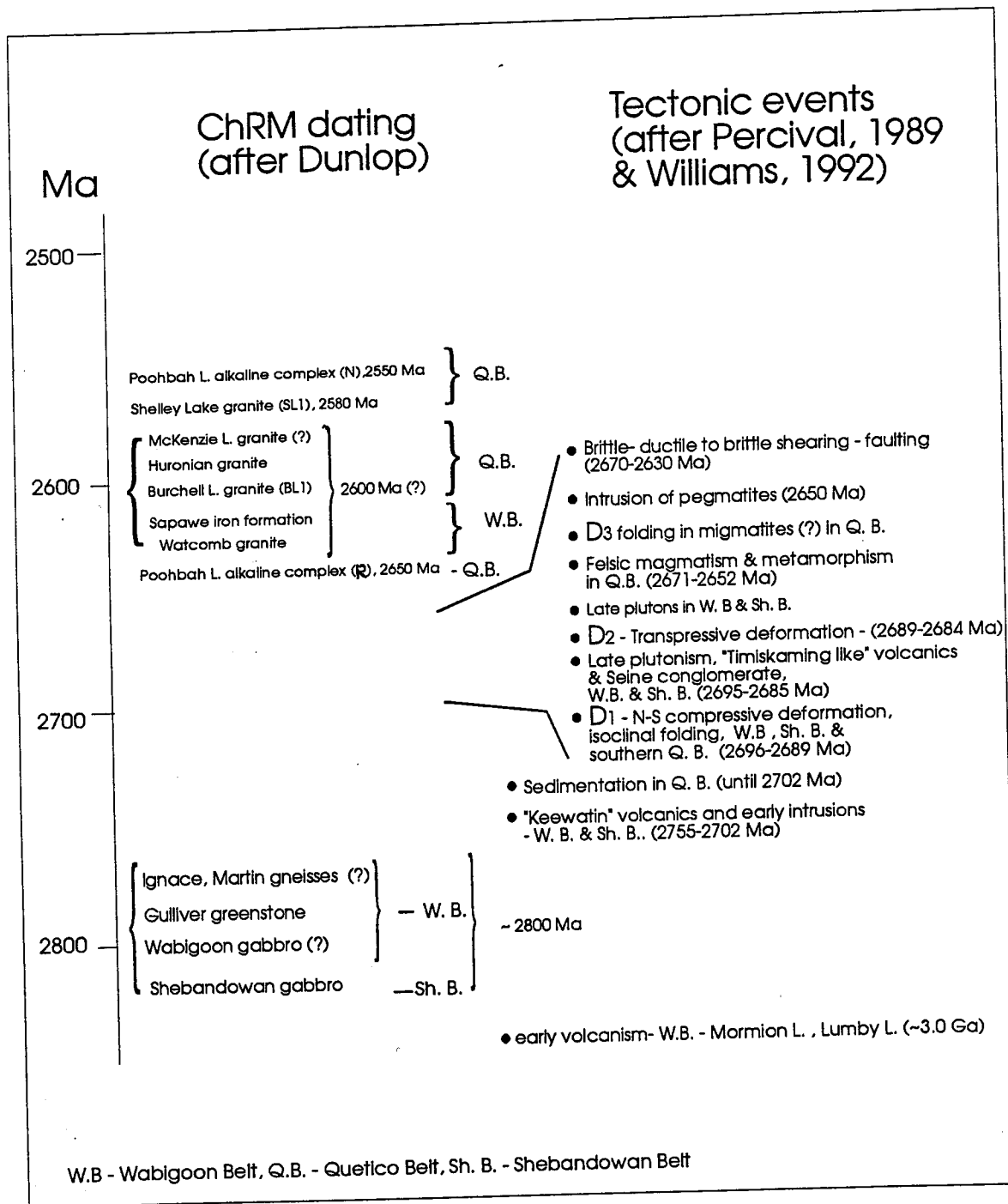


Table 3.4. The comparison of estimated times of acquiring of ChRM by intrusive bodies with age relationships of tectonic events in the Quetico Belt and its surroundings.

the closure of the Quetico sedimentary trough at 2685 Ma (all dating after Percival 1989)- see Table 3.4.

With the exception of No 2 direction in Table 3.2 the post-tectonic mean NRM directions for the listed rock units group closely around  $Dec=005^\circ$ ,  $Inc=55^\circ$  (Fig. 3.3) and can be interpreted as acquired during cooling after syntectonic recrystallization. Some earlier remanence determinations (Dunlop 1979) show a more scattered pattern. At first inspection one might interpret these as poorly defined NRM mean directions due to a small number of samples. On the other hand, they are located in ENE-WSW quadrants and could be regarded as pre-tectonic and reoriented from their primary positions by tectonic strain or stress (Borradaile et al., 1993). The mechanism of the reorientation of existing remanence directions due to the transpressive shear deformation will be discussed later.

## Chapter 4.

### Present project.

#### 4.1. The scope of this study.

The project is a continuation of the wider study program of magnetic fabrics and the structure of late Archean metamorphic belts - mainly Wabigoon, Quetico and Shebandowan Belts northwest from Thunder Bay performed in Lakehead University. The study investigates the structure of the interior of Quetico Belt, the distribution of tectonic and magnetic fabrics along the traverse across highly metamorphosed schist - migmatite - pegmatite outcrops along Highway 11 from Atikokan to Huronian Lake and an effect of transpressive deformation on paleomagnetic data from the area (Fig. 4.1). I have investigated possible correlations between the directions of tectonic fabrics (schistosity, gneissic layering and extension lineations) with the anisotropy of magnetic susceptibility (AMS) and the anisotropy of anhysteretic remanent magnetization (AARM) for the areas of low metamorphic grade at the belt margins (Atikokan area and Huronian Lake - Kashabowie Lake area) and in the belt core of higher metamorphic grade east of Atikokan toward the Huronian Lake.

The determinations of characteristic remanence directions and anisotropy of ARM were performed on the previously collected

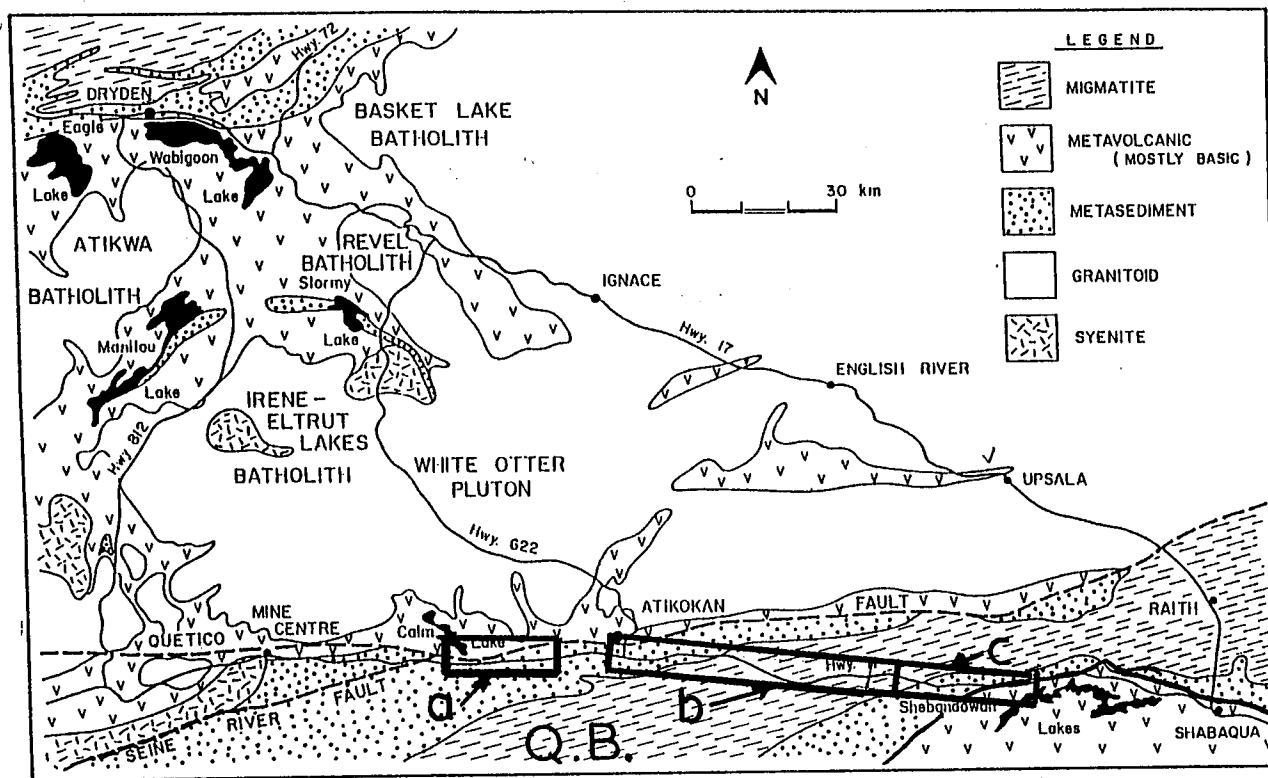


Fig. 4.1. Areas under study within the metasedimentary - migmatitic Quetico Belt (Q.B.).

- a) - Calm Lake - Perch Lake area - low grade metasediments at the northern margin with metavolcanic Wabigoon Belt;
- b) - traverse Atikokan - Huronian Lake;
- c) - traverse Huronian Lake (migmatites in Quetico Belt) to Kashabowie Lake in low grade metavolcanics in Shebandowan Belt.

specimens from Quetico - Wabigoon belt boundaries (west of Atikokan) and Quetico - Shebandowan belt boundary (Kashabowie - Huronian Lake traverse). Samples and hand specimens used previously for AMS studies by Sarvas (1988) and Spark (1990) had not been exposed to high fields and were used here for NRM determinations and ARM anisotropy determinations. Newly obtained results are compared with mineral fabrics and AMS directions determined in the two previous projects (opus cit.).

The study checks the validity of models of generating new para/diamagnetic and ferrimagnetic fabrics in an area undergoing a transpressive shear deformation and the use of magnetic fabrics as kinematic indicators of progressive deformation. I attempt also to explain the behaviour of ChRM directions in deformed rock units due to effects of the reorientation or resetting of the predeformational remanence. The further problem is the contribution of newly crystallized ferrimagnetic minerals (such as pyrrhotite) to the postdeformational NRM.

I conducted the field observations and laboratory experiments that included:

- (1) reconnaissance mapping of tectonic fabrics and lithology within the interior of Quetico Belt - the traverse W-E from Atikokan to Huronian Lake along Highway 11 - in 77 outcrops;

- (2) collecting oriented hand specimens (92 from outcrops in the traverse above and 20 additional hand specimens from outcrops from Kashabowie - Huronian Lake area) for the laboratory measurements and mineralogical studies. Specimens

were not drilled in the field - oriented specimens but were brought to the laboratory and drilled there.

(3) preparation of 294 cylindrical cores for AMS, ARM and NRM studies from collected material (175 from the interior of Quetico Belt and 119 from Quetico - Shebandowan belts boundary);

(4) determination and analysis of bulk magnetic susceptibility and its anisotropy (AMS) of cylindrical cores from the interior of Quetico Belt and Quetico -Shebandowan belt boundary;

(5) demagnetization of NRM in 237 selected samples from all three collections using thermal and alternating magnetic field methods of demagnetization. Calculation of characteristic remanence directions and analysis of their distribution.

(6) studies and interpretation of anisotropy of anhysteretic remanent magnetization (AARM) for 154 selected cylindrical samples from all three traverses;

(7) correlations of anisotropy of ARM and AMS fabrics with tectonic fabrics and distribution of characteristic magnetic remanence directions;

(8) correlation between anisotropy of saturation isothermal remanent magnetization (SIRM) and anisotropy of ARM for some selected samples;

(9) mineralogical studies of ferrimagnetic minerals within samples by means of magnetic hysteresis and Curie point determinations;

(10) analysis of the metamorphic grade and magnetic minerals based on thin sections of several selected localities;

(11) correlation of AMS, anisotropy of ARM and RM data with magnetic mineralogy.

#### 4.2. Field areas under investigation.

The studied traverse within the interior of Quetico Belts runs from wacke - mudstones, chlorite and biotite schist just south of Atikokan and adjacent to the Quetico Fault going east along Highway 11B and 11 through a very steep metamorphic gradient (Percival, 1989, Pirie and Mackasey, 1978). It crosses biotite, almandine and staurolite isograds extending toward Sapawe and Eva Lake and enters the migmatite and pegmatite zone. Further east, it leads through massive pegmatites east of Windigoostigwan Lake toward the Atlantic - Arctic Ocean watershed just east of Huronian Lake (map - Fig. 4.2), again in the migmatites.

Sampling was done regularly, at least every 1 km with minor exceptions in poorly exposed areas, along Highway 11 with 10 additional outcrops visited north of highway 11 along unmapped logging roads or minor highways 633 and 623 (map - Fig. 4.3). Most exposures were fresh roadcuts along the highways with both tops and sides of outcrops easily accessed. There is extremely little weathering of most outcrops.

The additional hand specimens came from an E-W traverse across Shebandowan - Quetico Belts boundary previously studied by Spark (1990) and Borradaile and Spark (1990). This transect extends from Kashabowie near Shebandowan Lake in low metamorphic grade greenschist facies metavolcanics on the east through biotite schist into migmatites within the high grade



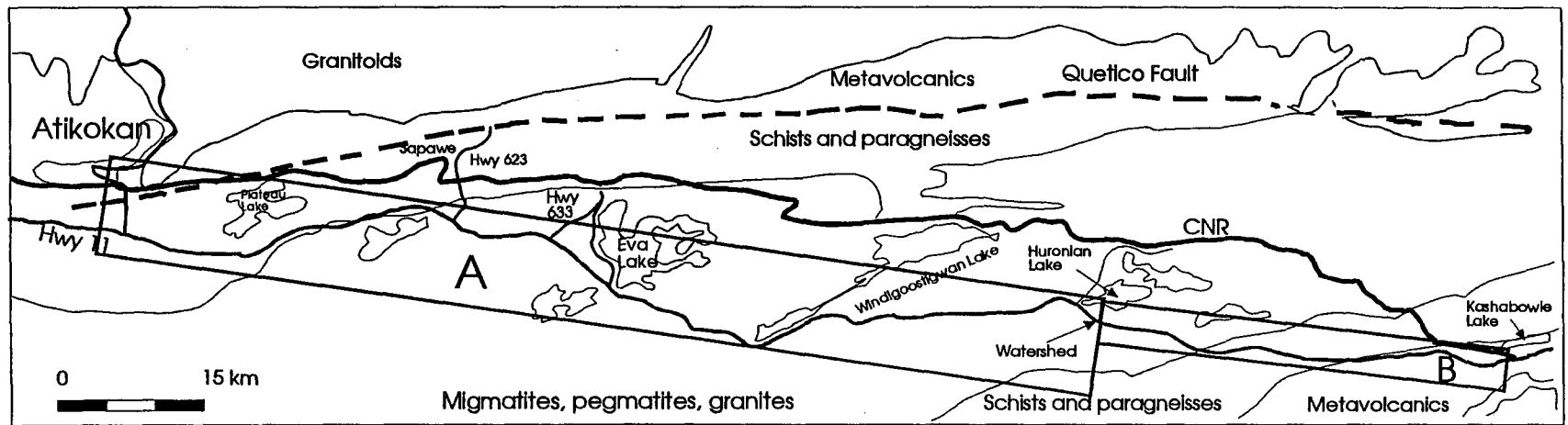


Fig. 4.2. Detailed subdivision of studied area correlated with lithology:  
 A - traverse Atikokan - Huronian Lake;  
 B - traverse Huronina Lake - Kashabowie Lake.

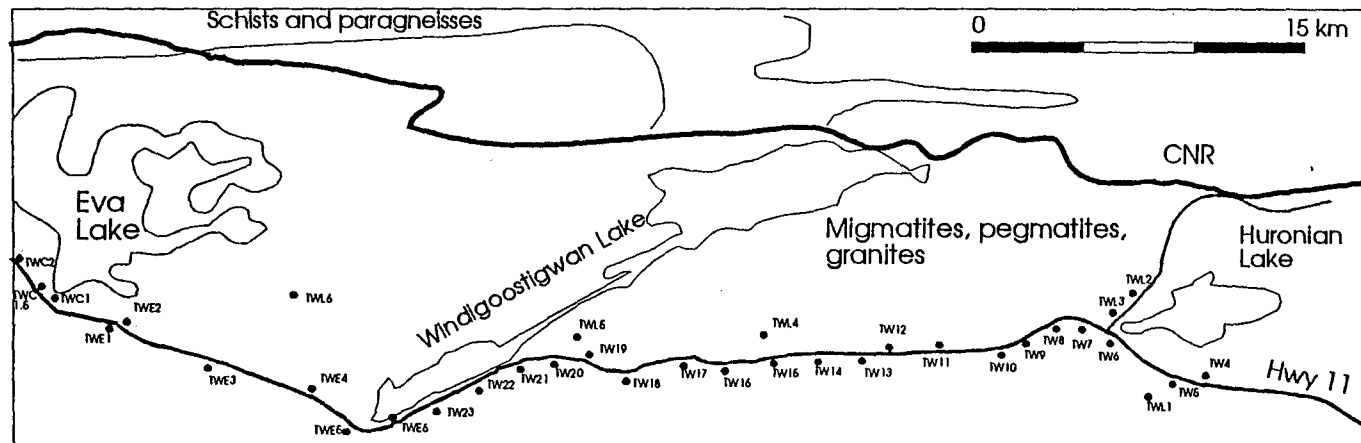
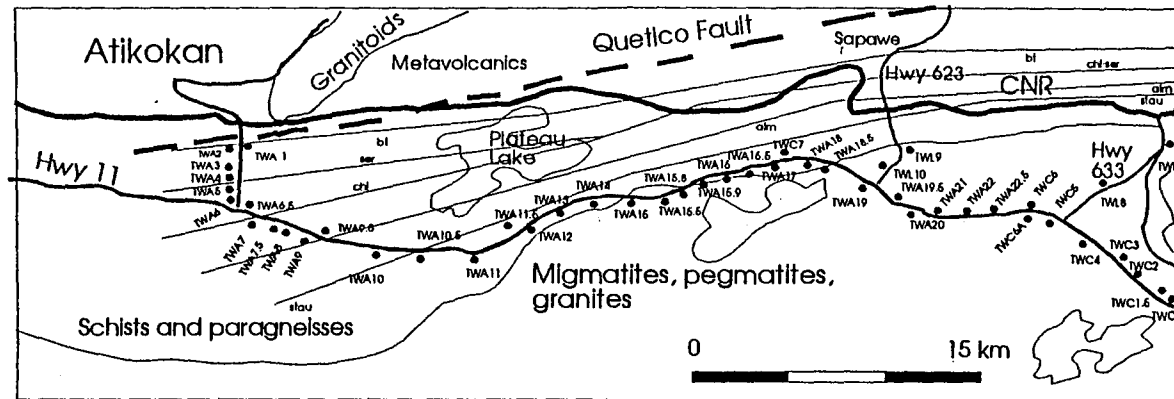


Fig. 4.3. Sampling sites within Quetico Belt - traverse Atikokan - Huronian Lake correlated to metamorphic isograds and lithology.

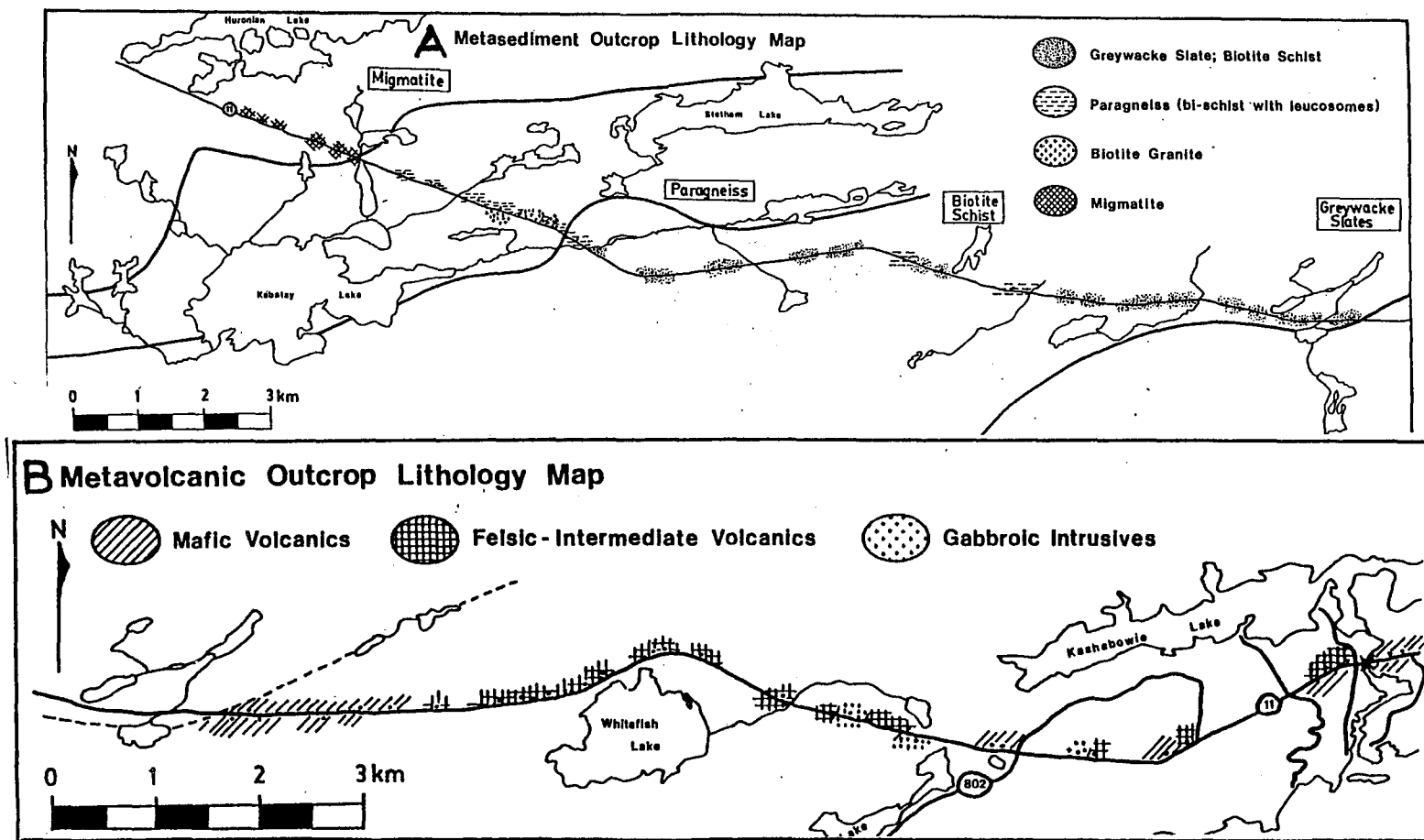


Fig. 4.4. Lithology at the Quetico B. - Shebandowan B. margin along Huronian L. - Kashabowie L. traverse (from Spark, 1990).

metamorphosed metasedimentary interior of Quetico Belt and terminates at the Atlantic- Arctic watershed near Huronian Lake (Fig. 4.2 and 4.4). This area was revisited and a new collection of 20 oriented hand specimens was obtained due to insufficient number of oriented cores (total 58) for AMS and ARM studies remaining from the previous project by Spark.

Previously collected (by Spark, 1990) cores (see localities on the map - Fig 4.5) were used also for determinations of ChRM directions and ARM studies (these were not a part of Spark's (1990) project). These were only used by Spark for low - field magnetic susceptibility measurements (AMS). Therefore it can be assumed that the low magnetic field ( $48 \text{ A/m} = 0.6 \text{ Oe}$ ) that was applied to these specimens has not influenced their NRM.

In addition, a set of 244 oriented cylindrical core samples from the Quetico - Wabigoon Belt boundary was also used as the material for ARM anisotropy and NRM determinations. The material was collected by Sarvas (1988) and Borradaile and Sarvas (1989) in two transects along Quetico Fault in the Calm Lake - Perch Lake area, west of Atikokan, mostly within the Quetico belt.

The southern traverse (also along Highway 11) extended from low grade chlorite schist and phyllites next to belt boundaries west from Calm Lake, crossing the isograds at a low angle as it passed into the higher grade metamorphism in the interior of Quetico belt to the west. The observed lithologies were metamorphosed mainly from sandstones and mudstones (Sarvas, 1988). The northern traverse (along CNR rail track) also crossed

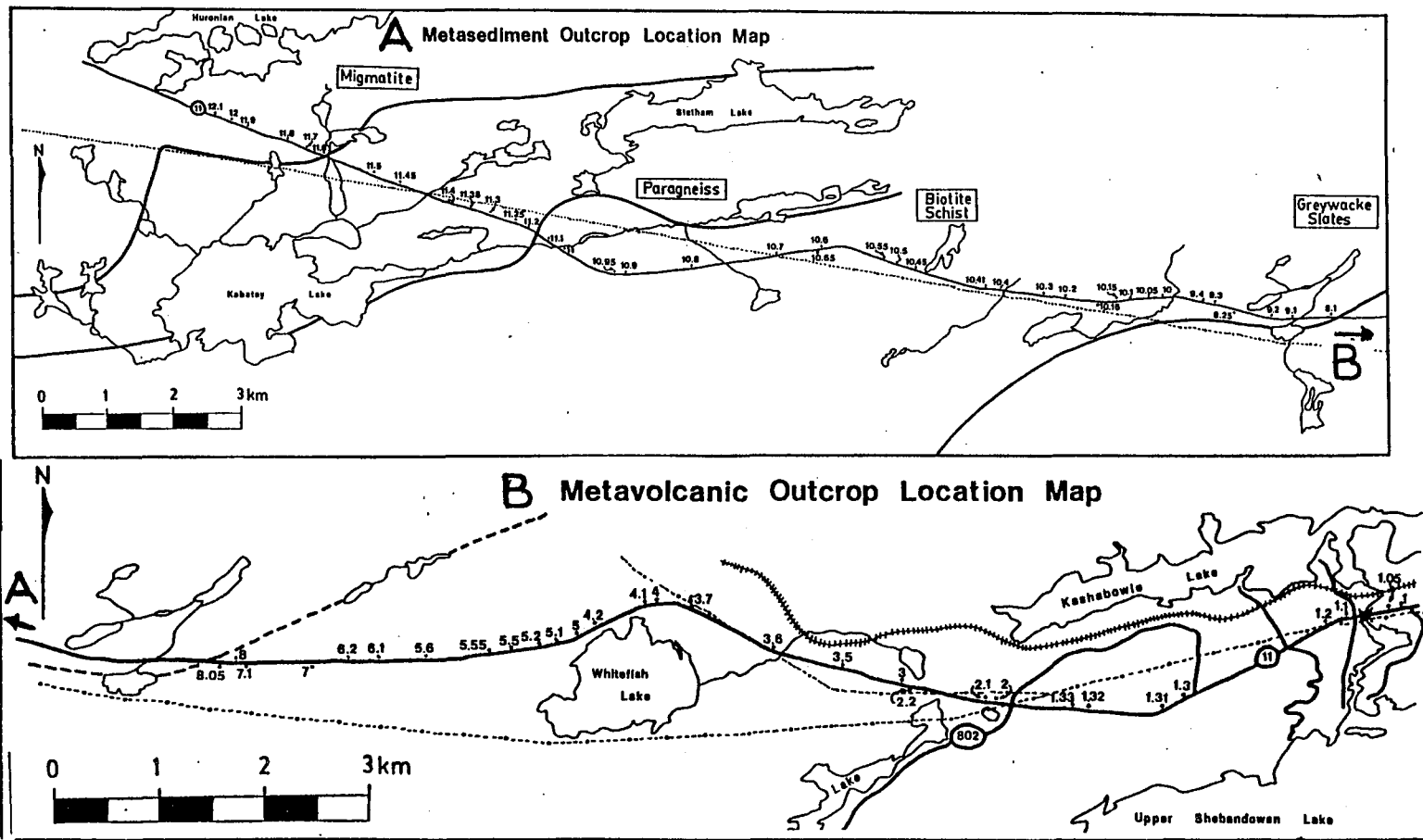


Fig. 4.5. Sampling sites along Huronian L. - Kashabowie L. traverse (from Spark, 1990).

the Quetico Belt and led through metavolcanics derived mainly from mafic flows and more felsic volcanoclastics with Quetico Belt metasediments recurring east of Banning Lake. Both transects were terminated around Perch Lake about 10 km west of Atikokan, in biotite schist.

Samples from this collection were only previously used for low magnetic field AMS studies and thus remained suitable for my NRM determinations and ARM studies described here.

The areas outside the transportation lines (such as highways and rail tracks) were not sampled and studied. Within the interior of Quetico Belt only a few outcrops away from the highways were visited. Usually only a flat upper surface was available for structural measurements. Collection of hand specimen in the massive recrystallized migmatites and pegmatites was extremely difficult. Thus poorly exposed off - road outcrops could be only sampled with use of back- pack drill, but this was too time consuming. Nor were the logging roads in the Quetico belt easily accessible for the sort of rental vehicles used during the field work.

#### 4.3. Field and laboratory methods of study - collection of material for laboratory studies.

The transect within the interior of Quetico Belt was visited, mapped and sampled during about one month of field work. The lithology of outcrops were investigated in a reconnaissance study. The length of outcrops that I visited varied from 20 to 100 m.

Structural measurements were performed in each sampled outcrop about every 1 -1.5 km and in some localities at closer spacing and involved:

- bedding surface determinations (where preserved) - near Atikokan where they were sometimes oblique enough to the schistosity to be recognized readily.

- primary tectonic schistosity or cleavage measured in about 70 outcrops. Some measurements were repeated in the same outcrop to average variations of the foliation plane within larger outcrops. In the schist outcrops the schistosity plane was measured, in more gneissic or migmatitic units only the orientation of gneissic layering was recorded. The dips were generally almost vertical throughout.

In some migmatitic outcrops the schistosity plane was preserved in biotite schist paleosome. However, it is realized that this is late- formed biotite. Subhorizontal lineations, generally dipping gently eastwards were often observed as a preserved orientation of mica or amphibole grains within

foliation planes. This is interpreted as the maximum finite extension direction during crystallization.

In most outcrops one to three hand specimens were collected with oriented surfaces (for which strike and dip was recorded). Only about one third of specimens were taken with an oriented horizontal surface. Samples were chosen only from more mafic areas of migmatitic outcrops (in case of migmatites and gneiss). This approach was deliberate, due to planned studies of ferromagnetic fabrics and NRM in the specimens collected.

In the laboratory, hand specimens were reoriented in their natural site orientation and horizontal cuts were made to facilitate vertical laboratory drilling. Then the samples were drilled to yield cylindrical cores - all of them with their long axis vertical and the north direction marked on the top surface. As a result all the prepared cylindrical cores with dimensions: 2.5 cm diameter and about 2.2 cm height were oriented in their geographical coordinates and could be used for determination of magnetic fabrics and NRM (Fig. 4.7a). Locations of sampled outcrops and collected samples are shown on the map (Fig. 4.3) and are listed in Appendix A.

Some other cylindrical cores from the Quetico - Wabigoon belt boundary collected in Sarvas' project (Sarvas 1988, Fig. 4.6) were oriented perpendicular to the mineral foliation (schistosity) in the outcrop with an arrow pointing the strike direction (Fig. 4.7b). The directional data obtained from them (as a NRM vector for example) had to be rotated to the



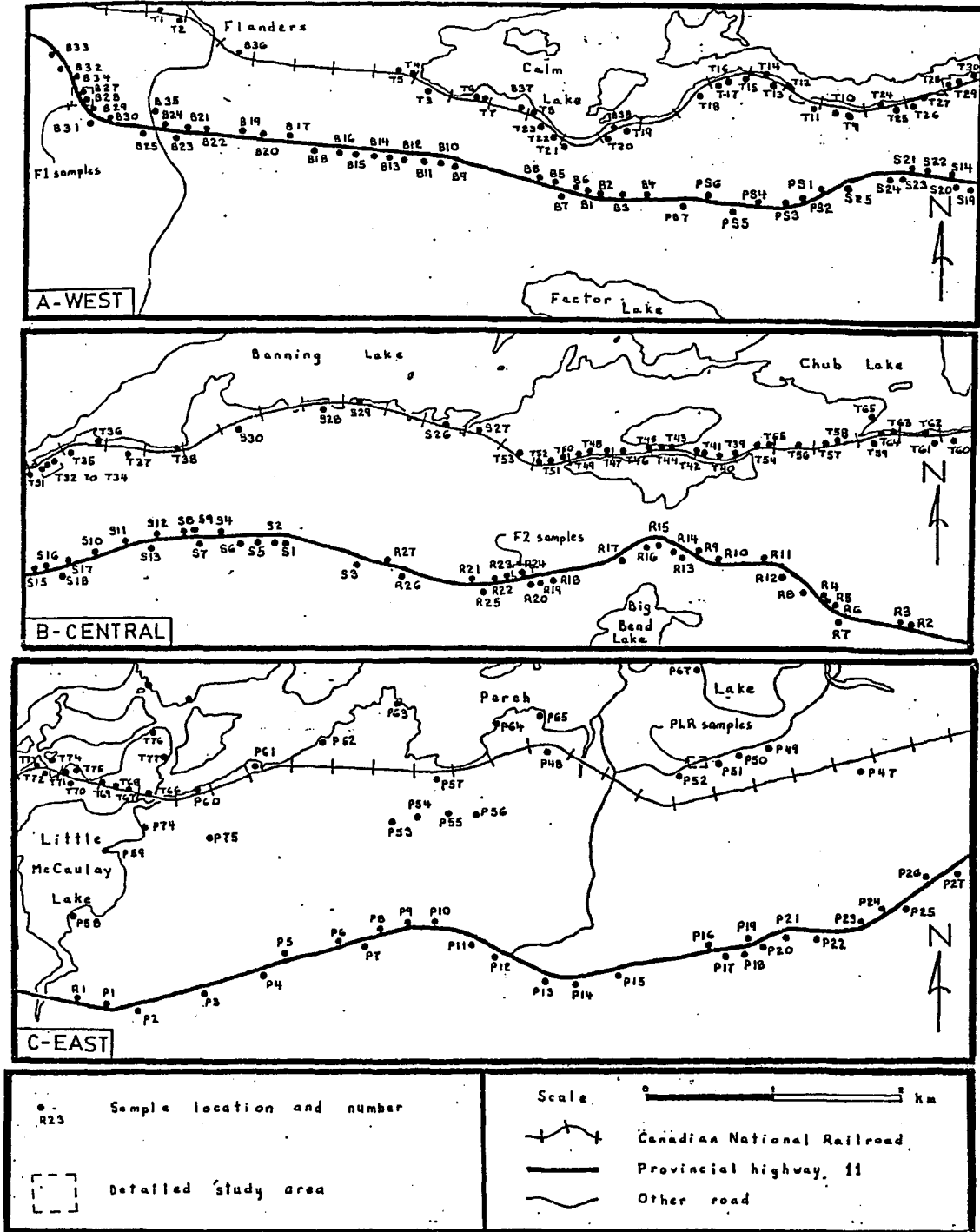


Fig. 4.6. Sampling sites in Calm Lake - Perch Lake area (from Sarvas, 1988).

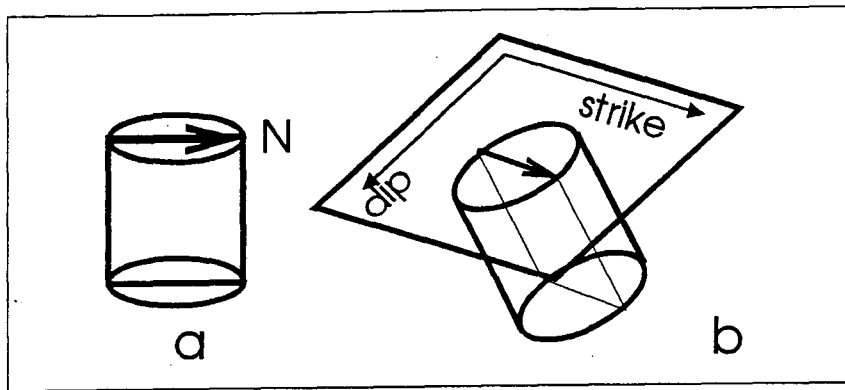


Fig. 4.7. The conventions of orienting of drilled cores.

a) - a core is drilled vertically with its top horizontal. The arrow on the top surface points to the North.

b) - a core is drilled perpendicular to schistosity plane in the outcrop. The top surface of the core is parallel to the schistosity plane. The orientation of schistosity plane is recorded (strike and dip) and its strike direction is transferred onto the top surface of the core. An arrow points toward the strike of schistosity plane.

A core with such orientation must have its all directional parameters (e.g. magnetic lineations and foliations) measured in sample coordinates recalculated in the true geographical coordinates.

geographical coordinates. The computer program COORD2.BAS was used to perform this task (see Appendix E).

The additional set of 20 hand specimens collected along the transect going through Quetico - Shebandowan Belts boundary as well as some hand specimens collected in Spark's project (Spark 1990) were used to drill a further 119 cores already oriented in the geographic coordinates.

The intensity of NRM was measured for a total of 294 cores with the use of MOLSPIN spinner magnetometer (a noise level of about 0.03 mA/m and a sensitivity much better than 0.5 mA/m). Bulk magnetic susceptibility was determined with an SI-2 induction coil (Sapphire Instruments). The theoretical principles of both methods as well as demagnetization procedures and methods of determinations of anisotropy of magnetic susceptibility and ARM are presented in later chapters.

The magnetic susceptibility of cores were high enough (at least  $10^{-5}$  SI units, mean MS was  $1.3 \pm 4.7 \cdot 10^{-3}$  SI for N=294 samples) that AMS could be measured for all 294 cores with use of Sapphire Instrument SI - 2 inductive coil and 12 - orientation of the sample within the coil (Stupavsky 1984).

The intensity of NRM was widely distributed from less than 1 mA/m to more than 10 A/m (mean NRM was 232 mA/m for N=589 samples but for 336 samples it was less than 10 mA/m). Therefore only cores with magnetization higher then 10 or 20 mA/m (total of 237) were selected for the alternating field or thermal demagnetization procedures. Samples chosen for AF treatment were

geographical coordinates. The computer program COORD2.BAS was used to perform this task (see Appendix E).

The additional set of 20 hand specimens collected along the transect going through Quetico - Shebandowan Belts boundary as well as some hand specimens collected in Spark's project (Spark 1990) were used to drill a further 119 cores already oriented in the geographic coordinates.

The intensity of NRM was measured for a total of 294 cores with the use of MOLSPIN spinner magnetometer (a noise level of about 0.03 mA/m and a sensitivity much better than 0.5 mA/m). Bulk magnetic susceptibility was determined with an SI-2 induction coil (Sapphire Instruments). The theoretical principles of both methods as well as demagnetization procedures and methods of determinations of anisotropy of magnetic susceptibility and ARM are presented in later chapters.

The magnetic susceptibility of cores were high enough (at least  $10^{-5}$  SI units, mean MS was  $1.3 \pm 4.7 \cdot 10^{-3}$  SI for N=294 samples) that AMS could be measured for all 294 cores with use of Sapphire Instrument SI - 2 inductive coil and 12 - orientation of the sample within the coil (Stupavsky 1984).

The intensity of NRM was widely distributed from less than 1 mA/m to more than 10 A/m (mean NRM was 232 mA/m for N=589 samples but for 336 samples it was less than 10 mA/m). Therefore only cores with magnetization higher then 10 or 20 mA/m (total of 237) were selected for the alternating field or thermal demagnetization procedures. Samples chosen for AF treatment were

- intensity of SIRM studies using alternating gradient force magnetometer Micromag 2900 from Princeton Measurements Corporation.

5 selected samples were crushed and the magnetic minerals separations were performed. The powdered magnetic phase was then viewed under binocular petrographic microscope and single grains were selected for experiments listed above. In addition, the approximate apparent content of magnetic minerals could be estimated from the magnetic phases. Also small pieces of host rock from the same hand specimens (about 200 mg each) were studied in the same experimental procedures on a Princeton Instruments, alternating gradient force magnetometer Micromag 2000.

The recognition of magnetic minerals and their preferred orientation gives some idea when they were formed with respect to the tectonic transpressive deformation and whether or not their magnetic fabrics can be regarded as kinematic indicators of shear component in the deformation history.



Plate 5.1. Pillow lavas in the metabolcanic Shebandowan Belt. Station RS8.05, next to the contact with the Quetico Belt metasediments. Greenschist facies metamorphic grade.

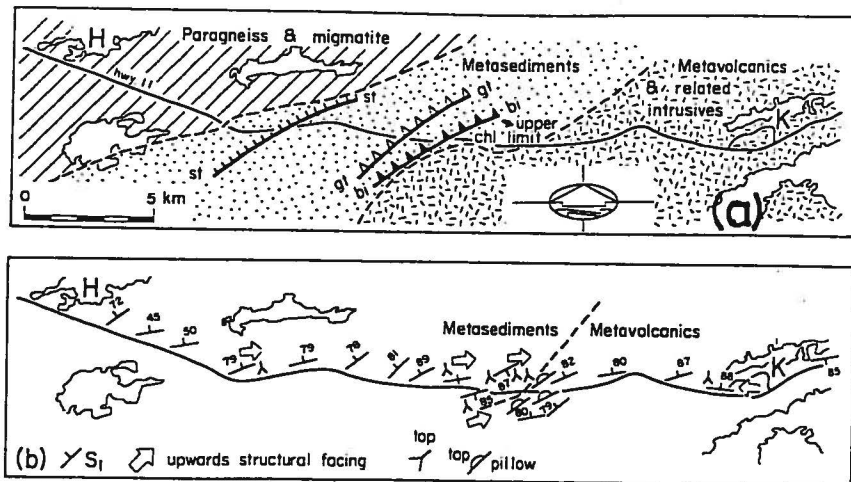


Fig. 5.2. (a) Schematic lithology and metamorphic isograds in Kashabowie L. - Huronian L. area; st - staurolite, gt - garnet, bi - biotite, chl - chlorite  
 (b) structural data - foliations, structural facing.  
 (modified after Borradaile and Spark, 1991).

## Chapter 5.

### Lithology and structure of studied areas.

#### 5.1. Review of lithology and structural observations on the Quetico Belt boundaries.

##### 5.1.1. Shebandowan - Quetico belts boundary.

The Kashabowie - Huronian Lake transect traverses the contact between metavolcanic Shebandowan Belt and metasedimentary Quetico Belt. It cuts the contacts and the metamorphic isograds in the area at a low angle (Pirie and Mackasey, 1978). Sampled outcrops in the Shebandowan Belt (studied in detail by Spark, 1990 and those revisited in this study for additional sampling) consist mainly of chlorite - actinolite - epidote rich mafic metavolcanic greenstones west of Kashabowie metamorphosed from massive or pillow lavas flows and pyroclastics with locally preserved graded bedding and pillows. Some minor outcrops of sheared felsic pyroclastic metavolcanics were observed west of Kashabowie.

Further west the traverse encounters a larger cluster of felsic metavolcanics around Whitefish Lake (outcrops 3 to 5.6 - Spark, 1990, see map - Fig. 4.4, 4.5), originating mainly from rhyolites, agglomerates and tuffs. More mafic flows grading into pillow lavas are present next to the subprovince boundary (Plate 5.1).

In the Quetico Belt the traverse passes through some clastic greywacke slates with well preserved graded bedding. Some smaller mafic volcanic flows are interbedded with greywackes just west of the subprovince boundary. Usually bedding is subparallel to the penetrative,  $S_1$  cleavage and can be recognized up to outcrop No. RS10 (Spark 1990). Further, the traverse leads through higher metamorphic grade biotite and hornblende schist (from outcrop no. 10.4); almandine garnet - sillimanite schist (from station no. 10.65) derived from greywackes with partly preserved relict graded bedding, into biotite - garnet paragneisses and migmatites west of Stetham Lake (map - Fig 5.2a).

Lower grade paragneisses are of calc- silicate types inter-layered with biotite schist. With higher grade metamorphism granite leucosomes can be observed within paragneisses. They gradually merge into migmatites with some pegmatite and quartz monzonite intrusions that are common west of outcrop RS11 (Spark, 1990).

More extensive studies of metamorphic grade in the area revealed that isograds are subparallel to the contact of belts (Pirie and Mackasey, 1978) with steep, lateral metamorphic gradients ranging from 50 to 100 °C/km (Percival, 1989) along the traverse in the vicinity of the contact.

The structural observations of the subprovince contacts (Spark, 1990, Borradaile and Spark, 1991, Percival, 1988) showed that along the area only first-phase penetrative tectonic fabric



elements can be noticed. This fabric is consistent through the traverse with mainly subvertical, W-E striking foliation  $S_1$  (slaty cleavage, schistosity and gneissic and migmatitic layering (Fig. 5.2b)). Within the migmatite zone near Huronian Lake the orientation of layering is much more variable due to intrusions of pegmatite bodies and local heterogeneous deformation of granitic leucosome veins which define the layering in the outcrop.

Preferred orientation of traces of mineral grains in the schistosity plane define the extension direction of finite strain locally in the outcrop. This  $L_1$  fabric generally plunges gently to the east along the transect (Spark 1990, Borradaile and Spark 1991). Where preserved, bedding is subparallel to schistosity with northwards younging. Structural facing close to the subprovince boundary zone can be determined as uniform and steeply upwards and eastwards. The intersection lineations between bedding and cleavage are subparallel to extension lineations and plunge gently to the east - at an angle of about  $20^\circ$  (Borradaile and Spark, 1991).

Borradaile and Spark (1991) discussed whether all the fabric in the area is of the same age in both belts (as  $D_1$  - 2696-2689 Ma -Corfu and Scott, 1986, Percival, 1989). They supposed that the tectonic fabric could develop progressively during the transpression event  $D_1$  with shear component almost parallel to sheared strata and early steepening of strata to near-vertical orientation. Therefore, the observed tectonic

fabric could characterize the same finite tectonic event throughout the entire area.

#### 5.1.2. Wabigoon - Quetico Belt boundary.

The transect across the Wabigoon - Quetico subprovince boundary runs along the Quetico Fault from the Calm Lake on the west toward the Perch Lake on the east and was about 12 km long. The sampling, lithological and structural studies were done by Sarvas (1988) and Borradaile and Sarvas (1989) along two communications lines: CNR rail track and Highway 11. Almost the whole area was situated within the Quetico belt metasediments, with some metavolcanic outcrops in the Wabigoon greenstone belt along the railway track.

Metasediments south of Flanders and Calm Lake were originally feldspathic sandstones with well preserved bedding, sometimes graded or cross-bedding (Sarvas, 1988) mainly arkoses and silty pelites and mudstones. Due to low grade metamorphism they were metamorphosed to chlorite - sericite slates and phyllites of the greenschist facies. Further along Highway 11 to the east metamorphic grade increases with epidote and sphene appearing 1 km south of the Quetico Fault and biotite appearing 1 km further south and becoming a major constituent of biotite schist in the area.

Metavolcanics outcrops in the north near the Quetico Fault

zone and in the Wabigoon greenstone belt were derived mainly from felsic volcanoclastic tuff and mafic flows rich in actinolite, epidote, chlorite, quartz and altered feldspars.

Primary fabrics in the area can be easily mapped as well preserved - bedding in the Quetico metasediments. Several sedimentary features such as graded bedding, cross-stratification, load casts and ripple marks are common. Bedding surfaces are generally uniformly oriented with strike 080° and dipping steeply to the north or south. Local younging directions were mostly to the north but in some areas they dip steeply southwards due to a sequence of tight to isoclinal and asymmetric major folds ( $F_1$ ) with long limbs younging to the north.

Only a first, continuous cleavage  $S_1$  was observed consistently within the area and it is oriented W-E, dipping steeply and subparallel to bedding plane. Observed  $S_0/S_1$  intersection lineations can have variable orientation within the plane subparallel to  $S_1$  and  $S_0$  (Fig. 5.3) and changes of their orientations are correlated with local younging variations. Therefore they can help to determine the unexposed axial-plane traces of  $F_1$  folds if the structural facing direction remains unchanged and cleavage is axial planar.

Structural facing in the area changes remarkably from upwards through sideways to downwards (Fig. 5.4). It was concluded that  $F_1$  folds are curvilinear and sheath-like (Borradaile et al.,

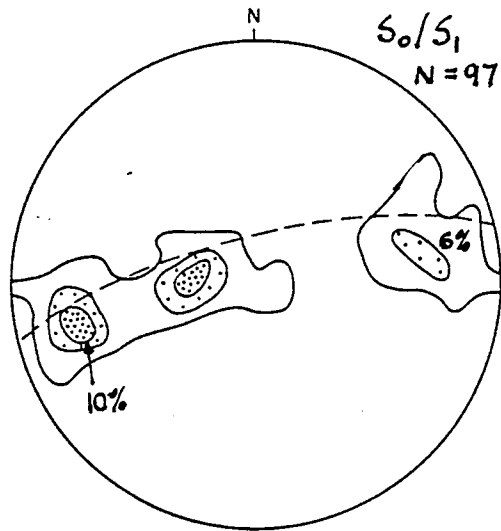


Fig. 5.3. Intersection lineations of bedding ( $S_0$ ) and cleavage ( $S_1$ ),  $n=97$ , contours: 2%, 6%, 10% (modified from Borradaile et al., 1988).

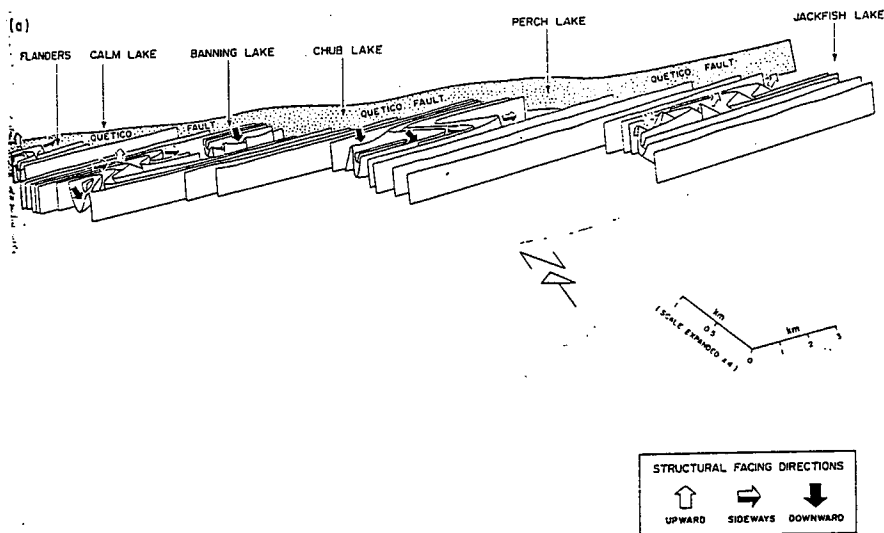


Fig. 5.4. Reconstruction of the form surfaces of bedding from field data between Flanders and Jackfish Lake (modified after Borradaile et al., 1988).

1988). In some outcrops minor asymmetric folds were observed also, as well as weak crenulation and kink bands indicative of post- $D_1$ , non-penetrative, local deformation.

The reconstruction of the set of curvilinear folds of sheath -like appearance with hinge axes slightly oblique to Quetico Fault (Fig. 5.4) (some are also exposed) led to the conclusion that the transpressive deformation with at least 70% shortening in N-S direction with dominant dextral shear was required in the area (Borradaile et al., 1988). It was also suggested that penetrative cleavage in this area can be synchronous with  $S_1$  from Shebandowan - Quetico Belt boundary as produced by the same tectonic event  $D_1$  (Borradaile and Spark, 1991) with mirror symmetry of lithology and metamorphism on both belt boundaries (Percival, 1989).

It should be noted that stratigraphic way up does not reflect this symmetry and is consistent to the north on both boundaries (Borradaile et al., 1988, Borradaile and Spark, 1991).

## 5.2. Studies of the interior of Quetico Belt.

Field studies of Quetico Belt traverse were completed in one month during the field season 1992. The pattern of changes of structural and magnetic fabric along whole the transect were studied but only more mafic parts of outcrops were investigated closely and sampled. Lithologically, outcrops in the area are very heterogenous on the outcrop scale. In many single outcrops 100 m long one finds schist, paragneiss and migmatite or pegmatitic intrusion. Therefore in those cases several samples (2 or 3) were collected from one outcrop and migmatitic layering fabric measured simultaneously with schistosity.

### 5.2.1. Lithology and sampling.

The Atikokan - Huronian Lake traverse, along Highway 11 led through low grade metamorphism chlorite - sericite greenschist facies, to high grade paragneisses, migmatites and pegmatite - quartz monzonite. The axis of maximum peak metamorphism was crossed and the traverse was completed east of Huronian Lake on the Arctic - Atlantic watershed, which is the west margin of Spark's (1988) study. At least one hand specimen was taken from each outcrop studied. In the area of higher metamorphic gradient, between Atikokan and Sapawe, structural measurements and sampling were made every 500 - 1000 m where possible (Fig.

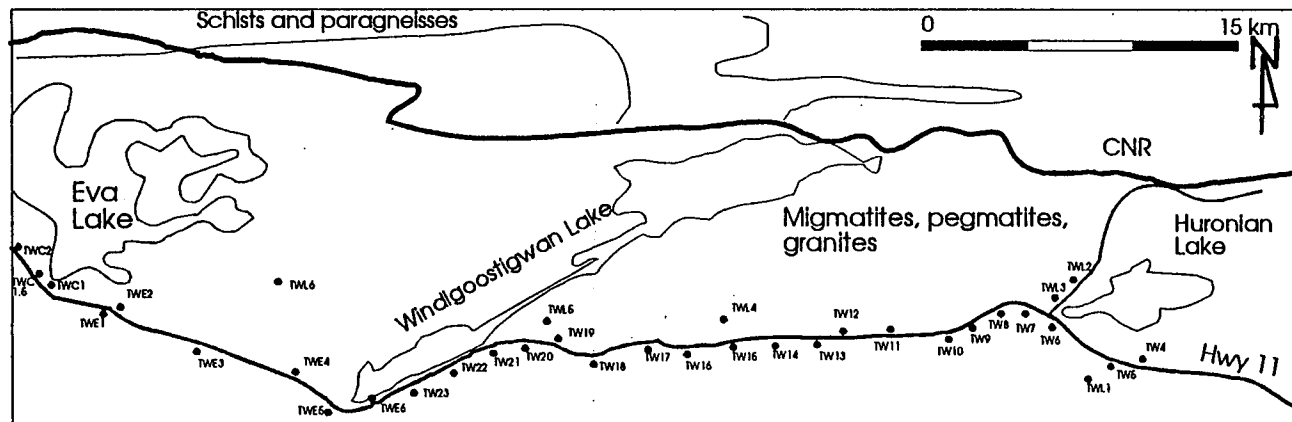
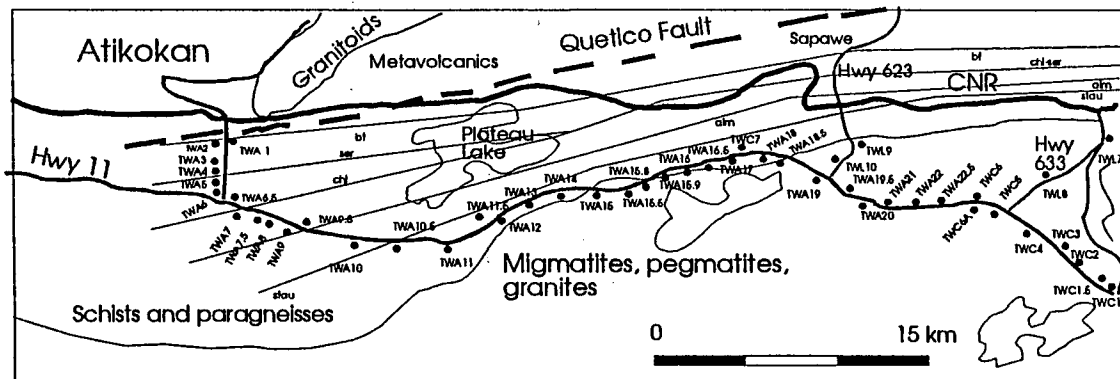


Fig. 5.5. Sampling sites in Atikokan - Huronian Lake area; with a schematic lithology and metamorphic isograds. bt - biotite (in), ser - sericite (out), chl - chlorite (out), alm - almandine garnet (in), stau - staurolite (in), going from W to E.

5.5), further east in high grade metamorphism outcrops distances between outcrops were a little greater.

Near Atikokan, 2 km south of the town and about 1 km south of Quetico Fault mylonitic zone, greenschist facies outcrops were sampled and studied (Plate 5.6). Rocks in these outcrops (TWA1 and TWA2) are mainly metasedimentary wacke turbidites grading into shales with preserved relict bedding,  $S_0$ , almost parallel to first penetrative slaty cleavage ( $S_1$ ). Parting of rocks is controlled by cleavage rather than by bedding and intersection lineations of bedding and cleavage are also easy to recognize. Beds are rather thin - of the order of 5 cm and relatively invariant in arkosic composition.

The fine grained matrix is mainly of chlorite and sericite with some opaque minerals recognized as pyrite and pyrrhotite.

Further south along Highway 11B the metamorphic grade increases steeply, crossing the biotite isograd and making primary sedimentary fabrics obscure. In outcrops TWA3 - TWA5 bedding is parallel to schistosity, biotite grains become visible (of 1 mm length) and gradually quartz veins appear parallel to schistosity. Some tension gashes filled with secondary quartz, perpendicular to extension lineations within schistosity plane were observed in paragneisses at station TWA4. As the transect along highway 11b is at right angles to the metamorphic isograds in the area (Pirie and Mackasey, 1978), further to the south biotite- chlorite assemblage was observed in thin-section studies (stations TWA5-7).





Plate 5.6. The deflection of foliation in amphibolite schist caused by the intrusion of pegmatite; station TWA15.5, Hwy 11, belt interior.



Plate 5.7. Massive monzonite intrusion with a contact with gently dipping biotite schist; station TWA18.5, Hwy 11, belt interior.

Large flakes of biotite become a major constituent of rock composition but they do not show a strong preferred orientation, in contrast to the fine grained chlorite - sericite matrix, which has a strong preferred crystallographic orientation (p.c.o.). This biotite phase grew late in the  $D_1$  history.

Further east, oblique to the WNW-ESE orientation of metamorphic isograds (Fig. 5.5), quartz veining and metamorphic differentiation are more common. In biotite schist and paragneisses, sericite decreases and biotite laths acquire stronger p.c.o. Primary bedding is not recognizable from layering developed by metamorphic differentiation. Chlorite is still abundant as a matrix component together with microcrystalline quartz. In less mafic outcrops (as TWA 9.5) the matrix is mainly composed of fine - grained quartz. Laths of chlorite and biotite are badly altered and show notable effects of radioactive damage (pleochroic haloes). Aggregates of Fe - bearing compounds become larger, up to 300  $\mu\text{m}$ , with weak preferred dimensional orientation (p.d.o.) subparallel to preferred orientation of the matrix.

Mica grains are visible to the naked eye around station TWA11, and metamorphic differentiation producing distinct quartz rich layers. Further east, only the more mafic parts of outcrops were sampled because the magnetic studies required higher contents of ferromagnetic minerals within samples.

From station TWA15 to the east (TWA17, 18) some massive amphibolite schist outcrops were observed with hornblende blasts

up to 5-8 mm size showing a weak preferred orientation. Feldspar grains are strongly altered to muscovite, and numerous biotite and muscovite inclusions are seen in the hornblende blasts. The highway locally enters a pegmatite zone, so some outcrops with small pegmatite intrusions were observed (TWA 15.5 - 15.8). Pegmatite bodies usually tilt older biotite schist - paragneiss layers during their intrusions causing the earlier schistosity to become less steep locally (Plate 5.6, 5.7) - outcrops TWA 15.5 - 18.5. Migmatites are common adjacent to pegmatite bodies, with schist layers 10 - 15 m west of Niobe Lake and highway 623 to Sapawe (e.g. TWC 7).

Further east of station TWA 18, samples show the existence of almandine garnet together with a biotite and muscovite assemblage. Preferred orientation in mica laths (p.c.o.) and p.d.o. in quartz grains is relatively high. Gradually, garnet blasts become fractured and altered along cracks to pennine chlorite (TWA22A).

East of Sapawe road outcrops are migmatitic with some pegmatite intrusions. Mafic paleosome (biotite schist) constitutes usually about 80% of the rock body. Some earlier foliation is preserved in these parts and often controls felsic layering and parting of the rock. Less mafic parts are comprised mostly of quartz - biotite and newly formed muscovite. Quartz veins (neosome) are often deformed in the schistosity plane, forming folds and boudinage (Plate 5.8). The felsic neosome often forms Augen or angular forms within outcrops giving the



Plate 5.8. Ptygmatic folds and quartz veins within migmatite; station TWC7, Hwy 11, belt interior.

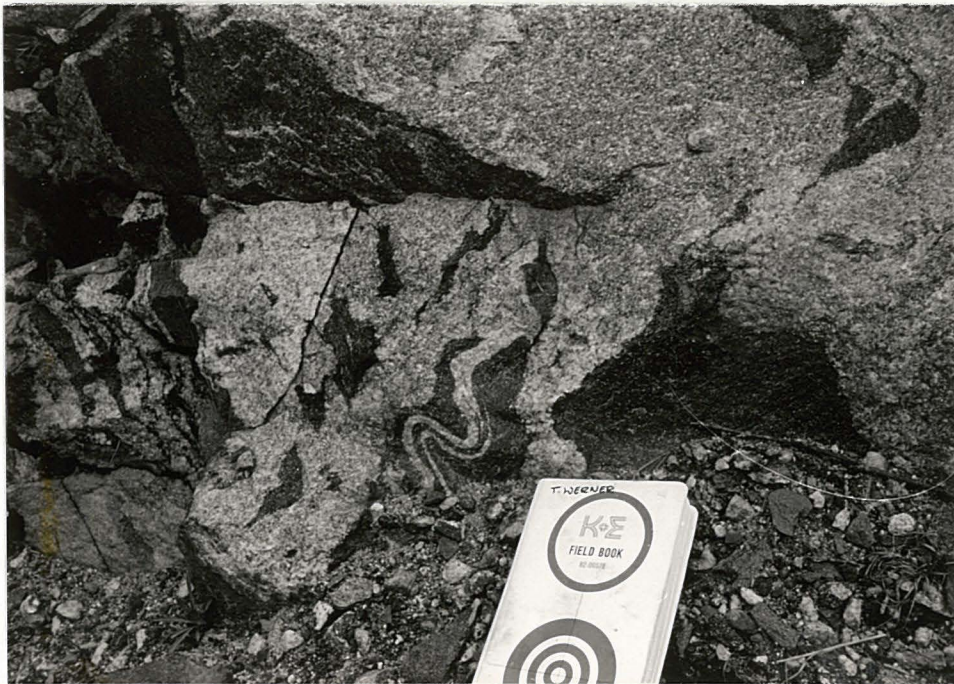


Plate 5.9. Anatexis in migmatite; relations between neosome and paleosome are seen; outcrop TWC4, interior of the belt.

appearance of multiphase or heterogeneous deformation on the outcrop scale (outcrops TWC4, TWC 1 - Plates 5.9, 5.10). Such felsic areas were not sampled, as they are known to be unsuitable for magnetic studies.

Near Duncan Lake a 1 km long granitic nebulite stock with some pegmatite veining is present (plate 5.11). A sequence of smaller granitic bodies next to pegmatites or migmatites was observed east of Eva Lake (stations TWE1-2). No consistent layering was measured in these outcrops. Layering changed remarkably at an outcrop scale, leading to the conclusion that the syn- deformational  $D_1$  fabric was disturbed by later intrusions of felsic rocks in the area. More mafic migmatitic outcrops near Eva lake still possessed distinct layering and p.c.o. of minerals (muscovite and biotite) consistent with the regionally developed  $S_1/L_1$  fabric beyond (Plate 5.12 - station TWE4).

Outcrops along the Quetico Park boundary, from Windigoostigwan Lake, are mostly pegmatitic with migmatite bodies among them. The size of migmatite units was sufficient (up to 100 m) to assume they are not strongly reoriented due to pegmatite and monzonite intrusions. Such outcrops were successfully sampled (station TW18).

Thin section studies revealed abundant muscovite, together with biotite (station TWE3). Staurolite appears (TWE4) west of Windigoostigwan Lake together with almandine garnet in biotite - muscovite - quartz matrices with strong preferred orientation

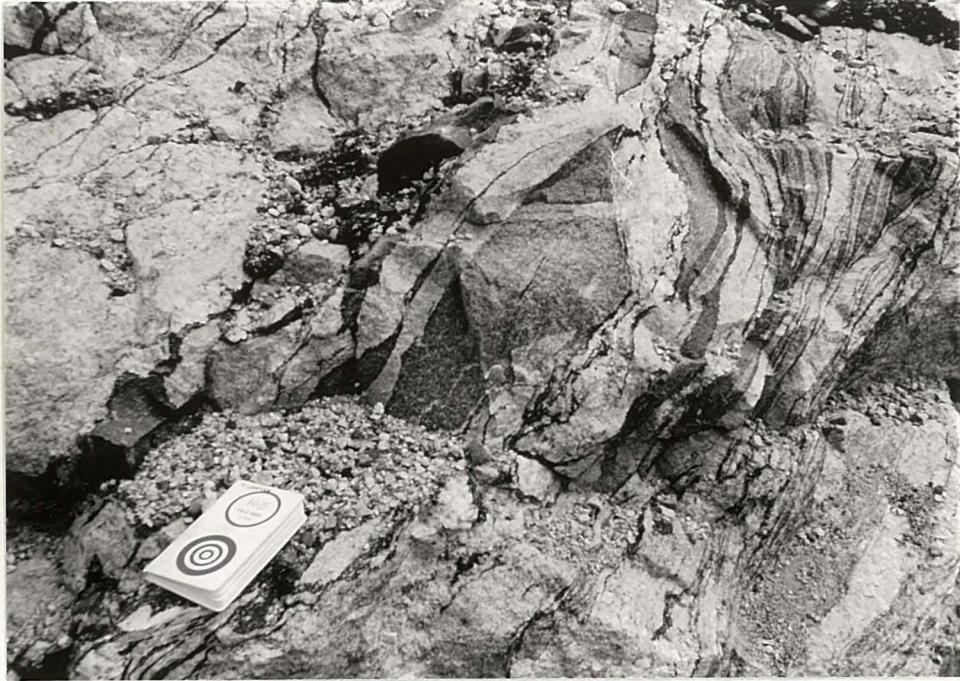


Plate 5.10. Anatexis in migmatite -an appearance of heterogeneous deformation; outcrop TWC1, interior of the belt.

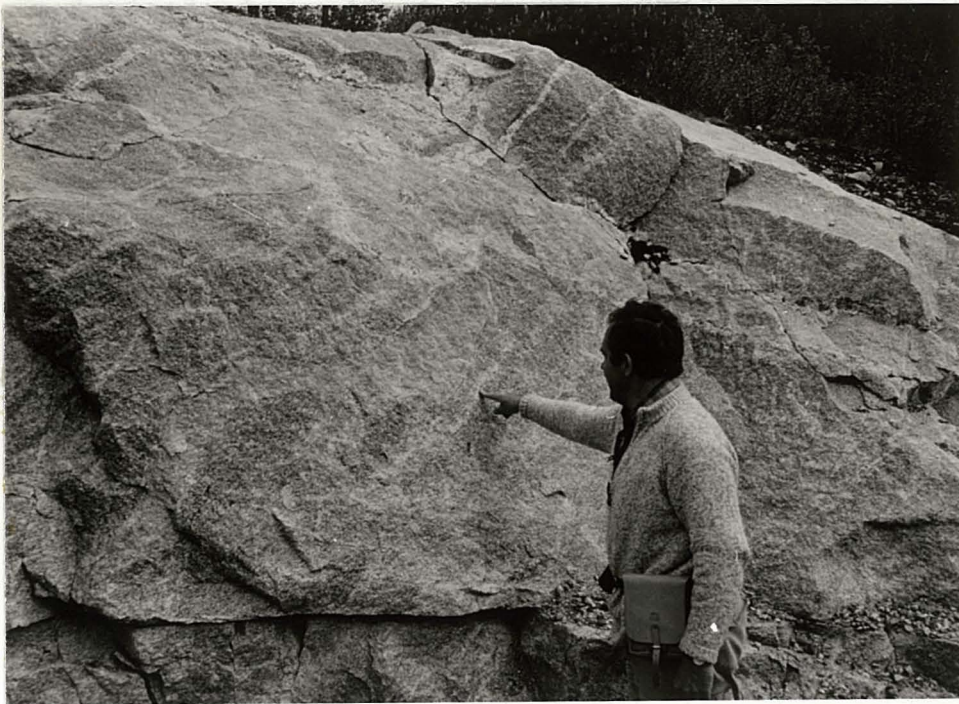


Plate 5.11. Nebulitic granite with some later pegmatitic veining; station TWC2, interior of the belt.



Plate 5.12. A typical migmatitic outcrop TWE4 with consistent metamorphic layering striking W-E. Boudinages and Augens can be noticed.



Plate 5.13. A minor open fold in biotite schist; outcrop TW12 east of Windigoostigwan L., interior of the belt.

east of this lake (TW23). It seems that the axis of peak metamorphism was crossed somewhere east of Eva Lake in the area occupied by felsic stocks.

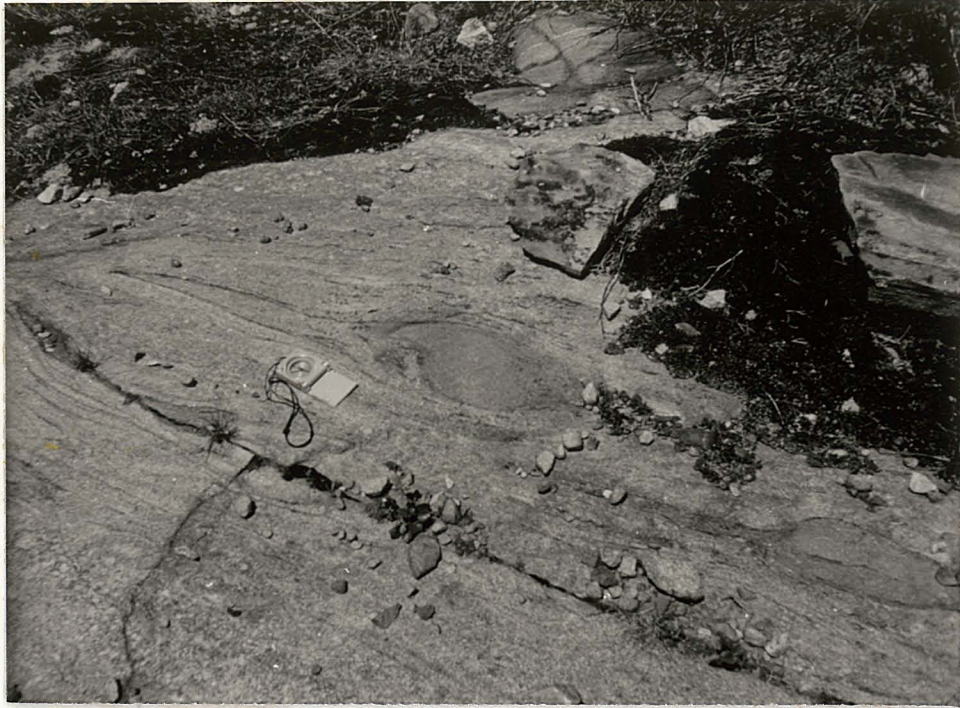
East of station TW17 pegmatite intrusions are less common. Migmatite outcrops have strong preferred orientation of layering with more mafic biotite - muscovite rich parts constituting about 70-80% of the outcrops. In biotite schist layers some early tectonic structures such as minor folds (Plate 5.13 - station TW12) persist despite higher migmatitic metamorphism in the area.

Near to Huronian Lake, the rocks are less migmatitic: paragneiss and biotite schist is observed. Some minor amphibolites also crop out (station TW8). Migmatitic layering shows a strong preferred orientation (Plate 5.14 - station TWL1) having a good correlation with schistosity in biotite schist outcrops. Some Augen structures showing competence contrast within layers in biotite paragneiss were also noticed (plate 5.15a,b - station TW4).





Plate 5.14. Migmatitic layering with strongly uniform orientation; outcrop TWL1 near Huronian Lake.



a)



b)

Plate 5.15. Augen structures preserved in biotite schist (a) and differentiated migmatite (b); outcrop TW4 near Arctic/Atlantic watershed east of Atikokan.

### 5.2.2. Structural observations in the Atikokan - Huronian Lake area.

Structural observations were made at 77 outcrops along the Atikokan - Huronian Lake traverse to complement earlier studies along the Quetico belt boundaries with adjacent belts (Sarvas, 1988, Spark, 1990). In low grade metamorphic rocks near Atikokan, primary fabrics such as bedding and younging could be determined, but in the more metamorphosed interior of the Quetico Belt only imposed planar and linear tectonic fabrics such as schistosity, extension lineations or gneissic and migmatitic layering were observed and recorded. Relationships among intrusive pegmatite and quartz monzonite bodies and earlier - formed metasedimentary schists were also investigated. Locally in the migmatitic zone, the effects of anatexis in migmatites, which produced veining and paleosome - neosome textures were also observed.

#### **Primary structures: $S_0$ - bedding and younging direction.**

Recognizable bedding which is not parallel to tectonic cleavage is preserved only in low grade greenschist facies rocks south of Atikokan. It was observed in some chlorite - sericite - biotite schist outcrops between stations TWA1 & TWA2 just south of the Quetico Belt crossing Highway 11B.  $S_0$  is very steep, practically vertical and striking W-E (Fig. 5.16). A younging direction to the north was determined in graded beds in station

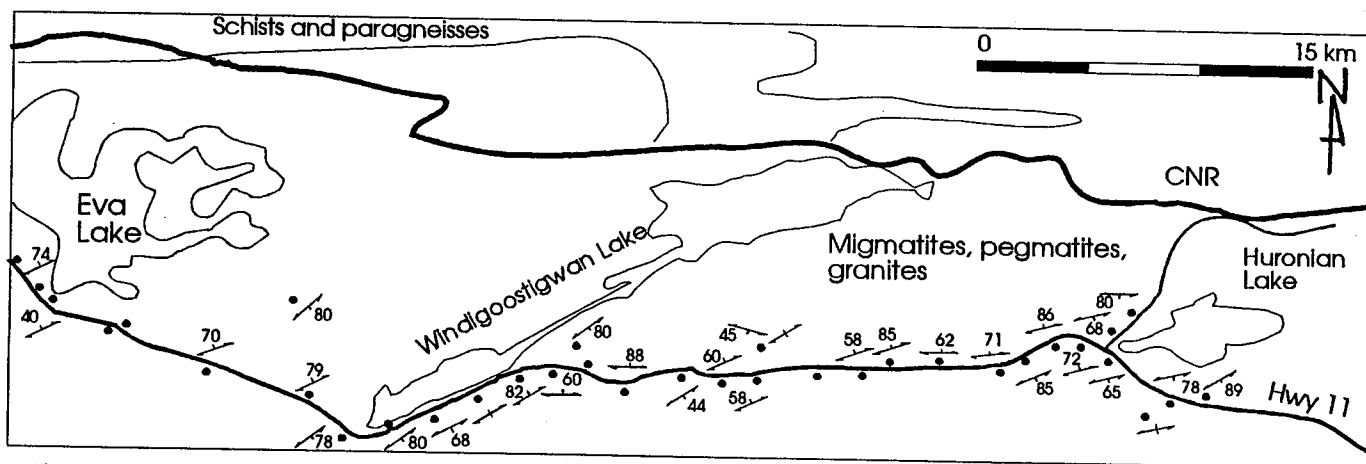
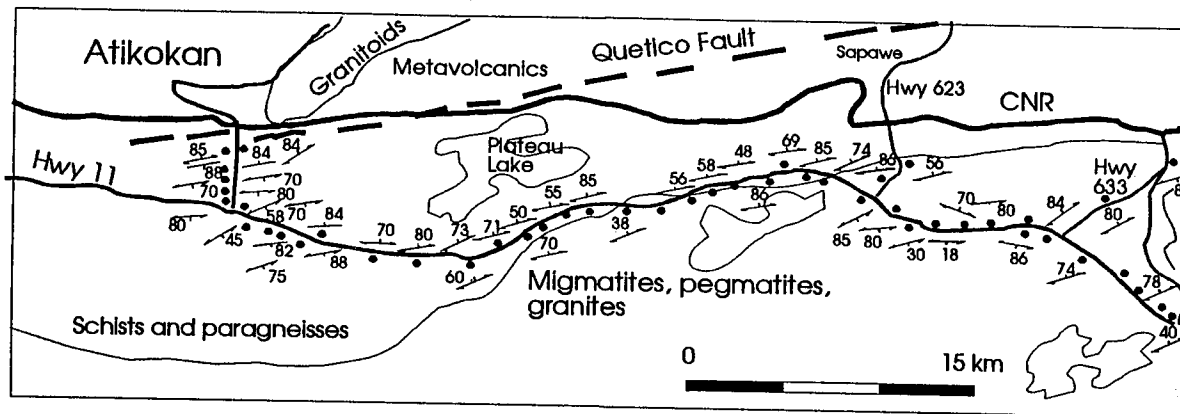
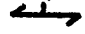




Fig. 5.16. Planar fabrics - bedding  $S_0$ , schistosity & migmatitic layering  $S_1$  in Atikokan - Huronian Lake area.

-  - schistosity;
-  - bedding;
-  - station.

TWA1 only.

Further south bedding becomes parallel or sub-parallel to schistosity and the younging direction is difficult to determine due to metamorphic differentiation in the schists which obscures the graded beds.

Locally in high - grade biotite schist layers small microfolds can be recognised folding the bedding (TW12, see Plate 5.13). However, bedding is not traceable along the outcrop and it can be mistaken with schistosity in fine grained biotite schist.

**S -fabrics: schistosity & layering in gneisses and migmatites.**

The first penetrative  $S_1$  tectonic cleavage can be easily observed within low- to medium - grade metasediments (schists and gneisses) within the Quetico belt. Variations in the orientation of the cleavage surface were observed commonly due to cleavage refraction in layers of different competence. These variations were usually of the order of  $10^\circ$ . In these cases, the orientation of two or three surfaces in one outcrop were measured and averaged.

In higher grade rocks, such as those with migmatitic and pegmatitic portions, a schistosity is still preserved in mafic biotite schists. Spaced layering of migmatites is generally controlled by existing schistosity, but preferred orientation of the layering is somewhat weaker than schistosity.

Numerous folds and boudins as well as Augen structures

occur within migmatite. They mark locally heterogenous deformation on the outcrop scale due to the strain-partitioning in partly melted felsic material and more stable biotite schist of different competencies. Therefore, the  $S_1$  fabric was measured on schistosity surfaces in migmatitic outcrops where possible. In some places, only the glaciated, smooth tops of outcrops were exposed for measurements; therefore the strike of near vertically dipping migmatitic layering was only recorded (TWL1 - Plate 5.15).

Through the whole traverse, only one tectonic  $S_1$  fabric was noticed. The cleavage is consistent generally throughout the area. The variations of strike were usually of 10-20° along the traverse for cleavage surfaces dipping steeply to NW as well as to SW (map -Fig. 5.16 and Fig. 5.17).

In dominantly pegmatitic outcrops, the remains of schist material are often tilted by intruding felsic bodies (TWC1, TWA6.5, TWA15.5, TWA16.5, TW23) and preserved schistosity may be much less steep (30-50°) than elsewhere.

Thin-section studies also revealed only one penetrative cleavage within schist samples. The cleavage is defined usually by chlorite and biotite grains (preferred crystallographic orientation - p.c.o) in greenschist facies. Quartz grains are small, show weak preferred dimensional orientation (p.d.o.) and are sometimes weakly strained. The rock composition often varies on the thin-section scale, showing the evidence of initial metamorphic differentiation and strain-partitioning. Areas

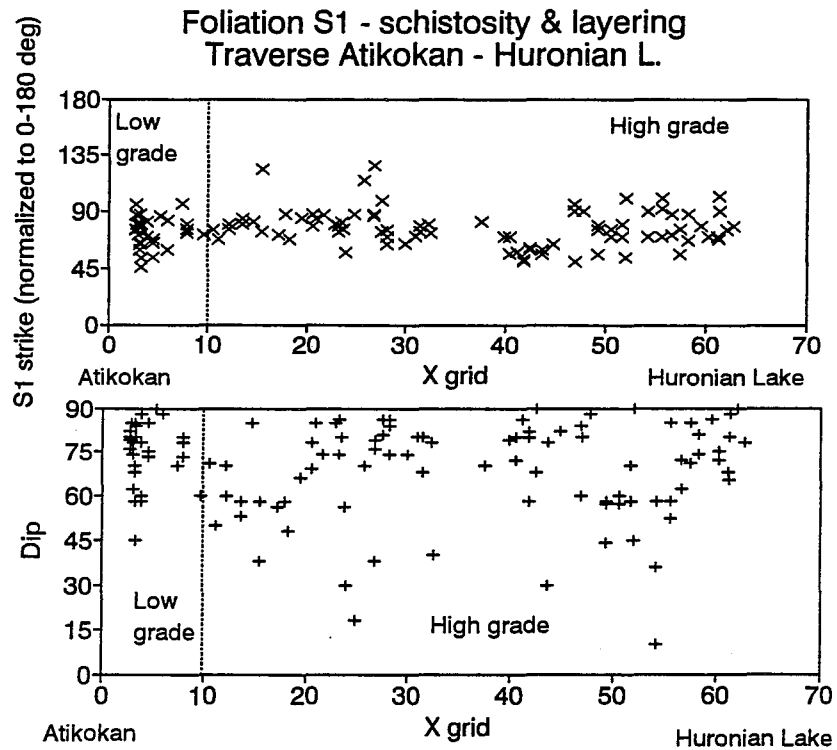


Fig. 5.17. Variations in the orientation of S<sub>1</sub> fabric.  
 a) - variations in strike (all samples had a strike from 0-180° sector compared, e.g. 70° instead of measured 250°).  
 b) - variations in dip.  
 Xgrid - X value of a kilometeric grid on the topographic map.

richer in sericite are usually more deformed than those with a quartz-rich matrix.

In low- grade schist samples some seams of pyrite oriented parallel to the continuous cleavage can be noticed. They may have been created when secondary material filled the spaces in the matrix already controlled by earlier continuous biotite cleavage and they do not indicate that pressure solution operated.

Higher grade amphibolite facies specimens from biotite - garnet - cordierite schist and migmatites are much more homogeneous on the thin-section scale and their biotite - quartz matrix does not show the effects of strain-partitioning so noticeably.

Samples from an amphibolite metagabbro at stations TWA15 - TWA19 do not show distinct cleavage; hornblende grains are somewhat aligned with weak p.c.o. and the biotite - quartz - cordierite matrix does not reveal any better developed preferred orientation.

#### **L- fabrics: mineral lineations.**

Lineations observed on schistosity surfaces were usually formed by the preferred orientation of large (sometimes 1-5 mm long) grains of biotite, muscovite or amphibole in greenschist and amphibolite schists. In lower grade outcrops, such as TWA1 and TWA2 with fine chlorite - biotite assemblages, indistinct bedding traces on cleavage planes were recognised instead.



Mineral lineations were observed only at 42 stations (52 measurements). They usually plunged gently to the east (map - Fig. 5.18 and Fig. 5.19). West plunging mineral lineations were measured only south of Atikokan in low grade greenschist facies rocks. In a few stations, lineations were anomalously steep; they were observed where the biotite schist units had been tilted by pegmatite intrusions.

#### **Bedding - cleavage relationships near Atikokan.**

Bedding surfaces were observed only in low grade greenschist facies rocks near Atikokan, in a few smaller outcrops between stations TWA1 and TWA2. Therefore traces of bedding on cleavage surfaces  $S_0/S_1$  were not recognised elsewhere.

The dihedral angle between steep subvertical bedding and cleavage is very small, less than  $10^\circ$ . Sub-parallelism of both fabrics is due partly to an effect of rotation of a passive bedding surface toward the principal axes of transpressive deformation. However it is also true that the principal planes (XY) of deformation were probably located subparallel to bedding, thereby permitting a large shearing component of deformation (Percival, 1988).

Traces of  $S_1$  on  $S_0$  surfaces were measured for both outcrops - their orientation is varying remarkably from one outcrop to another:

TWA1 :  $62^\circ/60^\circ$

TWA2:  $252^\circ/20^\circ$

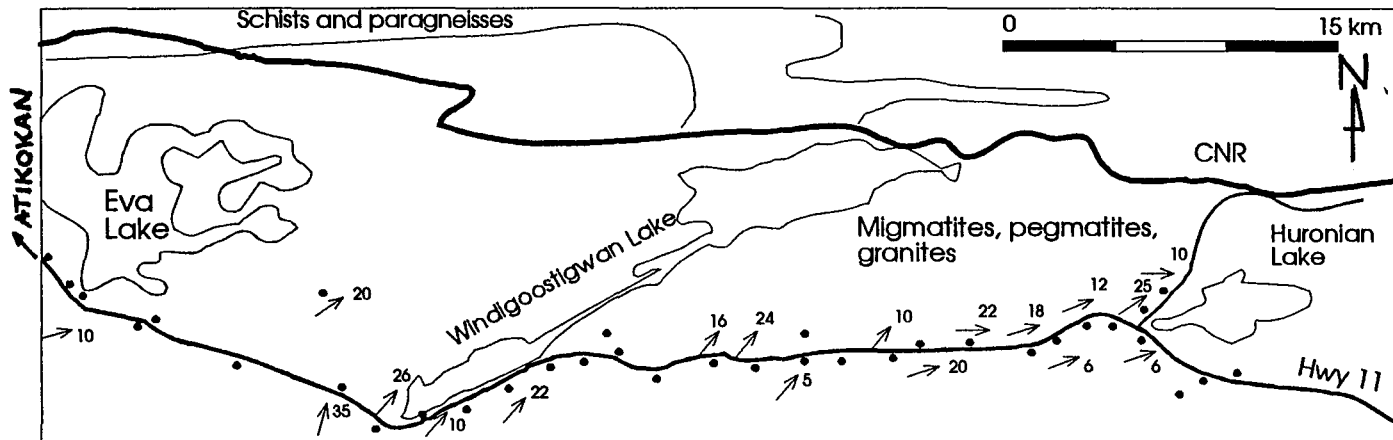
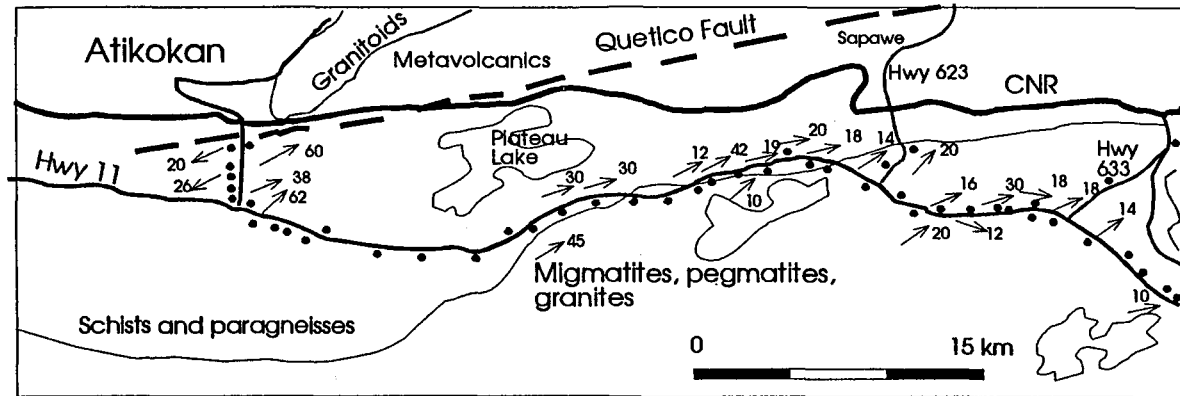


Fig. 5.18. Linear tectonic fabric - extension lineations  $L_1$  in Atikokan - Huronian Lake area.

- - lineation;
- - station.

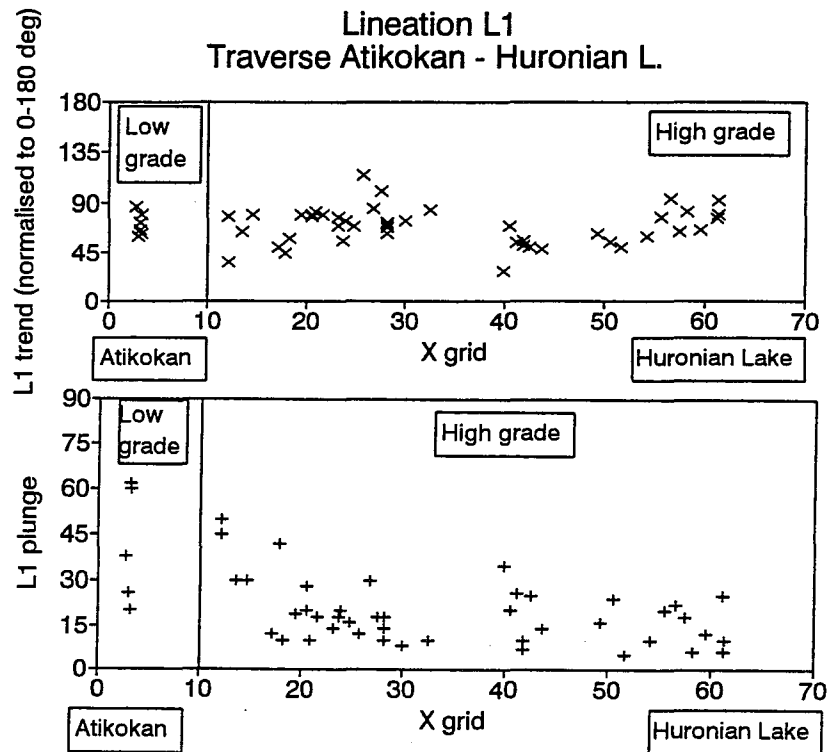


Fig. 5.19. Variations in the orientation of  $L_1$  fabric.  
 a) - variations in trend (all measured lineations had a direction of lination taken from 0-180° sector for a purpose of their comparison, e.g. 70° instead of measured 250°).  
 b) - variations in plunge.  
 Xgrid - X value of a kilometric grid on the topographic map.

and it is not very consistent with calculated direction of intersection of  $S_1$  and  $S_0$  surfaces (see table):

station	$S_0$	$S_1$	calculated intersection $S_0/S_1$	measured intersection $S_0/S_1$
TWA1	262/84NW	233/84NW	337-84	62-60
TWA2	78/88SE	258/85NW	258-0	252-20

This difference reflects the fact that small errors in measurement of orientation of two almost parallel surfaces can lead to much greater error in the direction of the calculated line of intersection of these two surfaces.

Measured  $S_0/S_1$  lineations are rather similarly oriented to those in the Calm Lake - Perch Lake area.

### 5.2.3. Relationships between tectonic fabric along the traverse.

#### Statistical methods employed to determine the mean positions of tectonic fabrics.

The clustering of poles to  $S_1$  was calculated with the use of computer program SpheriStat v1.1 (by Frontenac Wordsmiths, Canada, 1990; for details see Appendix E). This program calculates eigenvectors of the distribution of directions on the sphere by use of the Jacobi method (Press et al., 1986) and also finds  $\alpha_{95}$  confidence cones around calculated directions of

eigenvectors (Hext, 1963).

The program also draws density contour lines for a given distribution of points (e.g. poles to cleavage) using weighting spherical Gaussian function (Robin and Jowett, 1986). According to this algorithm, for each counting station all points are weighted by their angular distance from the station and counted.

If  $\sigma$  is a statistical dispersion of data, then contours for every  $2\sigma$ -step are drawn, starting from E - the expected value of the point density for random distribution. The program calculates the value of highest peak of point density in terms of multiples of  $\sigma$  above E value (see Appendix E).

Both procedures - eigenvector calculations and determination of the maximum peak of the density distribution by contouring the data, usually calculate the direction of the maximum cluster with less than  $5^\circ$  difference.

#### **The distribution of tectonic fabrics.**

The changes in metamorphic grade from low- grade greenschist facies at the belt margins to high grade migmatites in the interior of the Quetico Belt may be correlated with the distribution of tectonic and magnetic fabrics in the area as well as the orientation of the natural magnetic remanence. Therefore fabrics for 3 distinct areas will be studied separately.

These areas are:

a) - low grade metasediments in the Calm Lake - Perch Lake area and east of Atikokan till the staurolite isograd (up to the station TWA10.5, Xgrid=10). All these rocks are typical for the belt margin.

b) - higher grade metasediments in the interior of Quetico Belt often associated with pegmatites and granitoid intrusions (going east up to station RS10.7 near Stetham Lake east of Huronian Lake -where staurolite isograd is crossed again).

c) - low grade metasediments in the south margin of Quetico Belt and further east metavolcanics in the Shebandowan Belt (from station RS10.7 to the east). These rocks represent the belt margin rock units. The division of studied area into these 3 sub-areas is presented on the map - Fig. 5.20.

Schistosity  $S_1$  in low grade metasediments in Atikokan area at the northern margin of the Quetico Belt was determined only from studies east of Atikokan along Highway 11. The detailed tectonic data from the Calm Lake - Perch Lake area (collected by Sarvas, 1988) were not available. 34 orientations of  $S_1$  in chlorite and biotite schists have mean pole to  $S_1$  at  $345/9^\circ$  with confidence cone of  $7/4^\circ$  and the peak position from the counting procedure at  $346/9$  (Fig. 5.21a). A similar approach gave also well-defined positions for mean poles to  $S_1$  fabric in higher grade migmatitic interior and low grade metasediments and metavolcanics west of Kashabowie (Fig. 5.21b,c).

Mean schistosity planes have their strikes within a  $10^\circ$  range but in the centre of the belt  $S_1$  dips more gently (at  $68^\circ$ ,

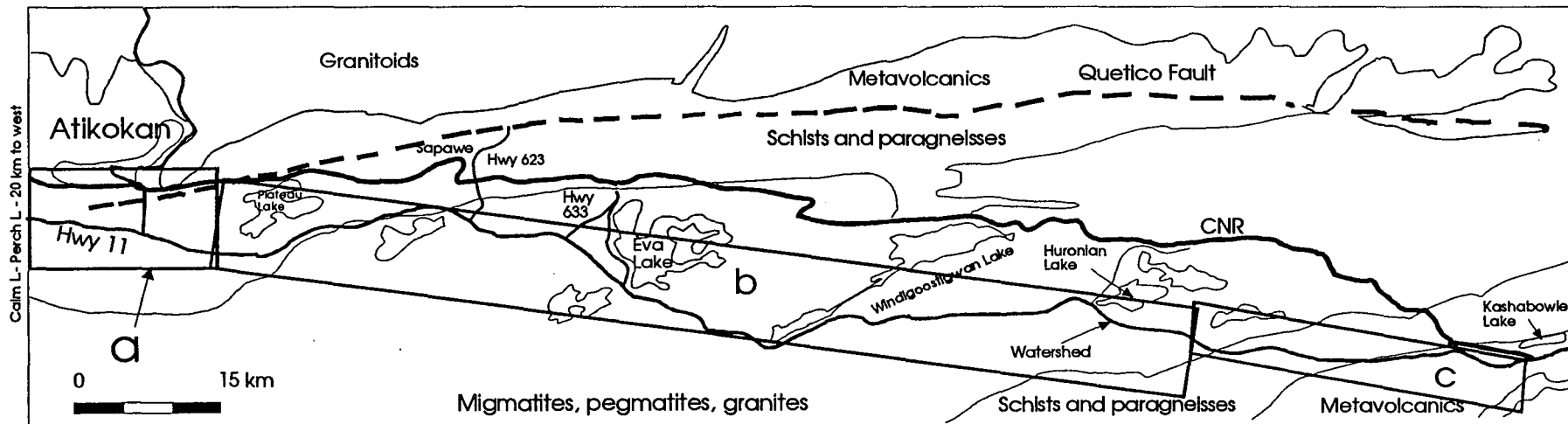


Fig. 5.20. The subdivision of studied areas according to the metamorphic grade.

- a) - low grade metasediments east of Atikokan (up to staurolite isograd, near station TWA11).
- b) - higher grade metasediments (amphibolite facies) and granitoid intrusives - "interior of the belt".
- c) - lower grade (below staurolite isograd) metasediments east of Huronian Lake and metavolcanics further east toward Kashabowie Lake - "Kashabowie area".

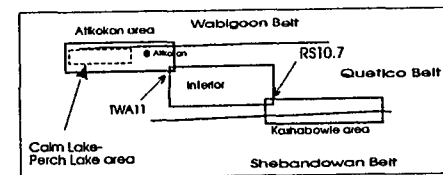
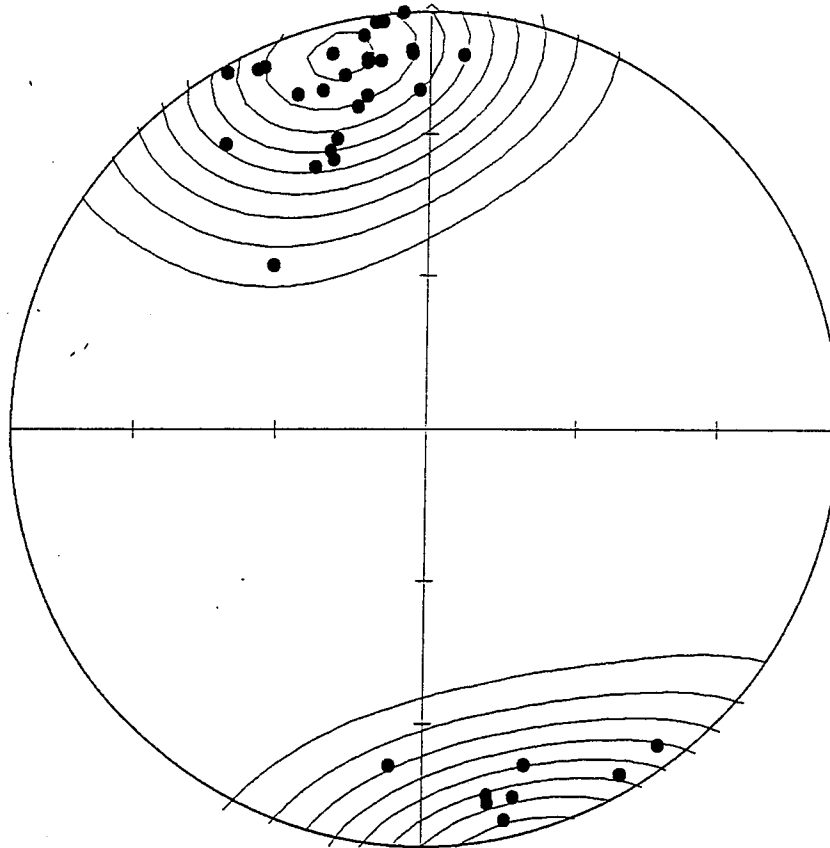


Fig. 5.21a.

Poles to S1 schistosity - Atikokan area

Low metamorphic grade metasediments



$N = 34$

$E = 3.56$

$k = 9.56$

$\text{Sigma} = 1.19$

$(\text{Peak} - E)/\text{Sigma} = 16.6$

Peak position :  $346.0^\circ / 9.2^\circ$

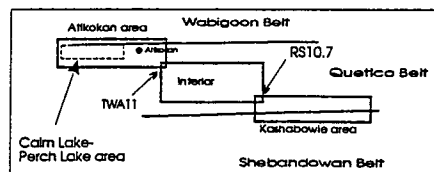
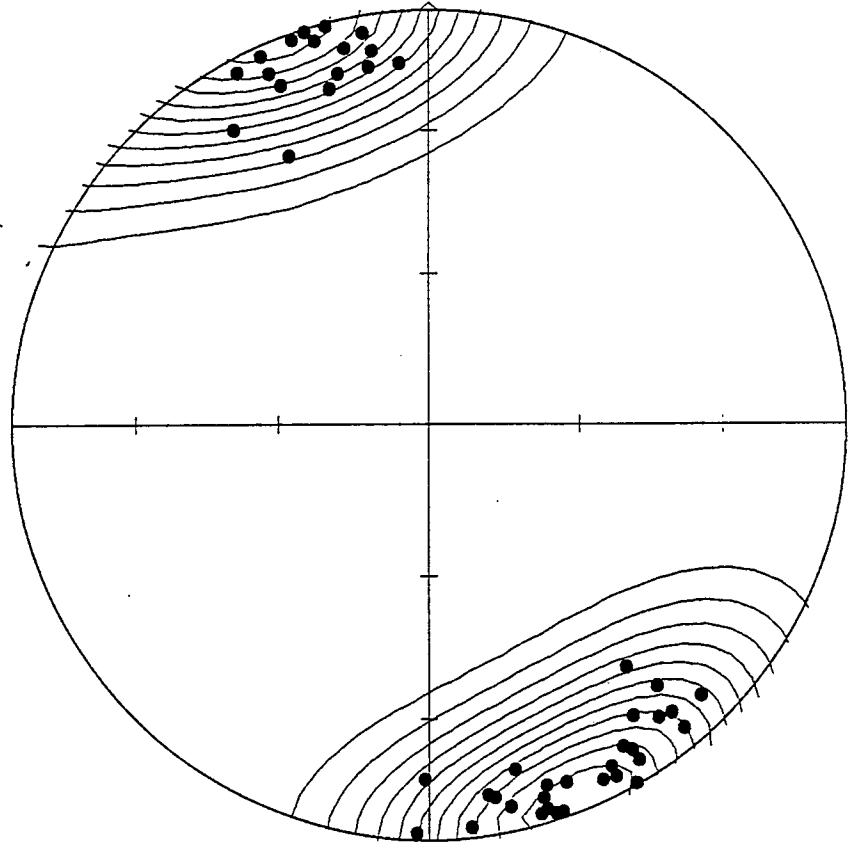




Fig. 5.21b.

Poles to S1 schistosity - Kashabowie - Huronian L.

Low metam. grade metavolcanics and metasediments



$N = 47$

$k = 12.44$

$(\text{Peak} - E)/\text{Sigma} = 22.0$

Peak position :  $157.6^\circ / 2.5^\circ$

$E = 3.78$

$\text{Sigma} = 1.26$

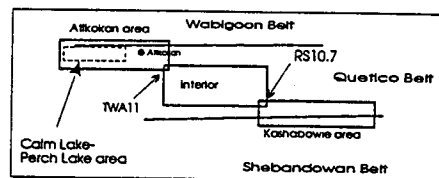
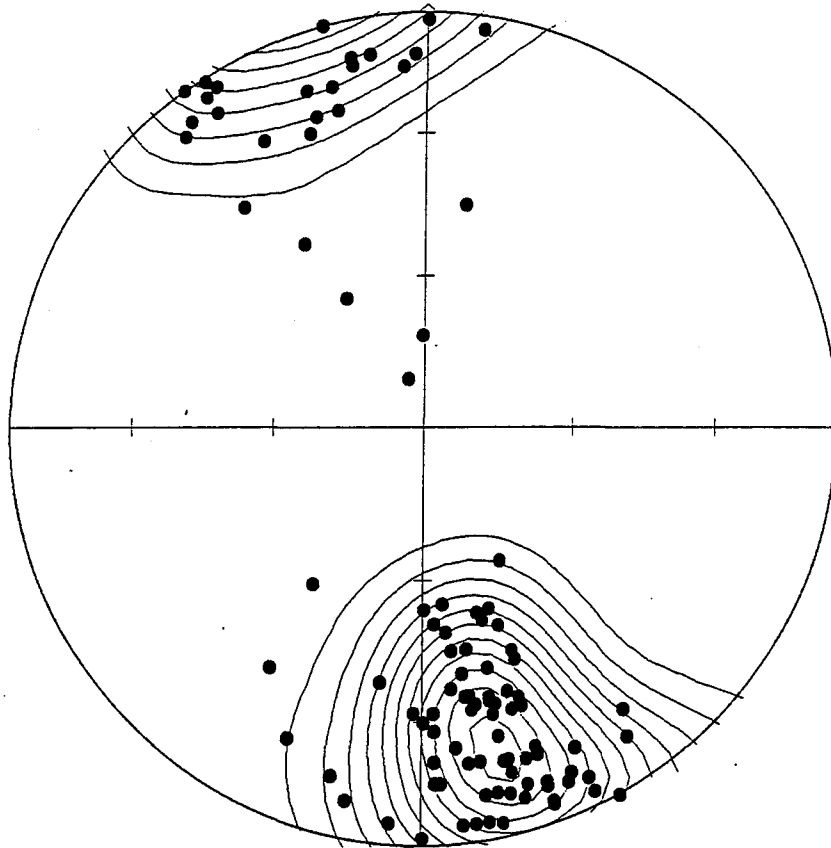


Fig. 5.21c.

Poles to S1 schistosity - the interior of Quetico

Medium and high metamorphic grade metasediments



$N = 106$

$E = 4.15$

$k = 25.56$

$\text{Sigma} = 1.38$

$(\text{Peak} - E)/\text{Sigma} = 20.8$

Peak position :  $167.9^\circ / 21.5^\circ$

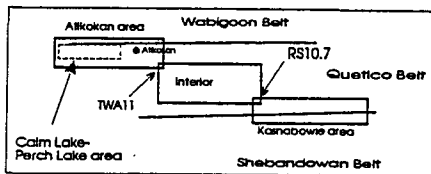
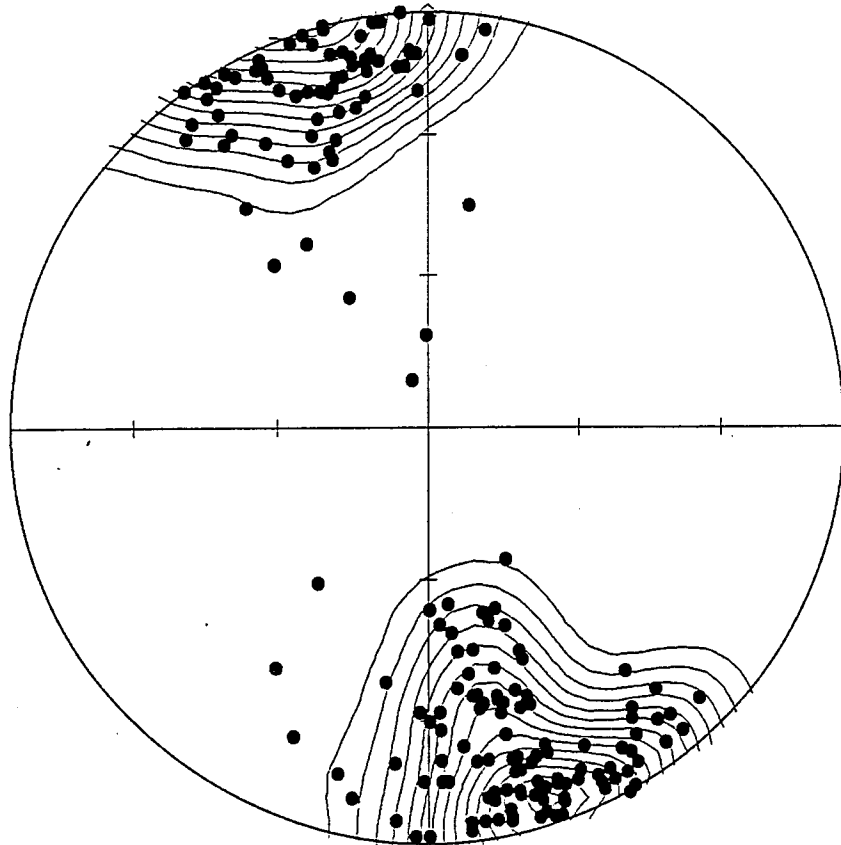


Fig. 5.21d.

Poles to S1 schistosity - Atikokan - Kashabowie L.  
Samples from Quetico belt margins and its interior



$N = 187$

$k = 43.56$

$(\text{Peak} - E)/\text{Sigma} = 26.7$

Peak position :  $162.6^\circ / 7.6^\circ$

$E = 4.29$

$\text{Sigma} = 1.43$

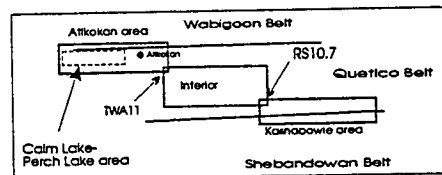


Table 5.22. The orientation of tectonic fabrics: poles to  $S_0$  and  $S_1$  and tectonic lineations  $L_1$  in three sub-areas: "Atikokan" - east of Atikokan in low grade metasediments; "interior" - medium and high grade metasediments; "Kashabowie" - low grade metasediments and metavolcanics east of Stetham L. toward Kashabowie L.

Area & fabrics (lineations $L_1$ & poles to planes $S_1$ & $S_0$ )	N	Peak position	$\sigma$	Eigen- vector	Conf. cone	Ref. fig.
$S_1$ - Atikokan	34	346/9	17	345/9	7/4	5.21a
$S_1$ - interior	106	168/22	21	166/17	6/3	5.21b
$S_1$ - Kashabowie	47	158/3	22	158/2	5/3	5.21c
$S_1$ - whole transect	187	163/8	27	163/7	4/2	5,21d
$L_1$ - Atikokan	7	76/52?	3	68/43?	43/17	5.23a
$L_1$ - interior	60	72/13	26	70/16	5/3	5.23b
$L_1$ - Kashabowie	32	74/20	16	72/21	8/4	5.23c
$L_1$ - whole transect	99	72/13	32	71/18	4/3	5.23d
$S_0$ - Atikokan	7	354/1	7	353/2	9/5	5.24a
$S_0$ - Kashabowie	11	164/2	10	163/3	6/3	5.24b

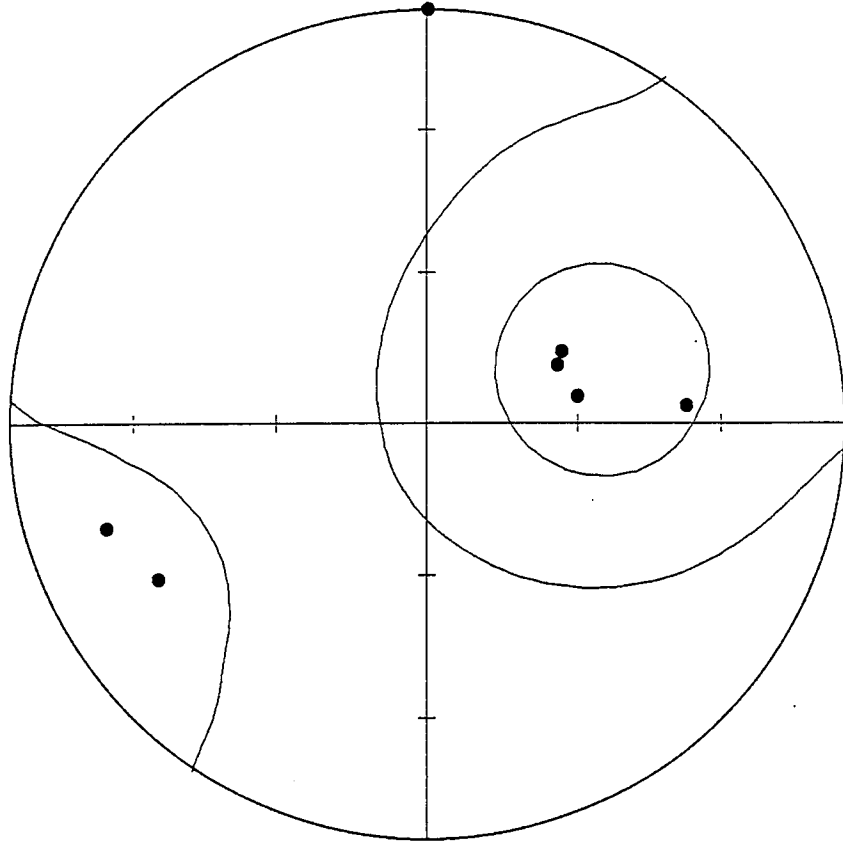
Table 5.22). The lower dips of  $S_1$  in the belt interior are caused probably by late intrusions of granitoid bodies and pegmatites within the area.  $S_1$  at the north margin dips to the S, but at the south margin to the N. The dip sense on the southern margin is much more consistent than on the northern one. Locally, the variations of  $S_1$  dip from to the S to the N are quite common in highly sheared chlorite and biotite schist just south of Atikokan.

Mineral lineations  $L_1$  in chlorite and biotite schist south of Atikokan are few and they have varying plunges (Fig. 5.23a). They were recognized as intersection lineations of  $S_0$  and  $S_1$

Fig. 5.23a.

Mineral lineations L1 - Atikokan area

Low grade metasediments



$N = 7$

$k = 3.56$

$(\text{Peak} - E)/\text{Sigma} = 2.9$

Peak position :  $76.0^\circ / 52.2^\circ$

$E = 1.97$

$\text{Sigma} = 0.66$

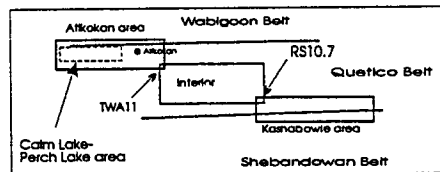
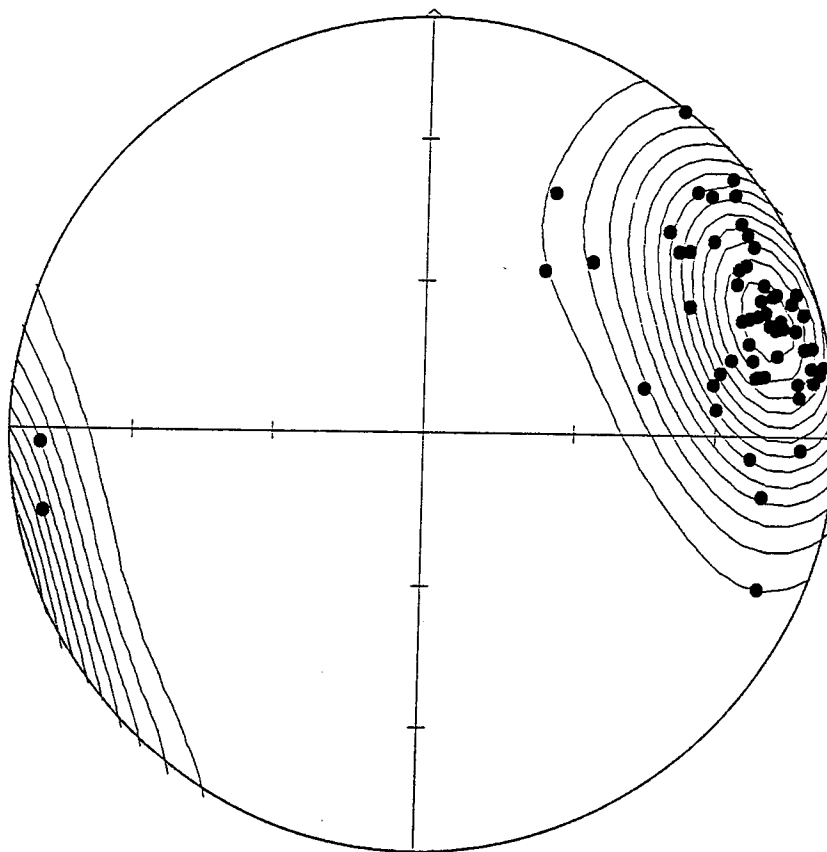


Fig. 5.23b.

Mineral lineations L1 - the interior of Quetico B

Medium and high metam. grade metasediments



$N = 60$

$E = 3.91$

$k = 15.33$

$\text{Sigma} = 1.30$

$(\text{Peak} - E)/\text{Sigma} = 25.8$

Peak position :  $71.6^\circ / 13.2^\circ$

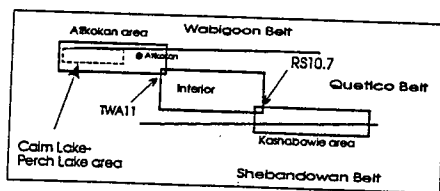
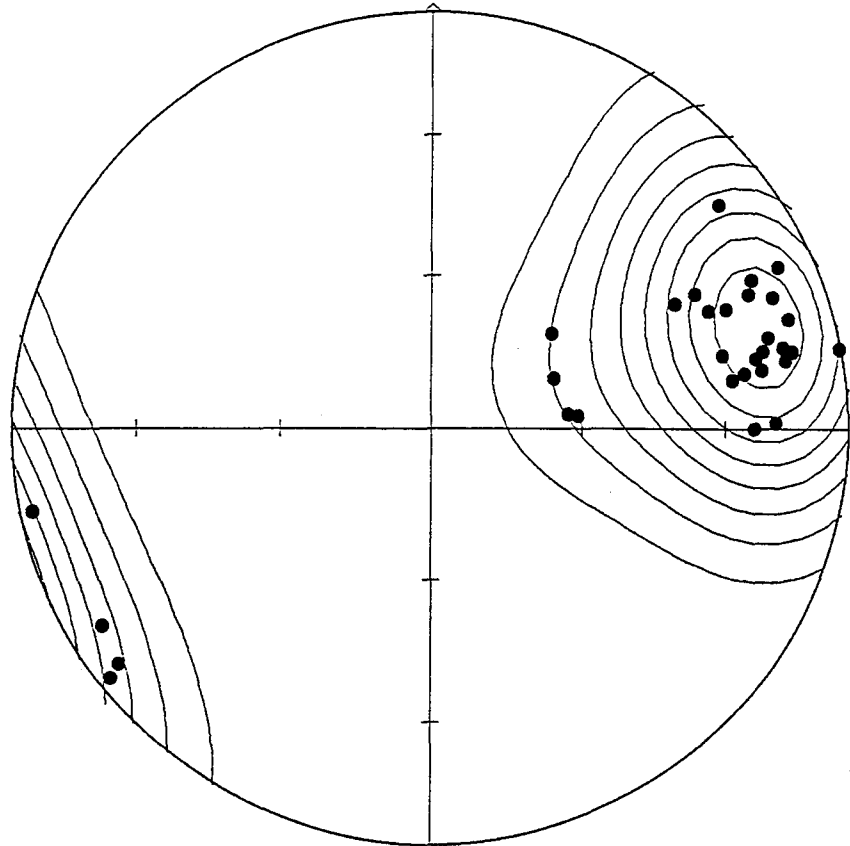


Fig. 5.23c.

Mineral lineations L1 - Kashabowie - Huronian L.

Low metam. grade metasediments and metavolcanics



$N = 32$

$E = 3.51$

$k = 9.11$

$\text{Sigma} = 1.17$

$(\text{Peak} - E)/\text{Sigma} = 15.8$

Peak position :  $74.1^\circ / 20.2^\circ$

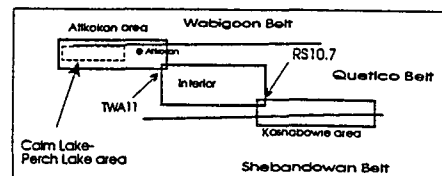
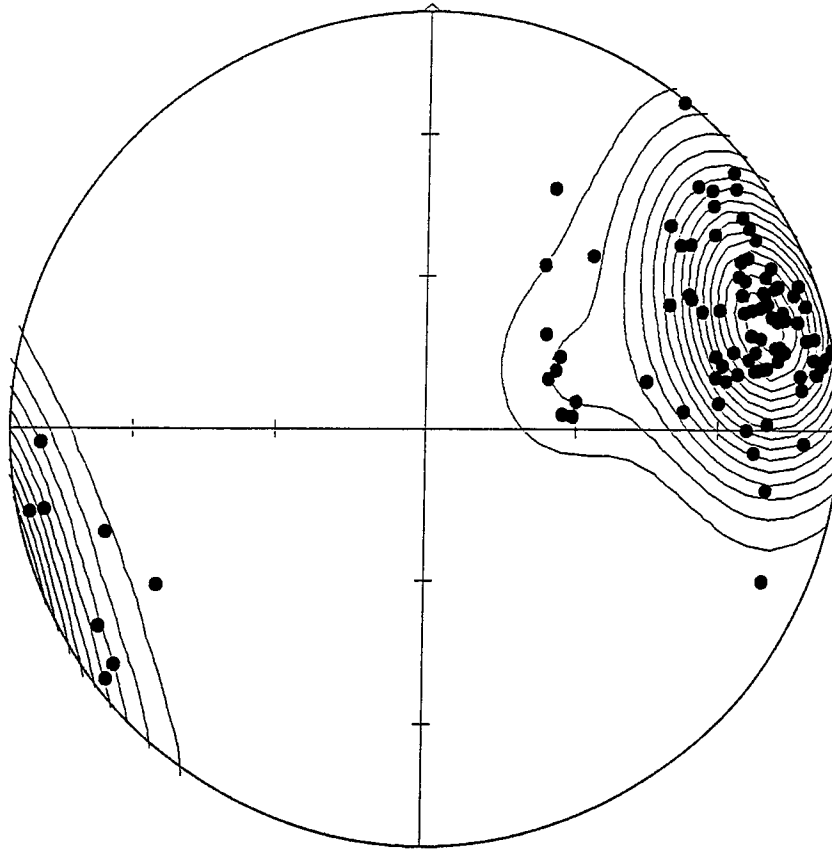


Fig. 5.23d.

Mineral lineations L1 - Atikokan - Kashabowie L.

Samples from the Quetico belt margins and interior



$N = 99$

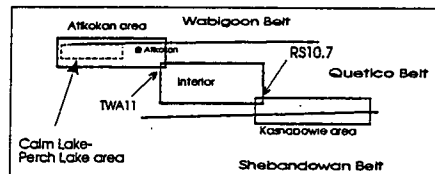
$E = 4.13$

$k = 24.00$

$\text{Sigma} = 1.38$

$(\text{Peak} - E)/\text{Sigma} = 31.7$

Peak position :  $71.6^\circ / 13.2^\circ$





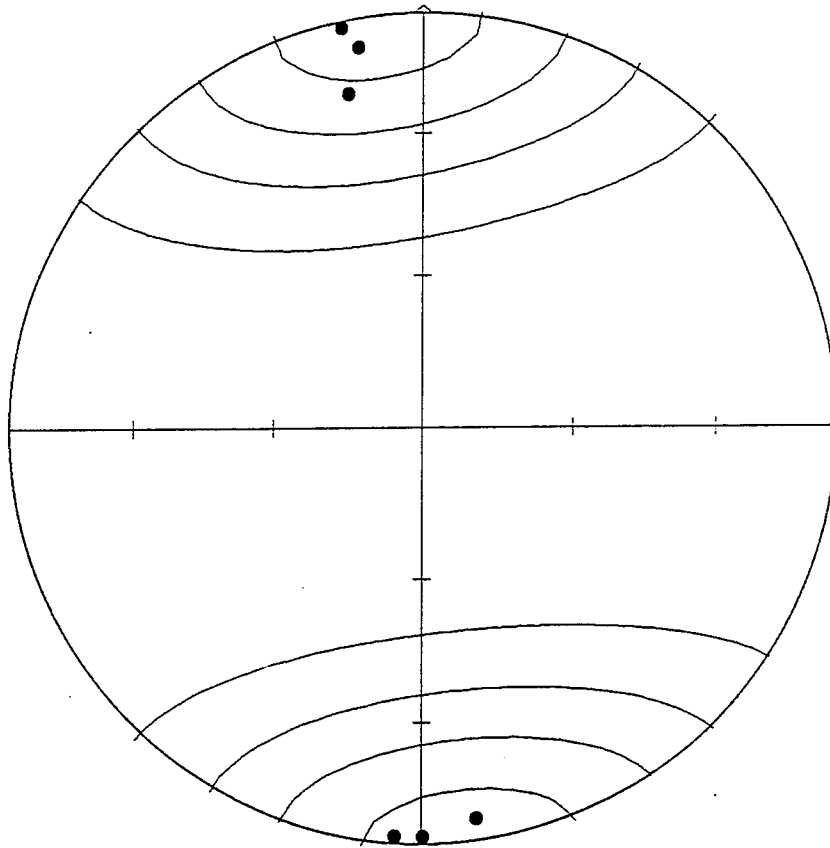
planes. Their erratic plunges are similar to those from the Calm Lake - Perch Lake area (Borradaile and Sarvas, 1989), correlated with sheath - like isoclinal folds. In higher grade rocks and metavolcanics  $L_1$  extension lineations cluster around well defined maxima (Fig. 5.23b,c), plunging gently to ENE (Table 5.22) and somewhat more steeply near the belt margins.

Primary bedding ( $S_0$ ) is preserved only in low- grade chlorite and biotite schists and is almost vertical at both belt margins (Fig. 5.24a, b). It is oriented clockwise with respect to  $S_1$  (Table 5.22). Its orientation is very consistent across each belt margin.

Fig. 5.24a.

Poles to bedding S0 - Atikokan area

Low metam. grade metasediments



$$N = 7$$

$$k = 3.56$$

$$(\text{Peak} - E)/\text{Sigma} = 7.1$$

$$\text{Peak position} : 353.7^\circ / 0.7^\circ$$

$$E = 1.97$$

$$\text{Sigma} = 0.66$$

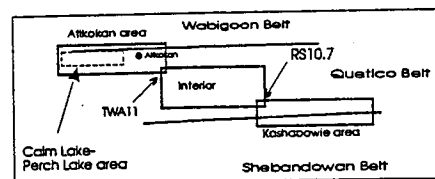
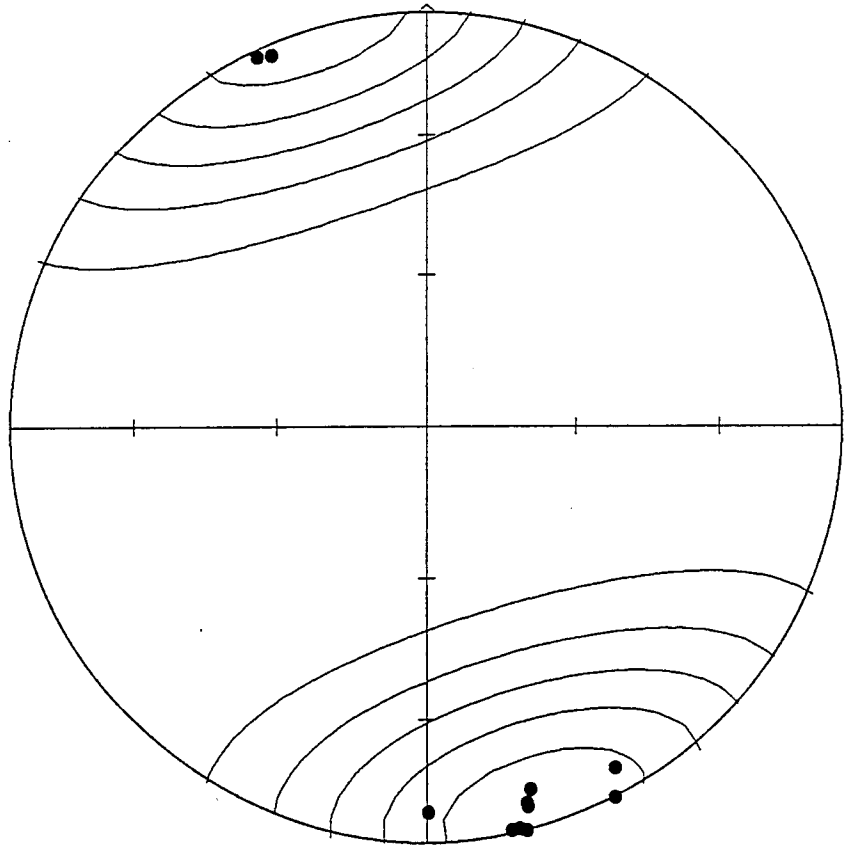


Fig. 5.24b.

Poles to S0 bedding - Kashabowie - Huronian Lake  
Low metam. grade metavolcanics and metasediments



$N = 11$

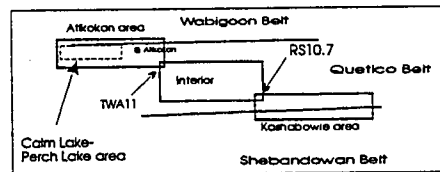
$k = 4.44$

$(\text{Peak} - E)/\text{Sigma} = 9.6$

Peak position :  $163.6^\circ / 1.8^\circ$

$E = 2.47$

$\text{Sigma} = 0.83$



## Chapter 6.

Review of magnetic properties of minerals and rocks.

Magnetic properties of all solid substances can be evaluated in terms of diamagnetic, paramagnetic or ferromagnetic (s.l.) behaviour, when the substance is exposed to an external magnetic field. This phenomenon can be used for several geophysical applications, such as paleomagnetism, geomagnetic mapping, magnetotellurics and rock-magnetic studies.

Studies presented here focus on the application of such magnetic properties as magnetic susceptibility of para- and ferromagnetic materials (hereafter s.l.) as well as magnetic remanence of ferromagnetic minerals (such as pyrrhotite and magnetite).

The acquired bulk magnetization  $M$  (per unit volume) of a sample exposed to an external magnetic field  $H$  is a function of both the external field  $H$  and the magnetic properties of the specimen. When the dependence of magnetization from the external field is linear, the material properties are characterized by a bulk magnetic susceptibility  $\chi$ , which can be a complex quantity in general. For a distant or low-frequency magnetic field the susceptibility is approximated by a set of real values; for a high frequency magnetic field the imaginary (out - of - phase) component of susceptibility is a decisive factor, reflecting more the conductivity of the material.

$$\bar{M} = \chi(\omega) \bar{H}_{ext}$$

- where:  $\chi$  - susceptibility,  $M$  - magnetization,  $H_{ext}$  - external magnetic field,  $\omega$  - frequency of external field.

Generally the contribution to magnetic properties of the sample can be given by diamagnetic, paramagnetic, ferromagnetic and ferrimagnetic (or antiferromagnetic) grains; these magnetic properties are considerably different.

Diamagnetic minerals owe their properties to the paired electron configuration of atoms. These have the resultant orbital and spin magnetic moments of filled electron shells equal zero (Kittel, 1971, p.499-501) in the absence of the external magnetic field. In the presence of the external field they acquire an orbital magnetic moment antiparallel to the direction of external magnetic field due to the interactions between the magnetic field and the existing orbital moments of single electrons. This is the diamagnetic effect. Their susceptibility is given as:

$$\chi = -\frac{N\mu_0 e^2 Z \langle r^2 \rangle}{6m_e} < 0 \text{ (O'Reilly, 1984)}$$

where:  $N$  - concentration of atoms,  $e$  - electron charge,  $Z$  - atomic number,  $m_e$  - electron mass,  $\langle r^2 \rangle$  - mean atom radius,  $\mu_0$  - permeability of free space.

The magnetic susceptibilities of diamagnetic minerals (eg.

quartz, calcite and dolomite) are about  $-10^{-6}$  to  $-10^{-5}$  SI and depend weakly on the temperature.

The diamagnetic minerals do not retain magnetization in the absence of external magnetic field. It should be pointed that all substances show the diamagnetic effect to the some degree as an effect of interactions of inner filled electron shells with the external magnetic field.

On the other hand, ferromagnetic, ferrimagnetic and antiferromagnetic minerals (hereafter sometimes ferromagnetic *s.l.*) and paramagnetic minerals have atoms of elements with odd atomic number in their crystal lattices which have uncoupled spins. Therefore the single atoms have the resultant non-vanishing magnetic moment even with the absence of external field. The bulk resultant magnetic moment of the sample vanishes due to thermal disorder of the individual spins. The acting of external field tends to orient the spin magnetic moment parallel to the external field as well as generating the diamagnetic orbital weak component of resultant magnetic moment.

In paramagnetic minerals the single atoms interact only with external field and not with themselves. Their densities of wave functions (or "orbitals" in classical approach) do not overlap, when compared to the standard distances of ions in the crystal lattice. The paramagnetic effect decreases with the temperature due to randomizing effect of thermal excitations.

Generally the dependence of the paramagnetic magnetization from the external magnetic field and temperature is given by

Brillouin function (see for example Stacey and Banerjee, 1974, eq. 1.18). For magnetic grains which usually contain a large number of atoms in the lattice, the magnetization can be approximated by Langevin model (eg. see Butler, 1991, p.22, Collinson, 1983, p.15). In low field and high temperature conditions when  $\mu_B H \ll kT$ , the magnetization is estimated as a linear function of external field and the susceptibility of a paramagnetic material is given by the equation:

$$\chi = \frac{C}{T}, \text{ where } C = \frac{N \mu_0 S(S+1) 4 \mu_B^2}{3 k} \quad \text{- Curie constant, (O'Reilly, 1984)}$$

- where S - total spin number of magnetic grain, k - Boltzmann constant, T - absolute temperature in kelvins,  $\mu_B$  - Bohr magneton, N - atom concentration.

When the paramagnetic material is present in a higher concentration, the exchange interaction among the atoms can lead to the creation of an additional molecular field  $H_{mol} = \lambda M$ , where M - magnetization,  $\lambda$  - constant. The dependence of the susceptibility from the temperature then becomes as follows:

$$\chi = \frac{C}{T-\theta}, \text{ where } C - \text{Curie constant: } C = N\mu_B^2/k; \theta - \text{an}$$

asymptotic Curie temperature:  $\theta = \lambda C$  (O'Reilly, 1984).

Atoms and ions of elements with uncompensated spins of electrons of the 3d shell have the strongest paramagnetic effect

- iron group elements, such as  $\text{Fe}^{3+}$  (with spin moment  $5\mu_B$ ),  $\text{Fe}^{2+}$  ( $4\mu_B$ ). They are a common constituent of rock forming silicates as amphiboles, micas, chlorites showing predominantly paramagnetic properties. The other strongly paramagnetic ions, such as  $\text{Mn}^{2+}$  (spin  $5\mu_B$ ) and  $\text{Cr}^{3+}$  (spin  $3\mu_B$ ) usually occur in small quantities in the magnetic minerals.

When the structure of crystallographic lattice permits the higher concentration of 3d ions at small distances (as in ferro-oxides and pyrrhotite) the interactions between the spins become significant, creating a new structure of aligning spins oriented parallel or antiparallel each to other. The exchange energy related to this alignment is negative and minimal for parallel alignment of spins (ferromagnetism), therefore the ferromagnetic materials can have strong spontaneous internal magnetization when the external magnetic field is absent.

In antiferromagnetic minerals, two antiparallel sublattices exist and tend to cancel the overall magnetization effect in the state of minimal exchange energy. In ideal antiferromagnetics the effects of two lattices cancel completely, but in natural minerals such as hematite the alignments are usually imperfect leading to weak spontaneous magnetism (in hematite above the Morin temperature  $\approx 263\text{K}$ ) - these minerals show canted antiferromagnetism.

In ferrimagnetic minerals one sub-lattice has stronger spontaneous magnetization than the other, generating weaker overall spontaneous magnetization than in the ferromagnetic



case.

The spontaneous magnetization vanishes above the specific temperature (Curie point  $\theta_C$  for a ferromagnetic and ferrimagnetic, Néel point  $\theta_N$  for a antiferromagnetic). In some ferrimagnetics (type N - Stacey and Banerjee, 1974) the self-reversal of magnetization (at the compensation point) can be observed due to the different rate of decrease of spontaneous magnetization for each sublattice (e.g. in some titanohematites), in other type of ferrimagnetics the overall magnetization can increase in some ranges of temperature (Fig. 6.1). In low temperatures the spontaneous magnetization in ferrimagnetics increases reaching maximum at 0 K.

The magnetic susceptibility is also strongly dependent on temperature:

- for ferromagnetics, in temperatures above Curie point  $\theta_C$ , where ferromagnetics behave as paramagnetics, the magnetic susceptibility decreases with temperature:  $\chi = \frac{C}{T - \theta_C}$ , where

$\theta_C > 0K$  and theoretically it is indefinite at  $\theta_C$  (Stacey and Banerjee, 1974); in ferromagnetic state the susceptibility slightly increases when the temperature approaches  $\theta_C$  (superparamagnetism), with the phase transition to paramagnetism in  $\theta_C$  (Fig.6.2);

- for ferrimagnetic minerals, in low temperatures ( $T < \theta_C$ ) the dependence of MS from T is as for ferromagnetics, above Curie

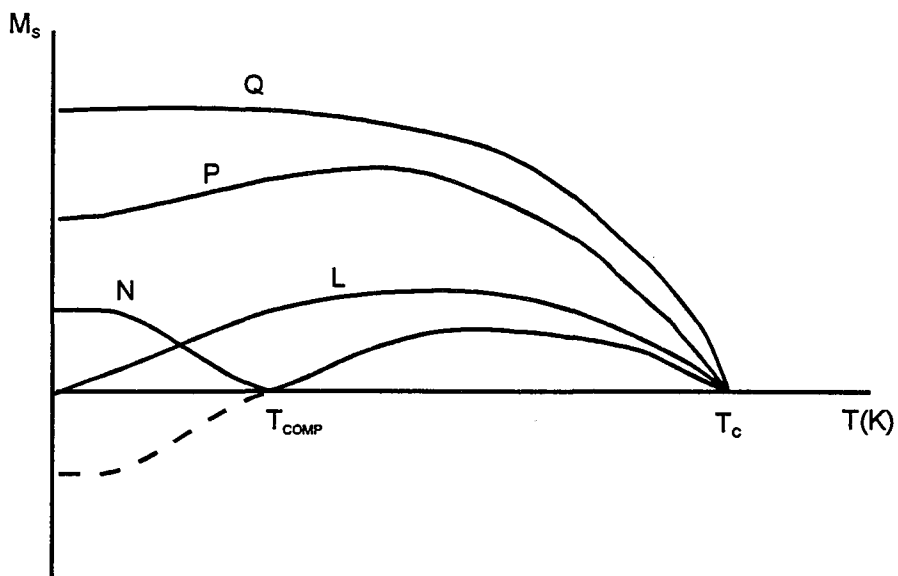


Fig. 6.1. Spontaneous magnetization curves for the three types of ferrimagnetics (types Q, N, L, P according to Néel terminology). Type Q model is also appropriate for ferromagnetics.

$T_c$  - Curie point,  $T_{comp}$  - temperature of compensation of spontaneous magnetization of both sublattices (modified from O'Reilly, 1984).

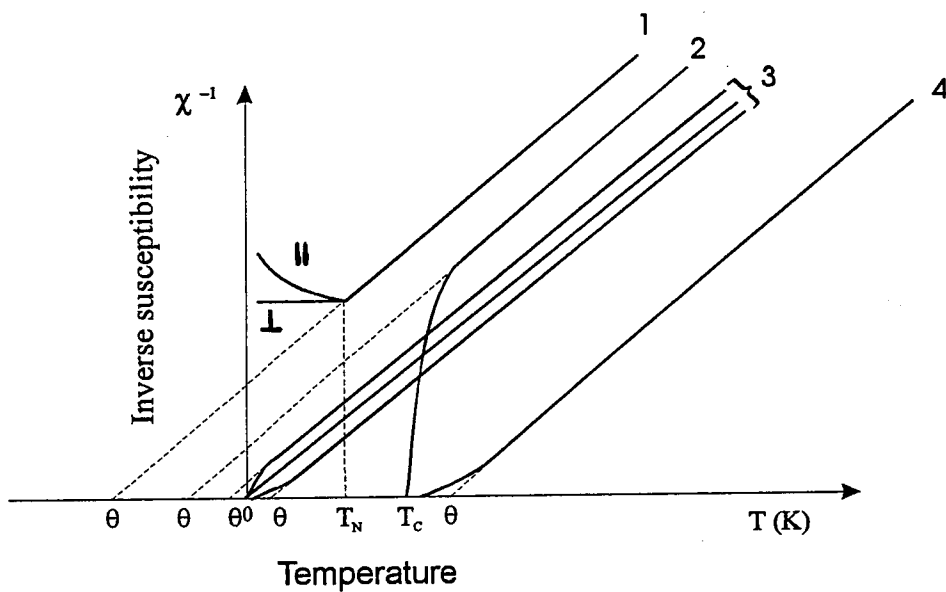


Fig. 6.2. Reciprocal susceptibility ( $1/\chi$ ) as a function of temperature.

1. anti-ferromagnetic,  $T_N$  - Néel temperature;
  2. ferrimagnetic,  $T_C$  - Curie temperature;
  3. para-magnetics, an ideal and real ones;
  4. ferromagnetic,  $T_C$  - Curie temperature;
- $\theta$  - asymptotic Curie temperature; (modified from O'Reilly, 1984).

temperature  $\chi$  decays as follows:  $\chi = \frac{C}{T-\theta'}$ , where  $\theta' < 0$  for  $T \gg \theta_c$

and as in case of ferromagnetism in theory  $\chi \rightarrow \infty$  when  $T \rightarrow \theta_c$ ; in fact there is a phase transition for  $\chi$  in Curie temperature;

- antiferromagnetics have the paramagnetic decay of susceptibility above the Néel temperature (as for ferrimagnetics), but at lower temperatures the susceptibility shows strong anisotropy with the direction of applied field with respect to the axis of spin alignment. The average susceptibility for an isotropic polycrystalline mineral can be

approximated as  $\chi = \frac{1}{3} \chi_{\parallel} + \frac{2}{3} \chi_{\perp}$ , where  $\chi_{\parallel}$  and  $\chi_{\perp}$  are

susceptibilities for a single crystal in directions parallel and perpendicular to the spin alignment (Stacey and Banerjee, 1974). When the orientation of polycrystalline grains of antiferromagnetic mineral is not isotropic in the sample, it can cause a large deviation from above formula.

The temperature dependence of susceptibility for all classes of materials is presented in Fig. 6.2.

The existence of remanent magnetization in ferro - ferri - and antiferromagnetic materials in the absence of external magnetic field and the process of the acquiring of magnetization by these material is explained on the basis on the ferromagnetic domain theory. The coupling interaction between spins leading to

the perfect alignment of spins minimizes the exchange energy  $E_{ex}$ . However because the grain possesses a magnetization  $M$ , which produces the external magnetic field around the grain, it also generates the internal self- demagnetizing field  $H_d$  in the grain. The magnetostatic self - energy of the grain due to this process  $E_{self} = -0.5*\mu_0M*H_d$  is a major component of the total magnetic energy of the grain. As magnetostatic forces are effective on the long range they distort the perfect spin alignment and produce the domain structure in the ferromagnetic (s.l.) minerals.

In each domain the magnetic moments tend to be aligned parallel each to other with a smooth transition of their orientation through the domain walls. When all magnetic moments are aligned, the domain has maximum possible magnetization of the material - saturation magnetization  $M_s$ . The number of domains and the direction of magnetic moment alignment in each domain is a function of grain shape, size and the crystallographic structure. This domain arrangement tends to minimize the overall magnetic energy of the grain and also eliminates the magnetic polarity from the external surface of the grain. However the building of domain wall increases the overall energy of the grain, therefore the number of domains in a single grain is usually of order 1 (SD) up to more than 30 (MD).

The third important term in the total magnetic energy of the grain comes from the magnetocrystalline anisotropy energy

$E_{anis}$ . Due to crystallographic structure of the magnetic material the coupling of spins have a preferred orientation (easy axis). The mechanisms responsible for that anisotropy are dipole - dipole interactions, anisotropy of the exchange energy integral and the single ion anisotropy (eg. O'Reilly, 1984 ch. 3.4). Depending on the crystallographic symmetry of the lattice, the anisotropy energy can have uniaxial (hematite) or cubic symmetry (magnetite).

As an effect of minimizing of the total energy, the configuration of domains in a magnetic grain is anisotropic and strictly depends on the shape and size of the grain as well as the saturation magnetization of the magnetic material. Therefore observed smaller magnetic grains are single domain (SD), larger ones are pseudo-single domain (PSD) or multidomain (MD). If the size of grain is too small to produce a stable alignment of magnetic moment within the grain, the grain is superparamagnetic, with susceptibility usually much larger than typical paramagnetics. The maximum size of SD - behaviour also increases with larger shape-ratio of the grain. An example schematic diagram for magnetite is shown on Fig 6.3.

Soffel (1971, 1977) found an approximately linear dependence between number of domains and grain size for pyrrhotite and titanomagnetite ( $x=0.55$ ). SD pyrrhotite grains are of size 2-3  $\mu\text{m}$ , 10 - 100  $\mu\text{m}$  long grains have 5-25 domains.

When the external field is acting on the ferromagnetic grain, the additional magnetic energy  $E_h = -0.5*\mu_0*M*H_{ext}$  is added

to the internal energy of the grain. The external field can not change the intensity of magnetization of a SD grain with saturation magnetization but tries to rotate the magnetic moment of the grain toward the applied field. In MD grains it can move the domain walls by the growth of one domain at the expense of the others. As the result the total magnetic moment of the grain changes. At higher fields the magnetic moments within single grains can rotate until the grain approaches the saturation magnetization.

The response of the grain to an external magnetic field is anisotropic. It can be magnetized (MD grains) or its magnetic moments reoriented (SD grains) easier in some directions ("easy" axes) or a plane ("easy" direction - plane perpendicular to "hard" axis) - see Fig 6.4 for the case of magnetite. There are several factors leading to this anisotropic behaviour, but two major ones are shape anisotropy and magnetocrystalline anisotropy. The others, such as alignment of magnetic domains or direct effects of exchange anisotropy are observed only in specimens exposed to high magnetic fields (Bhatal, 1971, Hrouda, 1982). Magnetostriction anisotropy (Hrouda, 1982, Stacey and Banerjee, 1974) is produced as an effect of elastic deformation of grain due to saturation magnetization of the grain.

The presence of demagnetizing field  $H_d$  within the grain leads to two basic effects:

1. - the difference between measured bulk volume susceptibility  $\chi$  and the intrinsic volume susceptibility  $\chi_i$ .

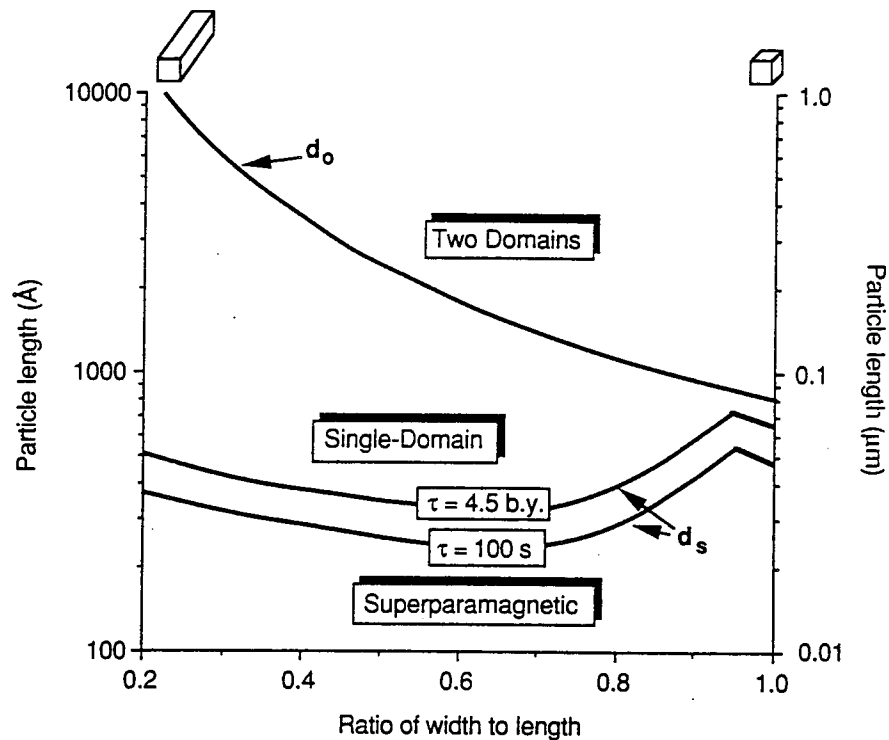


Fig. 6.3. Domain configuration of parallelepipeds of magnetite at 290 K as a function of shape and size.

$d_0$  - SD - MD threshold boundary;

$d_s$  - SPM - SD threshold boundary for different relaxation times  $\tau$  of remanent magnetization (from Butler, 1992).



2. - the producing of a hysteresis curve for the grain.

In a grain with magnetization  $M$ , the demagnetizing field is given as  $H_d = -N_i M$ , then the resultant intrinsic field  $H_i$  in the grain is  $H_i = H_{ext} - NM$ , where  $N_i$  is the demagnetizing factor along

the given axis. It leads to the dependence between observed  $\chi$

and intrinsic  $\chi_i$  susceptibilities : 
$$\chi = \frac{\chi_i}{1 + N_i \chi_i} .$$

The demagnetizing factor varies from 1 (for the axis perpendicular to the ideal disk) through 1/3 for a sphere to 0 for an axis along an infinite needle.

If intrinsic susceptibility is  $<1$ , the measured susceptibility is only slightly less than the intrinsic one. For strongly ferri- or ferromagnetic minerals intrinsic susceptibility is large ( $>10$ ) and  $N\chi \gg 1$ , therefore the measured susceptibility  $\chi \approx \frac{1}{N}$  is much lower than the high intrinsic

susceptibility. Spherical particles of magnetite with  $N=1/3$  have  $\chi \approx 3.3$ ; ellipsoidal grains of axis ratio 1.5:1 have  $N \approx 0.31$  and  $\chi \approx 3.2$ ; for aligned elongated particles of ratio 3:1,  $N=0.109$  (Collinson, 1983). Usually ferro- and ferrimagnetic minerals are only a minor constituent of the rock (volume fraction  $f \ll 1$ , usually of order 1%), which further decreases the measured

susceptibility. Intrinsic susceptibilities of hematite are of the order of  $10^{-3}$ , therefore the intrinsic susceptibility is actually measured, externally.

The behaviour of single- (SD) and multidomain (MD) magnetic grains in alternating magnetic field is usually different. Let us consider a MD sample which has initially no remanent magnetization. In the MD case the acting external field at first produces magnetization proportional to the external field (up to  $\sim 1$  mT - Fig. 6.5). In this range the initial or reversible susceptibility can be measured. In higher fields the domain walls are moved irreversibly, while some domains grow at the expense of the others. Finally, if the field is strong enough, the domains can rotate and the sample achieves saturation magnetization ( $M_s$ ).

Once the sample is magnetized when the external field is decreased to 0, the grain still possesses saturation isothermal remanent magnetisation (SIRM). The application of the field in reversed direction reduces the magnetization to zero with a reverse field equal to value of coercive force  $H_c$ .

However due to the existence of a self-demagnetizing field within the grain, the intrinsic field in the grain still exists; only the externally measured magnetization vanishes. Therefore to remove completely the remanent magnetization, a higher magnetic field (coercivity of remanence  $H_{cr}$ ) must be applied. The increase of magnetic field in a negative direction again increases magnetization up to saturation value. The processes

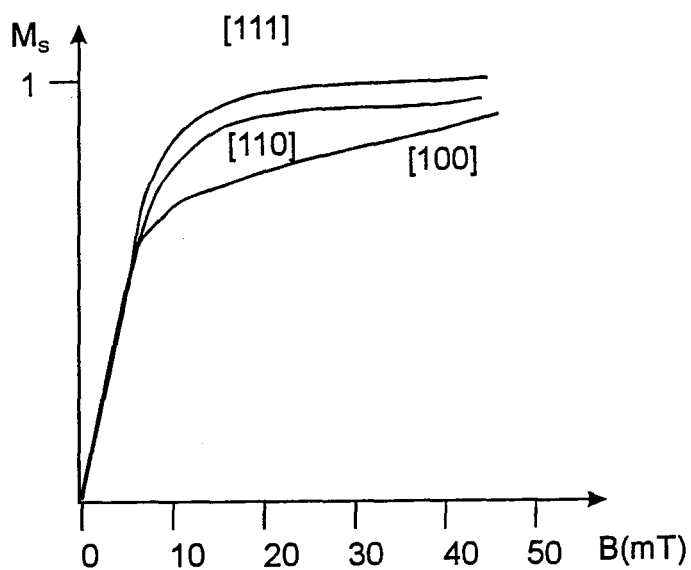


Fig. 6.4. Normalized magnetization of a single crystal of magnetite as a function of external magnetizing field for different crystallographic directions of magnetizing field:  
 [111] - along magnetocrystalline "easy" direction;  
 [100] - along "hard" direction, (modified from Butler, 1992).

are "symmetrical" as the field changes are continued in the opposite direction, producing the hysteresis loop. When the external field is insufficient to saturate the grain, remanent magnetization and coercivity have lower values also. In single domain grains, the shape of the hysteresis loop depends strongly on the orientation of the applied field with respect to the direction of easy axis of a given grain (Fig. 6.6). However for an assemblage of randomly oriented grains the bulk hysteresis loop is very similar to that of MD grains.

For the purpose of this paper SI units are preferred. Therefore often parameters  $B_c$ ,  $B_{cr}$  (in mT) appear instead of  $H_c$ ,  $H_{cr}$  (in mA/m) as the laboratory equipment used is often calibrated in units of induction instead of field intensity.

In multigrain assemblages of SD grains, coercive force values are lower than for a single grain (Butler, 1991) and for a randomly distributed assemblage it is equal to about 50% of the coercive force of the grain.

Non-magnetized specimens (with a total remanent magnetization equal to 0) can be exposed also to step-wise increasing external field and acquire isothermal remanent magnetization (IRM) up to saturation magnetization (SIRM). The intensity of SIRM should be equal to  $M_s$  in a given direction. The remanent acquisition coercivity  $H_{cr}$  (the external field needed to generate IRM of intensity of  $0.5 \cdot M_s$ ) can be determined also (Fig. 6.7).

The values of magnetic parameters for a given mineral, such

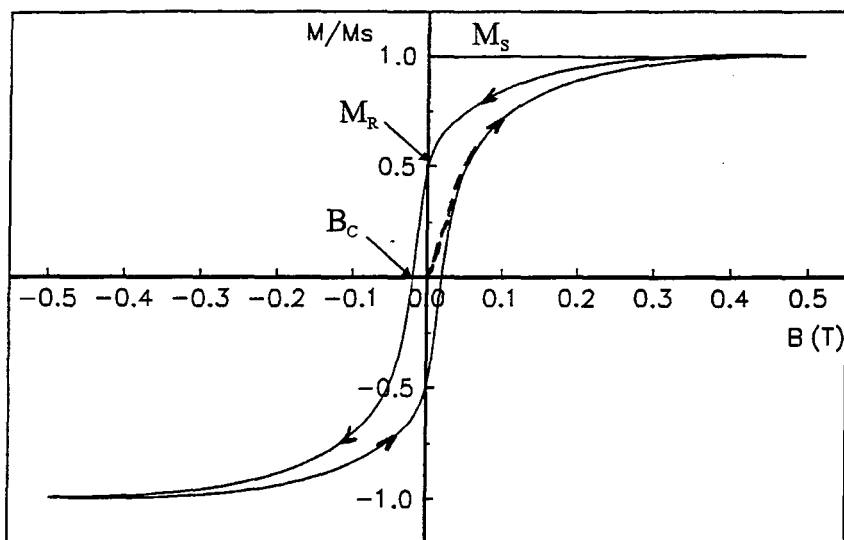


Fig. 6.5. Magnetization ( $M$ ) (normalized to saturation magnetization  $M_s$ ) of a magnetite-bearing sample in external magnetic field (expressed as magnetic induction  $B$ ).

$M_s$  - saturation magnetization;

$M_r$  - remanent magnetization (external field  $B=0$ );

$B_c$  - coercivity force (here in magnetic induction units, mT).

Initial curve of magnetization is shown as a dashed curve.

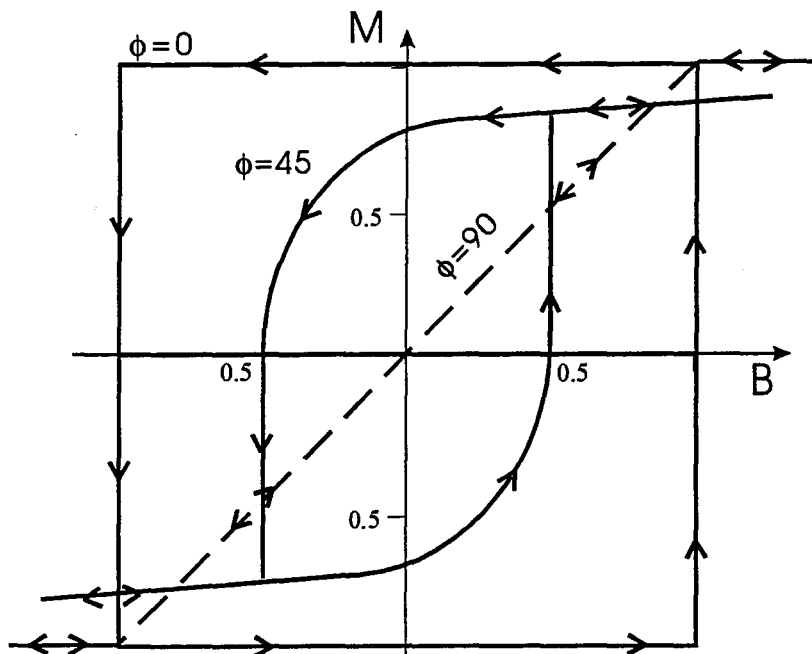


Fig. 6.6. Hysteresis loops for a single domain magnetite grain. The shape of each loop depends on the orientation of external field with respect to magnetocrystalline easy axis of the grain.

$\phi=0$  - field parallel to easy axis;

$\phi=90$  - field perpendicular to easy axis.

Magnetization  $M$  is normalized by saturation magnetization  $M_s$  and magnetic induction is normalized by  $\mu_0(N_b - N_a)M_s$ ,  $N_a$ ,  $N_b$  - demagnetization factors of an uniaxial grain.

IRM acquisition  
Sample TWA15

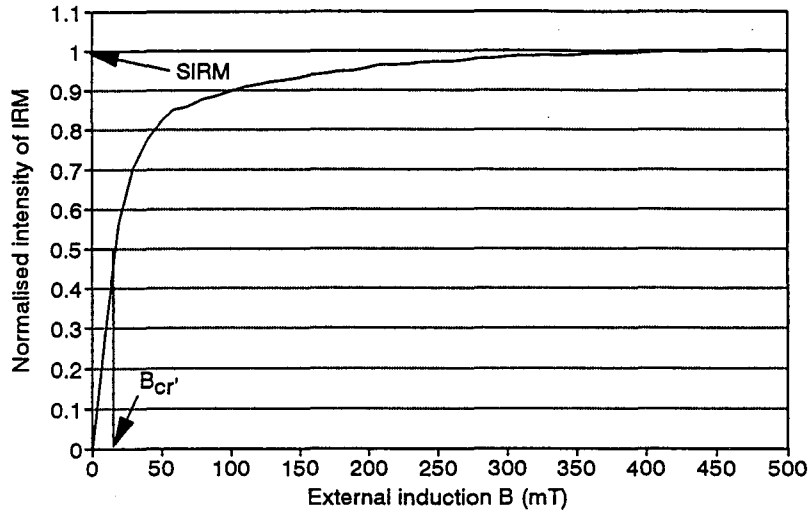


Fig. 6.7. A curve of acquisition of isothermal remanent magnetization (IRM) for magnetite bearing sample TWA15. Intensity of IRM is normalized by its saturation value SIRM). External magnetic field is expressed in induction B units (mT).  $B_{cr}$  (in mT) or  $H_{cr}$  (in A/m) is coercivity of acquisition of SIRM. This is a field required to generate a magnetization of 50% of SIRM in a sample.

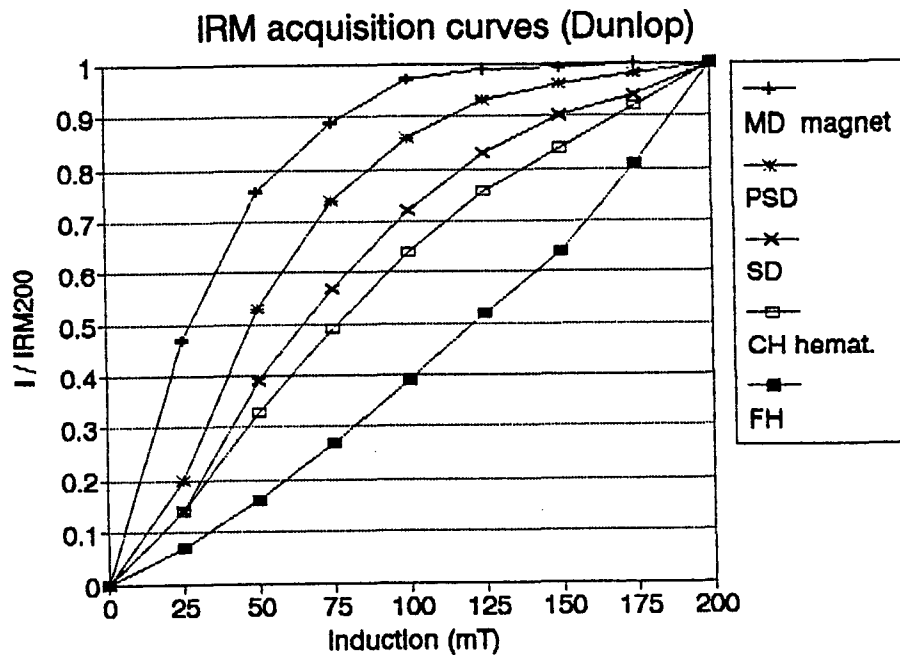


Fig. 6.8. IRM acquisition curves for PSD and SD magnetite, coarse (CH) and fine (FH) hematite (after Dunlop, 1971, 1972, 1973, 1981, 1983, 1986).

as  $H_c$ ,  $H_{cr}$ ,  $H_{cr}$ ,  $\chi$ ,  $M_r$  and  $M_s$  are different for assemblages of SD, PSD and MD grains and they are a function of grain size, shape and temperature. The SIRM acquisition curves for SD, PSD and MD assemblages of magnetite grains are shown on Fig. 6.8 (after Dunlop, 1981). Usually SD magnetite assemblages have the ratio  $H_c/H_{cr} > 0.5$ , for "true" MD grains :  $H_c/H_{cr} = 0.1 - 0.25$  (Fig 6.9, after Wasilewski, 1973).

The ratios  $M_r/M_s > 0.5$  are typical for SD particles, for MD grains the ratio is  $M_r/M_s < 0.05$  for magnetite,  $M_r/M_s < 0.1$  for  $x=0.6$  titanomagnetite (Dunlop, 1981). They can be often definitive of the domain structure of the grains (Dunlop, 1981 for magnetite). For MD particles Dunlop (1981) found  $B_c < 3$  mT for magnetite (originally  $H_c < 30$  Oe),  $B_c < 7$  mT for titanomagnetite; and initial susceptibility  $\chi_0 \approx 0.34$  to  $0.45$ .

SD grains gave higher values for coercive force: from 7 mT up to 40 mT for different rocks (diabases, basalts);  $H_c/H_{cr}$  ranged from 0.33 to 0.6;  $M_r/M_s$  are lower than theoretical values (0.5): 0.08 to 0.27, initial susceptibilities range from 0.18 to 0.28.

The direct relations between susceptibility, coercive force (or coercivity of remanence) and saturation magnetization are different for SD and MD particles (Dunlop, 1981), but they can vary also for different magnetic minerals. The formula for SD magnetite grains is:

$\chi = 0.349 M_s/H_{cr}$  (Dunlop, 1981), and for MD grains intrinsic susceptibility is used in above relation :  $\chi_i \propto M_s/H_c$ , thus the demagnetization factor must be determined as well. These

Domain structure classification  
after Wasilewski, 1973

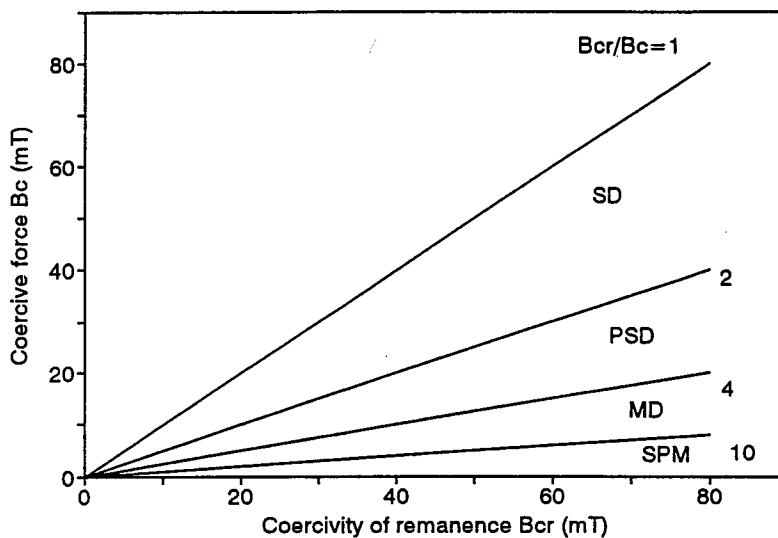


Fig. 6.9. The relation between coercive force  $B_c$  (or  $H_c$ ) and coercivity of remanence  $B_{cr}$  (or  $H_{cr}$  respectively) for magnetite as a function of domain structure of a grain.

Grains with  $B_c > B_{cr}$  do not exist.

SD - single - domain; PSD - pseudo - single - domain; MD - multi-domain; SPM - superparamagnetic grain;  
(modified from Wasilewski, 1973).



relations are not easily verified for unknown compositions or mixtures of magnetic phases. Therefore the ratios  $H_c/H_{cr}$  and  $M_r/M_s$  will be further used as an aid to domain structure determinations.

The domain structure is important when the stability of remanent magnetization is considered. Superparamagnetic (SP) grains cannot retain the stable magnetization (having a magnetic relaxation time that is too short). SD grains are suitable carriers of primary thermoremanent magnetization (TRM, Dunlop, 1981). MD grains can retain weaker secondary TRM or chemical remanence (CRM) (see Butler, 1992, Stacey and Banerjee, 1974).

The knowledge of other magnetic parameters such as coercive force, coercivity of remanence, Curie temperatures or blocking temperatures is necessary to perform suitable demagnetization treatments (alternating field demagnetization, thermal demagnetization and acid leaching techniques - Collinson, 1983).

## Chapter 7.

### Magnetic mineralogy of studied collections.

#### 7.1. Magnetic mineralogy of the belt boundaries.

Samples from the belt boundaries have been used in previous studies for determination of magnetic susceptibility and its anisotropy (Sarvas, 1988, Spark, 1990). As the contribution to MS and AMS varies for different minerals (Borradaile et al., 1987), initially the content of magnetic minerals had to be determined.

Three samples from Quetico - Wabigoon belt boundary (PSR 22, PSS 18 and PS 4) had their minerals separated using a Franz magnetic separator. The susceptibility of the fractions was measured by Sarvas (1988). Their compositions were determined by powder XRD technique and from grain mounts in polished sections examined under reflective-light microscopy (Sarvas, 1988).

Susceptibility results will be listed in chapter 9 as they are important primarily for AMS studies. Grain counts of strongly magnetic minerals in highly magnetic phase (pyrite, pyrrhotite and magnetite) for two grain mounts gave proportions as follows:

py : pyrrh : magn = 7:3:1 and 21:1:1 . The more extensive composition studies for the same collected material (Borradaile and Sarvas, 1989) showed average composition as 13:2.5:1, where

overall contribution of these minerals to whole volume of the rock is  $\ll 1\%$ .

The remaining part of the matrix is composed of diamagnetic minerals such as quartz and feldspar and paramagnetic ones: chloritic and micaceous phases as revealed by XRD. The bulk susceptibility was carried mainly by ferromagnetic phase, but the contribution of weakly paramagnetic phase was variable from 2% in PSS 18 up to 57% in PS 4. Here the only ferrimagnetic minerals under consideration are magnetite and pyrrhotite.

In the present study samples were demagnetized with the use of thermal demagnetization and AF demagnetization techniques (Collinson, 1983). Therefore initially studies of thermomagnetic curves were performed in the paleomagnetic laboratory of Institute of Geophysics in Poland. The small specimen (less than  $0.5 \text{ cm}^3$ ) of the host rock was magnetized in the field of electromagnet with ferromagnetic core providing up to 1 T, to produce an SIRM in the sample. Then the specimen was heated in the magnetically shielded space up to  $600^\circ \text{ C}$ . Continuous measurements of IRM intensity were performed for two cycles of heating (Fig 7.1 and Appendix C). The slope changes of the curves indicate of crossing of blocking temperatures for a given mineral or chemical changes during heating. The curve shape for the second cycle may indicate whether or not new magnetic phases (such as magnetite and hematite) were produced.

The curves for 4 samples (PSB 38, PST 63, PSR 1 and PSS 17 - Appendix C) showed mainly pyrrhotite content (blocking

Thermomagnetic curves for SIRM  
Sample: PSB38

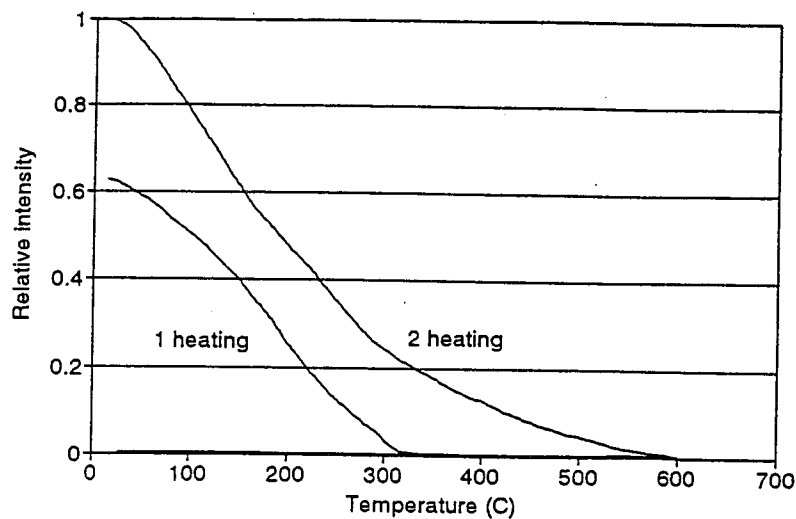


Fig. 7.1. Decrease of SIRM intensity during heating up to 600-700°C (above Curie point). Two heating cycles were performed. During cooling after each cycle there is no remaining remanence. The initial intensities are normalized to a higher one.

a) Mean susceptibility - Kashabowie Lake -  
- Huronian Lake - low grade rocks

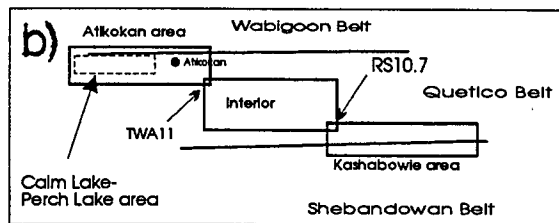
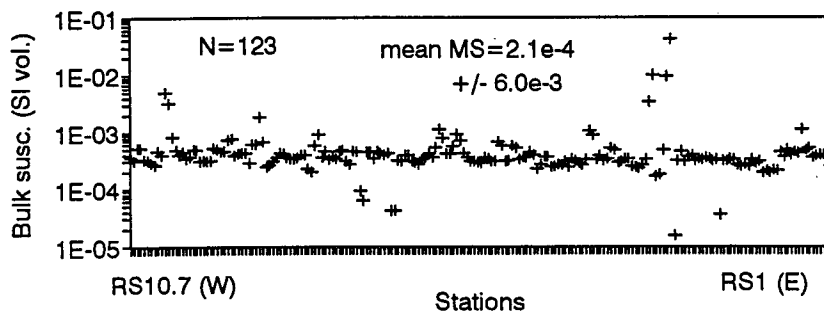


Fig 7.2. The distribution of mean magnetic susceptibility along traverses is studied areas (see fig. 7.2.b for locations). a) - low grade metasediments (Quetico Belt) and metavolcanics (Shebandowan belt) west of Kashabowie Lake - "Kashabowie area".

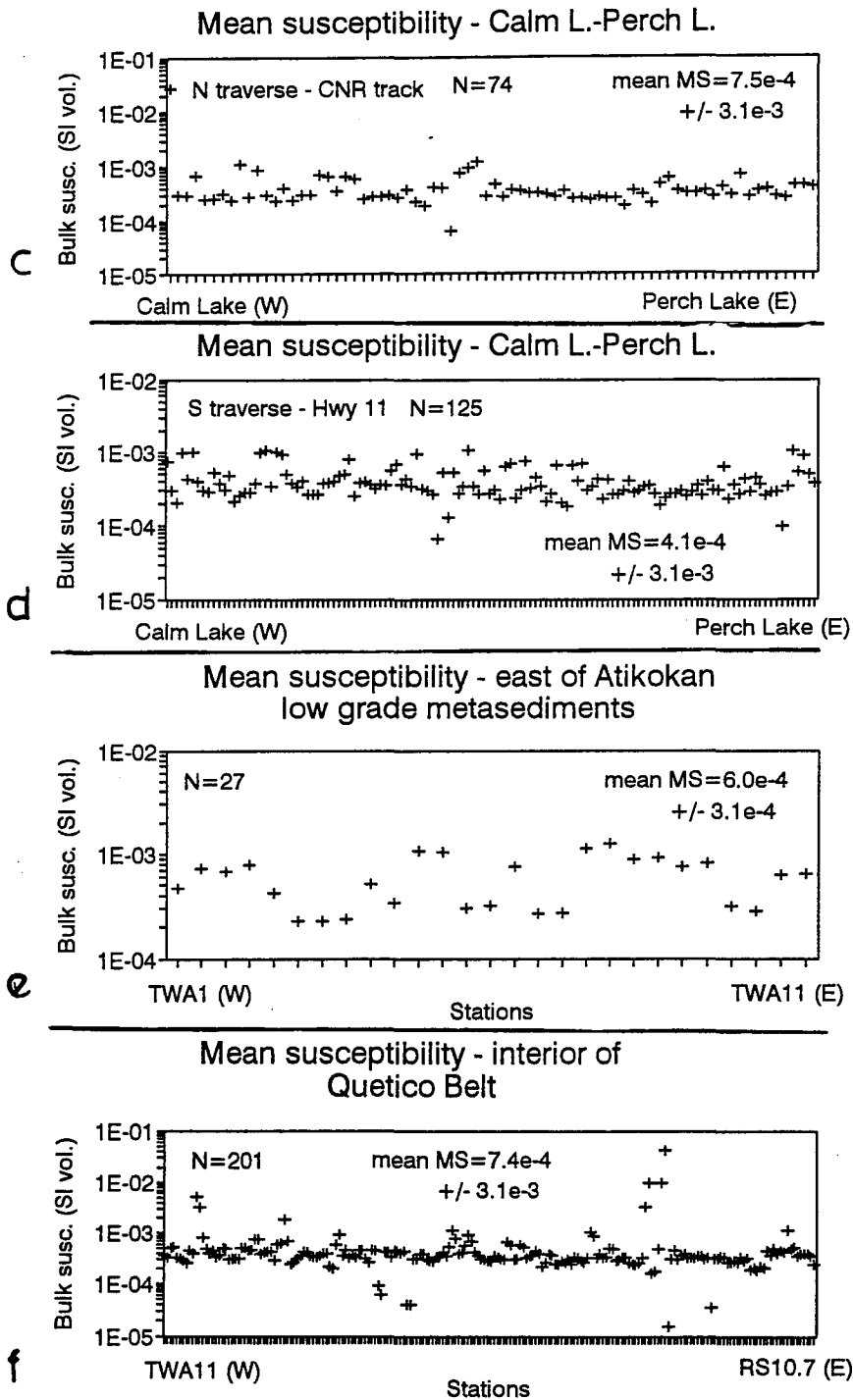


Fig. 7.2. continues.

c - e) low grade sediments on the northern margin of the Quetico Belt; f) - higher grade metasediments and felsic intrusives in the Quetico Belt interior.

temperatures about 320-350°C) with minor high-temperature magnetite content in PSR 1. The low temperature pyrrhotite phase ( $T_b \approx 150^\circ\text{C}$ ) can be also present in PST 63. The second heating curve shows the alteration of pyrrhotite and possibly also pyrite to magnetite due to oxidation processes. The more detailed presentation of magnetic properties of magnetite and pyrrhotite will be given in the next section.

At the Quetico - Shebandowan belt boundary the contribution of different minerals to MS and AMS was studied by Spark (1990). Mineral separation of 8 samples revealed content of ferromagnetic minerals as a fraction separated by hand magnet as  $\ll 1$  wt% (magnetite, hematite and pyrrhotite). The relative proportions of these minerals varied according to the different rock compositions. The ferromagnetic minerals were mainly magnetite and hematite in metabasalts (RS1 up to RS9 stations) and mainly pyrrhotite with minor magnetite in migmatites and paragneisses (RS10.5 and RS10.8). The contribution of dominantly paramagnetic separates (chlorite, biotite) to bulk susceptibility also varied from 23% (RS1.2) with an average of 70-80% up to 100%! An SEM study by Spark revealed also a significant contribution of garnet and some lesser contribution from staurolite and hornblende blasts to overall Fe ions map in highly metamorphosed units (Spark, 1990, SEM X-ray emission maps by EDA).

The bulk susceptibility along the Kashabowie Lake - Huronian Lake traverse varied from  $10^{-5}$  to  $10^{-2}$  (SI vol.) but did

not show the existence of any magnetic isograds (Rochette, 1987b) due to formation of a highly susceptible phase during metamorphism (Spark, 1991). The bulk susceptibility of the additional 119 samples collected along the traverse in my project also show a similar distribution to those of Spark. The only high peaks of susceptibility ( $10^{-2}$ - $10^{-1}$ ) are due to lithology of intrusive Fe - rich granitoid bodies (stations RS4- RS5 - Fig. 7.2a). In the other areas (metasedimentary Quetico Belt) the high values ( $>10^{-2}$ ) of susceptibility are correlated with amphibolite- rich rocks that are magnetite bearing (Fig. 7.2 b-f).

## 7.2. Magnetic properties of magnetite and pyrrhotite in the area.

This study focused on the magnetic properties of ferromagnetic minerals within the Quetico Belt and its margins. Observed minerals within the belt were mainly pyrrhotite and magnetite (with some hematite in low grade metavolcanics near Kashabowie - Spark, 1990). They are entirely responsible for the bulk magnetic properties of specimens such as natural remanent magnetization (NRM), Curie and blocking temperatures, coercivity and mean AF destructive field as well as anisotropy of ARM. They contribute also remarkably to the overall susceptibility and its anisotropy of specimens. However the contribution of different magnetic phases to susceptibility by means of separations made with the Franz magnetic separator were not examined in this project.

The other magnetic properties of ferromagnetic minerals that can be studied both for rock samples as well as for single grains are hysteresis properties, IRM acquisition, coercivity of remanence and changes of saturation magnetization  $M_s$  and SIRM with temperature.

Changes of SIRM with temperature were examined with the use of procedure as described in previous chapter. The method is capable to determine the presence of magnetite, hematite or one or 2 phases of pyrrhotite within the specimen. The Curie



temperature for crystalline magnetite is 575 - 580°C (Carmichael, 1982), for pyrrhotite 300-325°C (Soffel, 1981, Dekkers, 1990), and the Néel temperature for spin-canted antiferromagnetism in hematite is 675°C (Carmichael, 1982). However, thermomagnetic curves for SIRM which decay at 250-300°C can be also characteristic of intermediate compositions of titanomagnetites or titanohematites (Butler, 1992, p.98).

Thermomagnetic curves were obtained for 4 samples from the metavolcanic Shebandowan belt (TW1, RS1.3, TWR3.5 and TWR4.1). They showed a rapid decay of IRM at low temperatures with a characteristic bend near 150°C (titanomagnetite?, pyrrhotite?) and a steady gently decay at higher temperatures up to 575°C (TWR4.1, TW1 - magnetite - Fig. 7.3) or even up to 670°C (TWR3.5, RS1.3 - hematite - Fig. 7.4). Magnetite-bearing samples showed a significant increase in SIRM in a second heating cycle, therefore some pyrrhotite or pyrite might be present initially that was converted to magnetite during first heating cycle in temperatures more than 500°C. In second heating cycles, the inflexion point at 150°C was not observed which may support the conclusion that pyrrhotite (not titanomagnetite) was present initially. Thermal alteration of hematite-bearing samples led to a decrease in SIRM in the second heating cycle.

Low grade metasediments from Perch Lake - Calm Lake area (4 samples) and west of Shebandowan - Quetico belt contact (station RS10.5) as well as 16 of 17 samples from the Atikokan - Huronian Lake traverse (schists, gneisses and migmatites) showed the

Thermomagnetic curves for SIRM  
Kashabowie - Huronian - sample TW1

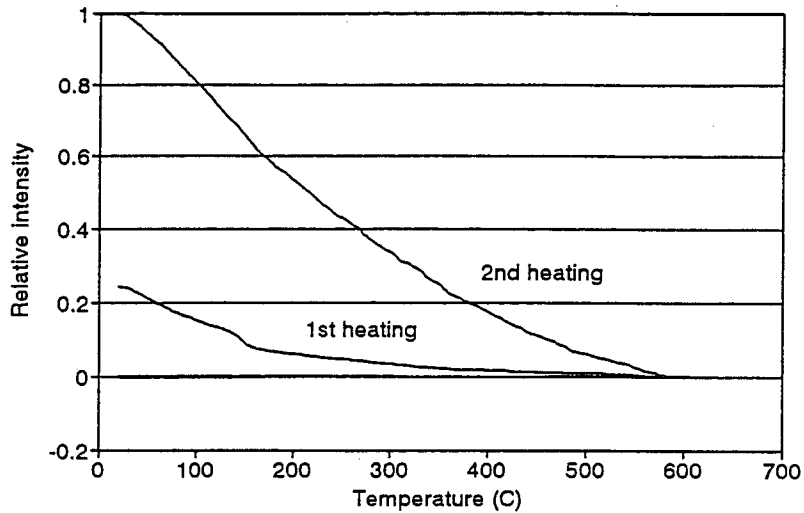


Fig. 7.3. SIRM decay during heating - sample TW1 - magnetite bearing. Note the increase of SIRM intensity after 1 heating. It indicate the mineralogical changes during heating - oxidization of pyrite and pyrrhotite to magnetite (?).

Thermomagnetic curves for SIRM  
Kashabowie - Huronian - sample RS1.3

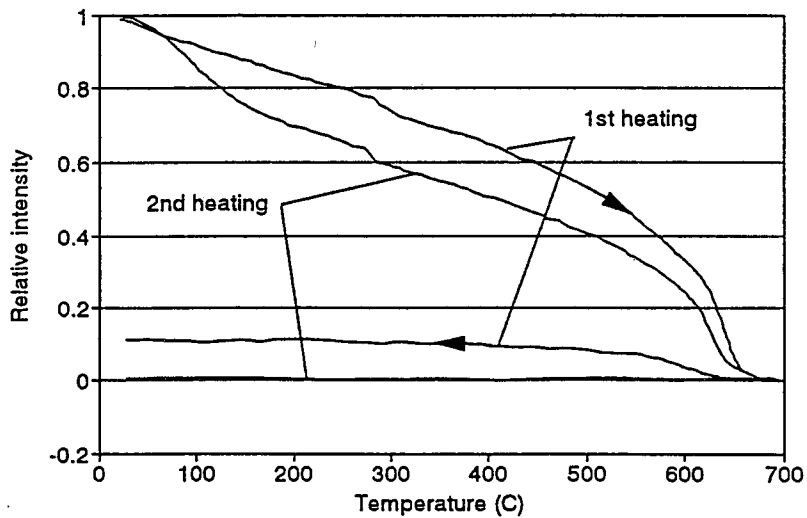


Fig. 7.4. SIRM decay during heating - sample RS1.3 - magnetite and hematite bearing. A heating cycle up to 700°C was not sufficient to demagnetize the sample completely. The second cycle (up to 750°C) demagnetized the sample.

presence of pyrrhotite alone on thermomagnetic SIRM curves (Fig. 7.5 and Appendix C). During a second cycle of heating the initial SIRM intensity increased up to 10-12 times or is of the same magnitude as at the beginning and only 10-20% of SIRM remains after heating to 350°C. The remaining SIRM decays at 580°C indicating the presence of magnetite. However, the principal increase in initial SIRM before the second heating cycle is due to the production of new pyrrhotite. This may be produced from pyrite which is abundant when observed in polished thin sections.

The only different thermomagnetic curve was obtained for an amphibolite sample (TWA 15). It contains magnetite and titanomagnetites only (Fig. 7.6 and Appendix C).

Generally, the dependence of SIRM with temperature for pyrrhotite can be somewhat complex in a range 100-300°C. Natural pyrrhotite can have varying chemical composition  $Fe_{1-x}S$  ( $0 < x < 0.125-0.13$ , with valence of S  $< 2$ ). It has the structure of NiAs and is composed of two parallel sublattices with vacancies grouped in one of sublattices. Magnetic properties of pyrrhotite are controlled by vacancies in layers forming superstructures (Dekkers, 1988).  $Fe_7S_8$  pyrrhotite has monoclinic crystal structure, a 4C superstructure of vacancies and is ferrimagnetic. For  $x < 0.1$  pyrrhotite is hexagonal, antiferromagnetic and can have 3 common superstructures (5C -  $Fe_9S_{10,11}$ C -  $Fe_{10}S_{11}$  and 6C -  $Fe_{11}S_{12}$ ).

In hexagonal pyrrhotite at the temperature 200-210°C the  $\lambda$

Ms decay with T - 2 heatings  
Sample TWE6A

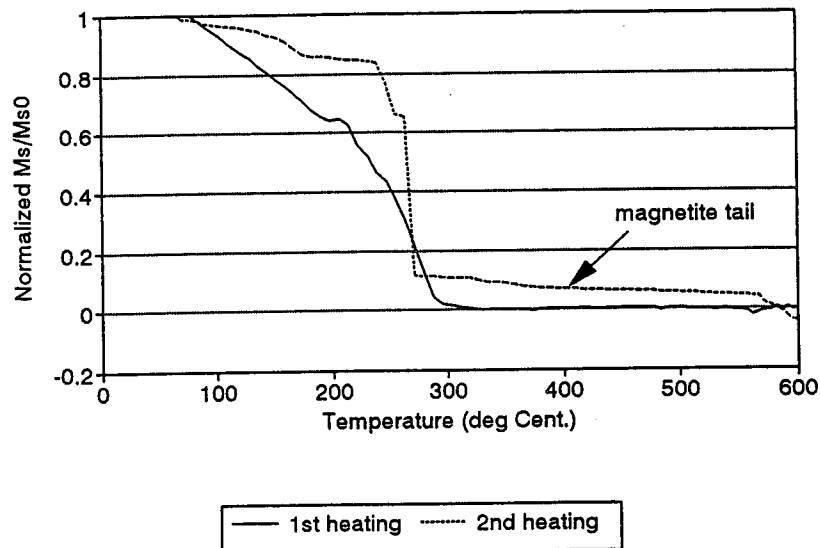


Fig. 7.5. SIRM decay during heating for pyrrhotite bearing sample (TWE6A) from the interior of the Quetico belt. Note newly produced after 1 cycle of heating. Only heating curves are shown.

Thermomagnetic curves for SIRM  
2 heatings - sample TWA 15 - 2

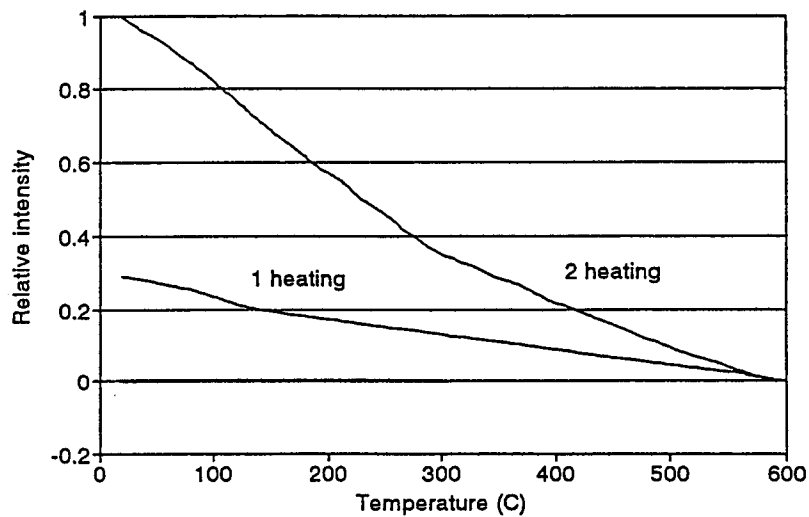


Fig. 7.6. SIRM decay during heating for amphibolitic sample from the interior of the belt. 1st heating curve indicates mainly magnetite (but some pyrrhotite can be also present). 2nd curve shows the presence of newly created magnetite (from pyrrhotite?).

transition to ferrimagnetic pyrrhotite with Curie temperature of 265°C can be observed due to a change of vacancy ordering (Schwarz, 1975, Dekkers, 1989). Because of this the magnetization sharply increases during heating. These transitions are reversible when the cooling cycle is slow. For higher cooling rates a high temperature superstructure can be quenched to lower temperatures depending on the cooling rate (Kissin and Scott, 1982).

Natural pyrrhotite is often a mixture of both magnetic phases and this composition can be semi-quantitatively determined if the HT superstructure is quenched (Schwarz, 1975) during cooling. However in single-phase monoclinic  $Fe_7S_8$  pyrrhotite no transition is observed.

In addition, during heating in air, pyrrhotite oxidizes to magnetite or hematite at temperatures above 500°C (Dekkers, 1990). Therefore, if a specimen primarily contains both pyrrhotite and magnetite then during thermal demagnetization of NRM above 500°C a newly produced magnetite can be magnetized by the field of magnetite already present. This could conceivably increase the overall remanent magnetization of the sample. However, in a specimen bearing pyrrhotite only, the thermal demagnetization procedure may be carried to lower temperatures and oxidization of pyrrhotite can be avoided.

The susceptibility of samples that were thermally demagnetized was also monitored. Any significant increase in

bulk susceptibility during heating may indicate mineralogical changes of para- and ferromagnetic minerals during heating, and also the alteration of pyrrhotite to magnetite. Changes of susceptibilities of paramagnetic minerals in the matrix due to heating are more difficult to estimate. Dekkers (1990) reported a ten-fold increase in bulk susceptibility of some pyrrhotite-bearing samples during heating, starting at 450°C.

In this study pyrrhotite-bearing samples were heated usually only up to 350-400°C, where they were entirely demagnetized. Therefore, the changes of susceptibility at lower temperatures were of prime concern, because they could monitor mineralogical changes that could have obscured the data from the thermal demagnetization of NRM.

36 samples from the Quetico metasediments, 1 of amphibolite and 7 from Shebandowan metavolcanics had their bulk susceptibility measured after each step of heating (at 20, 100, 200, 300, 350°C and for some samples in higher temperatures as well). 29 of 36 metasedimentary samples showed less than 30% changes in susceptibility (both increase and decrease) after steps of heating often with erratic changes in susceptibility for a given sample (Fig. 7.7 and Appendix C). However, 7 samples showed significant increase in susceptibility (up to 150% - Fig. 7.7 and Appendix C). This behaviour was taken into an account when I interpreted NRM demagnetization data after thermal treatment.

On the other hand, metavolcanics and amphibolite showed

### Susceptibility changes after heating

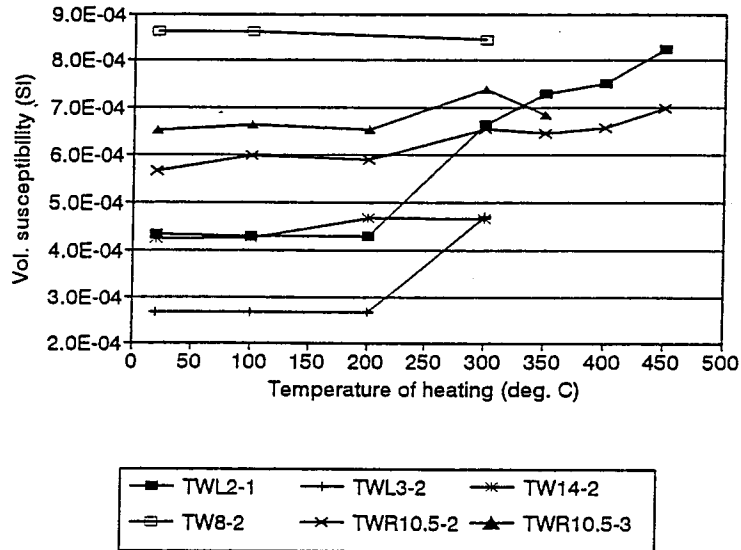


Fig. 7.7. Magnetic susceptibility as a function of temperature during heating samples that were thermally demagnetized up to 450°C. Metasedimentary samples - pyrrhotite bearing, interior of the Quetico belt.

### Susceptibility changes after heating

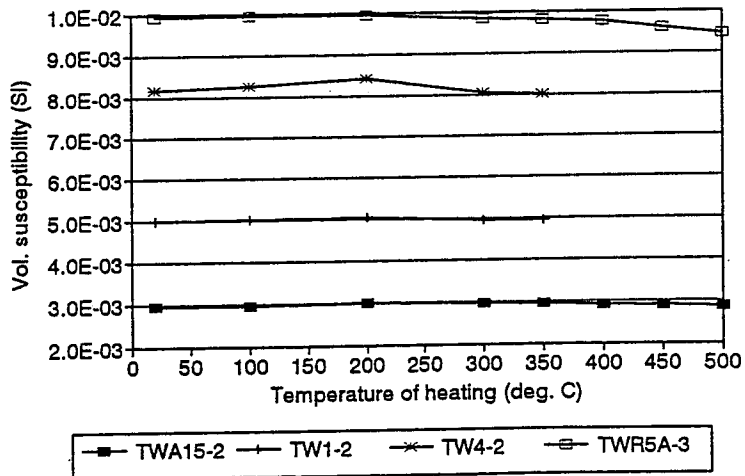


Fig. 7.8. Magnetic susceptibility as a function of temperature during heating samples that were thermally demagnetized up to 550°C. Samples TW1-1 and TWR5A-3 - from metavolcanics, TWA15-2 - amphibolite schist from the interior of Quetico Belt: all of them are magnetite bearing; TW4-2 - pyrrhotite bearing metasediment.

little variation of susceptibility with temperature (usually decrease of up to 10-15%), when even heated up to 500°C (Fig. 7.8. and Appendix C). Therefore I suggest that mineralogical changes of paramagnetic phyllosilicates are responsible for variations of bulk susceptibility of metasedimentary samples at temperatures below 400°C rather than oxidization of pyrrhotite having occurred.

5 metasedimentary samples from the interior of the belt and 1 felsic rhyolite (TWR4.1) were crushed and the magnetic phase was separated with a hand- magnet. Less magnetic phases were also obtained with the use of a Franz magnetic separator with 0.05A amperage.

The following samples were separated:

TWA5 - biotite schist;

TWA15 - amphibolite;

TWC1 - from granite - pegmatite zone;

TWE6A - from staurolite - garnet rich migmatite zone;

TW8 - biotite schist;

TWR4.1 - felsic rhyolite.

Observation of the phase separated by a hand- magnet, under petrographic microscope revealed that all but TWA15 and TWR4.1 contain mainly pyrrhotite of size  $>50 \mu\text{m}$ . Smaller grains of magnetite were not noticed in these separations. It is believed that the smaller grains of pyrrhotite and magnetite remained attached to biotite, quartz and feldspar grains during the



magnetic separation.

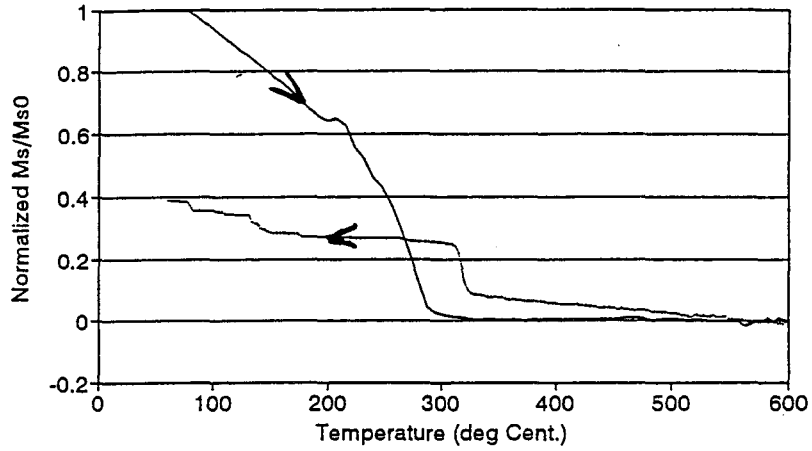
Magnetic phase of TWA15 contains mostly magnetite with less than 10% pyrrhotite and TWR4.1 is magnetite-bearing.

Strong - field thermomagnetic behaviour of all but TWA5 samples were studied with use of SI-8 Sapphire Instrument Curie balance with neodymium alloy permanent magnet producing a field of 590 mT. This field is sufficient to generate saturation magnetization  $M_s$  in magnetite and pyrrhotite. During the heating of the magnetic phase Curie points for remanence carrying minerals can be determined and the changes of saturation magnetization from temperature during heating and cooling cycle can be monitored. Samples were twice heated up to 600°C; a second thermomagnetic curve sometimes reveals the mineralogical changes (e.g. oxidization of pyrrhotite to magnetite) at elevated temperatures (Fig. 7.9a).

Curie balance results confirmed that metasedimentary samples (TWC1, TWE6A, TW8) carried mainly pyrrhotite, but contrary to the results of SIRM thermomagnetic curves pyrrhotite can be multi-phase in TW8 and TWE6A (Fig. 7.9b). These curves show a characteristic kink at a temperature of about 150°C and Curie temperature less than 300°C. The higher Curie temperatures obtained during cooling can be explained on the basis that high temperature phase prevails or monoclinic pyrrhotite is produced (Appendix C). New magnetite is also produced during heating.

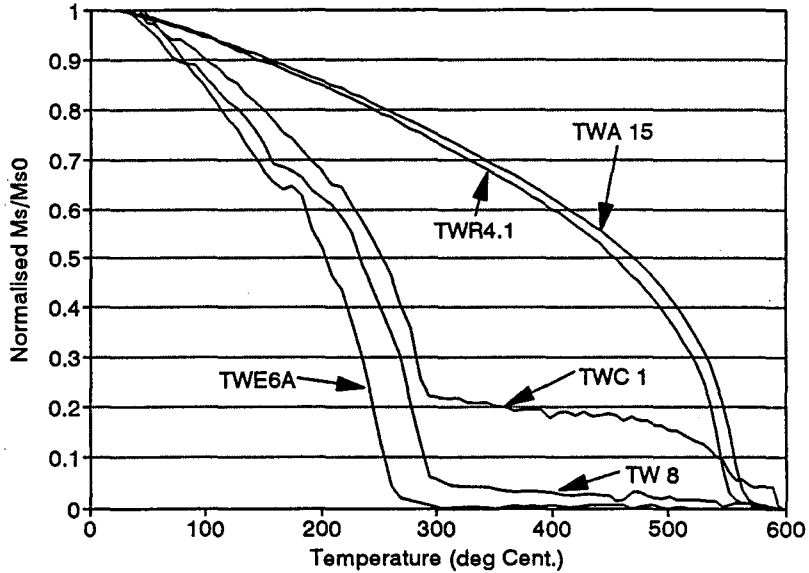
An anomalous content of magnetite in sample TWC1 maybe due to the contamination of measured material in a holder by residua

Ms changes during 1 cycle: heat. - cool  
Sample TWE6A



a)

Ms decay with temperature



b)

Fig. 7.9. Saturation magnetization  $M_s$  as a function of temperature (Curie balance).

a) -  $M_s$  changes during a heating - cooling cycle; pyrrhotite bearing metasedimentary sample from the interior of the belt. Note higher  $M_s$  intensities above  $300^\circ\text{C}$  during cooling - some magnetite might be created.

b) - heating curves for 5 samples: TWA15 and TWR4.1 are magnetite bearing, the others - pyrrhotite bearing. Detailed descriptions of sample in the text.

of magnetic phase TWA15, which was measured prior to TWC1.

The  $M_s$  thermomagnetic curves for samples TWA15 and TWR4.1 are typical for magnetite. The presence of a small fraction of pyrrhotite in TWA15 (amphibolite) could not be confirmed by thermomagnetic studies because the saturation magnetization of pyrrhotite is only 20% that of magnetite (Carmichael, 1982).

Hysteresis studies for the 6 samples selected above were performed with the use of alternating gradient force magnetometer MicroMag™ Model 2900 made by Princeton Measurements Corporation.

Samples of weight up to 30 mg were placed on the extension rod connected to the piezoelectric element. Around the holder both D.C. magnetic field and alternating field gradient of frequency near mechanical resonant frequency of the holder operated.

A periodic force acting on the sample was proportional to the magnitude of the gradient field, the intensity of D.C. field and the magnetic moment of the sample. Therefore magnetic moment of the sample could be calculated.

The equipment was used to study a hysteresis loop of the sample, acquisition of IRM and demagnetization remanence curves. From the hysteresis loop, such parameters as coercive force  $H_c$ , saturation magnetization  $M_s$  and saturation isothermal remanent magnetization  $M_r$  were measured (Fig. 6.5).

The magnetic moment of paramagnetic/ diamagnetic matrix component was easily subtracted as it increases linearly with an

applied field. The maximum intensity of applied field was  $4 \cdot 10^5$  A/m (5000 Oe - equivalent of 0.5 T induction) to ensure saturation conditions of magnetite and pyrrhotite phases. However this field is not sufficient to saturate hematite or goethite (Butler, 1992, Carmichael, 1982).

Coercivity of remanence  $H_{cr}$  was measured from demagnetization remanence curve with step-wise demagnetizing field up to 0.5 T acting on the sample with previously generated SIRM with the applied field of 0.5 T. SIRM acquisition curve was produced with step-wise increase of external field up to 0.5 T (Fig. 7.12). The remanence acquisition coercive force  $H_{cr}$  could be also obtained from that curve.

Measurements of saturation magnetization related rock - magnetic parameters were conducted for one to three rock fragments (10 - 35 mg in weight) from the 6 samples selected above as well as for sets of a few grains (4 - 13) from magnetic separates. Values of measured parameters are presented in Table 7.10.

The matrix effect was strictly paramagnetic. In high fields up to 0.5 T the magnetic moment of sample came mostly from the paramagnetic matrix. A linear increase of the magnetic moment in high field could be used to calculate the high field volume susceptibility of paramagnetic matrix  $\chi_1$ .

The total low-field (usually 0.1 mT) susceptibility  $\chi_0$  is a combination of field dependent ferromagnetic part  $\chi_f$  and para- or diamagnetic susceptibility  $\chi_1$ , that is not field dependent :

Table 7.10. The list of hysteresis properties obtained from AFGM2900 for 6 samples. a) - for rock fragments; b) - for magnetic phases separated by hand-magnet (hm) or Franz separator (Fs).

a) Hysteresis properties - rock pieces

Sample No	mass g	density g/cm <sup>3</sup>	Matrix	Mstotal /mass Am <sup>2</sup> /kg	Ms ferro /mass Am <sup>2</sup> /kg	Mr loop /mass Am <sup>2</sup> /kg	Mr dem /mass Am <sup>2</sup> /kg	Mr - IRM /mass Am <sup>2</sup> /kg	Mr/Ms	Hc mT	Hcr mT	Hcr/Hc	H1/2 mT	Hcr' mT	(Hcr' +H1/2) /2Hcr	mean susc. SI vol.	matrix susc. SI vol.	matrix /total susc.	
TWA5	1	0.0117	2.73	para	5.6E-02	2.9E-03	1.8E-04	1.7E-04	3.2E-04	0.063	9.8	34.5	3.52	7.5	95	1.49	4.2E-04	3.7E-04	0.87
	2	0.0139	2.73	para	4.8E-02	2.0E-03	1.7E-04	1.7E-04	2.9E-04	0.084	12.1	38.3	3.17	7.5	92	1.30	4.2E-04	3.2E-04	0.76
	3	0.0108	2.73	para	6.1E-02	4.0E-03	3.5E-04	3.8E-04	5.4E-04	0.087	12.2	43.3	3.55	7.5			4.2E-04	4.0E-04	0.95
TWA15	1	0.0354	3.02	para	1.3E-01	6.5E-02	3.5E-03	3.2E-03	4.2E-03	0.054	2.7	8.68	3.17	3.5	28	1.81	4.2E-03	5.0E-04	0.12
	2	0.0301	3.02	para	5.7E-02	1.0E-02	5.2E-04	6.6E-04	9.9E-04	0.050	2.7	10.7	3.93	3.5	68	3.34	4.2E-03	8.9E-04	0.21
	3	0.0297	3.02	para	4.9E-02	4.4E-03	2.2E-04	2.0E-04	4.9E-04	0.049	3.6	15.9	4.43	3.5	79	2.59	4.2E-03	8.5E-04	0.20
TWE6A	1	0.0181	2.61	para	3.0E-02	2.3E-03	1.6E-04	1.7E-04	3.8E-04	0.067	4.7	23	4.93	3	75	1.70	8.0E-04	4.5E-04	0.56
	2	0.0202	2.61	para	2.8E-02	1.7E-03	1.6E-04	1.4E-04	3.5E-04	0.095	5.1	14.3	2.79	3	80	2.90	8.0E-04	4.3E-04	0.54
	3	0.0268	2.61	para	2.5E-02	4.6E-04	7.6E-05	7.6E-05	2.3E-04	0.167	13.8	26.6	1.93	3	93	1.80	8.0E-04	4.1E-04	0.51
TWC1	1	0.0235	2.73	para	2.8E-02	2.3E-03	2.8E-04	2.4E-04	4.7E-04	0.121	7.5	22.3	2.96	8	84	2.06	4.5E-04	4.5E-04	1.00
	2	0.0170	2.73	para	3.7E-02	1.6E-02	8.5E-03	8.6E-03	9.2E-03	0.527	19.8	27.3	1.38	8	57	1.19	4.5E-04	3.6E-04	0.81
	3	0.0290	2.73	para	2.5E-02	7.1E-04	9.8E-05	9.5E-05	2.8E-04	0.138	8.1	17.2	2.13	8	95	2.99	4.5E-04	4.2E-04	0.93
TW8	1	0.0144	2.66	para	7.1E-02	4.5E-02	2.4E-02	2.4E-02	2.6E-02	0.539	15.9	22	1.38	3	46	1.11	9.5E-04	4.4E-04	0.46
	2	0.0215	2.66	para	3.0E-02	1.0E-02	3.6E-03	3.5E-03	4.1E-03	0.366	15.5	25.7	1.66	3	52	1.07	9.5E-04	3.4E-04	0.36
	3	0.0163	2.66	para	6.6E-02	3.8E-02	2.1E-02	2.0E-02	2.2E-02	0.547	14.1	18.6	1.32	3	38	1.10	9.5E-04	4.7E-04	0.49
TWR4.1	1	0.0191	2.52	para	2.8E-02	1.6E-02	1.2E-03	1.2E-03	1.5E-03	0.077	5.5	28.8	5.20	4.5	65	1.21	2.0E-02	1.9E-04	0.01

Note: term "magnetization" is used here for simplicity  
for magnetic moments (units mAm<sup>2</sup>) and mass magnetization (units . Am<sup>2</sup>/kg)

Table 7.10b) - hysteresis properties for magnetic phases.

Hysteresis properties - TW series - grains															
Sample No	No of grains	Ms total nAm	Ms ferro nAm	Mr loop nAm	Mr dem nAm	Mr IRM nAm	Mr/Ms	Hc mT	Hcr mT	Hcr/Hc	H? mT	Hcr' mT	(Hcr' +H?)/ 2Hcr	mass density g/cm <sup>3</sup>	Matrix
TWA5	hm	10	214.0	187.0	95.2	99.1	99.7	0.509	14.1	18.8	1.33	7.5	14.8	0.59	Ms-total (/mass)
	Fs	6	47.8	55.6	26.4	30.3	28.6	0.474	13.6	18.4	1.35	7.5	15.5	0.63	Ms-ferro (/mass)
TWA15	hm	12	797.0	770.0	50.3	46.7	59.0	0.065	4.2	12.7	3.01	3.5	17.8	0.84	Mr (/mass)
	Fs	5	620.0	597.0	24.7	23.8	32.3	0.041	3.0	12.3	4.17	3.5	30.0	1.36	Mr - dem (/mass)
TWC1	hm	9	415.0	344.0	168.0	177.0	172.0	0.489	19.4	24.6	1.27	8.0	17.0	0.51	Mr - IRM (/mass)
	Fs	5	620.0	597.0	24.7	23.8	32.3	0.041	3.0	12.3	4.17	3.5	30.0	1.36	Mr/Ms
TWE6A	hm	13	446.0	360.0	158.0	158.0	166.0	0.439	12.8	16.5	1.29	3.0	14.3	0.52	Hc
	Fs	5	620.0	597.0	24.7	23.8	32.3	0.041	3.0	12.3	4.17	3.5	30.0	1.36	Hcr
TW8	hm	5	133.0	121.0	52.0	57.4	52.7	0.429	11.2	14.6	1.30	3.0	12.4	0.53	Hcr/Hc
	Fs	5	91.7	84.0	38.1	44.1	38.9	0.453	16.8	24.2	1.44	3.0	17.2	0.42	H?
TWR4.1	sep1	4	2001.0	1920.0	22.1	19.3	37.1	0.012	1.2	10.8	9.15	4.5	16.3	0.96	Hcr'
	sep2	4	1490.0	1.4	16.0	11.5	23.2	0.011	1.3	9.31	7.45	4.5	16.4	1.12	(Hcr'+H?)/2Hcr

- g - mass of rock piece
- density of cylindrical core
- paramagnetic or diamagnetic
- saturation magnetization of whole sample
- satur. magnet. of ferromagn. phase
- saturation isothermal remanence
- initial SIRM before demagnetization
- maximum IRM after IRM acquisition
- ratio of SIRM to Ms of ferromagnet.
- coercive force
- coercivity of remanence
- ratio of coerc. of reman. to coerc. force
- field required to reduce ARM to half
- field required to impose of IRM=0.5\*SIRM
- Dankers's (1981) parameter
- bulk susceptibility of a cylindrical core
- high field susceptibility of matrix
- ratio of paramagnetic susc. to total susc.

$\chi_0 = \chi_f + \chi_l$  (Rochette, 1987a). The paramagnetic low-field component can be approximated with high field susceptibility, if the assumption of field independence holds.

High field volume susceptibility values were of order  $10^4$  for both magnetite and pyrrhotite bearing samples. They were compared with the overall bulk susceptibility of cylindrical cores drilled from the same hand specimens as rock fragments used in hysteresis studies. Susceptibilities of several cylindrical cores from the same hand sample varied of up to 25%, high field matrix susceptibilities of different rock pieces from the same sample showed also large variations in high field susceptibility (up to 80% in TWA15). Therefore the comparison of both susceptibilities is rather qualitative.

The ratio of matrix susceptibility to total susceptibility was 0.4 to 0.95 for pyrrhotite bearing rocks, 0.1-0.2 for amphibolite and about 0.01 for magnetite bearing rhyolite (see table 7.10). These results are in good correlation with direct measurements of contribution of different magnetic phases to bulk susceptibility performed by Spark (1991) for traverse Kashabowie - Huronian Lake.

Intensity of field related parameters (coercivity,  $H_{cr}$ ,  $H_{cr'}$ ) are here expressed in induction units (mT) for convenience, although it is not strictly correct. The symbols related to induction such as  $B_c$  instead of  $H_c$  are also used in some cases.

Coercive force  $H_c$  values are usually remarkably scattered for three different rock fragments from the same hand sample due to variations of paramagnetic content on the hand-sample scale.  $H_c$  ranged from 4.7 mT to 19.8 mT (3.7 - 15.8 kA/m) for pyrrhotite bearing rocks and from 2.7 to 5.5 mT for magnetite rich samples.

$H_c$  values for separated grains were much more uniform, 13.6 to 19.4 mT for pyrrhotite and 1.2 to 4.2 mT for magnetite. Coercivity values for pyrrhotite indicate that grain size is of the order of 20-80  $\mu\text{m}$  (Dekkers, 1988), which is in a good agreement with the observation under petrographic microscope in this study (of order 50 -100 $\mu\text{m}$ ).

Soffel (1981) considered pyrrhotite grains of that size as pseudo-single domain (PSD with grain size of 10-40 $\mu\text{m}$ ) and multidomain (MD with grain size >100 $\mu\text{m}$  ?).

The additional constrain for domain structure comes from the relation between ratios of  $M_r$  and  $M_s$  versus  $H_{cr}$  and  $H_c$  (Fig. 7.11). Clark (1984) found ratio of  $H_{cr}/H_c$  for different sizes of pyrrhotite grains of range: 1.02 for smaller (10-15 $\mu\text{m}$  in length grains) to 1.38 for 80 $\mu\text{m}$  long grains. Recorded here values of this ratio 1.27 - 1.44 for single grains suggest their size to be of more than 30 $\mu\text{m}$ .  $M_r/M_s$  ratios (here of range 0.43 - 0.51) are slightly higher than those recorded by Clark for grains larger than 20 $\mu\text{m}$ .

Soffel (1981) suggested that grains of pyrrhotite of size of 10-40 $\mu\text{m}$  are PSD and more than 100 $\mu\text{m}$  long ones are "true" MD. However, when regions of high inclusions densities within true



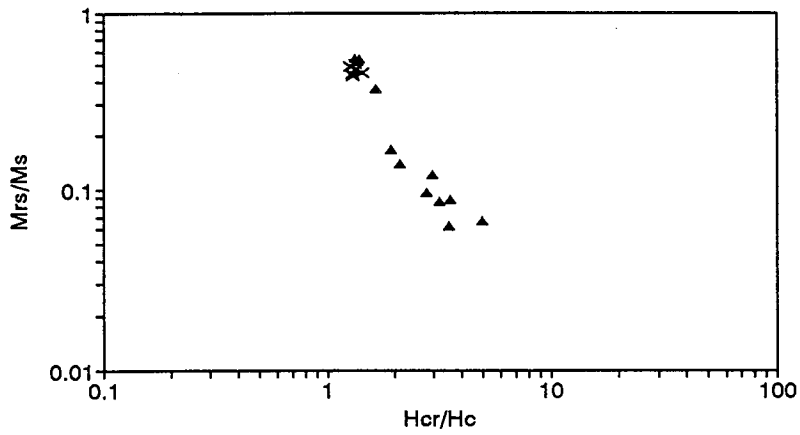
MD grains exists, they can have PSD properties (Soffel, 1981). Therefore I believe that most of studied here grains (50 to 100 $\mu$ m in length) are PSD ones.

Pyrrhotite grains from weaker magnetic fraction (symbol "Fs") have slightly higher values of  $H_{cr}/H_c$  ratio than hand-magnet separates ("hm" symbol) (see Table 7.10). If only rock pieces are taken under consideration, magnetic phase seems to be predominantly PSD as well (Fig. 7.11a). However none well established boundaries of SD/PSD and PSD/MD behaviour were listed in the literature for pyrrhotite.

The trend for pyrrhotite-bearing rock fragments to have lower ratios of  $M_r/M_s$  and higher ratios of the coercivity of remanence to coercive force than the highly magnetic phase is significant. It can be caused by the fact that highly magnetic phase separated by hand magnet cannot contain weaker magnetic MD grains. Therefore it should be expected that a larger population of MD grains exist in the specimen than is indicated by the content of higher magnetic phases. However, such MD grains can possess regions of PSD properties (Soffel, 1981) and therefore also retain stable TRM components.

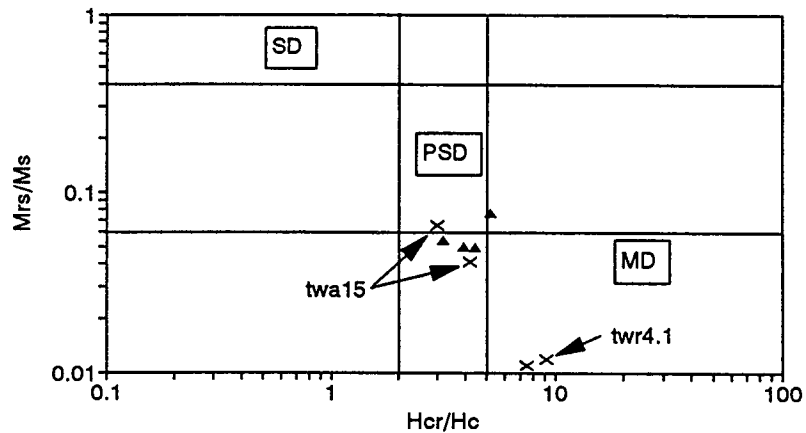
In the case of magnetite-bearing rocks grains of TWR4.1 can be located on the plot of both ratios as entirely MD and these of TWA15 as PSD/MD transition (Fig. 7.11b) according to Wasilewski (1973) and Dunlop (1981) classification for magnetite. Also low coercivity  $H_c$  values support this classification (Dunlop, 1986).

Hysteresis ratios- pyrrh. rich samples  
Atikokan - Huronian Lake traverse



▲ rock pieces × grains

Hysteresis ratios- magnet. rich samples  
Atikokan - Huronian Lake traverse



▲ rock pieces × grains

Fig. 7.11. Remanent magnetization to saturation magnetization ratio ( $M_{rs}/M_s$ ) versus coercivity of remanence to coercive force ratio ( $H_{cr}/H_c$ ).

a) for pyrrhotite-bearing samples TWC1, TWA5, TWE6A; this ratios are typical for PSD or MD grains.

b) for magnetite-bearing samples (TWA15 and TWR4.1).

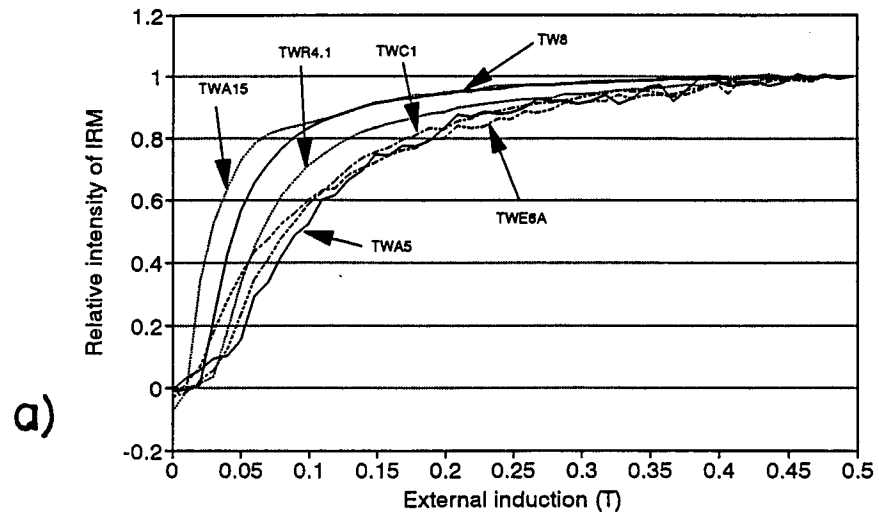
Fields of SD/PSD/MD after Borradaille, Chow et al., 1993. Magnetite samples are located in PSD - MD fields.

The IRM acquisition curves for rock fragments (Fig. 7.12a) and grains (Fig. 7.12b) are characteristic for large grains of pyrrhotite (40 - 100 $\mu$ m, Fig. 7.12c modified from Dekkers, 1988) and MD grains of magnetite ( $H_{cr}'$  of order 15-30 mT, Dunlop, 1971, 1972, 1973, 1981, see also Fig. 6.8). However a larger value of the field required to impart IRM of 50% of SIRM ( $H_{cr}$ ) for TWR4.1 (true MD?) than for TWA15 (rather PSD) is unusual.

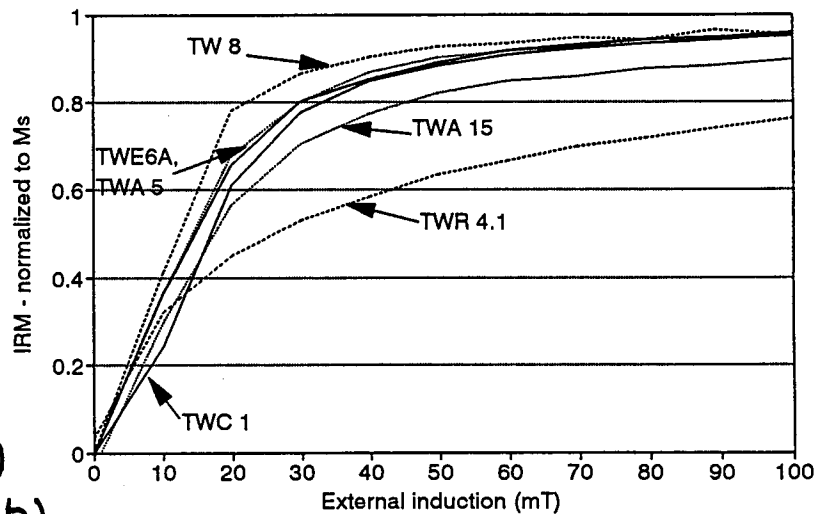
Magnetite grains from TWR4.1 and TWA15 samples require anomalously high fields to produce SIRM in a sample (typical saturating field for MD grains is 120-150 mT). It might be suggested that a small amount of hematite is also present in the separated phase (on the surfaces of magnetite grains). This would increase the values of coercivity remanence of magnetite grains as well. However the presence of hematite was not shown on thermomagnetic curves perhaps because the  $M_s$  (and SIRM) of hematite is much lower than that of magnetite.

All rock fragments with pyrrhotite show also much slower increases of IRM with field than the magnetically separated phases. Samples TWE6A, TWC1 and TWA5 are not saturated even in the field of 500 mT. This cannot be explained by the presence of hematite because of its low coercivity of remanence and very low values of median destructive field  $H_{1/2}$  required to AF demagnetize NRM or ARM (3 - 8 mT).

IRM acquisition-TW series - rock pieces  
AFGM apparatus



IRM acquisition - magnetic phases  
Quetico Belt



NATURAL PYRRHOTITE

Remanent Acquisition Curves

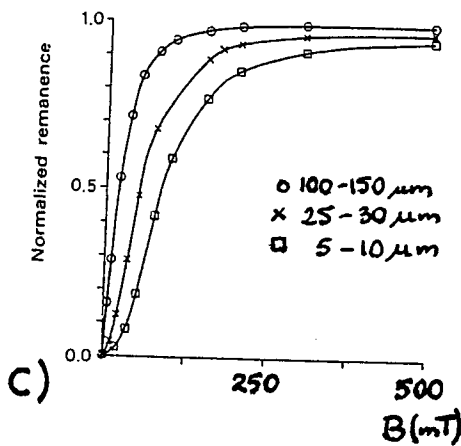


Fig. 7.12. IRM acquisition curves for rock fragments (a) and magnetically separated grains of pyrrhotite and magnetite (b). Note that IRM acquisition coercive force  $H_{cr}'$  is larger for rock fragments than for grains.

c) IRM acquisition curves for 3 grain -size fractions, modified from Dekkers, 1988.

Dankers' (1981) relation between parameters  $H_{cr}$ ,  $H_{cr}'$  and  $H_{1/2}$ :

$H_{cr}' + H_{1/2} = 2 H_{cr}$  was also tested for single grains (Table 7.10).

The relation generally does not hold. However because of large measurement errors for  $H_{1/2}$  (1.5 mT) it could not be decided whether this was a significant criticism.

## Chapter 8.

### Determinations of the directions of natural remanent magnetization (NRM).

#### 8.1. The record of natural remanence in metamorphic rocks.

Paleomagnetic studies generally focus on the determination of natural remanent magnetization which is primary and not disturbed by subsequent tectonic events or metamorphism (characteristic remanent magnetization). However, the primary remanence can be often completely remagnetized and a stable characteristic remanence can be a secondary one as well (e.g. of chemical origin). In many cases, several components of NRM may be found in one sample or at one specific site, indicating several episodes of partial resetting of the earlier NRM components (e.g. due to heating, fluid action or creating a new magnetic mineral phase), thereby imposing a new secondary NRM component.

If a pre-tectonic NRM direction is reoriented due to tectonic folding or tilting, involving simply rigid body rotation without strain, step-wise unfolding methods may be used in some situations to estimate the amount of deformation (e.g. Graham's (1949) fold test - Facer, 1983; method of Williamson & Robertson, 1976).

This is not the case if an area has undergone large scale

penetrative deformation, like transpression in the study area with overlapping low to high grade metamorphism. De-straining of remanence is a more complex, still poorly understood procedure (Cogné and Perroud, 1987, Borradaile and Mothersill, 1989).

Initially it was not known whether the NRM within samples was formed pre-tectonically, syn - tectonically or post - tectonically. Clearly, the direction of components of NRM may reflect not only the direction of the magnetic field at the time of generation of the magnetization in the sample but also later movements of the area as they occurred in weakly deformed or not deformed rock units (e.g. Dunlop' studies in Northwestern Ontario, 1979, 1983, 1984, 1985). The NRM direction can also be influenced by several processes associated with the progressive deformation and accompanying metamorphism.

Mineralogical changes like the growth of newly recrystallized magnetic phases such as pyrrhotite, magnetite or hematite or the increase of temperature within the area above the blocking temperatures of the relevant minerals can partly or completely reset any predeformational or pre- metamorphic NRM.

On the other hand, the mechanism of progressive deformation within the area can rotate individual magnetic grains (usually of prolate or rod- like shape) as passive markers (March rotation) or rigid markers toward the flow plane of deformation (Ramsay, 1967, Gosh & Ramberg, 1976, Borradaile, 1988) thereby causing the rotation of NRM vector itself (e.g. Kodama, 1988, Vetter et al., 1989).

The process of development of preferred orientation during deformation by rotation of grains or grain boundaries processes such as particulate flow (Borradaile, 1981) also leads to the reorientation of magnetic moments of individual single or multidomain grains. As preferred orientation of magnetic grains increases, the preferred orientation of primary magnetizations can be reduced. It results in decrease of macroscopic magnetization of the sample.

The third factor which must be taken under consideration is the anisotropy of remanent magnetization. When a specimen acquires a remanent magnetization (thermal - TRM, depositional - DRM or chemical - CRM) the direction of magnetization vector is usually different from the direction of external magnetic field acting on the specimen. The deflection of remanent magnetization from the direction of external magnetic field depends on orientation of the sample with respect to that field and on the anisotropy of magnetic remanence. Fuller (1963) showed experimentally that acquired TRM can be deflected more than  $50^\circ$  from external magnetic field direction for some rock samples with high anisotropy of remanence.

The anisotropy of remanent magnetization (thermal TRM, anhysteretic ARM or isothermal IRM) can be measured experimentally after exposing the sample to an external magnetic field during cooling from a temperature higher than its range of blocking temperatures (in case of TRM acquisition, Fuller 1963, Uyeda et al. 1962) or the combination of weak constant magnetic



field and stronger alternating field (ARM acquisition - McCabe et al., 1985) or finally by use of stronger constant magnetic field alone (IRM acquisition, Uyeda et al., 1962). Imposing a magnetization and consecutive measurements of the acquired magnetization  $M$  can be made for several orientations of the sample and as a result the tensor of anisotropy of remanence  $\hat{k}$  can be obtained.

$$\bar{M} = \hat{k} \bar{H}$$

where  $M$  - remanent magnetization,  $H$  - acting external field,  $k$  - tensor of apparent anisotropy.

The anisotropy degree for remanent magnetization  $M_r$ , usually exceeds the anisotropy of saturation magnetization  $M_s$  and anisotropy of magnetic susceptibility  $\chi$  (Hrouda, 1982).

$$\frac{\chi_{\max}}{\chi_{\min}} < \frac{M_{rS \max}}{M_{rS \min}} \quad ; \quad \frac{M_{S \max}}{M_{S \min}} < \frac{M_{rS \max}}{M_{rS \min}}$$

where:

$\chi_{\max}, \chi_{\min}$  - maximum and minimum susceptibility

$M_{rS \max}; M_{rS \min}$  - the maximum and minimum remanent magnetization (thermal TRM, anhysteretic ARM or isothermal IRM);

$M_{S \max}; M_{S \min}$  - the maximum and minimum saturation magnetization.

When an external field acts on a specimen with high

anisotropy of remanent magnetization, the magnetization vector is deflected toward the plane of maximum and intermediate axes of anisotropy of remanence (principal plane). The angle of deflection depends on the anisotropy degree and orientation of principal plane of anisotropy with respect to the acting field (Fig. 8.1). The angle of deflection was approximated theoretically for thermal RM and isothermal RM by Uyeda et al. (1963) with the assumption that anisotropy of susceptibility is the same as anisotropy of remanence.

$$\tan\alpha = \frac{M_{IRM_{\min}}}{M_{IRM_{\max}}} = \frac{1}{P_0} * \tan\beta \quad - \text{ for IRM}$$

$$\tan\alpha = \frac{1}{P_0 * P_B} * \tan\beta \quad - \text{ for TRM}$$

where  $\alpha$  - the angle between the magnetization vector and basal plane of anisotropy of susceptibility;

$\beta$  - the angle between the external field vector and basal plane of susceptibility;

$$P = \frac{\chi_{\max}}{\chi_{\min}} \quad \text{anisotropy degree for susceptibility}$$

$P_0, P_B$  - anisotropy of susceptibility degree for room and blocking temperature conditions. Theoretical calculations for IRM for different anisotropy degree for susceptibility are shown

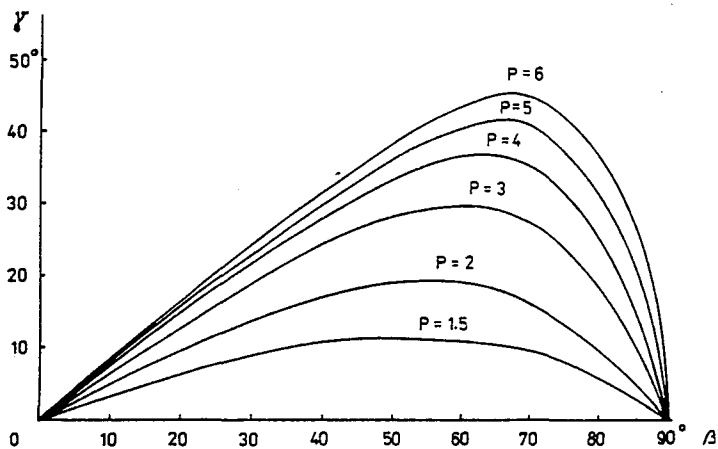


Fig. 8.1. The angle  $\gamma$  of deflection of isothermal remanence from the direction of external magnetic field toward the axis of maximum susceptibility as a function of angle  $\beta$  between a direction of external field and a direction of maximum susceptibility. A function of deflection angle is calculated for several values of anisotropy ratio  $P$  (from Hrouda, 1982).

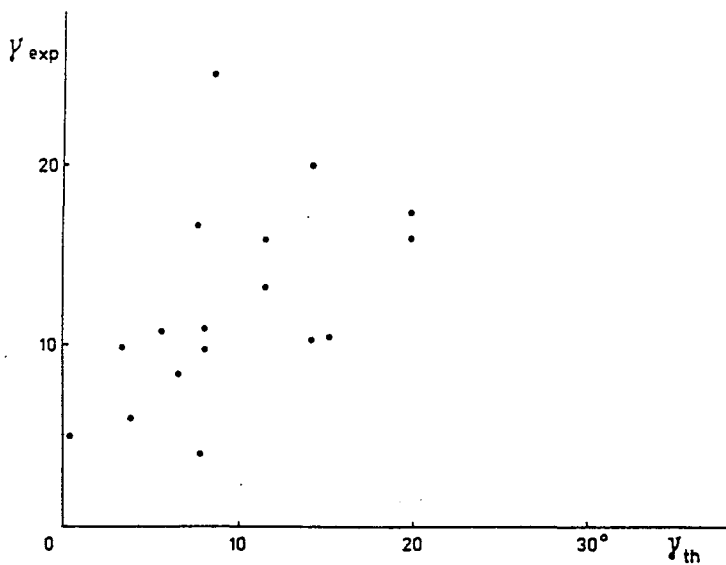


Fig. 8.2. The correlation between measured  $\gamma_{exp}$  and calculated  $\gamma_{th}$  angle of deflection of IRM vector from the external field toward the maximum susceptibility direction for several igneous and metamorphic rocks (from Hrouda, 1982). Note that measured angles are usually larger than predicted.

in Fig. 8.1.

In practice the measured deflection of the magnetization vector  $\gamma = \beta - \alpha$  is often larger (usually 10-20°) than theoretical values (based on anisotropy of susceptibility) - Fig. 8.2. (Janák, 1967, Stephenson et al., 1986, Fuller, 1963), e.g. for pyrrhotite-bearing limestone Fuller reports  $P_{AMS}=1.04$  and 50° of TRM deflection (Fig. 8.3). This happens because the degree of anisotropy for bulk susceptibility for a studied rock sample is usually much lower than anisotropy of remanent magnetization, especially for metamorphic rocks. Therefore the anisotropy parameter  $P$  for remanence should be used in the Uyeda' equations instead of  $P$  for AMS. The contribution to magnetic susceptibility (MS) and its anisotropy (AMS) in these rocks comes equally from rock-forming diamagnetic minerals and auxiliary paramagnetic phyllosilicates as well as from ferrimagnetic minerals (Borradaile et al., 1987, Borradaile et al., 1986). The highly anisotropic hematite and pyrrhotite (crystallographic anisotropy) and moderately anisotropic magnetite (shape anisotropy) are present usually as accessory minerals in trace  $\ll 1\%$  quantities, therefore the bulk susceptibility tensor reflects a lower anisotropy due to the large contribution of less anisotropic dia- and paramagnetic minerals (Jackson et al., 1989).

The observed deflection of remanent magnetization vector from a known direction of external magnetic field  $\gamma$  can have values from 10 - 15° (for  $P_{RM}=1.5$  up to even 50° for  $P_{RM}=6$ ); the

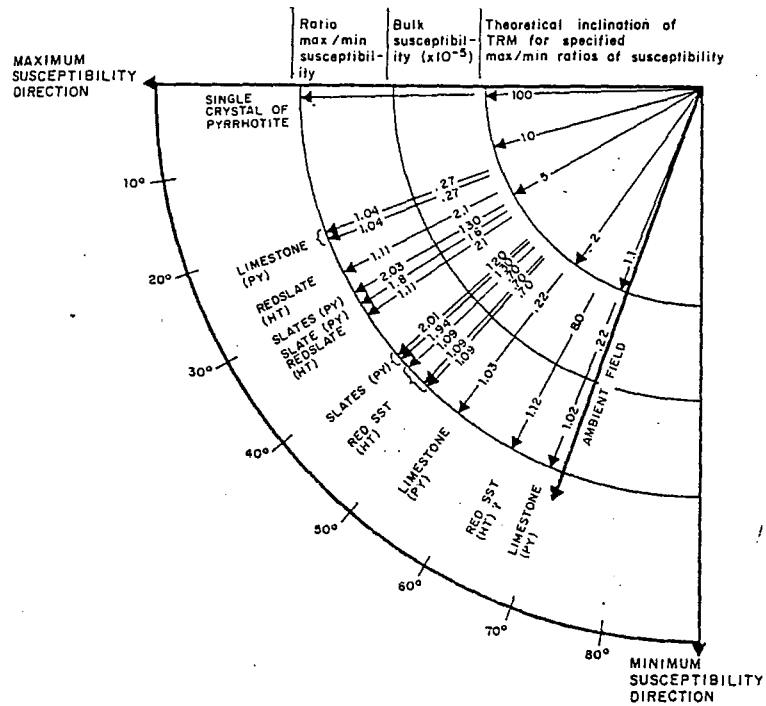


Fig. 8.3. The anisotropic acquisition of NRM by crystalline anisotropic rocks. The ratio of the max/min susceptibility is given and compared with the susceptibility anisotropy which should give the observed divergence of TRM. (from Fuller, 1963)

higher deflection was noticed for highly anisotropic hematite and pyrrhotite - rich samples (e.g. Fuller, 1963 for TRM, Janák, 1967 for IRM, Werner & Jeleńska, 1991 for TRM in hematite).

In this study AMS anisotropy degree  $P$  had mean value of  $1.35 \div 0.61$  ( $n=550$ ) and  $P$  parameter for ARM anisotropy was  $4.23 \div 2.79$  ( $n=123$ ). If anisotropy degree for natural remanent magnetization (thermal or chemical) is similar to that of ARM, then substantial deflections of natural remanence from the magnetic field may be expected. These deflections caused by anisotropy of remanence may be of value up to  $40 - 50^\circ$ , when the direction of magnetic field is at low angle ( $20-30^\circ$ ) to minimum axes of anisotropy of remanence (Fig. 8.1).

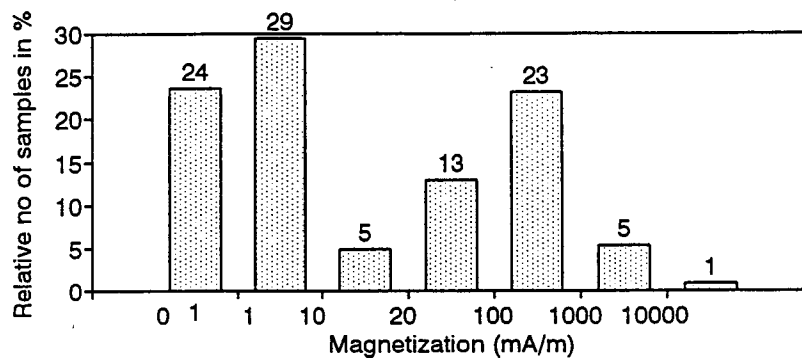
## 8.2. The initial natural remanence for the study area.

The three collections of cylindrical cores 25 mm in diameter and 22 mm in height were obtained from visited areas; 167 samples from Kashabowie - Huronian traverse (119 samples collected in this study and 58 by Spark (1990), 244 samples - from Perch Lake - Calm Lake traverse (Sarvas, 1988) and 175 samples from Atikokan Huronian Lake traverse (in this study) - for a total of 538 cores. Usually 2 - 4 cores were drilled from 1 or 2 hand-specimens collected from each outcrop.

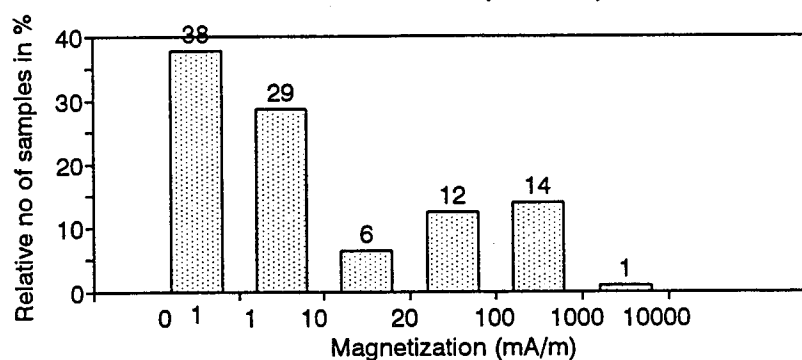
The initial natural remanent magnetization (NRM) of all samples was measured with the use of MOLSPIN spinner magnetometer with sensitivity better than 0.1 mA/m.

The intensity of NRM varied very much from one sample to another; intensities from 0.2 mA/m up to 13000 mA/m were recorded (Fig. 8.4). They differed remarkably from one outcrop to another (Fig. 8.5); even cores drilled from the same hand-specimen may possess NRM intensities differing by factor of 5 or more. As the content of ferrimagnetic minerals (mainly pyrrhotite) was less than 1% in a specimen, small variations of its content in the bulk composition was the main factor responsible for variations of NRM intensities.

Distribution of NRM intensities  
Atikokan area (N=226)



The interior of belt (N=202)



Kashabowic - Huronian L. area (N=114)

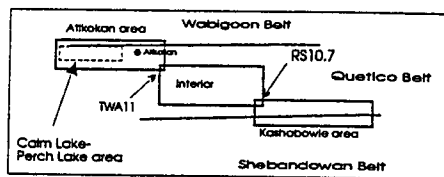
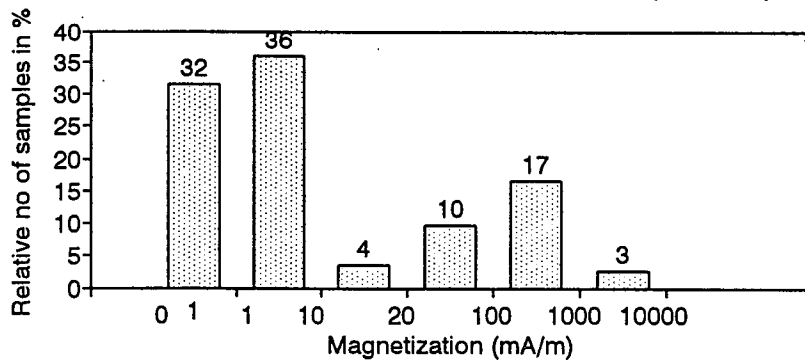


Fig. 8.4. Histograms of intensity of initial natural remanence (NRM) for samples from three areas of different metamorphic grade (see sketch map). 70% samples have NRM intensity less than 10 mA/m.



Intensities of natural remanence  
The Calm Lake- Perch Lake area

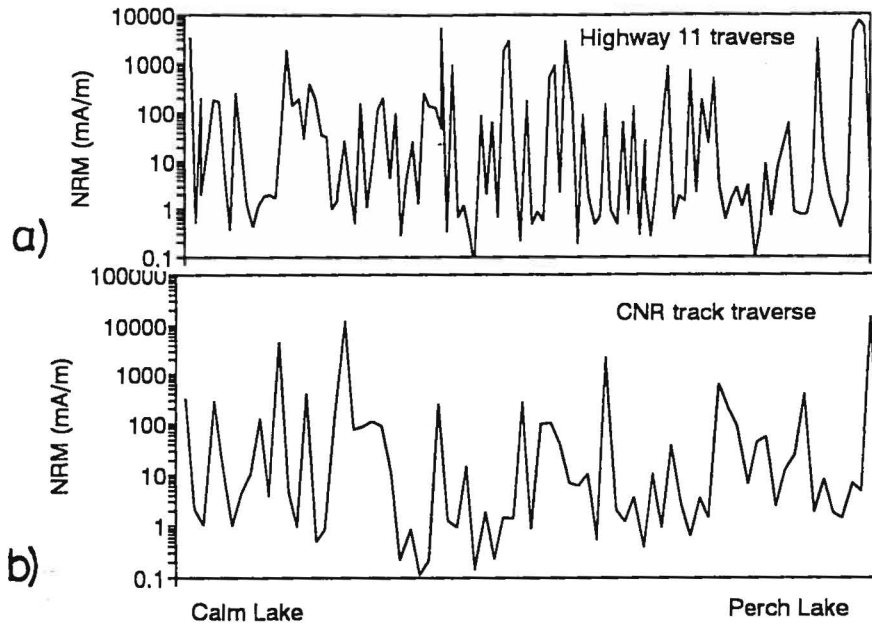
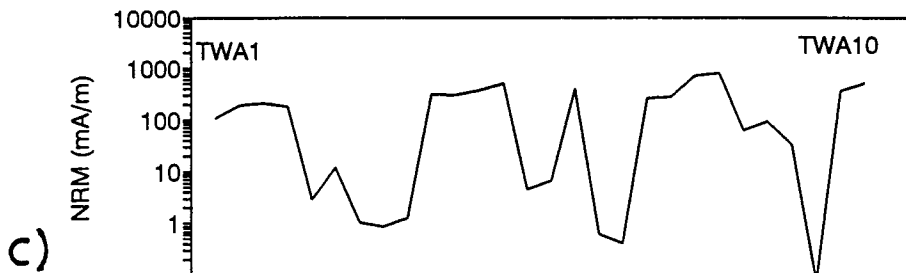


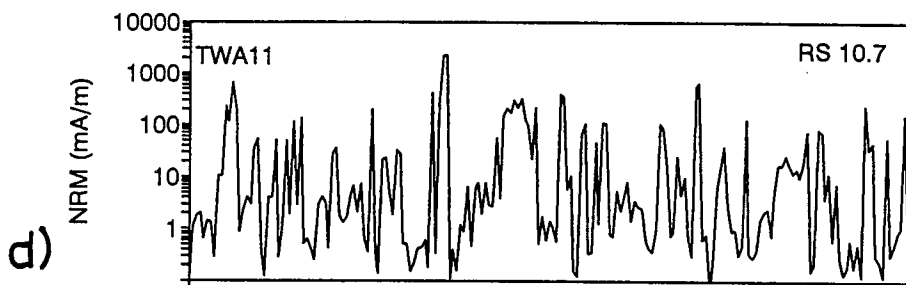
Fig. 8.5. The variations in NRM intensity along traverses. a) and b) - along hwy 11 and railway track in Calm Lake - Perch Lake area. c) - e) - along hwy 11 from Atikokan to Kashabowie Lake. (see sketch map). All traverses are from west to east. Variations are erratic and this indicates that NRM intensity is controlled mainly by the mineralogical composition of samples.

Intensities of natural remanence

Atikokan area



The interior of the Quetico Belt



The Kashabowie - Huronian Lake area

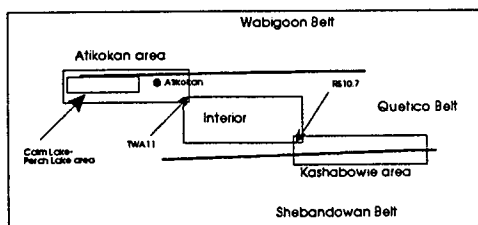
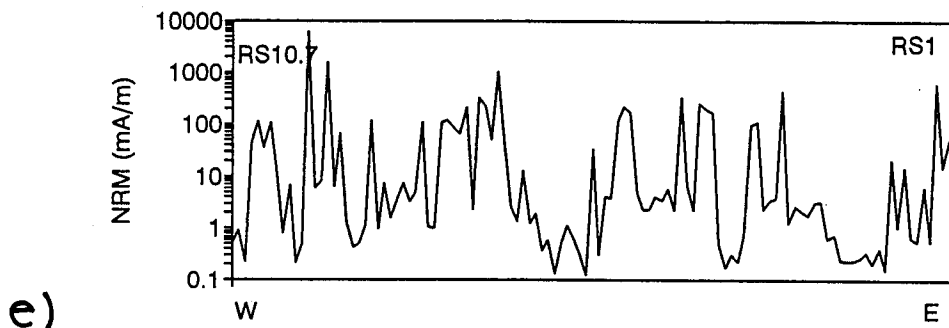


Fig. 8.5. continues.

### 8.3 Demagnetization of remanence - procedures.

More than 55% of specimen had an initial NRM too weak to be demagnetized (Fig. 8.4) and still measured reliably with the MOLSPIN spinner magnetometer. All but a few cores with intensities of magnetization higher than 10 mA/m (for the Atikokan - Kashabowie transects) or higher than 20 mA/m (for the Calm Lake - Perch Lake traverse) were selected for demagnetization procedures together with some weaker samples. These made a total of 176 for alternating field treatment and 58 for thermal treatment.

Alternating field, step-wise demagnetization was performed with the use of Sapphire Instrument SI-4 apparatus with maximum peak a.f. field of 200 mT. The initial magnetization of each core was measured in a MOLSPIN spinner magnetometer (Molyneux, 1971) before the first step of demagnetization. Then the core was exposed to alternating magnetic field inside a nest of three  $\mu$ -metal shields increasing to a peak value and then decaying. This procedure randomizes the magnetic domains of the coercivity less than the peak intensity reached by the alternating magnetic field. The procedure was repeated for the same sample in three mutually perpendicular directions. After the step of demagnetization the remaining remanence of core was measured again in the magnetometer. Repeating of these steps with the use of successively higher peak demagnetizing AF field produces the demagnetization path for the remanence vector (Zijderveld,

1967).

The remaining NRM can be plotted on the stereogram or projected onto the planes of a geographic coordinate system. In this way Zijdeveld plots were obtained for each demagnetized sample (Fig. 8.6).

The samples were demagnetized with steps of AF magnetic field from 1.5 mT up to the maximum field necessary to demagnetize the sample, which ranged from 20 mT up to 200 mT. If a sample possessed one or two components of magnetic remanence which are recorded by grains of different coercivity, the demagnetization path should consist almost linear segments as each NRM component is removed during AF treatment. If the coercivity spectra for components overlap, the demagnetization path is curved reflecting the simultaneous removal of both components (Collinson, 1983).

The errors of measurements of weak NRM vector as well as effects of viscous magnetization of low coercive grains in the sample internal field or residual Earth's magnetic field can introduce errors. It is also possible that a specimen may acquire a weak anhysteretic component during AF treatment, although a special cancellation circuit in the demagnetiser limits this problem. Finally some errors can be introduced by a gyromagnetic component in non-tumbling magnetometers like SI-4 (Stephenson, 1981). However, this only occurs at very high demagnetising fields (>150 mT).

The procedure of demagnetization was terminated when the

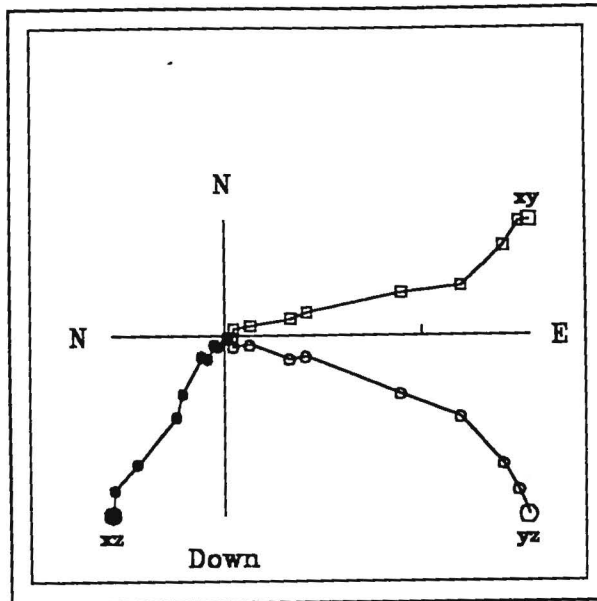


Fig. 8.6. An example of Zijderveld diagram for AF demagnetization path.

Remaining NRM vectors measured after each demagnetization step forming a demagnetization path are plotted in 2 or 3 projections on planes of coordinate system (X-Y, Y-Z or X-Z).

In a standard geographic coordinate systems it gives projections: N-E (X-Y plane), N-Down (X-Z plane) and E-Down (Y-Z plane). Projection in two planes is sufficient to describe any vector, but a convention for projection in three planes is employed here.

remaining demagnetization showed random changes of its direction after each step of demagnetization: this indicated that the remaining remanence had become unstable.

An analogous demagnetization procedure was performed with the use of a triple  $\mu$  - metal shielded cylindrical furnace in which a set of 15 samples was heated to the given temperature and then permitted to cool down. The samples were heated in steps of 50 or 25° C from room temperature up to a maximum temperature ranging from 350° C up to 600°C for a given sample. The measurements of magnetic remanence were performed after each heating - cooling cycle with use of the MOLSPIN magnetometer and also bulk magnetic susceptibility was measured at room temperature after every 100°C heating treatment to detect any possible mineralogical changes in the samples.

The maximum temperature of heating for each thermal demagnetization step was controlled with 10°C accuracy. The obtained demagnetization path for a sample was presented in the same way as for AF treatment. The heating procedure was terminated when the remaining magnetizations become randomly oriented, when changes in sample susceptibility were larger than 20%, or when the intensity of remanence vector dropped beneath 1-2% of its initial value.

The decay of one- component (uni-vectorial) remanent magnetization under AF treatment can be modelled by an exponential decay function. Therefore the median destructive field (MDF) can be defined as the AF peak field intensity

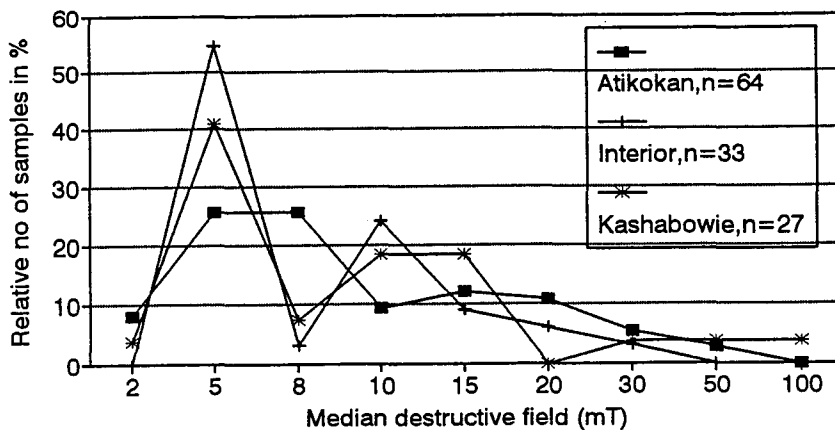
sufficient to decrease the remanence to 50% of its initial value. For the studied collections, the MDF for AF treatment was mostly in the range of 5 - 15 mT (Fig. 8.7). The maximum peak field used for demagnetization ranged mostly from 20 to 30 mT. Some (10% for TW and RS collections and 20% for PS collection - Fig. 8.8) samples with high coercivity (hematite?) were not demagnetized sufficiently even by field of 200 mT. They usually revealed a stable one-component characteristic remanence up to the 200 mT demagnetization field.

About 10% of samples showed a remagnetization effect during AF treatment at low AF fields (10 mT), with more than 50% of initial remanence intensity still existing. The observed demagnetization paths became random for these samples when AF field of higher intensity was applied. The pyrrhotite grains in these samples were probably multidomain with very low coercivity and they quickly acquired a viscous remanence as a result of self - magnetization in the residual intrinsic field (Fig. 8.9).

The remaining samples (about 150) were demagnetized at higher alternating fields and their demagnetization paths revealed variably defined, uni- or bi-vectorial component of remanence (Fig. 8.10).

The thermal demagnetization was usually terminated at temperatures of about 350 - 375° C, corresponding to the blocking temperatures of pyrrhotite (Fig 8.11), with only a few samples from low grade rocks carrying high temperature unstable remanence in magnetite and hematite grains.

Median destructive field for AF treatm.  
Distribution for belt bound. and inter.



Distribution for total collection

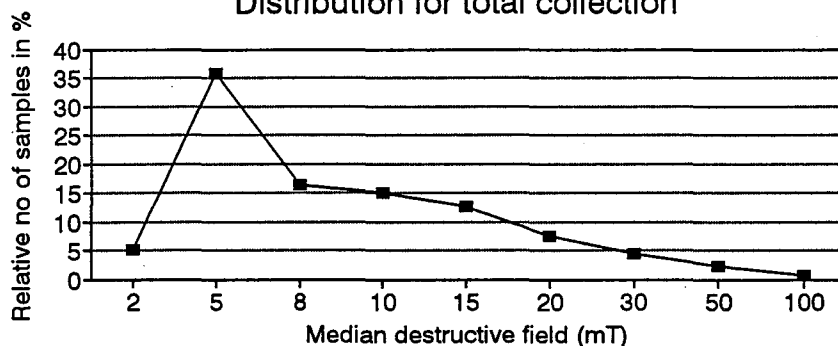
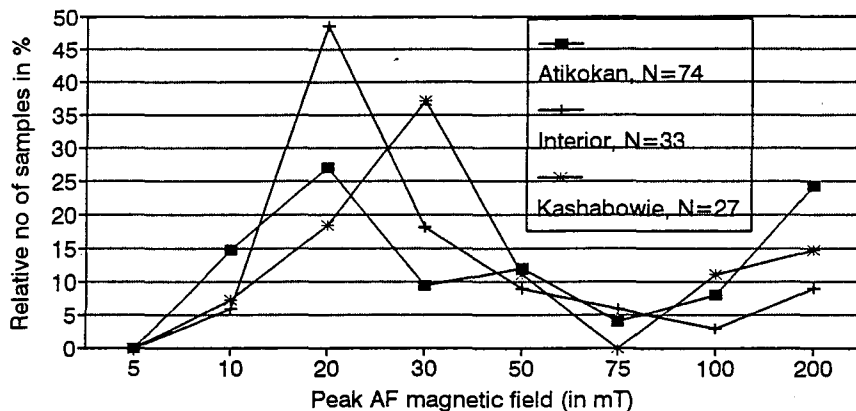


Fig. 8.7. A distribution of median destructive field (MDF) value used in AF demagnetization technique for collections of samples from three studied sub-areas (Atikokan, Interior and Kashabowie).  
a) MDF values for each of sub- areas separately;  
b) NDF values distribution for a whole studied area.  
MDF values are usually very low - less than 5 mT for interior and Kashabowie area, slightly higher for Atikokan area (smaller pyrrhotite grains?).



Peak magnetic field used in AF demag.  
Distribution for belt bound and inter.



Distribution for total collection

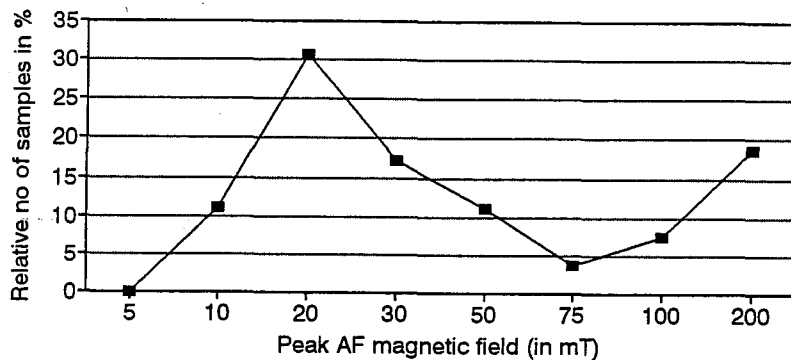


Fig. 8.8. Peak alternative field (used in the last a.f. demagnetization step before a remaining NRM became unstable). Most of peak field values are about 20 -30 mT, indicating PSD or MD remanence carrying grains. Some every high coercive samples are probably hematite bearing.

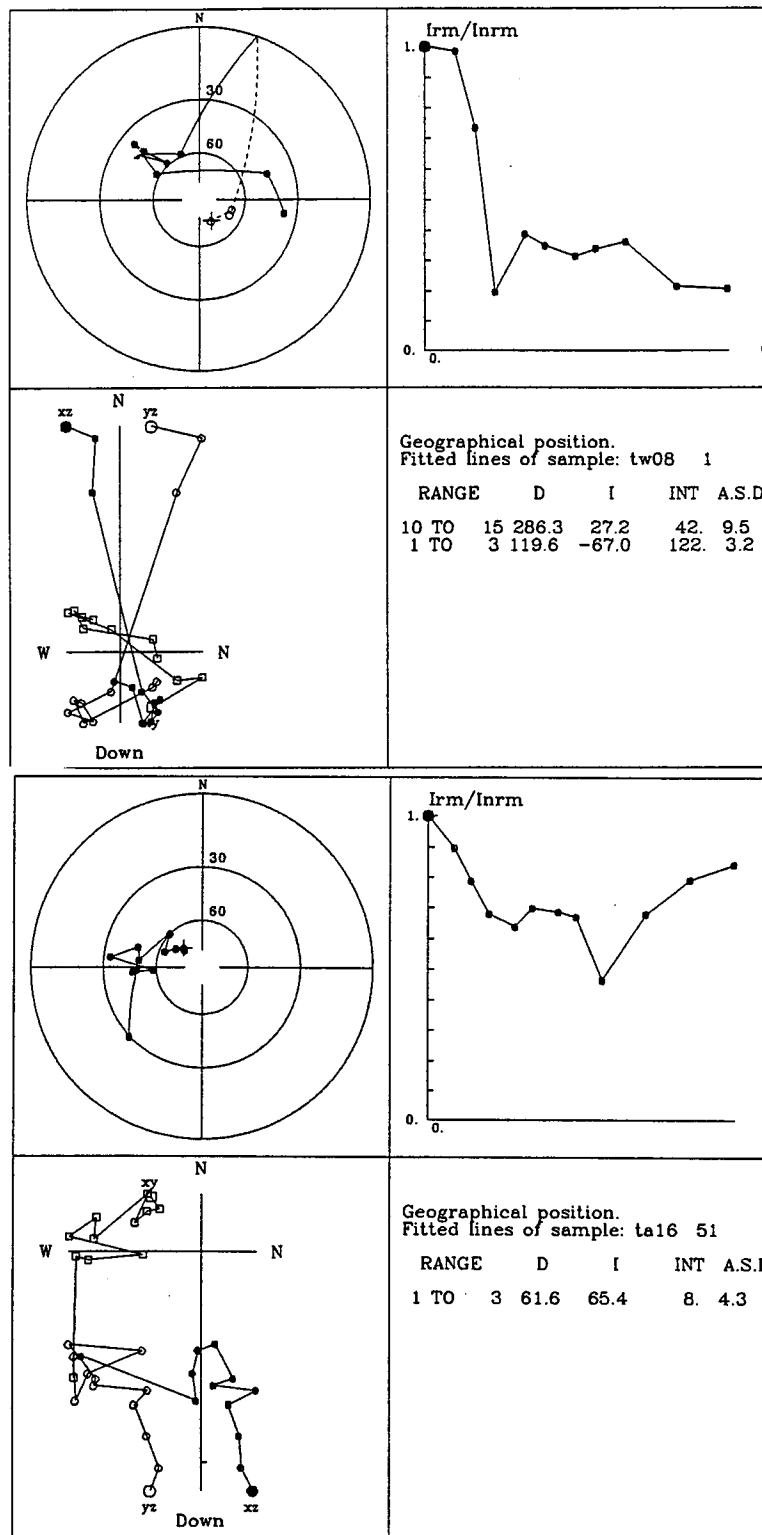
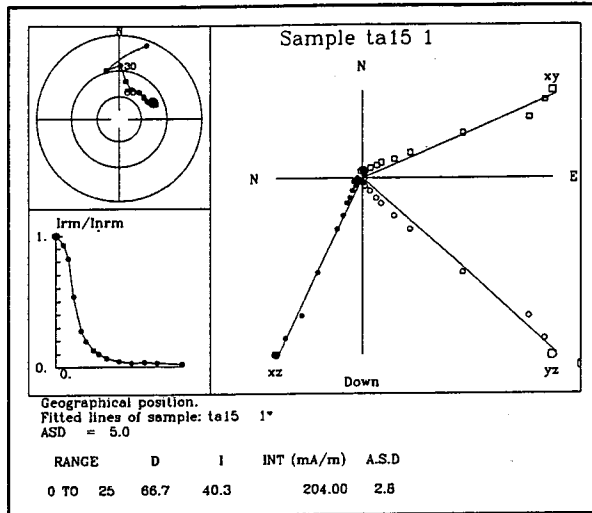
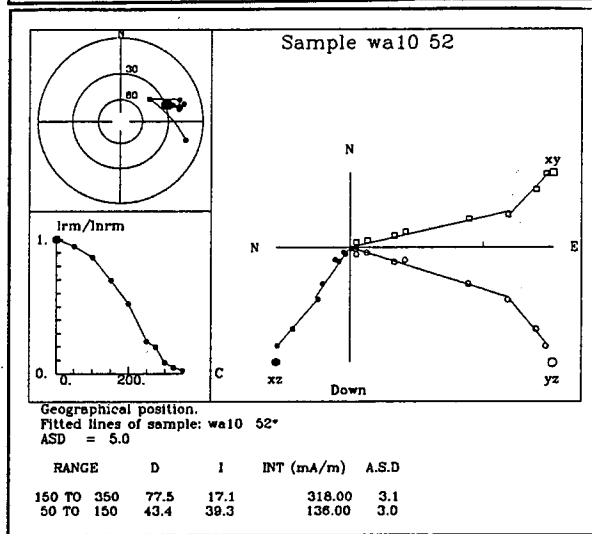


Fig. 8.9. Two examples of easily unstable NRM (when a field of about 10 mT was applied). Sample TW8-1 is pyrrhotite bearing; TWA16.5-1 has some amphibolite phase - can be magnetite bearing as well.

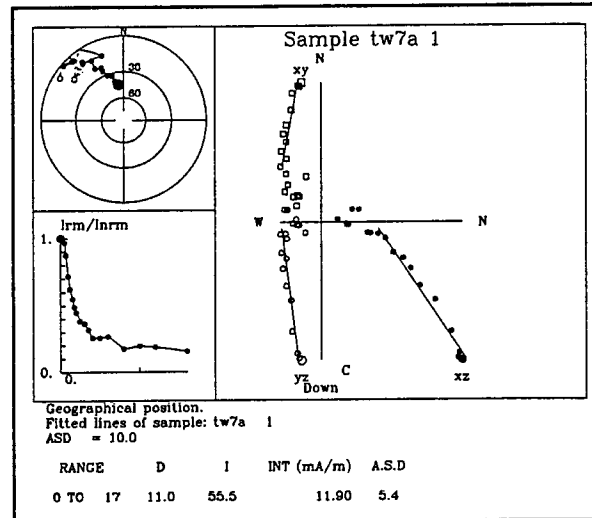
Fig. 8.10. Three examples of stable NRM during AF demagnetization procedure.  
 a) - magnetite bearing sample (TWA15-1) demagnetized up to 25 mT AF field; -uni - vectorial ChRM.



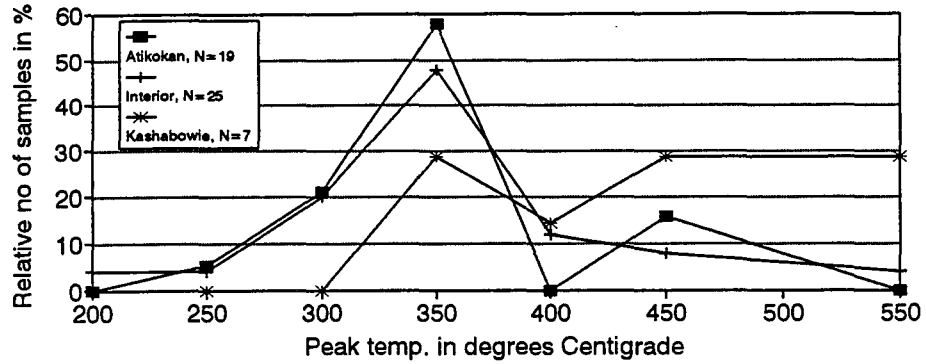
b) - pyrrhotite bearing sample (TWA10.5-2) demagnetized up to 35 mT AF field; bi- vectorial ChRM.



c) - pyrrhotite bearing sample (TW7A-1) demagnetized up to 17.5 mT AF field; uni- vectorial ChRM.



Peak temperature for thermal demagnet.  
Distribution for belt margins & inter.



Distribution for total collection

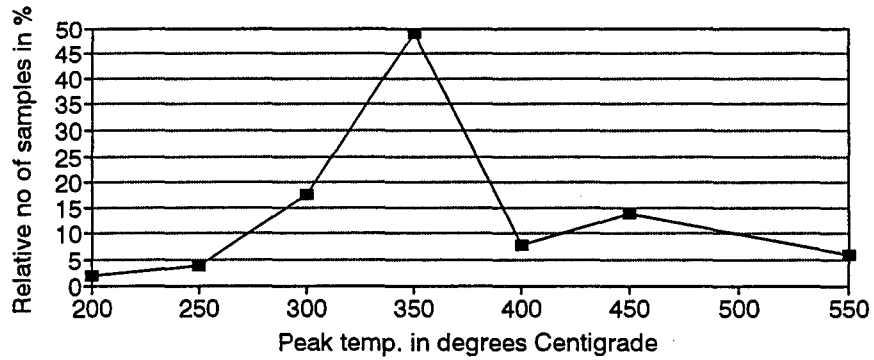


Fig. 8.11. A distribution of peak temperatures used for thermal demagnetization of NRM, employed before samples became unstable or mineralogical changes were noticed. Most samples were demagnetized with a peak temperature 350°C; however, thermal demagnetization was carried into higher temperatures for 60% of samples from Kashabowie area.

The computer algorithm based on principal component analysis (Kirschvink, 1980) was used to determine the segments of the demagnetization path for each sample. This can be approximated by a line with the error lower than a certain assumed accuracy (angular standard deviation - ASD, see for example Werner & Jeleńska, 1991).

The direction of the fitted line can be interpreted as the direction of magnetic remanence, only if one component of remanent magnetization was removed from the sample in a corresponding range of coercivity or blocking temperatures.

The algorithm uses a set of  $N$  consecutive points from demagnetization path to calculate their vector mean ("the centre of gravity"- CM) and then a matrix  $M_{ij}$  of the distances between the CM and points from the set was constructed.

$$M_{ij} = \sum_{k=1}^N (x_{k_i} - x_{CM_i}) * (x_{k_j} - x_{CM_j})$$

where: CM - centre of mass,

$x_{k_i}$  or  $x_{k_j}$  - X, Y or Z - component of a  $k$ -th vector

Eigenvalues  $\lambda_1 > \lambda_2 > \lambda_3$  and corresponding eigenvectors of this matrix are determined and the eigenvector corresponding to the greatest eigenvalue is taken as a direction of fitted line.

The scatter of points from a linear arrangement is tested in terms of ratio of the other eigenvalues and  $\lambda_1$ :

$$\tan(ASD) = \sqrt{\frac{\lambda_2 + \lambda_3}{\lambda_1}}$$



seemed not to reflect the real NRM and they were rejected.

The ChRM directions falling into classes A or B were plotted on a stereogram for results of AF treatment and thermal treatment separately. Some samples from Calm Lake - Perch Lake area that were not drilled in geographic coordinates had their ChRM directions reoriented into true geographic coordinates. This procedure was performed with use of algorithm COORD2.BAS written by the author.

First the obtained direction was rotated along the vertical axis of angle equal to the strike value for top surface of cylindrical core to restore the arrow on the core into strike direction. Then a rotation along the horizontal strike line of dip angle was performed. The same procedure is repeated for magnetic fabrics directions such as maximum and minimum axes of anisotropy of susceptibility or anisotropy of anhysteretic remanence.

#### 8.4. Distribution of characteristic magnetic remanences.

The ChRM directions were plotted on a stereogram (equal area projection) for results of AF treatment and thermal treatment. Data were grouped in three different suites: those from low grade metasediments in Atikokan area, those from the interior of the belt and those from Huronian Lake - Kashabowie Lake area (low grade metasediments and metavolcanics). They were plotted separately on the stereogram (Fig. 8.13, 8.14).

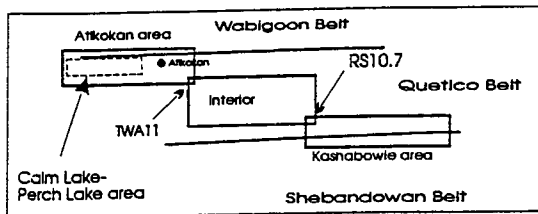
The distribution of characteristic remanence directions from the suites of samples studied can be analyzed in terms of the formation of either a cluster or a girdle.

Principal component analysis method (PCA) can be used to find the best fit of a great circle for weakly developed girdles of remanence directions. The direction of the eigenvector corresponding to the minimum eigenvalue of the PCA matrix characterizes the pole to fitted plane. Also the clustering pattern can be evaluated by means of Fisher's statistics on the sphere (Fisher, 1953, McElhinny, 1973).

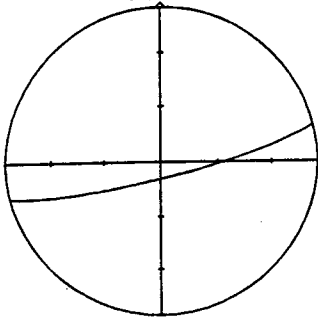
However Fisher's statistics can be successfully use only in case, when the distribution of directions on the sphere is assumed to be uni-vectorial and not orthorhombic. This assumption is not valid for studied data because direction are distributed along the girdle.

Procedures for fitting a plane and calculating the common direction were applied to following sets of directions:

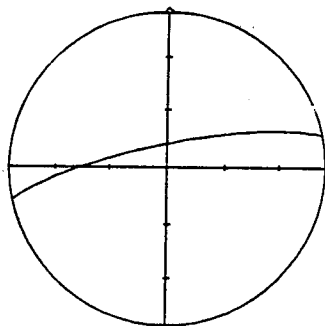




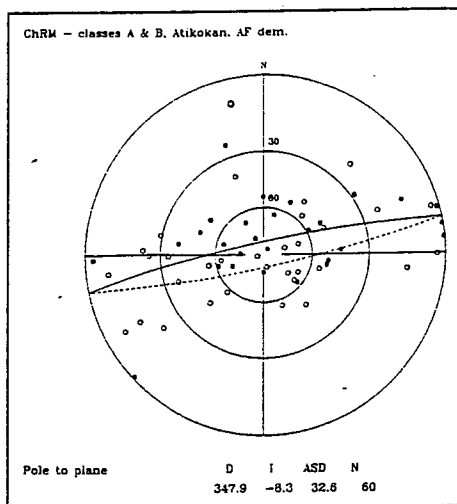
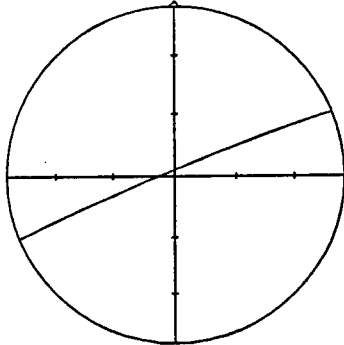
Mean S1 schistosity plane - Atikokan area



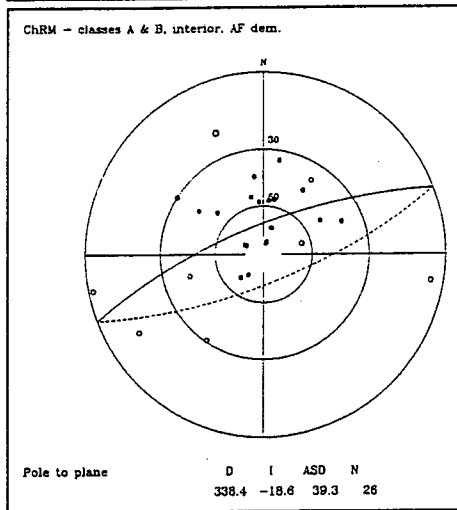
Mean S1 schistosity plane - Quetico Belt Interior



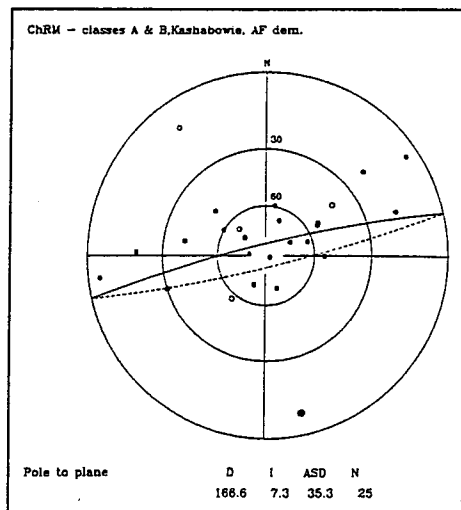
Mean S1 schistosity plane - Kashabowie area



a)

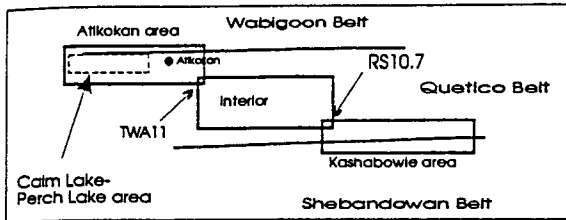


b)

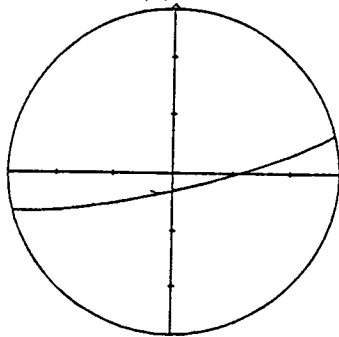


c)

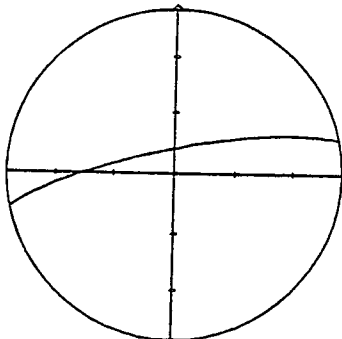
Fig. 8.13. A distribution of ChRM directions for classes A&B determined by AF demagnetization with fitted mean planes for three subareas - (Fig. a) - c)). Compare with mean S<sub>1</sub> planes.



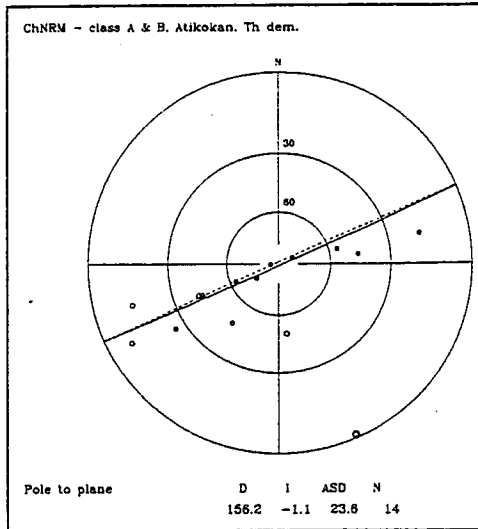
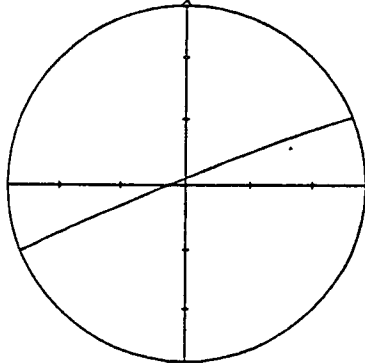
Mean S1 schistosity plane - Atikokan area



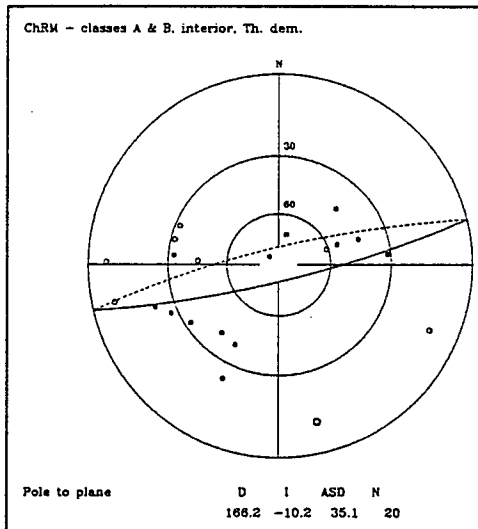
Mean S1 schistosity plane - Quietico Belt interior



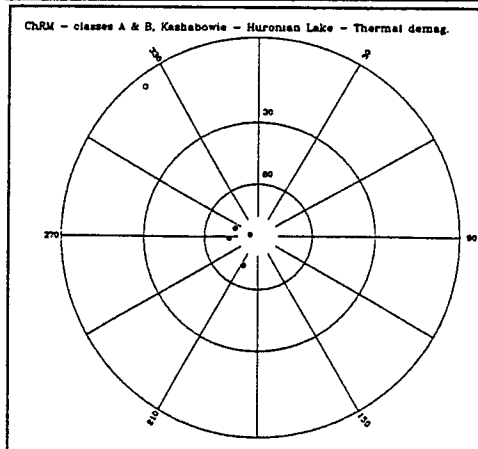
Mean S1 schistosity plane - Kashabowie area



a)



b)



c)

Fig. 8.14.  
A diagram as fig. 8.13 for thermally demagnetized samples.

- a) A and B classes together;
- b) A class directions only;
- c) all three classes of directions together.

Such approach can indicate whether elimination of the worst define directions (class C) improves the overall grouping of ChRM in a girdle or a cluster. Results of these calculations presented in Table 8.15. suggest that a weakly developed girdle distribution is formed both for class A directions alone as well as for collections containing all three classes of directions. Therefore the substantial scatter of ChRM direction is not correlated with measurement errors. This leads to the conclusion that even some class C directions (defined from the short 3-4 points segments of demagnetization path) may be statistically significant. Most of them are recorded in a samples with very low coercive pyrrhotite grains which are already unstable at AF peak field of only 10 mT. However there is not a method to decide which individual C class directions should be accepted as ChRM directions.

Table 8.15. The relation of poles to mean planes and mean Fisherian directions to the selection of classes of ChRM directions.

	PCA - pole to plane	Fisher's mean direction	PCA-cluster direction
ALTERNATING FIELD TREATMENT			
Atikokan area			
all classes, N=98	168/7 (33) <sup>1</sup>	45/36 (50) <sup>2</sup>	37/80
A & B, N=60	168/8 (33)	41/-16 (65)	42/76
A class, N=47	172/8 (32)	351/35 (76)	59/70
Quetico Belt interior			
all classes, N=54	168/14 (39)	324/61 (23)	10/75
A & B, N=26	158/19 (39)	341/65 (28)	11/68
A class, N=11	148/13 (34)	13/63 (38)	30/64
Kashabowie area			
all classes, N=31	169/9 (34)	337/69 (29)	40/76
A & B class, N=25	167/7 (35)	343/72 (28)	52/73
A class, N=12	170/9 (29)	353/74 (46)	53/71
THERMAL TREATMENT			
Atikokan area			
all classes, N=30	340/3 (26)	117/64 (40)	126/86
A & B, N=14	336/1 (24)	224/49 (49)	68/57
Quetico Belt interior			
all classes, N=40	342/8 (43)	203/70 (35)	78/36
A & B, N=20	346/10 (35)	251/46 (44)	77/7
Kashabowie area - CLUSTER ONLY	Spheristat - peak count	Fisher's mean	PCA - cluster
all classes, N=11	270/81 (7 $\sigma$ ) <sup>3</sup>	320/76 (23)	275/81
A & B class, N=5	243/80 (4 $\sigma$ )	294/69 (40)	256/79

1 - ASD value; 2 - Fisher's  $\alpha_{95}$ ;

3 - peak value for counting procedure (SpheriStat).

Fisher's means for each set of remanence directions and mean direction of clustering determined by PCA method are very poorly defined and strongly depend on the chosen class of remanence

directions. However the most of Fisherian means and directions of maximum clustering are rather steep (with inclination of 50 - 70°).

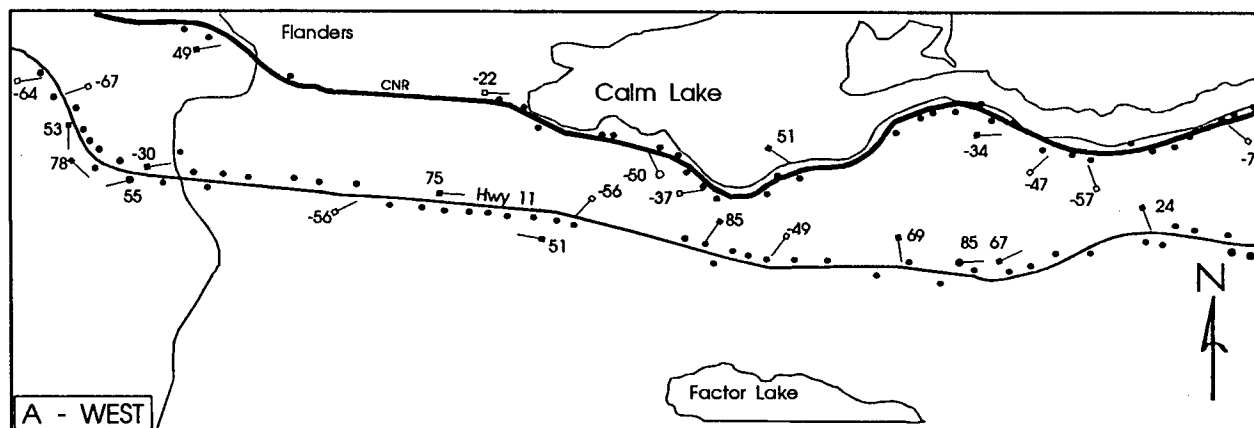
The calculated ChRM directions are distributed along great circles striking ENE-WSW and dipping steeply or to the NNW (for samples demagnetized by AF) or SSE (for those demagnetized thermally). Both steep and gently inclined individual NRM directions were observed.

When distributions of ChRM from three different suites are studied separately (Fig. 8.13 and 8.14) it can be noticed that for interior of the belt mean planes are less steep. Individual directions in the interior form less developed girdle than at belt margins. ChRM directions cleaned by AF method generally are distributed around the mean schistosity plane (Fig. 8.13), but those obtained after thermal demagnetization are somewhat deflected to the south (Fig 8.14).

Thermal demagnetization curves gave usually better defined linear segments of demagnetization paths with fewer cases of large remanence left after treatment (due to high blocking temperature mineral phases such as magnetite). ChRM directions after thermal demagnetization are very similar to those after AF demagnetization for an individual handspecimen. However, the number of demagnetized thermally sample is of 30% of those demagnetized by AF method (less than 20 samples were thermally demagnetized from each of three suites). Those results are less significant statistically, especially for data from Kashabowie

area (only 5 samples thermally demagnetized). The thermally demagnetized ChRM directions from Kashabowie area cluster around  $270/75^\circ$  and are not distributed along the girdle.

The possibility of a local common preferred orientation of natural remanence in some areas was also examined. The mapping of ChRM vectors along all three traverses did not show any common small scale alignment of ChRM directions from one outcrop to another (Fig.8.16, 8.17). Variations in ChRM directions can be of  $180^\circ$  for two outcrops at a distance of 1 km. However the ENE - WSW tendency for ChRM declination is characteristic for each outcrop.



- NRM direction after AF demagnetization
- NRM direction after thermal demagnetization
- 
- filled symbol - positive inclination;
- empty symbol - negative inclination

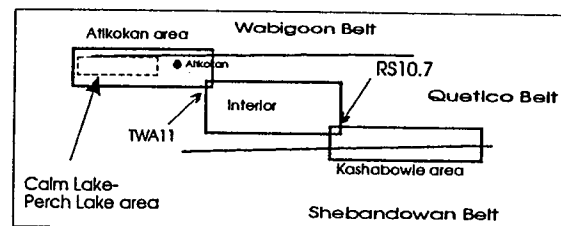
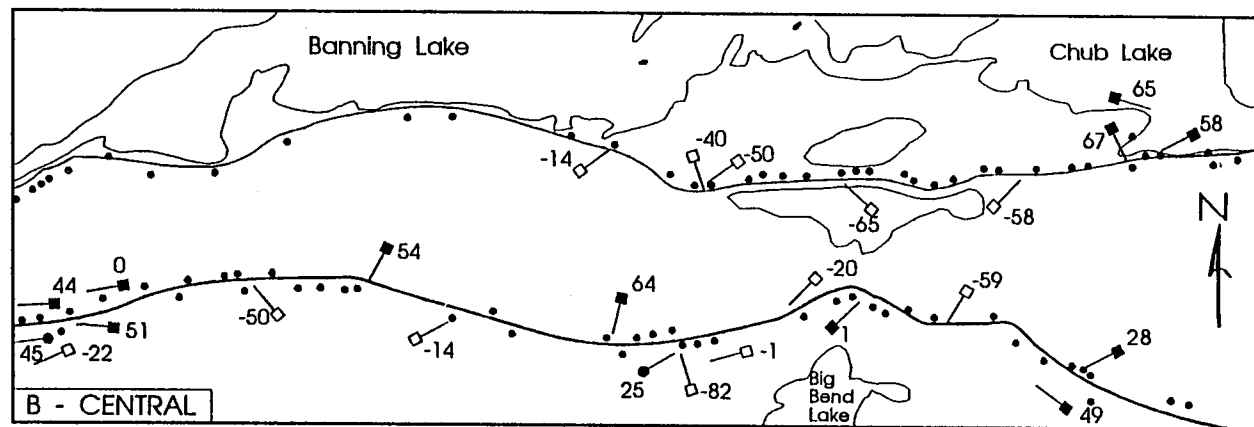


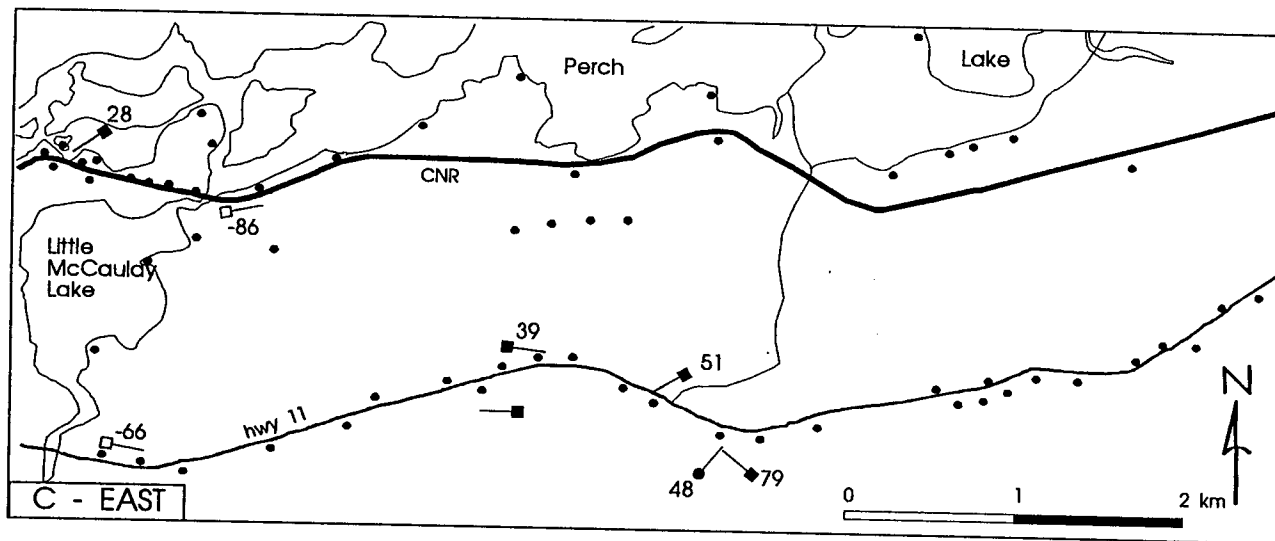
Fig. 8.16. A map of ChRM directions for sites from Calm Lake - Perch Lake area. Maps A,B,C cover three parts of that area from west to east. A - the western part on this page. Note different symbols used for AF and thermally demagnetized ChRM. Numbers next to symbols are inclination values that correlate to open or closed symbols, that indicate positive or negative inclinations. A scale on map C.



- NRM direction after AF demagnetization
- NRM direction after thermal demagnetization
- filled symbol - positive inclination;
- empty symbol - negative inclination

Fig 8.16 - continues; map B - the central part of the Calm Lake - Perch Lake area..





- NRM direction after AF demagnetization
- NRM direction after thermal demagnetization
- filled symbol - positive inclination;
- empty symbol - negative inclination

Fig 8.16 - continues; map C - the eastern part of the Calm Lake - Perch Lake area.

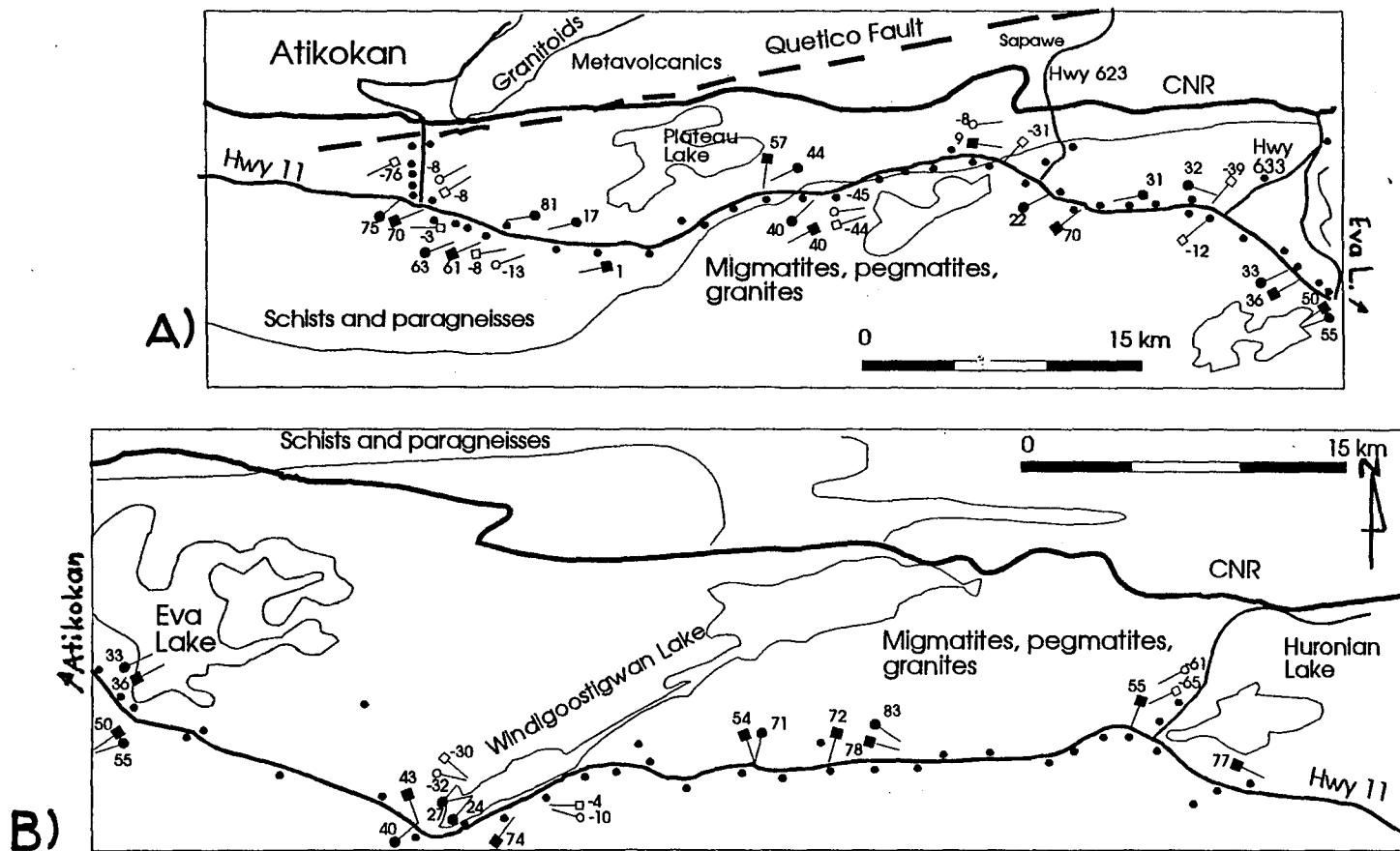
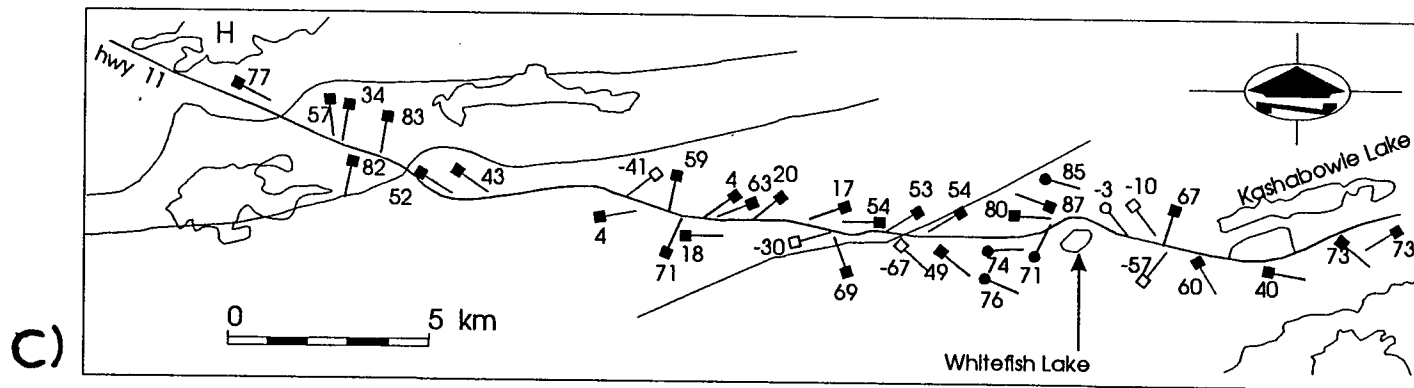


Fig. 8.17. A map of ChRM directions for Atikokan - Kashabowie L. traverse along Hwy 11. Maps A and B cover Atikokan - Huronian L. area, Map C - Huronian L. - Kashabowie L. area. Legend is shown under map C. The symbol convention is the same as for Fig. 8.16.



- NRM direction after AF demagnetization
- NRM direction after thermal demagnetization
- filled symbol - positive inclination;
- empty symbol - negative inclination

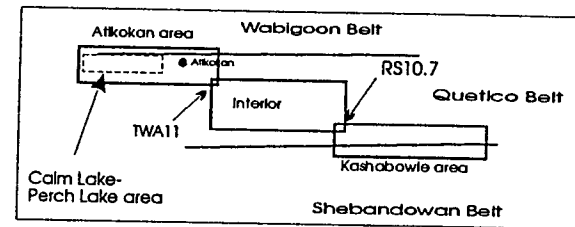


Fig 8.17. continues; Map C for Huronian Lake - Kashabowie Lake area.

### 8.5. Interpretation of the distribution of ChRM directions.

Determined ChRM directions do not cluster around a mean direction for any suite. The ChRM directions between neighbouring outcrops show also very large differences. Their orientations are also quite closely correlated with the overall planar tectonic fabric for each suite (especially for samples demagnetized by A.F. technique). Therefore it is obvious that recorded ChRM directions are deflected from the direction of the external magnetic field. Those large differences (especially in inclination) between outcrops cannot be explained by different ages of acquisition of remanent magnetization by individual rock units and substantial changes of paleogeographic position of the area during deformation.

Several factors can be discussed as responsible for observed distribution of ChRM directions.

1. The substantial anisotropy (mean  $P'$  of order 3 to 5) of ARM suggests that the anisotropy of acquired chemical or thermomagnetic remanence should be also of the same order. The foliation planes of ARM anisotropy were oriented almost parallel to mean schistosity  $S_1$  for each of 3 suites. Therefore ChRM directions can be deflected from the direction of the Earth's magnetic field at the time of acquisition of stable remanence. The mean ChRM directions for weakly deformed rock bodies in the area determined by Dunlop cluster around  $005^\circ/55^\circ$  (Borradaile et al., 1983, see also chapter 3.2 for details). That direction is

at angle of about 20-30° to the foliation planes of the anisotropy of remanence for individual samples. According to Uyeda et al. (1963) model for anisotropy parameter of the order of 3 to 5 the deflection of the remanence from the external field direction can be of order of 20-30° toward the foliation plane of anisotropy of remanence. For higher values of anisotropy parameter P those deflections could be up to 50°. Therefore I postulate that the overall distribution of the ChRM directions along planes of tectonic foliation and ARM anisotropy foliation planes can be caused by samples anisotropy of remanence.

However about of 10-30% of samples from each suite had very low inclinations of ChRM (less than 30°). These can be hardly explained by the anisotropy effect alone if it is assumed that all samples were exposed to the same external Earth' magnetic field direction.

The influence of anisotropy of remanence onto the direction of ChRM should be examined in future more thoroughly. The design can be as follows:

First one must assume that anisotropy of ARM is the same as anisotropy of thermomagnetic or chemical remanence for a given sample. The orientation of Earth's magnetic field for a given sample can be calculated when the anisotropy of remanence and direction of ChRM is known. If the directions of magnetic field for a collection of samples cluster, this can be indicative that the girdle distribution is caused by the

anisotropy of remanence alone. However, if a girdle distribution is still preserved, the other factors also might also be responsible.

The girdle distributions for ChRM directions from each suite were not well defined ( $ASD > 20^\circ$ ). It was mainly caused by the fact that only 10-30% of directions are widely spread along a girdle having low (less than  $30^\circ$ ) inclinations. The rest of ChRM direction rather cluster in a sector of high inclinations ( $> 60^\circ$ ) as can be expected when the anisotropy of remanence model is employed here to explain those distributions of ChRM directions.

2. The mineralogical observations confirmed also that remanence is carried mainly by pyrrhotite grains, which are usually of late metamorphic origin thus they do not carry predeformational remanence. No traces of magnetite were observed in samples prior to heating them to temperatures greater than  $350^\circ$ . It supports the conclusion that pyrrhotite is late-metamorphic and late-tectonic.

Pyrrhotite grain alignment seems to be controlled by matrix fabrics such as the preferred dimensional orientation of quartz and feldspar and the preferred crystallographic orientation of biotite grains. Grains are large (usually greater than  $50\mu\text{m}$ ) and pseudo-single- and multi-domain. Therefore the remanence is rather of chemical origin, acquired during the growth of pyrrhotite with substantial p.c.o. and has to be interpreted as late-tectonic.

3. The model of rotation of pre-existing remanence during a progressive deformation can be only employed to grains which are pre-metamorphic. Such models of passive line or rigid marker rotation were discussed extensively by Kodama, (1988), Borradaile and Mothersill (1989), Vetter et al., (1989), and Borradaile (1992, 1983) do not take effects of metamorphic recrystallization under consideration. They could be only used for magnetite bearing metavolcanic rocks in Kashabowie Lake, if the observed magnetite is pre-tectonic. Microscopic observations and multi-domain magnetic properties suggest however metamorphic origin of magnetite. Therefore it is not possible to separate clearly the rotational effect (if any exists) of deflection of the natural remanence from the external magnetic field direction.

4. Experimental studies for magnetite- and hematite-bearing synthetic samples showed that the effect of stress alone with low strain values (less than 30%) could reduce the overall isothermal remanence of the sample (Borradaile and Mothersill, 1989, Borradaile, 1992). The differential stress (not hydrostatic one) applied during experiments remagnetized the hematite grains with higher coercivity and low coercive multidomain magnetite (with coercivity of remanence less than 30 mT). Lower coercive hematite and single -domain magnetite were partially demagnetized. In case of multi-domain magnetite the process can be explained by irrecoverable domain wall movement controlled by the differential stress (Borradaile, personal

comm.). Directions of removed remanence were not correlated with stress axes. In the case of pyrrhotite, this effect was not studied.

In the studied area differential stress conditions during and after a transpressive deformation are not known. However the removal of primary natural remanences due to the action of such differential stresses cannot be discarded. If low-coercive grains had their initial remanence removed by stress field the secondary acquired remanence could be controlled by high overall anisotropy of remanence and as well be correlated with the direction of Earth' magnetic field characteristic for the time of resetting of remanence. It could be one of factors that produced low inclined remanence vectors in several samples.

Finally, I would like to emphasize that the collection of samples for NRM studies was rather small and further studies, especially on a site scale may be helpful to explain the processes leading to a post-tectonic distribution of NRM in the area.



## Chapter 9.

## Anisotropy of magnetic susceptibility - overview.

The anisotropy of low - field magnetic susceptibility (AMS) is used commonly as the qualitative, and in a few cases also as a quantitative indicator of bulk rock fabric of tectonic origin (Hrouda, 1982, Borradaile, 1988). The high correlation between tectonic fabric (orientation of schistosity and extension lineations) and axes of maximum and minimum susceptibility is typical, but the correlation between strain ratio and anisotropy of magnetic susceptibility degree ("magnetic strain gauge" - Jackson and Tauxe, 1991) is not commonly found (Borradaile, 1988) and seems to be mainly controlled by the bulk composition of the rock (Borradaile, 1988, Jackson and Tauxe, 1991) and the mechanism of deformation. The local correlations for strain estimates from AMS anisotropy were only considered to be reliable in a few cases (e.g., Hirt et al., 1988, Ruf et al., 1988, Borradaile, 1991).

Jackson pointed out that no correlation between the strain and AMS can be found when stress controlled recrystallization is responsible for the preferred orientation of magnetic grains (Jackson and Tauxe, 1991, see also Housen and van der Pluijm, 1990).

The advantage of AMS studies for a tectonic interpretation is the speed and the high precision of measurements (typically

less than 1% error for mean susceptibility of  $10^{-3}$  SI vol.), as well as the abundance of magnetic minerals in a rock even when conventional tectonic strain indicators are absent in the field.

The other geological and geophysical applications of AMS as discussed by Hrouda (1982) concern for example the influence of AMS on the deflection of the direction of remanent magnetization recorded in a rock. The intrinsic field within the specimen due to AMS is not parallel to the direction of the acting external magnetic field. Therefore, samples with high AMS have usually a substantial deflection of the remanence direction from the external field (Hrouda, 1982, Uyeda et al., 1962, Fuller, 1963). The quantitative models of this correlation are however rarely confirmed in experiment (Fuller, 1963, see also chapter 8).

Also anisotropy of remanence, eg. ARM is a better indicator of the deflection of remanence, since its effect are not diluted by the presence of paramagnetic minerals as is the case for AMS.

9.1. The method of the AMS determination and the contribution of different minerals into anisotropy of magnetic susceptibility - terms and definitions.

The acquired bulk magnetization of a sample exposed to an external magnetic field  $H$  is a function of both external field  $H$  and the magnetic properties of the specimen characterized by a bulk magnetic susceptibility  $\chi$ . This can be a complex quantity in general. For a distant or low-frequency magnetic field the susceptibility is approximated by a set of real values, for high frequency magnetic field the imaginary component of susceptibility becomes significant and indicates the conductivity response of the specimen.

$$\bar{M} = \hat{\chi}(\bar{H}_{ext}, \omega) \bar{H}_{ext}$$

- where:  $\chi$  - susceptibility,  $M$  - magnetization,  $H_{ext}$  - external magnetic field,  $\omega$  - frequency of external field.

In this study only low - frequency external field was used for magnetic susceptibility determination. The magnetic susceptibility meter used during MS and AMS investigation Sapphire Instrument SI-2 operated at a field frequency of 750 Hz and root-mean-square intensity of the field of 0.05 mT (0.5 Oe = 40 A/m).

### Magnetic susceptibility ellipsoid.

Magnetization is not in general a linear function of external field when a ferromagnetic (s. l.) phase is considered. It usually obeys the Raleigh law :

$$M = \chi H + \eta H^2 \quad , \quad \chi - \text{is a initial or reversible susceptibility}$$

and  $\eta$  is Raleigh parameter ,when the external field is low compared to coercive force and sample was initially demagnetized (e.g. Clark, 1984). If the initial remanent magnetization  $M_r$  exists the total magnetization  $M_{total}$  of the sample in the external field is given as :  $M_{total} = M_r + M_{appl}$  , where only magnetization

$M_{appl}$  generated by external field can have a linear component with the field. Usually also para- or diamagnetic minerals produce a linear term in overall value of  $M_{appl}$ . Therefore only when the external field is small (usually of order 0.05 - 0.1 mT) is the measured magnetization due to external magnetic field linear with field, and susceptibility is not dependent on external field. In case of whole rock composition susceptibility both para- and ferromagnetic contributions to susceptibility exist.

Then the susceptibility can be represented by the second - rank symmetric tensor  $\hat{\chi}$  , where tensor components  $\chi_{ij}$  are constant values not dependent on the intensity of external

magnetic field (Hrouda, 1982).

$$\hat{\chi} = \begin{bmatrix} \chi_{11} & \chi_{12} & \chi_{13} \\ \chi_{21} & \chi_{22} & \chi_{23} \\ \chi_{31} & \chi_{32} & \chi_{33} \end{bmatrix}$$

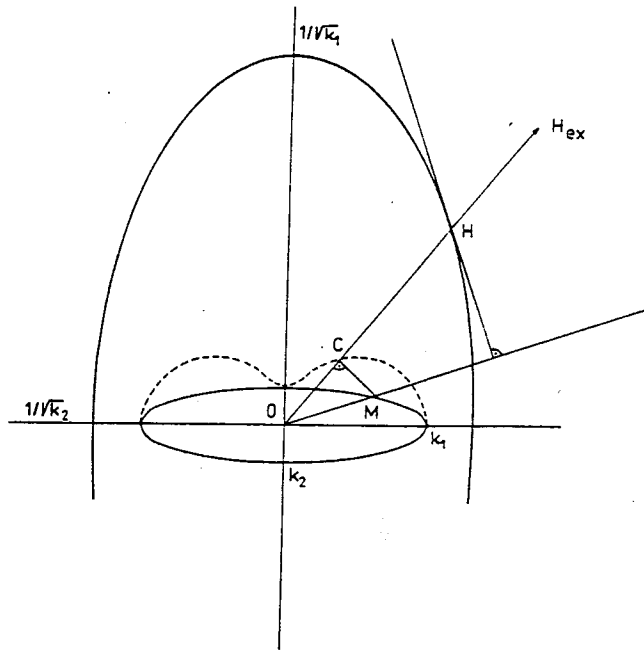
- where  $\chi_{ij} = \chi_{ji}$  - components of symmetric tensor.

Therefore only six different parameters are needed to define the tensor matrix. As a symmetric matrix the susceptibility has 3 eigenvectors and usually 3 different real eigenvalues. In the base coordinate system formed from the eigenvectors, the matrix reduces to the diagonal one with eigenvalues:  $\chi_{\max}$ ,  $\chi_{\text{int}}$ ,  $\chi_{\min}$ .

Thus the susceptibility tensor can be represented as an tri-axial ellipsoid with the length of its principal axes equal to eigenvalues of the susceptibility matrix oriented along the eigenvector directions (magnetization ellipsoid of Hrouda, 1982)

or by ellipsoid with principal axes of length  $\frac{1}{\sqrt{\chi_i}}$ , where  $\chi_i$  is a principal susceptibility (Nagata, 1961, definition of 'anisotropy of MS' by Hrouda, 1982, Fig. 9.1.).

The second definition can be a little confusing as it is not easily correlated with the strain ellipsoid representation (especially in three-dimensional studies). Therefore the first definition (with principal axis lengths equals to the corresponding eigenvalues of  $\chi$ , e.g. Jackson, 1990) will be used as the AMS ellipsoid in this thesis.



On the definition of the susceptibility ellipsoid and the magnitude ellipsoid. Legend:  $OH$  – direction of external magnetic field  $H_{ex}$ ,  $OM$  – anisotropic magnetization induced by  $H_{ex}$ ,  $OC$  – component of magnetization parallel to  $H_{ex}$  or the quantity measured by usual methods. If  $|H_{ex}| = 1$ ,  $OC$  is the susceptibility parallel to  $H_{ex}$  (directional susceptibility). Loci of  $H$ , where  $OH = 1/\sqrt{OC}$ , represents the susceptibility ellipsoid (heavy line) and the loci of  $M$  (thin line) is the magnitude ellipsoid. The dashed line represents the directional behaviour of the directional susceptibility (not represented by an ellipsoid).

Fig. 9.1. (from Hrouda, 1982).

parameters describing the anisotropy.

The anisotropy of magnetic susceptibility can be characterized by the shape of susceptibility ellipsoid as prolate, when  $\chi_{\max} > \chi_{\text{int}} > 1 > \chi_{\min}$  or oblate, when  $\chi_{\max} > 1 > \chi_{\text{int}} > \chi_{\min}$ . The degree of anisotropy (the deflection from spherical shape) and the sense of shape was described with numerous anisotropy parameters (see Hrouda, 1982 for detailed discussion), but two parameters are sufficient to describe the shape of the anisotropy ellipsoid.

One can choose anisotropy ratio  $P = \frac{\chi_{\max}}{\chi_{\min}}$ , or magnetic

lineation  $L$  and foliation  $F$ :  $L = \frac{\chi_{\max}}{\chi_{\text{int}}}$ ;  $F = \frac{\chi_{\text{int}}}{\chi_{\min}}$ , as analogues to Flinn's diagram parameters "a" and "b" for tectonic lineations and foliations (Flinn, 1962) to characterize susceptibility ellipsoid. However, we may alternatively use Jelinek's (1981) parameters  $P'$  -  $T$ , where

$$P' = \exp \sqrt{2 * \left[ \left( \ln \left( \frac{\chi_{\max}}{\bar{\chi}} \right) \right)^2 + \left( \ln \left( \frac{\chi_{\text{int}}}{\bar{\chi}} \right) \right)^2 + \left( \ln \left( \frac{\chi_{\min}}{\bar{\chi}} \right) \right)^2 \right]}$$

with geometric mean of susceptibility  $\bar{\chi} = (\chi_{\max} * \chi_{\text{int}} * \chi_{\min})^{\frac{1}{3}}$  and

$$T = \frac{\ln F - \ln L}{\ln F + \ln L}$$

The  $P'$ - $T$  parameters are superior. The parameter  $P'$  includes information from the intermediate axis, contrary to  $P$ . Moreover, the parameter  $T$  is symmetric and has the value  $T=1$  for prolate ellipsoid and  $-1$  for oblate one. The choice of Jelinek's plot  $P'$ - $T$  (Hrouda, 1982) gives the better resolution between prolate and oblate shapes of ellipsoids than Flinn diagram, especially for low values of anisotropy ( $P'$  of range 1-1.2). Values of parameter  $P'$  are almost equal values of  $P$  when samples are not strongly oblate or strongly prolate. In these extreme cases the difference is less than 10% (Fig. 9.2).

#### **Factors controlling AMS.**

The factors controlling the anisotropy of susceptibility of single grains and of a crystal lattice were discussed in some detail in Chapter 6. The overall magnetic fabrics of metamorphic rocks (especially sedimentary) are controlled practically by two of them :

1. magnetocrystalline anisotropy of grains located usually in a lattice with preferred crystallographic orientation (p.c.o.); e.g. paramagnetic silicates, hematite, pyrrhotite.
2. shape anisotropy of grains with relatively high intrinsic susceptibility and significant difference in demagnetization factors in principal directions of a grain (Hrouda, 1982), e.g. magnetite, titanomagnetites.

The minerals with significant shape anisotropy controlling AMS are ferrimagnetics : magnetite and some titanomagnetites



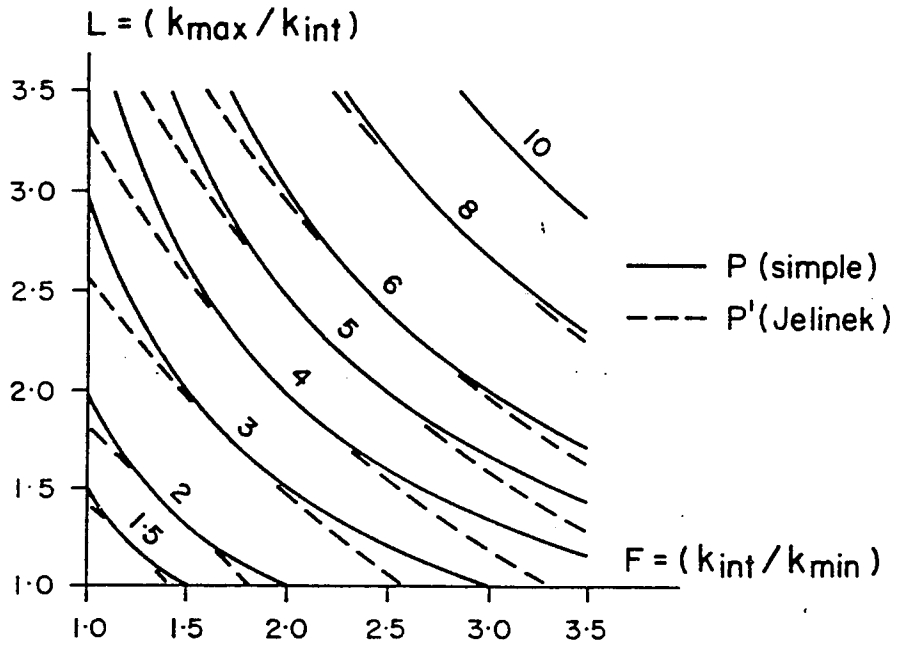


Fig. 9.2. A comparison between anisotropy parameters  $P'$  (Jelinek, 1981) and  $P = k_{max} / k_{min}$  (e.g. Hrouda, 1982) for different shapes of AMS ellipsoid (defined by lineation  $L$  and foliation  $F$  parameters). The difference between  $P'$  and  $P$  arises to about 10% for strongly oblate or strongly prolate samples (from Borradaile and Sarvas, 1990).

with elongated grains (Hrouda, 1982, Jackson, 1990). In such minerals SD grains have remanent magnetization parallel to their long axes but maximum axis of susceptibility is perpendicular to long axes ("inverse" magnetic anisotropy, Jackson 1990). It is caused by the effect that external field applied along long axis of a grain (and existing saturation magnetization of SD grain) cannot rotate the magnetization away from this position of minimum energy or increase the overall magnetization of already saturated grain. Therefore the external field applied along the long axis of a grain has no effect on this grain and minimum axis of AMS is parallel to long axis of the grain.

In MD grains with shape anisotropy the AMS fabric is not "inverse": they have the maximum axis of AMS parallel to the long axis of the grain. Potter and Stephenson (1988) indicated that when the effects due to shape anisotropy of a grain interact with the overall orientation fabric of a group of elongated grains, it results in four possible cases of bulk AMS fabric:

1. MD grains with an S-fabric (planar alignment of grains): the bulk minimum susceptibility is perpendicular to the plane,
2. SD elongated in a S -fabric: maximum susceptibility perpendicular to the plane.
3. MD grains in an L-fabric (linear alignment of grains): maximum susceptibility parallel to the direction of preferred orientation.
4. SD elongated grains in an L-fabric: minimum

susceptibility parallel to the fabric lineation.

The other common minerals which carry remanence are pyrrhotite and hematite. They have their anisotropy degree controlled mainly by magnetocrystalline anisotropy (anisotropy degree for these grains is  $>100$ , Hrouda, 1982). Antiferromagnetic (hexagonal) pyrrhotite usually has no shape anisotropy at all, and the monoclinic variety can reveal only a weak shape anisotropy in the basal plane due to its quite high susceptibility (Hrouda, 1982). When even a weak preferred orientation of these minerals exists in the rock, these minerals contribute significantly to the bulk AMS of the rock (Schwarz, 1974). Worm (1991) indicates that the AMS of pyrrhotite increases quickly with increasing field and although  $\chi_{\max}$ ,  $\chi_{\text{int}}$  and their ratio  $\chi_{\max}/\chi_{\text{int}}$  increases with field,  $\chi$  decreases and becomes sensitive of field frequency. A field of 1 mT and frequency 1 kHz can generate out of phase effects in the highly conductive pyrrhotite (Stupavsky, work in progress).

Paramagnetic platy minerals such as biotite, chlorite, hornblende and actinolite due to their abundance in the rock, contribute largely both to magnetic susceptibility and AMS (Borradaile et al., 1987). Hrouda (1982) gave values of anisotropy degree  $P'$  for metamorphic rocks as of range 1.1-1.3 but the minimum AMS of such single minerals common in metamorphic rocks can have  $P'$  as high as 1.7 (Borradaile et al., 1987). Magnetic fabric for these mineral is usually oblate (typical  $T$  values for biotite, chlorite, phlogopite: 0.3 - 0.95)

with some possible prolate fabric for hornblende and actinolite (Borradaile et al., 1987). However, Borradaile's technique for assembling and aligning individual grains in an approximate one and, moreover, the grains probably contain ferromagnetic inclusions. On theoretical grounds most of phyllosilicates should have oblate magnetic symmetry (Borradaile, pers. comm.). The minimum axis of susceptibility is usually perpendicular to the c-axis of crystals, but inverse fabrics can be observed in certain carbonate bearing rocks and in tourmaline-rich rocks (Rochette, 1988).

Mechanisms responsible for the formation of AMS fabric in the paramagnetic matrix are those normally responsible for the generation of p.c.o., e.g. rigid body (March) rotation in low temperatures, dynamic strain controlled recrystallization in higher temperatures, and stress-controlled crystallization during metamorphism.

#### **The overall AMS of rocks.**

In non-deformed sedimentary rocks, the initial AMS may be quite strong due to depositional conditions, current directions and compaction. The minimum axis of susceptibility in these rocks is usually perpendicular to bedding with an oblate fabric. However, in the case of current alignment, the maximum susceptibility can be oriented along the current direction or perpendicular to it (for some prolate grains, Hrouda, 1982) and the fabric may not be oblate parallel to bedding. Such

sedimentary AMS fabric can partly persist during later deformation or metamorphism, which can adversely influence any attempts at strain - AMS correlations (Borradaile, 1991).

AMS of volcanic rocks is rather low ( $P=1.0-1.05$ ) and is carried usually by titanomagnetites. It can correlate with lava flow directions where magnetic foliation is subparallel to the flow plane, but magnetic lineation can be oriented both parallel or perpendicular to the flow direction (Hrouda, 1982). In plutonic rocks low values of anisotropy ratio exist in plutons with flow fabric. High AMS with  $P'$  often greater than 2 are characteristic for plutons affected by ductile deformation. Ferrimagnetic minerals found in these rocks (magnetite, pyrrhotite) are usually younger than silicates and their preferred orientation and their shape is controlled by the surrounding matrix (Hrouda, 1982). However, the large-scale consistent magnetic fabric is rarely found.

#### **The measurement method of AMS in this study.**

Anisotropy of magnetic susceptibility of the collected cores was determined with the use of Sapphire Instrument SI-2 susceptibility meter. The apparatus has 8 x 5 cm solenoidal coil producing the relatively uniform field of 0.05 mT, with frequency 750 Hz. The cylindrical specimen occupied only 6% of coil volume, therefore the absolute precision of the equipment for 10 repeated measurements is about  $2.5 \cdot 10^{-6}$  SI vol. However 5 repeated measurements were only performed for each sample to

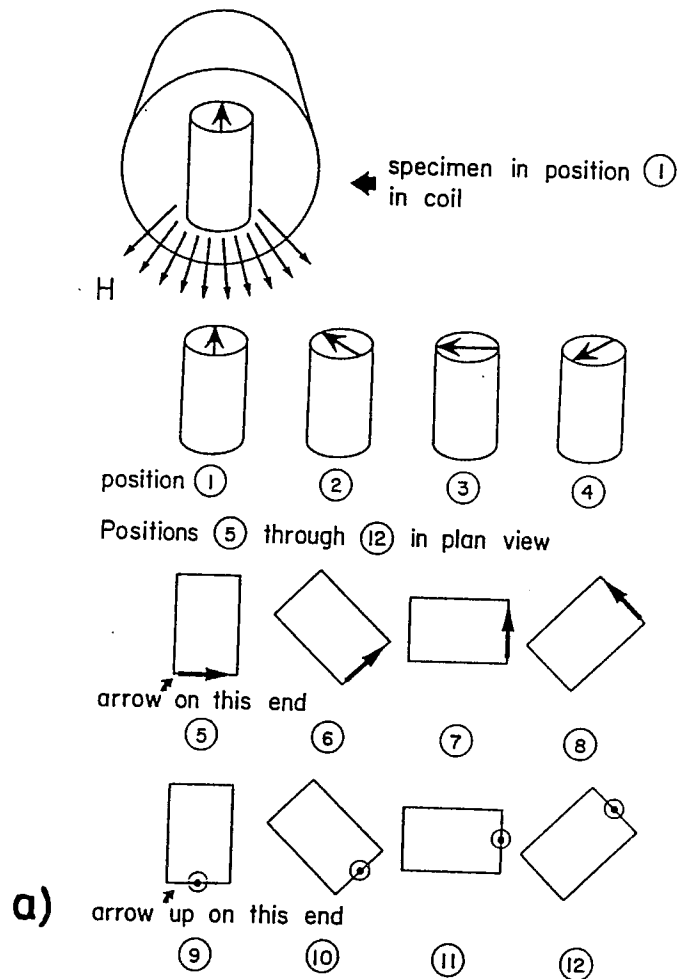
determine bulk susceptibility in this study. The relative measurement error for MS was less than 2-3 % for samples of susceptibility of order  $10^{-5}$ .

The AMS was measured with the use of Stupavsky' (1984) procedure in 12 positions (9 different positions, 3 repeated, with 1 measurement in each position) shown on Fig. 9.3a. Directions of applied field with respect to sample coordinate system are given on the stereoplot (Fig. 9.3b).

The coil measured the intensity of the component of induced magnetization along the direction of applied field, therefore at least 6 positions were necessary to determine the components of  $3 \times 3$  symmetrical tensor. The choice of 12 positions (9 different) helped to increase the accuracy of fitting the anisotropy tensor to data and gave the opportunity to estimate the error of estimation of the components of the anisotropy tensor.

This design of chosen applied field directions is similar to that of Girdler (1961) and a method analogous to the least squares estimate for anisotropy tensor is used to calculate principal axes of the tensor and their directions. The SI-2 algorithm calculates also the 95% confidence limit for the orientation of each axis ( $R_{95}$  angle) and the standard deviation for each principal susceptibility.

However, this method does not follow the estimation method proposed by Hext (1963). The error estimation algorithm used in SI-2 is based rather on the comparison of the results of calculation principal axes, when two sets of 6 measurements are



### Directions of axes of applied field in AMS measurements

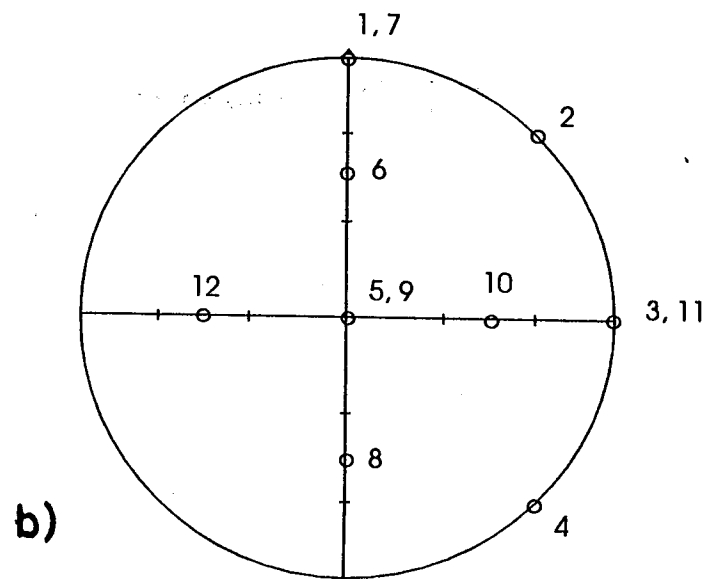


Fig. 9.3. An orientation of magnetic field with respect to a sample during AMS measurements.

a) 12 orientations of samples with respect to magnetic field that is applied along the axis of the coil.

b) the orientations of the magnetic field with respect to sample coordinates on the stereoplot.

used (from 12 measurements available). It can be the source of unrealistically large  $R_{95}$  values (usually 45 - 90°!) for the directions of two principal values which are very similar in magnitude (the oblate or the prolate case).

The chosen design of directions used in Stupavsky' (1984) applied field axes is not "rotational" (Hext, 1963), therefore Hext's formulae for a given design could be extremely complicated.



## Chapter 10.

### Results of AMS studies in the area.

#### 10.1. Earlier contributions to MS and AMS studies in the area.

Magnetic susceptibility and AMS fabric were previously studied at the margins of Quetico Belt in Calm Lake - Perch Lake area by Sarvas (1988) and in Kashabowie - Huronian Lake area by Spark (1991). Spark performed an MS survey with portable susceptibility meter (Czech Geophysica KT-2) along Kashabowie - Huronian Lake traverse. He also determined AMS fabric for 57 samples from the area with the use of SI-2 susceptibility meter (the same that was used in this study). The results (Borradaile and Spark, 1991) did not indicate any distinct magnetic isograds, e.g. "magnetite out" as found elsewhere by Rochette (1987b) with increasing metamorphic grade. Measured bulk susceptibility values were of  $3-4 \cdot 10^{-4}$  SI vol. for metasediments and ranged from  $2 \cdot 10^{-4}$  to  $8 \cdot 10^{-4}$  for metavolcanics.

The susceptibility variation were interpreted as solely due to lithological changes along the traverse. Borradaile and Spark (1991) showed that magnetite is not the major susceptibility contributor in the area, especially in metasediments, but MS is controlled by biotite and chlorite.

In Calm Lake - Perch Lake area the sampling in the area

done by Sarvas (1988) gave about 400 cylindrical samples and their AMS were determined with the SI-1 Sapphire Instrument susceptibility meter. SI-1 was the portable version of SI-2 coil, without PC computer interface. The results of AMS were accepted for 198 samples through the area (series PS\*) and 42 samples from fold closures (FA, FB series) and beds with refracted cleavage (PLR series). Borradaile and Sarvas (1990) and Borradaile et al. (1988) accepted only samples with very high principal axis direction accuracy ( $r_{95} < 5^\circ$ ) and sufficiently high susceptibility  $\chi > 6.2 \cdot 10^{-5}$  SI vol.

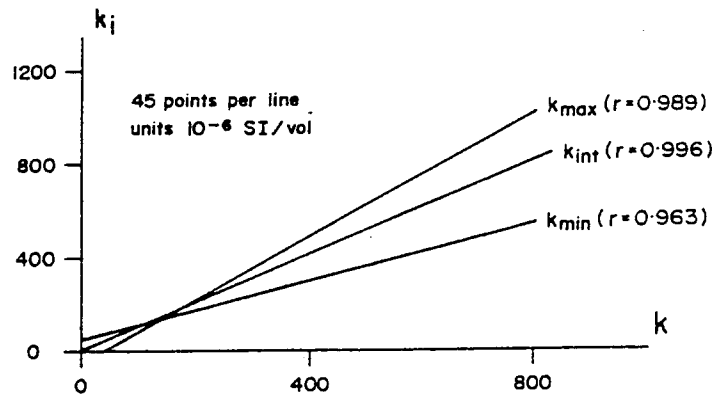
The magnetic minerals contributing to overall susceptibility were found to be magnetite (<2% wt) and paramagnetic sheet silicates (based on the study of separated phases from 3 samples). The authors (Borradaile and Sarvas, 1990) disregarded pyrrhotite contribution to the susceptibility as minor. However, they did not have access to equipment capable of studying remanence and this study revealed significant contributions from pyrrhotite to magnetic remanence. Thermomagnetic curves for 4 samples shown the presence only pyrrhotite as the magnetic phases carrying isothermal remanence (see chapter 6). However, the other samples could be mostly magnetite - bearing.

Some estimation of the multi-mineral contribution to AMS was performed with the use of the Henry (1983) plot of principal susceptibility versus mean susceptibility. The principal susceptibilities lines (fitted to data from 45 similar

greywackes) did not intersect in one common point, which usually suggests more than one mineral phase contributing to AMS (Sarvas, 1988, Fig. 10.1). However Henry's method was originally proposed for samples of a similar mineralogical composition of all samples (they came from a single handspecimen). That constraint seems unlikely to be realized in this case. Samples in Sarvas' (1988) study were taken from different outcrops of metasediments of low metamorphic grade. The inaccuracy of fitting the linear function to the experimental data could also effect the position of points of intersections.

Therefore the use of Henry's method cannot be very conclusive in a case of a set of samples from **different** locations.

The distribution of AMS fabric and bulk magnetic susceptibility data are reviewed in next sections when compared to AMS results from this study.



a) Values of principal susceptibilities ( $k_1$ ), and mean susceptibility ( $k$ ) for 45 similar greywackes. The correlation coefficients are shown each line for each of the principal values. The correlations are significant at the 95% level. If a single source of magnetic anisotropy is present the three lines should intersect at a single point (according to Henry, 1983) representing a theoretical, isotropic fabric with  $k_{\max} = k_{\text{int}} = k_{\min} = k$ .

Principal magnetic suscept. versus mean Atikokan area (N=226)

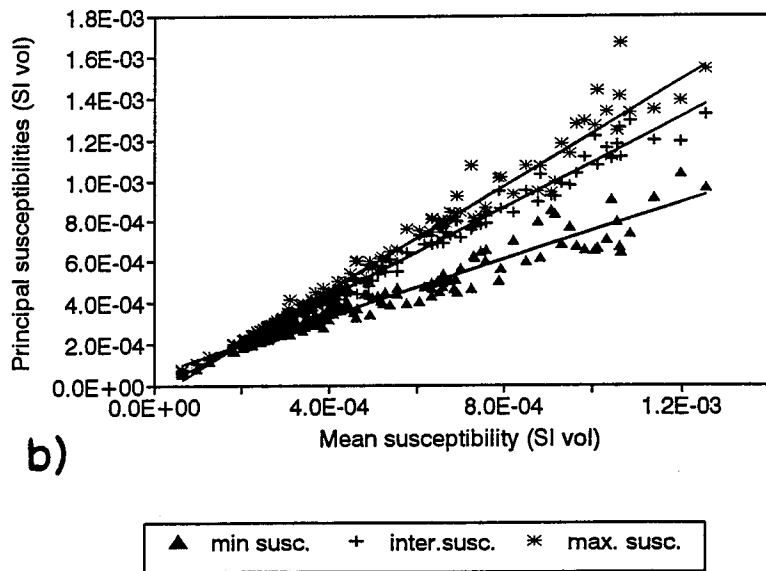


Fig. 10.1. The correlation between principal susceptibilities for metasediments from Atikokan area. a) 45 greywackes from Calm L. - Perch L. area. (from Borradaile and Sarvas, 1990). b) all 226 metasedimentary samples from Atikokan area. Lines do not transect in one point mainly due to variations in composition (see discussion in the text).

## 10.2. Sampling and selection of results in this study.

Kashabowie Lake - Huronian Lake traverse was revisited in this study to collect some additional material for NRM and anisotropy of ARM studies. The additional drilling of previously collected (Spark, 1991) hand samples was also performed. A new set of total 119 cores was prepared for further studies. Therefore additional MS and AMS determination were conducted on this material.

Anisotropy of magnetic susceptibility was measured for all 119 samples with SI-2 apparatus according to Stupavsky's (1984) 12 positions procedure without repetitions.

The accuracy of estimation of principal susceptibilities was up to 5% for some samples with average of 1-2%. The accuracy for the direction of the axes varied due to the shape of susceptibility ellipsoid. For almost uniaxial oblate ellipsoid the  $r_{95}$  angle (the angular error on the 95% confidence limit) could have values up to  $90^\circ$  for  $\chi_{\max}$  and  $\chi_{\text{int}}$ . There were also cases where both  $\chi_{\max}$  and  $\chi_{\min}$  were poorly defined. In cases where  $r_{95}$  was larger than  $20^\circ$ , the given principal axis data were rejected. There was usually a correlation between large values of  $r_{95}$  and standard deviation for principal susceptibility values. After evaluating the AMS data only 81 directions of  $\chi_{\min}$  and 61 directions of  $\chi_{\max}$  were accepted (appendix B).

These criteria were used also for AMS and anisotropy of ARM data for the other collections.

Most metasedimentary samples collected along the Hwy 11 from Atikokan to Huronian Lake through the zone of high metamorphic grade (total of 195) had their anisotropy of magnetic susceptibility studied **prior** to the AF demagnetization, but **after** the measurement of the initial NRM in samples. The procedure of AMS measurement does not disturb the magnetic remanence of samples as the applied field is approximately 0.05 mT and the minimum field chosen for AF demagnetization treatment was 1.5 mT.

The directions of maximum and minimum principal susceptibilities were studied on equal-area projection plot (in the same way as tectonic fabric). Their distribution was analyzed by two algorithms: counting and PCA in SpheriStat program (appendix E).

The problem remains, as to how to define the measurement error for the counting procedure to be easily comparable to an error ellipse from the PCA method. Therefore for comparison of different fabrics the eigenvector analysis results are chosen. Usually the 95% confidence cone for eigenvector analysis includes the position of contoured peak, therefore the choice between each method results seems to be insignificant in most cases.

### 10.3. The bulk magnetic susceptibility results.

The bulk mean susceptibility data for Calm Lake - Perch Lake traverse replotted after Sarvas (1988) do not show any substantial changes of susceptibility along the transect (Fig. 10.2). Susceptibilities are of order  $4 - 8 \cdot 10^{-4}$  SI vol. (mean  $SI = 5.3 \cdot 10^{-4} \pm 1.9 \cdot 10^{-3}$ ,  $N=199$ ) without any distinct zones of higher susceptibility (peaks of high MS were only noticed in single outcrops). It suggests that susceptibility is mainly controlled by phyllosilicates and confirms the minor content of highly susceptible ferrimagnetic minerals. The MS distribution in low metamorphic grade metasediments east of Atikokan is similar to that from Calm Lake - Perch Lake area (Fig. 10.3).

In the higher grade metasediments in the interior of the belt the bulk magnetic susceptibility calculated as the geometric mean of principal susceptibilities was of order  $2 \cdot 10^{-4}$  to  $10^{-3}$  SI vol. for all but 6 samples (mean  $MS = 7.1 \cdot 10^{-4} \pm 3.1 \cdot 10^{-3}$  for  $N=201$  samples, Fig. 10.3 and appendix B). No trend in susceptibility changes or metamorphic isograds along the traverse were noticed. The only higher susceptibility values ( $3 - 5 \cdot 10^{-3}$ ) were measured for the amphibolite sample (TWA 15). The least susceptible samples ( $10^{-5}$  SI vol.) came from the nebulitic intrusion near Eve Lake.

It is consistent with recognition that magnetite is mainly absent from the composition. Borradaile (1987) showed that small variations in magnetite concentration (around 1% wt base

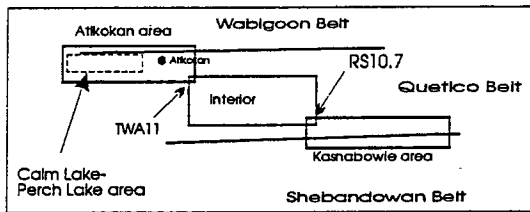
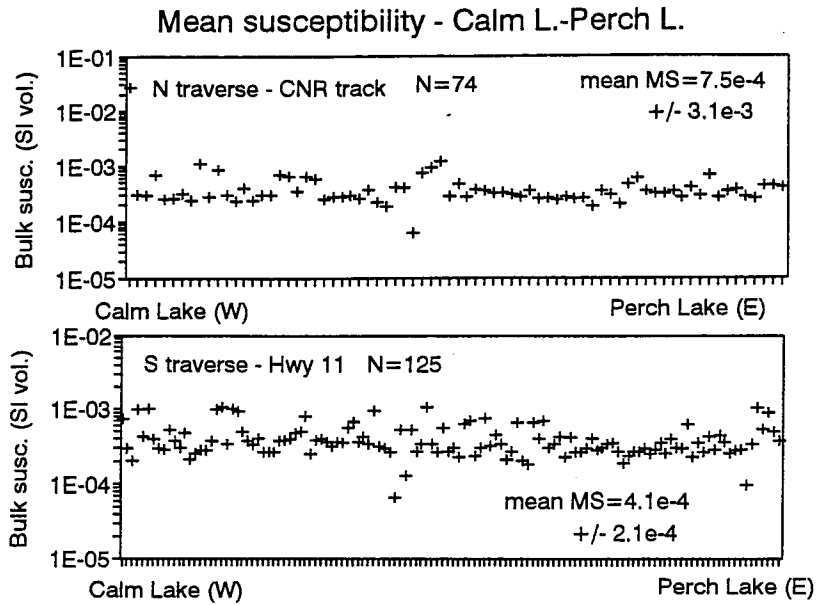
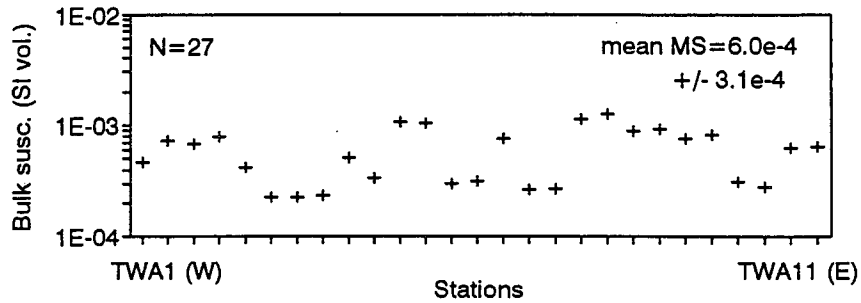


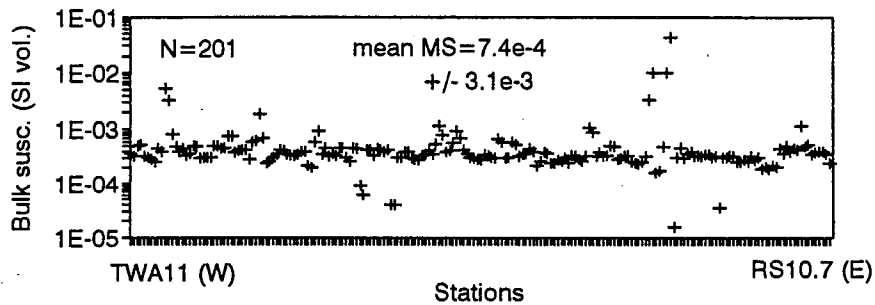
Fig. 10.2. Variations of magnetic susceptibility along the traverse in Calm Lake - Perch Lake area. Two traverses are mapped: North - along railway track and South - along highway 11. Note little variations in MS in metasediments. The only one high MS came from metavolcanics (station PST1), data from Sarvas, (1988).



Mean susceptibility - east of Atikokan  
low grade metasediments



Mean susceptibility - interior of  
Quetico Belt



Mean susceptibility - Kashabowie Lake -  
- Huronian Lake - low grade rocks

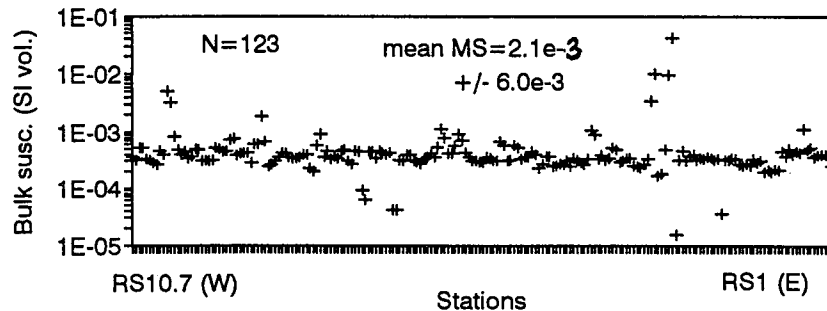


Fig. 10.3. Variations in magnetic susceptibilities along the traverse Atikokan - Huronian Lake. Subareas are chosen according to metamorphic grade (see sketch map on Fig 10.2). High values of MS are characteristic for magnetite bearing rocks and metavolcanics in general. Some data from Kashabowie area from Spark (1990)

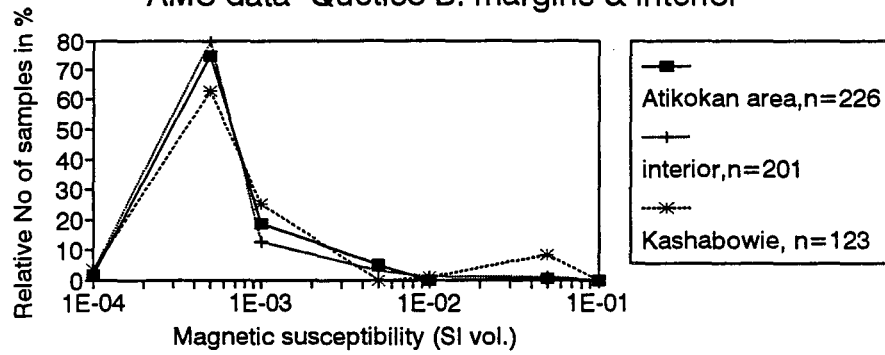
concentration) would be reflected in susceptibility. The sampling procedure in the field (sampling more mafic parts of outcrops) also ensured rather little variable composition of para- and ferromagnetic minerals.

The high values of MS for outcrops RS11.7 and TW4 in the migmatite zone can be caused by locally present, randomly distributed magnetite or high content of paramagnetic minerals due to low intensities of NRM and imposed ARM in tested specimens.

In low grade metasediments and metavolcanics at the Kashabowie - Huronian Lake area combined MS values (N =57 samples from Spark, 1991 study and N=66 from this study) are in the range  $10^{-4}$  to  $5 \cdot 10^{-2}$  for metavolcanics (high values are characteristic for outcrops RS4. - RS4.1, see Fig. 10.3 and appendix B). The large scatter is due to variation in Fe - silicates and magnetite content. In metasediments, the values of MS are much more uniform, usually of order  $10^{-4}$ , due to low content of magnetite.

The histograms of MS values (Fig. 10.4) indicate that both metavolcanics and the highly strained margin of the Quetico Belt near Atikokan had higher values of susceptibility than metasediments in Calm Lake - Perch Lake area and the interior of Quetico Belt. It can be caused by the higher content of magnetite (in metavolcanics) or phyllosilicates (in chlorite schist near Atikokan) when compared to more quartz- rich rocks from the other two areas.

Distribution of magn. susc.  
AMS data -Quetico B. margins & interior



AMS data -Quetico B. margins & interior

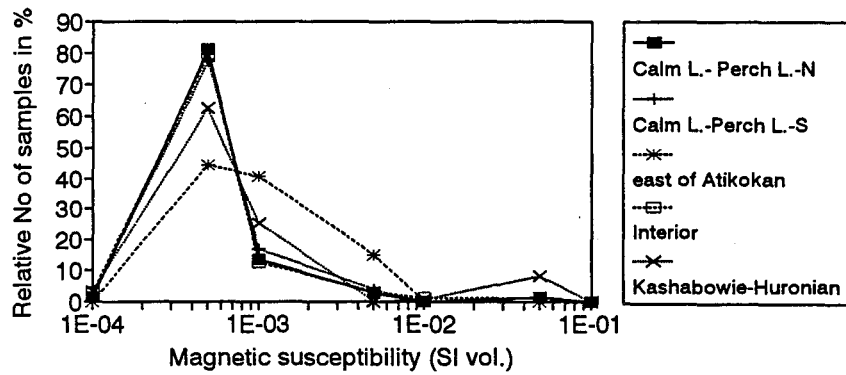


Fig. 10.4. A histogram of magnetic susceptibilities for studied areas. Windows  $<10^{-4}$ ;  $10^{-4}$ - $5 \cdot 10^{-4}$ ;  $5 \cdot 10^{-4}$ - $10^{-3}$ ;  $10^{-3}$ - $5 \cdot 10^{-3}$ ;  $5 \cdot 10^{-3}$ - $10^{-2}$ ;  $10^{-2}$ - $5 \cdot 10^{-2}$ ;  $5 \cdot 10^{-2}$ - $10^{-1}$  were used.

The most susceptible samples come from metavolcanics and high strained metasediments east of Atikokan.

## 10.4. Distribution of AMS anisotropy axes.

**Magnetic foliation - minimum axes of AMS.**

Poles to magnetic foliations were plotted for samples from all three suites, in the similar method as for tectonic fabrics. However the data from Calm lake - Perch Lake area (within low grade metasediments in the Atikokan area) were also considered separately, as the magnetic fabric was almost perfectly oblate there and magnetic lineations were poorly defined.

Magnetic fabric in the Calm Lake - Perch Lake showed that the orientation of magnetic foliation was uniform through the region (for N=116 samples, pole to plane: 163/17) with minimum susceptibility  $\chi_{\min}$  perpendicular to mean  $S_1$  cleavage (Borradaile et al., 1988). Data from larger collection (N=198, after Sarvas, 1988), without samples from fold closures gave the magnetic foliation almost vertical (Table 10.5, Fig. 10.6a).

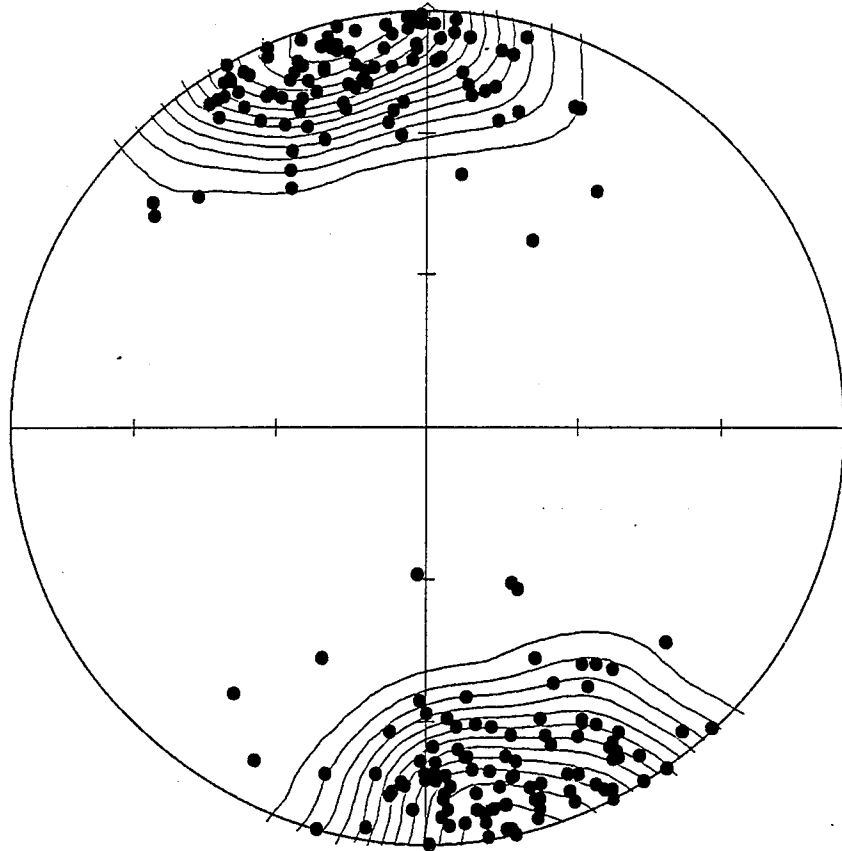
Table 10.5. The orientation of mean position of AMS minimum axes.

Area	N	Contoured peak	PCA - pole to plane
Calm L.-Perch L.	198	348/3 (24 $\sigma$ )	168/2 (3/3)
east of Atikokan	24	171/2 (13 $\sigma$ )	351/0 (8/6)
Atikokan area-total	222	351/2 (27 $\sigma$ )	168/2 (3/3)
Interior	168	164/20 (14 $\sigma$ )	165/23 (9/4)
Kashabowie area	91	155/5 (25 $\sigma$ )	154/3 (5/3)
Total: all 3 areas	481	163/8 (25 $\sigma$ )	164/7 (3/2)

Samples from chlorite schist rocks east of Atikokan have also almost vertical AMS foliation (Fig. 10.6b) but the

Fig. 10.6a. Data from Sarvas (1988).

AMS minimum axes - Calm Lake - Perch Lake area  
low grade metasediments



$N = 198$

$k = 46.00$

$(\text{Peak} - E)/\text{Sigma} = 23.7$

Peak position :  $347.5^\circ / 2.8^\circ$

$E = 4.30$

$\text{Sigma} = 1.43$

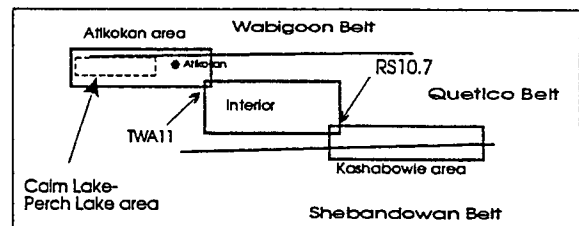
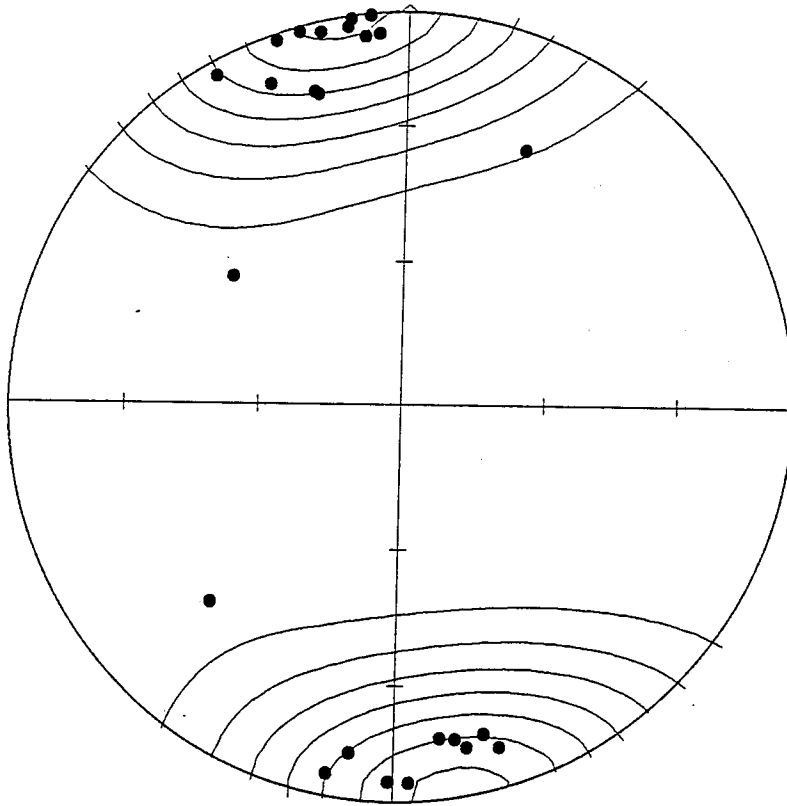


Fig. 10.6b.

AMS minimum axes - east of Atikokan area  
low grade metasediments



$N = 24$

$E = 3.27$

$k = 7.33$

$\text{Sigma} = 1.09$

$(\text{Peak} - E)/\text{Sigma} = 12.8$

Peak position :  $170.5^\circ / 1.6^\circ$

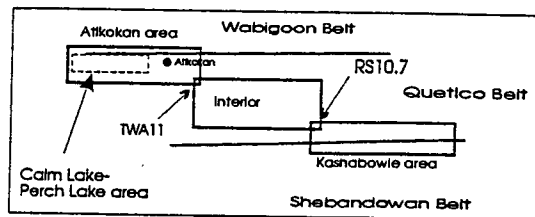
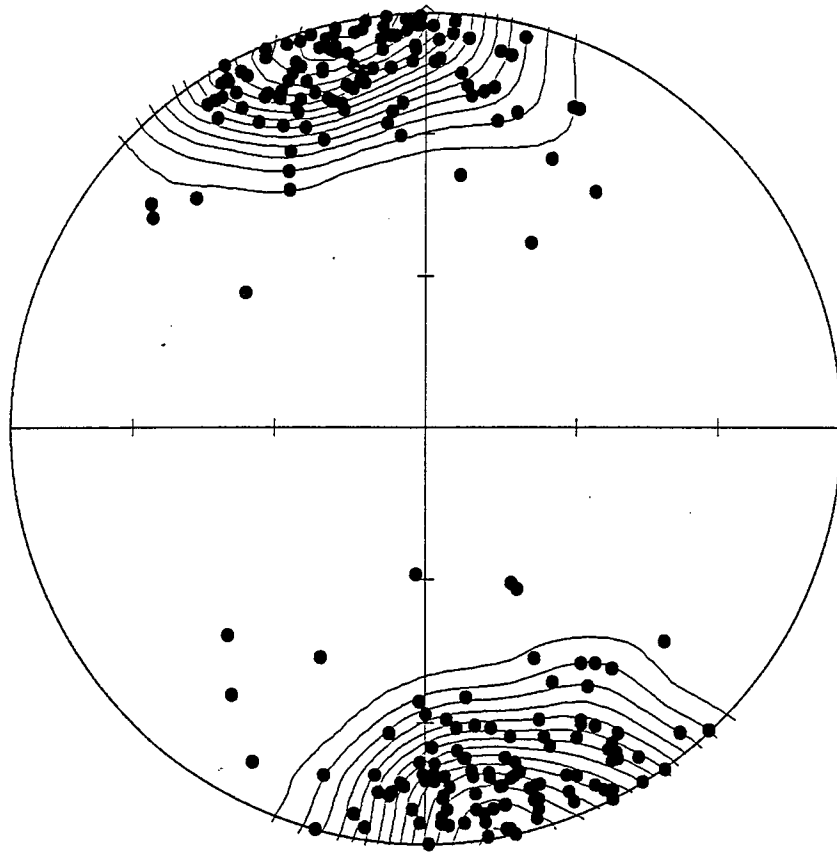


Fig. 10.6c. (combined data from Fig. 10.6a and b).

AMS minimum axes - Atikokan area  
low grade metasediments



$N = 222$

$E = 4.32$

$k = 51.33$

$\text{Sigma} = 1.44$

$(\text{Peak} - E)/\text{Sigma} = 26.6$

Peak position :  $350.5^\circ / 1.6^\circ$

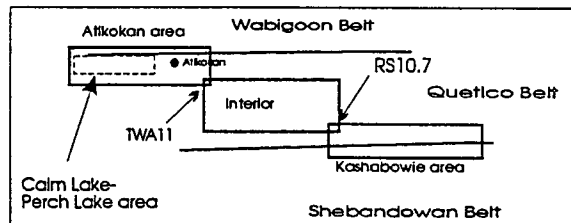
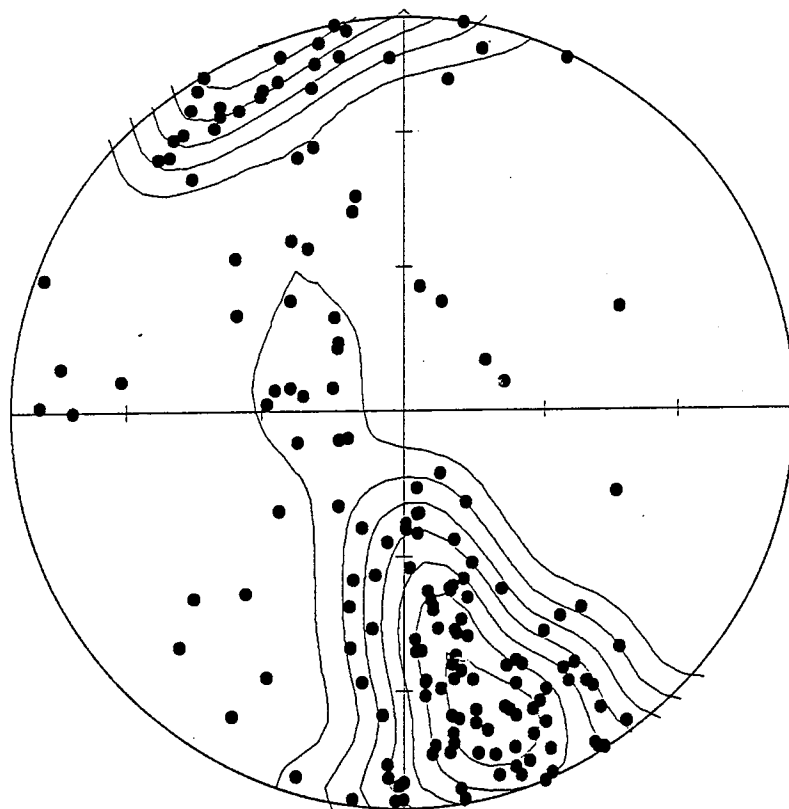


Fig. 10.6d.

AMS minimum axes - the interior of Quetico belt  
medium and high grade metasediments and intrusives



$N = 168$

$E = 4.27$

$k = 39.33$

$\text{Sigma} = 1.42$

$(\text{Peak} - E)/\text{Sigma} = 13.7$

Peak position :  $164.1^\circ / 20.2^\circ$

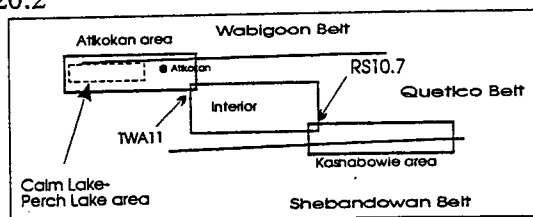
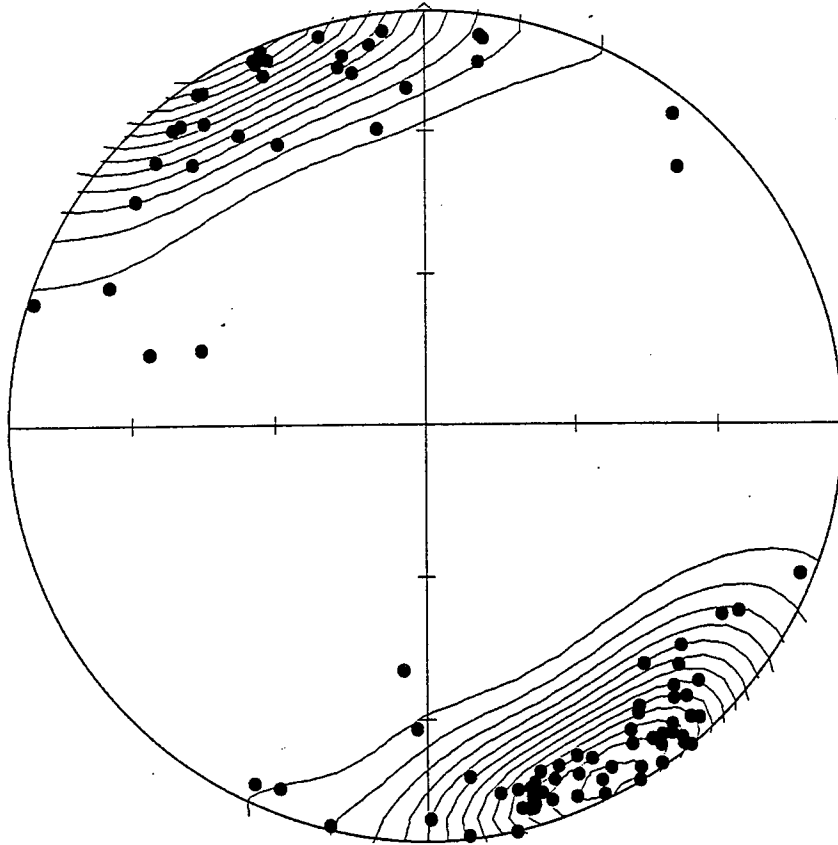




Fig. 10.6e. (data partly from Spark, 1990)

AMS minimum axes - Kashabowie - Huronian L. area  
 low grade metasediments and metavolcanics



$N = 91$

$E = 4.10$

$k = 22.22$

$\text{Sigma} = 1.37$

$(\text{Peak} - E)/\text{Sigma} = 25.0$

Peak position :  $154.8^\circ / 5.1^\circ$

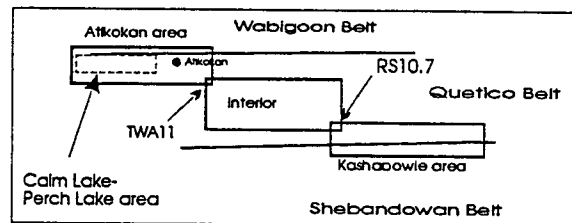
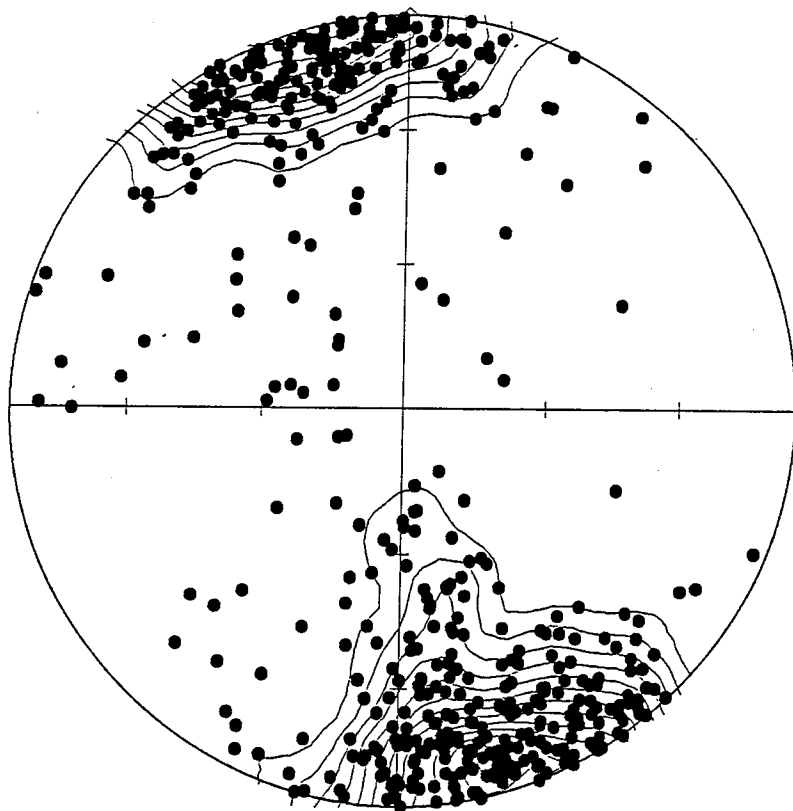


Fig. 10.6f. (combined data from fig. c, d,e).

AMS minimum axes - all areas



$N = 481$

$E = 4.42$

$k = 108.89$

$\text{Sigma} = 1.47$

$(\text{Peak} - E)/\text{Sigma} = 24.9$

Peak position :  $162.6^\circ / 7.6^\circ$

direction of dip for an AMS foliation plane varies from one outcrop to another (Fig. 10.10, outcrops near Atikokan).

In the interior of the belt the AMS determination was performed for 175 samples and detailed results of calculated principal susceptibilities and their directions are listed in appendix B. The accuracy of measurement of principal susceptibilities was at the range from 2% to 7% (appendix B). It can be partly due to the influence of field frequency on pyrrhotite in the samples and partly due to quite low susceptibilities.

The mean foliation plane for the rocks from the interior of the belt (for N=168 samples) has similar strike to that from Atikokan area but is much less steep (dip of 70°) than in Atikokan area (Fig. 10.6d), like for a mean schistosity planes. The clustering of AMS minimum axes is weaker than at belt margins (Table 10.5). A few individual samples had their AMS minimum axes oriented in the directions of overall mean direction of maximum or intermediate axes (mainly those from the centre of the belt). Some of them have weak anisotropy (amphibolite- rich ones - magnetite bearing), which may indicate the contribution of inverse AMS fabric from SD magnetite. Some others have weak overall susceptibility, therefore their directions of axes are poorly defined.

In low grade metasediments and metavolcanics in Kashabowie - Huronian Lake area the principal axes of susceptibility showed tight clustering for  $\chi_{\min}$ , with a steep mean magnetic foliation

plane (dip of  $85^\circ$ ), for  $N=91$  samples (Table 10.5, Fig. 10.6e). A few samples west of Kashabowie had their AMS maximum axes oriented more like intermediate or maximum axes of other samples but they had usually low susceptibility what can not explained by the effect of the presence of SD magnetite.

The distribution of AMS minimum axes for the whole area ( $N=481$ ) reflects the consistent ENE-WSW direction of magnetic foliation through the area and intermediate value ( $82^\circ$  to the N) of the dip of mean magnetic foliation is a result of changes of dip from one suite to another (Fig. 10.6f, Table 10.5).

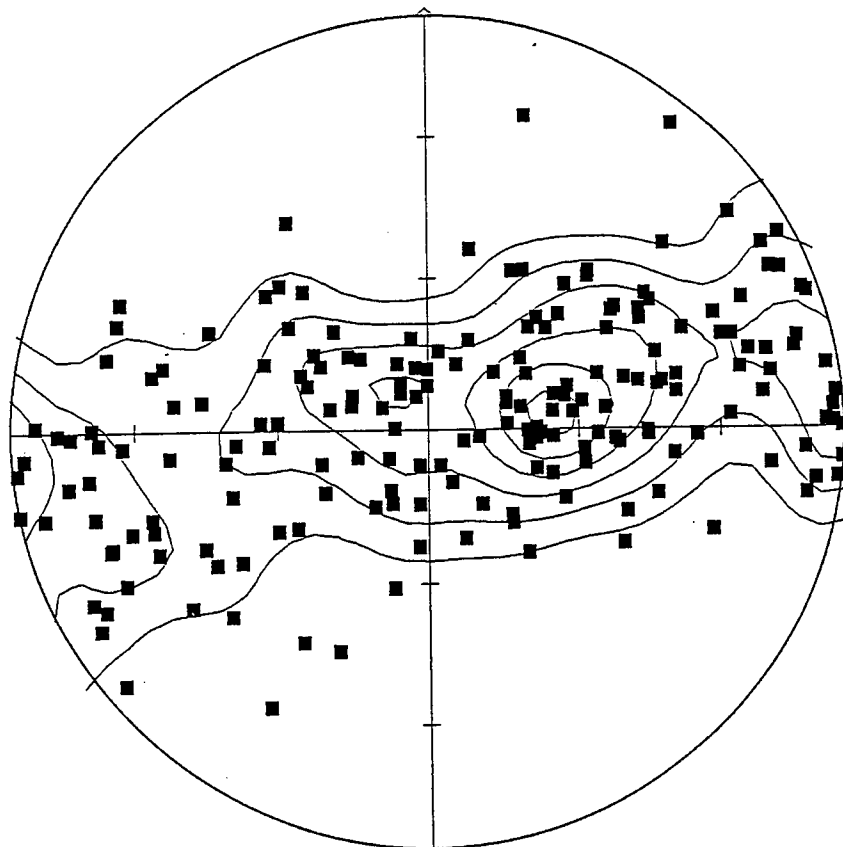
#### **Magnetic lineations - maximum axes of AMS.**

In Perch Lake - Calm Lake area AMS maximum axes do not cluster, but show a local grouping in a girdle along the magnetic foliation plane (Fig.10.7a, Table 10.8). No significant correlation with the  $S_0/S_1$  lineations (Fig. 10.7a,  $S_0/S_1$  stereonet, from Borradaile et al., 1990) or the orientation of fold axes was found. However, the accuracy of determination of the direction of  $\chi_{\max}$  is usually low due to almost uniaxial oblate magnetic fabric.

The orientation of maximum susceptibility along the hinge axis of the folds in the fold closure (FA and FB series) was interpreted as a possible effect of superposition of the initial sedimentary oblate magnetic fabric parallel to bedding with later tectonically driven magnetic fabric along the cleavage plane (Borradaile et al., 1988).

Fig. 10.7a. Data from Sarvas (1988).

AMS maximum axes - Calm Lake - Perch Lake area  
low grade metasediments



$N = 196$

$E = 4.30$

$k = 45.56$

$\text{Sigma} = 1.43$

$(\text{Peak} - E)/\text{Sigma} = 10.8$

Peak position :  $78.7^\circ / 66.9^\circ$

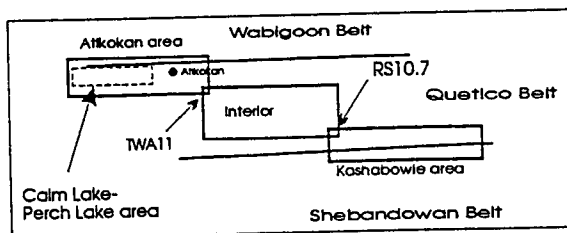
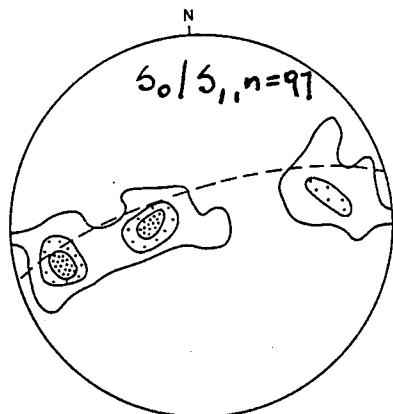
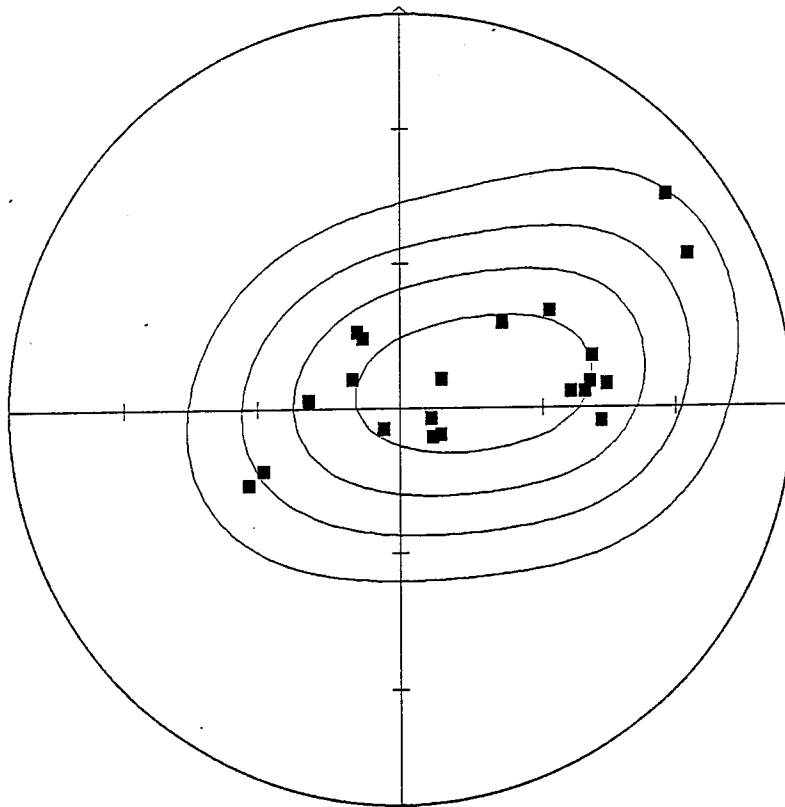


Fig. 10.7b.

AMS maximum axes - east of Atikokan area  
low grade metasediments



$N = 21$

$k = 6.67$

$(\text{Peak} - E)/\text{Sigma} = 7.4$

Peak position :  $71.6^\circ / 75.7^\circ$

$E = 3.15$

$\text{Sigma} = 1.05$

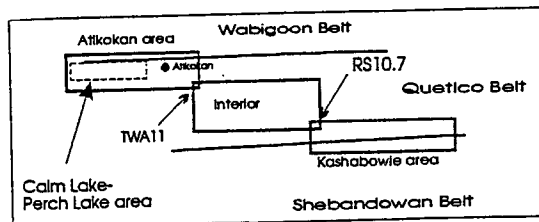
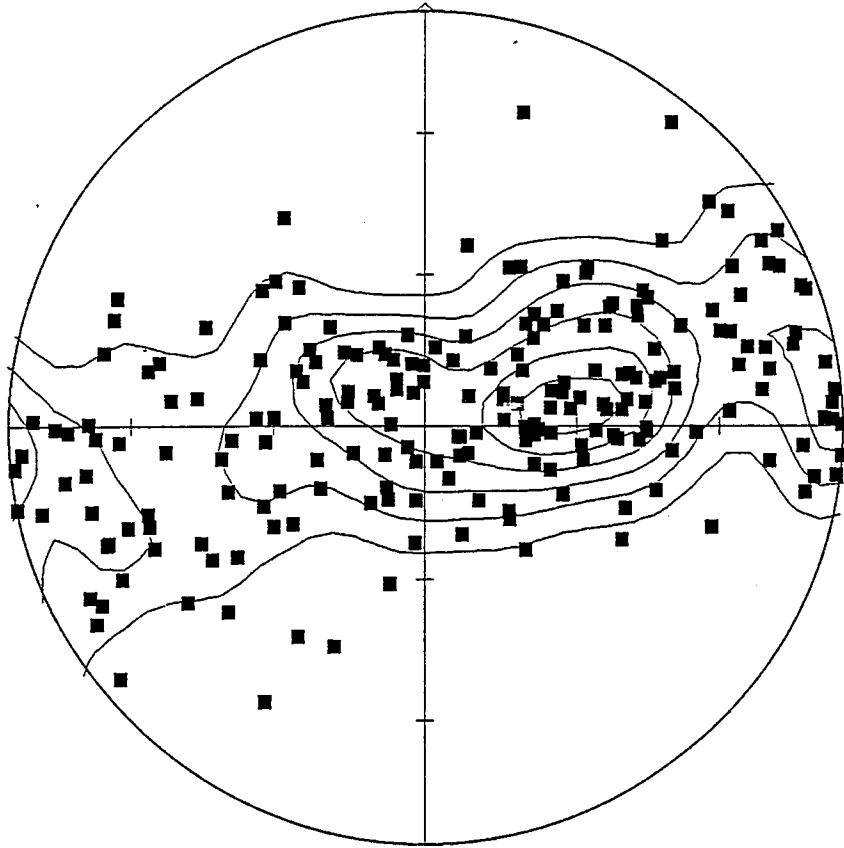


Fig. 10.7c. (combined data from Fig. 10.6a and b).

AMS maximum axes - Atikokan area  
 low grade metasediments



$N = 217$

$E = 4.32$

$k = 50.22$

$\text{Sigma} = 1.44$

$(\text{Peak} - E)/\text{Sigma} = 11.2$

Peak position :  $80.5^\circ / 62.4^\circ$

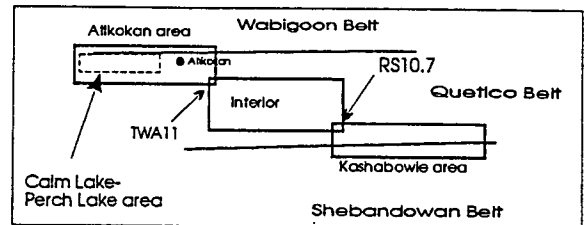
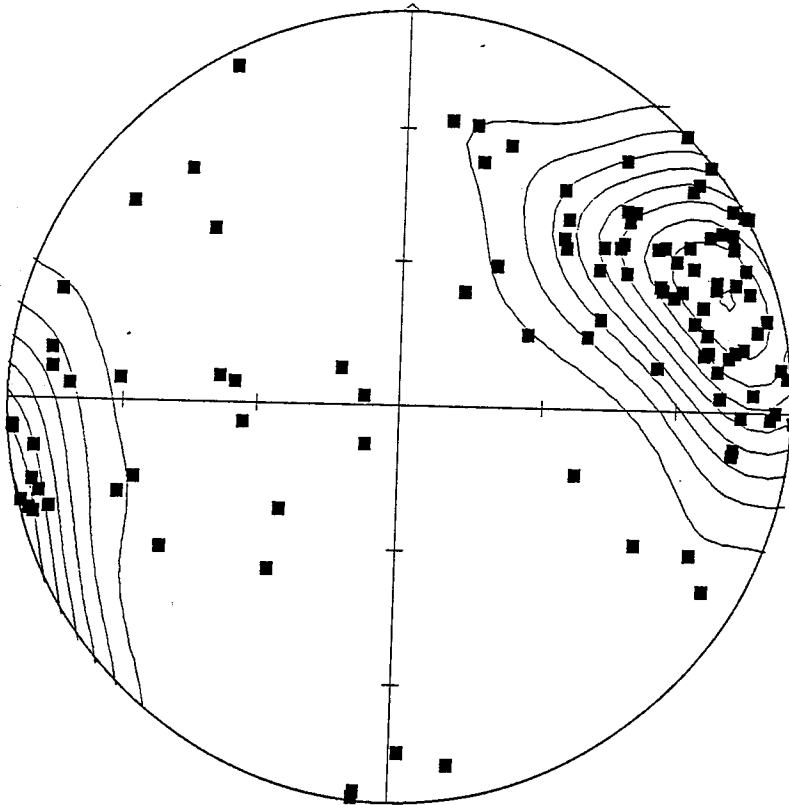


Fig. 10.7d.

AMS maximum axes - the interior of Quetico Belt  
medium to high grade metasediments and intrusives



$N = 106$

$E = 4.15$

$k = 25.56$

$\text{Sigma} = 1.38$

$(\text{Peak} - E)/\text{Sigma} = 16.2$

Peak position :  $71.6^\circ / 13.2^\circ$

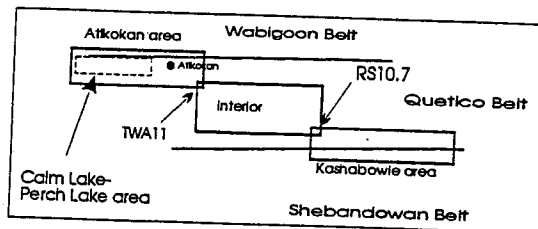
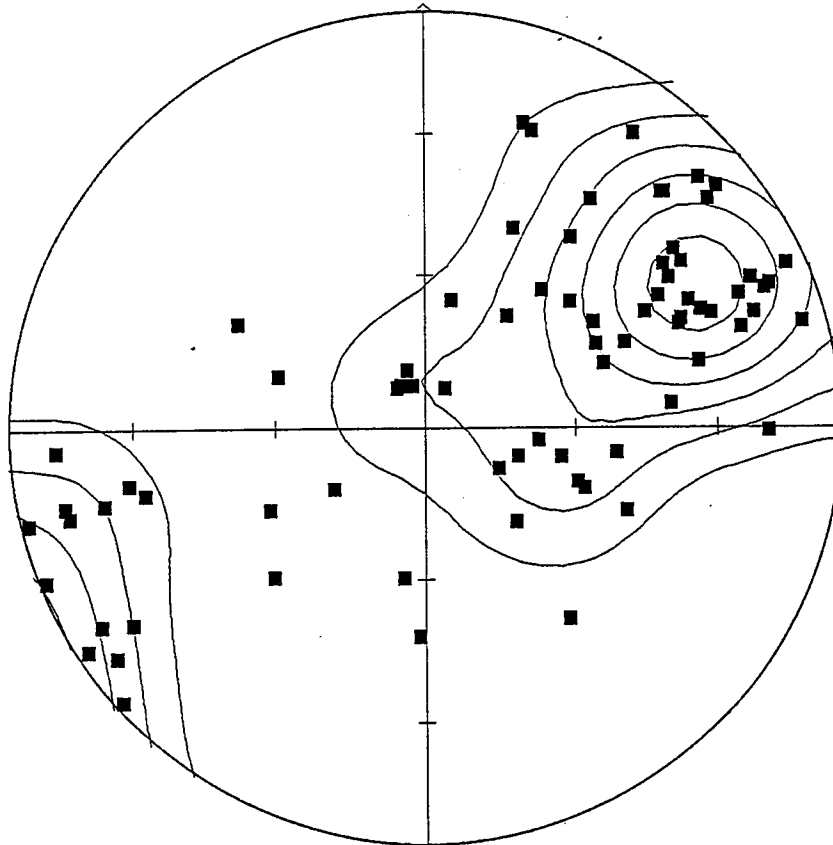




Fig. 10.7e. (data partly from Spark, 1990).

AMS maximum axes - Kashabowie - Huronian L. area  
 low grade metasediments and metavolcanics



$N = 77$

$E = 4.03$

$k = 19.11$

$\text{Sigma} = 1.34$

$(\text{Peak} - E)/\text{Sigma} = 11.5$

Peak position :  $63.4^\circ / 26.4^\circ$

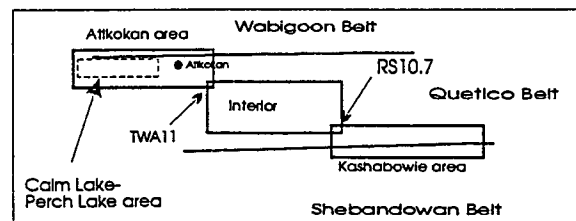
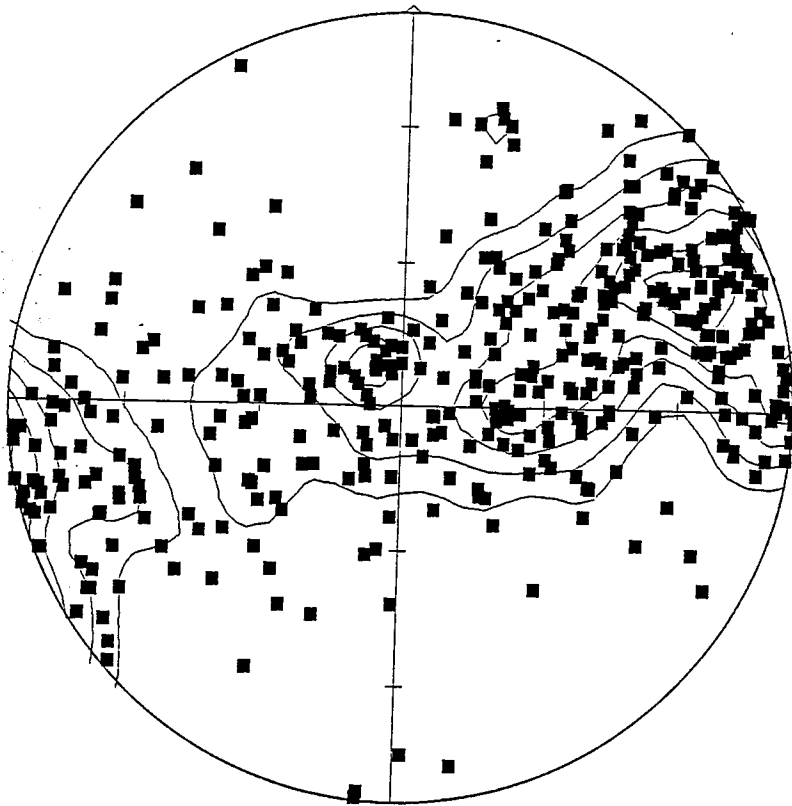


Fig. 10.7f. (combined data from fig. c, d,e).

AMS maximum axes - all areas



$N = 400$

$E = 4.40$

$k = 90.89$

$\text{Sigma} = 1.47$

$(\text{Peak} - E)/\text{Sigma} = 11.5$

Peak position :  $69.0^\circ / 23.7^\circ$

Table 10.8. The orientation of mean AMS maximum axes.

Area	N	Contoured peak	PCA - pole to plane
Calm L.-Perch L.	196	79/67 (11 $\sigma$ )	72/65 (23/4)
east of Atikokan	21	72/76 (7 $\sigma$ )	69/73 (19/6)
Atikokan area-total	217	81/62 (11 $\sigma$ )	72/67 (18/3)
Interior	106	72/13 (16 $\sigma$ )	70/14 (8/5)
Kashabowie area	77	63/26 (12 $\sigma$ )	63/32 (14/5)
Total all areas	400	69/24 (12 $\sigma$ )	70/33 (11/3)

In low grade chlorite schists east of Atikokan the position of AMS maximum axes is also poorly defined as individual directions of AMS lineations are distributed along the magnetic foliation plane (Fig. 10.7b). However the mean directions of AMS lineations are quite steep in Atikokan area (Fig. 10.7a-c , Table 10.8).

Within the interior of the belt AMS foliations are much less steep, plunging about 13° to ENE (Fig. 10.7d). Some individual inversions between AMS maximum and the other remaining axes were observed for samples from the centre of the belt.

In low grade metavolcanics and metasediments the gentle plunge (26°) of AMS lineations to the ENE also exists (Fig. 10.7e, Table 10.8). The individual AMS lineations are more scatter along the magnetic foliation plane than those for the interior of the belt. Some magnetic lineations are oriented similar to the mean direction of intermediate axes, but not perpendicular to mean magnetic foliation plane. Therefore the hypothesis of inverse AMS fabric (due to magnetite) in

metavolcanic area cannot be supported.

### **Variations of the orientation of magnetic fabrics along traverses.**

The variations of AMS fabric along the traverse from one outcrop to another was also studied, in an addition to fabric plots for each suite. The diagrams of changes of declination and inclination of AMS principal axes along the traverse for two W-E traverses in Calm Lake - Perch Lake area (along CNR track and along Highway 11) as well as for a W-E traverse from Atikokan to Kashabowie Lake along Highway 11 are presented for magnetic foliations and lineations at Fig. 10.9 and 10.10.

In low grade metasediments strikes of AMS foliations group around the mean strike of this fabric. However, the scatter of the AMS foliation directions increases toward the migmatite zone, with generally less steep magnetic foliations (Fig. 10.9).

Magnetic foliations are very steep at low grade rocks near Atikokan (Fig. 10.10 and Map 10.12), but are much more shallow when migmatite zone is entered from Plateau Lake toward Sapawe. They are steepened again around Eva Lake and again gently dipping in granitic zone east of Eva Lake. Further east their dips become more erratic. Strikes of magnetic foliations often are at high angle to the strike of mean AMS foliation for the interior of the belt but they are changing from one outcrop to another.

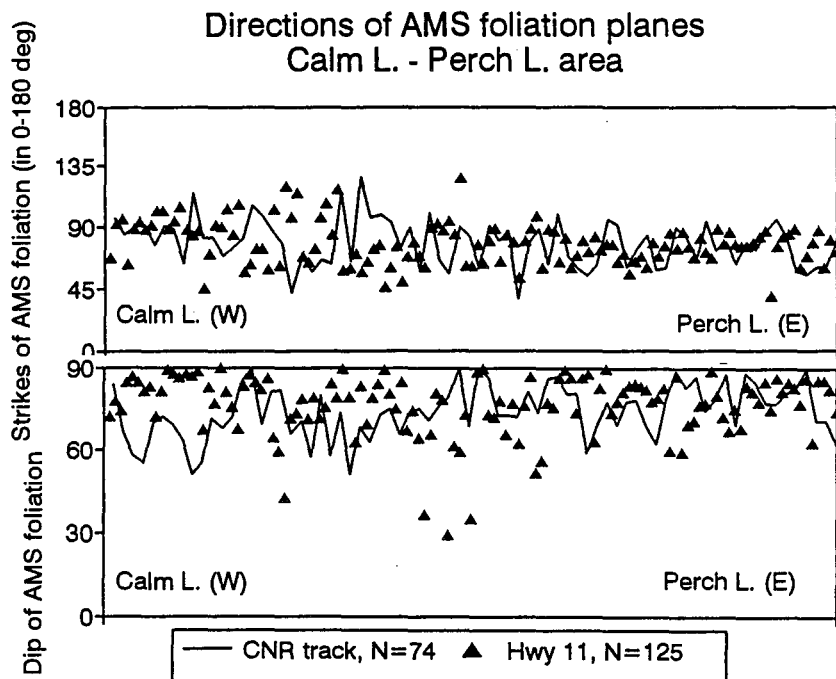


Fig. 10.9. Variations of strikes and dips of AMS foliation planes along traverses in Calm Lake - Perch Lake area. (strikes in 0-180° sector). Data from Sarvas (1988).

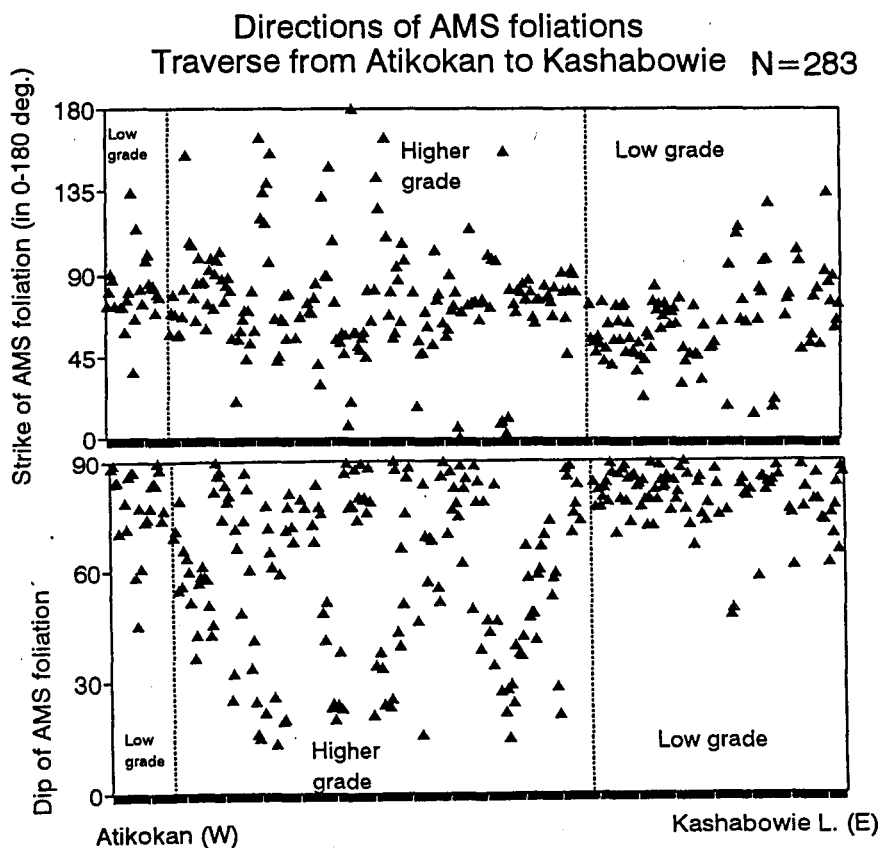


Fig. 10.10. Variations of AMS foliations along Atikokan - Kashabowie Lake traverse.

In low grade metasediments east of Huronian Lake AMS foliation are oriented rather consistently, but in metavolcanic zone they are again more scattered (Fig. 10.10).

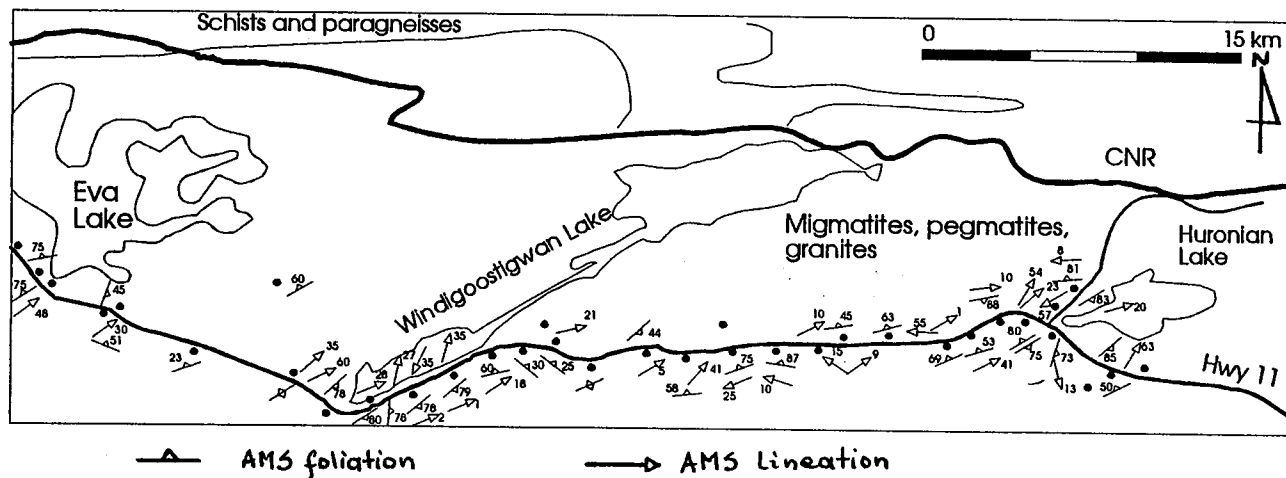
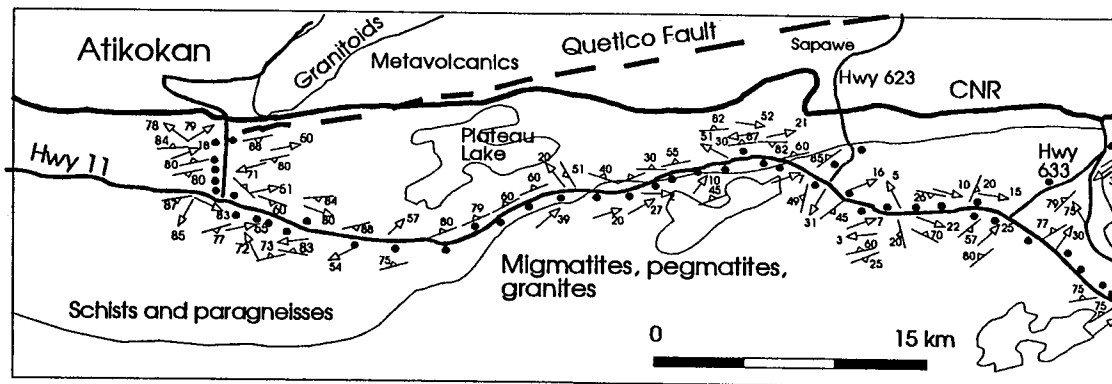
The trends of magnetic lineations in Calm Lake - Perch Lake area are much more uniform along the Hwy 11 traverse than on the contact with Wabigoon metavolcanics along CNR track (Fig. 10.11). However plunges of magnetic foliations in this area show strong local variations. This effect can be explained by the presence of late- tectonic sheath fold structures in the area (Borradaile et al., 1988).

Along the traverse from Atikokan to Kashabowie Lake magnetic lineations directions near Atikokan have rather uniform trends (map - Fig. 10.13) but can plunge both to north-east and south-west. Plunges of magnetic lineations are gentle in migmatite zones and more steep in low grade chlorite - biotite schist and areas with intruded granitoids and pegmatites (Fig. 10.12).

The distribution of AMS lineations becomes more erratic in low grade metavolcanics east of Stetham Lake (Fig. 10.12). Both steep and gently plunging AMS lineations are observed.



Fig. 10.13. Map of distribution of AMS foliations and lineations along Atikokan - Huronian Lake traverse.





## 10.5. The anisotropy ratios and shapes of AMS ellipsoids.

The shape of AMS ellipsoid was characterized in terms of Jelinek plot parameters  $P'$  and  $T$ . The anisotropy parameters were taken under consideration even for these samples that had poorly defined directions of principal axes due to almost perfect oblate AMS fabric. Only when all three AMS principal axes were poorly defined (with  $r_{95} > 20^\circ$ ), were those results rejected.

Table 10.14. Mean values of anisotropy parameters  $P'$  and  $T$ .

The area	N	$P'$ (mean $\pm$ std.dev.)	$T$ (mean $\pm$ std.dev.)
Atikokan area	225	1.36 $\pm$ 0.26	0.55 $\pm$ 0.31
the interior	199	1.44 $\pm$ 1.11	0.42 $\pm$ 0.38
Kashabowie area	123	1.29 $\pm$ 0.33	0.35 $\pm$ 0.43

In low- grade metasediments in Atikokan area (Calm Lake - Perch Lake samples and those east of Atikokan) samples showed strong oblate fabric and substantial anisotropy ratio (mean  $P'=1.36$ , Fig. 10.15a, Table 10.14, typical for anisotropic chlorites and biotites, Borradaile et al., 1987). The highest values of  $P'$  parameters are characteristic for samples from highly sheared area near Quetico Fault (stations TWA1-3, Fig. 10.15b). However, a few prolate fabrics were also observed (Fig. 10.15a, see also Borradaile and Sarvas, 1990). Thermomagnetic curve for one of those samples (PST63) did not reveal the existence of magnetite but pyrrhotite only. Therefore the prolate shape of those fabrics cannot be explained by a substantial content of magnetite.

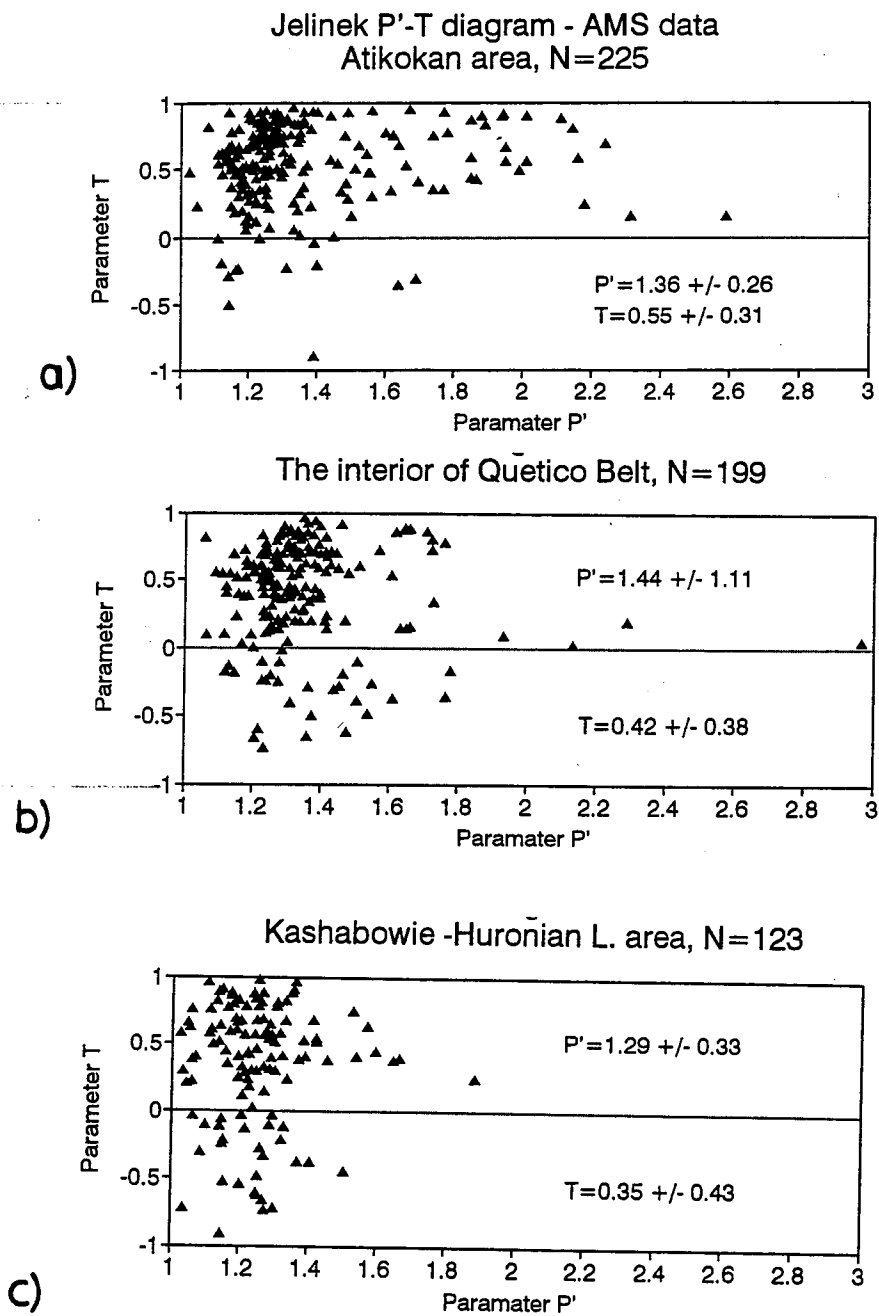


Fig. 10.15. Jelinek P'-T plot for AMS anisotropy parameters for three subareas. Mean values of P' and T for each area are also listed. Note higher values of anisotropy ratio P' in the belt interior and prolate fabric in metavolcanics.

In higher grade metamorphic rocks (amphibolite facies metamorphism) in the centre of the belt anisotropy ratios are slightly higher than for belt margins. The minimum anisotropy ratios  $P'$  are about 1.2, significantly larger than those from belt boundaries and maximum  $P'$  are about 2. The histogram of  $P'$  values reveals that anisotropy ratios for the interior are more tightly grouped than those for Atikokan area (Fig. 10.16).

The  $P'$ - $T$  diagram indicates that most of 199 samples have oblate fabric (Fig. 10.15b). However 28 samples revealed prolate magnetic fabric. When  $P'$ - $T$  plot results are compared to typical anisotropies for chlorite and biotite, observed values of  $T$  parameter for whole sample anisotropy are here somewhat smaller than for biotite (Borradaile et al., 1987), and typical for chlorite and muscovite.

The quantitative mineral composition data are not available for studied samples, but due to lower content of biotite in higher metamorphosed rocks than chlorite-muscovite matrix in greenschists and slightly more random p.c.o. of biotite, its contribution to AMS is smaller (Hrouda, 1982 discussed the correlation between p.c.o. and grain anisotropy).

Prolate fabrics are grouped only in few outcrops: amphibolites in TWA15 - TWA15.5, TWE6A, TWA18A, TWA19.5 and more felsic TWC1 (Fig. 10.17b). These seem to be correlated with later processes of an emplacement of felsic and mafic

Distribution of P' parameter  
AMS data -Quetico B. margins & interior

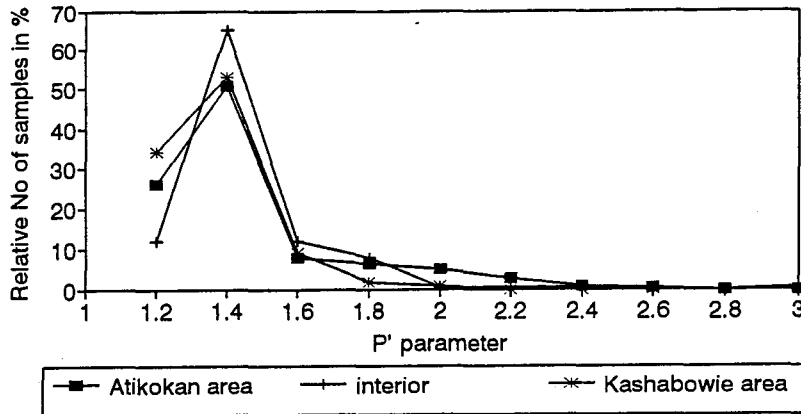


Fig. 10.16. A histogram of a distribution of anisotropy ratio P' for 3 sub-areas. In all 3 areas 45-65% samples have P' value from the range of 1.2 - 1.4 - typical for sheet- silicates. In metavolcanic Kashabowie area there is the largest fraction of low anisotropic AMS ( $P' < 1.2$ ). See text for detailed discussion.

intrusions in the area.

In the Kashabowie area anisotropy parameters  $P'$  and  $T$  plotted on the  $P'$ - $T$  diagram (for  $n=123$  samples) indicate mainly prolate AMS fabric. However, a substantial set (30) of samples with prolate fabric exists (Fig. 10.15c). Values of anisotropy ratio range from 1.05 to 1.9 (mean  $P'=1.29$ , and maximum of  $P'$  distribution for  $P'=1.2-1.4$ ; these are typical values for sheet silicates).

Sample with prolate magnetic fabric (20 overall) grouped mainly in more felsic metavolcanics (Fig. 10.17b). However they were accompanied by samples with oblate fabric in the same outcrops. Four of them had quite high susceptibility (greater than  $10^{-2}$  SI vol., Fig. 10.3) and thermomagnetic curves from the outcrop RS3.5 revealed mainly magnetite as remanence carrier. Therefore the prolate fabric together with low anisotropy can be explained as due to the magnetite content (Borradaile et al., 1987). However no inverse AMS fabric was observed, that suggest that magnetite is not SD. These specimen had also quite high anhysteretic susceptibility and ARM fabric was also mostly prolate. Some more extensive studies of correlation between different fabric will be presented in chapter 13.

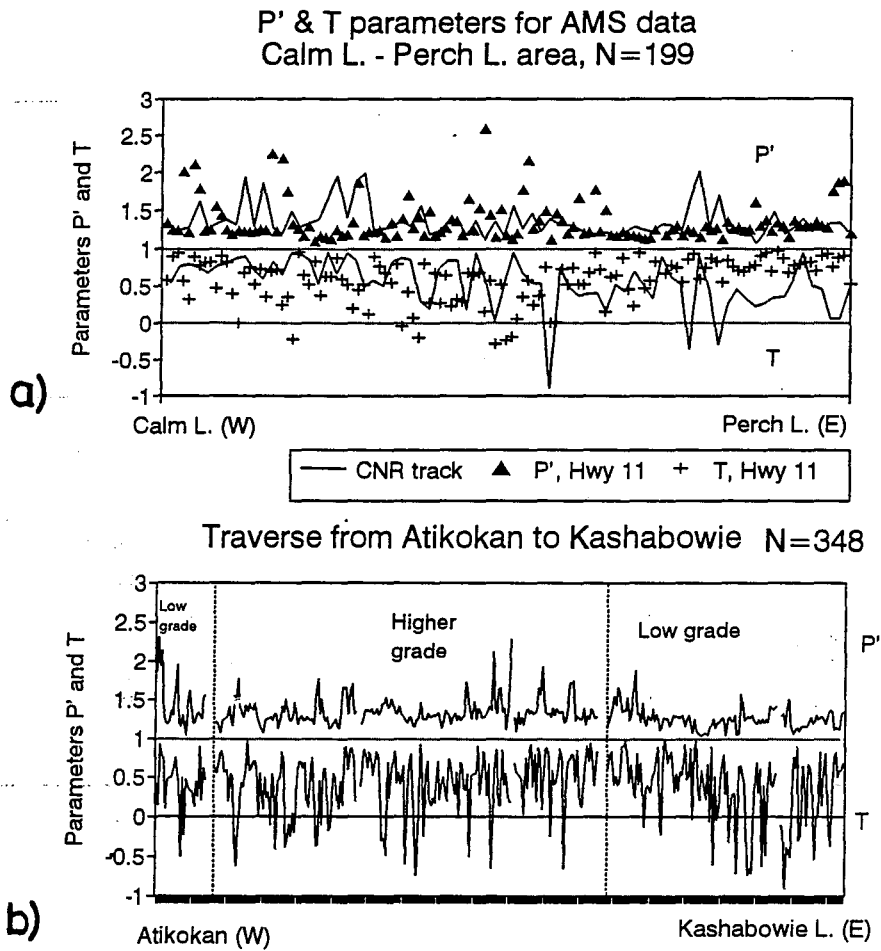


Fig. 10.17. A distribution of P' and T anisotropy parameters along traverses: a) in Calm Lake - Perch Lake area. b) along the Atikokan - Kashabowie Lake traverse. A traverse is divided into subareas according to metamorphic grade.

### The correlation between bulk susceptibility and AMS.

A correlation between the anisotropy ratio and bulk mean susceptibility was tested for all three suites (Fig. 10.18a-c). In low grade metasediments the overall magnetic anisotropy is controlled by p.c.o. of sheet silicates, as indicate the mean values of susceptibility and AMS anisotropy ratio  $P'$ . However, there is a small group of samples with low susceptibility but substantial prolate AMS fabric ( $T < 0$ , Fig. 10.18a). The knowledge of mineralogical composition of those samples is poor, as only a few samples from the whole collection had their ferromagnetic phase determined. At least one sample (PST63) showed the presence solely pyrrhotite as ferromagnetic minerals. Low values of bulk susceptibility also indicate that it is not magnetite that controls the susceptibility and the its anisotropy.

In the higher grade metasediments in the centre of the Quetico Belt the correlation between  $P'$  and MS indicates mainly paramagnetic contribution to AMS (as in the previous area, Fig. 10.18b). The group of prolate fabric is formed by samples mainly of amphibolite composition, with some content of MD or PSD magnetite. Some less susceptible samples ( $2-3 \cdot 10^{-4}$  SI vol.) show also weak prolate fabric ( $-0.25 < T < 0$ ), but it can be an effect of susceptibility measurement errors for weaker specimens.

In Kashabowie area, although most samples have their AMS fabric controlled by paramagnetic sheet silicates (Fig.

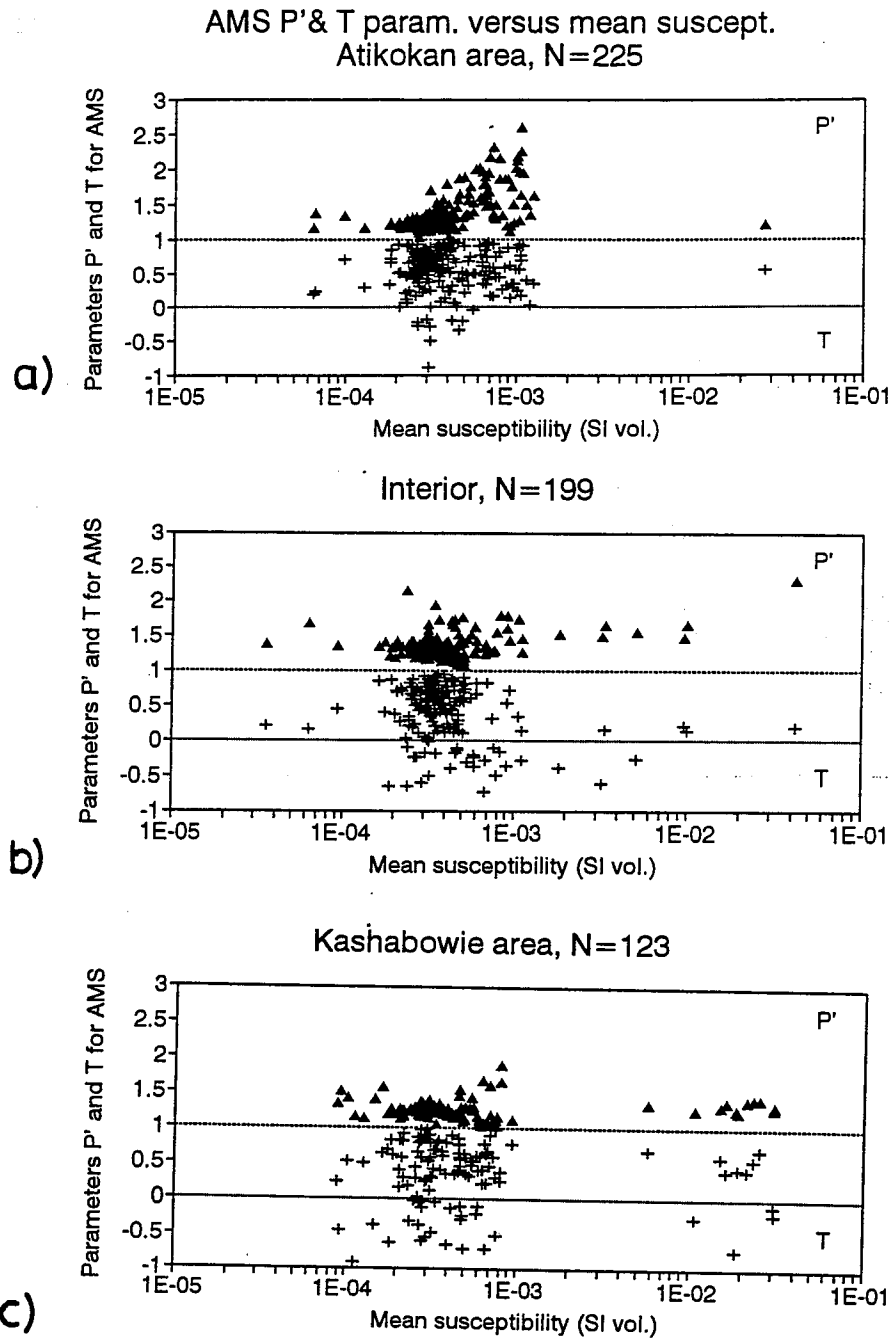


Fig. 10.18. A correlation between anisotropy parameters and susceptibility for 3 sub- areas. Note a group of highly susceptible samples in Kashabowie area (magnetite bearing ?).



10.18c), there is also a separate group of highly susceptible mostly metavolcanic samples with both prolate and oblate fabric present.

Those prolate fabric are believed to be controlled by magnetite, those oblate are controlled by sheet silicates, but with a substantial content of magnetite in the samples. There is a possibility that the arrangement of late- metamorphic magnetite can have weak preferred orientation, or that arrangement is controlled by the overall p.c.o. of paramagnetic matrix. In both cases the prolate fabric associated with shape anisotropy of prolate grains of magnetite may not be developed.

## Chapter 11.

### Anisotropy of ARM method.

#### 11.1. Anisotropy of remanence.

Contrary to magnetic susceptibility, the only magnetic phases responsible for the existence of remanent magnetization within the rock are ferromagnetic (s.l.). Usually due to chemical conditions only one or two ferromagnetic minerals are mineralogically stable in the rock and are therefore capable of carrying remanence (Jackson, 1991).

The magnetic fabric of ferromagnetic minerals can be tested with the use of one of several kinds of remanence that can be carried by the sample:

1. thermomagnetic remanence (TRM) - when applied field is acting on a sample during cooling in a defined range of temperature (eg. Collinson, 1983);
2. isothermal remanence (IRM) - when a strong D.C. field is applied to the specimen at room temperature (op. cit.);
3. anhysteretic remanence (ARM) - when a weak steady D.C. field acts on the sample simultaneously with a decreasing A.C. field, over a certain range of A.C. field or throughout the A.C. field range (Collinson, 1983, McCabe et al., 1985).

These remanences can be easily imposed on the sample under laboratory conditions.

The bulk anisotropy of remanence is therefore due to both anisotropy of the grains and the preferred orientation distribution of ferromagnetic grains.

The contribution of different ferromagnetic minerals to the bulk anisotropy can be more easily studied because a simpler mineralogical composition of ferromagnetic phases contributes to remanence in the sample than in case of a paramagnetic matrix contributing to low field susceptibility.

However the anisotropy of single grain can vary depending on the different magnetization processes employed. Also the different magnetic processes can generate magnetization in slightly different ferromagnetic phases (e.g. of different coercivity or blocking temperature), or in case of ARM in grains of different size.

The theoretical dependence between remanent magnetization and applied field is generally similar to that for susceptibility:

$$\bar{M}_r = kf(\bar{H})$$

where  $M_r$  is remanent magnetization,  $k$  is second rank symmetric tensor and  $f(H)$  is a function of applied D.C. magnetic field. For a low intensity of applied field the relation is linear, but for high intensities of applied field, due to the Raleigh law, the overall increase of remanence with field is non-linear, especially near saturation remanent magnetization. However, the

space (anisotropic) dependence can still be described by second-rank tensor (Stephenson et al., 1986). This is different from the AMS case, where a dependence of AMS on intensity of applied field was reported for certain ferromagnetic phases (e.g. for pyrrhotite, Worm, 1991, Stupavsky 1990/1991, work in progress).

The analogous approach to anisotropy of remanence tensor  $k$  results in the definition of anisotropy of the remanence ellipsoid with its principal axes to characterize this magnetic fabric. To sustain similarity with AMS ellipsoid the anisotropy tensor is given as isothermal, thermomagnetic or anhysteretic susceptibility (without units) when the measured remanent magnetization is normalized by the intensity of the applied field.

However in this thesis to retain a correlation between studied NRM values and imposed ARM, the calculated principal ARM were not normalized, but expressed in mA/m. It holds as long as the applied external field is the same for all studied samples (here 0.1 mT).

In any case we are principally concerned with directions of remanence, and ratios of magnitudes so that the absolute values are immaterial.

Anisotropy of remanence is generally greater than AMS for a given magnetic phase (Hrouda, 1982) as it is more difficult to impose the stable remanent magnetization along a high energy direction (hard axis) than to induce a magnetization in that direction (Jackson, 1991).

Ferromagnetic phases, that contribute to the overall remanent magnetization, have often different p.c.o /p.d.o fabric, different coercivity, blocking temperature or saturation remanent magnetization due to different grain size, or variation in composition (especially the latter in the case of titanomagnetites or pyrrhotite). Thus each phase may have a different contribution to the overall anisotropic fabric.

The dependence of anisotropy of remanence on the constituent mineral phases can be studied for ARM or TRM when partial TRM (pTRM) or ARM (pARM) are imposed in a defined window (of temperature or A.F. field respectively, Jackson, 1991, Jackson et al., 1988). For IRM, only the anisotropy of resultant IRM can be studied with increasing applied field. The changes of PIRM with increasing field can only be analyzed by examining the derivative of the final curve or by using vector difference. The imposing of partial IRM in window  $H_1-H_2$  is somewhat more complicated than for ARM or TRM - the A.F. demagnetization step with peak A.F. field  $H_1$  should be performed after applying of D. C. field of  $H_2$  intensity.

Jackson et al. (1988) indicated that partial remanence method produces less noise than differentiating of  $M_r=f(H)$  curve. In this study I shall be concerned only with ARM.

The results for partial ARM for 2 magnetite phases of different size and orientation present in the same specimen (Jackson et al., 1988) shows that the total anisotropy of ARM fabric is a resultant tensor of both phases. Most ferromagnetic

minerals reveal the strong dependence of coercivity on grain size (Dunlop, 1986 for magnetite, Dekkers, 1988 for pyrrhotite), therefore the acquired ARM strongly depends on the intensity of A.F. field during ARM acquisition.

The A.F. intensity for ARM also influences the number of phases which acquire the remanence. Small grain, SD magnetite with higher coercivities (e.g. 80-100 mT) can contribute to ARM fabric only if sufficient intensity of applied field is used to energise their spin moments.

(N.B. For SD magnetite, AMS fabric is "inverse" (Stephenson et al., 1986), but ARM fabric should give "normal" fabric: with maximum ARM along the length of a grain (Jackson, 1991)).

### 11.2. The determination of the anisotropy of ARM (=AARM).

The scenario of calculation of the anisotropy matrix of ARM depends on the facilities to measure the remanent magnetization after ARM acquisition in the sample. Two designs are useful:

1. When the component of ARM along the direction of applied D.C. field is directly measured, at least 6 measurements in different orientations are required to calculate symmetrical anisotropy matrix (with 6 different elements in 3x3 matrix). A larger number of measurements increases the accuracy of determination of matrix component and allows one to calculate the errors of determination of principal values and their directions. However, the least squares method must be then employed to find the anisotropy matrix. Similar schemes were constructed for the anisotropy of MS matrix (Girdler, 1961 - 9 positions, Stupavsky, 1984 - 12 positions).

Hext, (1963) offered an approach to calculate confidence cones  $R_{95}$  for axis directions and standard deviation errors for principal values of the matrix.

2. If the full remanence vector (3 components) is measured for each step of ARM acquisition, then in theory only measurements in 2 directions are needed to reproduce the symmetrical matrix.

Stephenson et al. (1986) proposed measurements in only 3 orthogonal planes as sufficient design for IRM anisotropy.

Jackson (1991) noted that the accuracy of measurement of all 3 components of a remanence vector should be high to get

reliable values for off - diagonal components of anisotropy matrix. This is possible in IRM acquisition, where the intensities of remanence are large. This is more difficult for ARM, however, the resolution could be improved with a larger number of measurement orientations (e.g. 12 as in this study).

Jackson (1991) proposed a goodness-of-fit parameter to test matrix fitted to experimental data as root-mean-square residual normalized to mean susceptibility (or mean remanence). This formula is probably of the form:

$$p = \frac{\sqrt{\sum_{i=1}^N \frac{[\|\bar{r}_{i_{exp}} - \bar{r}_{i_{teor}}\|^2]}{N-6}}}{k_{mean}}$$

where  $\|\bar{r}_{exp} - \bar{r}_{teor}\|$  is the vector distance between calculated ( $\bar{r}_{teor}$ ) and measured ( $\bar{r}_{exp}$ ) remanence for each orientation (along the axis of applied field in method 1 and in 3 - dimensional space in method 2).

In this study only samples which revealed stable NRM and were previously successfully AF demagnetized were chosen for ARM fabric studies. ARM was imposed in a Sapphire Instruments SI-4 AF demagnetizer with 0.1 mT D.C field along the cylindrical shield axis. The employed peak A.C. demagnetization field was set at 100 (for most samples) to 200 mT (for those with high coercivity of remanence >100 mT revealed in AF treatment of NRM). The D.C. field was applied in a window from 100 mT (a.f.)



to zero (a.f.).

### **Step-wise ARM acquisition for test samples.**

Initially, the dependence of ARM on the A.C. demagnetizing field was investigated for two pyrrhotite bearing samples (TW17-1 and TW19-1) from biotite schist - migmatite zone. The A.F. was increased in steps of 5 mT when ARM was imposed (for the same position of a sample in each step) and ARM was measured in MOLSPIN spinner magnetometer. The intensities of ARM were as high as 200 mA/m. The pARM diagram (Fig. 11.1) indicates that the coercivity of remanence ranges up to 40 mT for both samples with maxima at 20 mT for TW17-1 and 5 mT for TW19-1. Above these fields both samples became unstable. Secondary peaks in the ARM spectrum were observed for both samples at 30 mT. These results are approximately consistent with known mean destructive field (MDF) values (usually 60% of  $H_{cr}$  for large pyrrhotite grains (Clark, 1984)), here up to 20 mT. The maximum A.C. field window in ARM acquisition set at 100 mT is therefore suitable to produce ARM in all present ferromagnetic grains in all samples with low MDF.

### **ARM acquisition and anisotropy tensor calculation in the study.**

The sample was initially demagnetized with the AF peak field of 200 mT which was sufficient for all but a few samples (with high coercivity of remanence). The residual NRM was

Spectrum of ARM  
 Samples: tw17-1 & tw19-1

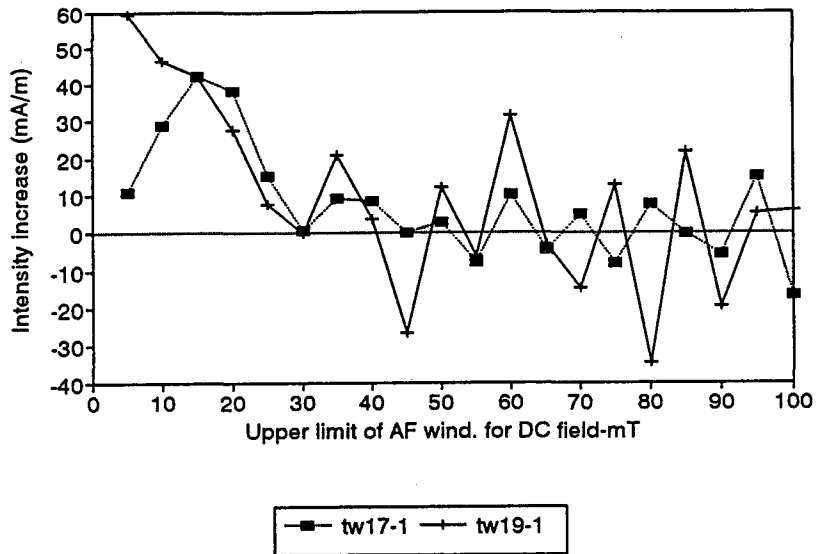


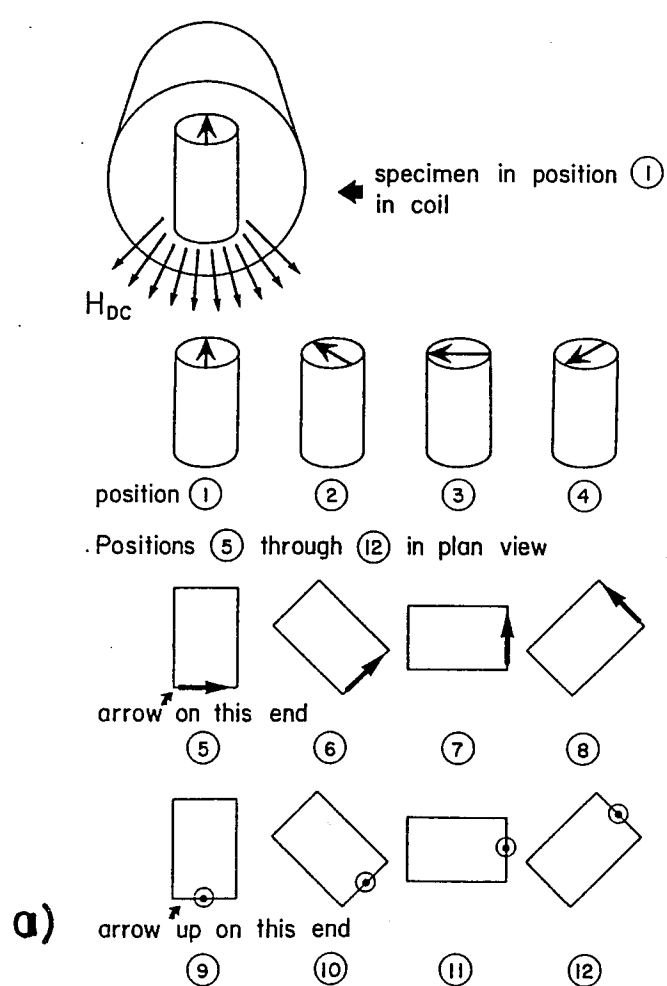
Fig. 11.1. Changes of anhysteretic remanence when a window of AF treatment, in which DC field is applied, becomes enlarged. X - axis - a value of upper limit of AF field for ARM acquisition. Results for two samples (pyrrhotite bearing) indicate that ARM is carried mainly by grains with coercivity of remanence less than 20 mT.

measured for all samples with MOLSPIN magnetometer. The sensitivity of the magnetometer is about 0.5 mA/m. Thus for ARM determination purposes, all samples with intensities lower than 0.5 mA/m can have significant measurement error (up to 20-30%) of each component of remanence vector. Therefore, only samples with previously determined stable NRM of intensity higher than 10 mA/m were used.

The procedure of ARM acquisition employed 12 orientations as designated by Stupavsky (1984). The change in orientation of sample for all but 4th to 5th orientation was at angle  $45^\circ$ ; from the 4th to 5th position it was  $90^\circ$  (Fig. 11.2a,b). The full vector of ARM was measured after each step of ARM acquisition with the Molspin magnetometer. Each sample was AF demagnetized in 3 orthogonal positions only after the 4th step, with the assumption that in mostly multidomain ferromagnetics the applied AF field of peak 100 mT during ARM acquisition is sufficient to unblock existing ARM which was imposed previously at angle of  $45^\circ$  to the actual orientation of demagnetizing field.

Four samples had their ARM imposed with demagnetization after every step of ARM acquisition. These tests did not reveal noticeable differences from those using full a.f. demagnetization after only the 4th step (see Table 11.3 and Fig. 11.4). Therefore further ARM acquisition was made with AF demagnetization only after the 4th step to save time.

As a result of this procedure, 12 vectors of ARM for the 12 Stupavsky orientations were obtained. This yields 36 equations



(a) ARM ACQUISITION DIRECTIONS

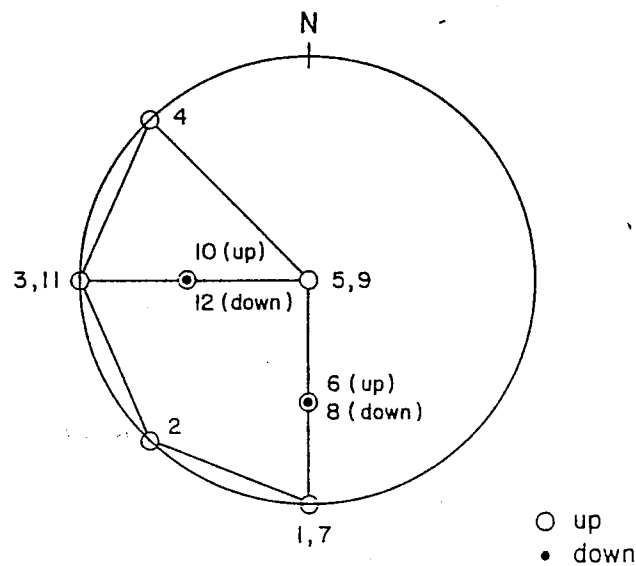


Fig. 11.2. The orientation of sample with respect to a component of distant magnetic field producing ARM. Magnetic field is out from the coil. a) 12 orientations of a specimen during ARM acquisition, when its anisotropy is measured. Changes of orientation are of  $45^\circ$  in each step except 4th to 5th step. b) a orientation of magnetic field in sample coordinates, numbers - orientations of a sample.

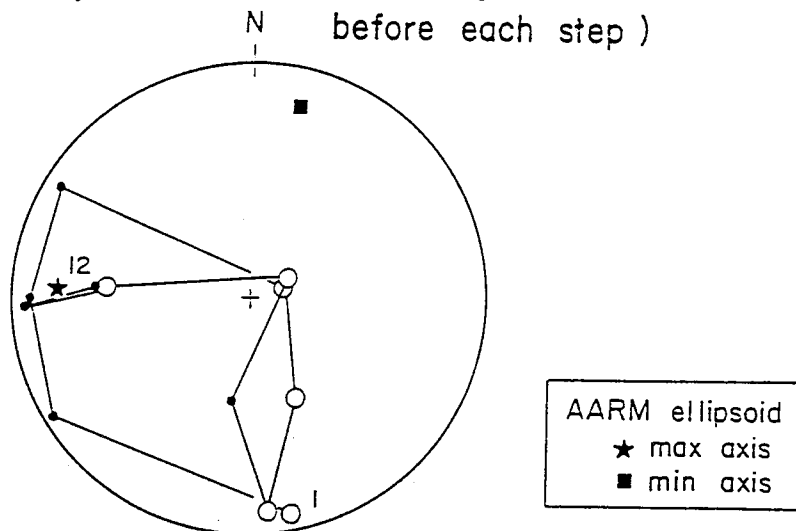
Table II.3. The comparison of ARM acquisition results for 2 discussed methods

I - AF demagnetization after 4th step

II - AF demagnetization after each step

	Method	Min			Int			Max			Mean ARM (mA/m)	
		Dec	Inc	Int	Dec	Inc	Int	Dec	Inc	Int	geom	aritm
TW8	I	346.1	10.2	1.72E+02	221.0	72.5	3.41E+02	78.6	14.0	7.10E+02	346.6	407.6
TW8	II	345.7	5.5	1.62E+02	228.8	77.9	3.29E+02	76.7	10.7	7.23E+02	338.0	404.8
TW14	I	6.7	7.0	6.11E+01	116.2	69.8	8.25E+01	274.3	18.8	1.32E+02	87.3	91.9
TW14	II	10.9	13.7	5.49E+01	136.9	67.4	8.11E+01	276.5	17.6	1.28E+02	83.0	88.1
TW17	I	318.0	44.6	8.94E+01	175.3	38.9	1.21E+02	68.6	19.6	1.81E+02	125.2	130.6
TW17	II	313.1	48.1	7.96E+01	176.6	33.1	1.20E+02	70.8	22.6	1.76E+02	118.7	125.0
TWA2	I	177.3	0.7	4.24E+01	267.6	23.5	5.13E+02	85.8	66.5	6.43E+02	241.0	399.6
TWA2	II	177.3	0.8	6.03E+01	267.6	19.2	5.42E+02	85.1	70.8	6.87E+02	282.0	429.6

a) TW14-1 ( AF demagnetisation  
before each step )



b) TW14-1 ( no AF demagnetisation  
between steps )

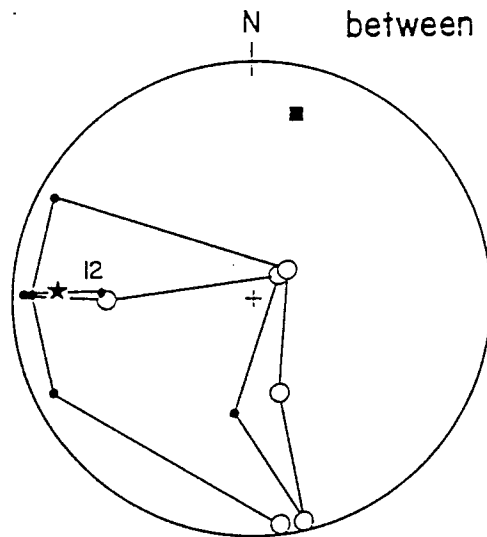


Fig. 11.4. ARM vectors after acquisition of ARM in each of 12 orientation. Two procedures were tested: a) with AF demagnetization before each step; b) - AF demagnetization only before 5th step, no AF demagnetization before the other steps. The orientation of principal axes of AARM ellipsoid are shown as well. Note that both method gave a similar orientation of acquired ARM vectors and directions of AARM fabric.

in the least squares method to find six parameters of the anisotropy matrix. Therefore two approaches to estimate the anisotropy matrix were adopted.

1. - The component of measured ARM along the direction of applied field was calculated to reduce the number of equations to 12 and to use the Stupavsky algorithm (SI-2 program) to estimate the anisotropy matrix and the error of fitting the matrix to experimental points.

2. - The full set of 36 equations was used to estimate the anisotropy matrix with least - squares method based on Hext (1963) approach. However the errors of calculated principal ARM and their orientation could not be estimated, due to the complex formulae necessary to be programmed for non - rotational design of specimen orientations (Hext, 1963).

The directions and values of principal anhysteretic remanences ( $ARM_{max}$ ,  $ARM_{int}$ ,  $ARM_{min}$ ) were calculated together with confidence cones ( $r_{95}$ ) for the directions estimate and the standard deviation (std) for an estimate of intensities of principal remanences.

The goodness-of-fit parameter (Jackson, 1991) was also calculated for both methods. These calculations were performed with the use of program FAMS4.BAS of Borradaile & Stupavsky modified by the writer. The comparison of results of both methods do not show any superiority of one approach over the other. The full vector approach employs many more experimental data therefore also goodness-of-fit can be affected by more

scattered results. For further studies, the Stupavsky approach (method 1) was used as it more easily calculates the error of the estimation of the principal values.

A total 89 samples from the Calm Lake - Perch Lake area, 30 samples from Atikokan - Huronian Lake traverse and 37 from Kashabowie Lake - Huronian Lake traverse were measured and most of them gave acceptable results for the ARM (with at least one direction of principal anhysteretic remanences with  $r_{95}$  less than  $20^\circ$ ) - see appendix B for tables.

Data with confidence cone  $r_{95} > 20^\circ$  were rejected from further interpretation of the distribution of directions of  $ARM_{max}$  and  $ARM_{min}$ . However they were used to determine the anisotropy parameters  $P'$ ,  $T$ . One should note that for samples with almost uniaxial prolate or oblate fabric the determination of directions of two principal axes (one of them is  $ARM_{int}$ ) naturally leads to high values of measurement "error".

Samples with substantial initial remanent magnetization after AF demagnetization at 200 mT prior to ARM acquisition had this remanent magnetization subtracted from the measured ARM remanence, as this was assumed to be unaffected by ARM acquisition.



## Chapter 12.

### ARM and its anisotropy (AARM) in the area.

#### 12.1. Intensity of ARM in the area.

The intensity of anhysteretic remanence can be used as a indicator of variations of ferromagnetic content through the transect. ARM intensity was calculated as a geometric mean of three principal values of AARM.

In Calm Lake - Perch Lake area 89 samples were examined (30 of them came from fold closures - series FA and FB and graded beds - series PLR and they were not used for further analysis of ARM fabric in the area). All but three had ARM intensities larger than 10 mA/m (the range 100-500 mA/m was the most common, mean ARM intensity is  $117 \pm 159$  mA/m,  $N=59$ , Fig. 12.1).

One sample with very high remanences came from western part of CNR track traverse from Wabigoon metavolcanic outcrops (Fig. 12.2a). It had also high susceptibility that can indicate the content of magnetite. The ARM intensity for remaining 58 metasedimentary samples showed local variations and was controlled by changes in pyrrhotite content and alignment. The content of magnetite in these samples is probably minor as none other extremely high ARM intensities were observed.

Samples from chlorite and biotite schist east of Atikokan had mostly high anhysteretic remanence (mean ARM intensity:  $211 \pm 96$  mA/m,  $N=10$ , Fig. 12.1, Fig. 12.2b). They contain pyrrhotite

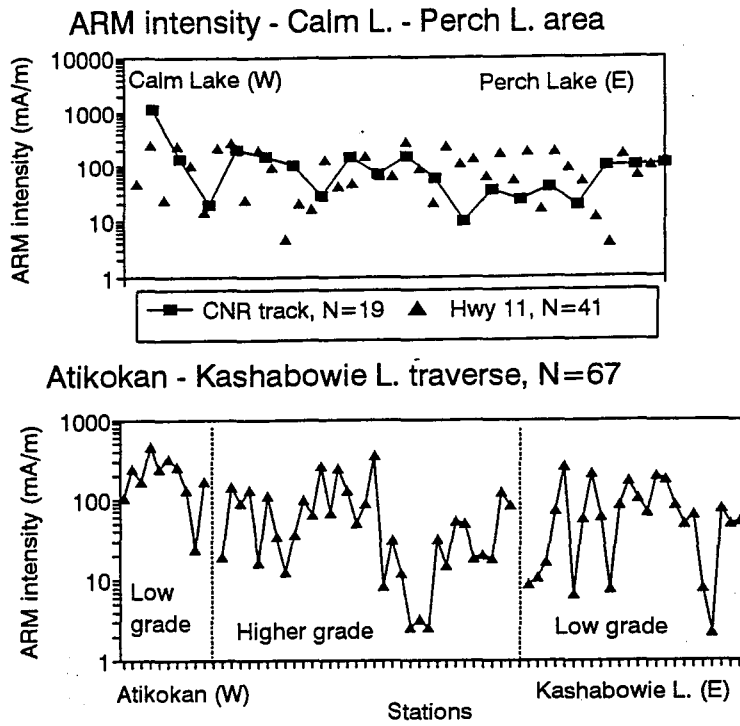


Fig. 12.2. Variations of ARM intensity along traverses. a) - Calm L. - Perch L. area; b) - traverse Atikokan - Kashabowie Lake.

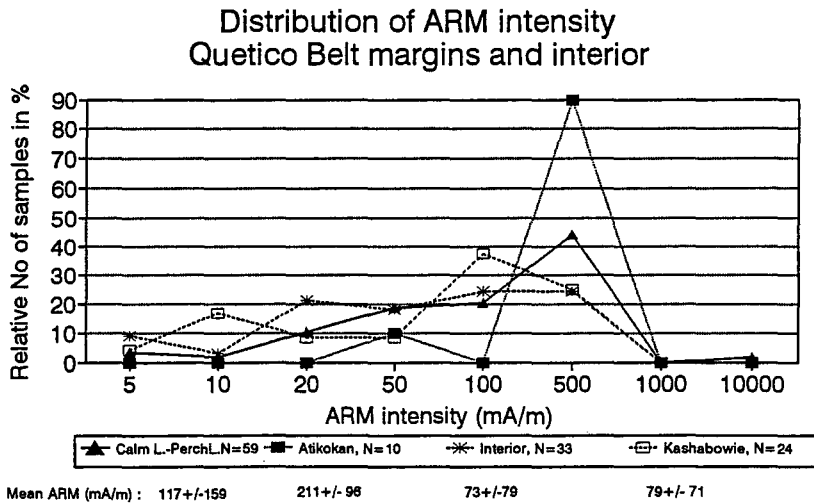


Fig. 12.1. A histogram of ARM intensity for 3 sub-areas. Atikokan area was divided into Calm L. - Perch L. area and area east of Atikokan. Note very high ARM intensity for samples near Atikokan.

only as ferromagnetic phase (see sample TWA5, appendix C).

ARM intensity for 33 samples from the interior of the belt are generally lower than at the northern margin of the belt (mean ARM:  $73 \pm 79$  mA/m Fig. 12.1) and local variations (especially low values of ARM are observed in more felsic outcrops, higher in amphibolites, Fig. 12.2b).

In low grade metasediments and metavolcanics of Kashabowie area ARM intensity is also low (mean ARM:  $79 \pm 71$  mA/m, N=24, Fig. 12.1). It is slightly higher in metavolcanics (Fig. 12.2b), but even the presence of magnetite in some samples does not cause higher ARM intensity. It can be explained by the fact that observed magnetite is MD and produced remanence is therefore low. None samples from felsic metavolcanics (stations RS 5.5 to 8) carried stable and consistent ARM fabric.

## 12.2. The distribution of directions of AARM foliations and lineations.

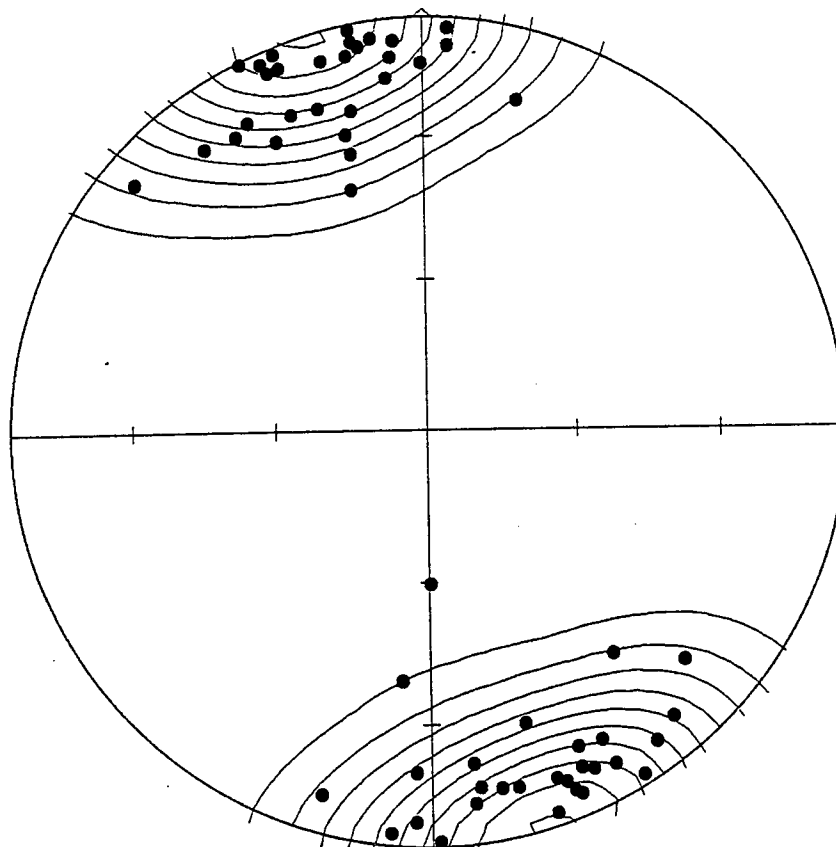
### **AARM foliations.**

In Calm Lake - Perch Lake area the  $ARM_{min}$  axes were accepted for 87 samples and  $ARM_{max}$  axes for 57 samples. However, data from fold closures and graded bed station cannot be used for overall distribution of directions as they may reflect combined sedimentary and tectonic fabric. Therefore they were excluded from the overall directional analysis. Remaining data plotted on the stereonet (Fig. 12.3a) indicate well developed AARM foliation almost vertical steeply dipping to the north.

AARM foliation planes for 10 samples from east of Atikokan suite group tightly around almost the same sub-vertical orientation (see Fig. 12.3b-c and Table 12.4). At the centre of the Quetico belt AARM foliation planes become less steep (mean dip of  $78^\circ$ ) than at northern margin (Fig. 12.3d and Table 12.4). However the scatter of orientation of AARM foliations for individual samples increases.

Fig. 12.3. Directions of AARM minimum axes - poles to AARM foliations. a) Calm Lake - Perch Lake area.

ARM anisotropy min axes - Calm L.-Perch L. area  
low grade metasediments



$N = 57$

$k = 14.67$

$(\text{Peak} - E)/\text{Sigma} = 18.3$

Peak position :  $163.6^\circ / 1.8^\circ$

$E = 3.89$

$\text{Sigma} = 1.30$

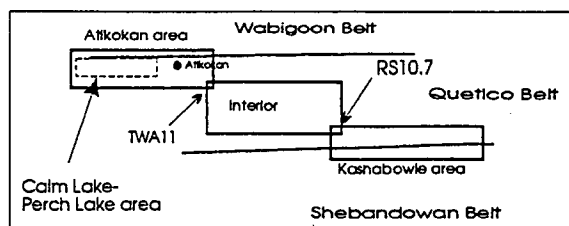
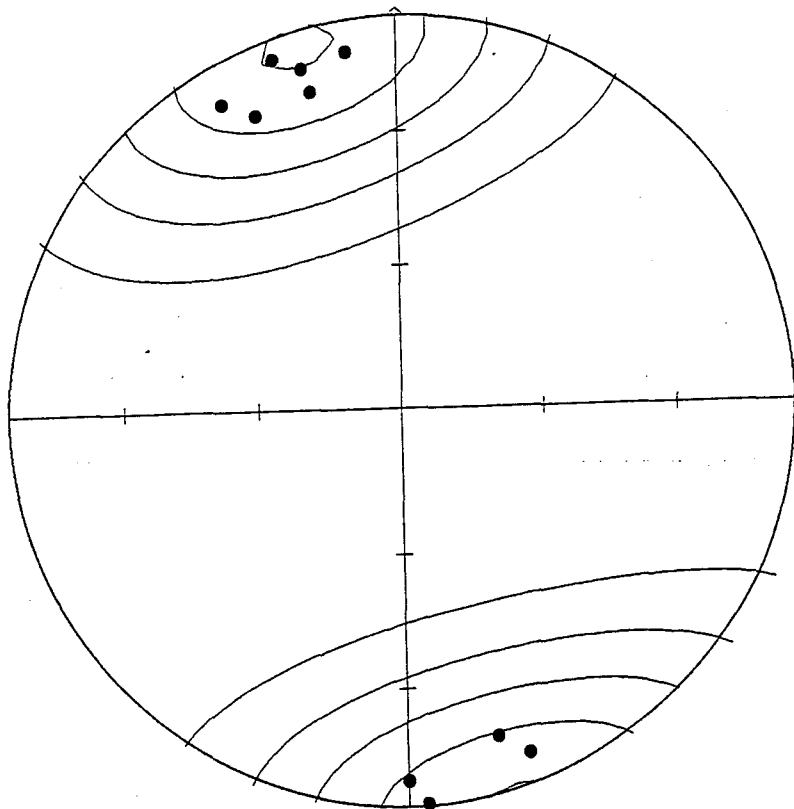


Fig. 12.3b.

ARM anisotropy minimum axes - east of Atikokan  
low grade metasediments



$N = 10$   
 $k = 4.22$   
 $(\text{Peak} - E)/\text{Sigma} = 8.2$   
Peak position :  $344.5^\circ / 4.4^\circ$

$E = 2.37$   
 $\text{Sigma} = 0.79$

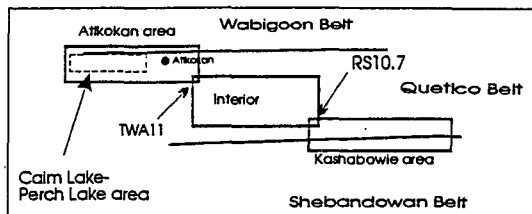
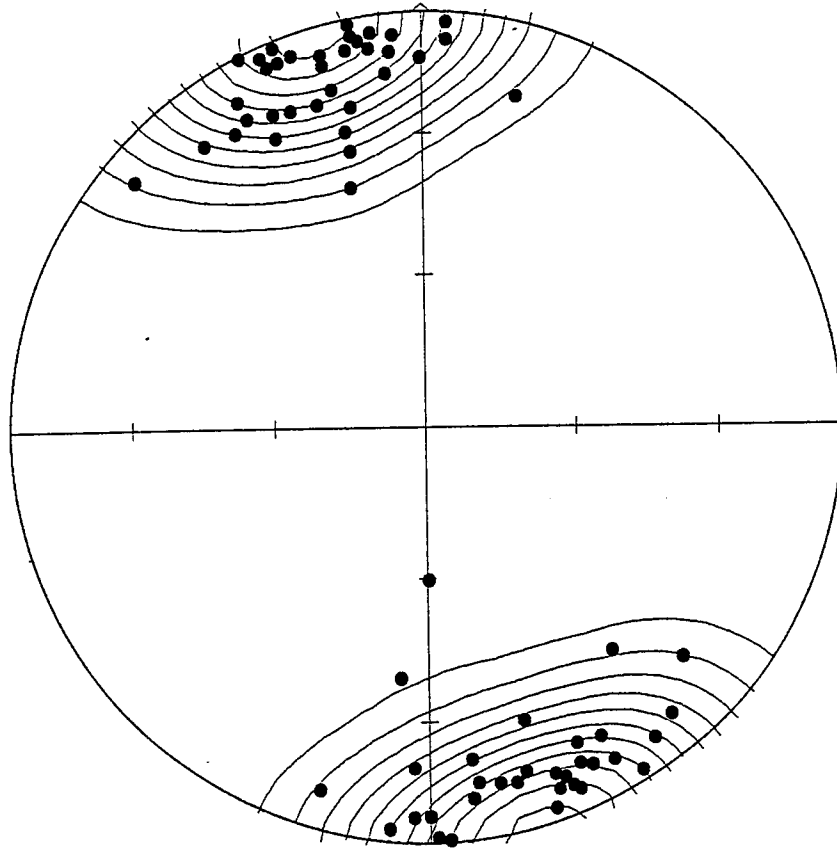


Fig 12.3c. Data from fig. 12.3a and 12.3b.

ARM anisotropy minimum axes - Atikokan area  
low grade metasediments



$N = 67$

$k = 16.89$

$(\text{Peak} - E)/\text{Sigma} = 21.0$

Peak position :  $343.6^\circ / 1.8^\circ$

$E = 3.97$

$\text{Sigma} = 1.32$

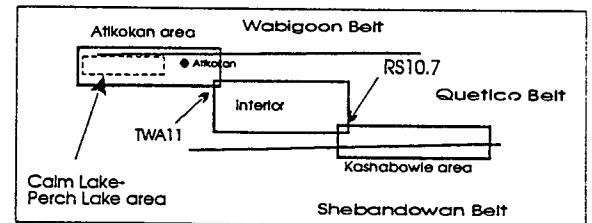
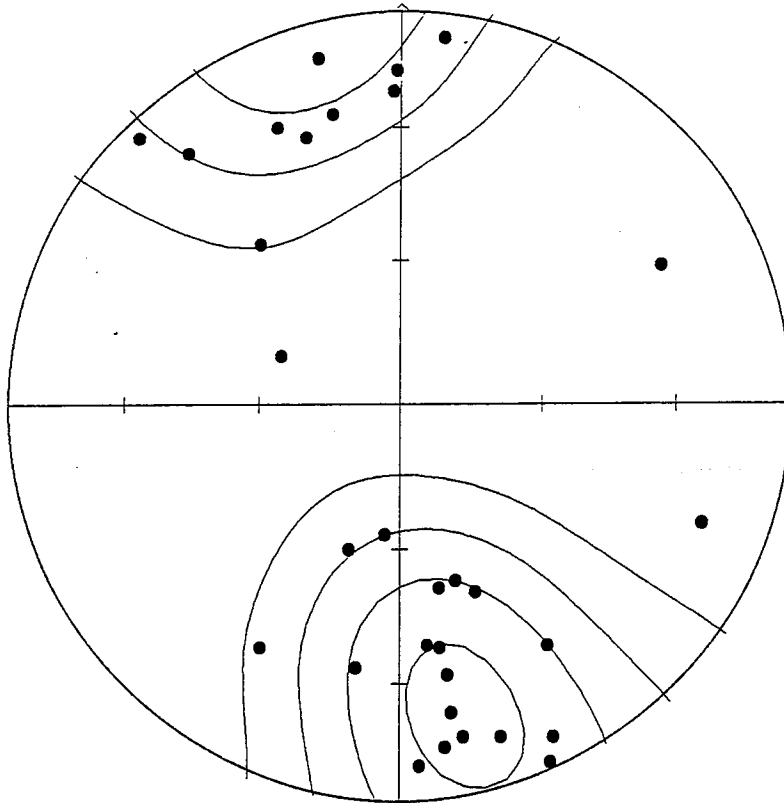


Fig. 12.3d.

ARM anisotropy minimum axes - the interior of  
Quetico B. -medium and high grade metased. & intr.



$N = 31$

$k = 8.89$

$(\text{Peak} - E)/\text{Sigma} = 6.7$

Peak position :  $167.9^\circ / 21.5^\circ$

$E = 3.49$

$\text{Sigma} = 1.16$

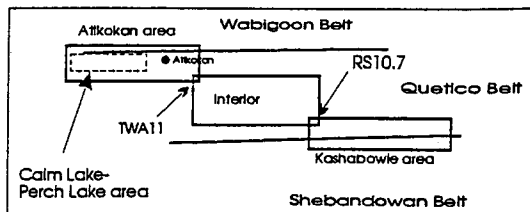
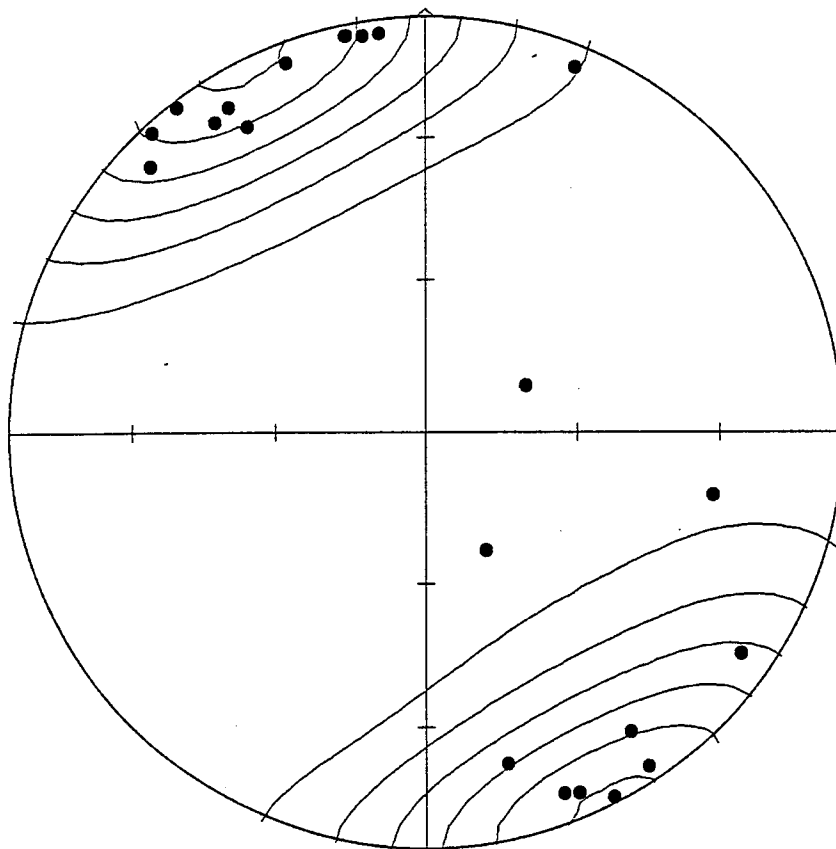




Fig. 12.3e.

ARM anisotropy min axes - Kashabowie - Huronian L.  
low grade metasediments and metavolcanics



$N = 22$   
 $k = 6.89$   
 $(\text{Peak} - E)/\text{Sigma} = 10.4$   
Peak position :  $333.4^\circ / 0.7^\circ$

$E = 3.19$   
 $\text{Sigma} = 1.06$

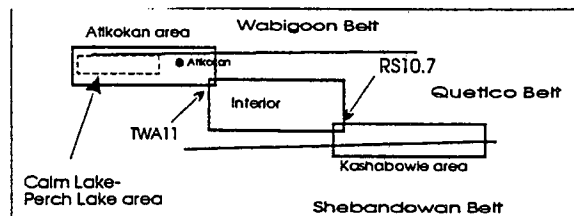
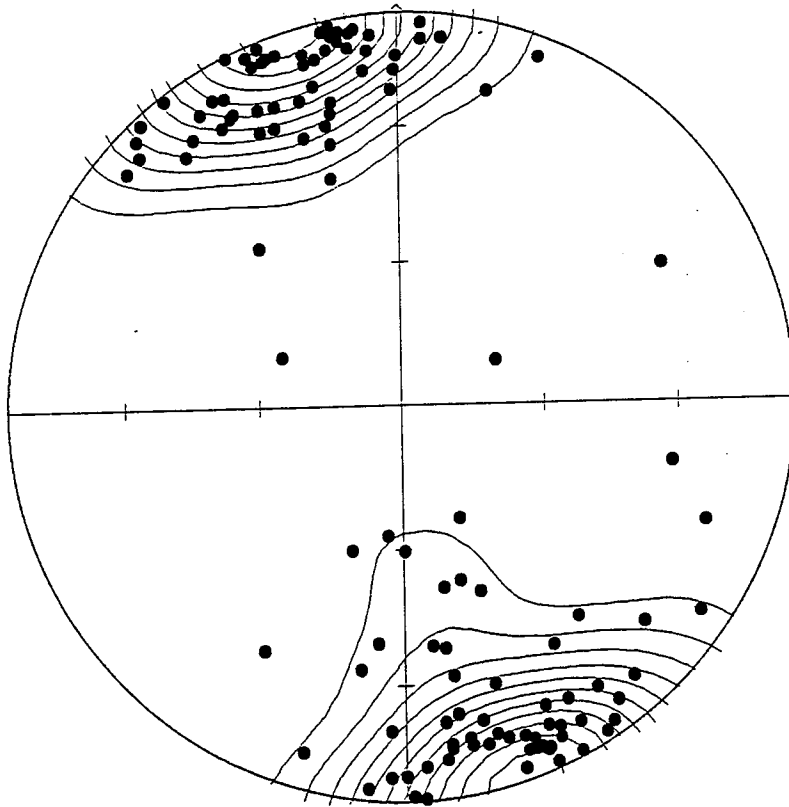


Fig. 12.3f. AARM min axes orientations - Data from all areas together.

ARM anisotropy minimum axes - Quetico Belt  
margins and interior - Atikokan area - Kashabowie



$N = 120$

$k = 28.67$

$(\text{Peak} - E)/\text{Sigma} = 21.3$

Peak position :  $160.6^\circ / 0.2^\circ$

$E = 4.19$

$\text{Sigma} = 1.40$

Table 12.4. The orientation of AARM minimum axes (poles to AARM foliations).

Area	N	Counting method	PCA method
Calm L.-Perch L.area	57	164/2 (18 $\sigma$ )	164/0 (6/5) ?
east of Atikokan	10	345/4 (8 $\sigma$ )	345/4 (10/6)
whole Atikokan area	67	344/2 (21 $\sigma$ )	344/0 (5/4) ?
interior	31	168/22 (7 $\sigma$ )	166/14 (19/9)
Kashabowie area	22	333/1 (10 $\sigma$ )	153/2 (10/7) ?
All areas total	120	161/0 (21 $\sigma$ )	162/2 (5/4) ?

? - distribution is not of Bingham type, the results of PCA method must be considered with caution.

On the southern margin AARM foliations become more steep in the low- grade metasediments of Quetico Belt and ARM foliation can dip to the north as well as to the south (Fig. 12.3e) with a mean foliation plane sub- vertical and striking slightly more to N-S direction than in the interior of the belt.

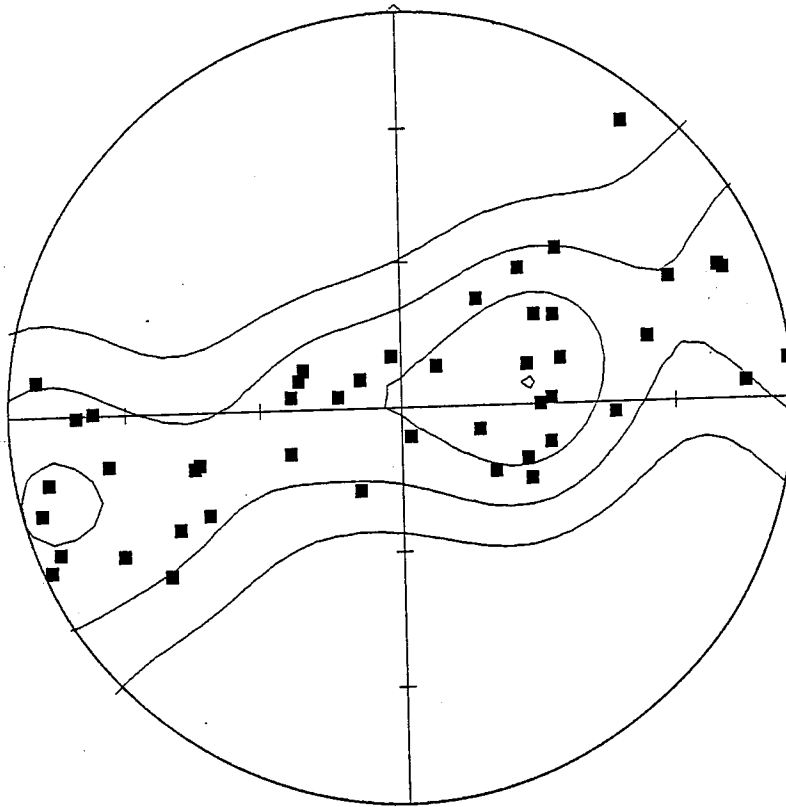
The overall AARM foliation plane for a whole area is subvertical (Fig. 12.3f) because there are more samples from margins of the belt than from the interior contributing to overall statistics.

#### AARM lineations.

In Calm Lake - Perch Lake area directions of maximum and intermediate principal axes of AARM are better defined than those for AMS axes. It is due to less perfectly oblate AARM fabric. Directions of AARM lineations are scattered along AARM foliation plane (Fig. 12.5a). However, a weak cluster of these lineations exists. The mean AARM lineation for that area is

Fig. 12.5. Directions of AARM maximum axes - AARM lineations. a)  
Calm Lake - Perch Lake area.

ARM anisotropy max axes - Calm L.-Perch L. area  
low grade metasediments



$N = 46$   
 $k = 12.22$   
 $(\text{Peak} - E)/\text{Sigma} = 6.0$   
Peak position :  $80.5^\circ / 62.4^\circ$

$E = 3.76$   
 $\text{Sigma} = 1.25$

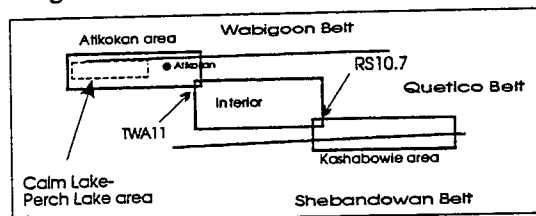
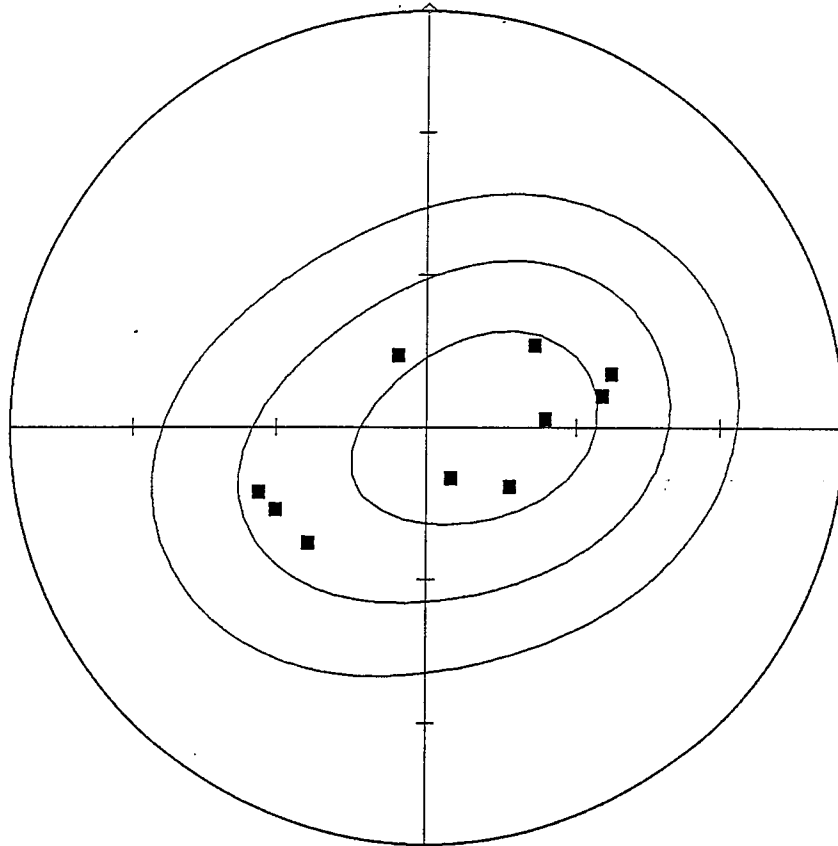


Fig. 12.5b.

ARM anisotropy maximum axes - east of Atikokan  
low grade metasediments



$N = 10$   
 $k = 4.22$   
 $(\text{Peak} - E)/\text{Sigma} = 5.2$   
Peak position :  $90.0^\circ / 76.5^\circ$

$E = 2.37$   
 $\text{Sigma} = 0.79$

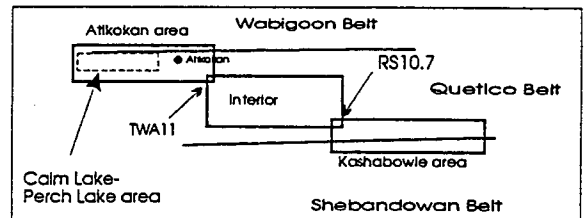
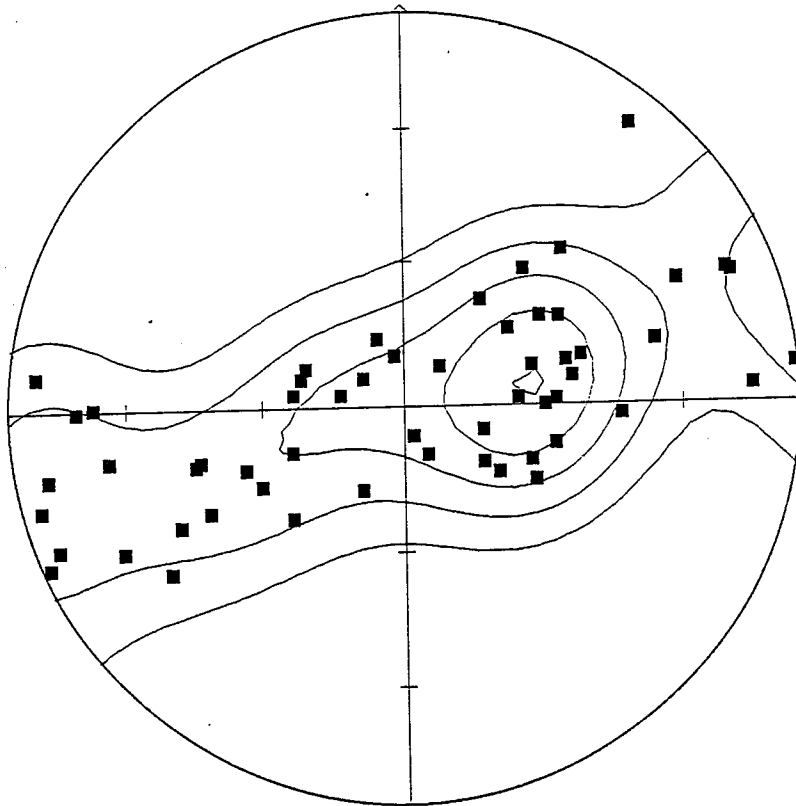


Fig 12.5c. Data from fig. 12.5a and 12.5b.

ARM anisotropy maximum axes - Atikokan area  
 Wabigoon-Quetico B. margin - low grade metasedim.



$N = 56$   
 $k = 14.44$   
 $(\text{Peak} - E)/\text{Sigma} = 8.1$   
 Peak position :  $80.5^\circ / 62.4^\circ$

$E = 3.88$   
 $\text{Sigma} = 1.29$

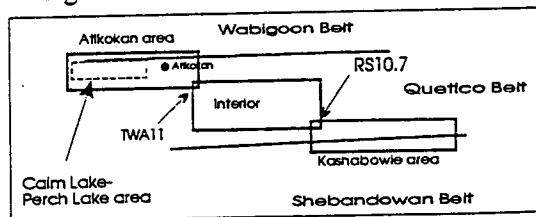
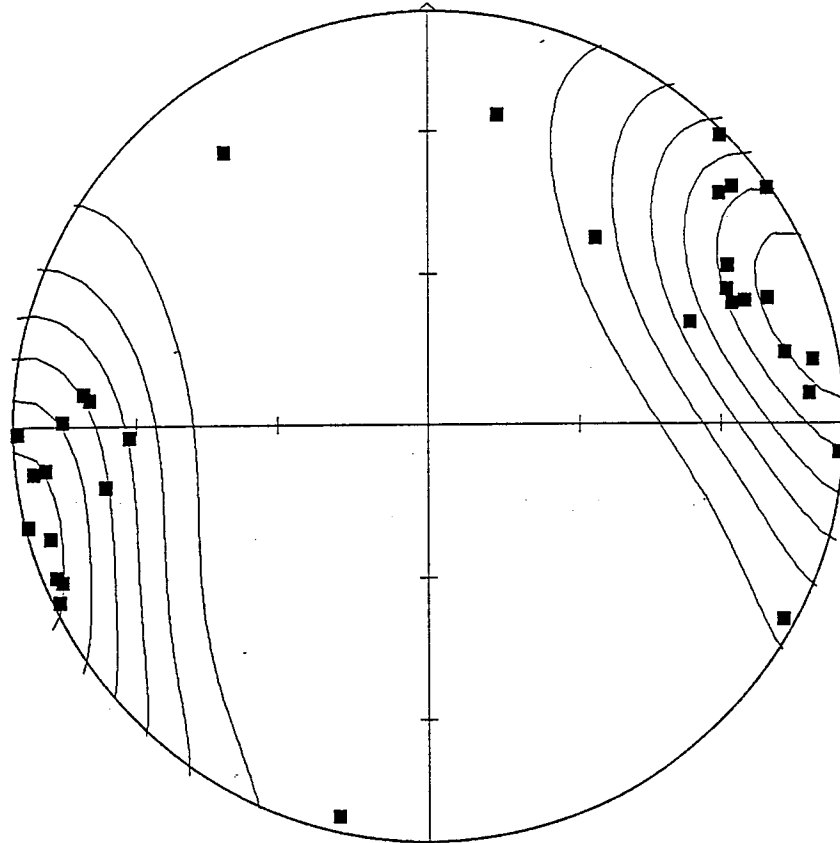


Fig. 12.5d.

ARM anisotropy max axes - the interior of Quetico  
medium to high grade metasediments and intrusives



$N = 32$   
 $k = 9.11$   
 $(\text{Peak} - E)/\text{Sigma} = 11.6$   
Peak position :  $74.5^\circ / 4.4^\circ$

$E = 3.51$   
 $\text{Sigma} = 1.17$

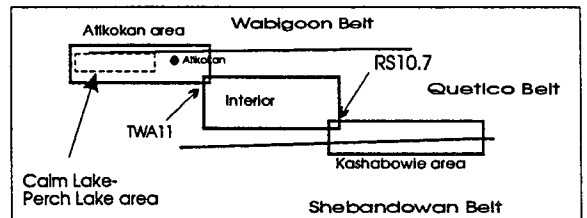
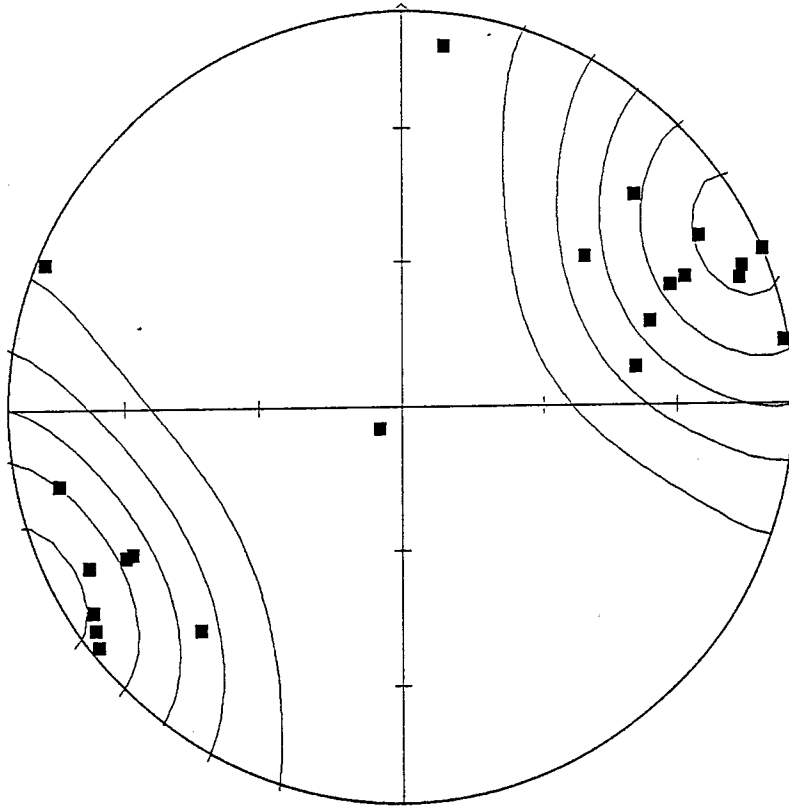


Fig. 12.5e.

ARM anisotropy max axes - Kashabowie - Huronian L.  
low grade metasediments and metavolcanics



$N = 22$

$k = 6.89$

$(\text{Peak} - E)/\text{Sigma} = 8.8$

Peak position :  $64.8^\circ / 5.1^\circ$

$E = 3.19$

$\text{Sigma} = 1.06$

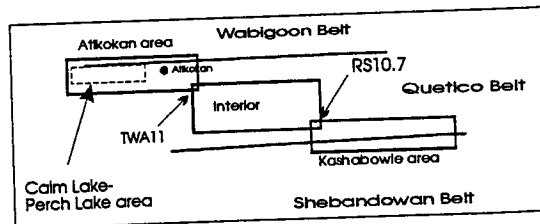
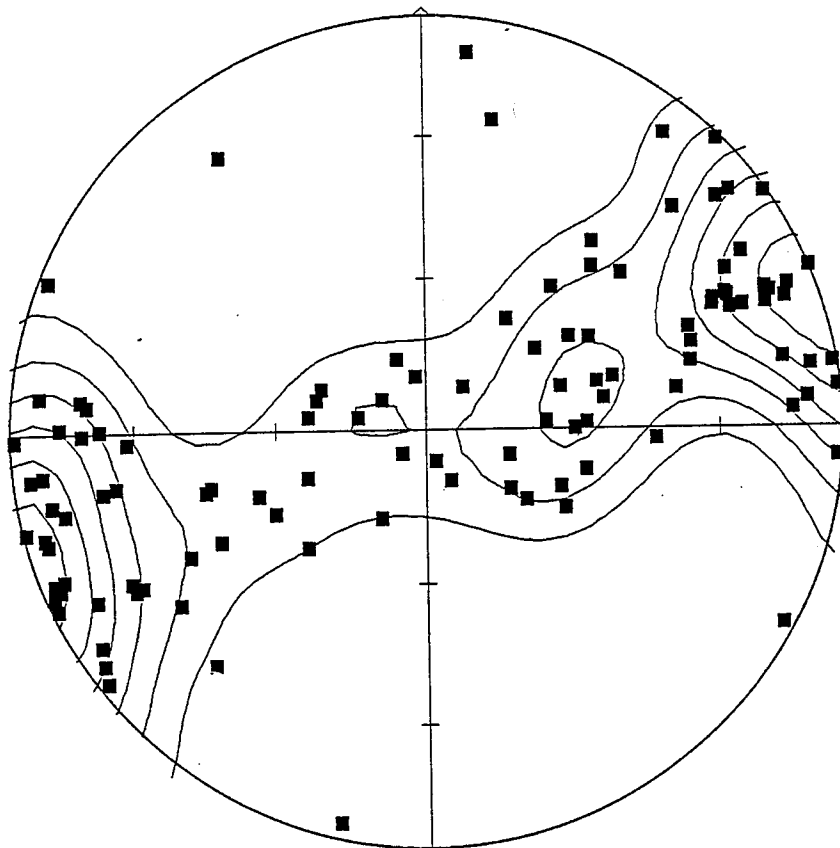




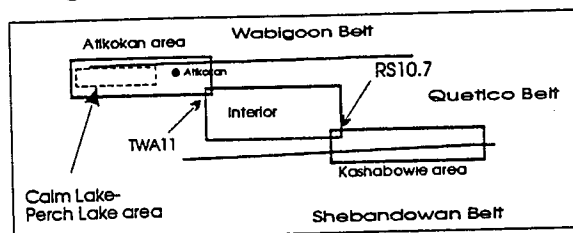
Fig. 12.5f. AARM max axes orientations - Data from all areas together.

ARM anisotropy maximum axes - Quetico Belt margins and interior



$N = 110$   
 $k = 26.44$   
 $(\text{Peak} - E)/\text{Sigma} = 11.5$   
 Peak position :  $70.6^\circ / 0.2^\circ$

$E = 4.16$   
 $\text{Sigma} = 1.39$



steep (plunge of  $62^\circ$ ) like the mean AARM lineation for low grade metasediments east of Atikokan (Fig. 12.5b).

In both remaining areas AARM lineations are very shallow and well grouped around their means, plunging gently ( $4-5^\circ$ ) to ENE (Fig. 12.5d-e, Table 12.6).

Table 12.6. The orientation of AARM maximum axes (AARM lineations).

Area	N	Counting method	PCA method
Calm L.-Perch L.area	46	81/62 ( $6\sigma$ )	73/62 (55/7)
east of Atikokan	10	90/77 ( $5\sigma$ )	110/84 (26/9)
whole Atikokan area	56	81/62 ( $8\sigma$ )	77/76 (33/5)
interior	32	75/4 ( $12\sigma$ )	73/4 (11/6) ?
Kashabowie area	22	65/5 ( $9\sigma$ )	63/5 (13/9) ?
All areas total	110	71/0 ( $12\sigma$ )	71/10 (15/5)

#### The variations of AARM fabric along the traverse.

In Calm Lake - Perch Lake area the orientation of AARM foliation planes show variations in plunge that may be of the order of up to  $30^\circ$  from one outcrop to another. However, these changes are not erratic but rather on a smaller scale the foliation orientations are similar. If strikes of those planes are normalized only to  $0-180^\circ$  sector, some consistent changes of the strike directions can be observed for both traverses (highway 11 and CNR track, Fig. 12.7a and Map 12.8).

On the traverse across the belt from Atikokan to Kashabowie Lake low grade metasediments have a uniform direction of AARM foliations (Fig. 12.7b and Maps 12.9 and 12.10). In the interior

of the belt the orientation of AARM foliations become more erratic and change rapidly from one outcrop to another (Fig. 12.7b, Map 12.9).

In the metavolcanic zone within Shebandowan Belt near Kashabowie AARM foliations vary remarkably along the traverses well (Fig 12.7, Map 12.10).

AARM lineations show large changes of its strike in Calm Lake - Perch Lake area, but changes in their plunges are much more ordered (Fig. 12.11a, Map 12.8). Going east those variations are getting minor for a steeply plunging lineations east of Atikokan and shallow lineations in the interior of the belt and Kashabowie Lake area (Fig. 12.11b, Maps 12.9 and 12.10).

This uniform orientation of AARM lineations along the traverse (except the narrow zone near northern margin of the belt) indicates that the mechanism that generated the AARM lineations fabric had to be also homogeneous throughout the area.

#### **The relations between sedimentary, tectonic and AARM fabric.**

Samples from three series from fold closures (FA and FB) and a graded bed (PLR) collected in Calm Lake - Perch Lake area show close grouping of their ARM fabric within the series at directions that are completely different than those of the whole

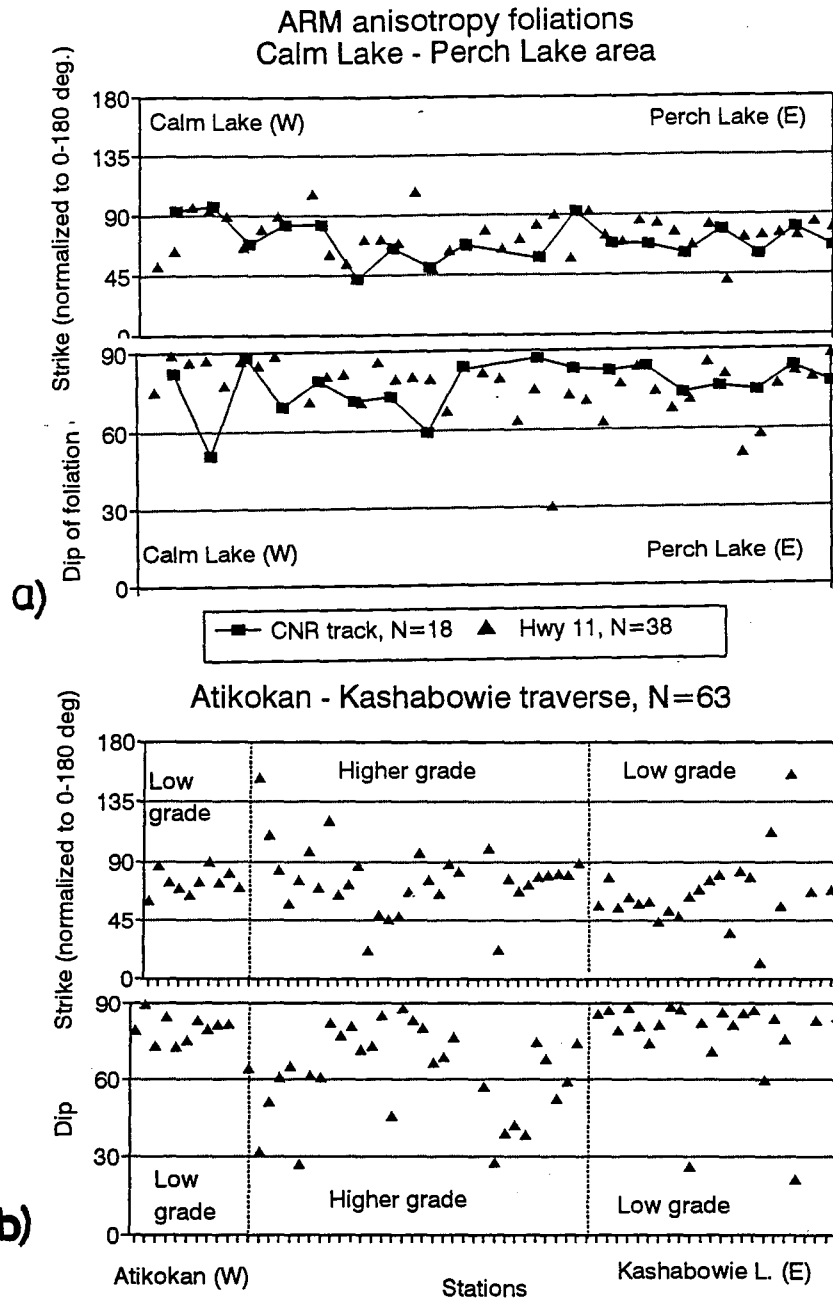
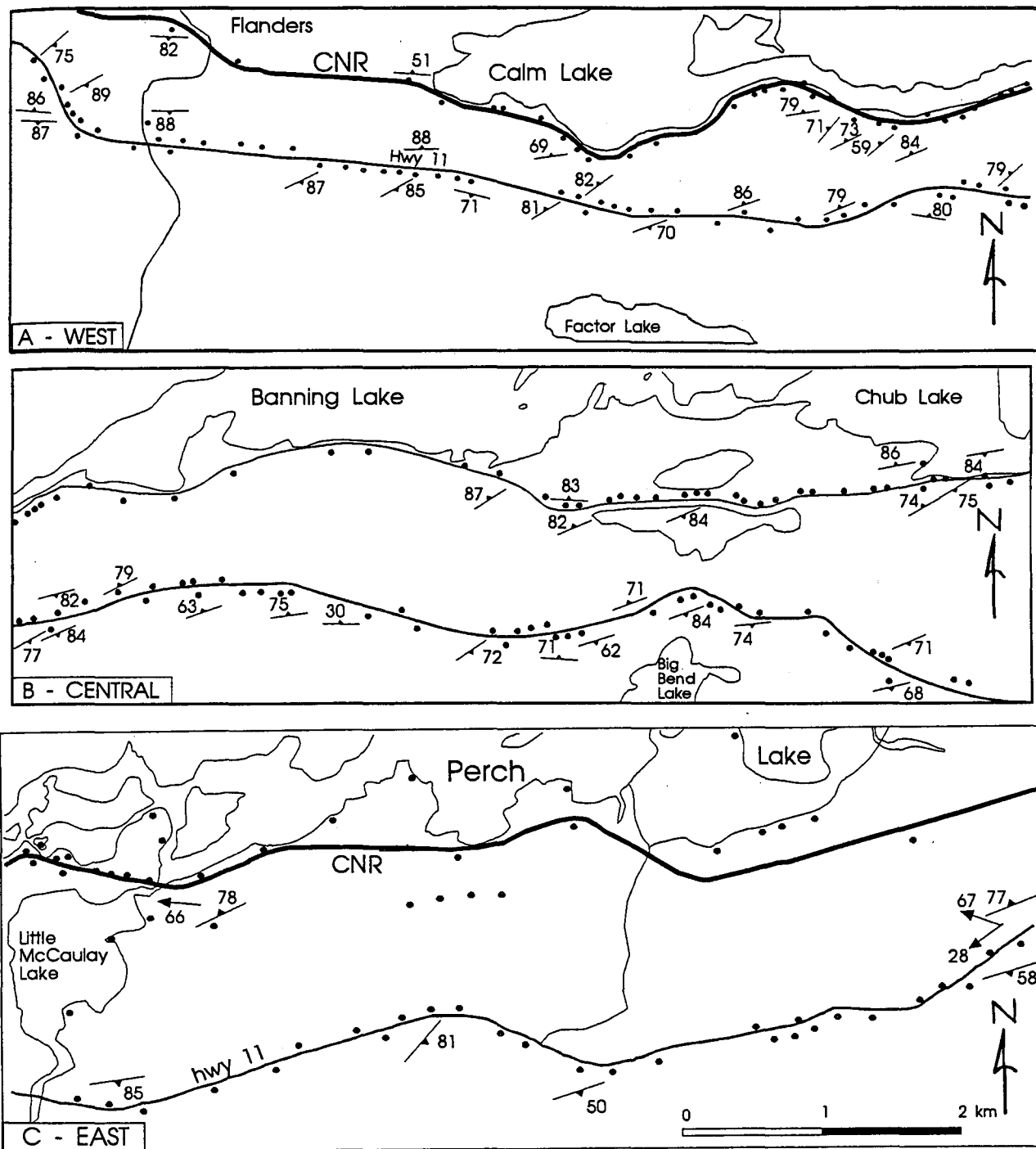


Fig. 12.7. Variations of directions of AARM foliations along traverses. a) - Calm L. - Perch L. traverse; b) Atikokan - Huronian L. traverse. Note more erratic dips of AARM foliations in the interior of the belt.



- ▲— ARM foliation
- ▶— ARM lineations - maximum axes of anisotropy

Fig. 12.8. Map of AARM fabric foliations and lineations in Calm Lake - Perch Lake area. AARM foliations for 3 sections of the area (west, central and east) and AARM lineations in eastern section of the area.

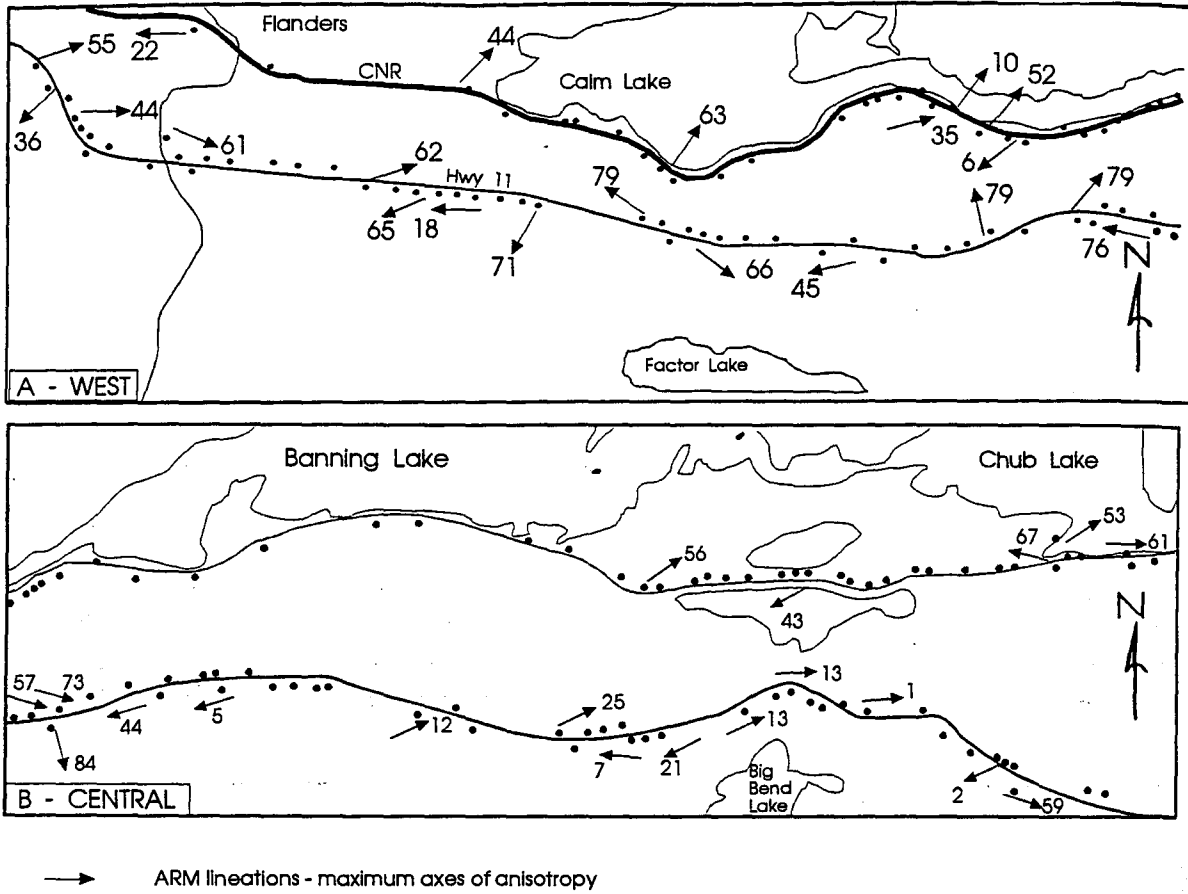
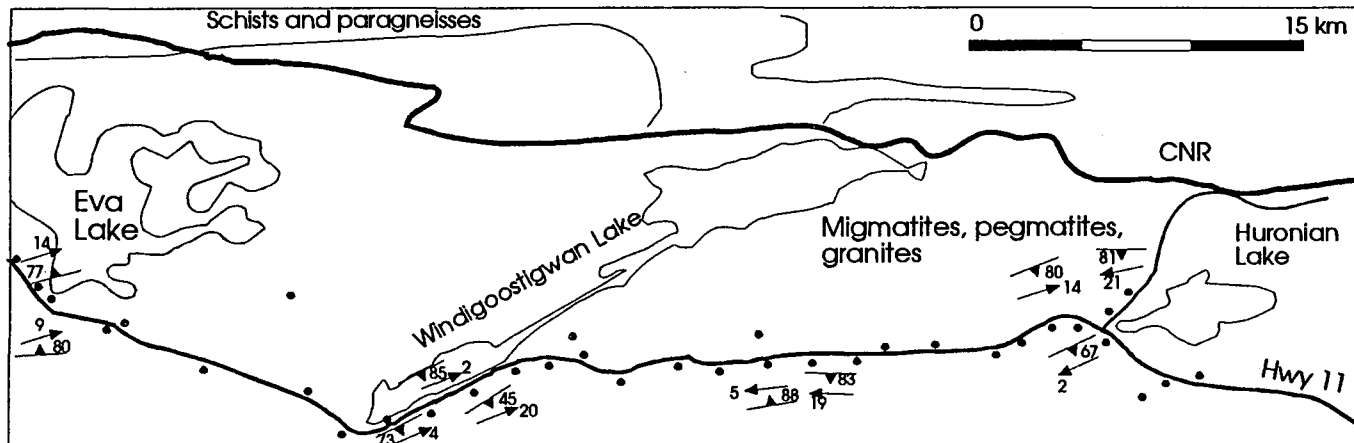
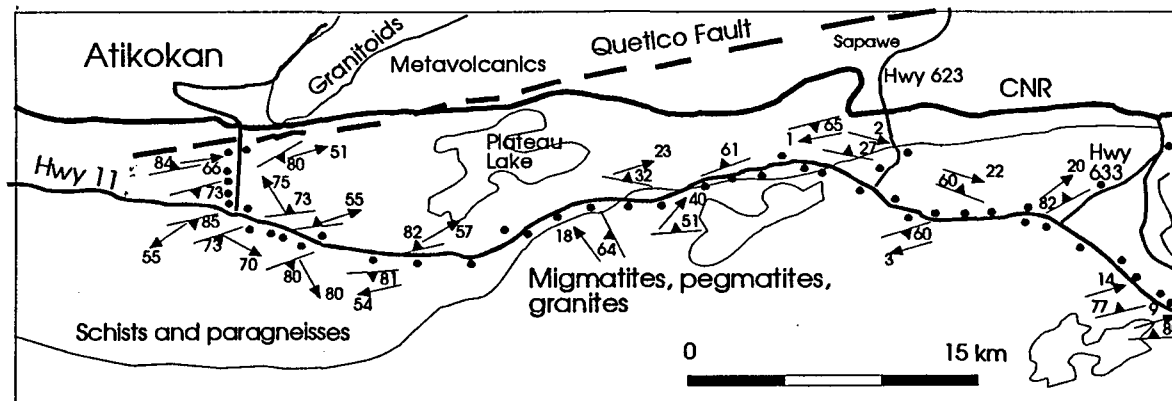
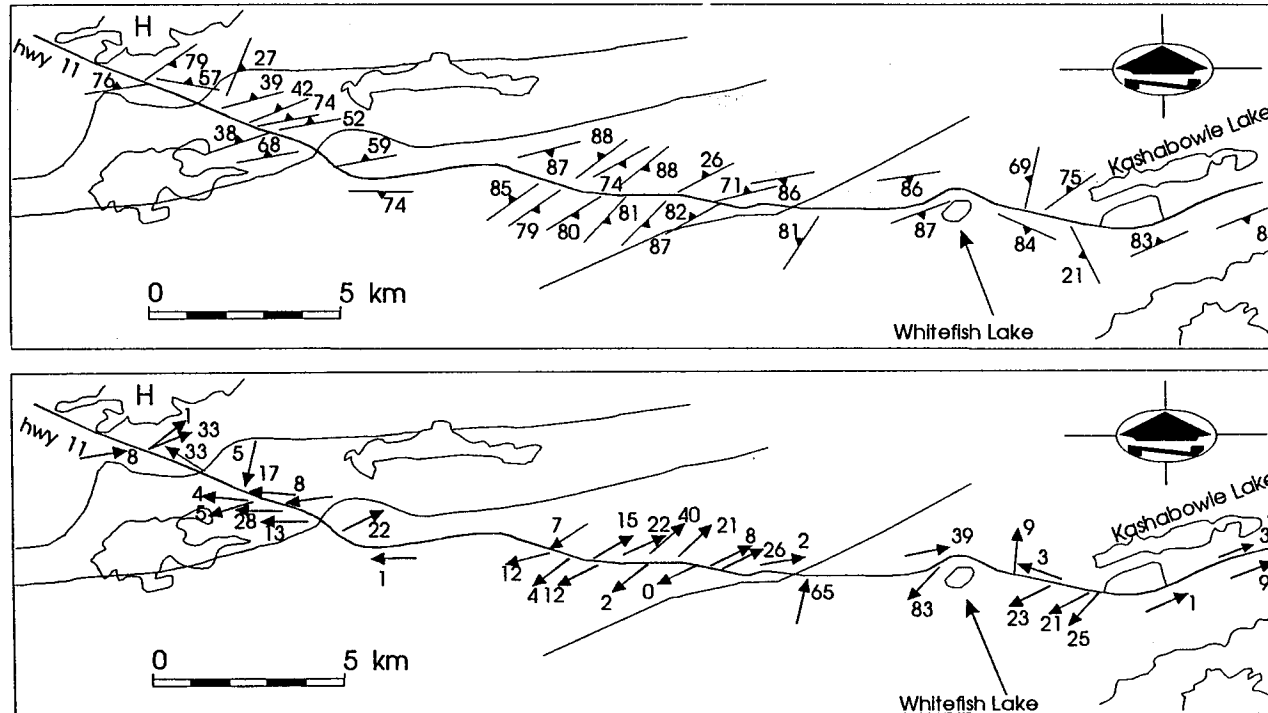


Fig 12.8. continues. AARM lineations in western and central sections of Calm Lake - Perch Lake area.

Fig. 12.9. Map of AARM fabric foliations and lineations along Atikokan - Huronian Lake traverse.

- ▲ - AARM foliations;
- ➔ - AARM lineations.





- ┘ ARM foliation
- ARM lineations - maximum axes of anisotropy

Fig. 12.10. Map of AARM fabrics, foliations and lineations along Huronian Lake - Kashabowie Lake traverse.



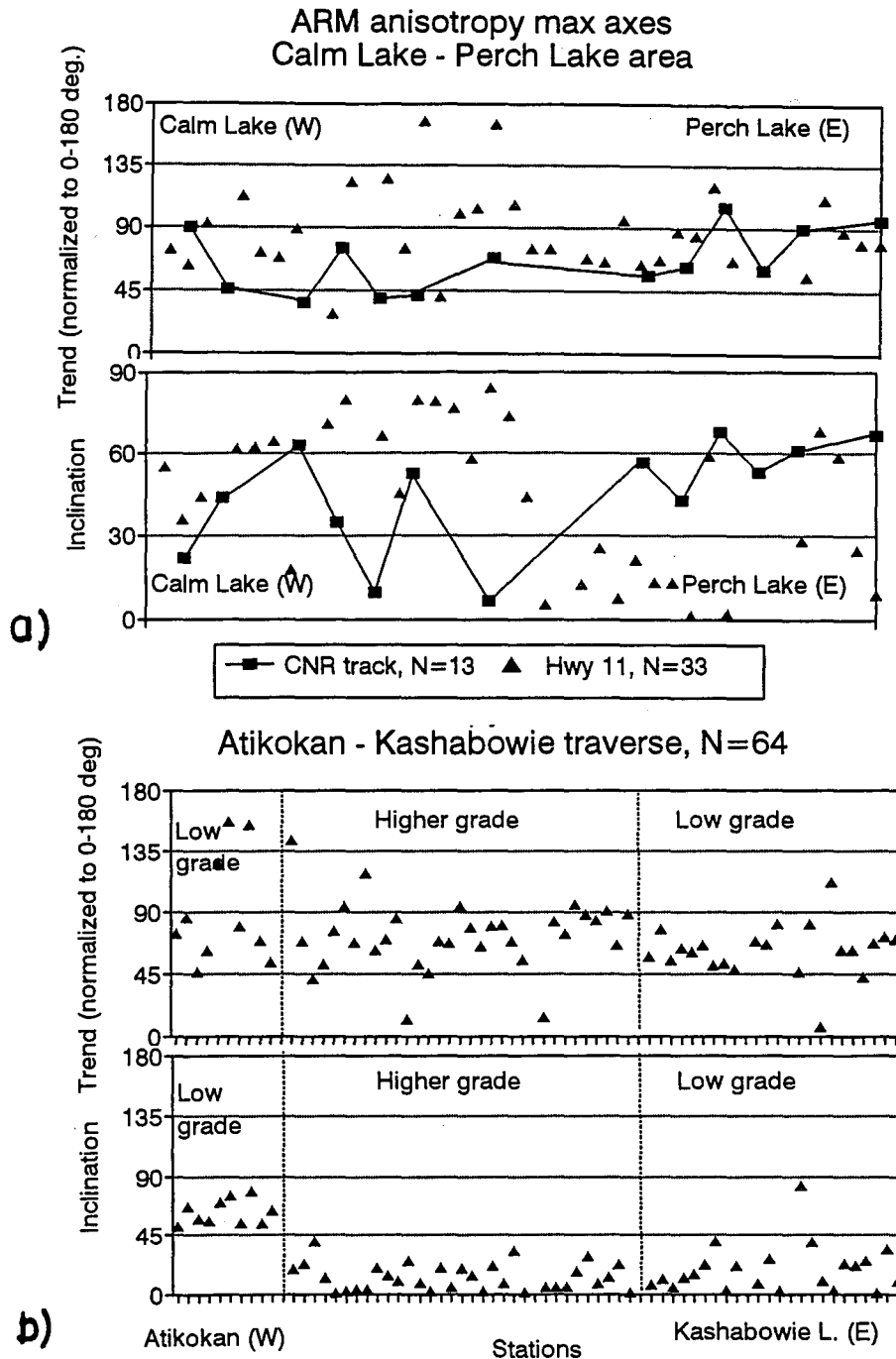


Fig. 12.11. Variations of directions of ARM lineations along traverses. a) - Calm L. - Perch L. traverse; b) Atikokan - Huronian L. traverse. Note very uniform plunges of ARM lineations along Atikokan - Kashabowic Lake traverse; steep east of Atikokan, shallow in the interior of the belt and Kashabowic area.

region data (Fig 12.12 - 12.14). The ferromagnetic phase in those rocks was recognized as pyrrhotite.

In fold closures AARM lineations group near  $S_0/S_1$  intersection lineations with some spread along the schistosity plane (Fig. 12.12 and 12.13). AARM foliations are not quite parallel to a pole to  $S_1$  plane, but deflected of about  $30^\circ$ . The orientation of bedding surfaces was not available, therefore the relations between  $S_0$  surfaces and AARM min axes were not examined.

In a graded bed with refracted cleavage the relation between AARM fabric and tectonic and sedimentary fabric is similar. AARM foliations are oriented along schistosity planes near  $S_0/S_1$  intersection lineations (Fig. 12.14). AARM foliations are more tightly grouped than  $S_1$  schistosity planes across the bed and largely offset from the bedding plane. That clustering suggest that AARM fabric is post-tectonic (and post-folding) and the growth of pyrrhotite was probably controlled by the orientation of recrystallized paramagnetic matrix. However, some effect of a sedimentary fabric on AARM still can be preserved as a weak grouping of AARM lineations near  $S_0/S_1$  exist. It was more prominent in case of AMS fabric (Borradaile et al., 1988) as paramagnetic phase is partly pre-tectonic.

Fig. 12.12. AARM fabric for a major fold in metasediment near Flanders. a) AARM lineations are near  $S_0/S_1$  intersection lineation, AARM foliation at low angle to  $S_1$ . b) distribution of AMS fabric for the same fold (from Borradaile et al., 1988).

AARM fabric - major fold near Flanders

Calm Lake - Perch Lake area

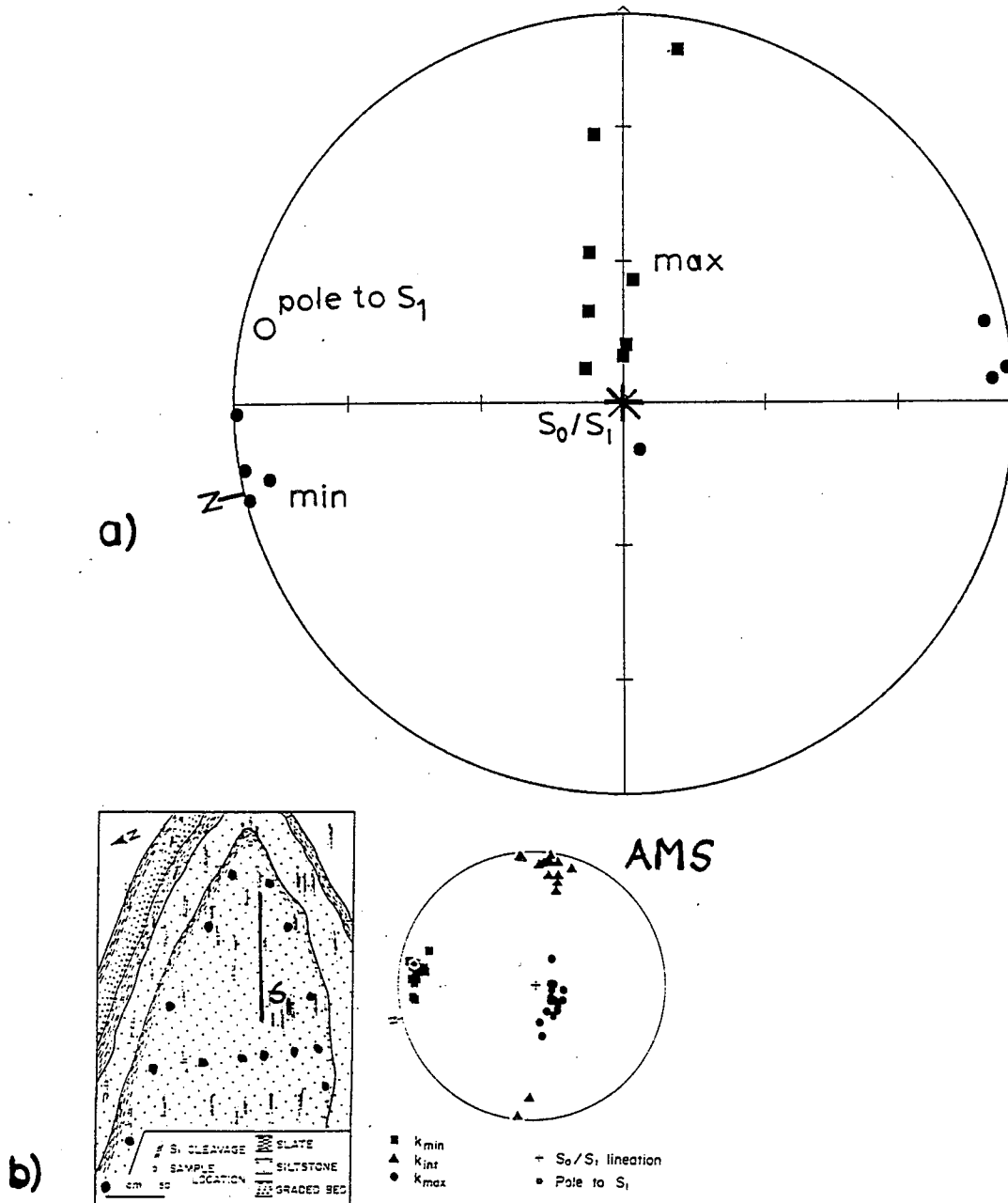


Fig. 12.13. AARM fabric for a minor fold in metasediment near Banning Lake. a) AARM lineations are near  $S_0/S_1$  intersection lineation, AARM foliation at low angle to  $S_1$ . b) distribution of AMS fabric for the same fold (from Borradaile et al., 1988).

AARM fabric - minor fold near Banning Lake

Calm Lake - Perch Lake area

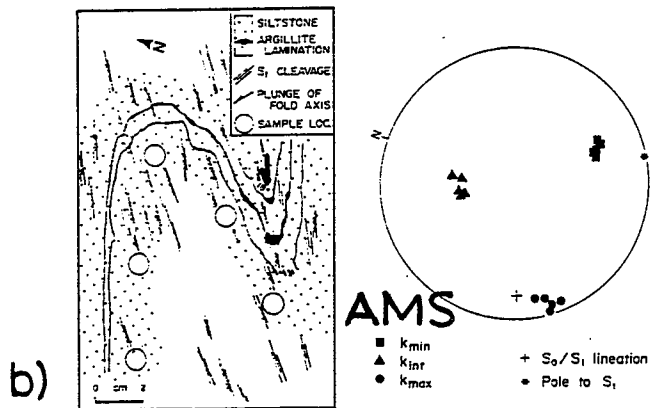
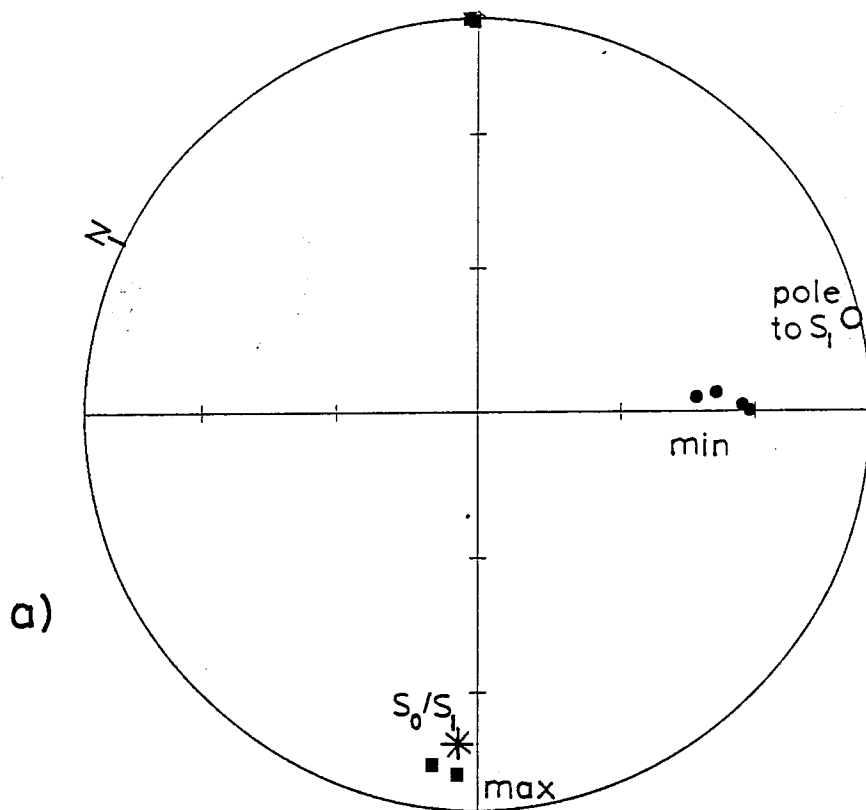
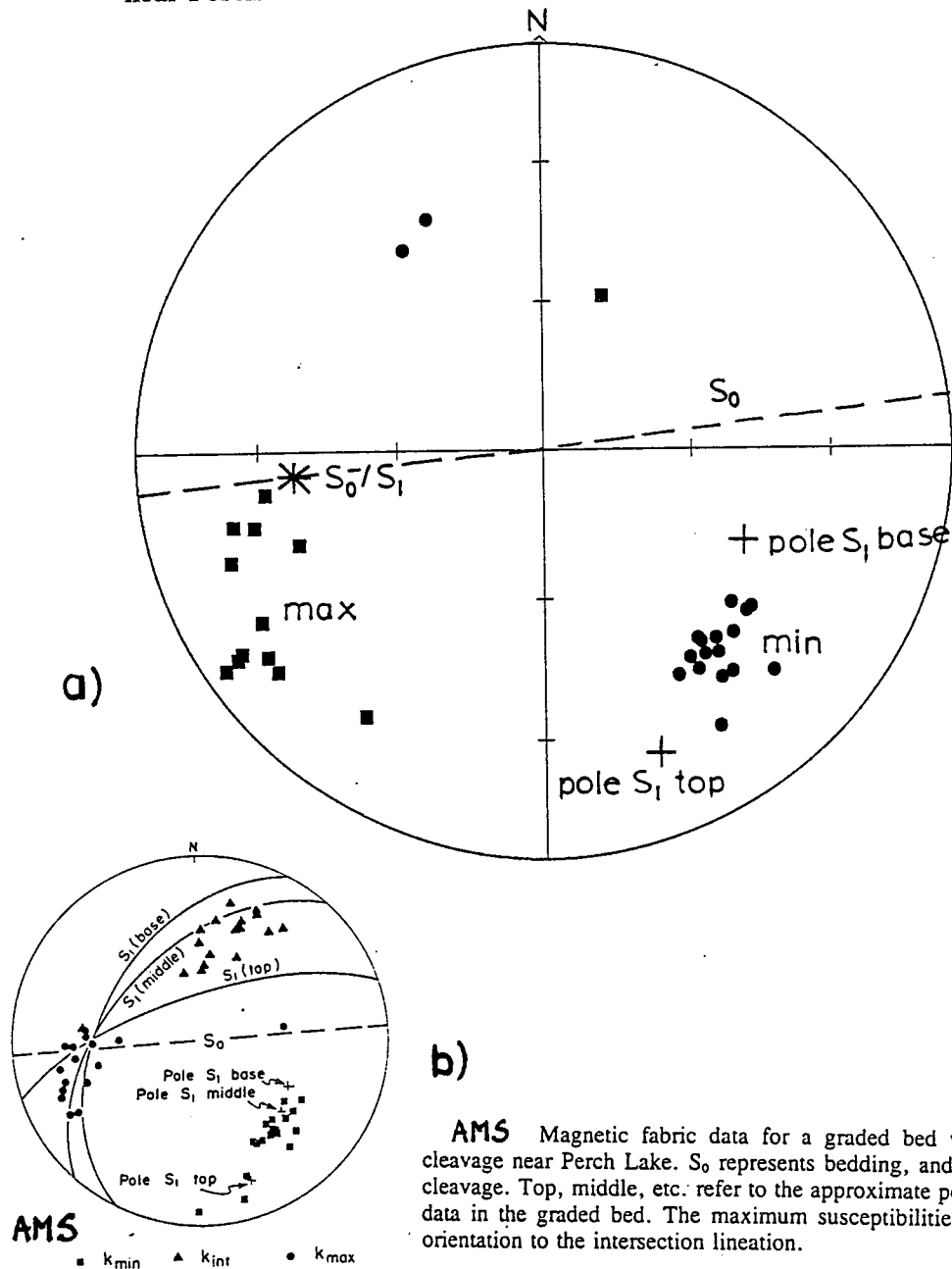


Fig. 12.14. AARM fabric for a graded bed with refracted cleavage near Perch Lake. a) AARM lineations are spread along  $S_1$  plane near a direction of  $S_0/S_1$  intersection lineation, AARM foliation between  $S_1$  of top and base of the bed; see text for discussion. b) AMS fabric for the same bed (from Borradaile et al., 1988).

AARM fabric - a graded bed with refracted cleavage  
near Perch lake - series PLR



AMS Magnetic fabric data for a graded bed with refracted cleavage near Perch Lake.  $S_0$  represents bedding, and  $S_1$  represents cleavage. Top, middle, etc. refer to the approximate positions of the data in the graded bed. The maximum susceptibilities are close in orientation to the intersection lineation.

### 12.3. Shape of AARM fabrics and anisotropy parameters.

The anisotropy parameters ( $P'$  and  $T$ ) were determined for all samples which possessed at least one well determined principal axis (that includes both perfect oblate and perfect prolate fabric).

The anisotropy parameter  $P'$  for ARM in all three areas is substantially larger than for susceptibility and suggests that the ferromagnetic phase carrying ARM may be mostly pyrrhotite and not magnetite (Fig. 12.15).

In the northern margin of the Quetico Belt (Atikokan area) anisotropy parameters for this area show quite a consistent distribution (Fig. 12.16). They are generally oblate with a high anisotropy ratio (greater than 2) typical for metasediments with pyrrhotite. High p.c.o. of pyrrhotite grains increases the overall mean anisotropy (mean  $P'=5.7 \pm 4.1$ , Fig. 12.16).

The highest values of anisotropy ratio ( $P' > 8$ ) are typical for those samples collected near the CNR track in the vicinity of Quetico Fault. A few samples with weakly developed prolate fabric ( $T > -0.2$ ) are not grouped together and are not significant (Fig 12.17a).

A highly anisotropic oblate fabric was present in the zone of the lowest grade metamorphic rock next to Quetico Fault near Atikokan ( $P'$  of values 15-20) due to very strong p.c.o. of matrix controlling p.c.o. of pyrrhotite grains (Fig. 12.17b).

Within the interior of the belt both prolate and oblate

Distribution of P' parameter - ARM data  
the Quetico Belt margins & interior

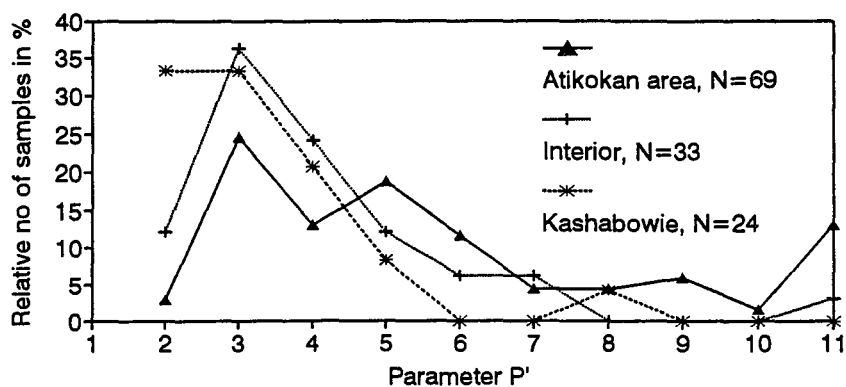


Fig. 12.15. A histogram of distribution of anisotropy ratio parameter P' for three sub-areas. Most of samples have P' from a range of 2 to 4 , with some higher anisotropies in Atikokan area.

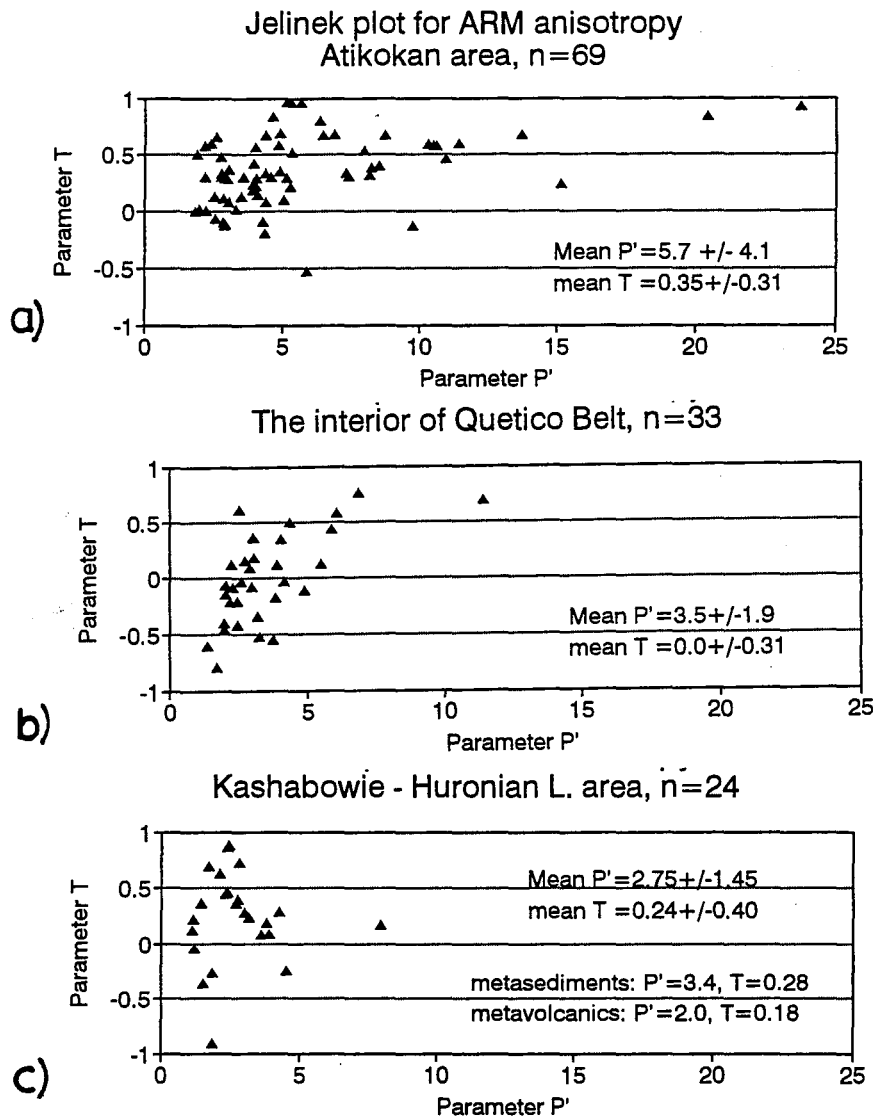
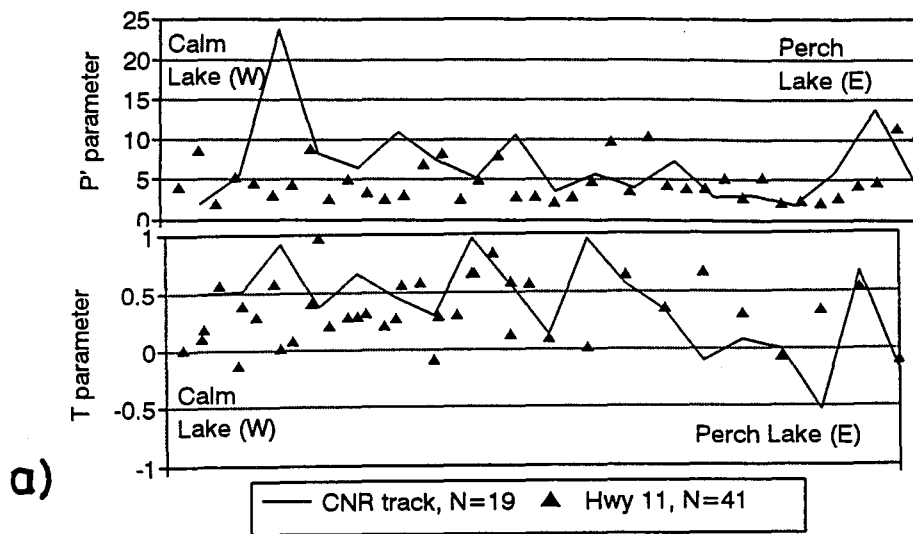


Fig. 12.16. Jelinek plot of anisotropy parameters P' and T for AARM fabric from three subareas (a-c). Note the highly anisotropic oblate fabrics in Atikokan area and common prolate fabric in the interior of the belt and metavolcanics. See text for discussion.



P' & T parameters for ARM anisotropy  
Calm Lake - Perch Lake area



Traverse Atikokan - Kashabowie L., N=67

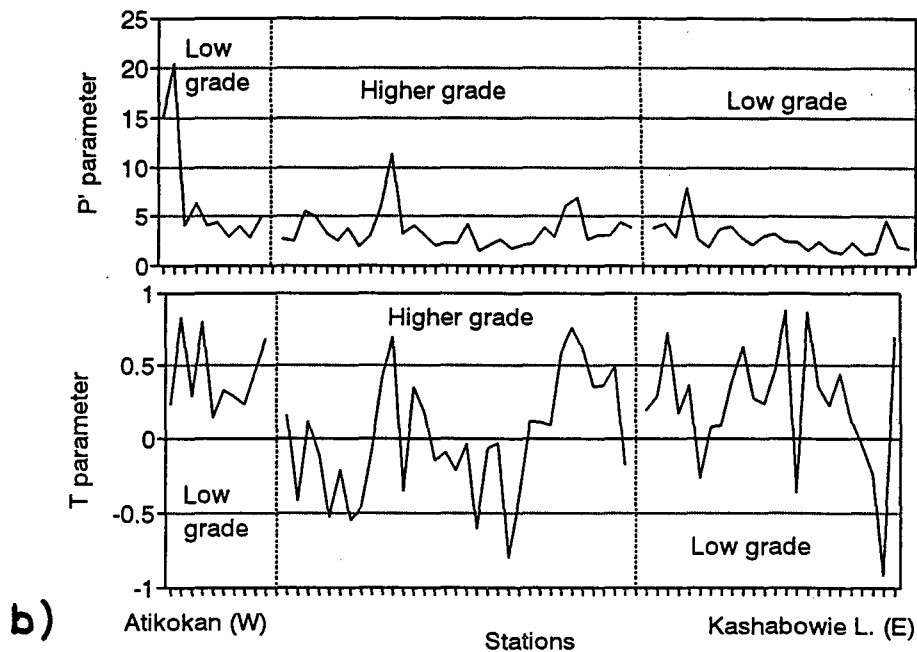


Fig. 12.17. Variations of anisotropy parameters  $P'$  and  $T$  for AARM fabric along traverses. a) - Calm L. - Perch L. area, b) Atikokan - Kashabowie L. traverse. Note significant changes in  $T$  parameter in the interior of the belt and the highest anisotropy in the vicinity of the Quetico Fault.

fabric are detected (Fig. 12.16b, mean  $T=0!$ ) with prolate ARM grouped next to Sapawe and Eva Lake and east of Windigoostigwan Lake (from station TW17 to the east) in lower grade migmatites as well (Fig. 12.17b). These prolate fabric are associated with lower anisotropy ratio (less than 4). Only some of these samples had amphibolite composition (magnetite bearing, although the anisotropy of ARM seems to be too high for magnetite only). However most of them did not reveal the presence of magnetite in thermomagnetic curves (see Appendix C). Therefore these prolate fabrics may have formed late, when the shearing component of deformation was much larger than the compressive one.

The other strong prolate fabric are reported in metasediments with very weak ARM as probably a measurement error (Fig. 12.17b).

In low- grade metasediments and metavolcanics in Kashabowie - Huronian Lake area the Jelinek  $P'$ - $T$  plot indicates that 5 (20%) samples have prolate fabric usually associated with low anisotropy ratio (less than 2, Fig. 12.16c). Two (of four) metavolcanic samples with substantial prolate fabric are magnetite -bearing (stations RS1.1, Spark, 1991 and RS1.3).

The distribution of  $P'$  parameter shows that for metasedimentary outcrops, the anisotropy ratio is larger than for metavolcanic ones (Fig. 12.16c). Metavolcanics do not possess strong p.c.o. and are more often magnetite- bearing with lower potential anisotropy of remanence for single grains. However, even in the metavolcanic rocks, high anisotropy is

observed in rocks with mostly magnetite (RS1.3, compare the thermomagnetic data in Appendix C).

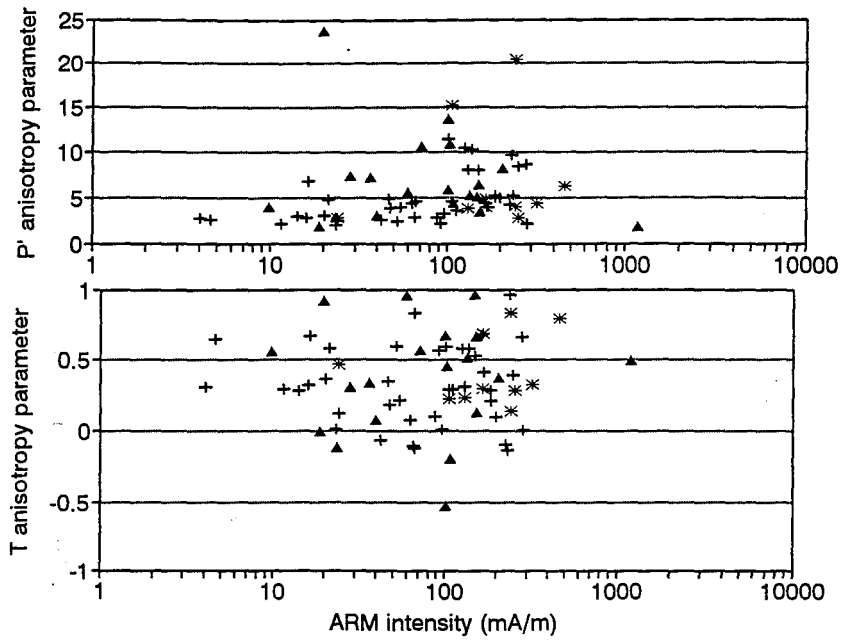
**Anisotropy of ARM and ARM intensity.**

The relation between the intensity of ARM and anisotropy parameters was also examined.

The weak trend of the increase of anisotropy ratio with ARM intensity can be postulated in all areas (Fig. 12.18). However there is no linear correlation between  $P'$  and ARM intensity.

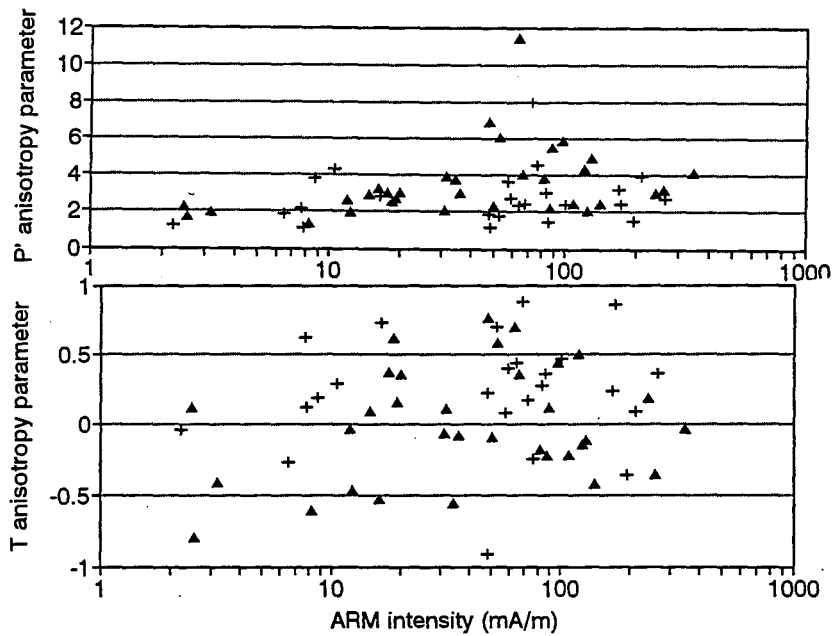
Neither was a dependence found between the parameter  $T$  and ARM intensity.

P' & T parameters versus ARM intensity  
Atikokan area - low grade rocks



▲ CNR track, N=19 + Hwy 11, N=41 \* east of Atik., N=10

Interior & Kashabowie area



▲ Interior, N=33 + Kashabowie, N=24

Fig. 12.18. A correlation between parameters of anisotropy of ARM and intensity of ARM. a) Atikokan area; b) Interior and Kashabowie area. Any correlation between P' or T and ARM intensity does not exist.

## Chapter 13.

### Tectonic and magnetic fabrics - discussion.

#### 13.1. The differences between fabrics in 3 separate suites.

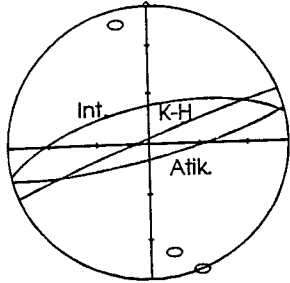
The studies of tectonic and magnetic fabric were performed for three separate areas: low grade metasediments at the northern margin of Quetico Belt ("Atikokan area"); higher grade (above staurolite isograd) metasediments ("Interior of belt") and lower grade metasediments and metavolcanics on the southern margin of the belt ("Kashabowie area"). The detailed results are reported in chapters 5, 8, 10 and 12.

#### **Tectonic fabrics.**

At the margins of the Quetico Belt  $S_1$  foliations are subvertical along the traverses. Only one pervasive schistosity ( $S_1$ ) is observed in each outcrop. The mean strike ENE - SWS is consistent along the traverses. In the centre of the belt  $S_1$  planes are less steep (mean dip is  $68^\circ$ ), however the mean direction of strike remains similar to those from the margins (Fig. 13.1a).

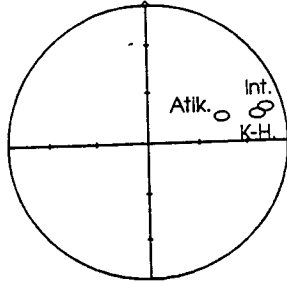
Schistosity is well developed in most mafic outcrops in the pegmatite - migmatite zone and it is weak in pegmatite and granitoid bodies. The more gentle plunge of schistosity planes in schistose parts of outcrops are associated typically with the

S1 foliations  
- all areas

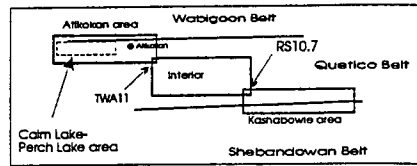


A

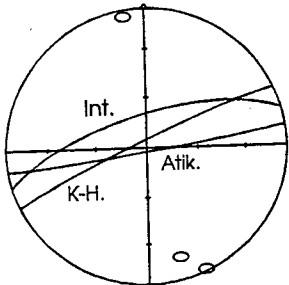
L1 lineations  
- all areas



B

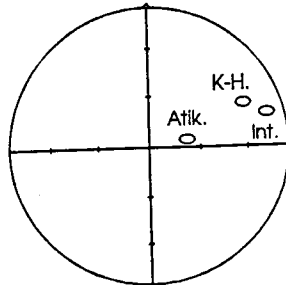


AMS foliations  
- all areas



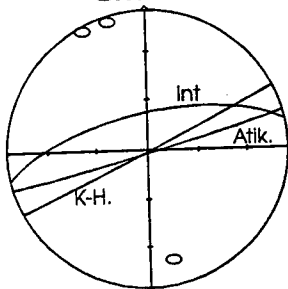
C

AMS lineations  
- all areas



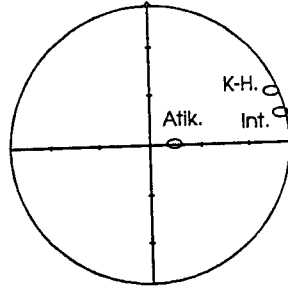
D

AARM foliations  
- all areas



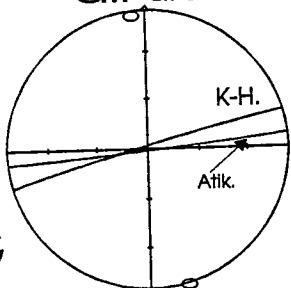
E

AARM lineations  
- all areas



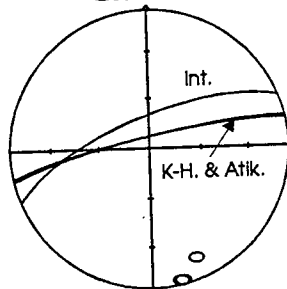
F

S0 bedding planes  
- all areas



G

ChRM directions  
- AF demag.  
- all areas



H

Fig. 13.1.  
A comparison  
of planar and linear  
fabric for different  
areas. Note variations  
in the orientation of  
each fabric  
in 3 sub - areas.  
An error of orientation  
of each fabric is not  
shown.

intrusions of more felsic bodies.

Observed lineations are mainly extension lineations in schists in higher metamorphic rocks or  $S_0/S_1$  intersection lineations in metasediments in Calm Lake - Perch Lake area ("Atikokan area").

$S_0/S_1$  lineations on the northern margin are weakly clustered and spread along  $S_1$  foliation plane. Extension lineations in chlorite and biotite schist east of Atikokan cluster weakly around a quite steep mean value (with a plunge of  $52^\circ$ ). In the interior of the belt and at the southern margin  $L_1$  fabric plunges gently to ENE (Fig. 13.1b).

The large scatter of  $S_0/S_1$  fabric in Calm Lake - Perch Lake area can be explained by the existence of a structure of sheath folds south of the Quetico Fault with varying plunges of fold axes and varying structural facing (Borradaile et al., 1988). A steeper orientation of  $L_1$  fabric in highly sheared zone south of Atikokan can be correlated with a compressive component of deformation in that area.

#### **AMS fabrics.**

AMS foliations at the northern margin of the Quetico Belt (in Calm Lake - Perch Lake and east of Atikokan) are almost vertical and near W-E striking (Fig. 13.1c). Also at the southern margin this fabric is subvertical and strikes slightly more to the south-west. In the interior of the belt AMS planes are less steep but the overall ENE-SWS strike prevails.

AMS lineations have a similar orientation to the tectonic  $L_1$  fabric (Fig. 13.1d). The plunges of these fabrics are steep and poorly defined in the Atikokan area, but shallow and consistent in the other areas (in the interior and in Kashabowie area).

#### **AARM fabrics.**

Both AARM foliations and lineations show a similar variations between three areas as AMS and tectonic fabrics (Fig. 13.1e,f). However due to a smaller number of samples the mean positions of AARM fabric are worse defined than those for AMS and tectonic fabric.

#### **$S_0$ bedding at the belt margins.**

Primary bedding is preserved only in low grade metasediments at the belt margins. It is subparallel to later  $S_1$  schistosity and as the other fabrics subvertical in both areas (Fig. 13.1g).

#### **The orientation of ChRM girdle.**

Planes fitted to ChRM directions of A & B classes are subvertical in the margin of the belt areas and more gentle dipping in the interior just like the other fabrics (Fig. 13.1h). However, their orientations are poorly defined (angular standard deviations of  $30^\circ$  or more). Those orientations exhibit the strong correlation between observed ChRM directions and AARM



foliations.

All fabrics, when their orientation in three areas is considered, show the subvertical orientation of planar fabrics at the belt margins and more gentle dips of these fabrics in the centre of the belt (usually dips are of value of 60-70°).

Linear fabrics plunge gently (plunges of values of 10-30° are typical) in the interior of the belt and at southern margin. However they are much more poorly clustered at the northern margin and the plunges of their mean orientations are quite steep (60 -70°). These fabrics usually are spread along the foliation plane. Although the accuracy of determinations of a mean direction of any linear fabric in the Atikokan area is poor, the similar orientation (gentle plunge to ENE) of all linear fabrics seems to be significant.

### 13.2. Detailed correlations of orientations of planar and linear fabrics.

It is not purpose of this study to examine the correlation between final strain in visited three areas and anisotropy ratios for ARM anisotropy and AMS. No strain data were available from Calm Lake - Perch Lake area and in the interior of the belt; reliable finite strain markers were not preserved due to high metamorphism in the area. Therefore fabric correlations in this study are based on the directional analysis of AMS, ARM and tectonic fabric as well as the correlation of  $S_1$ , AMS and ARM foliations for individual samples with all three fabrics known.

The anticlockwise (to the north) offset of ARM and AMS fabric with respect to tectonic fabric postulated in other studies as a kinematic indicator of the dextral shearing component (e.g. Spark, 1991, Dehls, 1992) was reexamined here for all three areas.

For each of three areas a relative orientation of tectonic fabric, AMS fabric and AARM were compared. The positions of poles to foliation planes and directions of lineations are plotted on the stereoplot. Positions of mean directions determined by principal component analysis (PCA) method together with a 95% confidence cone were taken as a mean orientation of each fabric. Confidence cones are drawn on the equal - area projection plot only approximately, as this projection distorts the shape of an ellipse.

The position of pole to ChRM direction was determined by PCA method as well with an angular standard deviation (ASD) cone around it. However, the ASD parameter is different than 95% cone limit. When the any planar fabric orientation is compared to ChRM plane orientation, the eventual non-overlap of the confidence cone for the planar fabric and an ASD circle for ChRM cannot answer the question whether their directions are truly different.

For any set of two planar fabric a such overlapping of confidence cones cannot also be decisive; the cones on the stereoplot are distorted.

#### **The northern margin of the Quetico Belt.**

Foliations for AMS, AARM and  $S_1$  fabric have very similar orientations, only about  $5^\circ$  apart one from another (Fig. 13.2). AMS and AARM planes are almost vertical,  $S_1$  plane dips steeply to south. However, the  $S_1$  fabric is not so well defined as the other ones because only tectonic data from outcrops east of Atikokan were available (measured in this study). AMS fabric is located between  $S_0$  and  $S_1$  fabric that can suggest that some component of primary sedimentary AMS fabric might persist. However,  $S_1$  and  $S_0$  data are collected from a smaller area than AMS.

The size of an confidence cone around AMS planar fabric may indicate that the difference between AMS and  $S_1$  fabric is significant. AARM fabric, on the other hand, is located closer

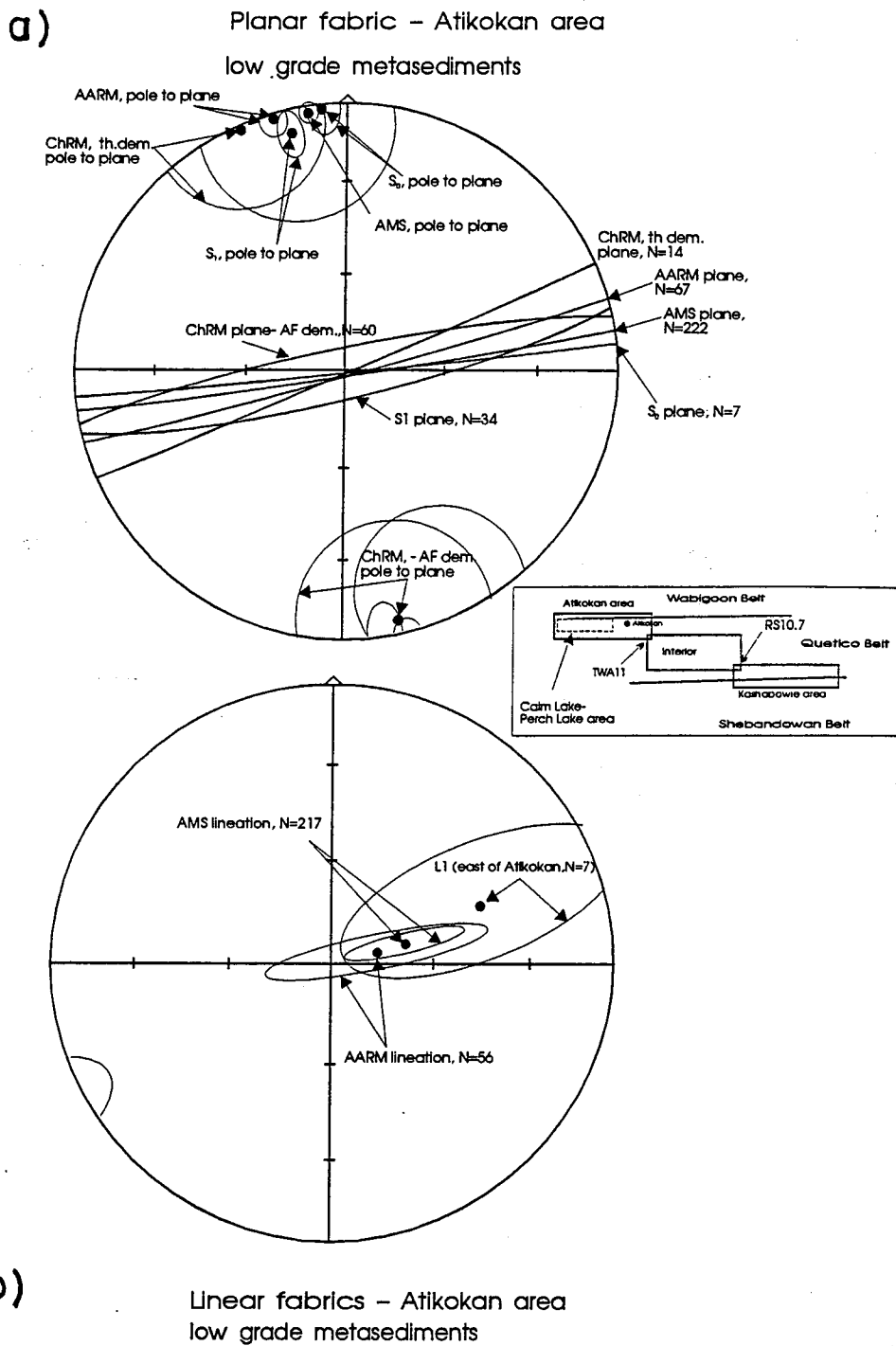


Fig. 13.2. Planar (a) and linear (b) fabric for northern margin of the belt - Atikokan area. Confidence cones are shown around poles to planes and directions of linear fabric. However, their shape is approximate.

to  $S_1$  and their confidence cones overlap (Fig. 13.2).

Those observations are consistent with Sarvas (1988) correlations between AMS foliations and  $S_1$  fabric in Calm lake - Perch Lake area. His AMS data from Calm Lake - Perch Lake area were used (198 of 222 samples) in this study as well. He found  $AMS_{min}$  axes perpendicular to  $S_1$  mean plane. However, the accuracy of determination of directions of both planar fabric was not listed.

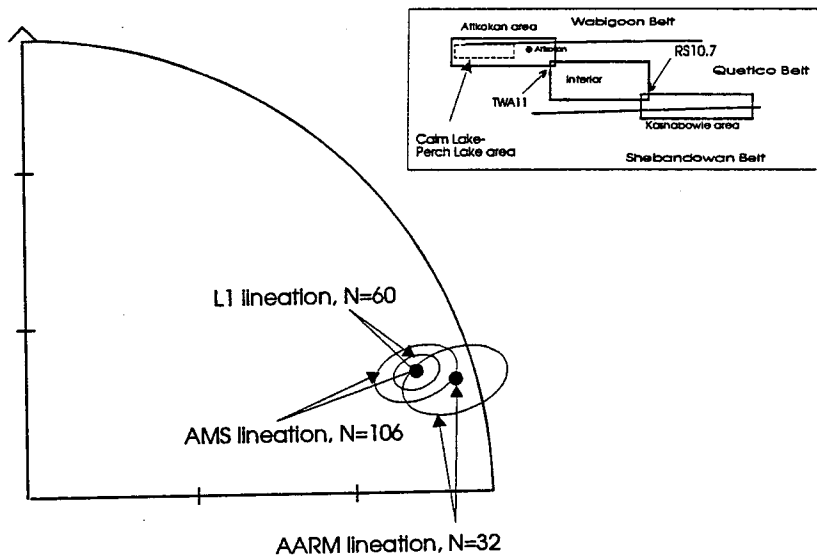
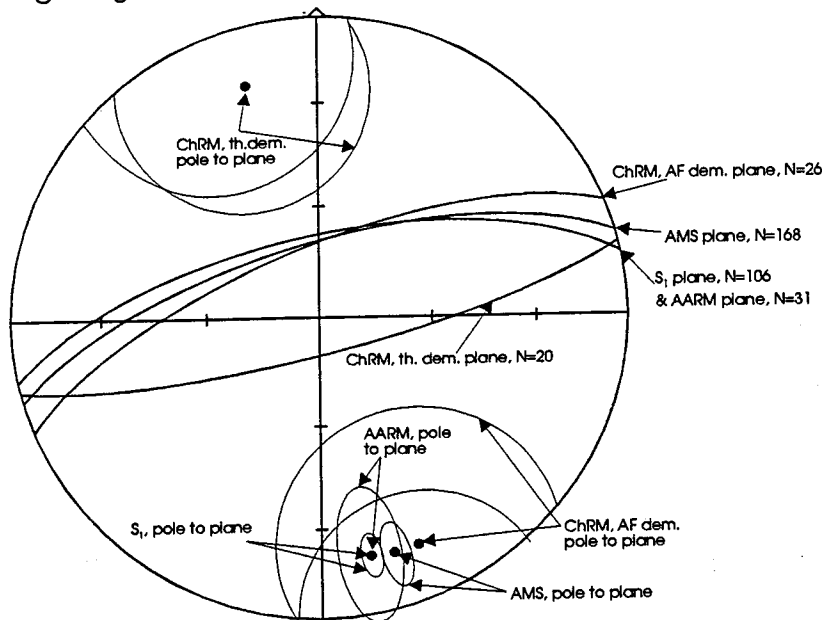
The intersections of  $S_0/S_1$  (after Sarvas, 1988) do not form any well developed cluster within  $S_1$  plane like the distribution of  $\chi_{max}$  axes that are also scattered along the AMS foliation plane (Fig. 5.3). Also extension lineations east of Atikokan form very weak cluster (compare Ch. 5). Similarly, AARM lineations do not cluster as well (compare Ch. 12). Orientations of mean directions of AARM, AMS and  $L_1$  lineations have large confidence cones ( $>30^\circ$  along the foliation planes, Fig. 13.2), but generally are quite steep in the area (plunges more than  $40^\circ$ ).

#### **The interior of the belt - higher metamorphic grade rocks.**

Orientations of tectonic fabrics:  $S_1$  and  $L_1$ , AMS and AARM magnetic fabrics were compared for metasediments from the interior of the belt (Fig. 13.3).

The strike of planar fabric in the area is almost the same with less than  $10^\circ$  variations. ARM foliation is parallel to schistosity and both dip at  $68^\circ$  to the north. AMS foliation is almost parallel to them as well. The difference of the

a) Planar fabric – the interior of Quetico Belt  
higher grade metasediments



b) Linear fabrics – the interior of Quetico Belt  
higher grade metasediments

Fig. 13.3. Planar (a) and linear (b) fabric for the interior of the belt. Confidence cones are shown around poles to planes and directions of linear fabric. See text for discussion.

orientation of AMS planar fabric with respect to two others may be significant if sizes of confidence cones are concerned. However AMS orientations in this area are further from  $S_1$  than the ARM foliations, as in the Atikokan area.

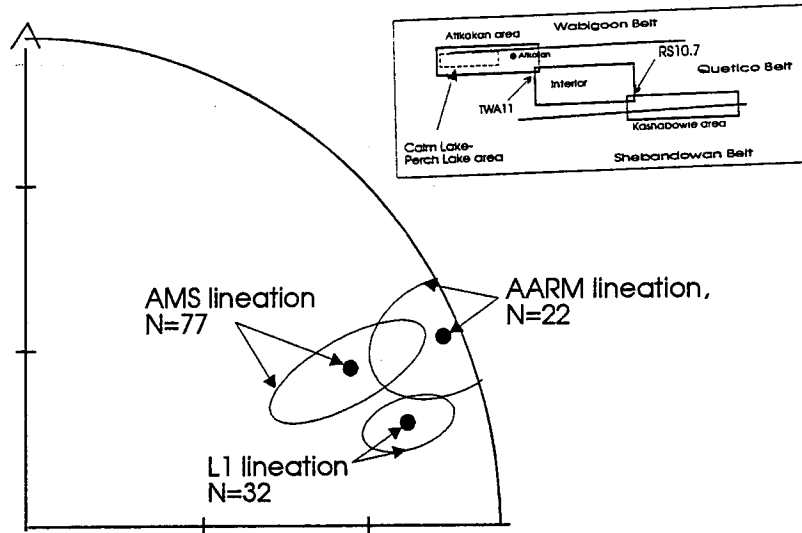
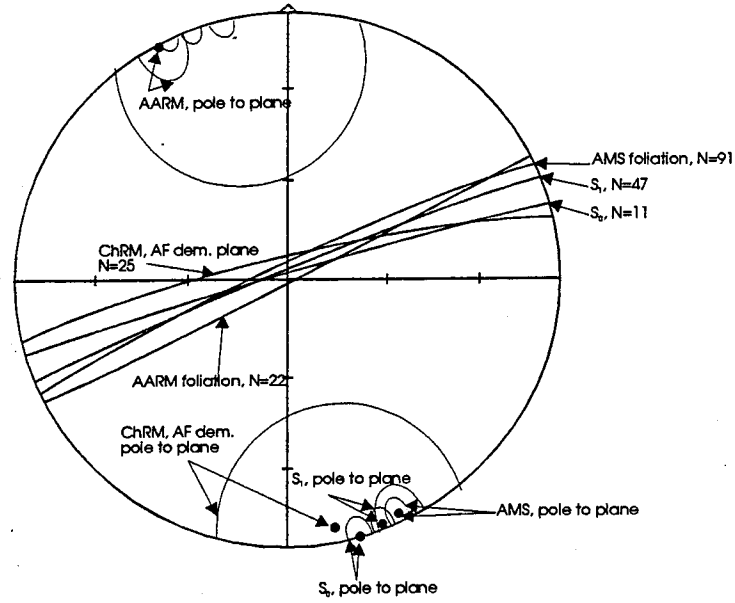
Linear fabrics are better defined than at the northern belt margin (e.g. in Calm Lake - Perch Lake area), indicating that the fabrics are not so uniaxially oblate as in the other area (Fig. 13.3b). The offset of AMS lineation with respect to the mineral lineation exists but remains within the confidence cone area. ARM lineation may be offset to the W-E from the  $L_1$  direction, but it can be non-significant statistically due to a substantially large confidence cone of AARM lineation.

#### **Kashabowie area - low grade metasediments and metavolcanics.**

Studies of fabric in the Kashabowie - Huronian Lake area resulted in the estimate of  $S_0$  and  $S_1$  plane and AMS fabrics by Spark (1990). My study led to the determination of ARM fabric, additional data for AMS fabric and determination of an distribution of ChRM directions for AF and thermal demagnetization procedure.

The orientation of all planar fabric in this area is much more consistent than at the northern margin of the belt (Fig. 13.4). Almost vertical planes of AMS and ARM foliations are close to  $S_1$ , and distances between poles to them are smaller than their confidence cones. The mean AARM foliation is slightly anticlockwise offset with respect to the AMS foliation when

a) Planar fabrics - Kashabowie area  
low grade metasediments & metavolcanics



b) Linear fabrics - Kashabowie area  
low grade metasediments & metavolcanics

Fig. 13.4. Planar (a) and linear (b) fabric for the southern margin of the belt - Kashabowie area. Confidence cones are shown around poles to planes and directions of linear fabric. See text for discussion.



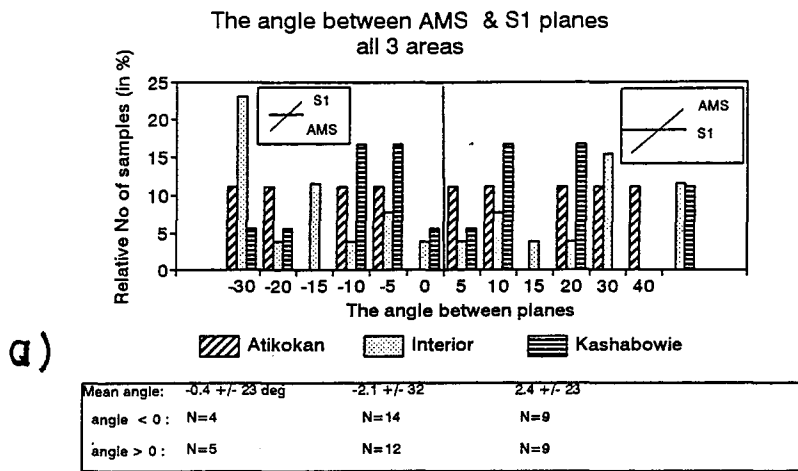
their strikes are compared. The same effect can be noticed for AMS fabric when compared to the mean direction of tectonic  $S_1$  schistosity. The position of primary bedding  $S_0$  is more offset from the other planes, but the bedding was measured only in 11 metasedimentary outcrops.

The linear fabric are oriented to the NE with very gentle plunges (Fig. 13.4b). The anticlockwise offset of ARM and AMS fabrics with respect to  $L_1$  (when their trends are considered) is believed to be statistically significant. However, AARM lineation plunges much more gently than other two fabrics, as in the interior of the belt.

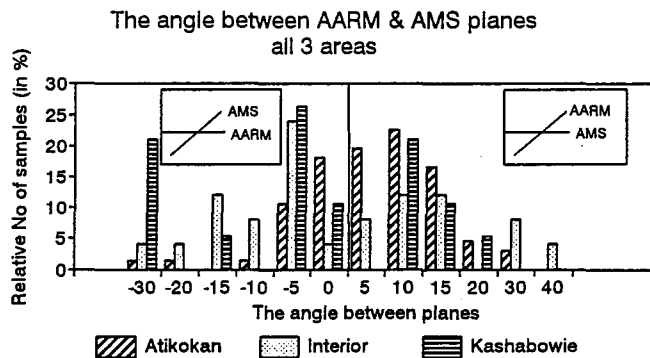
#### **Relations between planar fabrics ( $S_1$ , AARM and AMS) for individual samples.**

Relations between magnetic and tectonic fabrics of individual samples were also examined. The angle between corresponding foliations (AARM and AMS or AMS and  $S_1$ ) were calculated. When AARM fabric was offset to the north (anticlockwise) from AMS then the value of angle was taken as positive; when the offset was of opposite sense, the angle had a negative value (Fig 13.5a).

Orientations of the directions of intersections of two planar fabric (e.g. AARM and AMS) were also examined. The down plunge (filled circles on Fig. 13.6) of intersection line was taken when AARM was offset to the N-S (anticlockwise), and the plunge was up for an offset of an opposite sense (open circles

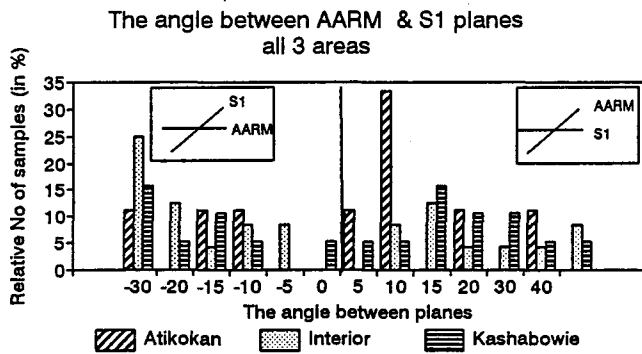


a)



b)

Mean angle: 3.2 deg +/- 10	-3.6 +/- 21	-11.8 +/- 24
angle < 0: N=22	N=14	N=12
angle > 0: N=44	N=11	N=7



c)

Mean angle: 2.3 +/- 18 deg	-5.8 +/- 34	-2.4 +/- 32
angle < 0: N=3	N=12	N=8
angle > 0: N=6	N=12	N=11

Fig. 13.5. Histograms of dihedral angles between planar fabrics for individual samples: a) - AMS foliation and S<sub>1</sub>, b) - AARM and AMS foliations, c) - AARM foliation and S<sub>1</sub>. An angle has a positive sign when a vector - product of poles to planes (e.g. AMS \* S<sub>1</sub>) has a positive inclination (AMS plane is anticlockwise offset with respect to S<sub>1</sub> plane). Therefore, positive values of an angle may indicate an effect of dextral shear. Tables below diagrams summarize the statistics. See text for detailed discussion.

on Fig. 13.6).

The effect of anticlockwise offset of AMS fabric with respect to the  $S_1$  schistosity plane is not more common than opposite situation for any collection of samples from all three areas (Fig. 13.5a). For single samples the angle between two fabric can be more than 20-30°. However, neither clockwise nor anticlockwise offset of one fabric with respect to another is common for any area. The mean values of that kind offset are of order of a few degrees (table on the Fig. 13.5a). Therefore there is no statistical significance in the distribution of the angles between individual AMS and  $S_1$  foliations in any area.

The directions of axes of intersections of AMS and  $S_1$  foliation planes are distributed along the plane for samples from the margins of the belt (Fig. 13.6a,c). However, because both planes are at small angle each to other, such distribution must be expected. In addition the error of determination of the direction of those intersection axes may be a quite large value. Therefore no significant conclusion can be drawn from such a distribution of intersection axes. On the other hand, samples from the interior of the belt have their intersection axes clustered near directions of AMS and  $L_1$  lineations (Fig 13.6b), because the foliations are less steep and at higher angles to one another.

The angles between AARM & AMS foliations for individual samples are usually smaller than those between AMS and  $S_1$  fabrics. They are usually less than 15° for all three areas

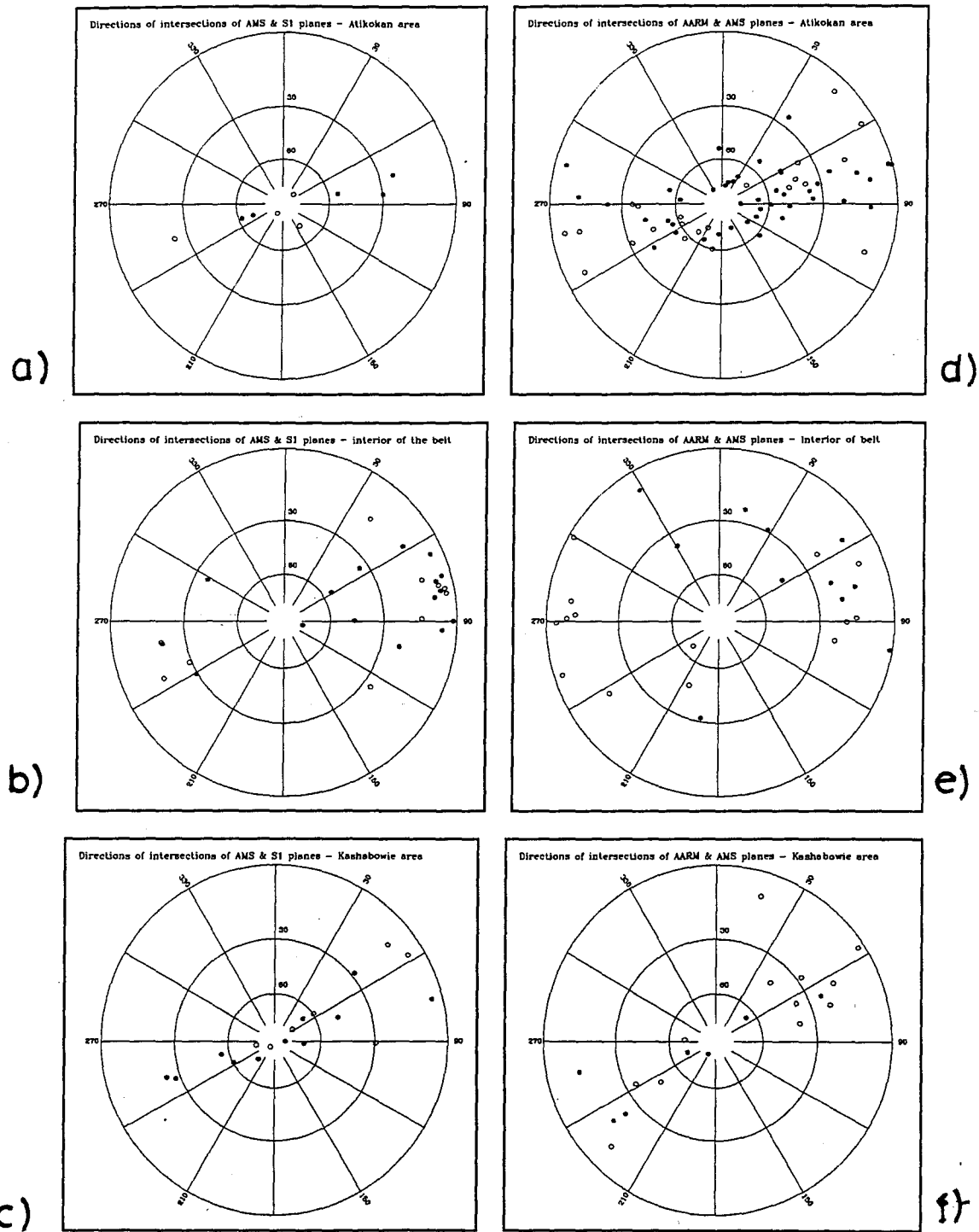


Fig. 13.6. Directions of vector cross-products of poles to planar fabrics (AMS\*S<sub>1</sub> - fig. a-c and AARM\*AMS - fig. d-f) for individual samples. They have a geometric interpretation as directions of intersections of two planar fabric for an individual sample. When they point down, a first fabric (from a pair) is anticlockwise with respect to other. That may indicate an effect of dextral shear. See text for discussion.

(Fig. 13.5b). In Atikokan area an anticlockwise offset of AARM planes with respect to AMS can be observed (44 samples with an anticlockwise offset and 22 with a clockwise one), but in the other two areas a weak opposite correlation exists (see table on Fig. 13.5b).

More than 20 % of samples from the Kashabowie area had a substantial angle (more than  $30^\circ$ ) between AARM and AMS foliations. It can be caused by the cases of inverse AMS fabric in some metavolcanic samples.

The axes of intersections of AMS and AARM foliations are scattered along the AMS or AARM planes (Fig. 13.6d-f). This scatter can be explained by a large error of determination of orientations of intersection axes for samples with almost parallel foliations.

#### **The relations between fabrics and a shear component of deformation.**

In earlier study some anticlockwise offset (of about  $5^\circ$ ) between mean directions of AMS and  $L_1$  lineations was determined by Spark (1990) for Kashabowie area (see also Borradaile and Spark, 1991). However the accuracy of determination of each mean direction was not reported. In this study two approaches are employed to test whether the significant difference between two fabric exists:

1. The comparison of mean orientations of examined fabrics with confidence cones for each orientation;

2. The comparison of angles between planar fabrics for individual samples.

It can be concluded that AMS planar fabric is slightly anticlockwise deflected from  $S_1$  schistosity in the interior of the belt and at the southern margin (based on the method 1). However, the separation of those two fabric is at the margin of overlap of their confidence cones. Method 2 does not indicate any significant offset of one of these fabrics with respect to another.

In Atikokan area AMS foliation is located between  $S_1$  and  $S_0$  fabrics and therefore can be partly of sedimentary and not tectonic origin.

AMS lineation show a substantial offset from  $L_1$  only in Kashabowie area. It confirms the observations of Spark (1990). In the interior of the belt it is parallel to  $L_1$ , in Atikokan area poorly defined.

These conclusions support an anticlockwise offset of AMS fabric with respect to tectonic fabric as a result of forming of AMS fabric during dextral transpression, **only** in the centre and on the southern margin of the Quetico Belt. However, for individual samples, an offset of AMS fabric from  $S_1$  fabric is not consistent along the traverse.

Mean AARM foliations are oriented more closely to  $S_1$  than AMS as well as AARM foliations for individual samples (Fig. 13.5c). However, confidence cones around poles to mean AARM foliations are larger and these relations can be artificial. An

analysis of results of method 2 suggests a slight anticlockwise offset of AARM planes with respect to  $S_1$  at the belt margins as well (table under Fig. 13.6c), compatible with dextral transpression.

AARM lineations are much less steep than other two fabrics ( $L_1$  and AMS lineations) in the interior of the belt and in the Kashabowie area. However, the confidence cones are quite large and therefore the real plunges of AARM lineations in these two areas can be steeper as well. In Atikokan area AARM lineations are much steeper, but the AARM fabric is more oblate and AARM lineations are consequently poorly defined.

The above observations suggest that although AMS and AARM fabrics correlate with tectonic fabric in this area, they only support dextral transpressive shear along the southern half of the Quetico Belt (see also Borradaile et al, 1988 for AMS fabric discussion).

13.3. The correlations between ARM and MS intensities and their anisotropy parameters.

The other parameters tested for correlations were anisotropy parameters  $P'$ ,  $T$  for ARM and AMS fabrics and mean susceptibility with mean anhysteretic remanence.

#### **Anhysteretic remanence and susceptibility.**

In the Atikokan area samples have a monotonic but non-linear increase of ARM intensity with susceptibility (Fig. 13.7a). This effect was observed for susceptibilities from range of  $2 \cdot 10^{-4}$  -  $10^{-3}$  SI vol. It suggest that the relative content of ferromagnetics and paramagnetics do not vary much from one sample to another. The content of magnetite is probably less than 2-3%, because susceptibilities are low. The small increase in pyrrhotite content produces slightly larger susceptibilities (of the same order as paramagnetic susceptibility,  $10_4$ ). The only sample with high susceptibility ( $>10^{-2}$  SI vol.) and remanence ( $>1$  A/m) is PST1 from Wabigoon metavolcanics.

In the interior of the belt the variations in the pyrrhotite content must be much larger, as from two samples with similar susceptibilities one can have 100 times larger ARM intensity than the other (Fig. 13.7b). Only two amphibolite samples have substantially larger susceptibilities (magnetite bearing).

In Kashabowie area variations in pyrrhotite content cause



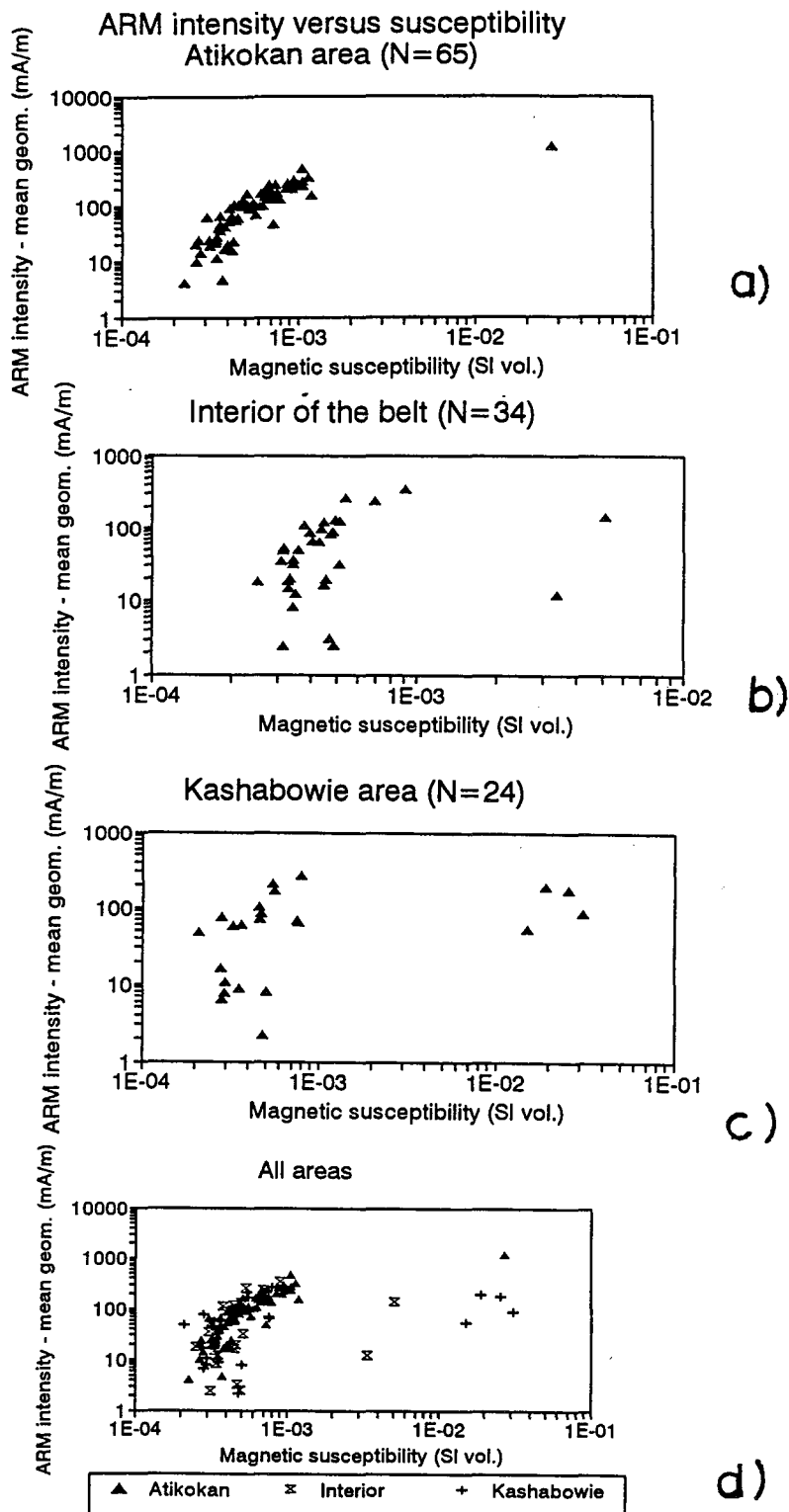


Fig. 13.7. Plots of ARM intensity as a function of magnetic susceptibility. Note a monotonic relation between ARM intensity and MS in Atikokan area and a group of highly susceptible samples with moderate ARM in Kashabowie area and in the interior of the belt (magnetite - bearing). In general low susceptible samples have similar composition in all three areas (fig. d).

similar variations in anhysteretic remanence as in the interior of the belt (Fig 13.7c). A group of magnetite-bearing metavolcanic samples is present as well. The observed correlations confirm that pyrrhotite is a major ferromagnetic phase in these collections, although detailed mineralogical studies were performed for less than 20 samples.

#### **The distribution of anisotropy parameters $P'$ and $T$ .**

Anisotropy of magnetic susceptibility increases from the belt margins to the interior of the belt (mean  $P'$  is 1.36 for Atikokan area, 1.29 for Kashabowie area and 1.44 for the belt interior, Fig. 10.15). However, there is also a large group of samples with highly anisotropic, almost perfectly oblate AMS fabric in Calm Lake - Perch Lake area. Those are samples from the vicinity of Wabigoon belt and shear zones of Quetico Fault. The lowest anisotropy ( $P'$  of order 1.05) is observed in metavolcanics of Kashabowie area, where prolate fabric is common (due to high content of magnetite).

Samples from Atikokan area have strongly oblate AMS fabric, typical for chlorite and biotite (and pyrrhotite as well). Within the interior of the belt a substantial set of prolate AMS fabric exists. They were correlated mainly with amphibolite-bearing samples with magnetite content and some samples with weak overall susceptibility, where measurement errors are important for determination of an AMS ellipsoid. Samples with prolate AMS come mainly from metavolcanics or felsic intrusions

(e.g. station RS11.3).

The anisotropy of ARM is the strongest in Atikokan area within metasediments with pyrrhotite as the only ferromagnetic phase ( $P'=5.7$ , Fig. 12.16). It indicates strong p.c.o. of this mineral. AARM fabric is almost entirely oblate there.

In the interior of the belt anisotropy of ARM is lower (mean  $P'=3.5$ ) and 50% of fabrics are prolate. Samples with prolate AARM fabric were mostly pyrrhotite-bearing (see chapter 12 for discussion). It suggests that although a single pyrrhotite crystal has a strong oblate anisotropy of remanence fabric (e.g. Dekkers, 1988), the p.c.o. of pyrrhotite assemblage in the rock may be of prolate (L) type, with the zone parallel to L.

In lower metamorphic grade metasediments in the Kashabowie area anisotropy is similar to that from the interior (mean  $P'=3.4$ ) but of oblate shape. In metavolcanics it is lower (mean  $P'=2$ ) and more samples have prolate fabric (discussion and details in chapter 12).

#### **Correlations between anisotropy parameters for AMS and AARM.**

The hypothesis whether anisotropy ratios of AMS and AARM are correlated with strain in the area are beyond the scope of interest in this thesis (there are few suitable finite strain markers). However, it can be examined whether there is a correlation between anisotropy ratios of both fabric and between their shapes.

In the Atikokan area only samples with an anisotropy ratio for AMS less than 1.6 can have both fabrics correlated (Fig 13.8a). There is a substantial scatter of anisotropy parameter  $P'$  for AARM when samples with very high anisotropy of AMS are considered. It suggests that a mechanism of ordering of pyrrhotite grains within some of these samples is much more effective than in samples with weaker AMS fabric. The overall factor of linear correlation  $R^2$  for that collection is only 0.38. In higher grade rocks the ARM fabric was determined only for samples with low AMS ( $P' < 1.7$ , Fig. 13.8b), therefore the correlation between anisotropy ratios for AARM and AMS is slightly higher ( $R^2 = 0.50$ ), but still insignificant. It also indicates that 4 samples with high AMS did not produced stable ARM. In Kashabowie area due to varying composition of ferromagnetic phase along the traverse, the correlation between ARM and AMS anisotropy ratios is negligible ( $R^2 = 0.35$ , Fig. 13.8c).

The shape of anisotropy ellipsoids can be easily examined when Jelinek' T parameters are compared for both (AMS and AARM) fabrics.

In Atikokan area the sense of fabric (prolate or oblate) is the same for all but 7 samples, that had prolate ARM but oblate AMS (Fig. 13.9a). Those samples came from metavolcanics outcrops on the contact with Wabigoon belt. The linear correlation between T parameters is strong. In the interior of the belt the shapes of anisotropy ellipses for both fabric were not correlated. 16

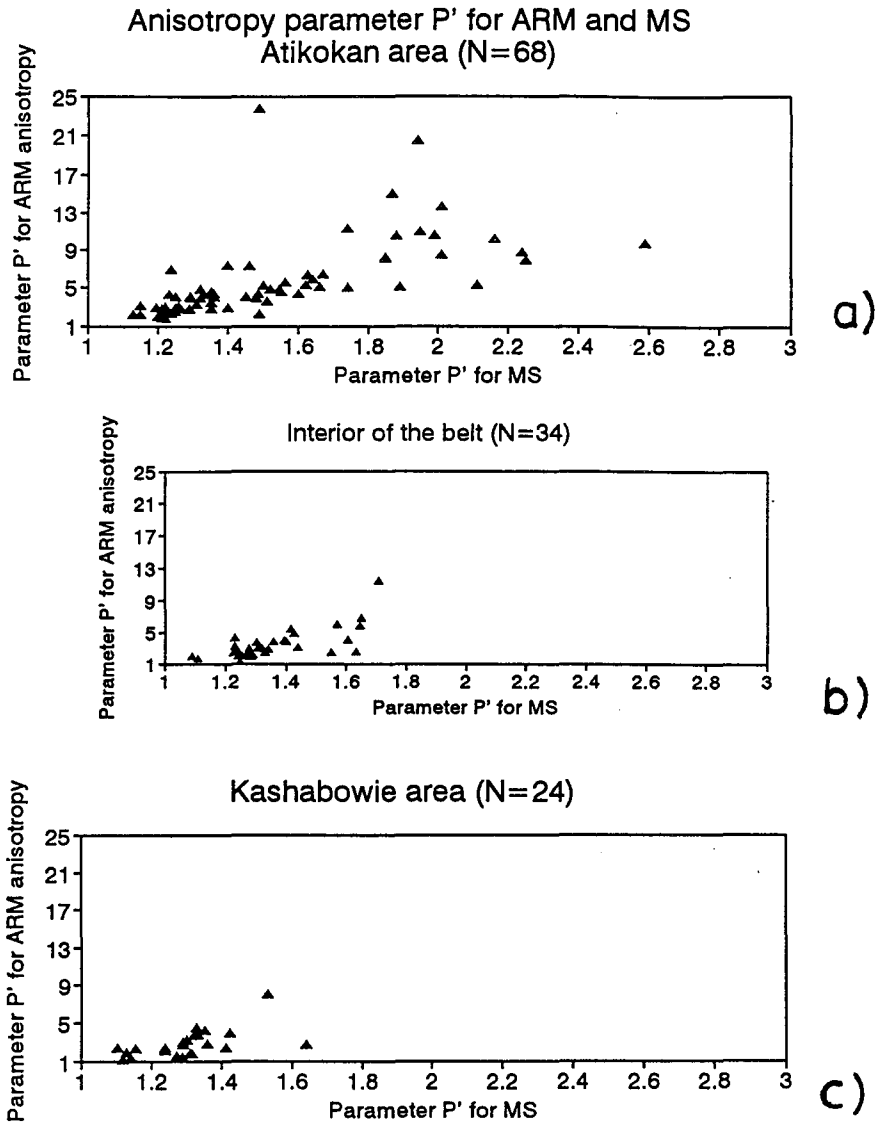


Fig. 13.8. A correlation between anisotropy parameters for AARM and AMS for three sub-areas: a) - Atikokan area, b) - Interior, c) - Kashabowie area. Note very weak correlation between fabric, especially for higher anisotropies.

of 34 samples showed prolate ARM fabric but oblate AMS (Fig. 13.9b). They were mainly amphibolite samples or with low ferromagnetic phase content. In the Kashabowie area the shape sense is often different for AMS and ARM fabric, with both cases of prolate AMS with oblate ARM as well as prolate ARM and oblate AMS observed (Fig. 13.9c). One almost uniaxially prolate ARM fabric was associated with substantial oblate ( $T_{AMS} > 0.5$ ) fabric for a sample from a metavolcanic outcrop.

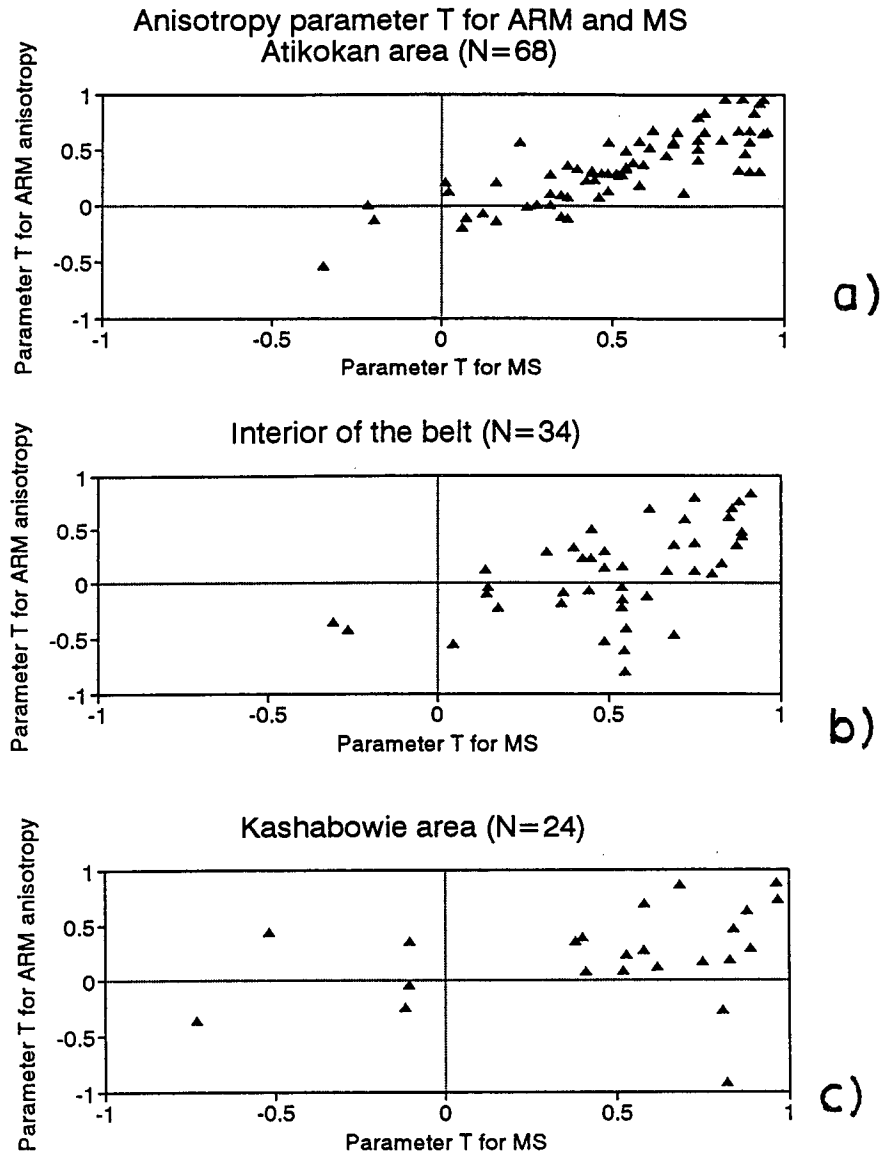


Fig. 13.9. A correlation of shapes of anisotropy ellipsoids for AMS and AARM for three sub- areas. Such correlation can be postulated only in Atikokan area. In other two areas lithology (mineralogical composition - presence of magnetite, pyrrhotite and sheet silicates) and metamorphic grade (presence of amphiboles and metamorphic magnetite) control relationship between fabrics. See text for detailed discussion.

13.4. The timing of development of the ferromagnetic phase and AARM fabric.

The observations of grain - grain relations in thin-sections and the comparison of different magnetic fabric suggest that mostly large pyrrhotite grains are responsible for ferromagnetic properties in metasedimentary units within three studied areas.

These grains are large but with low aspect ratios when separated fractions are viewed under petrographic microscope. They do not reveal well developed p.c.o. but anisotropy of ARM studies indicate very high overall anisotropy ratios. Therefore the p.c.o of grains must be substantial. It leads to suggestion that they were formed during post-metamorphic retrogressive conditions and did not experience any secondary reheating. The thermomagnetic curves did not indicate secondary magnetite in fresh, not heated grains. The ARM fabric is well developed and highly anisotropic what suggest that the alignment of grains was mainly controlled by the p.c.o. of the matrix. However, the stress conditions should prevail in the matrix during forming the pyrrhotite phase to ensure the suggested high overall p.c.o. of pyrrhotite. In the other situations, the crystallographic axes of pyrrhotite grains could be oriented more randomly.

If the position of AARM foliation more closely to the  $S_1$  fabric than AMS foliation is significant, this effect can be interpreted due to later formation of ferromagnetic phase (pyrrhotite) as post-metamorphic. The oxidization of pyrrhotite



takes place in temperatures more than 450° C, even when atmospheric air is absent (Dekkers, 1990). The oxygen in the matrix minerals can also cause oxidization of pyrrhotite to magnetite or hematite. Therefore it can be assumed that pyrrhotite was created in the matrix in retrogressive metamorphism conditions and its preferred orientation was controlled by the preferred orientation of highly deformed biotite - chlorite rich matrix. The model of rigid rotation of ferromagnetic grains does not apply here and the anisotropy of remanence cannot be used as kinematic indicator in this area. These speculations can be only supported by more extensive studies of ferromagnetic content of rocks through the area and thin - section studies of grain - matrix relations.

AARM lineations within the belt and at the southern margin are very consistent and almost horizontal. They can be produced as an effect of a substantial shearing component during the late stage of deformation. This can explain a different orientation of AARM lineations from tectonic and AMS lineations (which are steeper). The distribution of AARM lineation fabric in Atikokan area is controlled rather by the late- formed sheath folds and therefore generally steeper. In the Calm Lake - Perch Lake area the development of isoclinal to tight folds obliterated the direction of extension lineations. The flat fabric ( $T \rightarrow +1$ ) also made it difficult to define the lineation, as both the larger (maximum and intermediate) principal remanences (or susceptibilities) are similar.

This discussion indicates that both ARM and AMS fabric in this area correlate well with tectonic fabric, but they did not show features that could be helpful in the estimation of the sense of shearing component over the whole region. Only the southern half of the Quetico belt may be subject to consistent dextral transpression.

This study confirms that the leading factor which decides about the validity of use of magnetic fabric as the kinematic indicator of the shearing component of the deformation is the process of forming of both ferro - and paramagnetic phases and the development of preferred orientation in them. Because the paramagnetic and ferromagnetic fabric is controlled mainly by the processes of metamorphic recrystallization, for such rocks any quantitative correlations between strain, AMS and remanence fabrics cannot be undertaken (Stephenson et al., 1986).

### 13.5. The distribution of ChRM mean planes.

The position of planes fitted to the ChRM data by PCA algorithm is rather close to other planar fabric components. However, the error in estimating these planes is substantial (of the order of  $30^\circ$ ), therefore the dip values are not very precise. It can be postulated that both methods of demagnetization gave approximately the same orientation of ChRM girdle (within their measurement errors).

ChRM (after A.F. demagnetization) planes generally imitate the orientation of the ARM, AMS and schistosity planes. However, due to a much larger scatter of NRM vectors away from a girdle distribution, their positions are not so well defined.

The orientation of NRM vectors was also examined with respect to the ARM fabric orientation within samples. For most samples, NRM is deflected less than  $20^\circ$  from the ARM foliation plane (Fig. 13.10). The large overall anisotropies of ARM indicate that the p.c.o. of pyrrhotite grains within the basal plane is very high. The substantial deflection of NRM toward the basal plane of anisotropy (at large angles - more than  $30^\circ$ - $40^\circ$  from the Earth's magnetic field) is quite possible theoretically if the anisotropy of remanence is so high (see chapter 9 for a more theoretical discussion). The effective angle of deflection of ChRM direction from the magnetic field depends strongly on the relative orientation of the plane of anisotropy of remanence (determined) and external field (here unknown). For different

The distribution of angles between NRM  
and principal ARM axes - Quetico Belt

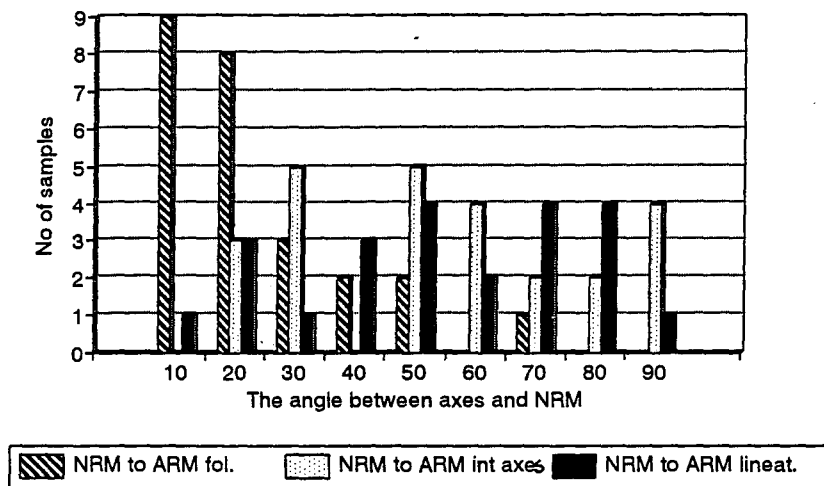


Fig. 13.10. A histogram of angles between directions of characteristic remanences and principal axes of anisotropy of ARM for individual samples (N=25) from the interior of the Quetico Belt. Note that angle between ChRM and AARM foliation plane is less than 30° for 80% of samples. ChRM are not deflected more toward AARM lineation than toward AARM intermediate axis.

samples such deflection can vary substantially (from  $0^\circ$  to  $30^\circ$ - $40^\circ$ ). This factor introduces additional disorder to the ChRM distribution.

Pyrrhotite grains do not have a substantial anisotropy within the basal plane. This supports the observation that ChRM vectors do not tend to orient themselves toward maximum or intermediate principal axes of ARM (Fig. 13.10).

The above discussion suggests that the rotations of ferromagnetic grains toward the  $S_1$  plane during deformation was a minor one, however ferromagnetic grains crystallized in that orientation. Therefore the ChRM in this case should be post- or syn-growth chemical remanence and post peak metamorphic. It is not pre-deformational and rotated toward the principal plane of finite deformation (e.g. Kodama et al., 1988, model). This leads to the hypothesis that the orientation of ChRM is controlled **mainly** by high basal anisotropy of pyrrhotite.

Individual ChRM directions are distributed along a plane, but with a weak clustering at high inclinations. The position of this weak cluster can be correlated with an effect of deflection of remanence away from Earth's field direction (for late Archean, see chapter 3.2) toward the anisotropy of remanence plane (see discussion in section 8.5) caused **mainly** by the anisotropy. However, a process of mechanical rotation of remanence of even stress- controlled deflection toward the principal plane of finite strain cannot be completely

disregarded. Some ChRM directions had low (or negative) inclinations (less than  $30^\circ$ ). The mechanism of rotation could be **partly** responsible for their final orientations.

However, any distribution of ChRM vectors for a given site (with no deformation or no substantial anisotropy of remanence) **always** has a significant scatter around a mean direction due to the influence of field- or laboratory related factors and measurement errors. Such a scatter was also observed for data obtained by Dunlop for weakly deformed or not- deformed granitoid bodies within the Belts. Therefore the presence of low- inclined ChRM directions could exhibit also the effect of these non-controllable factors. I did not find any factor (mineralogical, such as blocking temperature or coercivity, or site- related) to allow me to select low - inclined ChRMs as a separate set of directions (e.g. indicative of later acquired remanence).

## Chapter 14.

### Conclusions.

#### 14.1. Metamorphism, deformation and fabric in the area.

##### **The tectonic fabric and metamorphism of the interior of the Quetico Belt.**

1. The rocks along the transect from Atikokan to Huronian Lake along the Highway 11 have a steep metamorphic gradient between Atikokan and Sapawe ranging from low grade chlorite schist derived from greywackes through biotite schist, garnet - biotite schist, and locally staurolite- rich schist. Some higher grade mafic amphibolite units are met west of Sapawe. The interior of the belt contains mainly migmatites with well defined differentiated layering. In the highest grade rocks the effects of anatexis were observed, with abundant remnants of mafic biotite schist as paleosomes. The intrusions of one- or two- mica granitoid stocks are of size from tens of meters to 1- 2 km. Pegmatite bodies are common and they often locally deflect the existing tectonic planar fabric in the surrounding schists or migmatites.

For further studies the whole area from Calm Lake - Perch Lake through Atikokan and interior of the belt to Kashabowie

Lake was divided into 3 sub-areas:

1. low grade (below staurolite isograd) at the northern margin of the Quetico Belt: "Atikokan area";

2. Higher grade metasediments with common granitoids, pegmatites and migmatites in the interior of the belt: "Interior";

3. Lower grade metasediments (below staurolite isograd) at the southern margin of the Quetico Belt (east of Huronian Lake) and low grade metavolcanics within Shebandowan Belt west of Kashabowie Lake: "Kashabowie area". All studied fabrics were examined separately in each sub-area.

2. Only one pervasive tectonic fabric ( $S_1$ ) striking NE-SW was observed through the region. This is more consistent in orientation and steeper in schists than in migmatites but generally has the same orientation as the  $S_1$  fabric in adjacent belt margins. The more gentle dips ( $30-50^\circ$ ) of  $S_1$  fabric in higher grade rocks and more erratic orientation of tectonic fabric are associated mainly with the intrusions of granitoid and pegmatite bodies in the area. The intrusions produced a mechanical tilting of existing schists and paleosomes in migmatites. The tectonic lineation  $L_1$  (extension lineations) are much more uniformly oriented everywhere except in the Atikokan area and plunge gently to north-east. In the vicinity of the Quetico Fault, the  $L_1$  fabric is steep. The local structures such as boudins, ptygmatic folds, and minor folds were not



extensively investigated in the area and no outcrops were observed with two different tectonic fabrics ( $S_1$  and  $S_2$ ). Therefore, Sawyer's (1983) secondary fabric could not be confirmed. The single penetrative fabric observed here ( $S_1$  and  $L_1$ ) can be thus interpreted as equivalent to the  $D_2$  or  $D_3$  fabric in the OGS classification. (Williams, 1991).

**Magnetic mineralogy of ferromagnetic minerals in all three areas.**

3. The main ferromagnetic phase in metasedimentary rocks is pyrrhotite of sizes greater than 30-40  $\mu\text{m}$ . It is mainly pseudo-single-domain as deduced from hysteresis parameters, but a multidomain phase (with domains that have regions showing PSD properties, Soffel, 1981) may be also present. High field and zero - field thermomagnetic curves did not indicate significant contributions of magnetite to remanence in those rocks. It is in conflict with petrographic studies of Sarvas (1988) for 3 mineral separations from the Calm Lake -Perch Lake area; he found mostly magnetite grains. The pyrrhotite seems to be mostly a ferrimagnetic monoclinic phase, but the results can also support the presence of a hexagonal phase (because for a few samples, Curie temperatures are lower than 300°C). The coercivities of remanences are low and samples can be easily demagnetized by AF field.

Susceptibilities are of the order of  $10^{-4}$ - $10^{-3}$  and typical for chlorite, biotite and pyrrhotite. High field hysteresis studies indicate that 50 - 80% of susceptibility can be carried by paramagnetic matrix in those samples. Samples, that are magnetite rich (metavolcanics or amphibolites) have susceptibilities of order of  $10^{-3}$  -  $10^{-1}$ . Susceptibilities do not increase remarkably in low temperatures (<400°C), so that thermal demagnetization is of less use. In higher temperatures oxidization of pyrrhotite to magnetite takes place with 10-100 fold increase of remanence. The content of pyrrhotite was sufficient for ARM studies in more felsic outcrops from the granitic intrusions in the area as well.

The presence of a highly coercive phase (hematite?) was observed in a few samples, but thermomagnetic data were not available.

4. Samples from the metavolcanic Shebandowan Belt can have both magnetite and pyrrhotite (as minor constituents) as carriers of remanence and AARM fabric. Some samples with magnetite only were found near Kashabowie Lake. The coercivities and hysteresis parameters suggest that it is MD magnetite or from PSD/MD transition range. Some traces of hematite were noticed in a few samples.

5. The thin - section studies suggest that the orientation of pyrrhotite grains is controlled by the overall p.c.o. of biotite- rich matrix. The high p.c.o. of pyrrhotite was

confirmed by ARM anisotropy studies. During heating of pyrrhotite-rich samples above 450°C, pyrrhotite easily reacts to magnetite in the laboratory, even in an oxygen - poor atmosphere (Dekkers, 1990). The lack of magnetite in the metasedimentary samples together with the orientation of p.c.o. of pyrrhotite suggests that pyrrhotite phase is late to post-metamorphic.

#### **The AMS fabric in the studied areas.**

6. The AMS fabric studies in the Kashabowie area confirmed earlier results of Spark (1991) concerning the distribution of principal axes. AMS foliation is almost parallel to  $S_1$  fabric and subvertical at both margins of the Quetico belt. In Atikokan area AMS foliation is located between  $S_0$  and  $S_1$  fabric, and it might therefore be of composite sedimentary- tectonic origin due to transposition of bedding on isoclinal folds' limbs.

AMS fabric at the belt margins is mainly oblate and has anisotropy ratios ( $P' = 1.3-1.5$ ) characteristic for biotite and chlorite. Higher values of anisotropy were recorded in Atikokan area, where AMS is strongly oblate ( $T$  near 1). Some prolate fabrics with lower anisotropy were observed in magnetite-rich as well as in some pyrrhotite-bearing metavolcanics near Kashabowie Lake. The weak anticlockwise offset of mean AMS lineation from  $L_1$  lineation direction was observed only in

Kashabowie area, however the estimation error of both fabrics must be taken under consideration when both fabrics are compared. The approximate method of comparison of this offset was proposed for a single sample fabrics. However it has also statistical drawbacks, as the significance of the observed distribution is difficult to estimate.

At the northern margin AMS lineations are poorly defined, because of the almost perfect oblate fabric and stronger transposition and flattening deformation.

7. The AMS fabrics in the interior of the belt correlate with tectonic fabric and AMS foliation is slightly offset anticlockwise from  $S_1$ . AMS foliation is less steep than at the margins. AMS fabrics are generally oblate and have higher anisotropy ratios than those from metavolcanics in the Kashabowie area and at low grade metasediments on the belt margins. It is controlled by biotite and muscovite. The only prolate AMS fabrics are observed in some amphibolite-rich samples. There is no observed offset of mean AMS lineation with respect to mean  $L_1$  fabric, because the fabrics are dominantly oblate.

#### **The AARM fabric.**

8. AARM fabrics for individual samples (planar and linear) in all three areas are more weakly grouped than AMS fabrics.

Therefore it produces larger confidence cones around mean directions of the fabrics.

In the Atikokan area, AARM lineations for individual samples are spread along the AARM foliation plane. It is not an effect of a large error of determination of directions of AARM lineations for individual samples (only those with  $R_{95} < 30^\circ$  were considered). Such a girdle distribution is caused by heterogenous distribution in the area, that produces a similar girdle distribution for AMS lineations and  $S_0/S_1$  intersection lineations.

The principal axes of ARM correlate better with tectonic fabric than AMS when mean positions are examined. ARM foliations are steeper than those of AMS. ARM foliation is more erratic and less steep in the belt interior than at the margins.

Mean orientations of ARM lineations are almost horizontal in the interior of the Belt and in the Kashabowie area. In the Atikokan area, the mean AARM lineation is steeper but poorly defined due to a girdle distribution of individual AARM lineations.

More shallow AARM lineations and more steep AARM foliations than for AMS fabrics may confirm the later development of AARM fabric than AMS and tectonic ones. AARM fabrics might develop in subvertical position when earlier AMS and tectonic fabric were reoriented sub-vertically by North-South compressive components of deformation. Sub-horizontal plunges of AARM lineations can be correlated with the dominant horizontal shearing in a late

stage of deformation.

The comparison of AARM foliations with AMS and tectonic ones for individual samples is inconclusive as it is controlled by small - scale heterogeneous deformation; no statistically significant offset of AARM was observed.

The AARM fabric is generally oblate where pyrrhotite is determined as a ferromagnetic phase, and sometimes prolate in magnetite bearing samples. However, in the interior of the belt some pyrrhotite-bearing samples had also a prolate fabric.

9. Anisotropy ratios  $P'$  for ARM in metasediments are very high (typically 3 to 5) which indicates a well developed p.c.o. of pyrrhotite. Extremely high values of  $P'$  are typical for the vicinity of Quetico Fault near Atikokan. These indicate that the mechanism of development of p.c.o. in pyrrhotite was very effective near the Quetico Fault zone. Since pyrrhotite is believed to be formed as a late - metamorphic phase, this confirms the widely held view that the high strain correlated with faulting is also late - metamorphic.

10. The shapes of AARM and AMS ellipsoid correlate best in low grade metasediments. In high grade metasediments about 50% have prolate AARM fabric but oblate AMS fabric, although most of them are pyrrhotite bearing. In metavolcanics in Kashabowie area, AARM and AMS fabric often do not correlate when the shape of

ellipsoid is considered, due to prolate shapes of magnetite grains with strong shape anisotropy.

Weak correlations exist for anisotropy ratios  $P'$  from ARM and AMS fabrics for metasediments with AMS anisotropy less than 1.8, but there is no such correlation for metavolcanics and highly anisotropic metasediments. Intensities of ARM generally do not correlate with susceptibilities. It confirms the observations of Spark (1991) and Sarvas (1988) that susceptibility in the area is equally controlled by ferro- and paramagnetic phases.

14.2. The mechanisms of generation of ferromagnetic phase and relations between natural remanence and tectonic and metamorphic history of the area.

**ChRM components in the studied samples.**

1. The stable uni- or bi-vectorial demagnetization curves were obtained for sufficiently large collections of samples from all 3 areas. Determined vectors of ChRM during demagnetization were usually removed in more than 7 steps of demagnetization procedure (AF or thermal treatment were employed). Mean destructive fields were small (usually less than 20 mT) and blocking temperatures less than 350°C. Most samples were unstable in AF field of 50 mT, however samples stable to AF demagnetizations of up to 200 mT also were observed. These observations are in agreement with an hypothesis that the carrier of remanence is mostly pyrrhotite, as concluded from studies of magnetic phases.

A few samples from the Kashabowie Lake area had a substantial part of initial NRM not demagnetized after field of 200 mT was applied, indicating the presence of hematite.

2. Determined ChRM directions do not cluster around a mean direction for any suite but they form weakly-developed girdles. The ChRM directions between neighbouring outcrops show also very large differences. Their orientations are also quite closely



correlated with the overall planar tectonic fabric for each suite (especially for samples demagnetized by A.F. technique). The dips of planes fitted to girdles formed by thermally demagnetized samples differ more from the other fabrics. However, the error of estimating of ChRM planes is substantial (especially for thermal demagnetization data, usually more 30°) and such a difference may be insignificant. It is understandable, because the number of samples demagnetized thermally is very small.

The elimination of the worst defined ChRM vectors (class C, fitted to 3 or 4 points of demagnetization path) does not decrease the scatter of overall distribution of ChRM directions.

3. The method of automatic fitting of directions with PCA algorithm did not work well for some demagnetized samples which demagnetization paths had substantial noise in many cases.

4. Several mechanisms were considered for the control of the distribution of ChRM vectors. A high anisotropy ( $P'$  of order 3 to 5) of ARM suggests that the deflection of NRM toward the plane of maximum and intermediate anisotropy of remanence is the **most substantial** effect. It can produce a 30-40° deflection of NRM from the direction of Earth' magnetic field. The mean NRM direction recorded in other non-deformed units in the area (005°/55°) for the late Archean is located at angle of 20-30° to AARM foliation planes and the estimated deflection of NRM from

external field direction due to anisotropy can be of 20-30°, depending on the anisotropy ratio. However, low inclinations of some individual ChRM directions cannot be easily explained by this mechanism.

Observed low inclinations of some ChRM and overall poorly defined girdles can indicate that other processes may have taken part in controlling of the ChRM distribution. However, some scatter of ChRM directions (around a mean direction) exists also for weakly anisotropic and non-metamorphosed rock units in general (e.g. in Dunlop' studies), due to numerous factors originating in field or laboratory. A statistical analysis (as Fisher's statistics) helps to minimize their effect in such cases. In the case of anisotropic and metamorphosed rock units these factors can also contribute to a more scattered distribution of ChRM. Therefore the observed low - inclined ChRM may be statistically insignificant. There are too few samples with determined ChRM (usually 20 - 30 for each area) to examine a statistic significance for the observed distribution.

5. The model of rotation of rigid ferromagnetic grains toward the principal plane of deformation is much less probable, as the grains would have to be pre-tectonic. On the contrary, mineralogical studies indicate that pyrrhotite is late-metamorphic. Magnetite present in some metavolcanic or amphibolite-bearing samples is also probably late-metamorphic.

6. The effect of deflection of remagnetization of some components of primary NRM by late stress field cannot be rejected either. It may explain the presence of gently inclined ChRM directions in the collections as these directions can reflect a different (later) Earth's magnetic field direction. However, no effects of incremental stress-controlled remagnetization have been reported so far for pyrrhotite (only for magnetite and hematite).

7. It can be suggested that NRM is probably of chemical origin and could record an average magnetic field direction for a longer time. The single grains can achieve their threshold (to record stable remanence) size at different times as the rate of growth of pyrrhotite grains might be different for each outcrop and therefore record a different direction of magnetic field. Therefore, the averaged (through time) magnetic field directions for different grains can result in different directions of acquired NRM (enhanced by anisotropy of remanence).

8. There is no method to determine the quantitative contribution of each possible mechanism for causing the final orientation of ChRM vectors. However, it may be possible to calculate the position of ChRM vector when the effect of the anisotropy of remanence alone is removed (see chapter 8 for details).

**The model of forming the magnetic phase in metasedimentary rocks - other consequences.**

It has been proposed in this study that pyrrhotite was formed late during metamorphism - probably in temperatures lower than 300°C, under reducing conditions. The p.c.o of pyrrhotite was controlled by already existing penetrative cleavage in host biotite-rich matrix. It explains the high correlation between ARM anisotropy fabric and tectonic fabric and high values of ARM anisotropy. The orientation of an almost vertical ARM fabric with quite well developed ARM lineations corresponds to late dominate shearing in the area during transpressive deformation. It can explain also the different (almost horizontal) orientation of ARM lineations and AMS and tectonic lineations (steeper) in the interior of the belt and in the Kashabowie area. The linear AARM fabrics (poorly defined for some samples) in Atikokan area are not oriented like in the other areas (they are scattered along the AARM foliation plane), because of **locally heterogeneous** late- shearing and faulting deformation. This deformation additionally enhanced the AARM anisotropy ratio in the vicinity of the Quetico Fault.

The ferromagnetic phase was therefore developed later than the paramagnetic one. It can be assumed that the biotite - chlorite matrix was oriented along the schistosity plane and formed planes of weakness for further development of shear deformation in the area. This matrix (and not the direction of

maximum extension in the increment strain, Ramsay, 1967) controlled the orientation of crystallizing of ferromagnetic grains and allowed the development of a very high p.c.o. of pyrrhotite matrix.

This model is not relevant for the formation of magnetite which crystallized somewhat earlier during the metamorphism. It also suggests that AARM pyrrhotite fabric can only reflect a kinematic sense of deformation during the latest stages of primary deformation.

Finally, it is noted that an understanding of the process of development of ferromagnetic phase in the rock is critical if the method of determination of sense of shear based on AMS and ARM fabric is to be valid.

## References.

- Bauer, R.L. 1986. Multiple folding and pluton emplacement in Archean migmatites of the Southern Vermilion Complex, north-eastern Minnesota. *Canadian Journal of Earth Sciences* **23**, 1753-1764.
- Bauer, R. L., Hudleston, P. J., and Southwick, D. L. 1992. Deformation across the western Quetico subprovince and adjacent boundary regions in Minnesota. *Can. J. Earth Sci.* **29**, 2087-2103.
- Beakhouse, G.P. 1985. The relationship of supracrustal sequences to a basement complex in the western English River Subprovince; in *Evolution of Archean Supracrustal Sequences*, Geological Association of Canada, Special Paper 28, p. 169-178.
- Beakhouse, G.P., 1991. Winnipeg River Subprovince, In *Geology of Ontario*, Ontario Geological Survey, Special Volume 4, part 1, pp.279-301.
- Berger, G. W., and York, D. 1979.  $^{40}\text{Ar}$ - $^{39}\text{Ar}$  dating of multicomponent magnetizations in the Archean Shelley Lake granite, northwestern Ontario, *Canadian Journal of Earth Sciences* **16**, 1933-1941.
- Bhatal, R. S., 1971. Magnetic Anisotropy in Rocks. *Earth-Sci. Rev.* **7**, 227-253
- Birk, W. D. 1971. Progressive Metamorphism of the Kashabowie Group at Shebandowan, Ontario with Special Reference to Zoning in Garnets. B.Sc. thesis, Queen's University, Kingston, Ontario.
- Blackburn, C.E., Johns, G.W., Ayer, J. and Davis, D.W. 1991. Wabigoon Subprovince In *Geology of Ontario*, Ontario Geological Survey, Special Volume 4, part 1, pp.303-381.
- Borradaile, G.J. 1981. Particulate flow of rock and the formation of rock cleavage. *Tectonophysics*, **24**, 442-455.
- Borradaile, G.J. 1982. Comparison of Archean structural styles in two belts of the Superior Province. *Precambrian Res.*, **19**, 179- 189.
- Borradaile, G.J. 1988. Magnetic susceptibility, petrofabrics and strain. *Tectonophysics*, **156**, 1-20.

- Borradaile, G.J. 1991. Correlation of strain with anisotropy of magnetic susceptibility (AMS). *Pure and Applied Geophysics*, **135**, 15-29.
- Borradaile, G.J. 1992. Deformation of remanent magnetism in a synthetic aggregate with hematite. *Tectonophysics*, **206**: 203-218.
- Borradaile, G.J. 1993. Strain and magnetic remanence. *J. Struct. Geol.*, **15**, 383-390
- Borradaile, G.J. and Alford, C. 1987. Relationship between magnetic susceptibility and strain in laboratory experiments. *Tectonophysics*, **133**, 121-135.
- Borradaile, G.J. and Brown, H.G. 1987. The Shebandowan Group: "Timiskaming-like" Archean rocks in northwestern Ontario. *Can. J. Earth Sci.*, **24**, 185-188.
- Borradaile, G.J., and Hermes, J.J. 1980. Temporal changes in heat flow distribution associated with metamorphism in the SW Scottish Highlands and the Lepontine Alps. *Journal of Geology*, **88**, 87-95.
- Borradaile, G.J. and Mothersill, J.S. 1984. Coaxial deformed and magnetic fabrics without simply correlated magnitudes of principal values. *Physics of the Earth and Planetary Interiors*, **35**, 294-300.
- Borradaile, G.J. & Mothersill, J.S. 1989. Tectonic strain and paleomagnetism: experimental investigation. *Physics of the Earth and Planetary Interiors*, **56**, 254-265.
- Borradaile, G.J. and Mothersill, J.S. 1991. Experimental strain of isothermal remanent magnetisation in ductile sandstone. *Physics of the Earth and Planetary Interiors*, **65**, 308-318.
- Borradaile, G.J. and Sarvas, P., 1990. Magnetic susceptibility fabrics in slates: structural, mineralogical and lithological influences. *Tectonophysics*, **172**, 215-222.
- Borradaile, G. J. and Spark, R. N., 1991: Deformation of the Archean Quetico- Shebandowan subprovince boundary in the Canadian Shield near Kashabowie, northern Ontario. *Canadian Journal of Earth Science*, **28**, 116-125.
- Borradaile, G.J., Chow, N. & Werner, T., 1993. Magnetic hysteresis of limestones: facies control? *Phys. Earth. & Planet. Inter.*, **76**:241-252.

- Borradaile, G.J., Keeler, W., Alford, C. and Sarvas, P. 1987. Anisotropy of magnetic susceptibility of some metamorphic minerals. *Physics of the Earth and Planetary Interiors*, **48**, 161-166.
- Borradaile, G.J., MacKenzie, A. & Jensen, E. 1990. Silicate versus trace mineral susceptibility in metamorphic rocks. *J. Geophys. Res.*, **95**, 8447-8451.
- Borradaile, G.J., Mothersill, J.S., Tarling, D. and Alford, C. 1985/86. Sources of magnetic susceptibility in a slate. *Earth and Planetary Science Letters*, **76**, 336-340.
- Borradaile, G., Sarvas, P., Dutka, R., Stewart, R. and Stubley, M. 1988. Transpression in slates along the margin of an Archean gneiss belt, northern Ontario - magnetic fabrics and petrofabrics. *Canadian Journal of Earth Science*, **25**, 1069-1077.
- Borradaile, G.J., Stewart, R.A. & Werner, T. In Press. Uplift of an Archean subprovince boundary from magnetic fabrics. *Tectonophysics*....
- Borradaile, G. J., Werner, T., Dehls, J. F. and Spark, R. N., 1993. Archean regional transpression and paleomagnetism in northwestern Ontario, Canada. *Tectonophysics*, **220**, 117-125.
- Butler, R. F. 1991. *Paleomagnetism: magnetic domains to geologic terranes*. Blackwell Scientific Publications, 319 pp.
- Card, K. D. 1990. A review of the Superior Province of the Canadian Shield, a product of Archean accretion. *Precambrian Research*, **48**, 99-156.
- Card, K.D., and Ciesielski, A. 1986. Subdivisions of the Superior Province of the Canadian Shield. *Geoscience Canada*, **13**, 5-13.
- Card, K. D., and King, J. E. 1992. The tectonic evolution of the Superior and Slave provinces of the Canadian Shield: introduction. *Can. J. Earth Sci.* **29**, 2059 - 2065.
- Carmichael, R. S. 1982. *Handbook of Physical Properties of Rocks*. vol II. CRC Press, Inc., Boca Raton, Florida, 345 pp.
- Clark, D. A., 1984. Hysteresis properties of sized dispersed monoclinic pyrrhotite grains, *Geophys. Res. Lett.*, **11**, 173-176.
- Cogné, J.-P., and H. Perroud 1987. Unstraining paleomagnetic vectors: The current state of debate, *Eos Trans. Am. Geophys. Union*, **68**, 705-712.



- Collinson, D.W. 1983. Methods in rock magnetism and palaeomagnetism: techniques and instrumentation. Chapman and Hall, London, 503 pp.
- Corfu, F., and Stott, G.M. 1986. U-Pb ages for late magmatism and regional deformation in the Shebandowan belt, Superior Province, Canada. Canadian Journal of Earth Sciences, 23, 1075-1082.
- Dankers, P. H., 1981. Relationship between median destructive field and coercive forces for dispersed natural magnetite, titanomagnetite, and hematite, Geophys. J. R. Astr. Soc., 64, 447-461.
- Davis, D.W., Poulsen, K.H. and Kamo, S.L. 1989. New insights into Archean structural development from geochronology in the Rainy Lake area, Superior Province, Canada. J. Geology, 97, 379-398.
- Dehls, J., 1992. The Magnetic Fabrics and Strain History of the Archean Seine Group Metasedimentary Rocks near Mine Centre, Northwestern Ontario. M.Sc. Thesis, Lakehead University, Thunder Bay, Ont.
- Dekkers, M.J. 1988. Magnetic properties of natural pyrrhotite. I. Behaviour of initial susceptibility and saturation-magnetization-related rock magnetic parameters in a grain-size dependent framework. Phys. Earth. & Planet. Inter., 52, 376-393.
- Dekkers, M.J. 1989. Magnetic properties of natural pyrrhotite. II. High and low-temperature behaviour of  $J_s$  and TRM as a function of grain size. Phys. Earth & Planetary Interiors, 57, 266-283.
- Dekkers, M. J. 1990. Magnetic monitoring of pyrrhotite alteration during thermal demagnetization, Geophys. Res. Lett., 17, 779-782.
- Dickin, A. P., Mueller, E., McNutt, R. H., and Beakhouse, G. 1991. The role of the Winnipeg River belt in the tectonic evolution of the Superior Province. Geological Association of Canada - Mineralogical Association of Canada - Society of Economic Geologists. Program with Abstracts, 16, A23.
- Dunlop, D.J. 1971. Magnetic properties of fine particle hematite. Ann. Geophys., 27, 269-293.
- Dunlop, D.J. 1972. Magnetic mineralogy of unheated and heated red sediments by coercivity spectrum analysis. Geophys. J. Roy. Astron. Soc., 27, 37-55.

- Dunlop, D.J. 1973. Thermomremanent magnetization in submicroscopic magnetite. *J.Geophys. Res.*, **78**, 7602-7613.
- Dunlop, D. J., 1979: A regional paleomagnetic study of Archean rocks from the Superior Geotraverse area, northwestern Ontario. *Canadian Journal of Earth Science*, **16**, 1909-1919.
- Dunlop, D.J. 1981. The rock magnetism of fine particles. *Physics of the Earth and Planetary Interiors*, **26**, 1-26.
- Dunlop, D. J., 1983: Paleomagnetism of Archean rocks from northwestern Ontario: Wabigoon gabbro, Wabigoon Subprovince. *Canadian Journal of Earth Science*, **20**, 1805-1817.
- Dunlop, D. J., 1984a: Paleomagnetism of Archean rocks from northwestern Ontario: II. Shelley Lake granite, Quetico Subprovince. *Canadian Journal of Earth Science*, **21**, 869-878.
- Dunlop, D. J., 1984b: Paleomagnetism of Archean rocks from northwestern Ontario: IV. Burchell Lake granite, Wawa-Shebandowan Subprovince. *Canadian Journal of Earth Science*, **21**, 1098-1104.
- Dunlop, D. J., 1985: Paleomagnetism of Archean rocks from northwestern Ontario: V. Poohbah Lake alkaline complex, Quetico Subprovince. *Canadian Journal of Earth Science*, **22**, 27-38.
- Dunlop, D.J. 1986. Hysteresis properties of magnetite and their dependence on particle size: a test of pseudo-single-domain remanence models. *J. Geophys.Res.*, **91**, 9569-9584.
- Dutka, R.J.A. 1982. The structure and lithology of the Quetico sediments in the Atikokan area. B.Sc. thesis, Lakehead University, Thunder Bay, Ont.
- Facer, R. A., 1983. Folding, strain, and Graham's fold test in paleomagnetic investigations, *Geophys. J. R. Astr. Soc.*, **72**, 165-171.
- Fuller, M.D. 1963. Magnetic anisotropy and Paleomagnetism. *J. Geophys. Res.*, **68**, 293-309.
- Girdler, R.W., 1961. The measurement and computation of anisotropy of magnetic susceptibility in rocks. *Geophys. J. Roy. Astron. Soc.*, **5**, 34-44.
- Ghosh, S.K. & Ramberg, H. 1976. Reorientation of inclusions by combination of pure shear and simple shear. *Tectonophysics*, **34**, 1-70.

- Graham, J. W., 1949. The stability and significance of magnetism in sedimentary rocks, *J. Geophys. Res.*, **54**, 131-167.
- Graham, J. W., 1966. Significance of magnetic anisotropy in Appalachian sedimentary rocks, in *The Earth Beneath the Continents*, 10, edited by J. S. Steinhart, and T. J. Smith, pp. 627-648, American Geophysical Union, Geophysical Monograph Geophys. Monogr., Am. Geophys. Union, **10**, 627-648.
- Henry, B. 1983. Interprétation quantitative de l'anisotropie de susceptibilité magnétique. *Tectonophysics*, **91**, 165-177.
- Henry, B. 1989. Magnetic fabric and orientation tensor of minerals in rocks. *Tectonophysics*, **165**, 21-27.
- Hext, G.R. 1963. The estimation of second-order tensors, with related tests and designs. *Biometrika*, **50**, 353-373.
- Hirt, A.M., Lowrie, W., Clendenen, W.S. and Kligfield, R. 1988. The correlation of magnetic anisotropy with strain in the Chelmsford Formation of the Sudbury Basin, Ontario. *Tectonophysics*, **145**, 177-189.
- Hodgkinson, J.M. 1968. Geology of the Kashabowie Area. Ontario Department of Mines, Geological Report 53, 35pp with Map 2128 - Kashabowie Sheet.
- Hoffman, P.F. 1989. Precambrian geology and tectonic history of North America; in *The Geology of North America: An Overview*, *The Geology of North America*, Volume A, Geological Society of America, p. 447-512.
- Housen, B. A., and B. A. van der Pluijm, 1990. Chlorite control of correlations between strain and anisotropy of magnetic susceptibility, *Phys. Earth Planet. Inter.*, **61**, 315-323.
- Hrouda, F., 1982. Magnetic anisotropy of rocks and its application in geology and geophysics, *Geophys. Surv.*, **5**, 37-82.
- Hudleston, P.J., Schultz-Ela, D., and Southwick, D.L. 1988. Transpression in an Archean greenstone belt, northern Minnesota. *Canadian Journal of Earth Sciences*, **25**, 1060-1068.
- Jackson, M. J., 1990. Magnetic anisotropy of the Trenton Limestone revisited, *Geophys. Res. Lett.*, **17**, 1121-1124.
- Jackson, M. J., 1991. Anisotropy of magnetic remanence: A brief review of mineralogical sources, physical origins, and geological applications, and comparison with susceptibility anisotropy, *Pure Appl. Geophys.*, **136**, 1-28.

- Jackson, M. J. & Tauxe, L. 1991. Anisotropy of magnetic susceptibility and remanence: developments in the characterization of tectonic, sedimentary and igneous fabric. Rev. Geophysics Supplement, US National Report to International Union of Geodesy and Geophysics. pp. 371-376.
- Jackson, M. J., Banerjee, S. K., Marvin, J., Lu, R., and Gruber W. 1991. Detrital remanence, inclination errors, and anhysteretic remanence anisotropy: Quantitative model and experimental results, Geophys. J. Int., **104**, 95-103.
- Jackson, M. J., Gruber, W., Marvin, J. & Banerjee, S.K., 1988. Partial anhysteretic remanence and its anisotropy: Applications and grain size dependence, Geophys. Res. Lett., **15**, 440-443.
- Jackson, M. J., D. Sprowl, and B. Ellwood, 1989. Anisotropies of partial anhysteretic remanence and susceptibility in compacted black shales: Grain size- and composition- dependent magnetic fabric, Geophys. Res. Lett., **16**, 1063-1066.
- Janák, F. 1965. Determination of Anisotropy of Magnetic Susceptibility of Rocks. Studia geoph. geod., **9**, 290-301.
- Jirsa, M. A., Southwick, D. L., and Boerboom, T. J. 1992. Structural evolution of Archean rocks in the western Wawa subprovince, Minnesota: refolding of precleavage nappes during D<sub>2</sub> transpression. Can J. Earth Sci. **26**, 2146-2155.
- Kehlenbeck, M. M. 1986. Folds and folding in the Beardmore - Geraldton fold belt. Can. J. Earth Sci. **23**, 158-171.
- Kennedy, M.C. 1980. Metamorphism and structure across the Quetico structural subprovince, Raith, Ontario. B.Sc. thesis, Lakehead University, Thunder Bay, Ont.
- Kennedy, M.C. 1984. The Quetico Fault in the Superior Province of the southern Canadian Shield. M.Sc. thesis, Lakehead University, Thunder Bay, Ont.
- Kirschvink, J. L., 1980. The least-square line and plane and the analysis of palaeomagnetic data. Geophys. J. R. Astron. Soc., **62**, 699-718.
- Kissin, S. A. and Scott, S. C. 1982. Phase relations involving pyrrhotite below 350°C. Econ. Geol. **77**, 1739-1754.
- Kittel, C. 1971. Introduction to Solid State Physics. 4th ed., John Wiley & Sons, Inc, New York, 766 pp.

- Kodama, K.P. 1988. Remanence rotation due to rock strain and the stepwise application of the fold test. *J. Geophys. Res.*, **93**, 3357-3371.
- Lawson, A. C. 1888. Report on the geology of the Rainy Lake Region. *Geol. Nat. Hist. Surv. Can., Ann. Rept.*, vol. 3, pt. 1, rept. F, 183 pp.
- McCabe, C., Jackson, M. & Ellwood, B. 1985. Magnetic anisotropy in the Trenton Limestone: results of a new technique, anisotropy of anhysteretic susceptibility. *Geophys. Res. Lett.*, **12**, 333-336.
- McIlwaine, W. H. and Hillary, E. M. 1974. West half of Sapawe Lake Area. District of Rainy River. *in Summary of Field Work, 1974. Div. Mines, MP59*, 65-69.
- Mitchell, R. H. 1976. Potassium - argon geochronology of the Poohbah Lake alkaline complex, northwestern Ontario. *Canadian Journal of Earth Sciences*, **13**, 1456-1459.
- Molyneux, L. 1971. A complete results magnetometer for measuring the remanent magnetization of rocks. *Geophys. J. Roy. Astron. Soc.*, **24**: 429-433.
- Morin, J. A. 1973. Lower Shebandowan Lake area. *Ont. Div. Mines. Geol. Rep.* 110, 45 pp. with Map 2267.
- O'Reilly, W. 1984. *Rock and mineral magnetism*. Blackie @ Son Ltd., London, 220 pp.
- Osmani, I.A. 1991. Proterozoic Mafic Dike Swarms in the Superior Province of Ontario. *In The Geology of Ontario, Ontario Geological Survey, Special Volume 4, part 1, p.* 661-681.
- Owens, W.H. 1974. Mathematical model studies on factors affecting the magnetic anisotropy of deformed rocks. *Tectonophysics*, **24**, 115-131.
- Percival, J.A. 1988. Geological compilation of the Quetico (52B). *Geological Survey of Canada, Map 1682A, scale 1:250,000.*
- Percival, J.A. 1989. A regional perspective of the Quetico metasedimentary belt, Superior Province, Canada. *Canadian Journal of Earth Sciences*, **26**, 677-693.
- Percival, J. A., and Sullivan, R. W. 1988. Age constraints on the evolution of the Quetico Belt, Superior Province, Canada. *In Geological Survey of Canada, Paper 88-2, 97-108.*

- Percival, J. A., and Williams, H. R. 1989. The late Archean Quetico accretionary complex, Superior Province, Canada. *Geology*, **17**, 23-25.
- Pirie, J. 1977. Geology of Crooked Pine Lake area, District of Rainy River. Ont. Div. Mines, Open File Rep. 5223, 135pp.
- Pirie, J., and Mackasey, W.O. 1978. Preliminary examination of regional metamorphism in parts of Quetico metasedimentary belt, Superior Province, Ontario. In *Metamorphism in the Canadian Shield*. Geological Survey of Canada Paper 78-10, pp. 37-48.
- Potter, D.K. & Stephenson, A., 1988. Single domain particles in rocks and magnetic fabric analysis. *Geophys.Res. Lett.*, **15**, 1097-1100.
- Press, W.H., Flannery, B. P., Teukolsky, S. A., and Vetterling, W.T. 1986. *Numerical Recipes: The Art of Scientific Computing*. Cambridge University Press.
- Ramsay, J.G. 1967. *Folding and Fracturing of Rocks*. McGraw-Hill, New York, 578pp.
- Ramsay, J.G. & Huber, 1983. *The techniques of modern structural geology. Volume I: Strain analysis*. Academic Press, 307 pp.
- Robin, P.Y., & Jowett, E.C., 1986. Computerized density contouring and statistical evaluation of orientation data using counting circles and continuous weighting functions. *Tectonophysics*, **121**, 207-223.
- Rochette, P. 1987a. Magnetic susceptibility of the rock matrix related to magnetic fabric studies. *J. Struct. Geol.*, **9**, 1015-1020.
- Rochette, P. 1987b. Metamorphic control of the mineralogy of black shales in the Swiss Alps: toward the use of "magnetic isograds". *Earth and Planetary Science Letters*, **84**, 446-456.
- Rochette, P. 1988. Inverse magnetic fabric in carbonate-bearing rocks. *Earth Planet. Sci.Lett.*, **90**, 229-237.
- Ruf, A., Naruk, S.J., Butler, R.F., and Calderone, G.J. 1988. Strain and magnetic fabric in the Santa Catalina and Pinaleno Mountains metamorphic core complex mylonite zones, Arizona. *Tectonics*, **7**, 235-248.
- Sarvas, P.A., 1988. The structure and magnetic fabric of the Quetico metasedimentary rocks in the Calm Lake - Perch Lake area, NW Ontario. M.Sc. thesis, Lakehead University, Thunder Bay, Ont.

- Sawyer, E.W. 1983. The structural history of a part of the Archean Quetico metasedimentary belt, Superior Province, Canada. *Precambrian Research*, **22**, 271-294.
- Schwarz, E. J. 1974. Magnetic Fabric in Massive Sulfide Deposits. *Can. J. Earth Sci.*, **11**, 1669-1675.
- Schwarz, E. J., 1975. Magnetic properties of pyrrhotite and their use in applied geology and geophysics, *Geol. Surv. Can. Paper*, 74-59, 24 pp.
- Shklanka, R. 1972. Geology of the Steep Rock Lake area, District of Rainy River. *Ont. Dept. Mines, G.R. 93*, 114p., with Map 2217.
- Sleep, N. H. 1992. Archean plate tectonics: what can be learned from continental geology? *Can. J. Earth Sci.* **29**, 2066-2071.
- Soffel, H. C., 1971. The single-domain multidomain transition in intermediate titanomagnetites. *J. Geophys. (Z. geophys.)* **37**, 451-470.
- Soffel, H. C., 1977. Pseudo-single-domain effects and single-domain multidomain transition in natural pyrrhotite deduced from domain structure observations. *J. Geophys. (Z. geophys.)* **42**, 351-359.
- Soffel, H. C., 1981. Domain structure of natural fine-grained pyrrhotite in a rock matrix (diabase), *Phys. Earth Planet. Inter.*, **26**, 98-106.
- Spark, R.N. 1990. Magnetic fabrics and boundary structure at the Quetico/Shebandowan subprovince boundary, near Kashabowie, NW Ontario. M.Sc. thesis, Lakehead University, Thunder Bay, Ont.
- Stacey, F.D. & Banerjee, S.K. 1974. The physical principles of rock magnetism. *Developments in Solid Earth Geophysics*, vol. 5., Elsevier, Amsterdam, 195 pp.
- Stephenson, A., 1981. Gyromagnetic remanence and anisotropy in single-domain particles, rocks, and magnetic recording tape, *Phil. Mag. B*, **44**, 635-664.
- Stephenson, A., S. Sadikun, and D. K. Potter, 1986. A theoretical and experimental comparison of the anisotropies of magnetic susceptibility and remanence in rocks and minerals, *Geophys. J. R. Astr. Soc.*, **84**, 185-200.
- Stewart, R. W. 1984. The structure and lithology of the Quetico metasediments in the Chub Lake - Little McCauley Lake area. B.Sc. thesis, Lakehead University, Thunder Bay, Ont.

- Stesky, R.M. 1990. SpheriStat Version 1.1. Supplementary Operating Manual. Frontenac Wordsmiths, pp 34.
- Stott, G.M., and Schnieders, B.R. 1983. Gold mineralization in the Shebandowan belt and its relations to regional deformation patterns. *In* The geology of gold in Ontario. Ontario Geological Survey Miscellaneous Paper 110, 181-193.
- Stupavsky, M., 1984. Operating Manual for the SI-2 Magnetic Susceptibility Instrument. Sapphire Instruments, Ruthven, Ont.
- Tabor, J. R. 1988. Deformational and metamorphic history of Archean rocks in the Rainy Lake district, northern Minnesota. Ph. D. thesis, University of Minnesota, Minneapolis.
- Tabor, J. R., Hudleston, P. J. and Magloughlin, J. 1989. Metamorphism of the Quetico supracrustals north of the Vermilion granitic complex, northern Minnesota; *in* Geological Association of Canada - Mineralogical Association of Canada - Society of Economic Geologists. Program with Abstracts, 14, A38.
- Tanton, T. L. 1926. Recognition of the Couchiching near Steeprock Lake, Ontario. Roy. Soc. Can., Proc. and Trans., Third ser., vol. XX, pt. IV, 39-49.
- Thurston, P. C. 1985. Atikokan- Lakehead compilation project. *In* Summary of field work and other activities, 1985. Ontario Geological Survey, Miscellaneous Paper 126, 54-59.
- Thurston, P. C. 1990. The Superior Province - Emphasizing greenstone belts; *in* Gold and Base-metal Mineralization in the Abitibi Subprovince, Canada, with Emphasis on the Quebec Segment, Special Publication 24, Department of Geology, University of Western Australia, Perth, p.1-52.
- Thurston, P. C., and Davis, D. W. 1991. Tectonic subdivision of the northern Superior Province. Geological Association of Canada - Mineralogical Association of Canada - Society of Economic Geologists. Program with Abstracts, 16, A124
- Uyeda, S., Fuller, M.D., Belshe, J.C. and Girdler, R.W. 1963. Anisotropy of magnetic susceptibility of rocks and minerals. *J. Geophys. Res.*, 68, 279-291.
- Vandall, T.A. and Symons, D.T.A. 1990. Paleomagnetism of Archean granites and Matachewan dikes in the Wawa Subprovince, Ontario: reevaluation of the Archean apparent polar wander path. *Can. J. Earth. Sci.* 27, 1031-1039.



- Vetter, J.R., Kodama, K.P., & Goldstein, A. 1989. Reorientation of remanent magnetism during tectonic fabric development: an example from the Waynesboro Formation, Pennsylvania, U.S.A. *Tectonophysics*, **165**, 29-39.
- Wasilewski, P. J., 1973. Magnetic hysteresis in natural materials, *Earth Planet. Sci. Lett.*, **20**, 67-72.
- Werner, T. & Jelenska, M. 1992. The applicability of two computer techniques to separate the remanent magnetization (RM) components acquired in laboratory fields. *Physics of the Earth and Planetary Interiors*, **70**, 194-200.
- Williams, H.R., Stott, G.M., Thurston, P.C., Sutcliffe, R.H., Bennett, G., Easton, R.M. & Armstrong, D.K. 1992. Tectonic Evolution of Ontario: Summary and Synthesis. In *The Geology of Ontario*, Ontario Geological Survey, Special Volume 4, part 2, p.1255-1334.
- Williams, H. R. 1987. Structural studies in the Beardmore - Geraldton belt and in the Quetico and Wawa subprovinces. In *Summary of field work and other activities, 1987*. Ontario Geological Survey, Miscellaneous Paper 137, pp. 90-92.
- Williams, H.R. 1991. Quetico Subprovince. In *The Geology of Ontario*, Ontario Geological Survey, Special Volume 4, part 1, p.383-404.
- Williams, H.R., Stott, G.M., Heather, K.B., Muir, T.L. and Sage, R.P. 1991. Wawa Subprovince. In *The Geology of Ontario*, Ontario Geological Survey, Special Volume 4, part 1, p. 485-542.
- Williams, H.R. 1990. Subprovince accretion tectonics in the south-central Superior Province. *Can. J. Earth Sci.*, **27**, 570-581.
- Williamson, P. and Robertson, W. A. 1976. Iterative Method of Isolating Primary and Secondary Components of Remanent Magnetization Illustrated by Using the Upper Devonian Catombal Group of Australia. *Journal of Geophysical Research*, **81**, 2531- 2538.
- Worm, H.-U. 1991. Multidomain susceptibility and anomalously strong low field dependence of induced magnetization in pyrrhotite. *Phys. Earth Planet. Inter.*, **69**, 112-118.
- Zijderveld, J. D. A. 1967. A.C. demagnetization of rocks: Analysis of results. In *Methods in Paleomagnetism*, edited by D. W. Collinson, K. M. Creer, and S. K. Runcorn, pp. Elsevier, New York, 1967, p.254-256.

## Appendix A

Sampling and structural data for two areas:

1. Kashabowie - Huronian Lake traverse - outcrops revisited since Spark (1991) sampling.
2. Atikokan - Huronian Lake traverse - outcrops within the interior of the belt and in lower grade schist towards Atikokan.

Tables include:

the name of locality;  
grid reference for topographic maps;  
additional descriptions of locations;  
the description of rock unit, minerals, outcrop scale structures;  
bedding  $S_0$ ; schistosity  $S_1$  and extension lineations  $L_1$  data:  
direction of dip and dip are listed with some remarks;  
the name and orientation marks of hand samples collected for lab studies with some descriptions;  
No of taken photographs.

Sampling data - Kashabowie - Huronian traverse - additional sampling

Locality	Grid refer.	Map	Location	Rock unit	Minerals	Misc.	Structural fabrics			Lineation trend	Young plunge	Sample name	Sample coordinates	remarks		
							Bedding S0 dir of dip	Foliation dir of dip	remarks							
TW 1	90.5/92.2	52B/9	Kashabowie River	chlorite schist	feldspar			171	80	S-tect by feldspar			TW 1	68/8		
TW 2	89.5/91.8	52B/9	feldspar bombs	greenschist	feldspar bombs			165	76	ext lin	68	25	TW 2-1	H		
TW 2	89.5/91.8	52B/9											TW 2-2	H		
RS 1.32	87.6/90.9	52B/9	700m E from Rd 802 to lt	greenschist	chlorite			173	75				TWR 1.32	240/6		
RS 2.2	85.7/91.0	52B/9	W after powerline, S side	greenschist, more felsic				157	80	weak S1			TWR 2.2	348/50		
RS 3.5	85.2/91.2	52B/9	300m E from rt turn, N side	greenschist, granite layers(sec)				156	86				TWR 3.5	006/10		
RS 3.6	84.8/91.3	52B/9		coarse felsic veins				156	82				TWR 3.6	H		
RS 3.7	83.8/91.6	52B/9	lt turn, N side small 2 outcrops	greenschist, Qtz rich				348	86	no ext lin			TWR 3.7A	H		
RS 4.1	83.4/91.6	52B/10	lt turn, 200m E from Whitefish L.	greenschist Qtz coarse grains				180	79	S1 varies			TWR 3.7B	H		
RS 5	82.7/91.3	52B/10	rt turn, hilltop	greenschist, Fe rich, weathered				0	80				TWR 4.1A	346/15		
RS 6.1	81.4/91.1	52B/10	W from Whitefish Lake	greenschist, granite?				169	79				TWR 4.1B	H	more Fe?	
RS 8	79.8/90.9	52B/10	200m W from creek	granitic and some more mafic (amphib, oliv?)				170	80	in schist layers			TWR 5A	112/15		
RS 8.05	78.5/90.9	52B/10	300m E from belt bound	pillow lavas metam. to greenschist				354	81				TWR 5B	202/10	redishgreen	
RS 8.1	78.6/90.9	52B/10	100m W from *, S side	pillow lavas, slates,				334	88	weak and varying S1			TWR 6.1	266/12		
RS 9.4	77.5/91.2	52B/10	* mark	slate, strong S0 and S1				154	89	ext lin by chlorite	66	20	340	TWR 8.0		Pict 1,2
RS 10	76.9/91.2	52B/10	before lt turn, W of small creek	phyllite- actinolite, halos around feldspar				338	76	S1 in slates	76	22		TWR 8.05	H	Pict 6(2)
RS 10.3	75.0/91.2	52B/10	radioantenna	biotite phyllite or schist				338	76	slickensides?	72	20				
TW 3	75.1/91.2	52B/10	before RS 10.4	initial differentiation				346	76	S0/S1	344	77	N	TWR 8.1		Pict 3
RS 10.5	70.4/91.5	52B/10	hill top	Phyllite, metam nodules-actin				150	87	S0=S1, extlin by act	98	64		TWR 9.4	H	
RS 10.8	69.9/91.5	52B/10		basic dyke- amphibolite metagabbroic				168	87	no ext lin			TWR 10.0	90/22		
RS 11.25	67.4/92.0	52B/10		biotite schist				354	90							
TW 4	63.4/93.3	52B/10	Atlantic watershed	schist, staurolite in elong porphyroblasts				138	85	S0/S1, graded bedding	54	30	N	TWR 10.3	H	
				pegmatite, biotite schist				146	74	init diff, boudins				TW 3	H	
				pegmatite- deflection of S1 in contact				328	82	schistosity	235	5		TWR 10.5	75/6	
				migmatite augen structures				318	87	layering, ext lin in biotite						
								318	87					TWR 10.8	H	
								360	46	S1 in schist				TWR 11.25	348/44	
								350	64							
								147	89					TW 4	H	Pict 4,5,6

Traverse Atkokaan - Huronian Lake - the interior of the Quetico Belt

Sampling sites				Structural fabrics									
Locality	Grid refer.	Map	Location	Rock unit	Minerals	Bedding S0	Foliation dicrodip	remarks	Lineation	Sample	Sample orient	remarks	
TWA	1	03.3/00.2	52B/12 Hwy 11b	biotite schist		352 84	323 84	younging to N	62 60	TWA 1	H		
TWA	1	03.3/00.2	52B/12				350 80		80 60				
TWA	2	03.2/99.8	52B/12 Hwy 11b	biotite schist		168 88	348 85		252 20	TWA 2	H		
TWA	2	03.2/99.8	52B/12			360 88	330 85						
TWA	2	03.2/99.8	52B/12			4 88							
TWA	3	03.2/99.2	52B/12 Hwy 11b; Voyageur Bait Tackle	biotite schist			169 70	S0=S1		TWA 3	270/10		
TWA	3	03.2/99.2	52B/12				167 68						
TWA	3	03.2/99.2	52B/12				154 85						
TWA	3	03.2/99.2	52B/12				178 70						
TWA	4	03.0/98.9	52B/12 Hwy 11b; before rt turn	paragneiss, biotite schist	qtz veins extension gashes		162 62	ext lin	240 26	TWA 4	258/85		
TWA	4	03.0/98.9	52B/12				162 74						
TWA	4	03.0/98.9	52B/12				170 78						
TWA	5	02.7/98.0	52B/12 on lt turn Hwy 11b to 11 (3A)	biotite schist			166 76	ext lin diff to notice		TWA 5	132/8		
TWA	5	02.7/98.0	52B/12				177 80		86 38				
TWA	5	02.7/98.0	52B/12				165 82						
TWA	5	02.7/98.0	52B/12				185 79						
TWA	6	02.8/97.8	52B/12 Hwy 11b 100m before Hwy 11	biotite schist	Qtz veins, nodules		170 85			TWA 6	176/82		
TWA	6	02.8/97.8	52B/12				177 79	no ext lin					
TWA	6	02.8/97.8	52B/12				170 79						
TWA	6.5	03.2/97.6	52B/12 100m before TWA7	biotite schist			156 58	S1 varying	66 62	TWA 6.5	244/46		
TWA	7	03.3/97.6	52B/12	biotite schist	differ layering		136 45			TWA 7	134/47		
TWA	7.5	03.8/97.5	52B/12				172 88			TWA 7.5	118/12		
TWA	7.5	03.8/97.5	52B/12 200m after TWA7; moose sign	biotite schist	differ layering		160 60	no ext lin					
TWA	7.5	03.8/97.5	52B/12 turn 600m before motel		Qtz veins		172 78						
TWA	7.5	03.8/97.5	52B/12 100m before motel				160 58						
TWA	8	04.5/97.4	52B/12 motel	biotite schist			158 75			TWA 8	170/86		
TWA	8	04.5/97.4	52B/12 100m before antenna	biotite schist		170 82	155 85	no ext lin					
TWA	8	04.5/97.4	52B/12			167 71	144 73						
TWA	9	05.2/97.1	52B/12 antenna	biotite schist			176 90			TWA 9	H		
TWA	9.5	05.9/96.8	52B/12 100m after antenna		Qtz intrusions and veins II S1	352 84	150 88			TWA 9.5	H		
TWA	9.5	05.9/96.8	52B/12				173 88						
TWA	10	07.4/96.5	52B/12	biotite schist			6 70	weak foliation -varying		TWA 10	0/65		
TWA	10.5	07.9/96.4	52B/12	biotite schist			346 80			TWA 10.5	40/33		
TWA	10.5	07.9/96.4	52B/12				350 78						
TWA	10.5	07.9/96.4	52B/12 motel in construction	migmatite			343 73						
TWA	11	09.6/96.3	52B/12 lt turn road	biotite schist/gneiss			342 60	S1 varying		TWA 11	340/65		
TWA	11.5	10.5/96.7	52B/12 300m after TWA11	biotite schist/gneiss	S -tect, micas		345 71			TWA 11.5	166/24	schist	
TWA	12	11.1/96.9	52B/11 300m before rt turn	biotite schist/gneiss	initial diff		338 50			TWA 12	330/67		
TWA	13	12.1/97.5	52B/11 200m after power line	biotite schist	large micas		346 60	ext lin by micas	36 50	TWA 13	241/86		
TWA	13	12.1/97.5	52B/11 Murrain Rd	biotite gneiss	qtz veins		350 70		78 45				
TWA	14	13.5/98.0	52B/11 Ken Danard place Rd	gneiss	felsic		350 58		64 30	TWA 14	256/80		
TWA	14	13.5/98.0	52B/11				354 53						
TWA	15	14.6/98.2	52B/11 hill top before barrier	gneiss	biotite, amphibolite?, chlorite?		352 85	weak S1	80 30	TWA 15	85/35		
TWA	15.5	15.4/98.2	52B/11 Baptista place before lt turn	pegmatite, schist	biotite, granite intrusion musc. and fibrous dark? green		344 38			TWA 15.5	H	Pict 20	
TWA	15.5	15.4/98.2	52B/11				33 58						

Locality	Grid refer.	Map	Location	Rock unit	Minerals	Bedding 50	Foliation dirotdip	remarks	Location	Sample	Sample orient	remarks
TWA 15.8	16.2/98.4	S2B/11	before TWA16	granitic body, pegmatite, musc						TWA 15.8		
TWA 15.9	17.1/98.9	S2B/11		biotite schist			342 56		50 12	TWA 15.9	354/45	
TWA 16	17.8/99.2	S2B/11		biotite schist	large micas, staurolite?		358 58		44 42	TWA 16	354/11	
TWA 16.5	18.2/99.3	S2B/11		biotite/schist/pegmatite, farther granite			338 48		58 10	TWA 16.5	330/12	
TWA 17	19.4/99.7	S2B/11	400m after powerline	biotite schist, amphibolites			354 66		80 19	TWA 17	268/9	
TWC 7	20.5/99.9	S2B/11		staurolite schist, initial diff next to pegm			358 69	50=51	80 20	TWC 7	H	Pict 18,19
TWC 7	20.5/99.9	S2B/11					348 78		78 28			
TWA 18	20.9/99.8	S2B/11		schist/gneiss			354 85		82 10	TWA 18	H	gneiss
TWA 18	20.9/99.8	S2B/11								TWA 18-2	124/42	schist
TWA 18.5	21.6/99.6	S2B/11		biotite gneiss,	Qtz, amphibolite?		357 74		80 18	TWA 18.5A	H	biotite schist Pict 21
TWA 18.5	21.6/99.6	S2B/11								TWA 18.5B	H	amphibolite?
TWA 19	22.8/98.6	S2B/11		pegmatite			340 85	S1 very weak		TWA 19	334/12	
TWL 10	23.2/98.8	S2B/11	Rd 623, to N 500m from Hwy 11	migmatite, some pegmatic pebbles, musc slick.			348 86		70 14	TWL 10	10/6	
TWL 10	23.2/98.8	S2B/11					164 74		77 14			
TWA 19.5	23.5/98.2	S2B/11		pegmatite, biotite schist			171 80			TWA 19.5	86/12	Pict 22
TWL 9	23.7/99.2	S2B/11	Rd 623, to N 2km before dump	biotite schist, initial differ.			346 56		56 18	TWL 9	210/84	
TWL 9	23.7/99.2	S2B/11							63 20			
TWA 20	23.9/97.9	S2B/11		pegmatite, biotite schist			148 30	layering, micas lin	74 20	TWA 20A	90/10	Pict 15-17
TWA 20	23.9/97.9	S2B/11								TWA 20B	0/12	
TWA 21	24.8/98.0	S2B/11		pegmatite, schist			178 18	S1 in schist	70 16	TWA 21	92/20	
TWA 22	25.8/98.0	S2B/11	200m after road to rt	biotite schist			24 70		114 12	TWA 22A	124/10	
TWA 22	25.8/98.0	S2B/11								TWA 22B	130/18	
TWA 22.5	26.8/98.1	S2B/11	100m west from TWC6	pegmatite, gneiss?			178 79		85 30	TWA 22.5	92/12	
TWA 22.5	26.8/98.1	S2B/11					176 76					
TWA 22.5	26.8/98.1	S2B/11					36 38	other side of road no schistosity				
TWC 6A	27.6/97.9	S2B/11	S side	basic graywacke, pegmatite	epidote					TWC 6A	H	
TWC 6A	27.6/97.9	S2B/11		granitic veining	amphibolite?							
TWC 6	27.7/98.0	S2B/11		biotite schist/granite gneiss			188 86		100 18	TWC 6	112/14	
TWC 5	28.2/96.9	S2B/11		migmatite, pegmatite, biotite rich layers			340 84		70 18	TWC 5A	H	
TWC 5	28.2/96.9	S2B/11					344 81			TWC 5B	H	
TWC 5	28.2/96.9	S2B/11								TWC 5C	38/10	
TWC 4	30.0/96.8	S2B/11		migmatite from graywacke, new biotite			334 74	ext lin in schist.	74 8	TWC 4	H	Pict 13,14
TWC 4	30.0/96.8	S2B/11					334 86	plane	72 14			
TWC 4	30.0/96.8	S2B/11					345 74		68 10			
TWC 4	30.0/96.8	S2B/11							68 14			
TWL 8	31.0/98.2	S2B/11	Rd 633, 200m N from Hwy 11	pegmatite, large schist pebbles			340 80	near pegm S1 dip=30	62 14	TWL 8	154/34	
TWC 3	31.5/95.8	S2B/11		granite, granitic gneiss - K feldspar, Fe rich				shear zones		TWC 3A	H	
TWL 7	31.5/99.1	S2B/11	Rd 633, 1km S from Quetico Centre	pegmatite body with large biotite layers			168 80			TWL 7	250/14	
TWL 7	31.5/99.1	S2B/11					164 68					
TWC 2	32.0/95.5	S2B/11		granitic nebulite, homogeneous, musc second.				no layering		TWC 2	196/6	Pict 12
TWC 1.5	32.3/95.5	S2B/11		pegmatite, some biotite gneiss, schist layers			350 78	layering		TWC 1.5A	H	
TWC 1.5	32.3/95.5	S2B/11								TWC 1.5B	166/18	
TWC 1	32.6/94.8	S2B/11		pegmatite, schist layers, boudins			343 40	layering varies	84 10	TWC 1	108/10	schist layer Pict 10,11
TWC 1	32.6/94.8	S2B/11								TWC 1A	H	more felsic gneiss
TWE 1	34.7/93.8	S2B/11	100m after lt turn	granitic body, some paleosome? pebbles						TWE 1	120/24	mafic
TWE 2	35.2/93.8	S2B/11	300m to E	pegmatite, granite, mafic layers						TWE 2	165/50	
TWE 3	37.6/92.8	S2B/11	500m from Quetico park entrance	pegmatite			352 70	weak layering		TWE 3A	220/20	
TWE 3	37.6/92.8	S2B/11	to E							TWE 3B	H	

Locality	Grid refer.	Map	Location	Rock unit	Minerals	Bedding S0 dip/dip	Foliation remarks	Lineation	Sample	Sample orient	remarks
TWE	4 39.9/92.2	S2B/11	100m W from French River	migmatite	boudinages, porphyroblasts	340 79	layering, ext lin	28 35	TWE 4A	222/23	more mafic Pict 23-25
TWE	4 39.9/92.2	S2B/11							TWB 4B	H	more felsic
TWL	6 40.5/93.9	S2B/11	Barrier Rd to N, 2 km from Hwy	migmatite, pegmatite intrusions		146 80		70 20	TWL 6	336/24	
TWE	5 41.2/91.4	S2B/11	It turn of Hwy 11, S side	migmatite		340 72					
TWE	6 41.8/91.8	S2B/11		migmatite, biotite schist layers		148 86	layering, ext lin	54 26	TWE 5	H	
TWE	6 41.8/91.8	S2B/11				140 80	N-layer, ext lin.	52 7	TWE 6A	320/11	
TW	23 42.5/92.0	S2B/11	in the middle of Lake Windigoostigwan	pegmatite, 4m high, larg: set of joints		142 82	S-layer, ext lin.	56 10	TWE 6B	142/18	
TW	23 42.5/92.0	S2B/11				150 68			TW 23	350/18	
TW	22 43.7/92.6	S2B/11	small outcrop, S side	migmatite, felsic		140 58					
TW	22 43.7/92.6	S2B/11				326 78	ext lin in musc.	48 14	TW 22	H	
TW	21 44.8/93.0	S2B/11	beginning of Lake Windigoostigwan	pegmatite with some migmatite		331 90		50 25			
TW	21 44.8/93.0	S2B/11		in pegmatite grains of amphibolite, actinolite?		334 82	in migmatite		TW 21A	330/32	mafic
TW	20 45.8/93.3	S2B/11	300m before lt turn	pegmatite, Qtz, pink granite	more mafic layers, musc. incl.	330 30	on cont with pegmatite		TW 21B	320/20	felsic
TW	19 46.9/93.4	S2B/11	JD Hackman road to rt, N side	pegmatite body, very felsic, small		0 60	weak layering		TW 20	243/0	from paleosome?
TWL	5 47.0/93.9	S2B/11	JD Hackman Rd N under powerline	migmatite		140 80	varying layering		TW 19	242/40	
TW	18 47.8/93.0	S2B/10	sign 90 km/h, gravel pit on lt	pegmatite	amphibolite (yellow-green)?	0 88			TWL 5	71/26	
TW	18 47.8/93.0	S2B/10				5 84			TW 18	346/14	Pict 4 (2)
TW	17 49.3/93.4	S2B/10	200m before sign: rt turn	Migmatite, wide schist layers		146 44		62 16	TW 17	338/22	
TW	16 50.6/93.2	S2B/10	200m before rt turn	migmatite, pegmatite intr.	boudins in flow plane	340 60	ext lin in micas	55 24	TW 16	H	
TW	16 50.6/93.2	S2B/10				345 58					
TW	16 50.6/93.2	S2B/10				349 57					
TW	15 51.7/93.5	S2B/10	50m W of road to N	migmatite, wide schist layers		350 58		50 5	TW 15	70/12	
TW	15 51.7/93.5	S2B/10		boudins in ext dir.		346 57					
TWL	4 52.0/94.2	S2B/10	gravel pit on shore	migmatite, high differ, biotite layers		190 45	layering		TWL 4	124/27	
TWL	4 52.0/94.2	S2B/10				144 90	layering				
TW	14 52.8/93.5	S2B/10	700m before rd to rt	granite, pegmatite		340 58	S1-layering,		TW 14	50/10	
TW	13 54.2/93.7	S2B/10	small outcrop before hill top	migmatite	muscovite	340 70	ext lin by musc	60 10	TW 13	350/10	
TW	13 54.2/93.7	S2B/10				340 85	layering in fold				
TW	12 55.6/93.8	S2B/10	100m after lt bend	migmatite, minor fold on N side		160 10	A-bottom, B-top	77 20	TW 12A	H	Pict 2,3 (2)
TW	12 55.6/93.8	S2B/10				0 36	layer, N side		TW 12B	H	
TW	12 55.6/93.8	S2B/10				358 62	layering		TW 12C	350/22	
TW	11 56.6/93.8	S2B/10	before hill top, S-side	migmatite layered		10 52		94 22	TW 11	H	Pict 1(2)
TW	11 56.6/93.8	S2B/10				2 58					
TW	10 57.5/93.7	S2B/10	after rt bend, S side	migmatite, layered	biotite layers	346 71	layering	64 18	TW 10	66/27	
TW	10 57.5/93.7	S2B/10				342 72					
TW	9 58.3/93.9	S2B/10	Top of hill after bridge on Harbour Lake	migmatite	biotite, amphibolite	358 74	ext lin in biotite	82 6	TW 9	280/6	
TW	9 58.3/93.9	S2B/10				146 85					
TW	8 59.6/94.4	S2B/10	on lt turn, before Burn Creek	migmatite, granitic & Qtz intrusions	biotite, amphibolite	348 86		66 12	TW 8	15/20	
TW	8 59.6/94.4	S2B/10				337 81					
TW	7 60.3/94.4	S2B/10	before lt turn, S-side	migmatite, pegmatite intrusions	boudins, ext ll layering	340 72	schistosity		TW 7A	H	
TW	7 60.3/94.4	S2B/10			muscovite, biotite				TW 7B	60/14	
TWL	3 61.2/94.4	S2B/10	as 2, 300m from Hwy	biotite schist		160 68	schistosity, ext lin	76 25	TWL 3	H	
TW	6 61.3/94.0	S2B/10	300m west from watershed	migmatite/pegmatite	second muscovite, biotite	158 65	S1 in biotite	80 6	TW 6	8/6	
TW	6 61.3/94.0	S2B/10				160 75	layering				
TWL	2 61.4/94.7	S2B/10	login road to Huronian Lake, 800m from Hwy 11	biotite schist, migmatite		180 88	schistosity	92 10	TWL 2	252/5	
TWL	1 62.1/93.1	S2B/10	700 m west from watershed	migmatite, only top visible		165 90	layers steep				Pict 5(2)
TW	5 62.8/93.4	S2B/10	Aretic watershed	migmatite		168 78			TW 5A	H	Si depleted
TW	5 62.8/93.4	S2B/10		migmatite/pegmatite		12 80	layering		TW 5B	H	

## Appendix B

### Magnetic fabric AMS and ARM data :

1. <sup>X</sup>AMS data for Kashabowie - Huronian area:
  - The axes of principal susceptibilities;
  - The anisotropy parameters (Flinn A and B and Jelinek P' and T).
2. <sup>AF</sup>AMS data for Atikokan - Huronian area:
  - The axes of principal susceptibilities;
  - Measurement errors for AMS data;
  - The anisotropy parameters (Flinn A and B and Jelinek P' and T).
3. ARM data for all three areas - principal axes with errors and anisotropy parameters.
  - RS collection - Kashabowie - Huronian Lake traverse
  - TW collection - Atikokan - Huronian Lake traverse
  - PS collection - Calm Lake - Perch Lake area.

## AMS data for Kashabowie - Huronian Lake traverse

N=119

Sample	Susceptibility															Mean aritm	Mean geom	Rejected data
	MIN					INT					MAX							
	Dec	Inc	alfa95	Int	std dev	Dec	Inc	Int	Dec	Inc	Int	Dec	Inc	Int	std dev			
TW 1-1	335.9	1.7	0.6	1.29E-02	1.08E-05	243.3	56.4	1.59E-02	67.1	33.6	1.3	1.68E-02	6.16E-06	1.52E-02	1.51E-02			
TW 1-2	344.4	3.2	0.7	4.88E-03	1.23E-05	249.5	56.9	6.11E-03	76.4	32.9	0.6	6.38E-03	4.37E-07	5.79E-03	5.75E-03			
TW 2-1	179.7	6.2	25.2	1.19E-04	2.66E-06	276.8	48.9	1.29E-04	84.4	40.4	73.8	1.33E-04	1.2E-06	1.27E-04	1.27E-04			
TWR 1.3a	183.1	7.6	46.9	2.47E-04	4.26E-06	263.8	54.3	2.79E-04	67.8	34.6	20.1	3.28E-04	3.79E-06	2.85E-04	2.83E-04	min		
TWR 1.3b	182.1	27.9	31.3	2.38E-04	5.91E-07	285.5	23.5	2.61E-04	49.3	52.0	6.9	3.23E-04	8.78E-06	2.74E-04	2.72E-04			
RST 1.31a	333.7	11.7	49.4	1.82E-04	6.37E-06	149.2	78.3	2.08E-04	243.5	0.9	41.3	2.31E-04	1.56E-05	2.07E-04	2.06E-04	max,min		
RST 1.31b	173.1	16.3	17	1.89E-04	7.2E-06	30.6	69.8	2.23E-04	266.6	11.6	34.2	2.32E-04	9.88E-07	2.15E-04	2.14E-04			
TWR 1.32-1a	159.6	13.0	73.9	2.73E-04	5.18E-07	65.2	18.5	3.04E-04	282.7	67.1	36.7	3.25E-04	2.21E-05	3.01E-04	3.00E-04	max,min		
TWR 1.32-1b	145.5	58.0	90.4	2.76E-04	1.08E-05	39.4	9.8	2.88E-04	303.6	30.1	42.4	3.29E-04	4.41E-06	2.98E-04	2.97E-04	max,min		
TWR 1.32-1c	323.5	10.9	26.4	2.23E-04	1.1E-05	227.4	29.0	2.52E-04	71.9	58.6	16.5	2.88E-04	1.12E-06	2.54E-04	2.53E-04	max		
TWR 1.32-1d	147.9	3.6	12.4	2.40E-04	1.68E-06	243.9	58.5	2.68E-04	55.7	31.2	21.1	2.97E-04	7.71E-06	2.68E-04	2.67E-04			
RST 1.33-1a	320.5	7.6	30.4	3.33E-04	6.29E-06	215.6	62.6	3.82E-04	54.9	26.1	79.7	3.92E-04	1.54E-05	3.69E-04	3.68E-04	max		
RST 1.33-1b	333.8	11.5	42.2	3.27E-04	1.81E-05	190.4	75.8	3.93E-04	65.5	8.3	52	4.11E-04	5.58E-06	3.77E-04	3.75E-04	max,min		
RST 2ca	8.4	13.0	19.8	4.49E-04	8.21E-06	266.9	40.6	4.76E-04	112.4	46.5	15.6	5.12E-04	8.24E-08	4.79E-04	4.79E-04			
RST 2.1a	350.4	28.8	26.4	3.95E-04	1.34E-06	221.8	48.5	4.39E-04	96.7	27.0	39.2	4.42E-04	6.18E-06	4.25E-04	4.25E-04	max		
RST 2.1b	178.4	3.9	36.6	4.63E-04	5.43E-06	273.8	54.0	4.77E-04	85.8	35.7	61.8	5.03E-04	9.78E-06	4.81E-04	4.81E-04	max,min		
RST 2.1c	186.8	18.0	31.2	4.58E-04	6.92E-06	317.2	63.4	4.83E-04	90.4	18.9	20.9	5.26E-04	9.26E-08	4.89E-04	4.88E-04	min		
RST 2.1d	326.1	9.6	44.8	4.30E-04	1.95E-06	226.5	44.8	4.76E-04	65.4	43.7	84	4.87E-04	5.37E-08	4.65E-04	4.64E-04	max,min		
TWR 2.2-1	157.3	15.2	52	7.23E-04	6.57E-06	44.7	54.8	7.47E-04	256.7	30.9	15.3	8.30E-04	6.59E-06	7.67E-04	7.65E-04	min		
TWR 2.2-2	158.8	13.5	13.4	6.31E-04	7.39E-06	61.2	28.8	6.60E-04	271.2	57.6	77.6	6.64E-04	3.63E-06	6.52E-04	6.51E-04	max		
RST 3a	317.6	0.2	47.6	1.27E-04	8.34E-06	227.0	78.1	1.41E-04	47.6	11.9	23.7	1.77E-04	1.36E-05	1.48E-04	1.47E-04	min		
RST 3b	242.1	23.7	60.7	7.80E-05	1.12E-08	342.5	22.5	8.70E-05	110.9	56.3	16.1	1.16E-04	7.78E-07	9.36E-05	9.23E-05	min		
TWR 3.5-1	287.4	1.5	0.7	2.72E-02	3.02E-05	194.1	65.7	3.05E-02	18.1	24.2	0.5	3.50E-02	7.77E-05	3.09E-02	3.08E-02			
TWR 3.5-2	111.8	4.0	1.1	2.74E-02	3E-05	210.2	64.3	3.05E-02	19.9	25.3	0.5	3.61E-02	9.2E-05	3.13E-02	3.11E-02			
TWR 3.7a-1	38.8	5.3	9.7	4.72E-05	3.08E-05	278.6	79.6	1.09E-04	129.6	8.9	45.1	1.58E-04	5.01E-05	1.05E-04	9.32E-05	max		
TWR 3.7b-1	309.9	12.8	36.1	1.17E-05	1.72E-05	190.6	65.1	2.44E-05	44.9	21.0	24.7	4.40E-05	1.97E-05	2.67E-05	2.32E-05	min		
TWR 4.1a-1	179.3	35.8	41.7	2.97E-04	1.77E-05	305.6	39.3	3.14E-04	64.3	30.4	9.1	3.69E-04	9.14E-06	3.27E-04	3.25E-04	min		
TWR 4.1a-2	336.3	4.7	24.4	3.94E-04	2.83E-06	224.5	77.5	4.45E-04	67.3	11.5	26.7	4.73E-04	6.97E-06	4.38E-04	4.36E-04			
TWR 4.1b-1	353.6	4.9	0.3	2.10E-02	9.56E-06	261.6	21.6	2.76E-02	95.8	67.8	1.1	2.90E-02	3.2E-05	2.59E-02	2.56E-02			
TWR 4.1b-2	351.4	8.3	0.5	1.80E-02	1.7E-05	258.9	16.7	2.25E-02	106.8	71.2	1	2.47E-02	7.35E-06	2.17E-02	2.15E-02			
TWR 4.1b-3	8.0	5.9	0.8	1.38E-02	1.56E-05	276.4	15.2	1.70E-02	118.8	73.7	1.4	1.87E-02	4.79E-05	1.65E-02	1.64E-02			
TWR 4.1b-4	8.5	6.6	0.6	1.93E-02	2.67E-06	274.5	31.0	2.50E-02	109.3	58.1	1.6	2.69E-02	3.84E-05	2.37E-02	2.35E-02			
RST 4.2a	164.8	26.3	54.6	1.94E-04	1.02E-05	65.5	18.0	2.24E-04	305.1	57.3	58.2	2.41E-04	5.83E-06	2.20E-04	2.19E-04	max,min		
RST 4.2b	339.9	21.8	48.1	1.73E-04	3.82E-06	115.5	60.7	1.97E-04	242.2	18.6	58.4	2.04E-04	1.43E-05	1.91E-04	1.91E-04	max,min		
RST 4.2c	171.4	21.1	53.9	1.69E-04	3.37E-06	282.0	42.4	1.76E-04	62.4	40.1	20.3	2.09E-04	1.63E-06	1.84E-04	1.84E-04	min		
RST 4.2d	284.1	31.7	17	1.88E-04	9.75E-07	183.7	16.3	2.12E-04	70.5	53.5	59.1	2.24E-04	8.84E-06	2.08E-04	2.08E-04	max		
TWR 5a-1	202.5	6.6	1.5	1.75E-02	1.18E-06	111.9	5.6	1.81E-02	341.7	81.3	0.5	2.19E-02	1.8E-05	1.92E-02	1.91E-02			
TWR 5a-2	206.2	5.1	0.6	1.70E-02	4.75E-06	115.5	8.3	1.77E-02	327.2	80.2	0.5	2.13E-02	2.29E-05	1.87E-02	1.86E-02			
TWR 5a-3	156.4	9.5	1	9.85E-03	2.48E-05	66.0	2.2	1.02E-02	322.9	80.3	1	1.25E-02	1.75E-05	1.09E-02	1.08E-02			



Sample	Susceptibility														Mean aritm	Mean geom	Rejected data
	MIN					INT				MAX							
	Dec	Inc	alfa95	Int	std dev	Dec	Inc	Int	Dec	Inc	alfa95	Int	std dev				
TWR 5b-1	347.0	9.9	17.6	3.57E-04	1.56E-05	235.9	64.2	4.02E-04	81.4	23.6	36.8	4.37E-04	1.41E-06	3.98E-04	3.97E-04	max	
TWR 5b-2	334.8	8.1	2.4	4.56E-04	3.22E-06	190.2	80.1	5.22E-04	65.6	5.7	26.7	5.95E-04	4.77E-06	5.04E-04	5.03E-04		
RST 5.1a	124.2	43.8	49.7	2.07E-04	3.85E-06	247.4	29.7	2.39E-04	358.0	31.7	64.6	2.52E-04	1.03E-05	2.33E-04	2.32E-04	max,min	
RST 5.1b	110.5	45.8	55.5	1.80E-04	9.48E-06	203.6	3.0	1.74E-04	296.4	44.1	45.2	2.01E-04	2.49E-06	1.78E-04	1.77E-04	max,min	
RST 5.5a	185.8	40.4	21.7	1.27E-04	5.55E-06	78.5	19.3	1.79E-04	329.2	43.3	64.7	1.93E-04	7.97E-06	1.66E-04	1.64E-04	max	
RST 5.5b	187.0	30.8	81.5	8.34E-05	2.09E-06	283.3	10.5	1.08E-04	30.0	57.1	58.2	1.17E-04	2.28E-07	1.03E-04	1.02E-04	max,min	
TWR 6.1-1	243.3	57.7	87.3	6.85E-04	7.82E-06	129.1	14.5	6.68E-04	31.1	28.2	35.8	6.67E-04	1.12E-05	6.73E-04	6.73E-04	max,min	
TWR 6.1-2	288.2	42.3	23.8	6.55E-04	6.21E-06	35.6	18.2	6.80E-04	142.9	42.1	22.3	6.86E-04	4.62E-07	6.73E-04	6.73E-04		
RST 6.2-3a	129.5	5.9	82.6	2.16E-04	3.83E-05	34.1	42.3	2.33E-04	226.0	47.1	25.3	2.73E-04	3.93E-06	2.41E-04	2.40E-04	min	
RST 6.2-3b	157.7	9.4	38.9	2.85E-04	3.14E-06	256.0	41.0	3.00E-04	57.3	47.5	74.1	3.23E-04	1.5E-05	2.96E-04	2.95E-04	max,min	
RST 6.2-3c	47.2	34.4	87.5	2.36E-04	1.99E-05	142.2	7.3	2.66E-04	242.7	54.8	44.3	2.85E-04	1.27E-05	2.62E-04	2.61E-04	min	
RST 6.2-3d	155.5	13.9	7.2	2.80E-04	9.65E-06	251.4	22.7	3.31E-04	36.5	63.0	21.6	3.63E-04	7.99E-06	3.25E-04	3.23E-04		
RST 7-1a	139.4	19.2	82.1	2.59E-04	2.37E-06	235.1	18.9	2.70E-04	11.4	64.7	12.8	3.19E-04	4.54E-06	2.83E-04	2.82E-04	min	
RST 7-1b	122.6	16.8	19.6	2.85E-04	2.15E-06	29.6	10.0	3.13E-04	269.9	70.3	61.1	3.22E-04	3.28E-06	3.07E-04	3.06E-04	max	
RST 7-1c	153.6	11.8	15.5	2.80E-04	3.05E-06	243.9	1.5	2.84E-04	340.9	78.1	22.3	3.13E-04	5.85E-06	2.85E-04	2.85E-04		
RST 7-1d	143.1	18.4	73.5	2.83E-04	1.32E-05	237.8	14.0	3.14E-04	3.0	66.8	41.8	3.41E-04	9.83E-06	3.12E-04	3.11E-04	max,min	
RST 7-2a	149.3	17.6	33.3	2.96E-04	6.45E-06	44.1	39.8	3.56E-04	257.9	45.1	45.7	3.68E-04	2.57E-05	3.40E-04	3.39E-04	max,min	
RST 7-2b	141.0	2.3	14.1	3.09E-04	6.66E-06	50.1	21.8	3.62E-04	236.7	68.0	11.7	3.69E-04	1E-07	3.47E-04	3.46E-04		
RST 8-1	280.3	34.6	109.6	6.10E-04	3.19E-06	33.2	29.4	6.22E-04	152.9	41.3	74	6.25E-04	5.46E-06	6.19E-04	6.19E-04	max,min	
RST 8-2	137.7	23.3	18.2	5.85E-04	5.44E-06	254.3	46.1	6.09E-04	30.3	34.7	50.3	6.19E-04	9.15E-06	6.04E-04	6.04E-04	max	
RST 8c-1	156.5	22.2	74.2	6.47E-04	6.57E-06	57.6	20.9	6.70E-04	288.7	58.7	28	6.65E-04	4.57E-07	6.67E-04	6.67E-04	min	
TWR 8.05-1	120.8	13.8	24.9	7.10E-04	1.03E-06	225.7	46.8	7.73E-04	19.0	40.2	51.8	7.74E-04	4.52E-06	7.53E-04	7.52E-04	max	
RST 9c	140.9	8.5	76	3.30E-04	4.83E-06	232.7	11.9	3.40E-04	16.0	75.3	65.7	3.51E-04	1.86E-05	3.40E-04	3.40E-04	max,min	
RST 9.1a	160.2	10.7	6	4.88E-04	9.37E-06	288.1	72.9	5.71E-04	67.6	13.2	16.3	6.04E-04	5.18E-07	5.54E-04	5.52E-04		
RST 9.1b	162.6	8.5	5.1	4.85E-04	4.85E-06	268.7	61.7	5.87E-04	68.2	26.8	6	6.23E-04	6.97E-06	5.65E-04	5.62E-04		
RST 9.2-2a	184.2	7.8	9.1	4.67E-04	4.69E-06	43.0	75.2	5.49E-04	256.0	12.5	16.9	5.98E-04	1.42E-05	5.38E-04	5.35E-04		
RST 9.2-2b	151.8	7.3	1.8	4.09E-04	1.22E-06	258.2	65.8	4.91E-04	58.5	22.9	48.5	5.18E-04	9.1E-06	4.72E-04	4.70E-04	max	
RST 9.2-2c	157.9	4.2	14.8	4.50E-04	9.06E-06	357.1	85.5	5.25E-04	248.0	1.4	6.6	5.67E-04	9.28E-06	5.14E-04	5.11E-04		
RST 9.2-2d	164.9	5.2	6.9	4.41E-04	1.02E-05	291.6	81.4	5.26E-04	74.3	6.9	28.6	5.52E-04	1.54E-06	5.06E-04	5.04E-04		
RST 9.25a	326.9	18.0	9.5	2.65E-04	1.37E-06	71.6	38.1	3.22E-04	216.9	46.4	86.1	3.23E-04	4.38E-07	3.03E-04	3.02E-04	max	
RST 9.25b	140.7	8.0	9.1	2.92E-04	1.19E-05	242.2	55.0	3.48E-04	45.3	33.9	79.8	3.59E-04	1.39E-05	3.33E-04	3.32E-04	max	
TW 3-1	293.6	17.9	5.7	5.73E-04	1.19E-07	37.2	35.9	5.98E-04	182.1	48.5	20.9	6.30E-04	3.46E-06	6.01E-04	6.00E-04		
TW 3-2	314.1	10.3	17.5	5.58E-04	9.78E-06	70.0	67.3	5.89E-04	220.3	19.9	23.8	6.42E-04	8.66E-06	5.96E-04	5.95E-04	max	
TWR 9.4-1	319.2	7.2	15.4	2.83E-04	1.84E-06	202.2	74.6	3.23E-04	51.0	13.8	20.6	3.48E-04	4.56E-06	3.18E-04	3.17E-04		
TWR 9.4-2	137.8	6.4	20.4	2.57E-04	3.8E-06	244.3	68.5	3.26E-04	45.5	20.4	28	3.51E-04	1.33E-05	3.12E-04	3.09E-04		
TWR 9.4-3	307.6	12.7	26.3	2.83E-04	3.3E-07	58.2	57.3	3.27E-04	210.3	29.5	77	3.40E-04	7.25E-06	3.17E-04	3.16E-04	max	
TWR 9.4-4	143.7	5.6	12	2.70E-04	3.32E-06	45.8	54.8	3.36E-04	237.6	34.9	50.8	3.45E-04	1.4E-06	3.17E-04	3.15E-04	max	
TWR 10.0-1	317.9	17.0	2.9	3.79E-04	8.32E-06	207.3	49.1	4.13E-04	60.7	35.9	16.3	4.60E-04	1.86E-05	4.17E-04	4.16E-04		
TWR 10.0-2	334.5	4.5	6.6	3.59E-04	4.97E-06	241.1	37.3	3.96E-04	70.3	52.4	24.8	4.16E-04	2.08E-05	3.90E-04	3.90E-04		
TWR 10.3-1	157.9	16.5	34	2.30E-04	1.14E-05	293.0	67.3	2.64E-04	63.3	15.2	166.6	2.79E-04	1.95E-06	2.58E-04	2.57E-04	max,min	

Sample	Susceptibility															Mean aritm	Mean geom	Rejected data
	MIN					INT					MAX							
	Dec	Inc	alfa95	Int	std dev	Dec	Inc	Int	Dec	Inc	alfa95	Int	std dev					
TWR 10.3-2	130.9	20.2	11.5	2.31E-04	5.44E-06	272.2	64.8	2.81E-04	35.5	14.4	29.2	2.93E-04	9.79E-06	2.68E-04	2.67E-04			
TWR 10.5-1	137.9	12.7	8.2	4.47E-04	7.14E-06	327.1	77.2	5.78E-04	228.4	2.0	9	6.27E-04	1.77E-06	5.51E-04	5.45E-04			
TWR 10.5-2	147.1	10.0	1.9	4.79E-04	9.81E-06	10.8	78.3	6.78E-04	238.8	9.3	9.1	7.87E-04	1.34E-05	6.48E-04	6.34E-04			
TWR 10.5-3	142.7	7.5	4.8	5.35E-04	6.56E-07	10.1	78.9	7.42E-04	233.8	8.1	2.3	8.40E-04	5.52E-06	7.06E-04	6.93E-04			
TWR 10.8-1	157.3	1.5	12.1	3.08E-04	1.01E-05	298.5	88.0	3.82E-04	67.3	1.2	36	3.86E-04	1.58E-06	3.58E-04	3.57E-04	max		
TWR 10.8-2	137.1	19.6	7.7	3.36E-04	8.04E-06	43.7	9.5	3.99E-04	289.3	68.1	42.9	4.11E-04	6.96E-06	3.82E-04	3.80E-04	max		
TWR 10.8-3	172.3	14.5	6.9	3.27E-04	8.94E-06	277.2	45.0	4.31E-04	69.1	41.4	79.2	4.34E-04	1.78E-07	3.97E-04	3.94E-04	max		
TWR 10.8-4	183.0	11.9	5.8	3.31E-04	5.82E-06	48.3	73.2	4.13E-04	275.4	11.6	23.8	4.32E-04	1.19E-05	3.92E-04	3.89E-04			
TWR 10.8-5	181.0	6.6	7.7	3.12E-04	2.02E-06	79.4	60.2	3.65E-04	274.7	26.9	8.1	3.91E-04	8.93E-07	3.56E-04	3.54E-04			
RST 11-1a	173.5	68.8	20.3	3.80E-04	5.51E-06	343.0	20.9	4.68E-04	74.3	3.5	48.4	4.76E-04	8.52E-06	4.41E-04	4.39E-04	max		
RST 11-1b	153.3	56.7	4.1	3.80E-04	4.3E-06	344.8	32.8	4.32E-04	251.4	5.2	34.8	4.74E-04	3.66E-06	4.29E-04	4.27E-04	max,min		
RST 11.1-1a	169.4	31.9	8.3	2.88E-04	1.11E-05	282.0	31.7	4.17E-04	45.6	41.8	14.2	4.38E-04	5.16E-06	3.74E-04	3.68E-04			
RST 11.1-1b	165.5	30.7	1.9	3.83E-04	6.2E-06	301.8	50.6	5.75E-04	81.5	22.2	20.3	6.08E-04	1.64E-06	5.15E-04	5.03E-04			
RST 11.2-1a	166.9	20.3	16.3	1.77E-04	3.92E-06	287.7	54.1	2.23E-04	85.5	28.2	22.2	2.33E-04	6.85E-06	2.11E-04	2.10E-04			
RST 11.2-1b	62.6	67.5	60.8	1.75E-04	5.12E-06	336.7	0.8	1.80E-04	246.7	2.4	45.3	2.09E-04	7.9E-06	1.88E-04	1.87E-04	max,min		
RST 11.2-1c	344.6	22.4	45.7	1.93E-04	3.62E-06	156.1	67.5	2.20E-04	253.6	2.3	31.5	2.37E-04	9.64E-06	2.17E-04	2.16E-04	min		
RST 11.2-1d	174.7	16.5	7.7	1.70E-04	4.27E-06	275.0	31.2	2.23E-04	60.9	53.8	45.3	2.34E-04	3.68E-06	2.09E-04	2.07E-04	max		
TWR 11.25-1	157.8	31.2	11.4	2.32E-04	1.98E-06	288.4	47.0	2.91E-04	50.4	26.3	28.3	3.18E-04	1.2E-05	2.80E-04	2.78E-04			
TWR 11.25-2	154.7	30.0	14.3	2.61E-04	1.75E-05	283.2	47.2	3.24E-04	47.3	27.4	52.2	3.43E-04	1.15E-05	3.09E-04	3.07E-04	max		
RST 11.3a	166.7	41.8	19.9	2.31E-04	5.95E-06	0.0	47.4	2.52E-04	292.8	6.8	11.1	2.93E-04	2.64E-06	2.59E-04	2.57E-04			
RST 11.3b	177.5	41.8	16.7	2.28E-04	1.97E-05	313.7	38.9	2.92E-04	64.4	23.6	65.5	3.11E-04	1.56E-05	2.77E-04	2.74E-04	max		
RST 11.3c	171.5	48.7	8.2	2.20E-04	1.64E-05	330.4	39.3	2.83E-04	69.2	10.8	29.9	2.83E-04	7.83E-06	2.56E-04	2.54E-04			
RST 11.35a	175.5	32.0	10.6	2.64E-04	1.01E-06	8.3	57.4	3.55E-04	289.2	5.8	66.1	3.60E-04	1.4E-06	3.33E-04	3.31E-04	max		
RST 11.4-2a	160.1	53.1	10.4	2.44E-04	5.68E-06	327.2	36.2	3.49E-04	61.8	6.2	24.1	3.70E-04	1.32E-06	3.21E-04	3.16E-04			
RST 11.4a	310.6	10.6	51.8	2.54E-05	1.97E-06	65.5	66.0	3.63E-05	216.4	21.2	59.5	4.89E-05	1.45E-05	3.69E-05	3.56E-05	max,min		
RST 11.45a	171.7	47.9	9.6	2.90E-04	7.8E-06	57.3	20.5	3.50E-04	312.2	34.9	9.7	3.97E-04	3.46E-06	3.46E-04	3.43E-04			
RST 11.5a	279.1	62.3	21.5	2.74E-04	1.02E-05	76.3	25.9	3.39E-04	170.9	9.3	9.5	3.74E-04	5.8E-07	3.29E-04	3.26E-04			
RST 11.5b	246.8	75.1	22.7	2.96E-04	1.89E-05	103.9	12.0	3.74E-04	12.0	6.7	41.5	3.82E-04	4.36E-06	3.51E-04	3.48E-04	max		
RST 11.5c	272.9	60.9	14.4	2.90E-04	1.2E-05	14.3	6.2	3.76E-04	107.7	28.3	78.9	3.80E-04	6.53E-07	3.49E-04	3.46E-04	max		
RST 11.5d	281.2	65.5	14.4	2.71E-04	1.9E-06	94.3	24.3	3.26E-04	185.5	2.6	31.7	3.53E-04	6.92E-06	3.17E-04	3.15E-04			
RST 11.6-1a	188.9	43.8	1.5	2.58E-04	4.83E-06	308.6	27.3	3.19E-04	58.9	33.8	6.8	3.39E-04	9.01E-06	3.05E-04	3.03E-04			
RST 11.6-1b	174.7	45.9	37.5	3.39E-04	3.28E-06	352.5	44.1	3.81E-04	83.5	1.1	36.4	3.98E-04	5.69E-06	3.72E-04	3.71E-04	max,min		
RST 11.6-1c	167.9	62.9	7.5	3.41E-04	4.04E-07	335.2	23.3	4.04E-04	71.0	13.1	54.8	4.31E-04	1.4E-05	3.92E-04	3.90E-04	max		
RST 11.6-2a	178.7	51.1	35.6	2.94E-04	6.15E-06	12.8	38.0	3.19E-04	277.3	6.9	31.3	3.43E-04	2.36E-06	3.19E-04	3.18E-04	max,min		
RST 11.7-1a	345.0	46.7	0.4	2.70E-02	0.000309	187.2	41.1	4.40E-02	87.2	11.2	0.5	6.14E-02	2.98E-05	4.41E-02	4.18E-02			
RST 11.7-3a	334.6	19.0	64.9	3.09E-06	1.3E-06	77.4	32.9	2.63E-05	219.7	50.7	58.5	4.36E-05	4.05E-07	2.43E-05	1.52E-05	max,min		
RST 11.8-1a	144.7	60.6	37.4	1.47E-04	2.69E-06	274.6	19.9	1.84E-04	12.5	20.7	57.8	2.03E-04	4.56E-07	1.78E-04	1.76E-04	max,min		
RST 11.9a	336.0	11.5	26.4	4.62E-04	1.64E-05	235.6	41.5	4.99E-04	78.2	46.2	68.1	5.10E-04	5.12E-06	4.90E-04	4.90E-04	max		
TW 4-1	164.8	11.4		2.61E-03		348.5	78.6	3.46E-03	255.0	0.7		4.26E-03		3.44E-03	3.38E-03			
TW 4-2	165.1	5.9		7.77E-03		32.3	81.4	1.03E-02	255.7	6.3		1.28E-02		1.03E-02	1.01E-02			

## AMS parameters - Flinn and Jelinek - Kashabowie - Huronian lake traverse

Sample	AMS file code			K1/K2	K2/K3	ln(A)	ln(B)	P'	T	Rejected
	C	SN	Mean geom							
TW 1-1	1	1	1.51E-02	1.06	1.23	0.05	0.20	1.31	0.58	
TW 1-2	1	2	5.75E-03	1.04	1.25	0.04	0.22	1.33	0.68	
TW 2-1	1	1	1.27E-04	1.03	1.09	0.03	0.08	1.12	0.50	
TWR 1.3a	1	31	2.83E-04	1.17	1.13	0.16	0.13	1.33	-0.12	min
TWR 1.3b	1	32	2.72E-04	1.23	1.10	0.21	0.09	1.37	-0.38	
RST 1.31a	1	311	2.06E-04	1.11	1.15	0.10	0.14	1.27	0.15	max,min
RST 1.31b	1	312	2.14E-04	1.04	1.18	0.04	0.16	1.24	0.57	
TWR 1.32-1a	1	3211	3.00E-04	1.07	1.12	0.07	0.11	1.19	0.25	max,min
TWR 1.32-1b	1	3212	2.97E-04	1.14	1.04	0.13	0.04	1.20	-0.54	max,min
TWR 1.32-1c	1	3213	2.53E-04	1.14	1.13	0.13	0.12	1.29	-0.03	max
TWR 1.32-1d	1	3214	2.67E-04	1.11	1.11	0.10	0.11	1.24	0.02	
RST 1.33-1a	1	3311	3.68E-04	1.03	1.15	0.03	0.14	1.19	0.67	max
RST 1.33-1b	1	3312	3.75E-04	1.05	1.20	0.05	0.18	1.28	0.60	max,min
RST 2ca	2	31	4.79E-04	1.08	1.06	0.07	0.06	1.14	-0.11	
RST 2.1a	2	11	4.25E-04	1.01	1.11	0.01	0.11	1.14	0.89	max
RST 2.1b	2	12	4.81E-04	1.05	1.03	0.05	0.03	1.09	-0.30	max,min
RST 2.1c	2	13	4.88E-04	1.09	1.05	0.09	0.05	1.15	-0.24	min
RST 2.1d	2	14	4.64E-04	1.02	1.11	0.02	0.10	1.14	0.64	max,min
TWR 2.2-1	2	21	7.65E-04	1.11	1.03	0.10	0.03	1.15	-0.52	min
TWR 2.2-2	2	22	6.51E-04	1.01	1.05	0.01	0.05	1.06	0.78	max
RST 3a	3	1	1.47E-04	1.26	1.11	0.23	0.10	1.40	-0.38	min
RST 3b	3	2	9.23E-05	1.33	1.12	0.29	0.11	1.50	-0.45	min
TWR 3.5-1	3	51	3.08E-02	1.15	1.12	0.14	0.11	1.29	-0.10	
TWR 3.5-2	3	52	3.11E-02	1.18	1.11	0.17	0.11	1.32	-0.21	
TWR 3.7a-1	3	61	9.32E-05	1.46	2.30	0.38	0.83	3.45	0.38	max
TWR 3.7b-1	3	721	2.32E-05	1.80	2.09	0.59	0.74	3.78	0.11	min
TWR 4.1a-1	4	111	3.25E-04	1.17	1.06	0.16	0.06	1.25	-0.48	min
TWR 4.1a-2	4	112	4.36E-04	1.06	1.13	0.06	0.12	1.20	0.33	
TWR 4.1b-1	4	121	2.56E-02	1.05	1.31	0.05	0.27	1.41	0.69	
TWR 4.1b-2	4	122	2.15E-02	1.10	1.25	0.09	0.22	1.39	0.41	
TWR 4.1b-3	4	123	1.64E-02	1.10	1.24	0.09	0.21	1.37	0.39	
TWR 4.1b-4	4	124	2.35E-02	1.08	1.29	0.08	0.26	1.42	0.54	
RST 4.2a	4	21	2.19E-04	1.08	1.15	0.08	0.14	1.25	0.30	max,min
RST 4.2b	4	22	1.91E-04	1.03	1.14	0.03	0.13	1.19	0.61	max,min
RST 4.2c	4	23	1.84E-04	1.19	1.04	0.17	0.04	1.25	-0.62	min
RST 4.2d	4	24	2.08E-04	1.05	1.13	0.05	0.12	1.19	0.40	max
TWR 5a-1	5	11	1.86E-02	1.21	1.03	0.19	0.03	1.27	-0.73	
TWR 5a-2	5	12	3.97E-04	1.20	1.04	0.18	0.04	1.27	-0.66	max
TWR 5a-3	5	13	5.03E-04	1.23	1.04	0.21	0.03	1.30	-0.71	
TWR 5b-1	5	21	2.32E-04	1.09	1.13	0.08	0.12	1.23	0.18	max,min
TWR 5b-2	5	22	1.77E-04	1.02	1.14	0.02	0.13	1.19	0.69	max,min
RST 5.1a	5	11	1.91E-02	1.06	1.15	0.06	0.14	1.23	0.43	
RST 5.1b	5	12	1.08E-02	1.16	1.09	0.14	0.08	1.26	-0.27	
RST 5.5a	5	51	1.64E-04	1.08	1.41	0.08	0.35	1.57	0.64	max
RST 5.5b	5	52	1.02E-04	1.08	1.29	0.08	0.26	1.42	0.52	max,min
TWR 6.1-1	6	11	6.73E-04	1.03	1.00	0.03	0.00	1.04	-0.72	max,min
TWR 6.1-2	6	12	6.73E-04	1.01	1.04	0.01	0.04	1.05	0.63	
RST 6.2-3a	6	231	2.40E-04	1.17	1.08	0.16	0.08	1.27	-0.33	min
RST 6.2-3b	6	232	2.95E-04	1.08	1.13	0.08	0.12	1.22	0.24	max,min
RST 6.2-3c	6	233	2.61E-04	1.07	1.13	0.07	0.12	1.21	0.28	min
RST 6.2-3d	6	234	3.23E-04	1.10	1.18	0.09	0.17	1.30	0.29	
RST 7-1a	7	11	2.82E-04	1.18	1.04	0.17	0.04	1.25	-0.60	min
RST 7-1b	7	12	3.06E-04	1.03	1.10	0.03	0.09	1.14	0.52	max
RST 7-1c	7	13	2.85E-04	1.10	1.09	0.10	0.09	1.20	-0.03	
RST 7-1d	7	14	3.11E-04	1.09	1.11	0.08	0.10	1.21	0.11	max,min
RST 7-2a	7	21	3.39E-04	1.03	1.20	0.03	0.19	1.27	0.69	max,min
RST 7-2b	7	22	3.46E-04	1.02	1.17	0.02	0.16	1.22	0.79	
RST 8-1	8	1	6.19E-04	1.01	1.02	0.01	0.02	1.03	0.58	max,min
RST 8-2	8	2	6.04E-04	1.02	1.04	0.02	0.04	1.06	0.39	max
RST 8c-1	8	31	6.67E-04	1.02	1.04	0.02	0.03	1.06	0.22	min

## AMS parameters - Flinn and Jelinek - Kashabowie - Huronian lake traverse

Sample	AMS file code			K1/K2	K2/K3	ln(A)	ln(B)	P'	T	Rejected
	C	SN								
TWR 8.05-1	8	51		1.00	1.09	0.00	0.08	1.10	0.96	max
RST 9c	9	3		1.03	1.03	0.03	0.03	1.06	-0.04	max,min
RST 9.1a	9	11		1.06	1.17	0.06	0.16	1.25	0.47	
RST 9.1b	9	12		1.06	1.21	0.06	0.19	1.30	0.52	
RST 9.22a	9	221		1.09	1.18	0.09	0.16	1.29	0.31	
RST 9.22b	9	222		1.06	1.20	0.05	0.18	1.28	0.54	max
RST 9.22c	9	223		1.08	1.17	0.08	0.15	1.27	0.33	
RST 9.22d	9	224		1.05	1.19	0.05	0.18	1.27	0.57	
RST 9.25a	9	251		1.00	1.21	0.00	0.19	1.25	0.98	max
RST 9.25b	9	252		1.03	1.19	0.03	0.17	1.25	0.68	max
TW 3-1	3	1		1.05	1.04	0.05	0.04	1.10	-0.11	
TW 3-2	3	2		1.09	1.06	0.09	0.05	1.15	-0.22	max
TWR 9.4-1	9	41		1.07	1.14	0.07	0.13	1.23	0.30	
TWR 9.4-2	9	42		1.08	1.27	0.07	0.24	1.38	0.53	
TWR 9.4-3	9	43		1.04	1.15	0.04	0.14	1.21	0.57	max
TWR 9.4-4	9	44		1.03	1.24	0.03	0.22	1.30	0.79	max
TWR 10.-1	10	1		1.12	1.09	0.11	0.08	1.21	-0.13	
TWR 10.-2	10	2		1.05	1.11	0.05	0.10	1.16	0.35	
TWR 10.3-1	10	31		1.06	1.15	0.06	0.14	1.22	0.44	max,min
TWR 10.3-2	10	32		1.04	1.21	0.04	0.19	1.29	0.65	
TWR 10.5-1	10	51		1.08	1.29	0.08	0.26	1.42	0.52	
TWR 10.5-2	10	52		1.16	1.42	0.15	0.35	1.66	0.40	
TWR 10.5-3	10	53		1.13	1.39	0.12	0.33	1.59	0.45	
TWR 10.8-1	10	81		1.01	1.24	0.01	0.21	1.29	0.90	max
TWR 10.8-2	10	82		1.03	1.19	0.03	0.17	1.24	0.70	max
TWR 10.8-3	10	83		1.01	1.32	0.01	0.28	1.38	0.94	max
TWR 10.8-4	10	84		1.05	1.25	0.05	0.22	1.33	0.66	
TWR 10.8-5	10	85		1.07	1.17	0.07	0.16	1.26	0.39	
RST 11-1a	11	11		1.02	1.23	0.02	0.21	1.28	0.85	max
RST 11-1b	11	12		1.10	1.14	0.09	0.13	1.25	0.17	max,min
RST 11.11a	11	111		1.05	1.56	0.05	0.44	1.72	0.80	
RST 11.11b	11	112		1.06	1.58	0.06	0.46	1.76	0.78	
RST 11.21a	11	211		1.04	1.26	0.04	0.23	1.34	0.70	
RST 11.21b	11	212		1.16	1.03	0.15	0.03	1.21	-0.65	max,min
RST 11.21c	11	213		1.08	1.14	0.07	0.13	1.23	0.27	min
RST 11.21d	11	214		1.05	1.31	0.05	0.27	1.41	0.70	max
TWR 11.25-1	11	251		1.09	1.25	0.09	0.22	1.38	0.43	
TWR 11.25-2	11	252		1.06	1.24	0.06	0.22	1.34	0.59	max
RST 11.35a	11	351		1.02	1.25	0.02	0.22	1.31	0.87	
RST 11.3a	11	31		1.16	1.09	0.15	0.09	1.28	-0.25	max
RST 11.3b	11	32		1.07	1.28	0.06	0.25	1.39	0.59	
RST 11.3c	11	33		1.08	1.19	0.07	0.18	1.30	0.41	max
RST 11.42a	11	421		1.06	1.43	0.06	0.36	1.57	0.72	
RST 11.45a	11	451		1.13	1.21	0.13	0.19	1.37	0.20	max,min
RST 11.4a	11	41		1.35	1.43	0.30	0.36	1.93	0.09	
RST 11.5a	11	51		1.10	1.24	0.10	0.21	1.38	0.36	
RST 11.5b	11	52		1.02	1.26	0.02	0.23	1.33	0.84	max
RST 11.5c	11	53		1.01	1.30	0.01	0.26	1.36	0.92	max
RST 11.5d	11	54		1.08	1.20	0.08	0.18	1.31	0.39	
RST 11.61a	11	611		1.06	1.23	0.06	0.21	1.33	0.54	
RST 11.61b	11	612		1.04	1.13	0.04	0.12	1.18	0.52	max,min
RST 11.61c	11	613		1.07	1.19	0.06	0.17	1.27	0.45	max
RST 11.62a	11	621		1.08	1.08	0.07	0.08	1.17	0.03	max,min
RST 11.71a	11	711		1.40	1.63	0.33	0.49	2.29	0.19	
RST 11.73a	11	731		1.66	8.51	0.51	2.14	16.64	0.62	max,min
RST 11.81a	11	811		1.10	1.26	0.10	0.23	1.40	0.40	max,min
RST 11.9a	11	91		1.02	1.08	0.02	0.08	1.11	0.55	max
TW 4-1	4	1		1.23	1.32	0.21	0.28	1.63	0.15	
TW 4-2	4	2		1.24	1.33	0.21	0.28	1.65	0.14	

AMS anisotropy data - traverse Atikokan - Huronian Lake

Station	Sample	Grid X	DEC	MIN			INT			MAX			Mean susceptibility		Rejected	
				INC	INT	DEC	INC	INT	DEC	INC	INT	aritm	geom			
TWA1.0	twa	1	1	3.3	343.4	1.6	3.27E-04	251.9	41.8	5.03E-04	75.2	48.2	5.99E-04	4.76E-04	4.62E-04	
TWA1.0	twa	1	2	3.3	351.2	1.0	4.67E-04	260.3	40.2	7.58E-04	82.4	49.8	1.08E-03	7.67E-04	7.25E-04	
TWA2.0	twa	2	1	3.2	181.0	5.9	4.68E-04	89.9	10.2	8.21E-04	300.3	78.2	8.41E-04	7.10E-04	6.86E-04	
TWA2.0	twa	2	2	3.2	177.8	5.5	5.09E-04	268.6	8.4	9.51E-04	54.9	79.9	1.02E-03	8.25E-04	7.89E-04	
TWA3.0	twa	3	1	3.2	343.7	19.5	3.66E-04	88.2	35.3	4.50E-04	230.4	48.1	4.67E-04	4.28E-04	4.25E-04	max
TWA4.0	twa	4	1	3	154.8	10.0	2.08E-04	61.8	16.5	2.29E-04	274.8	70.5	2.49E-04	2.29E-04	2.28E-04	min
TWA4.0	twa	4	2	3	152.3	0.4	2.05E-04	243.4	71.6	2.30E-04	62.1	18.4	2.39E-04	2.25E-04	2.24E-04	min
TWA4.0	twa	4	3	3	162.7	11.4	2.12E-04	282.6	68.0	2.44E-04	68.8	18.6	2.56E-04	2.37E-04	2.37E-04	max
TWA5.0	twa	5	1	2.7	343.1	18.6	4.31E-04	81.9	24.5	5.37E-04	219.8	58.5	5.79E-04	5.16E-04	5.12E-04	max
TWA5.0	twa	5	2	2.7	329.3	4.1	2.89E-04	226.6	71.7	3.51E-04	60.6	17.8	3.71E-04	3.37E-04	3.35E-04	max
TWA6.0	twa	6	1	2.8	346.4	3.1	7.99E-04	76.6	4.4	1.18E-03	221.5	84.6	1.25E-03	1.08E-03	1.06E-03	
TWA6.0	twa	6	2	2.8	350.6	3.0	7.08E-04	260.3	5.8	1.16E-03	107.9	83.4	1.34E-03	1.07E-03	1.03E-03	
TWA6.5	twa	6.5	1	3.2	223.9	31.3	2.71E-04	327.3	20.8	3.03E-04	85.2	51.0	3.17E-04	2.97E-04	2.96E-04	
TWA6.5	twa	6.5	2	3.2	306.6	44.7	2.99E-04	154.9	41.6	3.09E-04	51.5	14.6	3.40E-04	3.16E-04	3.16E-04	min,max
TWA7.0	twa	7	1	3.3	336.4	12.8	6.48E-04	237.9	32.9	7.79E-04	84.8	54.1	8.30E-04	7.52E-04	7.48E-04	
TWA7.5	twa	7.5	1	3.8	25.1	29.4	2.49E-04	126.1	18.7	2.63E-04	244.0	54.1	2.89E-04	2.67E-04	2.66E-04	
TWA7.5	twa	7.5	2	3.8	117.9	8.0	2.66E-04	24.1	25.2	2.71E-04	224.2	63.3	2.72E-04	2.70E-04	2.70E-04	min,max
TWA8.0	twa	8	1	4.5	172.3	16.8	9.16E-04	80.2	6.7	1.20E-03	329.4	71.9	1.35E-03	1.15E-03	1.14E-03	
TWA8.0	twa	8	2	4.5	164.7	15.8	9.66E-04	73.7	3.7	1.32E-03	330.7	73.7	1.54E-03	1.28E-03	1.25E-03	
TWA9.0	twa	9	1	5.2	187.6	13.0	7.97E-04	289.2	41.0	8.95E-04	83.7	46.1	9.49E-04	8.80E-04	8.78E-04	
TWA9.0	twa	9	2	5.2	190.7	6.5	8.39E-04	286.5	41.8	9.24E-04	93.6	47.5	9.97E-04	9.20E-04	9.18E-04	
TWA9.5	twa	9.5	1	5.9	355.4	5.9	6.58E-04	264.6	7.7	7.88E-04	122.5	80.3	8.45E-04	7.64E-04	7.59E-04	
TWA9.5	twa	9.5	2	5.9	353.1	6.5	7.05E-04	262.5	5.8	8.42E-04	131.1	81.3	9.36E-04	8.27E-04	8.22E-04	
TWA10.0	twa	10	1	7.4	354.2	0.5	2.69E-04	263.3	60.6	3.33E-04	84.4	29.4	3.37E-04	3.13E-04	3.11E-04	max
TWA10.0	twa	10	2	7.4	339.7	2.1	2.50E-04	71.0	31.6	2.86E-04	246.3	58.3	3.13E-04	2.83E-04	2.82E-04	
TWA10.5	twa	10.5	1	7.9	169.6	16.2	4.95E-04	270.2	32.4	6.90E-04	57.2	52.8	7.46E-04	6.43E-04	6.34E-04	
TWA10.5	twa	10.5	2	7.9	167.9	13.4	5.06E-04	263.9	23.4	6.92E-04	50.5	62.6	7.75E-04	6.58E-04	6.47E-04	
TWA11.0	twa	11	1	9.6	148.1	20.9	3.25E-04	262.6	47.4	3.72E-04	42.6	35.1	3.85E-04	3.61E-04	3.60E-04	max
TWA11.0	twa	11	2	9.6	159.5	19.2	2.87E-04	254.7	14.5	3.28E-04	19.5	65.6	3.41E-04	3.19E-04	3.18E-04	max
TWA11.5	twa	11.5	1	10.5	169.1	35.1	4.75E-04	67.9	15.4	5.28E-04	318.3	50.7	5.38E-04	5.14E-04	5.13E-04	max
TWA11.5	twa	11.5	2	10.5	338.8	11.0	5.05E-04	73.1	21.2	5.30E-04	222.9	65.9	5.32E-04	5.22E-04	5.22E-04	max
TWA12.0	twa	12	1	11.1	147.1	34.2	2.88E-04	315.2	55.3	3.41E-04	53.3	5.6	3.46E-04	3.25E-04	3.24E-04	max
TWA12.0	twa	12	2	11.1	147.8	24.2	2.77E-04	306.2	64.2	3.26E-04	54.0	8.4	3.41E-04	3.15E-04	3.13E-04	max
TWA13.0	twa	13	1	12.1	157.4	26.5	2.49E-04	294.0	55.5	2.98E-04	56.7	20.4	3.13E-04	2.87E-04	2.85E-04	max
TWA13.0	twa	13	2	12.1	172.5	30.2	2.15E-04	288.2	36.7	2.64E-04	54.7	38.7	3.03E-04	2.61E-04	2.58E-04	
TWA14.0	twa	14	1	13.5	64.5	38.5	4.03E-04	205.7	44.4	4.73E-04	317.2	20.5	4.96E-04	4.57E-04	4.56E-04	
TWA14.0	twa	14	2	13.5	51.8	23.6	3.61E-04	157.5	31.8	4.00E-04	292.2	48.6	4.13E-04	3.92E-04	3.91E-04	min,max
TWA15.0	twa	15	1	14.6	197.5	53.4	4.20E-03	334.0	28.3	4.92E-03	76.0	21.2	6.48E-03	5.20E-03	5.12E-03	
TWA15.0	twa	15	2	14.6	196.3	47.6	2.80E-03	337.6	35.5	3.01E-03	82.7	20.1	4.04E-03	3.28E-03	3.24E-03	
TWA15.5	twa	15.5	1	15.4	167.5	33.3	6.34E-04	291.6	40.4	8.05E-04	53.5	31.8	1.12E-03	8.54E-04	8.31E-04	
TWA15.5	twa	15.5	2	15.4	155.6	31.4	4.03E-04	289.5	48.6	4.91E-04	49.8	24.0	5.70E-04	4.88E-04	4.83E-04	
TWA15.9	twa	15.9	1	17.1	175.8	28.7	3.43E-04	352.0	61.2	4.16E-04	84.9	1.6	4.49E-04	4.03E-04	4.00E-04	
TWA15.9	twa	15.9	2	17.1	189.1	31.4	3.85E-04	332.5	52.8	4.51E-04	87.7	18.0	4.85E-04	4.41E-04	4.39E-04	max
TWA16.0	twa	16	1	17.8	175.4	32.3	2.87E-04	269.9	7.1	3.71E-04	11.0	56.7	3.73E-04	3.44E-04	3.41E-04	max
TWA16.0	twa	16	2	17.8	175.9	39.3	3.01E-04	45.0	38.7	3.84E-04	290.7	27.1	4.07E-04	3.64E-04	3.61E-04	max
TWA16.5	twa	16.5	1	18.2	150.8	47.5	4.05E-04	298.3	37.7	5.30E-04	41.7	16.7	5.65E-04	5.00E-04	4.95E-04	
TWA16.5	twa	16.5	2	18.2	164.5	44.6	3.94E-04	286.6	28.3	5.20E-04	36.4	32.0	5.60E-04	4.91E-04	4.86E-04	
TWA17.0	twa	17	1	19.4	182.7	8.6	2.54E-04	290.7	64.0	3.25E-04	88.8	24.3	3.39E-04	3.06E-04	3.03E-04	max
TWA17.0	twa	17	2	19.4	8.8	0.4	2.50E-04	99.1	38.8	3.34E-04	278.3	51.2	3.52E-04	3.12E-04	3.09E-04	
TWC7.0	twc	7	1	20.5	161.8	4.1	2.68E-04	64.9	59.4	3.22E-04	254.2	30.3	3.38E-04	3.10E-04	3.08E-04	
TWC7.0	twc	7	2	20.5	180.3	2.8	2.84E-04	298.8	84.1	3.11E-04	90.0	5.2	3.41E-04	3.12E-04	3.11E-04	
TWA18.0	twa	18 a	1	20.9	7.5	16.2	4.78E-04	221.6	70.7	5.24E-04	100.5	10.3	5.38E-04	5.13E-04	5.13E-04	max
TWA18.0	twa	18 a	2	20.9	12.2	6.7	4.92E-04	276.8	38.9	5.09E-04	110.3	50.3	5.24E-04	5.08E-04	5.08E-04	min,max
TWA18.0	twa	18 b	1	20.9	357.5	11.1	3.99E-04	253.0	51.9	4.63E-04	95.6	35.9	4.87E-04	4.50E-04	4.48E-04	max
TWA18.0	twa	18 b	2	20.9	345.3	9.6	4.16E-04	232.8	66.2	4.77E-04	79.1	21.6	5.19E-04	4.71E-04	4.69E-04	
TWA18.5	twa	18.5	1	21.6	173.8	64.9	6.57E-04	356.5	25.1	7.61E-04	266.0	1.0	8.22E-04	7.46E-04	7.43E-04	
TWA18.5	twa	18.5	2	21.6	178.3	57.7	6.80E-04	351.5	32.1	7.58E-04	83.4	3.0	8.68E-04	7.68E-04	7.65E-04	

AMS anisotropy data - traverse Atikokan - Huronian Lake

Station	Sample	Grid X	DEC	MIN			INT			MAX			Mean susceptibility		Rejected		
				INC	INT	DEC	INC	INT	DEC	INC	INT	arim	geom				
TWA18.5	twa	18.5	a	1	21.6	171.2	18.8	3.38E-04	291.9	56.3	3.99E-04	71.3	26.8	4.11E-04	3.81E-04	3.80E-04	max
TWA18.5	twa	18.5	a	2	21.6	145.5	23.9	3.51E-04	307.4	65.0	4.21E-04	52.4	6.9	4.57E-04	4.10E-04	4.07E-04	
TWA19.0	twa	19		1	22.8	22.8	57.1	3.88E-04	115.9	2.0	4.19E-04	207.2	32.8	5.04E-04	4.37E-04	4.34E-04	max,min
TWA19.0	twa	19		2	22.8	110.4	41.4	4.05E-04	316.1	45.7	4.39E-04	212.3	13.1	4.53E-04	4.32E-04	4.32E-04	max
TWL9.0	twl	9		1	23.7	145.0	16.5	2.52E-04	312.4	73.2	2.95E-04	54.0	3.5	3.11E-04	2.86E-04	2.85E-04	max
TWL10.0	twl	10		1	23.2	149.5	3.3	4.95E-04	49.8	70.8	6.58E-04	240.6	18.9	6.77E-04	6.10E-04	6.04E-04	max
TWL10.0	twl	10		2	23.2	156.0	7.8	5.19E-04	253.2	42.3	6.47E-04	57.7	46.6	6.76E-04	6.14E-04	6.10E-04	max
TWA19.5	twa	19.5		1	23.5	340.6	30.0	1.54E-03	195.8	54.8	1.74E-03	80.6	16.8	2.30E-03	1.86E-03	1.83E-03	
TWA19.5	twa	19.5		2	23.5	313.8	56.6	5.95E-04	166.5	29.1	6.63E-04	67.9	15.1	8.07E-04	6.89E-04	6.83E-04	
TWA20.0	twa	20	a	1	23.9	161.0	48.9	2.18E-04	323.4	39.8	2.39E-04	60.8	8.8	2.68E-04	2.42E-04	2.41E-04	
TWA20.0	twa	20	a	2	23.9	322.8	65.5	2.39E-04	160.6	23.5	2.58E-04	67.7	6.7	2.93E-04	2.63E-04	2.62E-04	
TWA20.0	twa	20	b	1	23.9	171.2	74.0	2.68E-04	356.1	15.9	3.07E-04	265.7	1.3	3.49E-04	3.08E-04	3.06E-04	
TWA20.0	twa	20	b	2	23.9	149.8	75.2	2.96E-04	343.8	14.4	3.45E-04	253.0	3.4	4.33E-04	3.58E-04	3.54E-04	
TWA21.0	twa	21		1	24.8	262.9	75.9	3.84E-04	27.9	8.2	4.35E-04	119.5	11.4	4.49E-04	4.23E-04	4.22E-04	max,min
TWA21.0	twa	21		2	24.8	74.1	68.4	3.57E-04	240.9	21.1	4.31E-04	332.6	4.5	4.45E-04	4.11E-04	4.09E-04	
TWA22.0	twa	22		1	25.8	210.2	12.5	3.03E-04	332.8	67.7	3.69E-04	116.0	18.2	3.83E-04	3.52E-04	3.50E-04	
TWA22.0	twa	22		2	25.8	224.2	18.5	3.05E-04	83.1	66.8	3.56E-04	318.8	13.6	3.70E-04	3.44E-04	3.42E-04	max
TWA22.0	twa	22	a	1	25.8	208.0	25.1	2.96E-04	101.7	31.0	3.49E-04	329.6	48.1	3.60E-04	3.35E-04	3.34E-04	max
TWA22.0	twa	22	a	2	25.8	229.0	29.1	3.07E-04	352.6	44.8	3.54E-04	119.3	31.1	3.90E-04	3.50E-04	3.49E-04	
TWA22.5	twa	22.5		1	26.8	7.0	64.0	3.55E-04	214.8	23.4	4.00E-04	120.1	10.9	4.40E-04	3.98E-04	3.97E-04	
TWA22.5	twa	22.5		2	26.8	245.4	76.8	3.59E-04	353.8	4.2	4.14E-04	84.7	12.5	4.39E-04	4.04E-04	4.03E-04	max
TWC6.1	twc	6	a	2	27.6	328.4	38.7	1.94E-04	226.8	14.2	2.30E-04	120.6	47.9	2.36E-04	2.20E-04	2.19E-04	min,max
TWC6.1	twc	6	a	1	27.6	336.6	30.8	1.84E-04	173.7	58.0	2.05E-04	71.2	7.7	2.15E-04	2.01E-04	2.01E-04	
TWC6.0	twc	6		2	27.7	312.9	70.7	4.81E-04	189.6	10.9	5.57E-04	96.5	15.7	7.66E-04	6.02E-04	5.90E-04	
TWC6.0	twc	6		1	27.7	315.7	70.1	7.14E-04	190.8	11.7	8.53E-04	97.4	15.8	1.24E-03	9.37E-04	9.12E-04	
TWC5.0	twc	5	c	1	28.2	156.3	19.0	3.02E-04	264.5	42.2	3.64E-04	48.4	41.7	3.90E-04	3.52E-04	3.50E-04	max
TWC5.0	twc	5	b	2	28.2	335.1	12.9	3.85E-04	207.4	69.6	4.62E-04	68.8	15.6	5.80E-04	4.76E-04	4.69E-04	
TWC5.0	twc	5	b	1	28.2	349.4	9.1	2.85E-04	206.3	78.6	3.40E-04	80.5	6.7	3.56E-04	3.27E-04	3.25E-04	max
TWC5.0	twc	5	a	2	28.2	145.4	18.4	3.23E-04	256.7	47.5	3.76E-04	41.1	36.6	3.90E-04	3.63E-04	3.62E-04	
TWC5.0	twc	5	a	1	28.2	169.8	22.3	2.99E-04	302.9	59.0	3.52E-04	71.1	20.3	3.80E-04	3.44E-04	3.42E-04	
TWL7.0	twl	7		1	31.5	37.2	58.1	4.35E-04	143.3	9.8	4.56E-04	239.0	30.0	4.87E-04	4.59E-04	4.59E-04	min
TWL7.0	twl	7		2	31.5	342.7	25.5	4.47E-04	197.2	59.9	4.71E-04	79.9	14.8	5.05E-04	4.75E-04	4.74E-04	min
TWL8.0	twl	8		1	31	145.9	10.7	2.77E-04	255.4	60.5	3.18E-04	50.3	27.1	3.31E-04	3.09E-04	3.08E-04	max
TWL8.0	twl	8		2	31	141.2	13.8	2.35E-04	50.0	4.7	2.75E-04	301.4	75.4	2.91E-04	2.67E-04	2.66E-04	min
TWC4.0	twc	4		2	30	157.8	13.0	4.28E-04	268.1	56.4	4.66E-04	60.0	30.4	4.91E-04	4.62E-04	4.61E-04	max
TWC4.0	twc	4		1	30	313.6	15.7	4.22E-04	200.2	54.7	4.49E-04	53.2	30.7	4.72E-04	4.47E-04	4.47E-04	min
TWC3.0	twc	3	a	1	31.5	294.5	14.7	7.86E-05	189.1	45.4	9.70E-05	37.6	40.9	1.05E-04	9.36E-05	9.29E-05	max,min
TWC2.0	twc	2		1	32	223.4	26.4	4.83E-05	3.5	57.1	6.46E-05	124.0	18.2	8.00E-05	6.43E-05	6.29E-05	max,min
TWC1.5	twc	1.5	b	2	32.3	165.1	17.9	3.27E-04	29.1	65.8	5.00E-04	260.3	15.7	5.14E-04	4.47E-04	4.38E-04	max
TWC1.5	twc	1.5	b	1	32.3	161.0	22.1	3.28E-04	280.5	50.5	4.98E-04	56.9	30.8	5.11E-04	4.46E-04	4.37E-04	max
TWC1.5	twc	1.5	a	1	32.3	159.9	6.8	2.89E-04	65.1	35.3	3.53E-04	259.3	53.9	3.72E-04	3.38E-04	3.36E-04	max
TWC1.0	twc	1		2	32.6	167.5	12.8	3.46E-04	326.2	76.3	5.15E-04	76.4	4.8	5.32E-04	4.64E-04	4.56E-04	max
TWE1.0	twe	1		1	32.6	175.4	14.5	3.18E-04	277.3	38.5	4.97E-04	68.8	47.8	5.14E-04	4.43E-04	4.33E-04	
TWE1.0	twe	1		1	34.7	311.6	41.4	3.33E-04	179.7	37.1	4.13E-04	67.5	26.4	4.28E-04	3.92E-04	3.89E-04	
TWE1.0	twe	1		2	34.7	299.6	48.9	3.61E-04	184.9	20.1	4.29E-04	80.5	34.1	4.82E-04	4.24E-04	4.21E-04	
TWE2.0	twe	2		1	35.2	221.8	38.5	2.35E-05	130.8	1.3	4.16E-05	39.1	51.5	6.97E-05	4.49E-05	4.08E-05	max
TWE2.0	twe	2		2	35.2	292.8	22.5	1.92E-05	197.8	11.9	5.38E-05	81.9	64.2	6.34E-05	4.55E-05	4.03E-05	max,min
TWE3.0	twe	3	a	1	37.6	179.5	67.0	2.82E-04	341.3	22.0	3.16E-04	73.9	6.5	3.33E-04	3.10E-04	3.09E-04	max
TWE3.0	twe	3	a	2	37.6	179.4	65.8	2.73E-04	273.2	1.7	3.24E-04	4.0	24.1	3.31E-04	3.09E-04	3.08E-04	max
TWE3.0	twe	3	b	1	37.6	58.2	70.0	3.32E-04	238.4	20.0	4.27E-04	328.3	0.0	4.36E-04	3.98E-04	3.95E-04	max
TWE3.0	twe	3	b	2	37.6	18.8	66.1	3.32E-04	138.2	12.3	4.18E-04	232.8	20.2	4.41E-04	3.97E-04	3.94E-04	max
TWL6.0	twl	6		1	40.5	165.5	52.1	2.57E-04	17.5	33.5	3.21E-04	276.7	15.8	3.34E-04	3.04E-04	3.02E-04	max
TWL6.0	twl	6		2	40.5	145.6	67.3	2.38E-04	258.3	9.2	3.10E-04	351.7	20.6	3.18E-04	2.89E-04	2.86E-04	max
TWE4.0	twe	4	a	1	39.9	331.1	3.5	2.30E-04	61.7	10.2	2.93E-04	222.1	79.2	3.01E-04	2.75E-04	2.73E-04	min
TWE4.0	twe	4	b	1	39.9	143.7	3.5	2.76E-04	238.7	54.9	3.56E-04	51.3	34.9	3.73E-04	3.35E-04	3.32E-04	
TWE4.0	twe	4	b	2	39.9	328.9	0.7	3.03E-04	238.5	30.4	3.69E-04	60.1	59.6	3.93E-04	3.55E-04	3.53E-04	
TWE5.0	twe	5		1	41.2	316.9	13.1	3.56E-04	171.8	74.2	4.41E-04	49.0	8.7	4.53E-04	4.17E-04	4.14E-04	max
TWE5.0	twe	5		2	41.2	327.7	12.2	3.02E-04	216.8	58.7	3.69E-04	64.4	28.3	4.04E-04	3.58E-04	3.56E-04	
TWE6.0	twe	6	a	1	41.8	277.3	12.8	4.58E-04	164.5	59.6	5.18E-04	14.0	27.1	6.55E-04	5.44E-04	5.38E-04	
TWE6.0	twe	6	a	2	41.8	290.1	2.6	9.43E-04	195.4	60.7	1.08E-03	21.6	29.2	1.37E-03	1.13E-03	1.12E-03	
TWE6.0	twe	6	a	3	41.8	269.9	16.5	6.68E-04	152.6	57.2	7.42E-04	8.8	27.5	1.01E-03	8.06E-04	7.94E-04	
TWE6.0	twe	6	b	1	41.8	328.5	10.2	3.34E-04	154.5	79.7	4.34E-04	58.7	1.0	4.56E-04	4.08E-04	4.04E-04	max
TWE6.0	twe	6	b	2	41.8	148.6	1.0	3.41E-04	256.2	86.8	4.22E-04	58.6	3.1	4.81E-04	4.15E-04	4.11E-04	
TWE6.0	twe	6	b	3	41.8	321.1	10.8	4.48E-04	147.8	79.1	6.12E-04	51.3	1.2	6.61E-04	5.74E-04	5.66E-04	
TW23.0	tw	23		2	42.5	319.3	10.3	7.64E-04	58.8	42.3	1.01E-03	218.5	45.9	1.06E-03	9.46E-04	9.37E-04	
TW23.0	tw	23		1	42.5	325.8	14.3	5.94E-04	69.0	42.0	7.47E-04	221.3	44.5	7.63E-04	7.01E-04	6.97E-04	max
TW22.0	tw	22		2	43.7	149.4	2.1	3.68E-04	254.9	82.3	4.43E-04	59.1	7.4	4.77E-04	4.29E-04	4.27E-04	max
TW22.0	tw	22		1	43.7	315.4	11.3	2.96E-04	138.9	78.6	3.83E-04	45.5	0.7	4.11E-04	3.63E-04	3.60E-04	

AMS anisotropy data - traverse Atikokan - Huronian Lake

Station	Sample	Grid	DEC	MIN			INT			MAX			Mean susceptibility		Rejected	
				INC	INT	DEC	INC	INT	DEC	INC	INT	aritm	geom			
TW21.0	tw	21 a	2	44.8	172.0	69.0	2.62E-04	292.8	11.1	3.17E-04	26.4	17.6	3.44E-04	3.08E-04	3.06E-04	max
TW21.0	tw	21 a	1	44.8	155.5	55.6	2.67E-04	330.8	34.3	3.19E-04	62.3	2.2	3.31E-04	3.06E-04	3.05E-04	max
TW21.0	tw	21	2	44.8	233.8	72.2	2.71E-04	329.8	1.9	2.81E-04	60.4	17.7	3.27E-04	2.93E-04	2.92E-04	min
TW21.0	tw	21	1	44.8	172.6	52.2	2.56E-04	278.8	12.2	2.82E-04	17.5	35.1	3.05E-04	2.81E-04	2.81E-04	
TW20.0	tw	20	2	45.8	232.4	56.4	3.03E-04	329.3	4.5	3.64E-04	62.3	33.2	3.78E-04	3.48E-04	3.47E-04	max
TW20.0	tw	20	1	45.8	215.8	66.1	2.98E-04	3.9	20.6	3.61E-04	98.3	11.6	3.69E-04	3.43E-04	3.41E-04	max
TWL5.0	twl	5	1	47	139.1	21.6	2.85E-04	246.6	37.2	3.15E-04	25.7	45.0	3.28E-04	3.09E-04	3.09E-04	min,max
TWL5.0	twl	5	2	47	164.9	42.0	2.86E-04	61.0	14.9	3.02E-04	316.0	44.2	3.27E-04	3.18E-04	3.07E-04	min,max
TW19.0	tw	19	2	46.9	254.1	66.6	6.31E-04	163.6	0.4	6.47E-04	73.4	23.4	7.66E-04	6.81E-04	6.79E-04	
TW19.0	tw	19	1	46.9	200.7	64.5	5.31E-04	328.2	16.2	5.80E-04	64.0	19.1	6.63E-04	5.91E-04	5.89E-04	
TW18.0	tw	18	2	47.8	158.7	0.2	2.42E-04	248.8	5.9	3.33E-04	66.7	84.1	3.37E-04	3.04E-04	3.00E-04	max
TW18.0	tw	18	1	47.8	351.1	2.5	2.80E-04	81.9	15.9	3.28E-04	252.5	73.9	3.47E-04	3.18E-04	3.17E-04	max
TW17.0	tw	17	2	49.3	325.8	46.7	5.37E-04	160.7	42.3	5.82E-04	63.8	7.5	6.64E-04	5.94E-04	5.92E-04	
TW17.0	tw	17	1	49.3	328.7	50.3	4.56E-04	151.2	39.7	5.35E-04	60.1	1.2	5.61E-04	5.17E-04	5.16E-04	
TW16.0	tw	16	2	50.6	184.3	24.2	2.77E-04	91.9	5.3	3.44E-04	350.3	65.2	3.58E-04	3.27E-04	3.25E-04	max
TW16.0	tw	16	1	50.6	177.4	39.0	3.14E-04	289.8	25.1	3.62E-04	43.4	40.6	3.98E-04	3.58E-04	3.57E-04	
TW15.0	tw	15	1	51.7	155.1	14.7	3.17E-04	38.2	59.9	3.64E-04	252.3	25.6	4.04E-04	3.61E-04	3.60E-04	
TW14.0	tw	14	2	52.8	197.1	4.6	3.92E-04	81.7	79.3	4.59E-04	287.9	9.6	5.07E-04	4.52E-04	4.50E-04	
TW14.0	tw	14	1	52.8	188.1	1.9	3.46E-04	88.0	79.0	4.01E-04	278.4	10.9	4.45E-04	3.97E-04	3.95E-04	
TW13.0	tw	13	2	54.2	142.2	37.7	1.88E-04	31.8	24.3	2.35E-04	277.3	42.5	2.45E-04	2.23E-04	2.21E-04	max,min
TW13.0	tw	13	1	54.2	148.6	50.8	2.38E-04	337.3	38.8	2.71E-04	243.9	4.3	2.93E-04	2.67E-04	2.67E-04	max,min
TW12.0	tw	12 c	2	55.6	178.5	29.1	3.51E-04	322.6	55.5	3.80E-04	78.8	16.8	3.93E-04	3.75E-04	3.74E-04	max,min
TW12.0	tw	12 c	1	55.6	171.2	43.8	3.26E-04	320.9	42.0	3.77E-04	65.6	15.7	3.95E-04	3.66E-04	3.65E-04	max
TW12.0	tw	12 b	2	55.6	179.1	65.6	2.06E-04	41.3	18.6	2.52E-04	306.0	15.3	2.79E-04	2.45E-04	2.44E-04	min
TW12.0	tw	12 b	1	55.6	287.4	74.3	2.12E-04	144.9	12.6	2.51E-04	52.8	9.3	2.80E-04	2.48E-04	2.46E-04	
TW12.0	tw	12 a	2	55.6	324.4	6.6	2.34E-04	217.0	68.9	2.88E-04	56.8	19.9	2.98E-04	2.73E-04	2.72E-04	max
TW12.0	tw	12 a	1	55.6	317.2	21.0	2.40E-04	63.6	36.4	2.73E-04	203.7	46.1	2.81E-04	2.65E-04	2.64E-04	max
TW11.0	tw	11	2	56.6	137.4	33.2	2.65E-04	356.7	49.8	3.14E-04	241.2	20.0	3.33E-04	3.04E-04	3.03E-04	max
TW11.0	tw	11	1	56.6	160.3	21.1	2.11E-04	53.5	36.9	2.51E-04	273.5	45.6	2.77E-04	2.46E-04	2.45E-04	max
TW10.0	tw	10	2	57.5	152.5	21.9	2.99E-04	51.1	26.1	3.49E-04	277.2	54.7	3.64E-04	3.38E-04	3.36E-04	
TW10.0	tw	10	1	57.5	150.8	8.6	2.83E-04	329.2	81.4	3.20E-04	60.7	0.2	3.64E-04	3.22E-04	3.21E-04	min
TWL4.0	twl	4	1	52	136.0	39.1	2.53E-04	257.3	32.6	2.97E-04	12.8	34.0	3.05E-04	2.85E-04	2.84E-04	min,max
TW9.0	tw	9	2	58.3	142.3	34.7	2.27E-04	344.8	53.1	2.73E-04	240.0	10.9	2.84E-04	2.61E-04	2.60E-04	max
TW9.0	tw	9	1	58.3	193.4	38.6	2.82E-04	305.0	24.7	3.33E-04	58.8	41.3	3.60E-04	3.25E-04	3.23E-04	max
TW8.0	tw	8	2	59.6	346.7	4.4	7.86E-04	228.7	80.8	1.13E-03	77.3	8.1	1.35E-03	1.09E-03	1.06E-03	
TW8.0	tw	8	1	59.6	349.5	0.4	6.93E-04	257.7	77.2	9.80E-04	79.6	12.8	1.09E-03	9.21E-04	9.04E-04	
TW7.0	tw	7 b	2	60.3	147.7	18.7	2.84E-04	270.1	57.7	3.07E-04	48.5	25.3	3.86E-04	3.26E-04	3.23E-04	min
TW7.0	tw	7 b	1	60.3	154.6	20.0	3.35E-04	255.7	27.9	3.93E-04	33.7	54.6	4.14E-04	3.81E-04	3.79E-04	
TW7.0	tw	7 a	2	60.3	326.9	3.0	2.55E-04	230.0	66.8	3.41E-04	58.2	23.0	3.71E-04	3.22E-04	3.19E-04	
TW7.0	tw	7 a	1	60.3	330.9	13.6	3.02E-04	213.9	62.0	3.55E-04	67.1	24.0	3.73E-04	3.44E-04	3.42E-04	
TWL2.0	twl	2	1	61.4	180.2	7.4	4.52E-04	289.7	68.8	5.30E-04	87.5	19.8	5.64E-04	5.15E-04	5.13E-04	
TWL2.0	twl	2	2	61.4	161.5	11.8	4.17E-04	16.0	75.8	5.09E-04	253.1	7.8	5.18E-04	4.81E-04	4.79E-04	
TWL3.0	twl	3	1	61.2	343.8	15.4	2.50E-04	82.4	28.6	3.02E-04	228.9	56.9	3.15E-04	2.89E-04	2.88E-04	
TWL3.0	twl	3	2	61.2	170.9	1.5	2.58E-04	79.9	33.4	3.11E-04	263.2	56.6	3.46E-04	3.05E-04	3.03E-04	
TW6.0	tw	6	2	61.3	276.0	28.1	2.79E-04	18.3	21.6	3.70E-04	140.3	53.2	3.75E-04	3.41E-04	3.38E-04	max
TW6.0	tw	6	1	61.3	270.7	7.7	2.87E-04	29.9	74.4	3.46E-04	178.9	13.4	3.85E-04	3.39E-04	3.37E-04	
TW5.0	tw	5 a	2	62.8	340.5	4.9	2.06E-04	83.3	69.0	2.70E-04	248.6	20.4	2.85E-04	2.54E-04	2.52E-04	max
TW5.0	tw	5 a	1	62.8	167.9	21.2	2.16E-04	264.3	16.0	2.27E-04	28.5	63.0	2.88E-04	2.44E-04	2.42E-04	min
TW5.0	tw	5	2	62.8	122.9	44.5	1.60E-04	17.3	15.2	2.37E-04	273.4	41.5	3.42E-04	2.46E-04	2.35E-04	max,min
TW5.0	tw	5	1	62.8	164.1	40.6	2.13E-04	32.7	37.6	2.78E-04	279.8	26.8	2.88E-04	2.60E-04	2.58E-04	max

AMS data for Atikokan - Huronian area:

Measurement errors for AMS data



SAMPLE TWA SITE 1 CORE 1 SPEC 1 UNITS= SI v M= 12 NR= 2 1  
 SUSC. DEC INC R95 EV SDEV  
 TWA 1-1 MIN 343.38 1.61 3.2 3.2677E-04 2.840E-05  
 INT 251.94 41.78 3.8 5.0323E-04 1.348E-05  
 MAX 75.18 48.18 4.5 5.9891E-04 1.711E-05

TWA SITE 2 CORE 1 SPEC 2 UNITS= SI v M= 12 NR= 2  
 SUSC. DEC INC R95 EV SDEV  
 TWA 1-2 MIN 351.20 1.01 2.5 4.6725E-04 4.861E-06  
 INT 260.35 40.15 1.8 7.5758E-04 6.534E-06  
 MAX 82.39 49.83 1.8 1.0776E-03 1.314E-05

TWA SITE 3 CORE 2 SPEC 1 UNITS= SI v M= 12 NR= 2  
 SUSC. DEC INC R95 EV SDEV  
 TWA 2-1 MIN 180.96 5.86 3.3 4.6792E-04 1.003E-05  
 INT 89.87 10.17 24.4 8.2053E-04 2.031E-06  
 MAX 300.29 78.16 24.6 8.4150E-04 1.056E-05

TWA SITE 4 CORE 2 SPEC 2 UNITS= SI v M= 12 NR= 2  
 SUSC. DEC INC R95 EV SDEV  
 TWA 2-2 MIN 177.81 5.53 3.6 5.0881E-04 5.972E-06  
 INT 268.62 8.43 19.5 9.5122E-04 7.523E-06  
 MAX 54.90 79.89 19.9 1.0164E-03 1.483E-05

TWA SITE 5 CORE 3 SPEC 1 UNITS= SI v M= 12 NR= 2  
 SUSC. DEC INC R95 EV SDEV  
 TWA 3-1 MIN 343.66 19.55 17.9 3.6609E-04 1.246E-05  
 INT 88.24 35.34 37.6 4.4992E-04 9.477E-07  
 MAX 230.37 48.08 33.3 4.6670E-04 4.967E-06

TWA SITE 6 CORE 4 SPEC 1 UNITS= SI v M= 12 NR= 2  
 SUSC. DEC INC R95 EV SDEV  
 TWA 4-1 MIN 154.80 10.05 35.4 2.0778E-04 4.333E-07  
 INT 61.79 16.53 35.8 2.2947E-04 6.815E-06  
 MAX 274.82 70.50 16.6 2.4861E-04 1.720E-06

TWA SITE 7 CORE 4 SPEC 2 UNITS= SI v M= 12 NR= 2  
 SUSC. DEC INC R95 EV SDEV  
 TWA 4-2 MIN 152.27 0.37 59.8 2.0456E-04 5.207E-06  
 INT 243.37 71.60 79.5 2.2967E-04 7.641E-06  
 MAX 62.15 18.40 68.4 2.3950E-04 6.392E-07

TWA SITE 8 CORE 4 SPEC 3 UNITS= SI v M= 12 NR= 2  
 SUSC. DEC INC R95 EV SDEV  
 TWA 4-3 MIN 162.71 11.36 15.7 2.1239E-04 8.428E-06  
 INT 282.56 68.01 60.3 2.4382E-04 1.193E-06  
 MAX 68.84 18.57 58.7 2.5562E-04 1.636E-05

TWA SITE 9 CORE 5 SPEC 1 UNITS= SI v M= 12 NR= 2  
 SUSC. DEC INC R95 EV SDEV  
 TWA 5-1 MIN 343.10 18.63 14.1 4.3114E-04 2.724E-05  
 INT 81.92 24.45 53.4 5.3676E-04 3.466E-06  
 MAX 219.75 58.47 52.1 5.7884E-04 9.946E-06

TWA SITE 10 CORE 5 SPEC 2 UNITS= SI v M= 12 NR= 2  
 SUSC. DEC INC R95 EV SDEV  
 TWA 5-2 MIN 329.27 4.14 17.2 2.8851E-04 1.920E-05  
 INT 226.65 71.66 75.7 3.5132E-04 2.175E-06  
 MAX 60.60 17.83 74.0 3.7143E-04 2.900E-06

TWA 6-1

TWA SITE 11 CORE 6 SPEC 1 UNITS= SI v M= 12 NR= 2						
SUSC.	DEC	INC	R95	EV	SDEV	
MIN	346.36	3.09	4.6	7.9920E-04	2.166E-06	
INT	76.60	4.40	23.3	1.1802E-03	6.580E-06	
MAX	221.46	84.61	23.2	1.2473E-03	2.096E-06	

TWA 6-2

TWA SITE 12 CORE 6 SPEC 2 UNITS= SI v M= 12 NR= 2						
SUSC.	DEC	INC	R95	EV	SDEV	
MIN	350.58	3.03	2.5	7.0831E-04	2.546E-06	
INT	260.27	5.83	6.6	1.1628E-03	1.707E-05	
MAX	107.93	83.42	6.3	1.3382E-03	4.184E-06	

TWA 6.5-1

TWA SITE 13 CORE 6 SPEC 51 UNITS= SI v M= 12 NR= 2						
SUSC.	DEC	INC	R95	EV	SDEV	
MIN	223.87	31.35	9.8	2.7085E-04	7.946E-06	
INT	327.26	20.82	27.2	3.0270E-04	4.623E-06	
MAX	85.21	50.95	26.7	3.1716E-04	2.581E-06	

TWA 6.5-2

TWA SITE 14 CORE 6 SPEC 52 UNITS= SI v M= 12 NR= 2						
SUSC.	DEC	INC	R95	EV	SDEV	
MIN	306.56	44.74	78.7	2.9906E-04	1.206E-06	
INT	154.94	41.59	93.2	3.0886E-04	4.039E-06	
MAX	51.55	14.62	47.9	3.4028E-04	1.196E-06	

TWA 7-1

TWA SITE 15 CORE 7 SPEC 1 UNITS= SI v M= 12 NR= 2						
SUSC.	DEC	INC	R95	EV	SDEV	
MIN	336.40	12.84	8.9	6.4803E-04	4.952E-06	
INT	237.93	32.86	18.6	7.7883E-04	7.279E-06	
MAX	84.76	54.10	19.9	8.2969E-04	5.825E-06	

TWA 7.5-1

TWA SITE 16 CORE 7 SPEC 51 UNITS= SI v M= 12 NR= 2						
SUSC.	DEC	INC	R95	EV	SDEV	
MIN	25.13	29.39	21.2	2.4855E-04	4.488E-06	
INT	126.11	18.69	28.9	2.6321E-04	9.815E-07	
MAX	243.98	54.12	29.3	2.8858E-04	1.143E-05	

TWA 7.5-2

TWA SITE 17 CORE 7 SPEC 52 UNITS= SI v M= 12 NR= 2						
SUSC.	DEC	INC	R95	EV	SDEV	
MIN	117.94	8.01	116.3	2.6617E-04	3.391E-07	
INT	24.14	25.24	96.7	2.7075E-04	6.069E-07	
MAX	224.23	63.34	84.8	2.7237E-04	7.146E-06	

TWA 8-1

TWA SITE 18 CORE 8 SPEC 1 UNITS= SI v M= 12 NR= 2						
SUSC.	DEC	INC	R95	EV	SDEV	
MIN	172.27	16.79	6.5	9.1577E-04	4.897E-06	
INT	80.25	6.66	7.8	1.1987E-03	2.212E-06	
MAX	329.36	71.86	4.8	1.3459E-03	1.217E-05	

TWA 8-2

TWA SITE 19 CORE 8 SPEC 2 UNITS= SI v M= 12 NR= 2						
SUSC.	DEC	INC	R95	EV	SDEV	
MIN	164.71	15.83	3.4	9.6554E-04	1.126E-05	
INT	73.65	3.73	7.9	1.3241E-03	1.222E-05	
MAX	330.74	73.72	7.1	1.5444E-03	1.922E-06	

TWA 9-1

TWA SITE 20 CORE 9 SPEC 1 UNITS= SI v M= 12 NR= 2						
SUSC.	DEC	INC	R95	EV	SDEV	
MIN	187.61	12.99	12.3	7.9738E-04	9.669E-06	
INT	289.17	40.97	19.5	8.9468E-04	1.454E-05	
MAX	83.73	46.12	17.2	9.4943E-04	5.832E-06	

TWA 9-2

TWA SITE 21 CORE 9 SPEC 2 UNITS= SI v M= 12 NR= 2						
SUSC.	DEC	INC	R95	EV	SDEV	
MIN	190.70	6.50	7.0	8.3852E-04	7.671E-07	
INT	286.54	41.77	5.0	9.2448E-04	1.640E-05	
MAX	93.56	47.49	8.2	9.9718E-04	2.409E-06	

SAMPLE

TWA SITE 22 CORE 9 SPEC 51 UNITS= SI v M= 12 NR= 2  
 SUSC. DEC INC R95 EV SDEV  
 TWA 9.5-1 MIN 355.39 5.86 3.9 6.5793E-04 5.913E-06  
 INT 264.60 7.66 7.6 7.8825E-04 1.866E-07  
 MAX 122.47 80.33 6.7 8.4461E-04 5.813E-06

TWA SITE 23 CORE 9 SPEC 52 UNITS= SI v M= 12 NR= 2  
 SUSC. DEC INC R95 EV SDEV  
 TWA 9.5-2 MIN 353.12 6.52 9.4 7.0483E-04 1.848E-05  
 INT 262.46 5.80 14.2 8.4186E-04 3.252E-06  
 MAX 131.09 81.25 12.6 9.3563E-04 3.500E-06

TWA SITE 24 CORE 10 SPEC 1 UNITS= SI v M= 12 NR= 2  
 SUSC. DEC INC R95 EV SDEV  
 TWA 10-1 MIN 354.18 0.46 18.7 2.6907E-04 6.863E-06  
 INT 263.35 60.64 100.3 3.3282E-04 4.772E-06  
 MAX 84.44 29.36 101.1 3.3705E-04 1.247E-05

TWA SITE 25 CORE 10 SPEC 2 UNITS= SI v M= 12 NR= 2  
 SUSC. DEC INC R95 EV SDEV  
 TWA 10-2 MIN 339.70 2.11 18.4 2.4960E-04 4.221E-06  
 INT 71.00 31.59 21.7 2.8639E-04 1.452E-05  
 MAX 246.28 58.32 15.3 3.1309E-04 5.927E-06

TWA SITE 26 CORE 10 SPEC 51 UNITS= SI v M= 12 NR= 2  
 SUSC. DEC INC R95 EV SDEV  
 TWA 10.5-1 MIN 169.62 16.15 5.4 4.9509E-04 1.473E-06  
 INT 270.24 32.37 5.0 6.8957E-04 7.286E-06  
 MAX 57.15 52.84 6.8 7.4566E-04 2.487E-05

TWA SITE 27 CORE 10 SPEC 52 UNITS= SI v M= 12 NR= 2  
 SUSC. DEC INC R95 EV SDEV  
 TWA 10.5-2 MIN 167.94 13.44 5.5 5.0613E-04 8.257E-06  
 INT 263.87 23.39 9.2 6.9211E-04 1.651E-05  
 MAX 50.47 62.61 8.8 7.7457E-04 6.087E-06

TWA SITE 28 CORE 11 SPEC 1 UNITS= SI v M= 12 NR= 2  
 SUSC. DEC INC R95 EV SDEV  
 TWA 11-1 MIN 148.10 20.86 11.2 3.2469E-04 7.107E-06  
 INT 262.62 47.45 31.1 3.7247E-04 9.577E-06  
 MAX 42.57 35.10 33.0 3.8510E-04 2.940E-07

TWA SITE 29 CORE 11 SPEC 2 UNITS= SI v M= 12 NR= 2  
 SUSC. DEC INC R95 EV SDEV  
 TWA 11-2 MIN 159.50 19.21 26.0 2.8692E-04 1.163E-06  
 INT 254.68 14.53 49.2 3.2833E-04 3.141E-06  
 MAX 19.45 65.56 45.2 3.4139E-04 4.090E-06

TWA SITE 30 CORE 11 SPEC 51 UNITS= SI v M= 12 NR= 2  
 SUSC. DEC INC R95 EV SDEV  
 TWA 11.5-1 MIN 169.09 35.11 12.0 4.7487E-04 6.816E-06  
 INT 67.94 15.39 44.4 5.2801E-04 5.529E-06  
 MAX 318.29 50.69 42.8 5.3832E-04 2.134E-06

TWA SITE 31 CORE 11 SPEC 52 UNITS= SI v M= 12 NR= 2  
 SUSC. DEC INC R95 EV SDEV  
 TWA 11.5-2 MIN 338.76 11.05 58.0 5.0508E-04 5.929E-06  
 INT 73.10 21.18 77.9 5.2980E-04 6.350E-06  
 MAX 222.93 65.86 71.1 5.3245E-04 5.967E-07

TWA SITE 32 CORE 12 SPEC 1 UNITS= SI v M= 12 NR= 2  
 SUSC. DEC INC R95 EV SDEV  
 TWA 12-1 MIN 147.08 34.17 11.9 2.8848E-04 4.876E-06  
 INT 315.23 55.25 53.3 3.4086E-04 7.917E-07  
 MAX 53.30 5.56 52.7 3.4618E-04 2.975E-06

SAMPLE

TWA 12-2 TWA SITE 33 CORE 12 SPEC 2 UNITS= SI v M= 12 NR= 2  
 SUSC. DEC INC R95 EV SDEV  
 MIN 147.81 24.21 24.2 2.7718E-04 1.737E-05  
 INT 306.21 64.19 67.9 3.2584E-04 7.742E-08  
 MAX 54.00 8.41 62.9 3.4098E-04 4.098E-06

TWA 13-1 TWA SITE 34 CORE 13 SPEC 1 UNITS= SI v M= 12 NR= 2  
 SUSC. DEC INC R95 EV SDEV  
 MIN 157.41 26.54 13.9 2.4865E-04 7.496E-06  
 INT 294.00 55.50 50.9 2.9832E-04 5.457E-06  
 MAX 56.72 20.38 51.9 3.1269E-04 1.317E-06

TWA 13-2 TWA SITE 34 CORE 13 SPEC 2 UNITS= SI v M= 12 NR= 2  
 SUSC. DEC INC R95 EV SDEV  
 MIN 172.47 30.18 6.5 2.1541E-04 1.240E-07  
 INT 288.15 36.69 9.5 2.6408E-04 1.121E-05  
 MAX 54.74 38.66 7.1 3.0278E-04 6.620E-06

TWA 14-1 TWA SITE 36 CORE 14 SPEC 1 UNITS= SI v M= 12 NR= 2  
 SUSC. DEC INC R95 EV SDEV  
 MIN 64.47 38.52 3.9 4.0335E-04 2.696E-06  
 INT 205.73 44.41 14.2 4.7300E-04 2.629E-06  
 MAX 317.18 20.47 14.1 4.9598E-04 1.255E-05

TWA 14-2 TWA SITE 37 CORE 14 SPEC 2 UNITS= SI v M= 12 NR= 2  
 SUSC. DEC INC R95 EV SDEV  
 MIN 51.75 23.55 57.4 3.6103E-04 7.055E-06  
 INT 157.46 31.84 82.6 4.0023E-04 1.362E-05  
 MAX 292.17 48.56 59.9 4.1348E-04 2.248E-06

TWA 15-1 TWA SITE 38 CORE 15 SPEC 1 UNITS= SI v M= 12 NR= 2  
 SUSC. DEC INC R95 EV SDEV  
 MIN 197.49 53.44 0.6 4.2000E-03 2.072E-05  
 INT 333.98 28.27 0.7 4.9247E-03 6.975E-07  
 MAX 76.01 21.17 0.8 6.4766E-03 5.710E-06

TWA 15-2 TWA SITE 39 CORE 15 SPEC 2 UNITS= SI v M= 12 NR= 2  
 SUSC. DEC INC R95 EV SDEV  
 MIN 196.27 47.56 3.5 2.8013E-03 8.099E-05  
 INT 337.63 35.53 3.9 3.0068E-03 5.776E-05  
 MAX 82.74 20.06 2.0 4.0435E-03 2.931E-05

TWA 15.5-1 TWA SITE 40 CORE 15 SPEC 51 UNITS= SI v M= 12 NR= 2  
 SUSC. DEC INC R95 EV SDEV  
 MIN 167.52 33.30 3.6 6.3388E-04 1.228E-05  
 INT 291.55 40.44 4.1 8.0454E-04 5.509E-06  
 MAX 53.47 31.82 2.4 1.1241E-03 4.633E-06

TWA 15.5-2 TWA SITE 41 CORE 15 SPEC 52 UNITS= SI v M= 12 NR= 2  
 SUSC. DEC INC R95 EV SDEV  
 MIN 155.60 31.43 3.4 4.0312E-04 3.537E-06  
 INT 289.49 48.61 3.3 4.9119E-04 1.210E-05  
 MAX 49.82 23.99 3.4 5.7022E-04 7.197E-07

TWA 15.9-1 TWA SITE 42 CORE 15 SPEC 91 UNITS= SI v M= 12 NR= 2  
 SUSC. DEC INC R95 EV SDEV  
 MIN 175.76 28.73 14.2 3.4305E-04 3.604E-06  
 INT 351.98 61.22 19.8 4.1584E-04 1.094E-05  
 MAX 84.88 1.60 19.0 4.4904E-04 9.989E-06

TWA 15.9-2 TWA SITE 43 CORE 15 SPEC 92 UNITS= SI v M= 12 NR= 2  
 SUSC. DEC INC R95 EV SDEV  
 MIN 189.13 31.36 14.3 3.8476E-04 9.852E-06  
 INT 332.49 52.78 37.4 4.5149E-04 8.495E-06  
 MAX 87.74 17.95 35.0 4.8548E-04 8.232E-06

TWA 16-1

SUSC.	DEC	INC	R95	EV	SDEV
MIN	175.40	32.33	3.6	2.8731E-04	3.422E-06
INT	269.94	7.13	80.4	3.7109E-04	1.424E-06
MAX	11.01	56.69	80.3	3.7302E-04	1.138E-06

TWA 16-2

SUSC.	DEC	INC	R95	EV	SDEV
MIN	175.94	39.28	8.0	3.0091E-04	1.710E-07
INT	44.95	38.73	51.8	3.8382E-04	1.144E-05
MAX	290.70	27.12	51.2	4.0688E-04	1.279E-05

TWA 16.5-1

SUSC.	DEC	INC	R95	EV	SDEV
MIN	150.75	47.48	5.0	4.0454E-04	7.237E-06
INT	298.33	37.74	16.4	5.2969E-04	7.665E-06
MAX	41.72	16.65	15.7	5.6536E-04	2.114E-05

TWA 16.5-2

SUSC.	DEC	INC	R95	EV	SDEV
MIN	164.51	44.63	4.4	3.9358E-04	1.947E-06
INT	286.64	28.32	7.1	5.1998E-04	3.560E-06
MAX	36.35	32.04	7.3	5.5990E-04	5.539E-07

TWA 17-1

SUSC.	DEC	INC	R95	EV	SDEV
MIN	182.73	8.56	19.3	2.5420E-04	1.147E-05
INT	290.73	64.03	61.5	3.2457E-04	6.878E-06
MAX	88.83	24.32	59.4	3.3852E-04	2.944E-07

TWA 17-2

SUSC.	DEC	INC	R95	EV	SDEV
MIN	8.77	0.39	7.6	2.5027E-04	5.963E-06
INT	99.08	38.76	14.4	3.3438E-04	3.747E-06
MAX	278.28	51.24	12.6	3.5200E-04	6.066E-07

TWA 18A-1

SUSC.	DEC	INC	R95	EV	SDEV
MIN	7.47	16.18	30.8	4.7793E-04	9.555E-06
INT	221.56	70.70	60.1	5.2389E-04	5.034E-07
MAX	100.48	10.25	57.2	5.3807E-04	2.969E-06

TWA 18A-2

SUSC.	DEC	INC	R95	EV	SDEV
MIN	12.24	6.68	46.5	4.9227E-04	2.877E-07
INT	276.82	38.94	95.7	5.0926E-04	1.546E-06
MAX	110.34	50.27	87.7	5.2370E-04	2.062E-06

TWA 18B-1

SUSC.	DEC	INC	R95	EV	SDEV
MIN	357.45	11.09	7.7	3.9895E-04	3.328E-06
INT	253.00	51.86	42.8	4.6271E-04	9.083E-06
MAX	95.62	35.94	43.4	4.8689E-04	1.964E-07

TWA 18B-2

SUSC.	DEC	INC	R95	EV	SDEV
MIN	345.27	9.60	13.6	4.1637E-04	4.115E-06
INT	232.75	66.18	12.4	4.7697E-04	6.075E-07
MAX	79.11	21.59	12.8	5.1911E-04	3.150E-07

SAMPLE

TWA 18.5-1 TWA SITE 54 CORE 18 SPEC 51 UNITS= SI v M= 12 NR= 2  
 SUSC. DEC INC R95 EV SDEV  
 MIN 173.81 64.88 3.0 6.5680E-04 2.218E-07  
 INT 356.49 25.10 22.5 7.6068E-04 7.518E-06  
 MAX 266.00 1.03 22.3 8.2157E-04 6.477E-06

TWA 18.5-2 TWA SITE 55 CORE 18 SPEC 52 UNITS= SI v M= 12 NR= 2  
 SUSC. DEC INC R95 EV SDEV  
 MIN 178.26 57.73 2.0 6.7950E-04 2.631E-06  
 INT 351.52 32.09 4.4 7.5799E-04 4.663E-07  
 MAX 83.43 3.04 4.4 8.6799E-04 3.318E-06

TWA 18.5A-1 TWA SITE 56 CORE 18 SPEC 511 UNITS= SI v M= 12 NR= 2  
 SUSC. DEC INC R95 EV SDEV  
 MIN 171.22 18.81 10.6 3.3829E-04 1.083E-05  
 INT 291.93 56.30 87.3 3.9312E-04 1.195E-05  
 MAX 71.30 26.85 88.0 4.1129E-04 7.185E-06

TWA 18.5A-2 TWA SITE 57 CORE 18 SPEC 512 UNITS= SI v M= 12 NR= 2  
 SUSC. DEC INC R95 EV SDEV  
 MIN 145.47 23.89 7.6 3.5138E-04 3.040E-06  
 INT 307.39 65.02 8.9 4.2069E-04 6.298E-06  
 MAX 52.40 6.88 10.5 4.5696E-04 1.241E-06

TWA 19-1 TWA SITE 58 CORE 19 SPEC 1 UNITS= SI v M= 12 NR= 2  
 SUSC. DEC INC R95 EV SDEV  
 MIN 22.82 57.11 67.8 3.8755E-04 3.030E-05  
 INT 115.89 1.99 59.6 4.1912E-04 1.362E-05  
 MAX 207.18 32.81 61.6 5.0413E-04 1.543E-05

TWA 19-2 TWA SITE 59 CORE 19 SPEC 2 UNITS= SI v M= 12 NR= 2  
 SUSC. DEC INC R95 EV SDEV  
 MIN 110.40 41.35 10.4 4.0483E-04 3.603E-06  
 INT 316.11 45.67 30.0 4.3938E-04 4.029E-06  
 MAX 212.27 13.15 30.0 4.5327E-04 2.785E-06

TWA 19.5-1 TWA SITE 60 CORE 19 SPEC 51 UNITS= SI v M= 12 NR= 2  
 SUSC. DEC INC R95 EV SDEV  
 MIN 340.58 29.98 1.8 1.5428E-03 7.892E-06  
 INT 195.83 54.77 1.9 1.7422E-03 1.712E-05  
 MAX 80.59 16.76 1.4 2.2972E-03 6.849E-06

TWA 19.5-2 TWA SITE 61 CORE 19 SPEC 52 UNITS= SI v M= 12 NR= 2  
 SUSC. DEC INC R95 EV SDEV  
 MIN 313.79 56.56 6.0 5.9519E-04 1.753E-06  
 INT 166.49 29.06 11.3 6.6342E-04 8.742E-06  
 MAX 67.88 15.08 10.1 8.0734E-04 1.104E-05

TWA 20A-1 TWA SITE 62 CORE 20 SPEC 11 UNITS= SI v M= 12 NR= 2  
 SUSC. DEC INC R95 EV SDEV  
 MIN 160.96 48.87 22.5 2.1832E-04 1.307E-05  
 INT 323.41 39.78 27.1 2.3941E-04 3.495E-06  
 MAX 60.79 8.77 20.9 2.6790E-04 2.017E-07

TWA 20A-2 TWA SITE 63 CORE 20 SPEC 12 UNITS= SI v M= 12 NR= 2  
 SUSC. DEC INC R95 EV SDEV  
 MIN 322.76 65.46 23.8 2.3884E-04 1.477E-06  
 INT 160.58 23.49 31.1 2.5794E-04 3.353E-06  
 MAX 67.66 6.69 23.4 2.9274E-04 3.687E-06

SAMPLE

TWA 20B-1  
 TWA SITE 64 CORE 20 SPEC 21 UNITS= SI v M= 12 NR= 2  
 SUSC. DEC INC R95 EV SDEV  
 MIN 171.19 74.03 18.8 2.6774E-04 3.946E-06  
 INT 356.07 15.92 23.0 3.0735E-04 4.772E-06  
 MAX 265.70 1.29 14.7 3.4864E-04 2.043E-06

TWA 20B-2  
 TWA SITE 65 CORE 20 SPEC 22 UNITS= SI v M= 12 NR= 2  
 SUSC. DEC INC R95 EV SDEV  
 MIN 149.81 75.21 19.5 2.9624E-04 1.162E-05  
 INT 343.83 14.37 20.2 3.4536E-04 1.827E-06  
 MAX 252.95 3.44 13.4 4.3335E-04 8.054E-06

TWA 21-1  
 TWA SITE 66 CORE 21 SPEC 1 UNITS= SI v M= 12 NR= 2  
 SUSC. DEC INC R95 EV SDEV  
 MIN 262.92 75.89 46.5 3.8419E-04 3.938E-06  
 INT 27.88 8.20 85.0 4.3533E-04 2.661E-06  
 MAX 119.54 11.41 72.8 4.4915E-04 9.468E-06

TWA 21-2  
 TWA SITE 67 CORE 21 SPEC 2 UNITS= SI v M= 12 NR= 2  
 SUSC. DEC INC R95 EV SDEV  
 MIN 74.13 68.38 12.8 3.5711E-04 7.807E-07  
 INT 240.86 21.09 25.1 4.3077E-04 3.393E-06  
 MAX 332.61 4.53 26.3 4.4505E-04 1.652E-06

TWA 22-1  
 TWA SITE 68 CORE 22 SPEC 1 UNITS= SI v M= 12 NR= 2  
 SUSC. DEC INC R95 EV SDEV  
 MIN 210.15 12.47 20.1 3.0304E-04 1.308E-05  
 INT 332.81 67.71 44.1 3.6913E-04 9.810E-06  
 MAX 115.99 18.17 40.0 3.8273E-04 7.146E-06

TWA 22-2  
 TWA SITE 69 CORE 22 SPEC 2 UNITS= SI v M= 12 NR= 2  
 SUSC. DEC INC R95 EV SDEV  
 MIN 224.23 18.46 10.6 3.0513E-04 4.051E-06  
 INT 83.12 66.78 66.9 3.5603E-04 4.999E-06  
 MAX 318.85 13.57 66.4 3.6979E-04 3.817E-06

TWA 22A-1  
 TWA SITE 70 CORE 22 SPEC 11 UNITS= SI v M= 12 NR= 2  
 SUSC. DEC INC R95 EV SDEV  
 MIN 208.02 25.11 5.6 2.9630E-04 3.982E-06  
 INT 101.66 31.01 48.9 3.4901E-04 9.910E-07  
 MAX 329.55 48.13 49.0 3.6001E-04 1.362E-05

TWA 22A-2  
 TWA SITE 71 CORE 22 SPEC 12 UNITS= SI v M= 12 NR= 2  
 SUSC. DEC INC R95 EV SDEV  
 MIN 228.97 29.15 22.4 3.0655E-04 3.099E-07  
 INT 352.58 44.79 30.1 3.5448E-04 5.175E-06  
 MAX 119.32 31.09 20.1 3.8980E-04 5.306E-06

TWA 22.5-1  
 TWA SITE 72 CORE 22 SPEC 51 UNITS= SI v M= 12 NR= 2  
 SUSC. DEC INC R95 EV SDEV  
 MIN 7.00 63.95 8.5 3.5528E-04 6.225E-06  
 INT 214.84 23.37 15.5 4.0011E-04 9.785E-06  
 MAX 120.09 10.85 17.0 4.3992E-04 4.193E-06

TWA 22.5-2  
 TWA SITE 73 CORE 22 SPEC 52 UNITS= SI v M= 12 NR= 2  
 SUSC. DEC INC R95 EV SDEV  
 MIN 245.42 76.77 16.0 3.5890E-04 1.011E-05  
 INT 353.79 4.24 41.2 4.1350E-04 7.805E-06  
 MAX 84.73 12.51 40.1 4.3943E-04 1.556E-05

SAMPLE

TW 6-1

TW SITE 12 CORE 6 SPEC 1 UNITS= SI v M= 12 NR= 2						
SUSC.	DEC	INC	R95	EV	SDEV	
MIN	270.72	7.75	18.9	2.8703E-04	3.894E-07	
INT	29.90	74.41	17.9	3.4631E-04	4.717E-06	
MAX	178.85	13.45	19.7	3.8464E-04	1.220E-05	

TW 6-2

TW SITE 13 CORE 6 SPEC 2 UNITS= SI v M= 12 NR= 2						
SUSC.	DEC	INC	R95	EV	SDEV	
MIN	276.04	28.15	12.3	2.7948E-04	1.013E-05	
INT	18.27	21.61	67.0	3.6972E-04	2.412E-05	
MAX	140.31	53.24	67.1	3.7501E-04	5.417E-06	

TW 7A-1

TW SITE 14 CORE 7 SPEC 11 UNITS= SI v M= 12 NR= 2						
SUSC.	DEC	INC	R95	EV	SDEV	
MIN	330.95	13.58	15.6	3.0238E-04	3.319E-06	
INT	213.91	62.02	23.3	3.5547E-04	2.162E-05	
MAX	67.12	23.97	22.2	3.7277E-04	2.772E-06	

TW 7A-2

TW SITE 15 CORE 7 SPEC 12 UNITS= SI v M= 12 NR= 2						
SUSC.	DEC	INC	R95	EV	SDEV	
MIN	326.94	2.96	5.1	2.5544E-04	1.224E-05	
INT	230.01	66.77	19.6	3.4090E-04	6.308E-06	
MAX	58.20	23.02	18.9	3.7106E-04	1.605E-05	

TW 7B-1

TW SITE 16 CORE 7 SPEC 21 UNITS= SI v M= 12 NR= 2						
SUSC.	DEC	INC	R95	EV	SDEV	
MIN	154.58	20.04	6.3	3.3464E-04	1.810E-05	
INT	255.69	27.86	16.9	3.9306E-04	1.047E-06	
MAX	33.72	54.59	16.5	4.1420E-04	2.964E-05	

TW 7B-2

TW SITE 17 CORE 7 SPEC 22 UNITS= SI v M= 12 NR= 2						
SUSC.	DEC	INC	R95	EV	SDEV	
MIN	147.70	18.68	61.7	2.8445E-04	4.980E-08	
INT	270.11	57.71	66.7	3.0687E-04	2.425E-05	
MAX	48.51	25.29	25.7	3.8587E-04	1.172E-05	

TW 8-1

TW SITE 18 CORE 8 SPEC 1 UNITS= SI v M= 12 NR= 2						
SUSC.	DEC	INC	R95	EV	SDEV	
MIN	349.51	0.41	6.2	6.9304E-04	1.169E-05	
INT	257.70	77.21	15.5	9.8035E-04	1.356E-05	
MAX	79.60	12.78	15.3	1.0882E-03	2.275E-05	

TW 8-2

TW SITE 19 CORE 8 SPEC 2 UNITS= SI v M= 12 NR= 2						
SUSC.	DEC	INC	R95	EV	SDEV	
MIN	346.68	4.36	1.8	7.8623E-04	9.176E-06	
INT	228.75	80.76	2.0	1.1253E-03	8.255E-06	
MAX	77.31	8.14	2.2	1.3459E-03	3.757E-06	

TW 9-1

TW SITE 20 CORE 9 SPEC 1 UNITS= SI v M= 12 NR= 2						
SUSC.	DEC	INC	R95	EV	SDEV	
MIN	193.40	38.62	16.1	2.8186E-04	8.418E-06	
INT	304.95	24.69	29.5	3.3279E-04	5.892E-06	
MAX	58.80	41.32	30.7	3.6016E-04	4.926E-07	

TW 9-2

TW SITE 21 CORE 9 SPEC 2 UNITS= SI v M= 12 NR= 2						
SUSC.	DEC	INC	R95	EV	SDEV	
MIN	142.31	34.73	30.2	2.2727E-04	3.048E-06	
INT	344.83	53.12	58.5	2.7284E-04	9.922E-06	
MAX	239.98	10.89	57.7	2.8401E-04	1.674E-06	



SAMPLE

TW10-1

SUSC.	DEC	INC	R95	EV	SDEV
MIN	150.78	8.57	40.8	2.8298E-04	2.027E-05
INT	329.20	81.42	46.3	3.2031E-04	1.669E-05
MAX	60.74	0.23	27.4	3.6410E-04	3.583E-06

TW10-2

SUSC.	DEC	INC	R95	EV	SDEV
MIN	152.50	21.94	5.5	2.9932E-04	3.345E-06
INT	51.12	26.10	18.6	3.4899E-04	1.787E-06
MAX	277.24	54.75	18.5	3.6444E-04	5.693E-06

TW11-1

SUSC.	DEC	INC	R95	EV	SDEV
MIN	160.31	21.10	13.8	2.1068E-04	6.750E-06
INT	53.48	36.87	45.2	2.5135E-04	9.537E-06
MAX	273.51	45.59	45.5	2.7726E-04	3.293E-06

TW11-2

SUSC.	DEC	INC	R95	EV	SDEV
MIN	137.41	33.15	11.0	2.6529E-04	5.866E-06
INT	356.72	49.83	72.2	3.1383E-04	7.562E-06
MAX	241.17	20.00	73.2	3.3347E-04	1.731E-05

TW12A-1

SUSC.	DEC	INC	R95	EV	SDEV
MIN	317.20	20.97	18.5	2.4005E-04	3.165E-05
INT	63.62	36.42	76.8	2.7295E-04	5.019E-06
MAX	203.72	46.12	75.3	2.8075E-04	1.105E-05

TW12A-2

SUSC.	DEC	INC	R95	EV	SDEV
MIN	324.44	6.58	23.5	2.3422E-04	9.558E-06
INT	217.03	68.94	66.4	2.8826E-04	6.898E-06
MAX	56.84	19.92	65.6	2.9757E-04	1.080E-06

TW12B-1

SUSC.	DEC	INC	R95	EV	SDEV
MIN	287.41	74.27	19.5	2.1221E-04	1.027E-05
INT	144.87	12.60	18.6	2.5071E-04	2.275E-06
MAX	52.78	9.26	10.4	2.8025E-04	2.818E-07

TW12B-2

SUSC.	DEC	INC	R95	EV	SDEV
MIN	179.07	65.60	51.1	2.0571E-04	7.127E-06
INT	41.31	18.57	56.9	2.5208E-04	3.191E-06
MAX	306.05	15.26	31.8	2.7864E-04	2.472E-05

SAMPLE:

TW12C-1

TW SITE 30 CORE 12 SPEC 31 UNITS= SI v M= 12 NR= 2  
SUSC. DEC INC R95 EV SDEV  
MIN 171.22 43.77 17.8 3.2578E-04 9.424E-06  
INT 320.86 42.01 67.8 3.7672E-04 6.222E-06  
MAX 65.56 15.73 67.7 3.9519E-04 9.105E-06

TW12C-2

TW SITE 31 CORE 12 SPEC 32 UNITS= SI v M= 12 NR= 2  
SUSC. DEC INC R95 EV SDEV  
MIN 178.46 29.11 76.8 3.5095E-04 1.207E-05  
INT 322.65 55.53 79.2 3.7985E-04 5.566E-06  
MAX 78.77 16.82 40.8 3.9285E-04 1.982E-05

TW13-1

TW SITE 32 CORE 13 SPEC 1 UNITS= SI v M= 12 NR= 2  
SUSC. DEC INC R95 EV SDEV  
MIN 148.62 50.85 43.7 2.3831E-04 6.038E-07  
INT 337.31 38.83 54.5 2.7074E-04 6.309E-06  
MAX 243.87 4.26 36.9 2.9343E-04 1.014E-05

TW13-2

TW SITE 33 CORE 13 SPEC 2 UNITS= SI v M= 12 NR= 2  
SUSC. DEC INC R95 EV SDEV  
MIN 142.22 37.72 35.6 1.8761E-04 1.501E-05  
INT 31.75 24.32 83.9 2.3540E-04 9.948E-06  
MAX 277.30 42.48 86.0 2.4494E-04 1.180E-05

TW14-1

TW SITE 34 CORE 14 SPEC 1 UNITS= SI v M= 12 NR= 2  
SUSC. DEC INC R95 EV SDEV  
MIN 188.07 1.93 10.7 3.4557E-04 4.542E-06  
INT 87.97 78.96 10.6 4.0093E-04 3.903E-06  
MAX 278.44 10.85 6.3 4.4475E-04 1.328E-06

TW14-2

TW SITE 35 CORE 14 SPEC 2 UNITS= SI v M= 12 NR= 2  
SUSC. DEC INC R95 EV SDEV  
MIN 197.14 4.64 12.8 3.9179E-04 1.057E-05  
INT 81.67 79.30 25.3 4.5884E-04 1.686E-06  
MAX 287.92 9.61 23.4 5.0666E-04 1.017E-05

TW15-1

TW SITE 36 CORE 15 SPEC 1 UNITS= SI v M= 12 NR= 2  
SUSC. DEC INC R95 EV SDEV  
MIN 155.07 14.66 21.2 3.1655E-04 7.480E-06  
INT 38.21 59.92 25.1 3.6374E-04 3.116E-06  
MAX 252.28 25.63 13.5 4.0372E-04 2.194E-05

TW16-1

TW SITE 37 CORE 16 SPEC 1 UNITS= SI v M= 12 NR= 2  
SUSC. DEC INC R95 EV SDEV  
MIN 177.43 39.04 20.2 3.1417E-04 2.075E-05  
INT 289.77 25.11 21.0 3.6235E-04 3.504E-06  
MAX 43.43 40.58 10.4 3.9822E-04 1.471E-05

TW16-2

TW SITE 38 CORE 16 SPEC 2 UNITS= SI v M= 12 NR= 2  
SUSC. DEC INC R95 EV SDEV  
MIN 184.29 24.19 11.7 2.7746E-04 1.009E-05  
INT 91.89 5.33 34.9 3.4450E-04 5.976E-07  
MAX 350.27 65.16 33.1 3.5786E-04 9.840E-06

TW17-1

TW SITE 39 CORE 17 SPEC 1 UNITS= SI v M= 12 NR= 2  
SUSC. DEC INC R95 EV SDEV  
MIN 328.66 50.28 10.5 4.5647E-04 8.808E-06  
INT 151.17 39.69 14.2 5.3503E-04 9.587E-06  
MAX 60.14 1.23 12.2 5.6100E-04 8.495E-06

SAMPLE:

TW 17-2

TW SITE 40 CORE 17 SPEC 2 UNITS= SI v M= 12 NR= 2  
SUSC. DEC INC R95 EV SDEV  
MIN 325.80 46.73 13.2 5.3725E-04 7.714E-06  
INT 160.73 42.29 28.7 5.8206E-04 2.080E-06  
MAX 63.85 7.50 26.1 6.6397E-04 1.777E-05

TW 18-1

TW SITE 41 CORE 18 SPEC 1 UNITS= SI v M= 12 NR= 2  
SUSC. DEC INC R95 EV SDEV  
MIN 351.15 2.47 28.1 2.7984E-04 8.400E-06  
INT 81.85 15.89 30.2 3.2825E-04 2.384E-06  
MAX 252.54 73.91 36.7 3.4677E-04 9.158E-06

TW 18-2

TW SITE 42 CORE 18 SPEC 2 UNITS= SI v M= 12 NR= 2  
SUSC. DEC INC R95 EV SDEV  
MIN 158.74 0.21 15.1 2.4178E-04 2.023E-06  
INT 248.76 5.89 53.4 3.3253E-04 5.953E-06  
MAX 66.72 84.09 55.0 3.3739E-04 2.035E-05

TW 19-1

TW SITE 43 CORE 19 SPEC 1 UNITS= SI v M= 12 NR= 2  
SUSC. DEC INC R95 EV SDEV  
MIN 200.67 64.49 14.5 5.3086E-04 8.886E-06  
INT 328.22 16.21 13.9 5.8012E-04 8.402E-06  
MAX 64.01 19.14 4.9 6.6302E-04 8.116E-06

TW 19-2

TW SITE 44 CORE 19 SPEC 2 UNITS= SI v M= 12 NR= 2  
SUSC. DEC INC R95 EV SDEV  
MIN 254.14 66.59 30.1 6.3077E-04 4.854E-06  
INT 163.60 0.44 30.0 6.4733E-04 1.787E-06  
MAX 73.40 23.41 8.0 7.6581E-04 8.659E-06

TW 20-1

TW SITE 45 CORE 20 SPEC 1 UNITS= SI v M= 12 NR= 2  
SUSC. DEC INC R95 EV SDEV  
MIN 215.76 66.07 7.0 2.9756E-04 1.159E-05  
INT 3.85 20.64 75.5 3.6108E-04 3.678E-06  
MAX 98.29 11.57 75.8 3.6921E-04 1.181E-05

TW 20-2

TW SITE 46 CORE 20 SPEC 2 UNITS= SI v M= 12 NR= 2  
SUSC. DEC INC R95 EV SDEV  
MIN 232.41 56.43 5.9 3.0312E-04 3.815E-06  
INT 329.28 4.54 56.1 3.6411E-04 2.518E-06  
MAX 62.26 33.18 56.0 3.7781E-04 2.582E-06

TW 21-1

TW SITE 47 CORE 21 SPEC 1 UNITS= SI v M= 12 NR= 2  
SUSC. DEC INC R95 EV SDEV  
MIN 172.60 52.24 22.2 2.5617E-04 8.603E-06  
INT 278.80 12.20 30.2 2.8213E-04 6.314E-06  
MAX 17.53 35.08 26.3 3.0546E-04 1.561E-05

TW 21-2

TW SITE 48 CORE 21 SPEC 2 UNITS= SI v M= 12 NR= 2  
SUSC. DEC INC R95 EV SDEV  
MIN 233.76 72.23 77.5 2.7100E-04 1.287E-05  
INT 329.77 1.94 72.4 2.8144E-04 7.952E-06  
MAX 60.39 17.66 28.0 3.2671E-04 1.597E-06

TW 21A-1

TW SITE 49 CORE 21 SPEC 11 UNITS= SI v M= 12 NR= 2  
SUSC. DEC INC R95 EV SDEV  
MIN 155.54 55.61 7.4 2.6714E-04 8.521E-07  
INT 330.84 34.30 49.6 3.1908E-04 2.925E-06  
MAX 62.33 2.19 49.1 3.3138E-04 5.277E-06

SAMPLE

TW 21A-2

TW SITE 50 CORE 21 SPEC 12 UNITS= SI v M= 12 NR= 2  
SUSC. DEC INC R95 EV SDEV  
MIN 172.04 68.97 7.1 2.6167E-04 8.586E-07  
INT 292.83 11.13 32.7 3.1717E-04 6.246E-06  
MAX 26.41 17.60 32.5 3.4381E-04 1.150E-06

TW 22-1

TW SITE 51 CORE 22 SPEC 1 UNITS= SI v M= 12 NR= 2  
SUSC. DEC INC R95 EV SDEV  
MIN 315.35 11.34 6.3 2.9613E-04 1.459E-06  
INT 138.92 78.63 26.1 3.8266E-04 1.104E-05  
MAX 45.49 0.69 26.1 4.1110E-04 8.401E-06

TW 22-2

TW SITE 52 CORE 22 SPEC 2 UNITS= SI v M= 12 NR= 2  
SUSC. DEC INC R95 EV SDEV  
MIN 149.36 2.07 21.6 3.6782E-04 1.014E-06  
INT 254.91 82.35 59.9 4.4257E-04 1.381E-05  
MAX 59.10 7.38 59.6 4.7674E-04 1.567E-05

TW 23-1

TW SITE 53 CORE 23 SPEC 1 UNITS= SI v M= 12 NR= 2  
SUSC. DEC INC R95 EV SDEV  
MIN 325.79 14.26 5.3 5.9416E-04 9.849E-06  
INT 69.02 41.98 75.7 7.4696E-04 1.207E-05  
MAX 221.31 44.54 75.7 7.6313E-04 8.243E-06

TW 23-2

TW SITE 54 CORE 23 SPEC 2 UNITS= SI v M= 12 NR= 2  
SUSC. DEC INC R95 EV SDEV  
MIN 319.29 10.29 3.3 7.6429E-04 4.526E-06  
INT 58.80 42.31 8.7 1.0129E-03 1.718E-06  
MAX 218.50 45.86 8.1 1.0623E-03 3.415E-06

SAMPLE

TWC 1-1

TWC SITE 1 CORE 1 SPEC 1 UNITS= SI v M= 12 NR= 2  
 SUSC. DEC INC R95 EV SDEV  
 MIN 175.39 14.48 5.1 3.1802E-04 2.460E-06  
 INT 277.25 38.53 6.5 4.9685E-04 1.018E-06  
 MAX 68.82 47.84 4.6 5.1380E-04 5.783E-06

TWC 1-2

TWC SITE 2 CORE 1 SPEC 2 UNITS= SI v M= 12 NR= 2  
 SUSC. DEC INC R95 EV SDEV  
 MIN 167.55 12.83 5.3 3.4551E-04 1.997E-06  
 INT 326.25 76.26 36.9 5.1539E-04 1.078E-05  
 MAX 76.44 4.83 37.2 5.3201E-04 5.042E-06

TWC 1.5A-1

TWC SITE 3 CORE 1 SPEC 511 UNITS= SI v M= 12 NR= 2  
 SUSC. DEC INC R95 EV SDEV  
 MIN 159.90 6.77 23.2 2.8898E-04 6.386E-07  
 INT 65.08 35.29 86.7 3.5306E-04 6.105E-06  
 MAX 259.26 53.87 84.5 3.7169E-04 7.582E-06

TWC 1.5B-1

TWC SITE 4 CORE 1 SPEC 521 UNITS= SI v M= 12 NR= 2  
 SUSC. DEC INC R95 EV SDEV  
 MIN 160.96 22.14 4.0 3.2793E-04 2.067E-06  
 INT 280.53 50.49 42.3 4.9823E-04 3.072E-06  
 MAX 56.91 30.82 42.4 5.1060E-04 7.526E-07

TWC 1.5B-2

TWC SITE 5 CORE 1 SPEC 522 UNITS= SI v M= 12 NR= 2  
 SUSC. DEC INC R95 EV SDEV  
 MIN 165.11 17.89 3.8 3.2738E-04 8.235E-07  
 INT 29.15 65.82 52.6 5.0016E-04 2.672E-06  
 MAX 260.33 15.73 52.6 5.1393E-04 1.686E-06

TWC 2-1

TWC SITE 6 CORE 2 SPEC 1 UNITS= SI v M= 12 NR= 2  
 SUSC. DEC INC R95 EV SDEV  
 MIN 223.43 26.43 53.2 4.8254E-05 9.250E-06  
 INT 3.53 57.06 69.1 6.4630E-05 2.585E-06  
 MAX 124.02 18.20 44.3 7.9982E-05 7.737E-08

TWC 3A-1

TWC SITE 7 CORE 3 SPEC 11 UNITS= SI v M= 12 NR= 2  
 SUSC. DEC INC R95 EV SDEV  
 MIN 294.52 14.66 35.2 7.8573E-05 1.283E-05  
 INT 189.12 45.43 72.9 9.6960E-05 1.425E-06  
 MAX 37.62 40.89 70.5 1.0517E-04 6.854E-06

TWC 4-1

TWC SITE 8 CORE 4 SPEC 1 UNITS= SI v M= 12 NR= 2  
 SUSC. DEC INC R95 EV SDEV  
 MIN 313.57 15.74 40.8 4.2174E-04 2.033E-06  
 INT 200.16 54.65 41.4 4.4866E-04 9.611E-06  
 MAX 53.22 30.73 11.6 4.7156E-04 1.330E-05

TWC 4-2

TWC SITE 9 CORE 4 SPEC 2 UNITS= SI v M= 12 NR= 2  
 SUSC. DEC INC R95 EV SDEV  
 MIN 157.78 13.01 8.6 4.2765E-04 4.855E-06  
 INT 268.09 56.37 68.7 4.6598E-04 8.973E-06  
 MAX 59.99 30.41 68.7 4.9133E-04 3.086E-05

TWC 5A-1

TWC SITE 10 CORE 5 SPEC 11 UNITS= SI v M= 12 NR= 2  
 SUSC. DEC INC R95 EV SDEV  
 MIN 169.82 22.31 16.6 2.9910E-04 4.830E-06  
 INT 302.94 59.02 9.7 3.5210E-04 4.369E-06  
 MAX 71.07 20.34 13.7 3.7972E-04 6.027E-06

TWC 5A-2

TWC SITE 11 CORE 5 SPEC 12 UNITS= SI v M= 12 NR= 2  
 SUSC. DEC INC R95 EV SDEV  
 MIN 145.43 18.39 20.2 3.2317E-04 8.640E-06  
 INT 256.73 47.54 35.3 3.7588E-04 1.356E-05  
 MAX 41.11 36.65 31.3 3.8986E-04 2.946E-07

SAMPLE

TWC 5B-1

TWC SITE 12 CORE 5 SPEC 21 UNITS= SI v M= 12 NR= 2						
SUSC.	DEC	INC	R95	EV	SDEV	
MIN	349.38	9.13	23.1	2.8463E-04	4.360E-06	
INT	206.26	78.64	46.3	3.4022E-04	1.254E-06	
MAX	80.46	6.71	42.3	3.5566E-04	1.023E-05	

TWC 5B-2

TWC SITE 13 CORE 5 SPEC 22 UNITS= SI v M= 12 NR= 2						
SUSC.	DEC	INC	R95	EV	SDEV	
MIN	335.13	12.86	12.9	3.8517E-04	3.928E-06	
INT	207.37	69.56	12.5	4.6249E-04	9.764E-06	
MAX	68.79	15.62	3.2	5.7978E-04	1.723E-06	

TWC 5C-1

TWC SITE 14 CORE 5 SPEC 31 UNITS= SI v M= 12 NR= 2						
SUSC.	DEC	INC	R95	EV	SDEV	
MIN	156.27	19.01	5.2	3.0156E-04	7.401E-07	
INT	264.47	42.19	53.8	3.6367E-04	1.215E-05	
MAX	48.38	41.72	52.4	3.9030E-04	1.137E-06	

TWC 6-1

TWC SITE 15 CORE 6 SPEC 1 UNITS= SI v M= 12 NR= 2						
SUSC.	DEC	INC	R95	EV	SDEV	
MIN	315.67	70.14	3.4	7.1374E-04	3.991E-06	
INT	190.78	11.68	3.7	8.5343E-04	1.268E-05	
MAX	97.41	15.84	1.9	1.2446E-03	1.567E-05	

TWC 6-2

TWC SITE 16 CORE 6 SPEC 2 UNITS= SI v M= 12 NR= 2						
SUSC.	DEC	INC	R95	EV	SDEV	
MIN	312.88	70.69	5.7	4.8139E-04	5.778E-06	
INT	189.57	10.90	4.2	5.5723E-04	5.536E-06	
MAX	96.46	15.75	5.1	7.6647E-04	1.491E-05	

TWC 6A-1

TWC SITE 17 CORE 6 SPEC 11 UNITS= SI v M= 12 NR= 2						
SUSC.	DEC	INC	R95	EV	SDEV	
MIN	336.62	30.82	63.1	1.8400E-04	8.884E-06	
INT	173.74	58.02	73.1	2.0469E-04	9.136E-06	
MAX	71.24	7.69	48.8	2.1486E-04	2.547E-06	

TWC 6A-2

TWC SITE 18 CORE 6 SPEC 12 UNITS= SI v M= 12 NR= 2						
SUSC.	DEC	INC	R95	EV	SDEV	
MIN	328.43	38.66	15.0	1.9414E-04	1.374E-05	
INT	226.77	14.18	53.9	2.2996E-04	3.657E-07	
MAX	120.55	47.85	55.0	2.3576E-04	7.852E-07	

TWC 7-1

TWC SITE 19 CORE 7 SPEC 1 UNITS= SI v M= 12 NR= 2						
SUSC.	DEC	INC	R95	EV	SDEV	
MIN	161.83	4.10	24.5	2.6846E-04	3.967E-06	
INT	64.88	59.36	19.6	3.2245E-04	3.792E-06	
MAX	254.23	30.31	22.8	3.3768E-04	1.416E-05	

TWC 7-2

TWC SITE 20 CORE 7 SPEC 2 UNITS= SI v M= 12 NR= 2						
SUSC.	DEC	INC	R95	EV	SDEV	
MIN	180.31	2.83	24.7	2.8367E-04	4.259E-08	
INT	298.79	84.07	30.0	3.1104E-04	3.171E-07	
MAX	90.03	5.21	22.3	3.4080E-04	1.874E-07	

SAMPLE:

TWE 1-1 TWE SITE 1 CORE 1 SPEC 1 UNITS= SI v M= 12 NR= 2 1  
 SUSC. DEC INC R95 EV SDEV  
 MIN 311.57 41.40 13.0 3.3338E-04 5.152E-06  
 INT 179.67 37.13 31.1 4.1283E-04 3.564E-06  
 MAX 67.48 26.36 30.1 4.2848E-04 6.308E-06

TWE 1-2 TWE SITE 2 CORE 1 SPEC 2 UNITS= SI v M= 12 NR= 2 1  
 SUSC. DEC INC R95 EV SDEV  
 MIN 299.64 48.92 5.7 3.6106E-04 2.869E-05  
 INT 184.85 20.08 19.7 4.2919E-04 4.648E-06  
 MAX 80.54 34.08 20.1 4.8222E-04 3.180E-05

TWE 2-1 TWE SITE 3 CORE 2 SPEC 1 UNITS= SI v M= 12 NR= 2 1  
 SUSC. DEC INC R95 EV SDEV  
 MIN 221.81 38.49 18.0 2.3482E-05 2.594E-06  
 INT 130.75 1.34 38.9 4.1558E-05 1.312E-05  
 MAX 39.06 51.48 41.1 6.9657E-05 6.029E-06

TWE 2-2 TWE SITE 4 CORE 2 SPEC 2 UNITS= SI v M= 12 NR= 2 1  
 SUSC. DEC INC R95 EV SDEV  
 MIN 292.80 22.54 29.5 1.9221E-05 7.825E-06  
 INT 197.78 11.92 68.5 5.3789E-05 6.141E-06  
 MAX 81.90 64.18 65.3 6.3374E-05 6.043E-06

TWE 3A-1 TWE SITE 5 CORE 31 SPEC 1 UNITS= SI v M= 12 NR= 2  
 SUSC. DEC INC R95 EV SDEV  
 MIN 179.50 66.99 20.2 2.8183E-04 1.359E-05  
 INT 341.31 21.96 52.0 3.1602E-04 5.103E-06  
 MAX 73.94 6.50 51.8 3.3256E-04 1.703E-06

TWE 3A-2 TWE SITE 6 CORE 31 SPEC 2 UNITS= SI v M= 12 NR= 2  
 SUSC. DEC INC R95 EV SDEV  
 MIN 179.43 65.79 9.6 2.7277E-04 1.356E-06  
 INT 273.19 1.69 34.5 3.2365E-04 7.468E-06  
 MAX 3.97 24.14 34.5 3.3095E-04 3.831E-06

TWE 3B-1 TWE SITE 7 CORE 32 SPEC 1 UNITS= SI v M= 12 NR= 2  
 SUSC. DEC INC R95 EV SDEV  
 MIN 58.24 70.02 7.5 3.3156E-04 2.528E-06  
 INT 238.35 19.98 38.9 4.2728E-04 6.980E-06  
 MAX 328.28 0.00 38.5 4.3608E-04 1.620E-06

TWE 3B-2 TWE SITE 8 CORE 32 SPEC 2 UNITS= SI v M= 12 NR= 2  
 SUSC. DEC INC R95 EV SDEV  
 MIN 18.76 66.07 9.6 3.3223E-04 6.800E-06  
 INT 138.22 12.32 34.6 4.1838E-04 5.182E-06  
 MAX 232.83 20.19 34.3 4.4128E-04 1.019E-05

TWE 4A-1 TWE SITE 9 CORE 41 SPEC 1 UNITS= SI v M= 12 NR= 2  
 SUSC. DEC INC R95 EV SDEV  
 MIN 331.09 3.54 28.2 2.3018E-04 1.428E-05  
 INT 61.72 10.15 67.5 2.9346E-04 1.792E-05  
 MAX 222.10 79.23 61.0 3.0057E-04 4.621E-06

TWE 4B-2 TWE SITE 10 CORE 42 SPEC 1 UNITS= SI v M= 12 NR= 2  
 SUSC. DEC INC R95 EV SDEV  
 MIN 143.73 3.46 12.6 2.7641E-04 5.855E-06  
 INT 238.66 54.89 11.8 3.5648E-04 4.206E-06  
 MAX 51.32 34.89 15.3 3.7255E-04 6.688E-06

SAMPLE:

TWE 4B-2  
TWE SITE 11 CORE 42 SPEC 2 UNITS= SI v M= 12 NR= 2  
SUSC. DEC INC R95 EV SDEV  
MIN 328.90 0.71 7.1 3.0257E-04 1.291E-05  
INT 238.48 30.35 22.2 3.6915E-04 1.442E-06  
MAX 60.10 59.64 21.7 3.9255E-04 1.920E-05

TWE 5-1  
TWE SITE 12 CORE 5 SPEC 1 UNITS= SI v M= 12 NR= 2  
SUSC. DEC INC R95 EV SDEV  
MIN 316.94 13.10 9.5 3.5609E-04 1.526E-06  
INT 171.79 74.16 90.5 4.4088E-04 1.114E-05  
MAX 48.98 8.72 90.2 4.5308E-04 1.347E-05

TWE 5-2  
TWE SITE 13 CORE 5 SPEC 2 UNITS= SI v M= 12 NR= 2  
SUSC. DEC INC R95 EV SDEV  
MIN 327.74 12.23 15.0 3.0249E-04 1.659E-05  
INT 216.82 58.72 24.4 3.6895E-04 1.207E-06  
MAX 64.44 28.29 20.0 4.0361E-04 2.134E-05

TWE 6A-1  
TWE SITE 14 CORE 61 SPEC 1 UNITS= SI v M= 12 NR= 2  
SUSC. DEC INC R95 EV SDEV  
MIN 277.27 12.81 21.8 4.5780E-04 1.306E-05  
INT 164.49 59.57 20.8 5.1816E-04 6.039E-06  
MAX 13.95 27.09 8.6 6.5474E-04 7.366E-06

TWE 6A-2  
TWE SITE 15 CORE 61 SPEC 2 UNITS= SI v M= 12 NR= 2  
SUSC. DEC INC R95 EV SDEV  
MIN 290.12 2.63 3.2 9.4346E-04 1.430E-05  
INT 195.44 60.69 3.6 1.0766E-03 1.337E-05  
MAX 21.59 29.17 2.2 1.3651E-03 3.294E-06

TWE 6A-3  
TWE SITE 16 CORE 61 SPEC 3 UNITS= SI v M= 12 NR= 2  
SUSC. DEC INC R95 EV SDEV  
MIN 269.92 16.54 12.0 6.6758E-04 3.789E-06  
INT 152.57 57.17 12.1 7.4196E-04 7.023E-06  
MAX 8.82 27.49 2.3 1.0098E-03 1.689E-05

TWE 6B-1  
TWE SITE 17 CORE 62 SPEC 1 UNITS= SI v M= 12 NR= 2  
SUSC. DEC INC R95 EV SDEV  
MIN 328.50 10.21 4.3 3.3421E-04 1.254E-05  
INT 154.49 79.74 33.6 4.3420E-04 1.653E-07  
MAX 58.69 1.04 33.4 4.5550E-04 2.530E-06

TWE 6B-2  
TWE SITE 18 CORE 62 SPEC 2 UNITS= SI v M= 12 NR= 2  
SUSC. DEC INC R95 EV SDEV  
MIN 148.64 0.99 7.6 3.4135E-04 6.899E-06  
INT 256.19 86.76 14.6 4.2198E-04 4.926E-06  
MAX 58.59 3.11 14.4 4.8148E-04 1.582E-05

TWE 6B-3  
TWE SITE 19 CORE 62 SPEC 3 UNITS= SI v M= 12 NR= 2  
SUSC. DEC INC R95 EV SDEV  
MIN 321.11 10.79 3.2 4.4813E-04 2.032E-07  
INT 147.80 79.14 19.6 6.1177E-04 1.083E-05  
MAX 51.35 1.23 19.3 6.6132E-04 1.109E-06



SAMPLE:

TWL 2-1

TWL SITE 1 CORE 2 SPEC 1 UNITS= SI v M= 12 NR= 2  
SUSC. DEC INC R95 EV SDEV  
MIN 180.21 7.37 8.8 4.5163E-04 4.542E-06  
INT 289.68 68.79 10.8 5.3014E-04 3.338E-06  
MAX 87.54 19.77 13.7 5.6396E-04 1.110E-05

TWL 2-2

TWL SITE 2 CORE 2 SPEC 2 UNITS= SI v M= 12 NR= 2  
SUSC. DEC INC R95 EV SDEV  
MIN 161.46 11.78 19.3 4.1669E-04 6.263E-06  
INT 15.98 75.80 34.2 5.0855E-04 2.244E-06  
MAX 253.10 7.84 32.5 5.1815E-04 1.088E-06

TWL 3-1

TWL SITE 3 CORE 3 SPEC 1 UNITS= SI v M= 12 NR= 2  
SUSC. DEC INC R95 EV SDEV  
MIN 343.75 15.35 20.2 2.4975E-04 7.373E-06  
INT 82.35 28.57 36.9 3.0170E-04 1.203E-05  
MAX 228.88 56.86 33.8 3.1540E-04 6.811E-06

TWL 3-2

TWL SITE 4 CORE 3 SPEC 2 UNITS= SI v M= 12 NR= 2  
SUSC. DEC INC R95 EV SDEV  
MIN 170.93 1.53 21.6 2.5795E-04 3.673E-06  
INT 79.92 33.38 18.2 3.1065E-04 9.165E-08  
MAX 263.24 56.58 12.3 3.4562E-04 4.521E-06

TWL 4-1

TWL SITE 5 CORE 4 SPEC 1 UNITS= SI v M= 12 NR= 2  
SUSC. DEC INC R95 EV SDEV  
MIN 135.99 39.11 36.6 2.5339E-04 8.474E-06  
INT 257.26 32.56 91.1 2.9669E-04 1.191E-05  
MAX 12.76 33.99 87.1 3.0548E-04 1.148E-05

TWL 5-1

TWL SITE 6 CORE 5 SPEC 1 UNITS= SI v M= 12 NR= 2  
SUSC. DEC INC R95 EV SDEV  
MIN 139.06 21.64 45.2 2.8467E-04 3.329E-06  
INT 246.56 37.16 55.4 3.1458E-04 1.224E-05  
MAX 25.73 44.96 32.1 3.2845E-04 3.010E-06

TWL 5-2

TWL SITE 7 CORE 5 SPEC 2 UNITS= SI v M= 12 NR= 2  
SUSC. DEC INC R95 EV SDEV  
MIN 164.85 41.96 51.2 2.8552E-04 7.540E-06  
INT 61.00 14.91 77.7 3.0199E-04 1.148E-05  
MAX 315.98 44.24 74.2 3.2738E-04 2.334E-06

TWL 6-1

TWL SITE 8 CORE 6 SPEC 1 UNITS= SI v M= 12 NR= 2  
SUSC. DEC INC R95 EV SDEV  
MIN 165.51 52.07 18.6 2.5726E-04 3.735E-07  
INT 17.47 33.47 63.3 3.2069E-04 3.063E-06  
MAX 276.72 15.75 60.3 3.3391E-04 9.267E-06

TWL 6-2

TWL SITE 9 CORE 6 SPEC 2 UNITS= SI v M= 12 NR= 2  
SUSC. DEC INC R95 EV SDEV  
MIN 145.58 67.30 17.0 2.3835E-04 3.773E-06  
INT 258.26 9.17 44.4 3.1027E-04 3.896E-06  
MAX 351.73 20.58 41.8 3.1788E-04 1.097E-06

SAMPLE!

TWL 7-1

TWL SITE 10 CORE 7 SPEC 1 UNITS= SI v M= 12 NR= 2						
SUSC.	DEC	INC	R95	EV	SDEV	
MIN	37.23	58.11	48.4	4.3471E-04	1.680E-05	
INT	143.30	9.78	48.8	4.5567E-04	4.959E-06	
MAX	239.01	30.02	23.2	4.8711E-04	1.235E-05	

TWL 7-2

TWL SITE 11 CORE 7 SPEC 2 UNITS= SI v M= 12 NR= 2						
SUSC.	DEC	INC	R95	EV	SDEV	
MIN	342.66	25.53	35.7	4.4689E-04	1.205E-05	
INT	197.15	59.91	37.1	4.7129E-04	1.270E-05	
MAX	79.93	14.85	21.6	5.0532E-04	1.378E-06	

TWL 8-1

TWL SITE 12 CORE 8 SPEC 1 UNITS= SI v M= 12 NR= 2						
SUSC.	DEC	INC	R95	EV	SDEV	
MIN	145.87	10.69	29.6	2.7700E-04	1.285E-05	
INT	255.36	60.50	89.9	3.1835E-04	4.771E-06	
MAX	50.32	27.14	86.5	3.3135E-04	3.458E-06	

TWL 8-2

TWL SITE 13 CORE 8 SPEC 2 UNITS= SI v M= 12 NR= 2						
SUSC.	DEC	INC	R95	EV	SDEV	
MIN	141.16	13.80	86.9	2.3495E-04	1.639E-05	
INT	49.99	4.75	87.6	2.7543E-04	1.612E-06	
MAX	301.42	75.37	27.7	2.9089E-04	9.813E-06	

TWL 9-1

TWL SITE 14 CORE 9 SPEC 1 UNITS= SI v M= 12 NR= 2						
SUSC.	DEC	INC	R95	EV	SDEV	
MIN	268.26	45.48	85.9	5.0360E-05	2.430E-04	
INT	175.62	2.59	50.3	2.7637E-04	1.063E-05	
MAX	83.07	44.41	67.3	5.5497E-04	2.516E-04	

TWL 9-2

TWL SITE 14 CORE 9 SPEC 2 UNITS= SI v M= 12 NR= 2						
SUSC.	DEC	INC	R95	EV	SDEV	
MIN	144.98	16.46	35.5	2.5249E-04	1.913E-05	
INT	312.36	73.15	69.3	2.9537E-04	4.597E-06	
MAX	53.95	3.48	58.0	3.1140E-04	1.808E-05	

TWL 10-1

TWL SITE 15 CORE 10 SPEC 1 UNITS= SI v M= 12 NR= 2						
SUSC.	DEC	INC	R95	EV	SDEV	
MIN	149.48	3.34	2.5	4.9534E-04	9.525E-06	
INT	49.80	70.82	53.8	6.5845E-04	3.071E-06	
MAX	240.62	18.87	53.8	6.7702E-04	2.833E-06	

TWL 10-2

TWL SITE 16 CORE 10 SPEC 2 UNITS= SI v M= 12 NR= 2						
SUSC.	DEC	INC	R95	EV	SDEV	
MIN	156.04	7.77	5.3	5.1885E-04	1.944E-06	
INT	253.19	42.35	45.8	6.4724E-04	1.571E-05	
MAX	57.74	46.60	45.5	6.7617E-04	6.954E-06	

AMS data - traverse Atikokan - Huronian Lake

Station	Sample	X grid	X grid	AMS file code		K1/K2	K2/K3	ln(A)	ln(B)	P'	T	
				CN	SN							
TWA1.0	TWA	1	1	3.3	1	1	1.19	1.54	0.17	0.43	1.87	0.43
TWA1.0	TWA	1	2	3.3	1	2	1.42	1.62	0.35	0.48	2.31	0.16
TWA2.0	TWA	2	1	3.2	2	1	1.03	1.75	0.03	0.56	1.94	0.91
TWA2.0	TWA	2	2	3.2	2	2	1.07	1.87	0.07	0.63	2.15	0.81
TWA3.0	TWA	3	1	3.2	3	1	1.04	1.23	0.04	0.21	1.30	0.70 max
TWA4.0	TWA	4	1	3	4	1	1.08	1.10	0.08	0.10	1.20	0.11 min
TWA4.0	TWA	4	2	3	4	2	1.04	1.12	0.04	0.12	1.18	0.47 min
TWA4.0	TWA	4	3	3	4	3	1.05	1.15	0.05	0.14	1.21	0.49 max
TWA5.0	TWA	5	1	2.7	5	1	1.08	1.25	0.08	0.22	1.36	0.49 max
TWA5.0	TWA	5	2	2.7	5	2	1.06	1.22	0.06	0.20	1.30	0.56 max
TWA6.0	TWA	6	1	2.8	6	1	1.06	1.48	0.06	0.39	1.62	0.75
TWA6.0	TWA	6	2	2.8	6	2	1.15	1.64	0.14	0.50	1.95	0.56
TWA6.5	TWA	6.5	1	3.2	6	51	1.05	1.12	0.05	0.11	1.18	0.41
TWA6.5	TWA	6.5	2	3.2	6	52	1.10	1.03	0.10	0.03	1.14	-0.50 min,max
TWA7.0	TWA	7	1	3.3	7	1	1.07	1.20	0.06	0.18	1.29	0.49
TWA7.5	TWA	7.5	1	3.8	7	51	1.10	1.06	0.09	0.06	1.16	-0.23
TWA7.5	TWA	7.5	2	3.8	7	52	1.01	1.02	0.01	0.02	1.02	0.48 min,max
TWA8.0	TWA	8	1	4.5	8	1	1.12	1.31	0.12	0.27	1.48	0.40
TWA8.0	TWA	8	2	4.5	8	2	1.17	1.37	0.15	0.32	1.61	0.34
TWA9.0	TWA	9	1	5.2	9	1	1.06	1.12	0.06	0.12	1.19	0.32
TWA9.0	TWA	9	2	5.2	9	2	1.08	1.10	0.08	0.10	1.19	0.13
TWA9.5	TWA	9.5	1	5.9	9	51	1.07	1.20	0.07	0.18	1.29	0.45
TWA9.5	TWA	9.5	2	5.9	9	52	1.11	1.19	0.11	0.18	1.33	0.25
TWA10.0	TWA	10	1	7.4	10	1	1.01	1.24	0.01	0.21	1.29	0.89 max
TWA10.0	TWA	10	2	7.4	10	2	1.09	1.15	0.09	0.14	1.26	0.21
TWA10.5	TWA	10.5	1	7.9	10	51	1.08	1.39	0.08	0.33	1.54	0.62
TWA10.5	TWA	10.5	2	7.9	10	52	1.12	1.37	0.11	0.31	1.55	0.47
TWA11.0	TWA	11	1	9.6	11	1	1.03	1.15	0.03	0.14	1.20	0.61 max
TWA11.0	TWA	11	2	9.6	11	2	1.04	1.14	0.04	0.13	1.20	0.55 max
TWA11.5	TWA	11.5	1	10.5	11	51	1.02	1.11	0.02	0.11	1.14	0.69 max
TWA11.5	TWA	11.5	2	10.5	11	52	1.01	1.05	0.01	0.05	1.06	0.81 max
TWA12.0	TWA	12	1	11.1	12	1	1.02	1.18	0.02	0.17	1.22	0.83 max
TWA12.0	TWA	12	2	11.1	12	2	1.05	1.18	0.05	0.16	1.24	0.56 max
TWA13.0	TWA	13	1	12.1	13	1	1.05	1.20	0.05	0.18	1.27	0.59 max
TWA13.0	TWA	13	2	12.1	13	2	1.15	1.23	0.14	0.20	1.41	0.20
TWA14.0	TWA	14	1	13.5	14	1	1.05	1.17	0.05	0.16	1.24	0.54
TWA14.0	TWA	14	2	13.5	14	2	1.03	1.11	0.03	0.10	1.15	0.52 min,max
TWA15.0	TWA	15	1	14.6	15	1	1.32	1.17	0.27	0.16	1.55	-0.26
TWA15.0	TWA	15	2	14.6	15	2	1.34	1.07	0.30	0.07	1.48	-0.61
TWA15.5	TWA	15.5	1	15.4	15	51	1.40	1.27	0.33	0.24	1.78	-0.17
TWA15.5	TWA	15.5	2	15.4	15	52	1.16	1.22	0.15	0.20	1.42	0.14
TWA15.9	TWA	15.9	1	17.1	15	91	1.08	1.21	0.08	0.19	1.32	0.43
TWA15.9	TWA	15.9	2	17.1	15	92	1.08	1.17	0.07	0.16	1.27	0.38 max
TWA16.0	TWA	16	1	17.8	16	1	1.01	1.29	0.01	0.26	1.35	0.96 max
TWA16.0	TWA	16	2	17.8	16	2	1.06	1.28	0.06	0.24	1.38	0.61
TWA16.5	TWA	16.5	1	18.2	16	51	1.07	1.31	0.07	0.27	1.43	0.61 max
TWA16.5	TWA	16.5	2	18.2	16	52	1.08	1.32	0.07	0.28	1.45	0.58
TWA17.0	TWA	17	1	19.4	17	1	1.04	1.28	0.04	0.24	1.36	0.71 max
TWA17.0	TWA	17	2	19.4	17	2	1.05	1.34	0.05	0.29	1.44	0.70
TWC7.0	TWC	7	1	20.5	7	1	1.05	1.20	0.05	0.18	1.27	0.60
TWC7.0	TWC	7	2	20.5	7	2	1.10	1.10	0.09	0.09	1.20	0.00
TWA18.0	TWA	18 a	1	20.9	18	11	1.03	1.10	0.03	0.09	1.13	0.55 max
TWA18.0	TWA	18 a	2	20.9	18	12	1.03	1.03	0.03	0.03	1.06	0.10 min,max
TWA18.0	TWA	18 b	1	20.9	18	21	1.05	1.16	0.05	0.15	1.23	0.49 max
TWA18.0	TWA	18 b	2	20.9	18	22	1.09	1.15	0.08	0.14	1.25	0.23
TWA18.5	TWA	18.5	1	21.6	18	51	1.08	1.16	0.08	0.15	1.26	0.31
TWA18.5	TWA	18.5	2	21.6	18	52	1.15	1.12	0.14	0.11	1.28	-0.11

AMS data - traverse Atikokan - Huronian Lake

Station	Sample	X grid	AMS file		K1/K2	K2/K3	ln(A)	ln(B)	P'	T	
			code	SN							
TWA18.5	TWA 18.5 a 1	21.6	18	511	1.05	1.16	0.05	0.15	1.23	0.54	max
TWA18.5	TWA 18.5 a 2	21.6	18	512	1.09	1.20	0.08	0.18	1.31	0.37	
TWA19.0	TWA 19 1	22.8	19	1	1.20	1.08	0.18	0.08	1.31	-0.40	max,min
TWA19.0	TWA 19 2	22.8	19	2	1.03	1.09	0.03	0.08	1.12	0.45	max
TWL9.0	TWL 9 1	23.7	9	1	1.05	1.17	0.05	0.16	1.24	0.50	max
TWL10.0	TWL 10 1	23.2	10	1	1.03	1.33	0.03	0.28	1.41	0.82	max
TWL10.0	TWL 10 2	23.2	10	2	1.04	1.25	0.04	0.22	1.33	0.87	max
TWA19.5	TWA 19.5 1	23.5	19	51	1.32	1.13	0.28	0.12	1.50	-0.39	
TWA19.5	TWA 19.5 2	23.5	19	52	1.22	1.11	0.20	0.11	1.38	-0.29	
TWA20.0	TWA 20 a 1	23.9	20	11	1.12	1.10	0.11	0.09	1.23	-0.10	
TWA20.0	TWA 20 a 2	23.9	20	12	1.13	1.08	0.13	0.08	1.23	-0.24	
TWA20.0	TWA 20 b 1	23.9	20	21	1.13	1.15	0.13	0.14	1.30	0.05	
TWA20.0	TWA 20 b 2	23.9	20	22	1.25	1.17	0.23	0.15	1.47	-0.19	
TWA21.0	TWA 21 1	24.8	21	1	1.03	1.13	0.03	0.13	1.18	0.80	max,min
TWA21.0	TWA 21 2	24.8	21	2	1.03	1.21	0.03	0.19	1.27	0.70	
TWA22.0	TWA 22 1	25.8	22	1	1.04	1.22	0.04	0.20	1.29	0.89	
TWA22.0	TWA 22 2	25.8	22	2	1.04	1.17	0.04	0.15	1.23	0.81	max
TWA22.0	TWA 22 a 1	25.8	22	11	1.03	1.18	0.03	0.16	1.23	0.88	max
TWA22.0	TWA 22 a 2	25.8	22	12	1.10	1.16	0.10	0.15	1.27	0.21	
TWA22.5	TWA 22.5 1	26.8	22	51	1.10	1.13	0.09	0.12	1.24	0.11	
TWA22.5	TWA 22.5 2	26.8	22	52	1.08	1.15	0.08	0.14	1.23	0.40	max
TWC6.0	TWC 6 a 2	27.7	6	12	1.03	1.18	0.02	0.17	1.24	0.74	min,max
TWC6.0	TWC 6 a 1	27.7	6	11	1.05	1.11	0.05	0.11	1.17	0.37	
TWC6.0	TWC 6 2	27.7	6	2	1.38	1.16	0.32	0.15	1.61	-0.37	
TWC6.0	TWC 6 1	27.7	6	1	1.48	1.20	0.38	0.18	1.78	-0.36	
TWC5.0	TWC 5 c 1	28.2	5	31	1.07	1.21	0.07	0.19	1.31	0.45	max
TWC5.0	TWC 5 b 2	28.2	5	22	1.25	1.20	0.23	0.18	1.51	-0.11	
TWC5.0	TWC 5 b 1	28.2	5	21	1.05	1.20	0.04	0.18	1.27	0.80	max
TWC5.0	TWC 5 a 2	28.2	5	12	1.04	1.18	0.04	0.15	1.22	0.81	
TWC5.0	TWC 5 a 1	28.2	5	11	1.08	1.18	0.08	0.16	1.28	0.37	
TWL7.0	TWL 7 1	31.5	7	1	1.07	1.05	0.07	0.05	1.12	-0.17	min
TWL7.0	TWL 7 2	31.5	7	2	1.07	1.05	0.07	0.05	1.13	-0.13	min
TWL8.0	TWL 8 1	31	8	1	1.04	1.15	0.04	0.14	1.21	0.55	max
TWL8.0	TWL 8 2	31	8	2	1.08	1.17	0.05	0.16	1.25	0.49	min
TWC4.0	TWC 4 2	30	4	2	1.05	1.09	0.05	0.09	1.15	0.24	max
TWC4.0	TWC 4 1	30	4	1	1.05	1.06	0.05	0.08	1.12	0.11	min
TWC3.0	TWC 3 a 1	31.5	3	11	1.08	1.23	0.08	0.21	1.35	0.44	max,min
TWC2.0	TWC 2 1	32	2	1	1.24	1.34	0.21	0.29	1.86	0.16	max,min
TWC1.5	TWC 1.5 b 2	32.3	1	522	1.03	1.53	0.03	0.42	1.86	0.88	max
TWC1.5	TWC 1.5 b 1	32.3	1	521	1.02	1.52	0.02	0.42	1.85	0.89	max
TWC1.5	TWC 1.5 a 1	32.3	1	511	1.05	1.22	0.05	0.20	1.30	0.59	max
TWC1.0	TWC 1 2	32.6	1	2	1.03	1.49	0.03	0.40	1.62	0.85	max
TWC1.0	TWC 1 1	32.6	1	1	1.03	1.56	0.03	0.45	1.71	0.86	
TWE1.0	TWE 1 1	34.7	1	1	1.04	1.24	0.04	0.21	1.31	0.70	
TWE1.0	TWE 1 2	34.7	1	2	1.12	1.19	0.12	0.17	1.34	0.19	
TWE2.0	TWE 2 1	35.2	2	1	1.68	1.77	0.52	0.57	2.97	0.05	max
TWE2.0	TWE 2 2	35.2	2	2	1.18	2.80	0.16	1.03	3.85	0.73	max,min
TWE3.0	TWE 3 a 1	37.8	31	1	1.05	1.12	0.05	0.11	1.18	0.38	max
TWE3.0	TWE 3 a 2	37.8	31	2	1.02	1.19	0.02	0.17	1.24	0.77	max
TWE3.0	TWE 3 b 1	37.8	32	1	1.02	1.29	0.02	0.25	1.36	0.85	max
TWE3.0	TWE 3 b 2	37.8	32	2	1.05	1.28	0.05	0.23	1.35	0.82	max
TWE4.0	TWE 4 a 1	39.9	41	1	1.02	1.28	0.02	0.24	1.34	0.82	max
TWE4.0	TWE 4 b 1	39.9	42	1	1.05	1.29	0.04	0.25	1.38	0.70	max
TWE4.0	TWE 4 b 2	39.9	42	2	1.08	1.22	0.08	0.20	1.31	0.53	min
TWL6.0	TWL 6 1	40.5	6	1	1.04	1.25	0.04	0.22	1.32	0.69	
TWL6.0	TWL 6 2	40.5	6	2	1.02	1.30	0.02	0.26	1.38	0.83	
TWE5.0	TWE 5 1	41.2	5	1	1.03	1.24	0.03	0.21	1.30	0.77	max
TWE5.0	TWE 5 2	41.2	5	2	1.09	1.22	0.09	0.20	1.34	0.38	
TWE6.0	TWE 6 a 1	41.8	61	1	1.28	1.13	0.23	0.12	1.44	-0.31	
TWE6.0	TWE 6 a 2	41.8	61	2	1.27	1.14	0.24	0.13	1.45	-0.29	
TWE6.0	TWE 6 a 3	41.8	61	3	1.36	1.11	0.31	0.11	1.54	-0.49	
TWE6.0	TWE 6 b 1	41.8	62	1	1.05	1.30	0.05	0.26	1.40	0.69	max
TWE6.0	TWE 6 b 2	41.8	62	2	1.14	1.24	0.13	0.21	1.41	0.23	
TWE6.0	TWE 6 b 3	41.8	62	3	1.08	1.37	0.08	0.31	1.51	0.60	
TW23.0	TW 23 2	42.5	23	2	1.05	1.33	0.05	0.28	1.43	0.71	
TW23.0	TW 23 1	42.5	23	1	1.02	1.26	0.02	0.23	1.32	0.83	max
TW22.0	TW 22 2	43.7	22	2	1.08	1.20	0.07	0.19	1.31	0.43	max
TW22.0	TW 22 1	43.7	22	1	1.07	1.29	0.07	0.26	1.41	0.56	
TW21.0	TW 21 a 2	44.8	21	12	1.08	1.21	0.08	0.19	1.32	0.41	max
TW21.0	TW 21 a 1	44.8	21	11	1.04	1.19	0.04	0.18	1.28	0.85	max
TW21.0	TW 21 2	44.8	21	2	1.18	1.04	0.15	0.04	1.22	-0.80	min
TW21.0	TW 21 1	44.8	21	1	1.08	1.10	0.08	0.10	1.19	0.10	
TW20.0	TW 20 2	45.8	20	2	1.04	1.20	0.04	0.18	1.27	0.86	max

AMS data - traverse Atikokan - Huronian Lake

Station	Sample	X	grid	AMS file		K1/K2	K2/K3	ln(A)	ln(B)	P'	T	
				code	CN SN							
TW20.0	TW	20	1	45.8	20 1	1.02	1.21	0.02	0.19	1.27	0.79	max
TWL5.0	TWL	5	1	47	5 1	1.04	1.11	0.04	0.10	1.16	0.40	min,max
TWL5.0	TWL	5	2	47	5 2	1.08	1.06	0.08	0.06	1.15	-0.18	min,max
TW19.0	TW	19	2	46.9	19 2	1.18	1.03	0.17	0.03	1.23	-0.73	
TW19.0	TW	19	1	46.9	19 1	1.14	1.09	0.13	0.09	1.25	-0.20	
TW18.0	TW	18	2	47.8	18 2	1.01	1.38	0.01	0.32	1.46	0.91	max
TW18.0	TW	18	1	47.8	18 1	1.06	1.17	0.05	0.16	1.25	0.49	max
TW17.0	TW	17	2	49.3	17 2	1.14	1.08	0.13	0.08	1.24	-0.24	
TW17.0	TW	17	1	49.3	17 1	1.05	1.17	0.05	0.16	1.24	0.54	
TW16.0	TW	16	2	50.6	16 2	1.04	1.24	0.04	0.22	1.32	0.70	max
TW16.0	TW	16	1	50.6	16 1	1.10	1.15	0.09	0.14	1.27	0.20	
TW15.0	TW	15	1	51.7	15 1	1.11	1.15	0.10	0.14	1.28	0.14	
TW14.0	TW	14	2	52.8	14 2	1.10	1.17	0.10	0.16	1.30	0.23	
TW14.0	TW	14	1	52.8	14 1	1.11	1.16	0.10	0.15	1.29	0.18	
TW13.0	TW	13	2	54.2	13 2	1.04	1.25	0.04	0.23	1.33	0.70	max,min
TW13.0	TW	13	1	54.2	13 1	1.08	1.14	0.08	0.13	1.23	0.23	max,min
TW12.0	TW	12	c 2	55.6	12 32	1.03	1.08	0.03	0.08	1.12	0.40	max,min
TW12.0	TW	12	c 1	55.6	12 31	1.05	1.16	0.05	0.15	1.22	0.50	max
TW12.0	TW	12	b 2	55.6	12 22	1.11	1.23	0.10	0.20	1.36	0.34	min
TW12.0	TW	12	b 1	55.6	12 21	1.12	1.18	0.11	0.17	1.32	0.20	
TW12.0	TW	12	a 2	55.6	12 12	1.03	1.23	0.03	0.21	1.30	0.73	max
TW12.0	TW	12	a 1	55.6	12 11	1.03	1.14	0.03	0.13	1.18	0.64	max
TW11.0	TW	11	2	56.6	11 2	1.06	1.18	0.06	0.17	1.27	0.47	max
TW11.0	TW	11	1	56.6	11 1	1.10	1.19	0.10	0.18	1.32	0.29	max
TW10.0	TW	10	2	57.5	10 2	1.04	1.17	0.04	0.15	1.23	0.56	
TW10.0	TW	10	1	57.5	10 1	1.14	1.13	0.13	0.12	1.29	-0.02	min
TWL4.0	TWL	4	1	52	4 1	1.03	1.17	0.03	0.16	1.22	0.69	min,max
TW9.0	TW	9	2	58.3	9 2	1.04	1.20	0.04	0.18	1.27	0.64	max
TW9.0	TW	9	1	58.3	9 1	1.08	1.18	0.08	0.17	1.28	0.36	max
TW8.0	TW	8	2	59.6	8 2	1.20	1.43	0.18	0.36	1.73	0.33	
TW8.0	TW	8	1	59.6	8 1	1.11	1.41	0.10	0.35	1.60	0.54	
TW7.0	TW	7	b 2	60.3	7 22	1.26	1.08	0.23	0.08	1.37	-0.50	min
TW7.0	TW	7	b 1	60.3	7 21	1.05	1.17	0.05	0.16	1.25	0.51	
TW7.0	TW	7	a 2	60.3	7 12	1.09	1.33	0.08	0.29	1.48	0.55	
TW7.0	TW	7	a 1	60.3	7 11	1.05	1.18	0.05	0.16	1.25	0.55	
TW6.0	TW	6	2	61.3	6 2	1.01	1.32	0.01	0.28	1.39	0.90	
TW6.0	TW	6	1	61.3	6 1	1.11	1.21	0.11	0.19	1.35	0.28	
TWL2.0	TWL	2	1	61.4	2 1	1.06	1.17	0.06	0.16	1.26	0.44	
TWL2.0	TWL	2	2	61.4	2 2	1.02	1.22	0.02	0.20	1.27	0.83	
TWL3.0	TWL	3	1	61.2	3 1	1.05	1.21	0.04	0.19	1.28	0.62	max
TWL3.0	TWL	3	2	61.2	3 2	1.11	1.20	0.11	0.19	1.34	0.27	
TW5.0	TW	5	a 2	62.8	5 12	1.05	1.31	0.05	0.27	1.41	0.67	max
TW5.0	TW	5	a 1	62.8	5 11	1.27	1.05	0.24	0.05	1.36	-0.65	min
TW5.0	TW	5	2	62.8	5 2	1.45	1.48	0.37	0.39	2.13	0.03	max,min
TW5.0	TW	5	1	62.8	5 1	1.04	1.31	0.04	0.27	1.39	0.77	max

ARM anisotropy axes - TW collection  
File: ARMTwsum.wq1

Sample		ARMTW*.sp	Min		Int				Max				Mean ARM (mA/m)								Rejected data	
			Dec	Inc	Dec	Inc	Dec	Inc	Dec	Inc	Dec	Inc	Dec	Inc	Dec	Inc	Dec	Inc	P'	T		
TWA	1	1 ARMTWA1	330.1	10.8	16.4	2.49E+01	232.0	36.2	1.30E+02	74.1	51.7	5.9	3.68E+02	106.2	174.5	2.82	5.24	1.04	1.66	15.13	0.23	
TWA	2	1 ARMTWA2	177.3	0.7	4.5	4.24E+01	267.6	23.5	5.13E+02	85.8	66.5	8.5	6.43E+02	241.0	399.6	1.25	12.10	0.23	2.49	20.45	0.83	
TWA	5	1 ARMTWA3s	344.5	17.1	5.1	7.81E+01	83.7	27.3	1.90E+02	226.3	57.0	4.7	3.09E+02	166.0	192.2	1.63	2.43	0.49	0.89	4.03	0.29	
TWA	6	1 ARMTWA4s	340.2	5.7	1.7	1.59E+02	74.0	33.9	7.18E+02	241.8	55.5	24.4	8.52E+02	459.7	576.1	1.19	4.52	0.17	1.51	6.35	0.80	max
TWA	7	1 ARMTWA5	334.1	17.5	3.6	1.17E+02	241.2	9.0	2.59E+02	125.2	70.2	10.3	4.73E+02	242.6	282.8	1.83	2.22	0.60	0.80	4.07	0.14	
TWA	8	1 ARMTWA6	164.5	15.0	4.6	1.43E+02	73.9	1.9	3.75E+02	336.8	74.9	4.6	6.09E+02	319.8	375.7	1.63	2.61	0.49	0.96	4.36	0.33	
TWA	9	1 ARMTWA7	180.1	7.2	6.7	1.44E+02	275.0	34.4	2.80E+02	79.9	54.6	3.1	4.07E+02	253.9	276.8	1.45	1.95	0.37	0.67	2.87	0.28	
TWA	9.5	1 ARMTWA8	344.2	10.7	3.9	6.33E+01	253.9	1.7	1.45E+02	154.7	79.2	8.6	2.44E+02	130.9	150.8	1.68	2.30	0.52	0.83	3.90	0.23	
TWA	10	1 ARMTWA9	351.7	8.9	10.6	1.37E+01	87.9	34.7	2.82E+01	249.3	53.9	23.5	3.64E+01	24.2	26.1	1.29	2.05	0.26	0.72	2.75	0.47	max
TWA	10.5	1 ARMTWA10	160.4	8.4	5.2	6.70E+01	254.4	25.0	2.32E+02	53.2	63.4	10.9	2.94E+02	166.0	197.7	1.26	3.47	0.24	1.24	4.90	0.68	
TWA	14	1 ARMTWA11	62.2	25.9	7	1.15E+01	201.2	57.2	2.04E+01	322.8	18.7	5.2	3.10E+01	19.4	21.0	1.52	1.78	0.42	0.57	2.72	0.16	
TWA	15	1 ARMTWA12	200.4	58.1	6.6	9.75E+01	328.8	21.1	1.26E+02	68.1	22.7	5	2.35E+02	142.3	152.6	1.86	1.29	0.62	0.25	2.47	-0.42	
TWA	15.5	2 ARMTWA13	173.5	38.7	7.1	3.67E+01	287.1	26.6	9.52E+01	41.6	39.8	4.6	2.01E+02	88.9	111.0	2.11	2.59	0.75	0.95	5.50	0.12	
TWA	16.5	1 ARMTWA14	148.2	29.2	3.9	6.07E+01	302.0	58.1	1.23E+02	51.5	11.8	8.4	2.96E+02	130.2	159.8	2.42	2.02	0.88	0.70	4.89	-0.11	
TWA	18	b 1 ARMTWA15	346.4	24.9	13.1	1.03E+01	164.9	65.1	1.34E+01	256.2	0.6	16.5	3.16E+01	16.3	18.4	2.36	1.31	0.86	0.27	3.24	-0.52	
TWA	18.5	a 1 ARMTWA16	187.4	62.9	6.9	7.22E+01	3.1	27.0	1.03E+02	94.0	1.8	6.7	1.77E+02	109.4	117.2	1.72	1.42	0.54	0.35	2.47	-0.21	
TWA	20	b 1 ARMTWA17	339.9	28.5	29.8	2.06E+01	151.9	61.3	2.73E+01	248.1	3.4	8.7	7.26E+01	34.5	40.2	2.66	1.33	0.98	0.28	3.75	-0.55	min
TWA	22	1 ARMTWA18	210.8	29.3	59.5	9.43E+00	22.7	60.5	1.12E+01	118.8	3.5	22.5	1.79E+01	12.4	12.8	1.60	1.19	0.47	0.17	1.94	-0.46	max,min
TWC	5	a 1 ARMTWC3	154.9	8.2	6.4	2.11E+01	266.2	68.4	3.49E+01	61.9	19.8	11.4	6.29E+01	35.9	39.7	1.80	1.65	0.59	0.50	2.98	-0.08	
TWC	1.5	b 1 ARMTWC2	162.9	13.2	8.6	3.66E+01	294.1	70.3	1.25E+02	69.5	14.3	6.8	2.02E+02	97.4	121.3	1.62	3.42	0.48	1.23	5.84	0.44	
TWC	1	1 ARMTWC1s	177.0	9.7	3	1.57E+01	312.1	76.5	1.07E+02	85.4	9.4	6	1.51E+02	63.3	91.1	1.41	6.79	0.35	1.92	11.43	0.69	
TWE	6	a 1 ARMTWE2	111.3	18.6	19	1.57E+02	234.2	58.2	2.27E+02	12.3	24.8	2.3	4.90E+02	259.3	291.2	2.16	1.45	0.77	0.37	3.19	-0.35	
TWE	6	b 1 ARMTWE3	319.3	17.1	11.6	3.09E+01	167.1	70.9	7.76E+01	51.9	8.4	5.5	1.21E+02	66.2	76.4	1.56	2.51	0.44	0.92	4.02	0.35	
TW	23	1 ARMTW10	315.2	5.1	1.6	1.34E+02	153.4	84.6	2.58E+02	45.3	1.7	4.5	4.06E+02	241.2	266.0	1.58	1.92	0.45	0.65	3.05	0.18	
TW	17	1 ARMTW7	318.0	44.6	3.8	8.94E+01	175.3	38.9	1.21E+02	68.6	19.6	6	1.81E+02	125.2	130.6	1.50	1.35	0.40	0.30	2.03	-0.15	
TW	15	1 ARMTW6	156.9	2.3	7.8	3.36E+01	40.1	84.9	4.89E+01	247.1	4.5	9.7	7.68E+01	50.2	53.1	1.57	1.46	0.45	0.38	2.29	-0.09	
TW	14	1 ARMTW5	6.7	7.0	11.1	6.11E+01	116.2	69.8	8.25E+01	274.3	18.8	3.5	1.32E+02	87.3	91.9	1.60	1.35	0.47	0.30	2.17	-0.22	
TW	8	1 ARMTW2	346.1	10.2	2.9	1.72E+02	221.0	72.5	3.41E+02	78.6	14.0	3.7	7.10E+02	346.6	407.6	2.08	1.99	0.73	0.69	4.13	-0.03	
TW	7	a 1 ARMTW1	335.4	23.5	60.7	7.30E+00	151.1	66.4	7.75E+00	244.7	1.6	22.8	9.89E+00	8.2	8.3	1.28	1.06	0.24	0.06	1.38	-0.61	max,min
TWL	2	1 ARMTWL1s	358.4	21.3	18.3	2.20E+01	128.7	58.9	3.05E+01	259.5	21.5	13.2	4.46E+01	31.0	32.3	1.46	1.39	0.38	0.33	2.03	-0.07	

Arm anisotropy axes - RS collection  
File: ARMrsum.wq1

ARM*.SPN	Station	Sample	Min			Int			Max			mean ARM										Rejected	
			Dec	Inc	alfa95	Int	Dec	Inc	Int	Dec	Inc	Int	Dec	Inc	alfa95	Int	geom	K1/K2	K2/K3	ln(A)	ln(B)		P'
ARM rs 1	1	tw 1-1	338.8	5.6	6.8	38.5	218.5	79.0	59.3	69.7	9.4	23.0	64.1	52.7	1.08	1.54	0.08	0.43	1.73	0.69			
ARM rs 2	1.1	rs 1.1			18.1	39.5	325.7	22.5	40.5	71.7	33.8	10.9	68.8	47.9	1.70	1.02	0.53	0.02	1.87	-0.91			
ARM twr 1	1.3	twr 1.3a	157.1	6.9	3.9	38.4	333.3	83.1	67.5	67.0	0.5	2.1	170.9	76.2	2.53	1.76	0.93	0.57	4.52	-0.24			
ARM rst 1	2	rst 2ca			72.8	2.0	3.5	59.0	2.2	222.8	24.9	30.8	2.4	2.2	1.10	1.09	0.10	0.09	1.20	-0.04	min		
ARM rs 3	2.1	rs 2.1	65.1	68.7	19.3	7.4	332.4	1.1	7.9	241.9	21.2	22.6	8.4	7.9	1.06	1.07	0.05	0.07	1.13	0.12			
ARM twr 2	2.2	twr 2.2-1	145.7	14.5	14.1	40.0	25.8	62.6	72.3	241.9	22.8	25.7	91.0	64.1	1.26	1.81	0.23	0.59	2.33	0.44			
ARM rs 4	3	rs 3c	22.2	6.2	9.9	44.2	180.4	83.4	48.8	291.9	2.6	5.7	51.9	48.2	1.06	1.10	0.06	0.10	1.18	0.22			
ARM twr 3	3.5	twr 3.5-1	102.2	30.5	18.4	70.6	261.3	57.8	89.6	6.6	9.4	24.2	100.4	85.9	1.12	1.27	0.11	0.24	1.43	0.36			
ARM twr 4	4.1	twr 4.1b-1	348.3	3.1	4.2	105.8	254.5	50.7	217.5	80.9	39.2	17.4	229.4	174.1	1.05	2.06	0.05	0.72	2.37	0.86			
ARM twr 5	5	twr 5a-1	353.0	4.0	21.1	162.8	83.4	5.4	185.5	226.5	83.3	3.1	245.1	194.9	1.32	1.14	0.28	0.13	1.52	-0.36			
ARM twr 6	8.05	twr 8.05-1	125.2	8.8	13.7	41.1			86.1	15.5	65.2	54.3	90.3	68.4	1.05	2.09	0.05	0.74	2.42	0.88	max		
ARM rs 9	8.1	rs 8.1	350.6	3.9	8.3	62.3	195.4	85.8	115.0	80.7	1.8	20.8	144.0	101.0	1.25	1.85	0.22	0.61	2.38	0.46			
ARM rs 12	9.1	rs 9.1s	166.3	19.3	18.5	91.1	288.4	56.6	185.0	66.4	26.1	8.8	286.1	169.0	1.55	2.03	0.44	0.71	3.17	0.24			
ARM rs 13	9.2	rs 9.2-2	159.3	8.0	11.8	46.2	295.6	79.0	92.6	68.2	7.5	6.1	137.2	83.7	1.48	2.01	0.39	0.70	3.01	0.28			
ARM rs 15	9.3	rs 9.3	153.6	64.0	23.2	5.0	334.2	26.0	9.0	244.1	0.3	50.3	10.2	7.7	1.14	1.78	0.13	0.58	2.13	0.63	max		
ARM rs 16	9.4	rs 9.4	317.3	2.7	9.0	34.1	220.5	68.4	67.6	48.3	21.4	9.9	91.0	59.4	1.35	1.98	0.30	0.68	2.74	0.39			
ARM twr 7	10.05	twr 10.05-1	322.3	1.8	8.0	104.7	88.5	87.1	219.8	232.3	2.4	2.2	408.7	211.1	1.86	2.10	0.62	0.74	3.91	0.09			
ARM rs 18	10.1	rs 10.1	313.8	8.7	1.5	29.7	213.7	48.9	59.6	51.2	39.8	4.3	107.5	57.5	1.80	2.00	0.59	0.69	3.62	0.08			
ARM rs 19	10.15	rs 10.15	329.3	16.0	9.8	4.9	206.3	62.2	6.2	66.0	22.1	5.4	9.0	6.5	1.47	1.25	0.36	0.22	1.85	-0.27			
ARM rs 20	10.2	rs 10.2	328.3	9.5	6.1	153.1	206.0	72.5	296.0	60.7	14.5	7.2	402.9	263.3	1.36	1.93	0.31	0.66	2.69	0.36			
ARM rs 21	10.3	rs 10.3	152.9	2.0	28.2	24.2	53.4	78.3	81.1	243.4	11.6	27.5	191.3	72.2	2.36	3.35	0.86	1.21	7.97	0.17			
ARM rs 22	10.4	rs 10.4	325.4	10.8	9.9	9.2	122.9	78.3	20.9	234.6	4.4	29.6	23.8	16.6	1.14	2.27	0.13	0.82	2.81	0.73			
ARM rs 23	10.45	rs 10.45	348.0	3.1	18.7	4.8	93.0	78.1	12.1	257.4	11.5	4.6	20.1	10.6	1.66	2.51	0.51	0.92	4.25	0.29			
ARM rs 24	10.55	rs 10.55	146.5	4.6	16.7	4.4	22.5	81.9	9.6	237.0	6.7	11.3	16.4	8.8	1.71	2.20	0.54	0.79	3.79	0.19			
ARM rs 25	10.9	rs 10.9	359.1	16.1	5.7	43.9	175.8	73.9	75.9	268.9	0.9	11.5	167.0	82.2	2.20	1.73	0.79	0.55	3.83	-0.18			
ARM rs 26	11.1	rs 11.1-1	170.0	31.2	2.7	53.2	306.1	49.9	152.6	65.5	22.4	10.7	217.2	120.8	1.42	2.87	0.35	1.05	4.32	0.50			
ARM rs 27	11.3	rs 11.3	170.7	37.7	3.5	9.8	15.7	49.5	20.4	270.6	12.6	8.8	28.7	17.9	1.41	2.08	0.34	0.73	3.00	0.36			
ARM rst 4	11.35	rst 11.35a	170.5	22.2	6.3	10.9	11.3	66.4	22.8	263.6	7.6	9.8	32.4	20.0	1.42	2.10	0.35	0.74	3.05	0.35			
ARM rs 28	11.35	rs 11.35	169.1	15.7	12.8	11.0	53.3	57.1	22.4	267.7	28.1	11.7	26.5	18.7	1.18	2.03	0.17	0.71	2.54	0.61			
ARM rs 29	11.4	rs 11.4-2	162.4	51.5	4.7	15.9	17.0	33.2	75.1	275.3	17.2	6.0	93.0	48.0	1.24	4.73	0.21	1.55	6.88	0.76			
ARM rst 5	11.4	rst 11.4-2a	157.8	47.8	5.4	19.1	348.6	41.6	73.8	253.8	5.4	11.0	105.1	52.9	1.42	3.86	0.35	1.35	6.04	0.58			
ARM rs 30	11.45	rs 11.45	167.8	51.0	7.6	8.6	356.8	38.6	15.3	263.3	4.4	23.7	24.8	14.9	1.62	1.78	0.48	0.58	2.88	0.09			
ARM rs 31	11.5	rs 11.5	291.9	62.6	8.4	15.6	100.9	27.0	33.1	193.2	4.5	8.2	60.4	31.5	1.82	2.12	0.60	0.75	3.88	0.11			
ARM rs 32	11.6	rs 11.6	190.0	33.0	38.5	1.6	67.8	39.5	2.6	305.2	33.2	59.7	3.6	2.5	1.43	1.57	0.35	0.45	2.24	0.12	max		
ARM rs 33	11.9	rs 11.9	324.8	11.2	60.1	2.4	151.2	78.7	2.9	55.0	1.2	29.9	4.6	3.2	1.59	1.22	0.46	0.20	1.97	-0.41	min		
ARM rst 8	11.9	rst 11.9a			43.1	2.1	176.0	24.9	2.2	68.6	32.9	20.4	3.4	2.5	1.53	1.05	0.42	0.05	1.68	-0.80	min		
ARM rs 35	12	tw 4-1	172.4	13.9	8.0	7.6	323.0	74.1	12.0	80.6	7.5	8.8	19.5	12.1	1.63	1.58	0.49	0.46	2.59	-0.03			





ARM anisotropy axes - PS collection  
 File : armpssum.wq1 - method 2

ARMps* file:	Sample	Geographic coordinates										Sample coordinates						Str	Dip	Mean ARM								Rejected	
		Min			Int			Max				Min		Int		Max				geom	K1/K2	K2/K3	ln(A)	ln(B)	P'	T			
		Dec	Inc	Int	alfa95	Dec	Inc	Int	Dec	Inc	Int	Dec	Inc	Dec	Inc	Dec	Inc												
ARM pst	10 pst	45	338.1	6.1	14.2	13.6	74.5	46.5	22.7	242.4	42.9	41.0	8.9	155.8	82.4	46.4	2.5	316.1	7.1	75	87	23.6	1.81	1.60	0.59	0.47	2.90	-0.11	
ARM pst	11 pst	51	158.2	7.8	12.2	12.7	253.1	32.5	45.0	56.3	56.4	86.1	7.1	213.9	75.8	30.2	14.2	120.4	0.9	260	74	36.2	1.91	3.69	0.65	1.30	7.31	0.34	
ARM pst	12 pst	52	182.6	6.8	4.5	9.3	286.4	63.4	12.5	89.3	25.6	16.7	30.0	5.5	80.4	245.6	4.8	154.9	8.3	263	84	9.8	1.34	2.80	0.29	1.03	4.01	0.56	max
ARM pst	14 pst	59	151.1	16.2	22.5	7.1	56.5	15.4	41.1	285.2	67.4	68.7	9.7	176.4	57.5	330.4	29.8	67.3	11.8	275	73	39.9	1.67	1.83	0.51	0.60	3.06	0.08	
ARM pst	15 pst	62	350.2	6.6	22.4	4.2	254.0	43.1	172.3	87.2	46.1	257.8	70.0	79.4	83.3	316.8	3.7	226.4	5.7	79	90	99.9	1.50	7.67	0.40	2.04	13.70	0.67	max
ARM pst	16 pst	63	330.1	15.4	50.4	13.7	233.0	24.0	75.0	89.8	60.9	274.3	9.6	206.3	46.6	30.8	41.3	298.8	2.2	278	88	101.2	3.66	1.49	1.30	0.40	5.89	-0.53	
ARM pst	17 pst	65	168.9	13.7	13.9	23.9	268.3	33.7	18.8	60.1	52.9	25.4	10.9	159.8	75.4	32.9	8.9	301.1	11.5	273	81	18.8	1.35	1.35	0.30	0.30	1.83	-0.01	
ARM psp	1 psp	1	352.2	4.8	59.7	9.4	85.9	37.8	105.5	256.0	51.8	123.5	77.7	352.2	4.8	85.9	37.8	256.0	51.8	H		92.0	1.17	1.77	0.16	0.57	2.15	0.57	max
ARM psp	2 psp	9	310.6	9.1	31.9	3.5	217.4	19.2	61.2	64.7	68.6	72.3	41.1	310.6	9.1	217.4	19.2	64.7	68.6	H		52.1	1.18	1.92	0.17	0.65	2.37	0.59	max
ARM psp	4 psp	13a	342.7	39.4	7.5	26.0	210.4	39.3	12.4	96.6	26.3	16.3	48.1	342.7	39.4	210.4	39.3	96.6	26.3	H		11.5	1.31	1.65	0.27	0.50	2.20	0.30	max
ARM psp	5 psp	26	344.9	31.8	2.3	15.2	113.1	44.9	4.5	235.5	28.2	6.4	14.1	344.9	31.8	113.1	44.9	235.5	28.2	H		4.1	1.42	1.92	0.35	0.65	2.77	0.30	
ARM psp	6 psp	26a	166.4	13.1	70.3	8.5	72.1	17.7	221.1	291.1	67.7	277.7	23.8	166.4	13.1	72.1	17.7	291.1	67.7	H		162.8	1.26	3.14	0.23	1.15	4.36	0.67	
ARM psp	7 psp	32	344.3	8.1	27.4	5.8	249.5	30.2	97.1	87.7	58.5	108.7	17.4	344.3	8.1	249.5	30.2	87.7	58.5	H		66.1	1.12	3.55	0.11	1.27	4.63	0.84	
ARM psp	8 psp	38a	354.8	10.5	25.5	11.8	106.0	62.9	159.5	259.9	24.7	255.5	16.2	354.8	10.5	106.0	62.9	259.9	24.7	H		101.3	1.60	6.25	0.47	1.83	11.40	0.59	
ARM psp	9 psp	39	349.2	1.8	33.2	9.7	91.1	81.0	192.9	259.0	8.8	308.9	14.1	349.2	1.8	91.1	81.0	259.0	8.8	H		125.6	1.60	5.81	0.47	1.76	10.49	0.58	
ARM psp	10 psp	60	155.9	12.5	54.1	2.3	61.3	19.8	97.4	276.2	66.3	233.1	4.4	155.9	12.5	61.3	19.8	276.2	66.3	H		107.1	2.39	1.80	0.87	0.59	4.35	-0.19	
ARM psr	1 psr	5	337.0	18.6	77.5	6.9	150.4	71.3	209.3	246.3	2.0	401.3	9.8	110.0	70.1	265.4	18.2	358.0	7.7	74	90	186.7	1.92	2.70	0.65	0.99	5.24	0.21	
ARM psr	2 psr	7	347.0	22.3	9.2	6.9	248.1	20.6	17.8	119.7	58.8	25.0	14.3	131.7	71.8	335.1	16.8	243.0	6.8	90	81	16.0	1.40	1.94	0.34	0.66	2.77	0.32	
ARM psr	3 psr	10	353.8	15.7	76.8	4.8	178.6	74.3	216.2	84.1	1.3	385.8	8.4	304.2	73.1	94.0	14.7	186.2	8.1	74	60	185.8	1.78	2.81	0.58	1.03	5.13	0.28	
ARM psr	4 psr	15	355.5	6.3	26.0	9.3	240.7	75.3	59.9	87.0	13.3	103.0	19.4	286.2	69.9	75.5	17.4	168.5	9.6	260	77	54.4	1.72	2.30	0.54	0.83	4.00	0.21	
ARM psr	5 psr	17	160.2	12.2	79.1	4.6	291.6	71.8	203.1	67.3	13.2	300.8	9.1	163.2	82.0	255.0	0.3	345.0	8.0	258	80	169.1	1.48	2.57	0.39	0.94	3.94	0.41	
ARM psr	6 psr	18	344.9	27.3	29.7	5.7	120.8	54.3	65.5	243.4	21.1	129.1	9.1	288.4	57.9	112.1	32.0	21.1	1.7	244	87	63.1	1.97	2.21	0.68	0.79	4.36	0.08	
ARM psr	7 psr	20	182.8	19.2	36.8	8.2	25.1	69.4	211.7	275.3	7.2	335.6	13.0	285.0	51.6	76.8	34.9	176.8	13.9	89	72	137.8	1.59	5.75	0.46	1.75	10.29	0.58	
ARM psr	8 psr	21	327.2	16.9	56.2	2.3	207.1	58.8	126.5	65.5	25.4	197.5	2.2	251.1	58.4	62.1	33.3	154.8	4.2	248	75	112.0	1.56	2.25	0.45	0.81	3.57	0.29	
ARM ps	1 ps	1	159.0	10.6	41.8	4.6	249.2	1.5	162.0	347.4	79.3	329.1	5.2	158.5	74.1	0.2	14.8	268.8	5.7	264	85	130.6	2.03	3.88	0.71	1.36	8.15	0.31	
ARM ps	2 ps	6	161.7	3.9	5.4	6.1	67.8	44.7	24.5	255.6	45.0	32.9	12.3	342.8	83.0	135.6	6.2	225.9	3.2	245	84	16.4	1.35	4.49	0.30	1.50	6.88	0.67	
ARM plr	1 plr	1	324.6	39.3	239.4	3.1	102.7	42.3	917.4	214.8	22.4	961.5	20.6	324.6	39.3	102.7	42.3	214.8	22.4	H		595.5	1.05	3.83	0.05	1.34	4.85	0.93	
ARM plr	2 plr	2	139.6	35.1	66.6	4.2	339.4	53.2	313.6	236.4	9.5	374.2	17.3	139.6	35.1	339.4	53.2	236.4	9.5	H		198.5	1.19	4.71	0.18	1.55	6.68	0.80	
ARM plr	3 plr	3	127.4	36.8	45.4	3.6	7.5	33.6	413.3	249.4	35.3	462.5	7.7	127.4	36.8	7.5	33.6	249.4	35.3	H		205.5	1.12	9.11	0.11	2.21	13.71	0.90	
ARM plr	4 plr	5	145.0	38.0	26.0	3.5	1.7	45.7	185.4	250.8	19.2	235.7	20.2	145.0	38.0	1.7	45.7	250.8	19.2	H		104.3	1.27	7.14	0.24	1.97	11.25	0.78	
ARM plr	5 plr	6	129.5	40.7	23.2	5.9	340.6	44.9	71.3	233.9	16.1	90.6	21.4	129.5	40.7	340.6	44.9	233.9	16.1	H		53.1	1.27	3.07	0.24	1.12	4.29	0.65	
ARM plr	6 plr	7	137.9	37.7	31.6	4.3	340.4	50.1	110.2	236.7	11.2	124.1	25.5	137.9	37.7	340.4	50.1	236.7	11.2	H		75.6	1.13	3.49	0.12	1.25	4.55	0.83	
ARM plr	7 plr	11	134.1	23.4	19.9	2.2	3.9	56.2	54.6	234.7	23.0	61.1	48.9	134.1	23.4	3.9	56.2	234.7	23.0	H		40.5	1.12	2.74	0.11	1.01	3.44	0.80	max
ARM plr	8 plr	12	139.8	29.7	9.9	14.4	7.3	49.8	26.5	244.8	24.5	34.7	43.7	139.8	29.7	7.3	49.8	244.8	24.5	H		20.9	1.31	2.68	0.27	0.99	3.74	0.57	max
ARM plr	9 plr	13	147.6	21.3	8.9	13.9	247.7	24.3	19.2	21.2	56.8	24.1	27.7	147.6	21.3	247.7	24.3	21.2	56.8	H		16.0	1.26	2.16	0.23	0.77	2.84	0.54	
ARM plr	10 plr	b	141.1	40.3	28.4	3.7	15.7	34.3	84.8	261.6	30.8	108.6	4.9	141.1	40.3	15.7	34.3	261.6	30.8	H		63.9	1.28	2.99	0.25	1.09	4.17	0.63	
ARM plr	11 plr	d	145.0	34.9	33.5	3.5	14.0	43.3	132.1	255.6	26.8	150.9	6.3	145.0	34.9	14.0	43.3	255.6	26.8	H		87.5	1.14	3.94	0.13	1.37	5.29	0.82	
ARM plr	12 plr	e	141.0	39.3	23.4	5.4	8.5	39.5	73.5	254.7	26.1	91.9	33.8	141.0	39.3	8.5	39.5	254.7	26.1	H		54.1	1.25	3.14	0.22	1.14	4.33	0.67	max
ARM plr	13 plr	f	149.4	36.2	31.1	3.3	11.1	45.5	109.2	256.7	22.1	139.6	5.8	149.4	36.2	11.1	45.5	256.7	22.1	H		78.0	1.28	3.51	0.25	1.26	5.01	0.67	
ARM plr	14 plr	g	128.8	37.0	40.3	4.2	339.8	48.7	136.3	231.0	15.8	160.7	13.0	128.8	37.0	339.8	48.7	231.0	15.8	H		95.9	1.18	3.39	0.16	1.22	4.54	0.76	
ARM plr	15 plr	h	142.3	30.3	9.3	6.7	17.7	44.1	30.4	252.6	30.7	34.9	60.5	142.3	30.3	17.7	44.1	252.6	30.7	H		21.4	1.15	3.28	0.14	1.19	4.30	0.79	max
ARM plr	16 plr	i	134.2	36.1	33.4	3.4	352.1	47.2	306.1	239.4	19.7	366.1	9.8	134.2	36.1	352.1	47.2	239.4	19.7	H		155.3	1.20	9.16	0.18	2.22	14.40	0.85	
ARM plr	17 plr	k	332.7	36.3	24.0	4.1	100.4	39.7	103.4	218.3	29.4	107.7	61.7	332.7	36.3	100.4	39.7	218.3	29.4	H		64.4	1.04	4.31	0.04	1.46	5.54	0.95	max
ARM plr	18 plr	l	141.9	36.7	49.5	2.3	333.2	52.7	152.5	236.0	5.5	174.0	18.2	141.9	36.7	333.2	52.7	236.0	5.5	H		109.5	1.14	3.08	0.13	1.13	3.98	0.79	

## Appendix C

### Petrographic data and magnetic mineralogy data

#### 1. Thermomagnetic curves in zero field for SIRM:

Kashabowie - Huronian Lake: TW1,RS1.3,TWR3.5,TWR4.1 -  
metavolcanics; TWR10.5 - metasediment in the Quetico Belt.

Atikokan - Huronian Lake: TWA5,TWC1,TWE6A,TW8 - pyrrhotite  
in metasediments; TWA15 - magnetite in amphibolite (3  
pieces);

Calm Lake - Perch Lake: PSB38,PSR1,PSS17,PST63 -  
pyrrhotite.

#### 2. Thermomagnetic curves in high field for $M_s$ (Curie balance), 2 curves during heating - cooling cycle:

Kashabowie - Huronian Lake: TWR4.1 - felsic rhyolite;

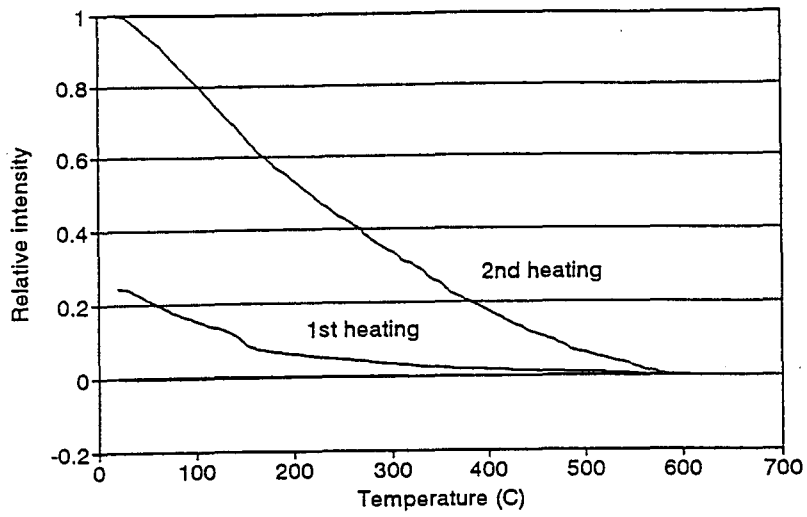
Atikokan - Huronian Lake: TW8 - biotite schist, TWE6A -  
migmatite, TWA15 - amphibolite;

#### 3. Susceptibility changes monitored after heating during step- wise thermal demagnetization

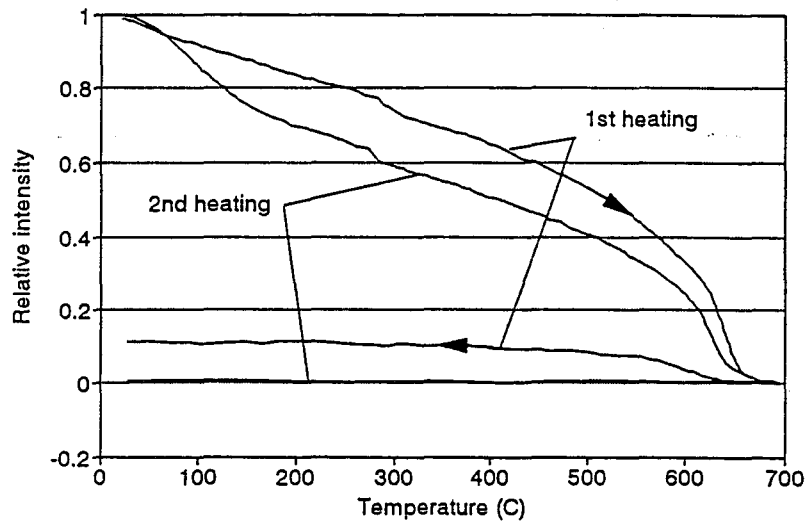
- see diagrams for descriptions

Thermomagnetic curves in zero field for SIRM:

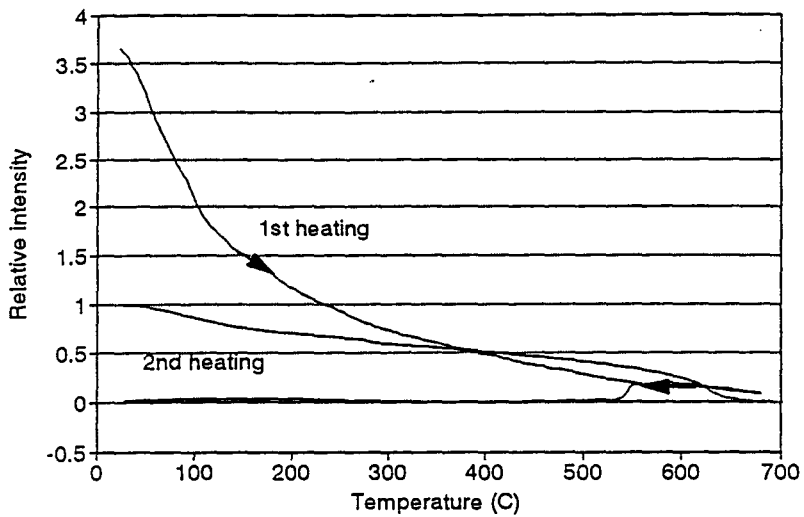
Thermomagnetic curves for SIRM  
Kashabowie - Huronian - sample TW1



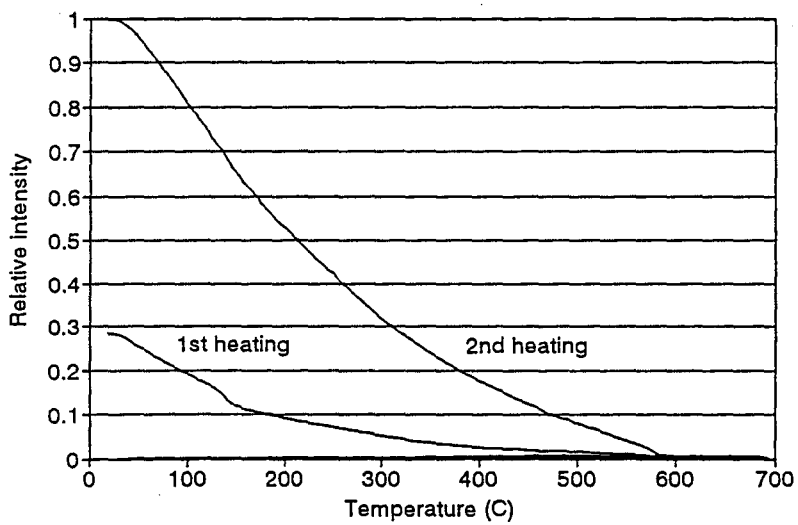
Thermomagnetic curves for SIRM  
Kashabowie - Huronian - sample RS1.3



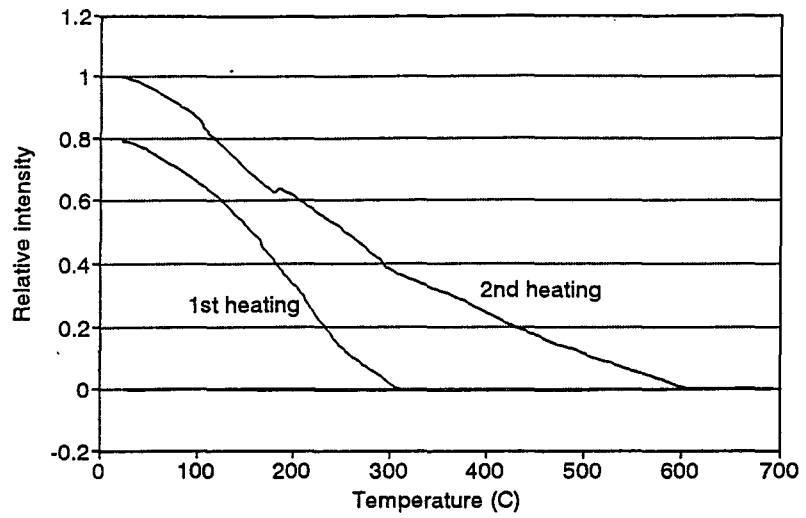
Thermomagnetic curves for SIRM  
Kashabowie - Huronian - sample TWR3.5



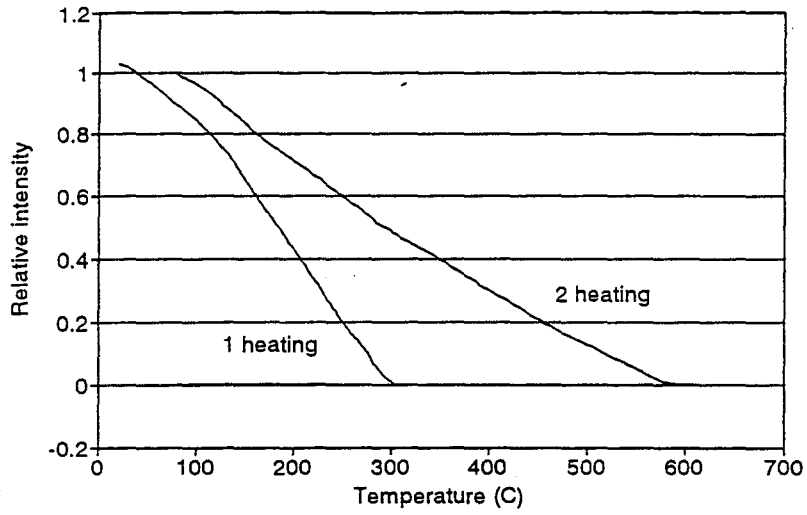
Thermomagnetic curves for SIRM  
Kashabowie - Huronian - sample TWR4.1



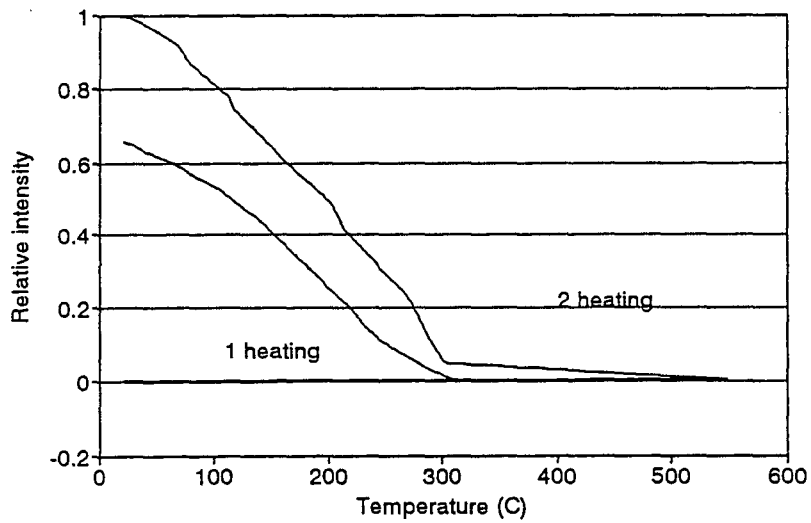
Thermomagnetic curves for SIRM  
Kashabowie - Huronian - sample TWR10.5



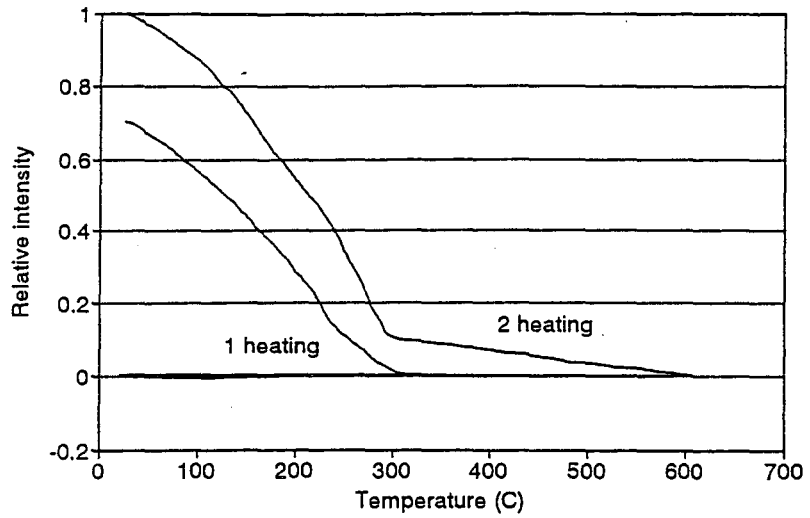
Thermomagnetic curves for SIRM  
2 heatings - sample TWC 1



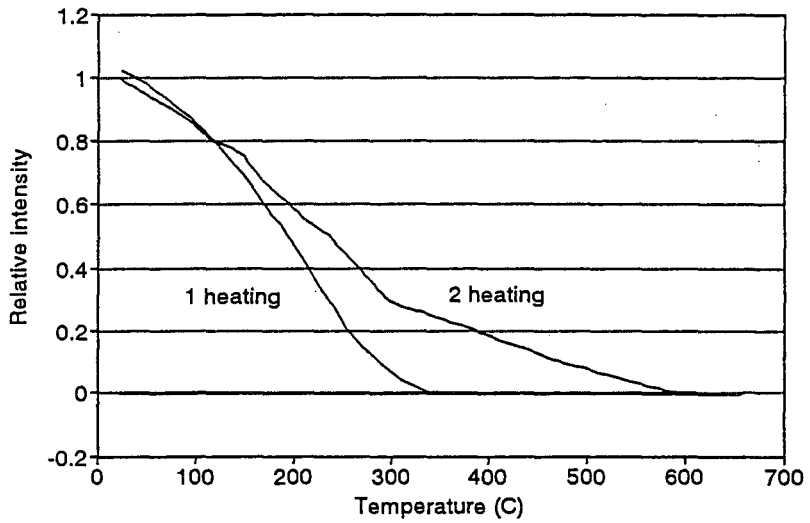
Thermomagnetic curves for SIRM  
2 heatings - sample TWE 6A



Thermomagnetic curves for SIRM  
2 heatings - sample TW 8

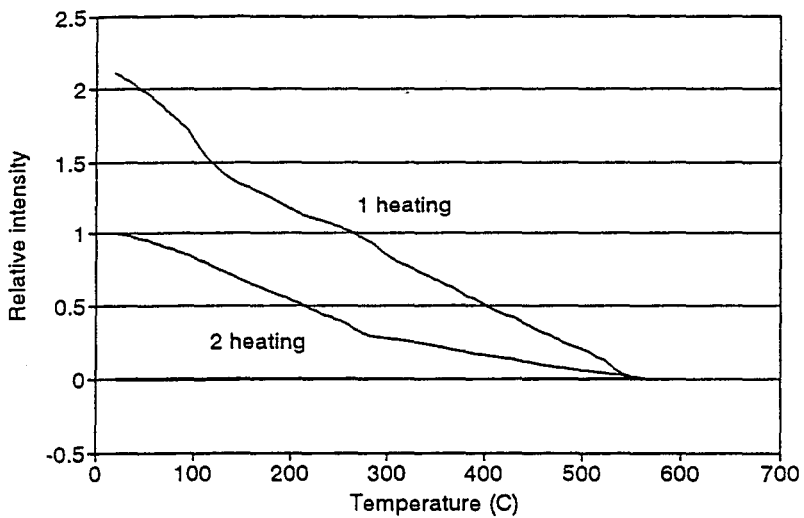


Thermomagnetic curves for SIRM  
2 heatings - sample TWA 5

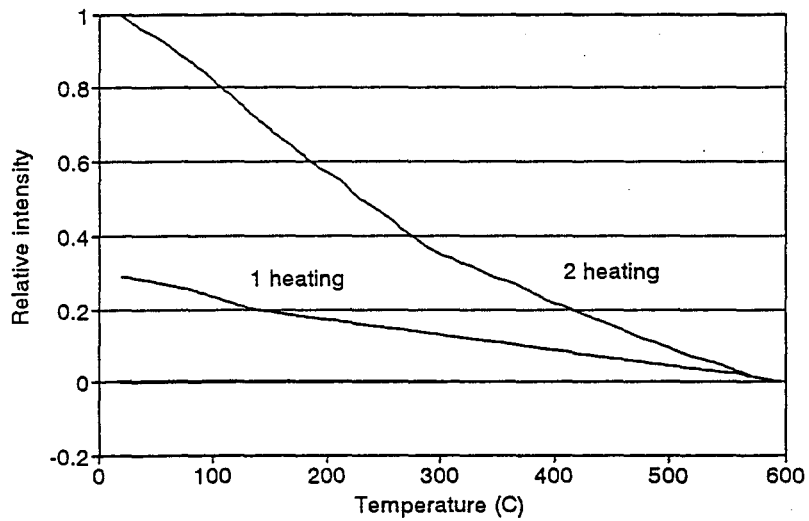




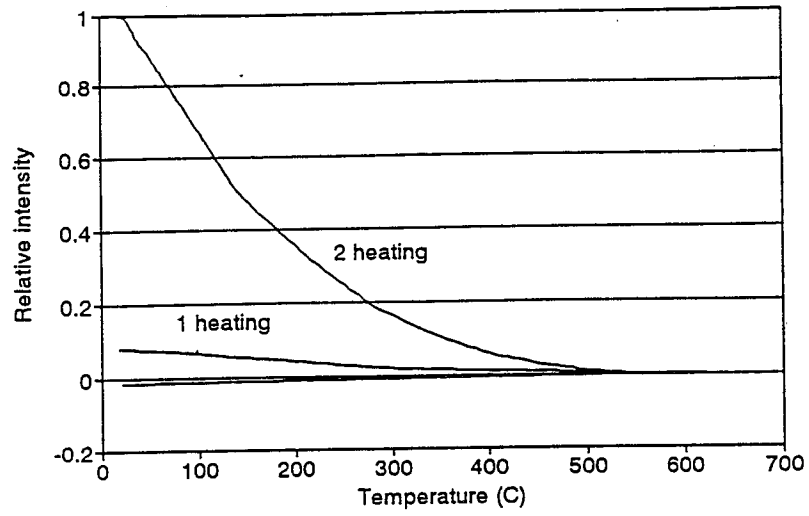
Thermomagnetic curves for SIRM  
2 heatings - sample TWA 15 -1



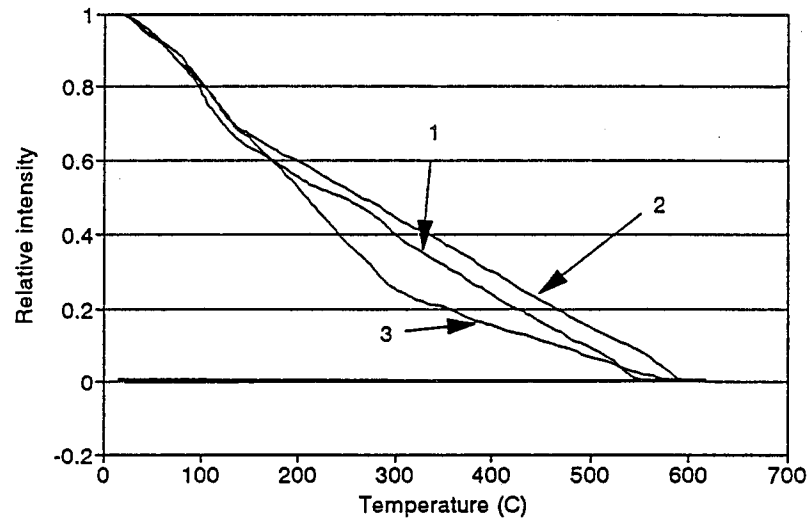
Thermomagnetic curves for SIRM  
2 heatings - sample TWA 15 - 2



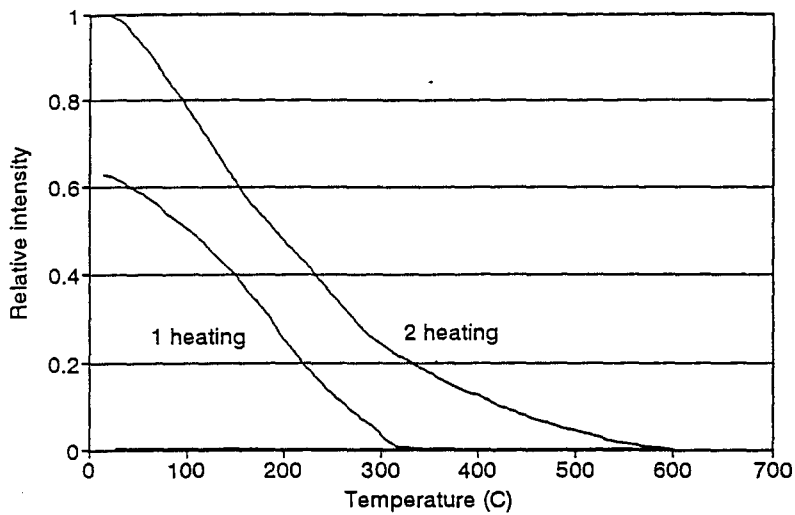
Thermomagnetic curves for SIRM  
2 heatings - sample TWA 15 - 3



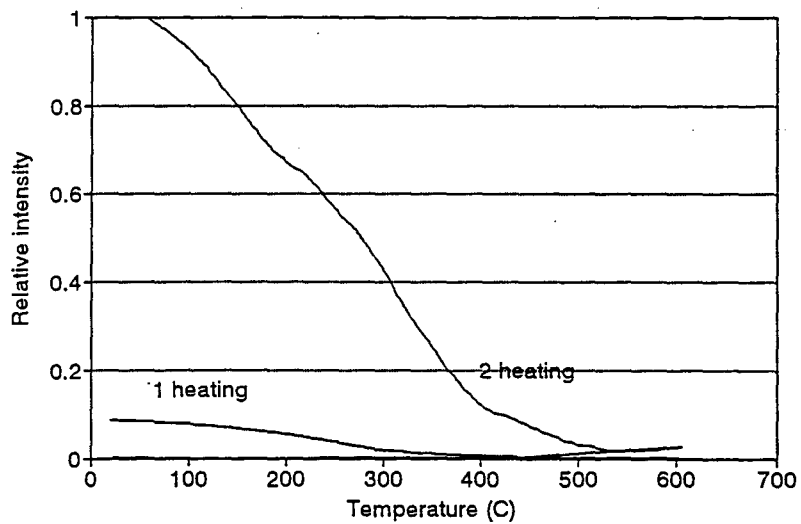
Thermomagnetic curves for SIRM  
Sample TWA15 - 3 pieces - 1 heating



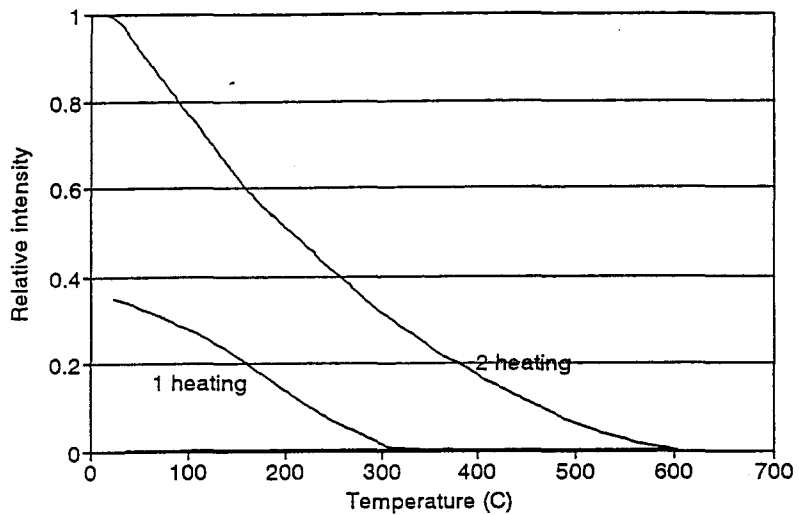
Thermomagnetic curves for SIRM  
Sample: PSB38



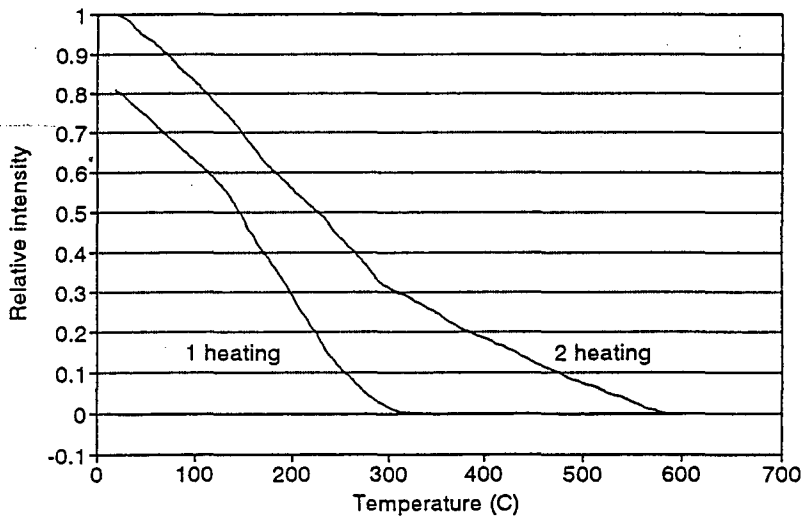
Thermomagnetic curves for SIRM  
Sample: PSR 1



Thermomagnetic curves for SIRM  
Sample: PSS 17

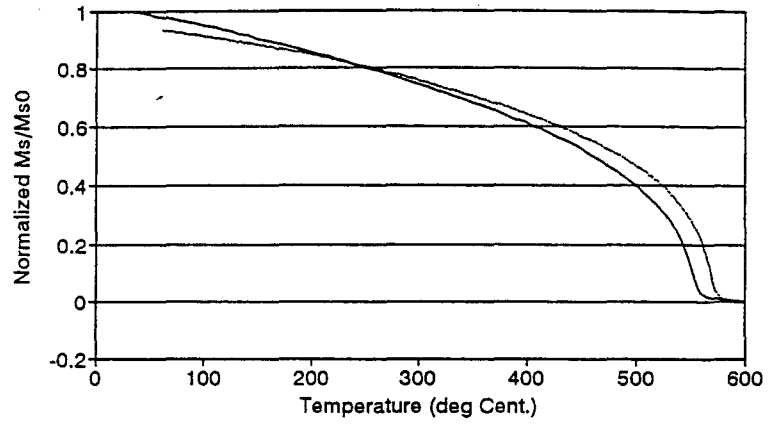


Thermomagnetic curves for SIRM  
Sample: PST 63



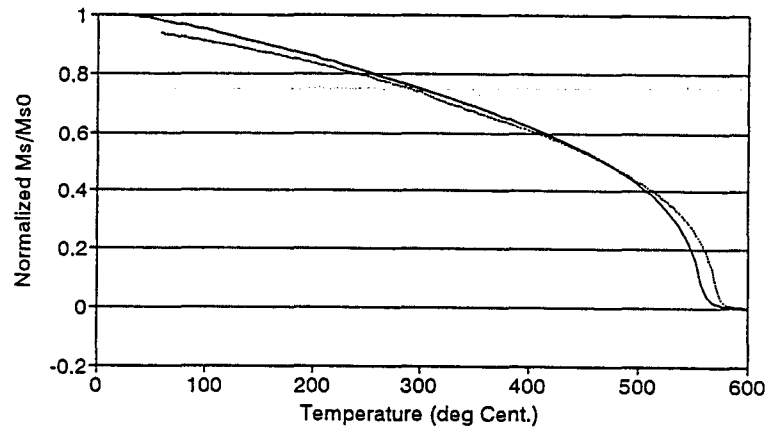
Thermomagnetic curves in high field for  $M_s$  (Curie balance), 2  
curves during heating - cooling cycle:

Ms changes during 1 cycle: heat. - cool  
Sample TWR4.1



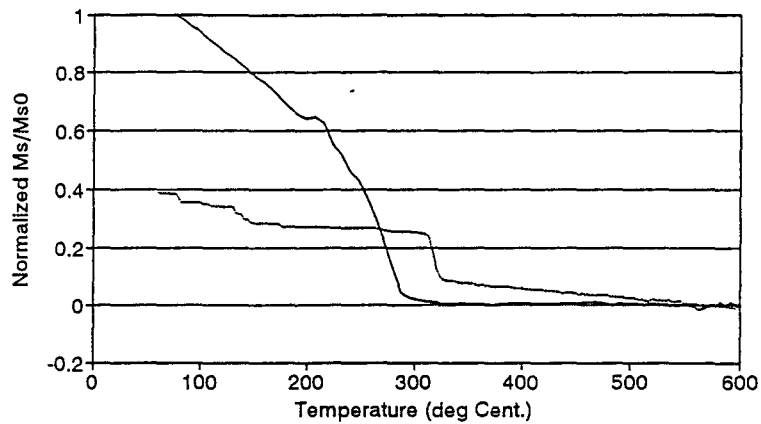
— 1st - heating — 1st - cooling

Ms changes during 1 cycle: heat. - cool  
Sample TWA15



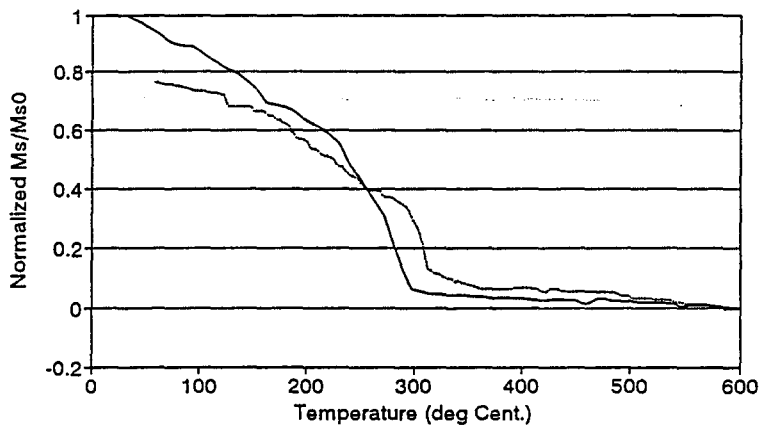
— 1st - heating — 1st - cooling

Ms changes during 1 cycle: heat. - cool  
Sample TWE6A



— 1st - heating — 1st - cooling

Ms changes during 1 cycle: heat. - cool  
Sample TW8

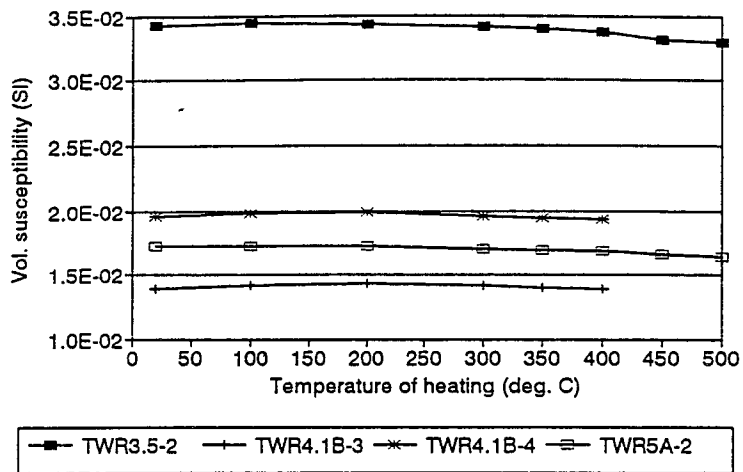


— 1st - heating — 1st - cooling

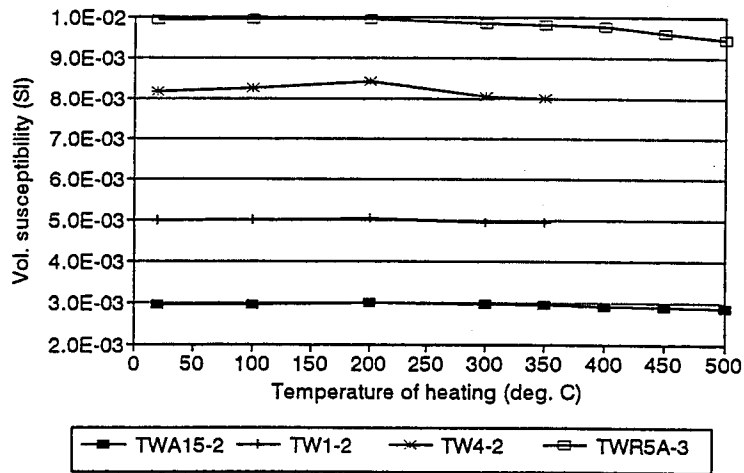
Susceptibility changes monitored after heating during step-wise thermal demagnetization



### Susceptibility changes after heating

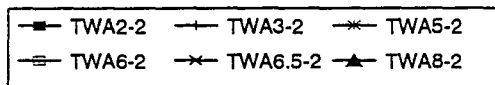
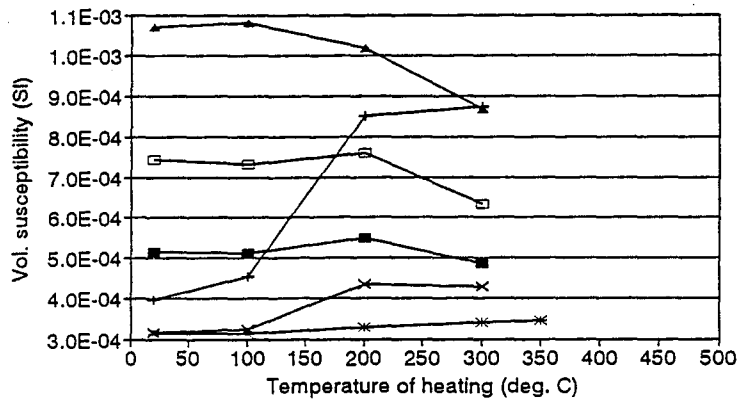


### Susceptibility changes after heating

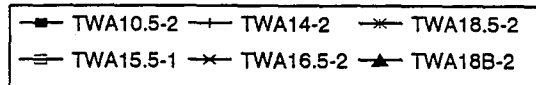
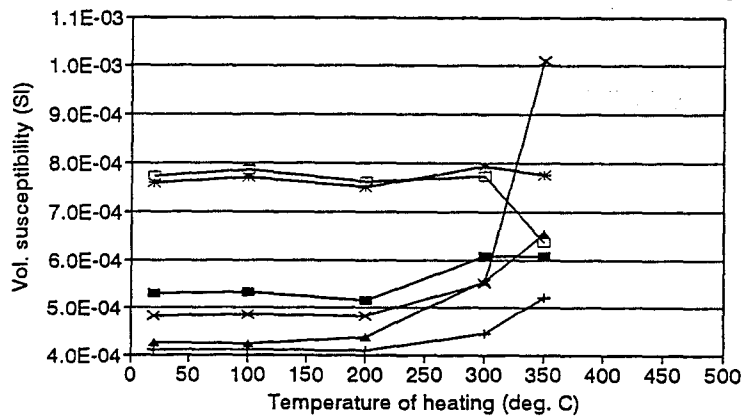


Metasediments from the Quetico Belt

### Susceptibility changes after heating

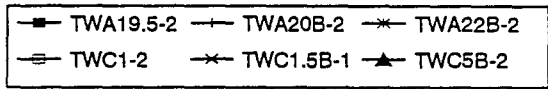
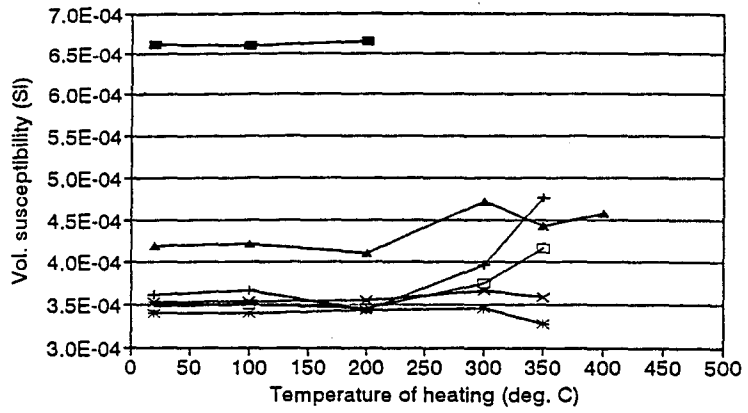


### Susceptibility changes after heating

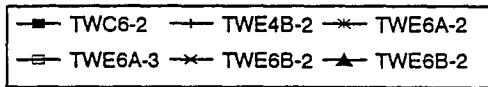
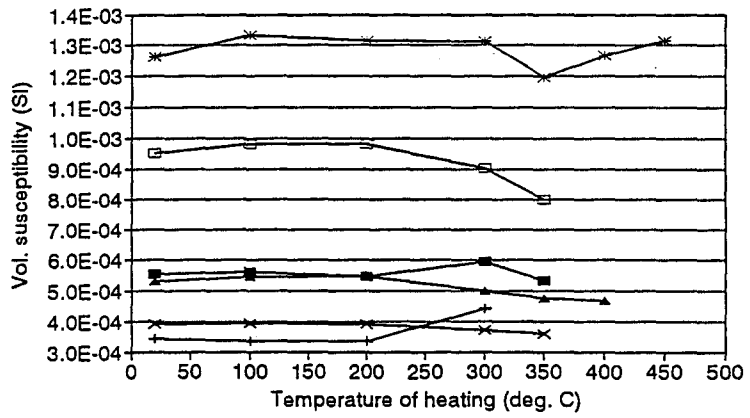


Metasediments from the Quetico Belt

### Susceptibility changes after heating

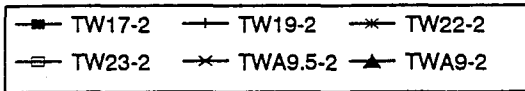
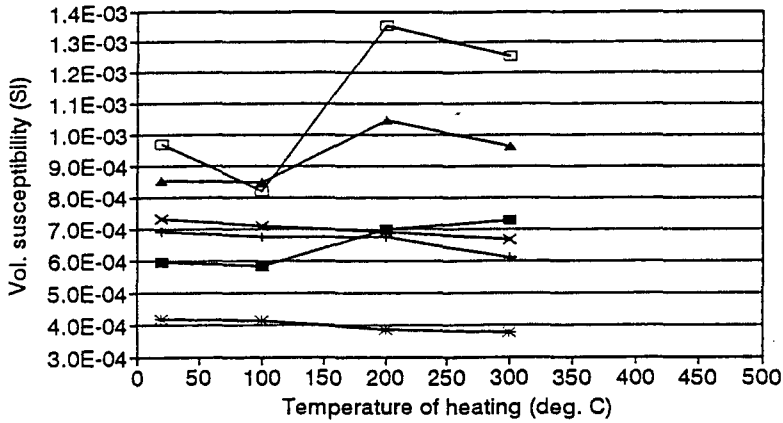


### Susceptibility changes after heating

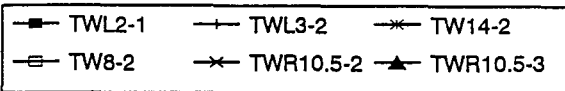
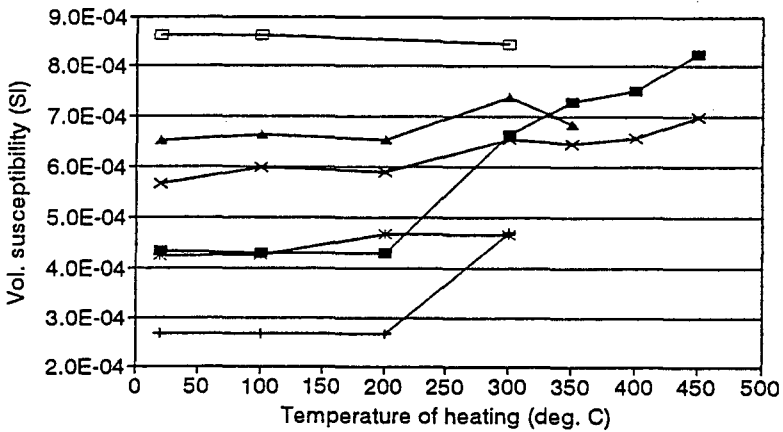


Metasediments from the Quetico Belt

### Susceptibility changes after heating



### Susceptibility changes after heating



Metavolcanics from Shebandowan belt  
(except TW4 - metasedimentary)

## Appendix D

### Natural remanent magnetization (NRM) studies data

A set of table for samples from each of three areas.

1. Initial NRM : declination (optional), inclination (optional), intensity, treatment (AF or thermal demagnetization).
2. Lines fitted to demagnetization path by Kirschvink's algorithm - AF treatment and thermal treatment.

Note that lines classified as C were rejected from further analysis.

ALL SAMPLES FROM KASHABOWIE - HURONIAN TRAVERSE - NRM INTENSITY

Sample	NRM int (mA/m)	NRM dem file	Sample	NRM int (mA/m)	NRM dem file	Sample	NRM int (mA/m)	NRM dem file
TW 1-1	52.87	TW 01-1	A TWR 6.1-2	3.92		RS 10.6	0.22	RS 10P6 .SPN A
TW 1-2	14.95	TW 1-2	T RS 6.2-1	34.09	RS 6P2-1 .SPN A	RS 10.65-2	0.94	RS 10P652 .SPN A
RS 1.1	616.13	RS 1P1 .SPN	A RS 6.2-3	0.30	RS 6P2-3 .SPN A	RS 10.7	0.51	RS 10P7 .SPN A
RS 1.2	0.55	RS 1P2 .SPN	A RS 7-1	0.12	RS 7-1 .SPN A			
RS 1.2-2C			RST 7-1A	0.13		TWR 10.8-1	0.49	
TW 2A-1	0.65		RST 7-1B	0.60		TWR 10.8-2	0.32	
TW 2B-1	0.56		RST 7-1C	0.37		TWR 10.8-3	153.76	
TW 2B-2	6.27		RST 7-1D	0.54		TWR 10.8-4	1.01	
RS 1.3	1.08	RS 1P3 .SPN	A RS 7-2	0.31	RS 7-2 .SPN A	TWR 10.8-5	0.9	
TWR 1.3A	20.54	RS 1P3A	A RST 7-2A	0.59		RS 10.9	56.76	RS 10P9 .SPN A
TWR 1.3B	15.14		RST 7-2B	1.16				
RS 1.31	0.20	RS 1P31 .SPN	A RS 7.1	1.98	RS 7P1 .SPN A	RS 11-1	0.31	RS 11-1 .SPN A
RST 1.31A	0.35		RST 8-1	1.38		RST 11-1A	0.24	
RST 1.31B	0.40		RST 8-2	2.66	RS 8-2 .SPN A	RST 11-1B	0.12	
RST 1.31C	0.16		RS 8.0	13.07	RS 8P0 .SPN A	RS 11.1-1	235.09	RS 11P1-1 .SPN A
TWR 1.32-1A	0.23		RS 8C			RST 11.1-1A	34.31	
TWR 1.32-1B	0.24		RST 8C-1	1.28		RST 11.1-1B	46.31	
TWR 1.32-1C	0.23		TWR 8.05-1	55.81	TWR 8P051	A RS 11.2-1	0.61	RS 11P2-1 .SPN A
TWR 1.32-1D	0.26		RS 8.1	1014.95	RS 8P1 .SPN A	RST 11.2-1A	0.18	
RS 2C	0.64	RS 2C .SPN	A RST 9C	48.77	RS 9C .SPN A	RST 11.2-1B	0.18	
RST 2CA	0.75	RS 2CA .SPN	RS 9.1	2.35	RS 9P1 .SPN A	RST 11.2-1C	0.12	
RS 2.1	1.80	RS 2P1 .SPN	A RST 9.1A	210.83		RST 11.2-1D	0.51	
RST 2.1A	2.13		RST 9.1B	214.04		TWR 11.25-1	0.29	
RST 2.1B	2.67		RS 9.1S	316.06	RS 9P1S .SPN A	TWR 11.25-2	0.13	
RST 2.1C	3.28		RS 9.2	1.00	RS 9P2 .SPN A	RS 11.3	11.46	RS 11P3 .SPN A
RST 2.1D	3.08		RS 9.2-1	1.06	RS 9P2-1 .SPN A	A RST 11.3A	3.80	
TWR 2.2-1	435.53	TWR 2P2-1	A RS 9.2-2	109.35	RS 9P2-2 .SPN A	RST 11.3B	7.42	
TWR 2.2-2	1.26		RST 9.2-2A	107.25		RST 11.3C	0.60	
RST 3A	3.58		RST 9.2-2B	64.42		RS 11.35	81.25	RS 11P35 .SPN A
RST 3B	2.34		RST 9.2-2C	82.23		RST 11.35A	71.08	RS 11P35A .SPN A
RST 3C	3.66	RS 3C .SPN	A RST 9.2-2D	120.81		RS 11.4-2	73.90	RS 11P4-2 .SPN A
TWR 3.5-1	93.58	TWR 3P5-1	A RS 9.25	7.38	RS 9P25 .SPN A	RST 11.4-2A	18.62	RST 11P42A .SPN A
TWR 3.5-2	110.64	TWR 3P5-2	T RST 9.25A	3.25		RST 11.4A	0.21	
TWR 3.6-1	0.77		RST 9.25B	4.89		RST 11.4B	0.16	
TWR 3.7A-1	0.17		RS 9.3	3.83	RS 9P3 .SPN A	RS 11.45	14.24	RS 11P45 .SPN A
TWR 3.7A-2	0.51		RS 9.4	118.05	RS 9P4 .SPN A	RST 11.45A	9.79	
TWR 3.7B-1	0.32		TWR 9.4-1	1.15		RS 11.5	16.77	RS 11P5 .SPN A
TWR 3.7B-2	0.22		TWR 9.4-2	0.95		RST 11.5A	16.62	
TWR 4.1A-1	2.19		TWR 9.4-3	1.55		RST 11.5B	25.79	
TWR 4.1A-2	6.42		TWR 9.4-4	7.52		RST 11.5C	11.77	
TWR 4.1B-1	322.27	TWR 4P1B1	A			RST 11.5D	16.91	
TWR 4.1B-2	251.8		TWR 10-1	0.42		RS 11.6-1	2.12	RS 11P6-1 .SPN A
TWR 4.1B-3	170.16	TWR 4P1B3	T TWR 10-2	0.51		RST 11.6-1A	1.59	
TWR 4.1B-4	191.32	TWR 4P1B4	T RS 10.05	1.29	RS 10P05 .SPN A	RST 11.6-1B	2.44	
RST 4.2A	3.38		RS 10.1	66.81	RS 10P1 .SPN A	RST 11.6-1C	4.66	
RST 4.2B	4.05		RS 10.15	6.25	RS 10P15 .SPN A	RS 11.6-2	0.74	RS 11P6-2 .SPN
RST 4.2C	2.35					RST 11.7-1A	130.26	
RST 4.2D	2.22		RS 10.2	1591.65	RS 10P2 .SPN A	A RST 11.7-3A	0.48	
RST 4.2E	5.83		RS 10.3	5981.70	RS 10P3 .SPN A	RST 11.7-3B	0.35	
TWR 5A-1	164.32	TWR 5A-1	A TWR 10.3-1	5.99		RST 11.7-3C	0.38	
TWR 5A-2	218.98	TWR 5A-2	T TWR 10.3-2	8		RST 11.7-3D	0.28	
TWR 5A-3	113.53	TWR 5A-3	T RS 10.4	6.77	RS 10P4 .SPN A	RS 11.8-1	0.97	RS 11P8-1 .SPN A
TWR 5B-1	2.3		TW 3-1	0.21		RST 11.8-1A	0.32	RST 11P81A .SPN
TWR 5B-2	4.91		TW 3-2	0.5		RS 11.9	2.93	RS 11P9 .SPN A
TWR 6.1-1	4.08		RS 10.41-1	0.81	RS 10P411 .SPN A	A RST 11.9A	0.94	RST 11P9A .SPN
			RS 10.45	10.04	RS 10P45 .SPN A	A RS 12.1	6.39	RS 12P1 .SPN A
			TWR 10.5-1	112.68	TWR 10P51	A TW 4-1	17.26	TW 04-1 A
			TWR 10.5-2	106.47	TWR 10P52	T	38	TW 4-2 T
			TWR 10.5-3	34.87	TWR 10P53	T		
			RS 10.55	42.77	RS 10P55 .SPN A	A		

A - demagnetized by AF field  
T - demagnetized by heating

Initial Natural Remanent Magnetization for samples from the interior of Quetico Belt

Sample	Dec	Inc	Int	Treatment	Sample	Dec	Inc	Int	Treat	Sample	Dec	Inc	Int	Treatment
TWA 05-1	241.5	-8.4	312.2	A	TWA 18.5A-1	28.5	66.4	1.9	TWE	06B-1	299.1	-29.4	210.2	A
TWA 05-2	241.0	-6.1	298.4	T	TWA 18.5-1	216.3	-26.2	112.1	A	TWE 06B-2	302.9	-31.5	185.3	T
TWA 06-1	235.1	62.8	365.9	A	TWA 18.5A-2	320.1	76.1	2.9	TWE	06A-2	294.5	67.4	299.7	T
TWA 06-2	238.3	77.2	490.2	T	TWA 18.5-2	199.0	-29.1	135.7	T	TWE 06A-3	310.9	70.3	208.6	T
TWA 04-1	190.4	80.3	1.0		TWA 19-1	281.3	-88.1	0.5	TWE	06B-3	297.3	-38.5	317.1	T
TWA 04-2	129.4	70.5	0.9		TWA 19-2	161.1	78.1	0.7	TW	23-1	200.8	74.6	118.9	A
TWA 04-3	159.2	71.3	1.3		TWL 10-1	0.0	53.4	0.4	TW	23-2	250.0	35.4	95.5	T
TWA 02-1	86.2	-79.9	210.7	A	TWL 10-2	208.9	-55.1	0.3	TW	22-1	111.8	-1.0	21.6	A
TWA 02-2	87.5	-45.2	186.5	T	TWA 19.5-1	150.0	63.4	3.0	TW	22-2	112.3	-11.6	214.5	T
TWA 03-1	17.3	66.4	2.9		TWA 19.5-2	134.3	86.7	4.3	T	TW 21A-1	67.9	71.3	0.5	
TWA 03-2	119.9	-75.6	12.1	T	TWL 09-1	85.6	33.3	3.1	TW	21-1	147.5	68.5	1.8	
TWA 06.5-1	56.5	82.3	4.4		TWA 20A-1	161.8	-32.0	0.4	TW	21A-2	248.1	37.7	0.6	
TWA 06.5-2	310.0	72.9	6.4	T	TWA 20B-1	83.1	62.0	27.8	A	TW 21-2	177.5	52.2	1.5	
TWA 01-1	79.9	60.0	106.3	A	TWA 20B-2	275.8	80.5	36.7	T	TW 20-1	338.9	39.2	1.1	
TWA 01-2	83.4	51.5	194.2		TWA 20A-2	213.1	67.0	2.0	TW	20-2	85.3	62.3	0.6	
TWA 07-1	96.7	32.5	375.5	A	TWA 21-1	282.9	8.9	1.3	TW	19-1	28.5	48.8	384.8	A
TWA 07.5-1	281.3	81.5	0.6		TWA 21-2	75.5	7.9	1.7	TW	19-2	36.6	41.1	347.9	T
TWA 07.5-2	255.1	71.1	0.4		TWA 22-1	294.6	18.2	4.9	TWL	05-1	55.5	66.7	5.6	T
TWA 08-1	249.0	64.9	260.9	A	TWA 22A-1	45.1	75.4	8.9	TWL	05-2	52.0	50.0	10.5	
TWA 08-2	252.9	64.1	274.2	T	TWA 22-2	146.4	29.3	2.1	TW	18-1	287.5	54.6	0.2	
TWA 09-1	261.0	-6.4	713.0	A	TWA 22A-2	354.7	12.3	7.4	T	TW 18-2	255.5	9.2	0.1	
TWA 09-2	255.9	-10.4	781.0	T	TWA 22.5-1	244.1	74.9	0.7	TW	17-1	12.2	47.5	63.9	
TWA 09.5-1	266.4	49.9	81.6	A	TWA 22.5-2	168.0	41.6	0.4	TW	17-2	18.4	68.4	102.0	T
TWA 09.5-2	351.1	80.3	89.7	T	TWC 06-1	73.0	20.5	201.3	A	TW 16-1	2.5	73.7	0.4	
TWA 10-1	346.3	15.6	32.2	A	TWC 06A-1	256.9	-13.1	0.3	TW	16-2	240.0	-9.7	0.4	
TWA 10-2	233.1	49.0	0.1		TWC 06A-2	266.2	-20.1	0.1	TW	15-1	357.3	77.5	45.8	A
TWA 10.5-1	86.4	10.0	350.0	A	TWC 06-2	348.2	-17.6	22.2	T	TWL 04-1	313.0	38.6	1.3	
TWA 10.5-2	83.7	6.2	501.1	T	TWC 05B-1	274.6	-18.4	22.6	A	TW 14-1	276.2	77.8	108.0	A
TWA 11-1	270.1	45.0	0.1		TWC 05C-1	60.4	73.3	5.6	TW	14-2	324.6	79.5	105.5	T
TWA 11-2	198.1	-20.1	1.1		TWC 05A-1	357.3	-7.8	1.9	TW	13-1	142.1	35.6	0.8	
TWA 11.5-1	266.2	53.8	1.9		TWC 05B-2	302.9	31.5	31.8	T	TW 13-2	22.1	-63.9	0.7	
TWA 11.5-2	215.5	36.5	2.1		TWC 05A-2	299.4	-68.3	26.6	A	TW 12C-1	276.0	31.4	5.5	
TWA 12-1	304.5	51.3	0.7		TWC 04-1	280.9	-43.8	0.5	TW	12C-2	96.7	-15.3	2.2	
TWA 12-2	274.5	76.5	1.4		TWC 04-2	196.3	-57.1	0.5	TW	12A-1	219.9	73.5	3.5	A
TWA 13-1	2.9	67.1	1.4		TWL 08-1	101.9	56.6	0.2	TW	12B-1	299.0	30.7	8.2	A
TWA 13-2	219.6	63.9	0.3		TWL 08-2	282.3	61.0	0.2	TW	12C-2	90.9	-15.3	1.5	A
TWA 14-1	32.2	52.0	10.7	A	TWC 03A-1	255.1	6.5	0.4	TW	12A-2	204.9	35.3	3.5	
TWA 14-2	38.3	48.3	10.6	T	TWL 07-1	82.2	5.5	0.5	TW	11-1	246.6	53.1	2.8	A
TWA 15-1	66.6	41.2	227.5	A	TWL 07-2	70.8	32.1	0.6	TW	11-2	202.8	54.1	2.5	
TWA 15-2	67.4	38.0	114.8	T	TWC 02-1	247.2	38.8	0.2	TW	10-1	250.5	44.9	0.6	
TWA 15.5-1	262.3	-45.4	665.4	T	TWC 01.5B-1	252.8	45.1	407.1	T	TW 10-2	290.4	53.3	0.5	
TWA 15.5-2	256.8	-43.4	196.0	A	TWC 01.5A-1	310.4	27.5	0.4	TW	09-1	76.8	38.3	0.4	
TWA 15.9-1	68.4	-77.1	0.9		TWC 01.5B-2	246.3	39.1	248.5	A	TW 09-2	332.8	46.4	1.0	
TWA 15.9-2	196.4	-44.9	2.4		TWC 01-1	58.8	50.5	2178.3	A	TW 08-1	147.8	-76.9	105.5	A
TWA 16-1	17.9	78.7	4.3		TWC 01-2	81.2	53.9	2255.4	T	TW 08-2	160.0	-57.9	85.0	T
TWA 16-2	38.7	59.6	3.0		TWE 01-1	0.0	70.6	0.1	TW	07A-1	349.9	44.2	14.6	A
TWA 16.5-1	323.7	70.1	35.6	A	TWE 01-2	259.6	-4.2	0.4	TW	07B-1	135.0	84.5	0.8	
TWA 16.5-2	16.1	50.7	54.3	T	TWE 02-1	238.6	-56.2	0.2	TW	07B-2	311.3	68.2	0.9	
TWA 17-1	281.3	77.6	0.4		TWE 02-2	141.9	56.8	1.2	TW	07A-2	24.5	57.0	25.0	
TWA 17-2	5.0	36.4	0.1		TWE 03A-1	311.8	68.5	0.9	TWL	03-1	133.6	78.2	4.3	
TWC 07-1	343.7	78.1	4.1		TWE 03B-1	302.3	16.9	6.4	TWL	03-2	207.9	72.9	10.0	T
TWC 07-2	355.1	76.2	4.1		TWE 03A-2	295.5	47.3	0.5	TW	06-1	6.4	-28.3	0.7	
TWA 18B-1	285.6	7.0	51.8	A	TWE 03B-2	305.7	18.9	6.3	T	TW 06-2	208.8	8.7	0.3	
TWA 18A-1	347.5	56.2	0.3		TWE 04B-1	56.2	22.2	7.8	TWL	02-1	61.6	-65.3	571.5	T
TWA 18A-2	316.4	-33.9	1.1		TWE 04A-1	354.8	50.2	1.9	TWL	02-2	76.2	-64.8	645.8	A
TWA 18B-2	258.6	4.7	50.2	T	TWE 04B-2	91.4	70.5	7.8	T	TW 05-1	208.3	72.2	0.6	
			1.9		TWL 06-1	82.7	77.3	2.8	TW	05A-1	323.5	80.8	0.8	
			112.1		TWL 06-2	103.9	78.8	2.7	TW	05-2	194.0	-31.2	0.0	
			2.9		TWE 05-1	351.1	43.2	56.5	A	TW 05A-2	282.5	82.7	0.3	
			135.7		TWE 05-2	49.2	49.4	3.9						
			0.5		TWE 06A-1	300.6	75.2	141.9	A					

Inkital NRM - Calm Lake - Perch Lake area

Sample	Dec	Inc	Int	Trtmnt	Sample	Dec	Inc	Int	Trtmnt	Sample	Dec	Inc	Int	Trtmnt	Sample	Dec	Inc	Int	Trtmnt																																																																																																																																																																																																																																																																																																																																																																																																																																																																																																																																																																																																																																																																																																																																																																																				
<b>PLR series</b>					<b>PST series</b>					<b>OWN COORD</b>					<b>PS series</b>					<b>OWN COORD</b>					<b>PSR series</b>					<b>OWN COORD</b>																																																																																																																																																																																																																																																																																																																																																																																																																																																																																																																																																																																																																																																																																																																																																																									
PLR 01	107.7	71.6	1514.5	A	PST 01	133.5	8.7	324.0	A	PS	PS01	73.1	10.1	202.6	A	PSR 1	104.0	25.1	2.6	PLR 02	289.8	81.6	285.0	A	PST 02	226.3	0.8	2.3	PS	PS02	45.6	-18.6	4.6	PSR 2	35.4	-29.6	2.6	PLR 03	196.6	-7.9	487.8	A	PST 03	81.6	-36.6	14.8	PS	PS03	80.1	9.9	1111.0	T	PSR 3	48.4	15.2	0.3	PLR 04	328.4	61.0	135.3	A	PST 04	340.3	-19.7	279.6	A	PS	PS04	223.6	61.9	9.4	PSR 4	88.0	-3.8	0.8	PLR 05	300.3	52.3	57.6	A	PST 05	226.4	2.4	1.1	PS	PS05	271.9	41.9	1.1	PSR 5	19.7	12.5	132.7	A	PLR 06	289.0	56.7	100.7	A	PST 06	86.2	-20.4	1.0	PS	PS06	84.0	-13.6	132.9	A	PSR 6	326.4	-22.7	0.3	PLR 07	224.8	45.4	15.6	PST 07	76.0	14.1	4.4	<b>F2 series</b>					PSR 7	53.8	-17.7	27.5	A	PLR 08	289.8	82.2	1.8	PST 08	255.8	14.9	128.2	T	F2 1	28.1	-43.2	1736.0	A	PSR 8	230.2	-2.7	65.9	T	PLR 09	140.3	-76.3	1540.6	T	PST 09	251.1	-9.3	86.8	A	F2 3	26.3	-40.4	2981.7	A	PSR 9	261.2	50.3	0.7	PLR 10	137.0	-72.2	381.0	A	PST 10	283.9	4.5	113.9	A	F2 4	12.8	-34.1	3486.2	A	PSR 10	268.9	-10.3	148.8	A	PLR 11	135.6	-72.5	232.5	A	PST 11	305.8	-0.8	86.6	A	F2 5	18.2	-36.5	4379.2	A	PSR 11	322.9	-77.9	1.0	PLR 12	144.9	-70.6	130.1	A	PST 12	71.9	3.6	77.7	A	<b>F1 series</b>					PSR 12	12.9	-25.3	0.5	PLR 13	70.5	73.5	1.3	PST 13	328.6	-11.3	11813.1	A	F1 1	196.7	-81.0	16.8	PSR 13	283.6	-23.1	0.5	PLR 14	289.2	86.8	1.1	PST 14	169.3	2.3	129.0	T	F1 2	352.4	78.4	101.5	A	PSR 14	308.1	7.9	2.1	PLR 15	280.7	32.7	104.9	A	PST 15	38.9	43.4	0.9	F1 3	0.6	75.2	20.4	A	PSR 15	357.1	39.1	90.0	A	PLR B	281.5	55.1	93.8	T	PST 16	94.2	-9.7	0.5	F1 4	348.0	9.6	3.6	PSR 16	23.0	-10.4	0.2	PLR C	280.3	52.5	134.1	A	PST 17	259.0	31.9	4.8	F1 5	55.2	2.8	12.4	PSR 17	211.7	-30.0	164.7	A	PLR D	289.2	51.7	82.3	A	PST 18	324.9	-11.2	4482.6	A	F1 6	128.2	19.2	121.9	T	PSR 18	179.7	10.0	2893.4	A	PLR E	303.7	84.8	118.9	A	PST 19	104.8	-53.3	3.9	F1 7	104.9	10.1	51.8	A	PSR 19	342.2	5.0	2.3	PLR F	248.3	47.7	108.5	A	PST 20	29.1	-82.4	10.6	F1 8	115.1	13.7	10.7	PSR 20	270.3	-29.2	902.0	A	PLR G	256.1	48.8	22.4	A	PST 21	301.8	60.7	0.2	F1 9	126.1	2.1	167.5	A	PSR 21	108.9	-2.4	174.6	A	PLR HA	270.7	59.3	6.9	PST 22	118.3	-39.2	0.9	F1 10	199.5	53.2	4.1	PSR 22	71.4	-12.4	0.8	PLR I	276.6	57.0	285.1	A	PST 23	62.4	28.8	0.1	F1 11	113.2	78.5	10.8	PSR 23	71.7	9.9	0.9	PLR J	133.2	58.2	95.5	A	PST 24	7.9	-32.4	0.2	F1 12	98.5	-83.2	0.8	PSR 24	21.3	13.5	533.2	T	PLR K	281.6	52.7	185.1	A	PST 25	253.8	-2.5	252.9	A	F1 13	136.4	-34.4	65.6	A	PSR 25	288.9	8.9	0.5	PLR L	280.7	43.9	200.2	T	PST 26	247.0	-36.0	1.3	F1 14	119.1	5.9	465.2	A	PSR 26	322.6	63.0	0.2	<b>PSB series</b>					F1 15	142.9	24.9	208.5	A	PSR 27	313.7	-12.4	12.6	PSS 1	108.4	-18.1	1848.6	A	PSS 2	16.4	4.3	0.7	PSS 3	335.9	0.2	2885.0	A	PSS 4	46.4	-76.3	2.1	PSS 5	185.0	3.2	84.8	T	PSS 6	245.3	3.8	87.2	A	PSS 7	245.7	-46.8	0.3	PSS 8	225.0	-62.1	0.0	PSS 9	106.8	45.3	0.4	PSS 10	10.5	8.7	947.9	A	PSS 11	39.7	22.3	1.2	PSS 12	355.0	96.4	0.7	PSS 13	45.0	-7.6	243.1	T	PSS 14	46.6	7.4	136.2	A	PSS 15	52.2	6.0	5256.4	A	PSS 16	327.7	17.2	123.6	A	PSS 17	103.0	16.7	1.3	PSS 18	75.3	15.9	26.5	A	PSS 19	227.6	-3.3	4.0	PSS 20	185.0	26.9	0.3	PSS 21	57.0	-55.3	86.9	A	PSS 22	94.9	17.3	0.9	PSS 23	188.9	-5.1	98.6	A	PSS 24	137.1	61.8	1.4	PSS 25	258.8	2.4	270.7	A	PSS 26	278.4	20.4	1.5	<b>PSP series</b>					PSP 1	124.2	-81.2	894.8	A	PSP 2	120.3	71.4	0.6	PSP 3	232.4	87.8	2.0	PSP 4	5.8	65.3	1.5	PSP 5	280.7	11.7	700.7	A	PSP 6	25.6	17.0	2.3	PSP 7	63.7	52.3	178.7	A	PSP 8	220.6	50.7	24.4	T	PSP 9	136.6	62.3	504.0	A	PSP 10	24.8	65.8	2.8	PSP 11	250.1	87.9	0.6	PSP 12	137.3	89.5	1.8	PSP 13	43.7	49.8	2.9	PSP 14	15.1	-62.0	1.1	PSP 15	244.5	86.0	3.3	PSP 16	30.1	18.9	0.1	PSP 17	270.2	86.1	0.4	PSP 18	0.0	35.6	0.7	PSP 19	185.4	85.8	8.1	PSP 20	189.8	79.6	47.9	A	PSP 21	284.9	45.0	82.3	A	PSP 22	82.4	69.2	0.9	PSP 23	56.7	80.9	0.8	PSP 24	91.8	88.4	0.8	PSP 25	114.7	84.7	2.7	PSP 26	297.2	-11.9	3056.4	A	PSP 27	332.5	65.6	12.0	PSP 28	82.9	-42.5	1.9	PSP 29	18.4	51.7	0.9	PSP 30	341.8	20.3	0.4	PSP 31	18.4	88.8	1.4	PSP 32	288.6	2.4	4382.7	A	PSP 33	247.6	-36.0	7282.7	T	PSP 34	74.9	-1.2	5286.1	A	PSP 35	321.5	83.1	5.2	PSP 36	27.1	46.8	3.9	PSP 37	277.8	-86.0	14281.8	A



Lines fitted to demagnetization path by Kirschvink's  
algorithm - AF treatment

Traverse Kashabowie - Huronian Lake

NRM directions for RS collection - lines fitted to AF demagnetization paths

Sample	Dec	Inc	H1	H2	No of points	ASD	INT of comp.	Class	Peak AF	Residual NRM in %	MDF
TW1.0-1	248	76.4	0.0	2.0	3	2.9	20	C	40.0	12	5.0
TW1.0-1	61.2	72.6	2.0	7.0	5	2.3	20	B			
RS1.1	310.3	72.9	40.0	190.0	20	3.1	703	A	190.0	4	100.0
RS1.3a-1	279.8	40.6	0.0	25.0	11	4.8	12	B	40.0	19	15.0
RS2.1	353.6	85.7	2.5	15.0	6	8.9	1	C			
RS2.1	300.7	59.7	12.5	30.0	6	5.4	1	B	80.0	10	30.0
RS2.1	330.9	64.4	50.0	80.0	5	5.6	1	C			
RS2.2-1	218.7	-57.1	0.0	15.0	12	2.8	443	A	15.0	6	3.5
RS3C	21.5	66.9	2.5	17.5	7	4.9	3	B	100.0	6	6.0
RS3.5-1	324.9	-9.6	1.0	7.0	6	5.1	79	B	30.0	12	4.5
RS4.1b-1	106.7	86.9	0.0	30.0	16	5.3	254	A	30.0	5	4.5
RS5a-1	276.4	79.7	0.0	15.0	12	2	174	A	15.0	6	3.5
RS6.2-1	310.4	49.4	5.0	200.0	20	2.4	36	A	200.0	5	50.0
RS7.1	167.6	-57.9	1.5	3.5	3	0.9	1	C	10.0	63	10.0
RS8.0	60	53.7	0.0	27.5	13	1.5	1020	A	17.5	8	5.0
RS8.05-1	314.8	-67.1	1.0	17.0	11	5.1	53	A	25.0	20	9.0
RS8.1	61.4	-19.5	2.5	12.5	5	4	12	C	27.5	0.3	3.0
RS9C	58.3	52.8	0.0	160.0	23	1.9	49	A	160.0	5.6	12.5
RS9.1S	90.2	54.1	0.0	20.0	11	5	310	A	22.5	3	2.0
RS9.25	159.7	69.1	0.0	6.0	6	7	5	B	7.5	46	5.0
RS9.2-2	252.2	-30.2	0.0	6.0	6	3.8	79	B	15.0	4	3.5
RS9.2-2	265.2	-5	5.0	8.5	4	4.9	17	C			
RS9.4	71.5	16.5	10.0	40.0	8	6.3	47	B	50.0	14	10.0
RS10.1	49.4	20.3	3.5	22.5	12	6.5	21	B	22.5	10	5.0
RS10.15	71.8	62.8	1.5	12.5	7	6	3	B	30.0	18	10.0
RS10.2	273.8	-25.4	0.0	2.5	3	4.2	437	C	15.0	1.5	4.0
RS10.2	271.5	18.2	2.5	15.0	10	4.1	1220	A			
RS10.3	55	3.9	0.0	100.0	17	2.2	5840	A	100.0	0.6	8.0
RS10.4	201.2	71.3	1.5	17.5	9	8.8	4	B	30.0	73	13.0
RS10.45	10.7	59.4	0.0	10.0	7	7.4	6	B	25.0	44	12.5
RS10.55	262.6	3.8	0.0	110.0	17	2.3	42	A	110.0	3.2	10.0
RS10.5-1	53.2	-41	0.0	7.0	7	3.5	80	B	25.0	32	14.0
RS10.9	304.1	43	0.0	7.5	5	5.2	31	B	17.5	23	10.0
RS11.1-1	312	51.9	0.0	5.0	5	2.5	23	B	10.0	68	10.0
RS11.35	9.9	82.6	0.0	75.0	19	3.9	77	A	75.0	24	12.0
RS11.35A	12.9	81.6	0.0	45.0	18	3.2	66	A	60.0	14.5	12.5
RS11.4-2	9.4	34.4	0.0	15.0	11	5.6	60	A	30.0	10	4.0
RS11.4-2	355.2	57.4	0.0	6.5	6	6.5	21	B	12.5	99	12.5
TW4.0-1	297.2	76.8	1.0	10.0	8	4.4	13	B	20.0	12	4.0

H1,H2 - range of demagnetization path, where lines were fitted

Peak AF - maximum field used in AF demag. before sample were unstable

Residual NRM - Intensity of NRM remained after use of peak AF

A,B,C - my own classification of reliability of NRM directions

ASD - angular standard deviation (error) of fitted lines

Int - intensity of fitted component in mA/m

Lines fitted to AF demagnetization paths for TW collection  
 File: AFtwline.wql

Station	Sample	Kirsch. file	Dec sample	Inc coord	H1	H2	No o points	ASD	INT of comp.	Class	Residual			
											Peak AF	NRM in %	MDF	
TWA1.0	twa1	1	ta01	1	78.5	59.8	6	10	4	5.5	39			
TWA1.0	twa1	1	ta01	1	80.9	43.1	1	5	4	7.5	41	20.0	16	7.0
TWA2.0	twa2	1	ta02	1	270.5	-27.9	5	7	3	4.1	38			
TWA2.0	twa2	1	ta02	1	71.4	-76	0	6	6	4.2	171	12.5	22	2.0
TWA5.0	twa5	1*	ta05	1*	240.9	-7.3	0	130	19	1.9	3250	130.0	1	7.5
TWA6.0	twa6	1	ta06	1	53.6	6.3	8	12	3	4.9	24			
TWA6.0	twa6	1	ta06	1	249.7	69.5	0	10	9	4.9	335	12.5	11	2.0
TWA7.0	twa7	1	ta07	1	90	-2.7	3	10	6	3.6	155			
TWA7.0	twa7	1	ta07	1	122	66.1	0	2	3	3.6	151	17.5	6	3.0
TWA8.0	twa8	1	ta08	1	255.6	61.3	0	12	10	6.8	288	17.5	11	2.0
TWA9.0	twa9	1	ta09	1	262.8	-7.8	0	50	17	2.5	683	60.0	5	5.0
TWA9.5	twa9.5	1	ta09	51	239.3	62.3	3	7	4	4.6	21			
TWA9.5	twa9.5	1	ta09	51	295.7	51.3	1	5	4	8.4	17	12.5	36	6.5
TWA10.	twa10	1	ta10	1	210.5	79.2	8	12	3	8.9	6			
TWA10.	twa10	1	ta10	1	354.6	5.3	1	5	4	5.1	28	20.0	5	3.0
TWA10.	twa10.5	1	ta10	51*	84.5	0.3	1	15	11	2.8	436	15.0	2	3.0
TWA14.	twa14	1	ta14	1	6	56.6	0	12	10	4.5	7	25.0	31	9.0
TWA15.	twa15	1*	ta15	1*	66.7	40.3	0	25	15	2.8	204	25.0	2	3.5
TWA15.	twa15.5	1	ta15	52	67.1	18.4	12	20	3	3.6	15			
TWA15.	twa15.5	1	ta15	52	253.8	-43.7	1	12	9	3.9	191	20.0	16	4.0
TWA16.	twa16.5	1	ta16	51	61.6	65.4	1	3	3	4.3	8	17.5	83	10.0
TWA18.	twa18	b 1	a18b	1	258	-1.5	20	70	7	7.7	19			
TWA18.	twa18	b 1	a18b	1	304.2	-28.8	100	140	3	5.1	4			
TWA18.	twa18	b 1	a18b	1	273.5	8.6	1	6	5	9.7	9	200.0	12	22.0
TWA18.	twa18	b 1	a18b	1	269.2	19.4	8	12	3	4.5	5			
TWA18.	twa18.5	1	ta18	51	213.7	-31	0	8	8	4	86	15.0	7	3.0
TWA20.	twa20	b 1	a20b	1	223.5	69.5	0	6	6	5.1	23	12.5	30	4.0
TWC6.0	twc6	1	tc06	1	84.8	14.9	1	3	3	1	126	12.5	18	3.0
TWC5.0	twc5	a 2	tc5a	2	32.8	-37.8	1	8	7	7.1	21	25.0	27	10.0
TWC5.0	twc5	a 2	tc5a	2	236.1	-48.1	7	12	4	1.6	12			
TWC5.0	twc5	a 2*	tc5a	2*	238.3	-11.8	15	25	5	8.5	17			
TWC5.0	twc5	b 1	tc5b	1	257.4	-11.9	7	10	3	6.5	15			
TWC5.0	twc5	b 1	tc5b	1	350.8	-13.1	1	3	3	2.3	6			
TWC5.0	twc5	b 1	tc5b	1	24.6	8.9	5	7	3	4.2	6	17.5	41	18.0
TWC1.5	twc1.5	b 2	c15b	2	282.4	66.7	17	25	3	8.4	21			
TWC1.5	twc1.5	b 2	c15b	2	202.1	80	8	12	3	6.5	37			
TWC1.5	twc1.5	b 2	c15b	2	249	36.3	1	7	6	3	168	50.0	10	4.5
TWC1.0	twc1	1*	tcw1	1*	58.6	50	0	200	24	1.1	2230	200.0	2	8.0
TWE5.0	twe5	1	te05	1	42.2	63.8	8	12	3	7.7	5			
TWE5.0	twe5	1	te05	1	353.3	43	0	7	6	4	47	15.0	14	3.0
TWE6.0	twe6	a 1	te6a	1	271	70.8	1	3	3	4.2	54	30.0	11	3.0
TWE6.0	twe6	b 1	te6b	1	259.6	-34.9	12	17	3	3.1	15			
TWE6.0	twe6	b 1	te6b	1	303.6	-30.3	0	8	8	4.5	182	15.0	15	3.0
TW23.0	tw23	1	tw23	1	215.8	74	0	7	7	4.9	85	50.0	15	3.5
TW22.0	tw22	1	tw22	1	110.1	44.4	8	12	3	3.7	3			
TW22.0	tw22	1	tw22	1	99.1	-4	0	7	7	5.6	18	20.0	22	4.0
TW19.0	tw19	1	tw19	1	31.2	44.9	0	12	9	3.5	387	20.0	4	3.0
TW19.0	tw19	1*	tw19	1*	245.5	39.7	17	20	3	2.9	32			
TW17.0	tw17	1	tw17	1	348.1	54	2	8	6	6.7	34			
TW17.0	tw17	1	tw17	1	357.5	5.3	0	2	3	2.3	19	15.0	12	5.0
TW15.0	tw15	1	tw15	1	64	38.4	7	12	4	9.5	11			
TW15.0	tw15	1	tw15	1	281.7	68.5	5	7	3	5.4	6			
TW15.0	tw15	1	tw15	1	16.4	72.3	0	8	8	6.5	23	25.0	23	8.5
TW14.0	tw14	1	tw14	1	250.2	26.8	15	20	3	4	10			
TW14.0	tw14	1	tw14	1	297.6	78.2	0	17	12	3.5	93	50.0	6	4.0
TW12.0	tw12	c 2	w12c	2	86.9	-20	3	7	4	3.2	2	7.5	8	5.0
TW11.0	tw11	1	tw11	1	264	71.7	2	5	3	8.7	1	12.5	30	8.5
TW8.0	tw8	1	tw08	1	286.3	27.2	10	15	3	9.5	42			
TW8.0	tw8	1	tw08	1	119.6	-67	1	3	3	3.2	122	15.0	21	3.0
TW7.0	tw7	a 1	tw7a	1	11	55.5	0	17	12	5.4	12	80.0	16	8.5
TWL2.0	twl2	2*	tl02	2*	73.2	-65.1	0	200	21	2.1	645	200.0	53	20.0

H1,H2 - range of demagnetization path, where lines were fitted  
 Peak AF - maximum field used in AF demag. before sample were unstable  
 Residual NRM - Intensity of NRM remained after use of peak AF  
 A,B,C - my own classification of reliability of NRM directions  
 ASD - angular standard deviation (error) of fitted lines  
 Int - intensity of fitted component in mA/m

PS collection - traverse Calm Lake - Perch Lake

Lines fitted to AF demagnetization path - all classes A-C

Sample	Dec sample coord	Inc sample coord	H1	H2	No of points	ASD	INT of comp.	Class	Peak AF	Residual			Sample orient		Dec geogr. coord	Inc geogr. coord
										NRM in %	MDF		Strike	Dip		
PSB 2	235.3	-58.7	1.0	15.0	7	6.2	16	A	40.0	12.0	12.5	280	64	37.0	-49.3	
PSB 5	86.6	4.6	0.0	40.0	16	2.1	29	A	40.0	15.0	7.5	74	88	36.5	85.7	
PSB 8	282.9	29.4	0.0	3.0	4	2.1	27	C	12.5	46.0	10.0	64	88	354.5	-56.3	
PSB 9	297.4	13.4	0.0	10.0	9	3.8	201	A	12.5	6.0	3.5	81	83	44.2	-56.0	
PSB 11	52.9	-12.1	1.0	10.0	8	3.8	38	A	12.5	17.0	3.0	80	90	99.6	51.2	
PSB 12	109.5	9.1	0.0	3.0	4	1.5	192	C	12.5	14.0	2.0	78	90	283.6	68.6	
PSB 13	66.4	-10.8	0.0	3.0	4	1.3	136	C	29.0	11.0	7.5	70	79	112.1	58.0	
PSB 13	294.3	-12.3	5.0	7.0	3	9.7	35	C				70	79	75.6	-66.2	
PSB 16	104.2	7.2	2.0	200.0	19	3.5	1890	A	200.0	8.0	35.0	80	86	273.4	75.5	
PSB 18	236.5	-3.8	1.0	50.0	12	4.9	34	A	80.0	10.0	25.0	68	78	259.1	-55.9	
PSB 27	89.4	37.7	0.0	7.0	7	7.1	9	B	15.0	53.0	12.5	89	89	359.8	53.3	
PSB 28	95.6	13.4	0.0	7.0	7	4.5	116	A	25.0	6.0	5.0	92	87	334.3	78.2	
PSB 33	244.1	-2.6	0.0	200.0	21	1.4	3280	A	200.0	1.4	12.5	72	82	262.4	-63.7	
PSB 34	292.3	-4.7	0.0	7.0	7	7.3	104	B				60	90	72.2	-67.2	
PSB 34	280.2	-11	12.0	17.0	4	10.7	51	C	30.0	13.0	10.0	72	82	107.7	-75.0	
PSB 35	210	2.2	0.0	25.0	14	3.5	281	A	20.0	5.2	4.0	95	84	281.0	-29.5	
PSB 38	120.4	26.2	0.0	25.0	13	4.8	436	A	50.0	1.8	6.5	80	90	304.2	50.7	
PSB 38	56	17.5	20.0	30.0	3	4.9	26	C				80	90	50.6	52.2	
PSP 1	116.6	-65.6	5.0	140.0	19	2.2	834	A	140.0	3.0	10.0	H		116.6	-65.6	
PSP 9	280.1	-53.2	3.0	7.0	3	6.4	173	C	140.0	3.0	16.0	H		280.1	-53.2	
PSP 9	277.5	38.9	10.0	140.0	15	3.3	583	A				H		277.5	38.9	
PSP 12	60.4	50.8	1.0	180.0	19	2.1	179	A	180.0	10.0	26.0	H		60.4	50.8	
PSP 13a	129.9	62.5	0.0	180.0	20	1.1	504	A	180.0	1.0	11.0	H		129.9	62.5	
PSP 26*	179.7	78.7	0.0	180.0	20	1.9	48	A	180.0	7.0	20.0	H		179.7	78.7	
PSP 26a	293.5	50.9	1.0	3.0	3	1.6	27	C	6.0	24.0	3.5	H		293.5	50.9	
PSP 26a	270.9	38.3	3.0	6.0	3	4.7	17	C				H		270.9	38.3	
PSP 32	269.3	-25	0.0	190.0	20	1.9	3020	A	190.0	3.0	10.0	H		269.3	-25.0	
PSP 38a	268.2	2.7	0.0	190.0	22	1.4	4480	A	190.0	1.0	6.5	H		268.2	2.7	
PSP 39	73.6	-2.4	0.0	190.0	23	1.8	5520	A	190.0	3.0	7.5	H		73.6	-2.4	
PSP 60	257.4	-86.4	0.0	190.0	23	1.4	14800	A	190.0	1.0	11.0	H		257.4	-86.4	
PSR 5	28.4	9.7	0.0	8.0	8	3.4	135	B	8.0	21.0	3.0	74	90	63.0	28.0	
PSR 7	57.5	-16.6	0.0	20.0	13	4.7	17	A	40.0	28.0	20.0	90	81	128.4	48.9	
PSR 7	13.5	7.7	25.0	40.0	3	2	4	C				90	81	84.3	14.4	
PSR 10	292.3	-7.4	2.0	15.0	9	5.3	93	B	15.0	35.0	11.0	74	60	31.3	-59.2	
PSR 15	352.4	32.5	2.0	10.0	7	4.3	54	B	10.0	39.0	6.0	260	77	226.7	0.7	
PSR 17	198.1	-36.1	0.0	8.0	8	5	140	B	12.0	19.0	3.0	258	80	43.1	-20.5	
PSR 17	262.1	1.2	8.0	12.0	3	10	20	C				258	80	132.5	-76.3	
PSR 18	181.3	10.3	0.0	190.0	21	1.6	3070	A	190.0	4.0	5.0	244	87	74.4	-0.7	
PSR 20	271.5	-26.1	0.0	40.0	17	2.5	1010	A	40.0	2.0	11.0	83	72	163.5	-81.8	
PSR 21	105.3	-6.5	0.0	15.0	11	4.9	149	A	20.0	14.0	7.5	248	75	14.3	63.7	
PSR 21	133.4	29.9	15.0	20.0	3	3	12	C				248	75	96.1	47.5	
PSS 1	109.1	-18	0.0	190.0	22	2	2090	A	190.0	2.0	15.0	265	77	26.7	53.7	
PSS 3	336.9	0.8	0.0	30.0	16	2.1	2980	A	30.0	1.0	3.5	260	40	241.4	-14.0	
PSS 7	249.6	10	0.0	17.0	9	5.9	43	A	60.0	5.0	25.0	262	65	139.9	-49.7	
PSS 7	272.7	11.3	20.0	30.0	3	1.6	17	C				262	65	176.5	-53.6	
PSS 7	237.4	-8.4	30.0	60.0	5	5.7	36	B				262	65	104.4	-54.8	
PSS 11	37.2	11.3	0.0	2.0	3	3	240	C	30.0	4.0	4.0	88	86	76.8	37.2	
PSS 11	359.8	7.8	2.0	30.0	12	1.9	846	A				88	86	80.2	0.3	
PSS 16	43.9	4.4	0.0	6.0	6	1.8	128	A	6.0	18.0	2.0	85	82	86.6	44.1	
PSS 17	50.5	4.2	0.0	200.0	24	3.2	6010	A	200.0	2.0	9.0	95	84	95.7	50.6	
PSS 18	334.8	15.7	0.0	25.0	14	4.7	176	A	25.0	10.0	5.5	88	84	68.3	-22.3	
PSS 20	75.2	15.7	0.0	3.0	4	3.3	7	C	8.0	55.0	17.5	241	72	248.0	75.7	
PSS 20	109.2	-4.5	6.0	8.0	3	5.5	5	C				241	72	12.9	60.6	
PSS 24	57.8	-55.4	0.0	40.0	17	1.9	102	A	40.0	6.0	5.5	270	85	340.7	24.0	
PSS 27	194.3	-6.6	0.0	17.0	12	4.2	85	A	120.0	25.0	5.5	60	90	233.2	-14.2	
PSS 27	177.3	-7.4	1.0	3.0	3	0.8	25	C				60	90	232.6	2.7	
PSS 27	201.1	-5.8	3.0	12.0	7	1.9	56	B				60	90	233.8	-21.0	
PSS 29	74.8	-22	0.0	5.0	4	5.3	146	C	50.0	20.0	30.0	?				
PSS 29	256.8	10.1	5.0	50.0	14	2.8	384	A				?				
PST 1	156.3	-8.4	1.0	3.0	3	2.7	77	C	50.0	2.0	7.0	92	83	259.9	22.1	
PST 1	131	17.2	3.0	50.0	16	3.4	236	A				92	83	290.2	48.7	
PST 4	345.6	-21	0.0	8.0	7	4.2	262	B	8.0	8.0	2.5	260	60	272.1	-22.3	
PST 9	310.3	-3.8	0.0	2.0	3	6	16	C	6.0	43.0	5.0	240	78	231.8	-49.3	
PST 9	245.2	-11.9	2.0	6.0	4	1.9	43	C				240	78	57.6	-65.7	
PST 10	280.6	1.9	0.0	10.0	9	6.7	62	B	10.0	47.0	7.5	230	60	159.5	-56.5	
PST 11	234.8	16.7	0.0	2.0	3	9.8	11	C	30.0	31.0	12.0	243	70	107.2	-39.6	
PST 11	311.6	-4.6	2.0	17.0	10	6	53	A				243	70	227.8	-46.7	
PST 11	302.3	-3.9	20.0	30.0	3	9.7	6	C				243	70	220.2	-54.7	
PST 12	89.5	1.8	1.0	6.0	5	3.3	66	C	7.0	21.0	3.0	215	65	303.7	66.8	
PST 12	67.4	-0.5	5.0	7.0	3	1.6	16	C				215	65	261.0	56.4	
PST 13	326.8	-11.8	0.0	80.0	22	1.5	12300	A	80.0	1.0	7.0	260	82	268.9	-34.0	
PST 22	323.9	-10.9	0.0	90.0	22	1.6	4560	A	90.0	1.0	6.5	250	75	252.4	-37.4	

Sample	Dec sample coord	Inc sample coord	H1	H2	No of points	ASD	INT of comp.	Class	Peak AF	Residual			Sample orient			Dec geogr. coord	Inc geogr. coord
										NRM in %	MDF		Strike	Dip			
PST 30	252.9	-2.4	0.0	17.0	12	2.6	232	A	17.0	9.0	4.0	279	78	127.2	-70.5		
PST 45	331	-15.9	2.0	5.0	3	5	1950	C	200.0	1.0	20.0	75	87	91.5	-28.7		
PST 45	265.3	-23.3	5.0	200.0	30	5.9	2140	A				75	87	130.2	-64.9		
PST 51	228.2	-21.2	1.0	8.0	7	6.8	30	B	7.0	43.0	6.5	260	74	65.9	-50.2		
PST 52	286.5	6.5	0.0	2.0	3	4.6	3	C	100.0	14.0	20.0	263	84	226.1	-69.3		
PST 52	286.5	-54.4	5.0	100.0	16	4.3	91	A				263	84	340.8	-39.8		
PST 54	296.4	8.3	0.0	190.0	17	3.4	40	A	190.0	19.0	50.0	257	80	223.1	-58.0		
PST 59	77.4	-2.9	0.0	12.0	10	4.7	37	A	12.0	37.0	8.5	275	73	331.8	66.5		
PST 62	239.4	2.3	0.0	5.0	5	2.2	182	C	10.0	33.0	2.0	79	90	263.5	-59.3		
PST 62	57	-2.9	5.0	10.0	4	8.3	42	C				79	90	84.3	56.9		
PST 63	116.2	-16.4	0.0	100.0	17	1.6	641	A	100.0	3.0	10.0	278	88	61.6	58.3		
PST 65	65.1	2.9	0.0	40.0	14	5.2	36	A	60.0	7.0	17.0	273	81	285.3	64.5		
PST 65	102.7	19.4	40.0	60.0	3	6.6	6	C				273	81	134.6	73.9		
PST 74	34.7	33.6	1.0	100.0	16	2.4	25	A	100.0	4.0	18.0	95	90	58.1	28.3		
f1 2	138	87.1	0.0	2.0	3	2.2	26	C	5.0	34.0	3.5	H		138.0	87.1		
f1 2	8.1	52.4	2.0	5.0	3	2	55	C				H		8.1	52.4		
f1 2	202.9	40.4	6.0	8.0	3	4.9	11	C				H		202.9	40.4		
f1 3	24.3	73.2	0.0	7.0	7	7	14	B	7.0	37.0	6.5	H		24.3	73.2		
f1 3	8.1	87.2	5.0	7.0	3	5.1	7	C				H		8.1	87.2		
f1 7	107.8	4.6	0.0	7.0	7	5.3	49	B	7.0	13.0	3.0	H		107.8	4.6		
f1 9	113.7	-12.4	0.0	3.0	3	4.1	122	C	6.0	22.0	3.0	H		113.7	-12.4		
f1 9	131.5	1.9	3.0	8.0	3	1.3	53	C				H		131.5	1.9		
f1 13	127.3	-46.2	0.0	3.0	4	4.7	25	C	8.0	30.0	5.0	H		127.3	-46.2		
f1 13	142.2	-28.3	3.0	6.0	3	1.9	18	C				H		142.2	-28.3		
f1 13	128.2	-5	6.0	8.0	3	4.1	7	C				H		128.2	-5.0		
f1 14	130.2	12.1	3.0	8.0	5	2.4	250	B	8.0	17.0	4.0	H		130.2	12.1		
f1 15	116.1	13.3	1.0	3.0	3	3.8	46	C	15.0	12.0	5.0	H		116.1	13.3		
f1 15	142.9	26	3.0	10.0	6	4.5	112	B				H		142.9	26.0		
f1 15	151.9	41.4	10.0	15.0	3	1.3	36	C				H		151.9	41.4		
f1 16	83.5	22.8	0.0	2.0	3	4.5	43	C	12.0	18.0	7.5	H		83.5	22.8		
f1 16	72.8	-0.2	8.0	12.0	3	6.2	54	C				H		72.8	-0.2		
f2 1	28.5	-44.7	0.0	130.0	21	1.4	1810	A	130.0	3.0	7.0	H		28.5	-44.7		
f2 3	31.1	-40.5	0.0	110.0	22	2.3	3050	A	110.0	4.0	7.5	H		31.1	-40.5		
f2 4	18.2	-34.2	0.0	110.0	22	1.8	3590	A	110.0	1.0	8.0	H		18.2	-34.2		
f2 5	20.5	-36.5	0.0	110.0	22	1.9	4470	A	110.0	2.0	8.5	H		20.5	-36.5		
plr 1	88.5	66.1	2.0	20.0	11	2.8	1090	A	20.0	8.0	3.5	H		88.5	66.1		
plr 2	260.9	46.8	3.0	10.0	6	5.9	77	B	35.0	3.0	5.5	H		260.9	46.8		
plr 2	277.4	42.2	20.0	35.0	3	4.9	48	C				H		277.4	42.2		
plr 3	187.3	-18.6	0.0	5.0	5	4.4	390	C	12.0	18.0	3.5	H		187.3	-18.6		
plr 3	220.4	10.3	7.0	12.0	3	3.9	35	C				H		220.4	10.3		
plr 5	31.8	44.9	0.0	2.0	3	6	42	C	12.0	30.0	8.0	H		31.8	44.9		
plr 5	277.1	38.7	3.0	8.0	5	3.3	54	C				H		277.1	38.7		
plr 5	326.3	59.2	8.0	12.0	3	4.9	22	C				H		326.3	59.2		
plr 6	31.1	47.8	1.0	3.0	3	4.7	6	C	15.0	53.0	18.0	H		31.1	47.8		
plr 6	312.8	49.2	6.0	15.0	8	6.3	19	B				H		312.8	49.2		
plr 7	275.7	54.8	5.0	27.0	11	7.5	61	A	27.0	34.0	21.0	H		275.7	54.8		
plr 11	117.1	-71.3	7.0	100.0	15	2	213	A	100.0	2.0	8.0	H		117.1	-71.3		
plr 12	122.3	-71.1	5.0	80.0	16	1.7	203	A	80.0	2.0	8.5	H		122.3	-71.1		
plr 13	141.3	-72.3	1.0	35.0	14	2.9	123	A	35.0	5.0	6.0	H		141.3	-72.3		
plr b	312	50.7	3.0	8.0	3	4.8	10	C	20.0	34.0	15.0	H		312.0	50.7		
plr b	263.9	40.3	15.0	20.0	3	4.6	20	C				H		263.9	40.3		
plr d	282.5	55.9	0.0	17.0	9	4.5	77	B	35.0	17.0	13.0	H		282.5	55.9		
plr d	283.3	45.8	20.0	35.0	4	6.6	37	C				H		283.3	45.8		
plr e	291.9	50.3	1.0	35.0	13	5.9	68	A	35.0	22.0	21.0	H		291.9	50.3		
plr f	299.6	60.2	0.0	60.0	17	5.4	118	A	60.0	7.0	17.0	H		299.6	60.2		
plr g	237.8	32	2.0	8.0	8	5.9	38	B	20.0	45.0	18.0	H		237.8	32.0		
plr g	296.6	41.6	8.0	12.0	3	4.9	13	C				H		296.6	41.6		
plr g	253	47.5	17.0	20.0	3	13.7	36	C				H		253.0	47.5		
plr h	262.4	38.3	2.0	5.0	3	5.4	2	C	25.0	30.0	16.0	H		262.4	38.3		
plr h	304.8	60.7	15.0	25.0	4	4.8	6	C				H		304.8	60.7		
plr i	20.8	70.7	0.0	2.0	3	5.4	59	C	25.0	28.0	8.5	H		20.8	70.7		
plr i	254.8	43.8	2.0	17.0	10	6.9	149	A				H		254.8	43.8		
plr i	322.8	33.1	17.0	25.0	3	9.8	41	C				H		322.8	33.1		
plr k	148.5	67.6	0.0	8.0	8	8.4	42	B	30.0	10.0	11.0	H		148.5	67.6		
plr k	196	65.3	20.0	30.0	3	6	20	C				H		196.0	65.3		
plr l	295.9	59.1	1.0	15.0	9	5.7	72	B	30.0	29.0	17.5	H		295.9	59.1		
plr l	271.7	47.1	20.0	30.0	3	8.9	26	C				H		271.7	47.1		
ps 1	67.9	11.7	0.0	7.0	7	4	144	B	20.0	4.0	5.0	284	85	245.5	67.1		
ps 1	71.2	2.4	10.0	20.0	5	4.3	48	C				284	85	271.2	71.1		
ps 6	96	-13.2	1.0	40.0	11	2.3	143	A	40.0	8.0	6.0	245	84	352.2	69.9		

H1,H2 - range of demagnetization path, where lines were fitted  
Peak AF - maximum field used in AF demag. before samples were unstable  
Residual NRM - intensity of NRM remained after use of peak AF  
A,B,C - my own classification of reliability of NRM directions  
ASD - angular standard deviation (error) of fitted lines  
Int - intensity of fitted component in mA/m

Lines fitted to demagnetization path by Kirschvink's  
algorithm - thermal treatment.

Lines fitted for Th. demagnetization path for RS collection  
 File: thrsline.wq1

Sample	Kirsch code	Dec geogr	Inc coord	H1	H2	No of ASD points	INT of comp.	Class T	Peak	Resid NRM in %
tw01	2 tw1x 2	354.6	79.1	0	100	3	2.8 10	C	325	16
tw01	2 tw1x 2	235.4	60.8	200	275	3	11 5	C		
twr03.5	2 twr3 52	322.8	-3.2	100	325	7	6.4 80	B	600	8
twr04.1b	3 twr4 123	206.2	71.5	0	375	11	3.6 154	A	425	6
twr04.1b	4 twr4 124	282.6	85.3	0	425	14	6.2 190	A	425	9
twr05a	2 twr5 12	249.8	81.6	0	100	3	4.6 64	C	600	5
twr05a	2 twr5 12	266.7	73.7	150	350	7	5.3 110	B		
twr05a	3 twr5 13	343.7	76.1	0	100	3	5.5 39	C	375	7
twr05a	3 twr5 13	291.1	76.2	150	300	5	7.7 45	B		
twr05a	3 twr5 13	346.8	79.5	500	550	3	2.8 6	C		
twr10.5	2 wr10 52	33.6	3.1	100	250	4	4.8 48	C	350	18

Lines fitted to TH. demagnetization paths for PS collection

File: THpsline.wq1

Sample	Kirsch	Dec	Inc	H1	H2	No of ASD	INT	Class	Peak	Residual	Orient	Dec	Inc			
	code	sample coord				points	of comp.		T	NRM	Strike	geogr. coord				
												Dip				
f1	06	f1xx	6	134.1	13.3	50	300	7	4	128	B	325	3.0	H	134.1	13.3
f1	17	f1xx	17	267.8	-28.8	100	200	3	4.6	114	C	300	6.0	H	267.8	-28.8
f1	17	f1xx	17	258.6	-30.9	250	300	3	3.9	82	C			H	258.6	-30.9
plr	10*	plr	10	124.4	-75.9	0	350	11	1.4	1570	A	350	2.0	H	124.4	-75.9
plr	m	plrm	1	251.9	31.6	100	300	6	3	183	B	325	0.7	H	251.9	31.6
plr	m	plrm	1*	318.8	58	275	325	4	1.7	50	C			H	318.8	58
ps	03	psxx	3*	85.1	10.8	50	325	9	4.8	113	B	325	4.0	278 80	268.1	85.1
ps	03*	psxx	3*	85.1	10.8	50	325	9	4.8	113	B			278 80	268.1	85.1
psb	10	psbx	10	56.5	-7.3	50	200	4	2.9	201	C			75 80	101.2	52.4
psb	10	psbx	10	73.4	4.9	200	275	3	2	138	C	350	1.0	75 80	91	72.7
psb	10	psbx	10	14.4	-3.3	275	325	3	3.7	42	C			75 80	80.9	13.6
psb	29	psbx	29	56.1	15	0	300	8	3	140	B	350	9.0	93 84	75.1	55.5
psb	29	psbx	29	105.1	5	275	325	3	3.4	23	C			93 84	269.9	74.9
psp	13	pspx	13	218	47.5	100	200	3	3.2	9	C			H	218	47.5
psp	13*	pspx	13	218.6	48.2	50	250	6	7.6	28	B	250	10.0	H	218.6	48.2
psp	38b	pspx	38	248.5	-42.1	0	300	8	1.7	6760	B	425	0.1	H	248.5	-42.1
psp	38b	pspx	38	247.5	-43.8	325	425	6	3.1	880	B			93 84	247.5	-43.8
psr	08	psrx	8	224.9	4.2	0	325	4	7.3	44	C	325	16.0	250 88	77.9	-44.5
psr	08	psrx	8	230.6	-7.9	50	200	4	2	40	C			250 88	60	-50.3
psr	24*	psrx	24	26	18.1	100	425	12	4.3	555	A	425	3.0	257 88	237.9	25.3
pss	05	pssx	5	183.2	3.1	100	200	3	0.6	31	C	300	12.0	257 72	80.9	-2.1
pss	15	pssx	15	46	-11.2	50	200	4	4.9	121	C	350	2.0	80 85	100.5	43.3
pss	15*	pssx	15	45.3	1.7	200	350	7	8.3	138	B			80 85	82.6	45.3
pst	08	pstx	8	261.1	4.3	150	325	6	5.4	129	B	325	11.0	277 55	173.2	-49.8



Lines fitted for demagnetization paths for TW collection

Thermal demagnetization

File: thtline.wq1

Sample	Dec	Inc	H1	H2	No of ASD points	INT	Class	Peak T	Resid.		
									geogr coord	(C)	of comp.
twa2	2	39.5	-58.2	50	150	3	3.5	31	C	300	8
twa2	2	99.2	-41.0	150	250	3	4	133	C		
twa3	2	157.8	67.1	0	100	3	2.6	1	C	275	28
twa3	2	66.0	-58.1	200	275	3	4.5	8	C		
twa5	2*	241.7	-8.0	0	425	14	2.3	307	A	425	0.8
twa6	2*	238.0	74.6	0	350	11	3.3	514	A	350	3
twa6.5	2	15.7	78.1	0	100	3	5.1	3	C	275	78
twa8	2	248.0	63.3	0	250	6	2.1	213	B	350	4
twa9	2*	254.4	-13.1	0	350	11	3.1	768	A	350	2
twa9.5	2	65.1	81.0	0	250	6	4.8	79	B	350	15
twa10.5	2	43.4	39.3	50	150	3	3	136	C	350	2
twa10.5	2	77.5	17.1	150	350	8	3.1	318	B		
twa14	2	72.0	43.8	0	300	8	4.2	31	B	325	6
twa15	2	208.4	39.5	0	250	6	5.4	86	B	575	4
twa15	2	88.5	56.0	300	350	3	7.2	13	C		
twa15	2	37.8	16.8	350	400	3	3.9	9	C		
twa15	2	93.4	36.6	400	475	4	6.8	27	C		
twa15.5	1	272.7	-44.6	150	325	6	4.3	483	B	350	2
twa15.5	1	269.5	-46.8	200	300	4	1.7	350	C		
twa16.5	2	284.5	44.2	50	150	3	4.2	37	C	325	12
twa16.5	2	326.1	43.7	150	250	3	1.8	18	C		
twa18	b 2	257.2	-7.5	0	300	8	5.5	54	B	325	41
twa18.5	2	69.8	24.2	0	100	3	4.4	19	C	325	25
twa18.5	2	195.9	-42.8	150	250	3	2.1	45	C		
twa18.5	2	151.7	-3.2	250	325	4	6.9	47	C		
twa19.5	2	251.1	21.5	0	200	5	4.4	6	B	275	17
twa19.5	2	123.7	58.1	200	275	3	11.6	1	C		
twa20	b 2	114.0	16.8	50	150	3	2.8	12	C	325	53
twa20	b 2	60.5	-15.6	200	300	4	6.9	14	C		
twa22	a 2	84.3	31.6	0	200	5	6.1	6	B	300	38
twc6	2*	271.0	-5.9	0	350	11	1.6	2350	A	350	1
twc5	b 2	275.1	32.8	0	400	12	3.8	728	A	400	3
twc1.5	b 1	236.5	32.7	0	350	11	1.7	1960	A	350	0.5
twc1	2*	70.4	54.6	0	350	11	1.4	251	A	350	0.8
twe4	b 2	218.8	28.2	0	150	4	2.6	12	C	250	23
twe4	b 2	179.4	66.9	150	250	3	2.3	14	C		
twe6	a 2	245.8	26.9	0	375	12	2.5	1560	A	450	3
twe6	b 2	169.9	23.2	0	100	3	4.9	26	C	325	4
twe6	a 3	206.0	23.5	0	200	5	4.8	303	B	275	4
twe6	b 3	239.2	-5.4	50	150	3	5.5	75	C	375	6
twe6	a 3	219.8	40.8	100	275	6	4.4	343	B		
twe6	b 2	292.0	-32.2	100	325	8	3.1	123	B		
twe6	b 3	284.0	-32.0	150	300	5	4.9	214	B		
twe6	a 2	32.6	23.8	350	400	3	1.6	64	C		
tw23	2	236.9	79.1	0	100	3	6.7	48	C	275	29
tw22	2*	113.7	-9.5	0	350	11	2.3	228	A	350	2
tw19	2	44.7	44.5	0	275	7	4.9	281	B	375	4
tw17	2	15.0	71.2	0	300	8	6.5	119	B	300	7
tw14	2	312.8	82.8	0	200	5	5.9	69	B	325	10
tw14	2	90.9	56.5	200	275	3	6.4	38	C		
tw8	2	149.9	-71.3	50	200	4	5.2	107	C	200	16
tw12	1	71.7	-60.7	0	400	12	3.1	532	A	450	3

## Appendix E

### Computer programs and algorithm review.

#### **Program COORD2.BAS**

The program converts a vector orientation, measured in the sample coordinates into geographic coordinates.

Usually such quantities as NRM vectors and the principal axes of anisotropy are measured with respect to the sample itself in a standard coordinate system, where +Z axis vertically down the sample and +X is north and +Y is east with respect to an arbitrary specimen orientation.

When a sample is drilled not from a horizontal surface but an inclined one, an arrow on the top of the sample marks one of three directions:

- a) - the direction of strike - then an arrow traces a horizontal line;
- b) - the direction of dip - then an arrow points down the dip direction;
- c) - the direction antiparallel to dip direction (Molyneux, 1971 convention, "Newcastle convention") - the arrow traces the up-dip direction.

The orientation of the top surface of the sample is also recorded in one of two methods: strike and dip or direction of

dip and dip. The program allows the user to choose the proper convention used during field drilling.

Next the direction of a vector, a line or a normal to the plane under consideration, is rotated around the strike axis of the plane to restore the inclination of the vector in the real inclined position of the sample. Finally, the rotation along the vertical axes is performed to restore the declination of vector (line, etc.) with respect to geographic North and not the direction of arrow on the sample.

If the structural data are concerned the "right-hand" convention used is that which present the data with its strike direction anticlockwise from the dip direction.

The program was used to restore the true orientation of NRM vectors and principal axes of ARM and MS for some series from the Calm Lake - Perch Lake area.

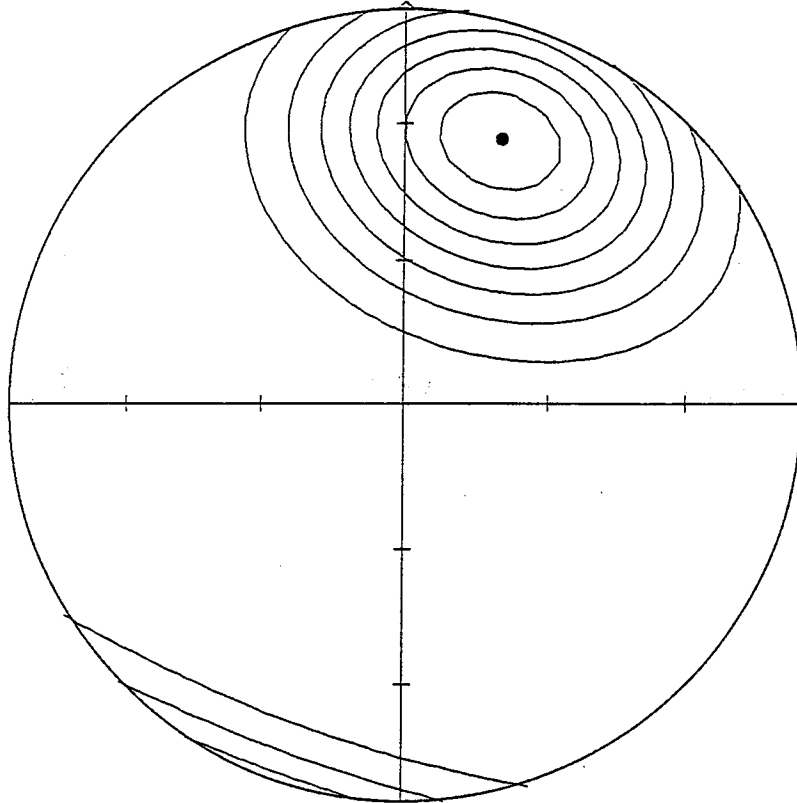
#### **Program SpheriStat (Frontenac Wordsmith) - remarks.**

The program uses two techniques to evaluate the distribution of data on the lower hemisphere: a contouring procedure and the principal component analysis (PCA) method.

The procedure of contouring calculates the distances from a given station to all points on the hemisphere. It uses the adjustable Gaussian spherical function as continuous (not discrete as counting circle) weighting function  $w = \exp [k(\cos\theta - 1)]$  to multiply the weight by the distance from the station for all data on the sphere (Robin and Jowett, 1986). The function value decreases rapidly with an angular distance away from the

Gauss weighting function

$N=16$  in the point : 1 20-30



$N = 16$

$k = 5.56$

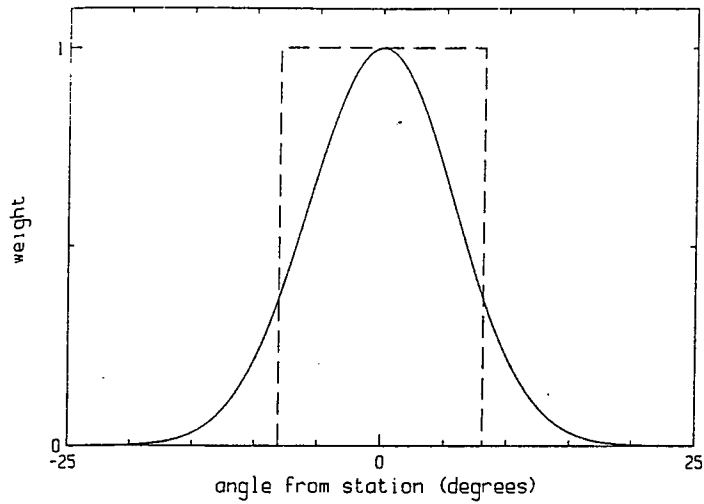
$(\text{Peak} - E)/\text{Sigma} = 13.6$

Peak position :  $18.4^\circ / 30.4^\circ$

$E = 2.88$

$\text{Sigma} = 0.96$

Fig. E1. A shape of spherical Gauss weighting function. The lowest contour level is  $E$ , following contours map an increase of count by  $2\sigma$ . The distance between a peak and the nearest contour is less than  $2\sigma$ .



Two contrasting weighting options which can be used for counting, schematically represented in two dimensions. The dashed line corresponds to the conventional counting circle.  $A = 0.005$  (fractional area of the whole sphere for polar data) or  $A = 0.01$  (non-polar data), i.e.  $\alpha = 8.11^\circ$ . The full curve is a spherical Gaussian curve (eqn. 10,  $k = 100$ ), with the same expected count value  $E$  as the conventional counting circle for points extracted randomly from a uniform population.

Fig. E2. (from Robin and Jowett, 1986).

Three principal directions with their associated 95% confidence cones. The long (major) axes of the elliptical cones are shown with zero orientation angle (measured relative to the line tangent to the great circles joining the principal directions). Note: this diagram is for illustration only; when plotted on an equal-area net, the cones will not appear as ellipses.

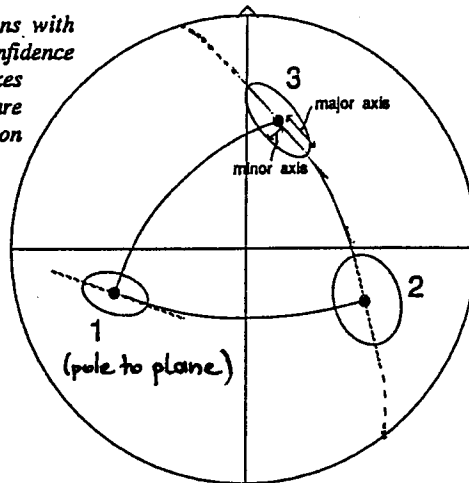


Fig. E4. A concept of confidence cone orientations for principal directions of Bingham orthorhombic distribution (from Stesky, 1990).

counting station (see Fig. E1 and E2). It produces smoother contours than the counting circle technique. The size of counting circle A is related to k value as  $A=1/k$ . Parameter k - the kurtosis of Gaussian function can be taken as a fixed value ( $k=100$ ) which produces the same count expected from a 1% counting circle for non-polar data (distributed on the half-sphere). This definition gives smoother contours for  $N > 450$  data points. For  $N < 450$  it is better to choose smaller  $k=2(1+N/9)$ . This is equivalent to the Kamb method (see Robin and Jowett, 1986 for discussion) and produces the expected count  $E=3\sigma$ , where  $\sigma$  is a statistical dispersion of data.

If  $\sigma$  is a statistical dispersion of data, then contours for every  $2\sigma$ -step are drawn, starting from E - the expected value of the point density for random distribution. The program calculates the value of highest peak of point density in terms of multiples of  $\sigma$  above E value.

For an example of a given distribution of poles to S1 surfaces (the data from the centre of the Quetico Belt) the results of contouring are:

number of points  $N=106$ ;

$E = 4.15$

$\sigma = 1.38$

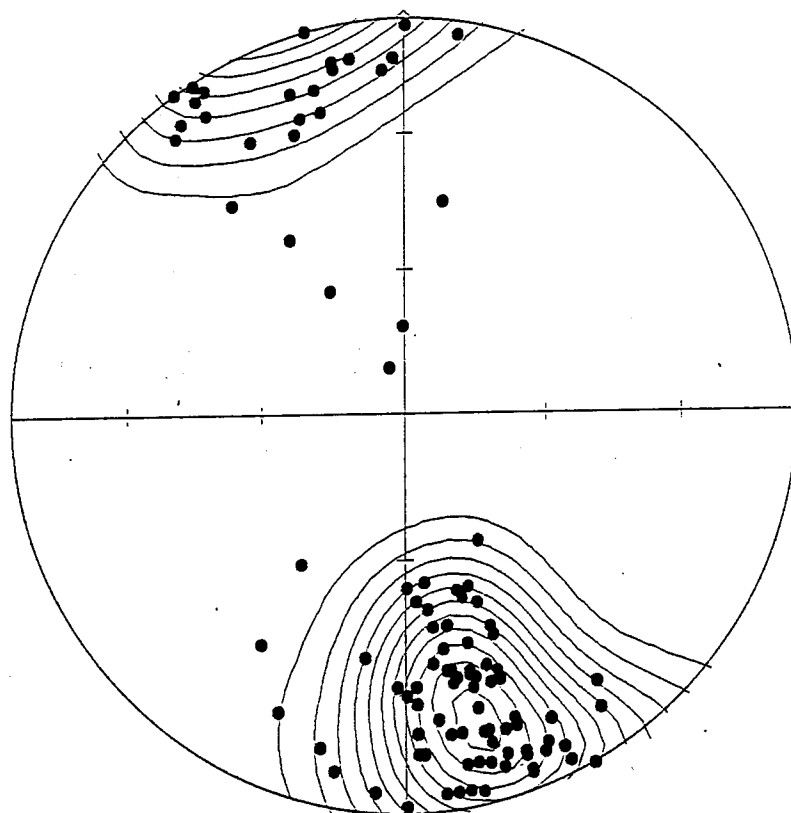
$(\text{peak value} - E)/\sigma = 20.8$

for a peak at  $168^\circ - 22^\circ$ .

It corresponds to mean S1 surface at  $258^\circ/68^\circ$  NW (Fig. E3).

The eigenvector technique determines eigenvectors of the sum matrix of products and cross-products of the directional

Poles to S1 schistosity - the interior of Quetico  
Medium and high metamorphic grade metasediments



$N = 106$                        $E = 4.15$   
 $k = 25.56$                        $\text{Sigma} = 1.38$   
 $(\text{Peak} - E)/\text{Sigma} = 20.8$   
Peak position :  $167.9^\circ / 21.5^\circ$

Fig. E3. Results of contouring procedure for a set of poles to S1 schistosity for interior of the Quetico Belt. Compare orientation of a peak with the orientation of principal direction: 166/17 with confidence cone 6/3.

cosines of each data point. The minimum eigenvector (correlated with minimum eigenvalue) indicates the direction normal to best-fitted plane to data and maximum eigenvector points into the direction of best-fitted line to data points. 95% confidence cones around these directions are determined from the Hext (1963) algorithm. The cones projected on the equal - area plot do not preserve their elliptical shape, however it can be approximated that the long axis of cone for the pole to best-fitting plane points toward that plane and the cone for maximum axis has its long axis approximately parallel to the trace of best fitting plane in that projection (Fig. E4).

The program calculates the real angles between cone axes and great circles joining the eigenvector directions as in general the cone can be deflected from the position listed above. If this deflection is greater than  $2-3^\circ$  it indicates that the distribution of points is not orthorhombic (Bingham distribution) and the positions of eigenvectors should be interpreted with caution.

#### **Program RMANISTW.BAS.**

The program calculates the positions and intensities of principal remanences when the anisotropy of remanence is studied.

It assumes that the applied field was imposed in 12 orientations as designed by Stupavsky (1984). The specimen should be oriented as shown at Fig. 11.2 with respect to the magnetizing D.C. field. The resultant remanence vector should be known in full;



all three components are required (as measured by MOLSPIN spinner magnetometer).

Two methods can be employed to calculate the principal remanence. The first utilizes the Stupavsky (1984) algorithm to find principal axes with angular confidence limit  $r_{95}$  and standard deviation for intensities of principal remanences, when the component of each remanence vector along the applied field direction is determined. The second, designed by the writer, uses the least squares method based on the all 3 components of remanence vector for each position.

#### **Stupavsky method:**

Let us take  $R_i$  as the remanence vector measured after the sample has the field applied in  $i$ -th position.  $H_i$  is the vector of applied D.C. magnetic vector. The component of remanence along the direction of applied field  $S_i$  is calculated as a scalar product of a remanence vector and a direction cosine of the applied field.

$$S_i = \overline{R}_i \cdot \frac{\overline{H}_i}{H}$$

Those products are used to construct the anisotropy matrix  $k$ :

$$\overline{R}_i = \hat{k} \frac{\overline{H}_i}{H}$$

(a combination of two  $S_i$  values to get 6 diagonal and off-diagonal elements of the matrix). The matrix is diagonalized and

eigenvectors and eigenvalues are determined. The method of calculation of errors of eigenvectors and eigenvalues in the Stupavsky procedure is original and was not fully understood by the writer. It creates two other anisotropy matrices for 6 measurements positions each and then compares the results of calculations of eigenvectors for them with the results for 12 positions' results.

#### **Least squares method.**

The method is based on Girdler's (1961) approach. The relation between the remanence and the directional cosine  $h_i$  of applied field ( $R_i = kh_i$ ) for a given directions of applied field gives three equations where 6 elements of anisotropy matrix  $k$  are unknown. The total of 12 measurements gives 36 equations with 6 unknown parameters. The least - squares method can find the expression for these parameters to minimize the sum of squares of differences between experimental values of  $R_i$  and the calculated ones. This was done algebraically as the design of directions of applied field is quite simple.

Then once the estimates of anisotropy matrix parameters are known, the eigenvectors and eigenvalues can be determined. However, the design to calculate the errors of those estimates is much more complicated, following the Hext (1963) approach. Therefore the program does not calculate the confidence limits and standard deviations for found principal remanences.

The only way to estimate the accuracy of anisotropy matrix

in this method is to verify the differences of calculated and measured remanence vectors for a set of 12 directions. This estimation is based on Jackson's (1991) parameter - see chapter 9 for details. The same estimate is additionally used for Stupavsky's design to have the possibility of comparing the results of both method.

## COORD.BAS

```

10 CLS : REM - Direct calculations; strike & dip mode; Writing and printing of results
20 PIF = ATN(1) / 45: 'rad to deg conversion factor
30 LOCATE 5, 10
40 PRINT "Vectors' conversion from sample coordinates"
50 LOCATE 6, 10
60 PRINT "into geographical coordinates."
70 LOCATE 8, 15: PRINT " Choose one of options:"
80 LOCATE 10, 20: PRINT "1 - Dec, Inc - direct calculations"
90 LOCATE 11, 20: PRINT "2 - Dec, Inc - calculations for data in file"
100 LOCATE 12, 20: PRINT "3 - structural data: planar & linear"
110 LOCATE 15, 20: PRINT "4 - QUIT"
120 LOCATE 17, 10: INPUT "Give me your option: ", op
130 CH = (op - 1) * (op - 2) * (op - 3) * (op - 4): IF CH = 0 GOTO 160: 'checking input number
140 CLS
150 LOCATE 5, 10: PRINT "WRONG CHOICE - TRY AGAIN": GOTO 70
160 IF op = 4 GOTO 1320
170 IF (op - 1) * (op - 2) <> 0 GOTO 1220
180 DECT$ = "DEC": INC$ = "INC": SOP = 0
190 IF op = 1 GOTO 270
200 CLS : LOCATE 5, 10: PRINT "Dec & Inc conversion for directions located in *.spn file"
210 LOCATE 7, 10: INPUT "Give me path for INPUT file (* - to repeat old path): "; pin$
211 IF pin$ = "*" THEN pin$ = pin1$ ELSE pin1$ = pin$
212 LOCATE 8, 10: INPUT "INPUT file name without extension "; infile$: infile$ = pin$ + infile$ + ".spn"
220 ON ERROR GOTO 240: OPEN "I", 2, infile$: lin = 0: IF EOF(2) GOTO 1170
230 GOTO 270
240 CLS : CLOSE #2: LOCATE 9, 10: PRINT "FILE DOES NOT EXIST - try again"
250 LOCATE 11, 10: PRINT "press any key to continue": CON$ = INKEY$: IF CON$ = "*" GOTO 250
260 GOTO 200
270 CLS : 'Choice of calculation mode
280 LOCATE 4, 20: IF op <> 2 THEN PRINT op; " - "; DECT$; " & "; INC$; " - direct calculations" ELSE PRINT "2 -
Dec, Inc calculations for *.spn file"
290 LOCATE 6, 20: PRINT "For given "; DECT$; " & "; INC$; " in sample coordinates"
300 LOCATE 7, 20: PRINT "and sample coordinates - "; DECT$; " & "; INC$; " are recalculated"
310 LOCATE 8, 20: PRINT "in geographic coordinates"
320 LOCATE 10, 20: PRINT "Choose sample coordinates mode:"
330 LOCATE 12, 20: PRINT "1 - strike & dip": LOCATE 13, 20: PRINT "2 - azimuth toward dip direction & dip"
340 LOCATE 14, 20: PRINT "3 - azimuth antiparallel to dip direction (Moleneaux) & dip": LOCATE 16, 20: PRINT "4
-RETURN TO MAIN MENU"
350 LOCATE 18, 20: INPUT "Which mode ? ", mo
360 IF mo = 4 GOTO 10
370 MOCHK = (mo - 1) * (mo - 2) * (mo - 3): IF MOCHK <> 0 GOTO 320
380 CLS
390 IF mo <> 1 GOTO 420
400 LOCATE 3, 20: PRINT "STRIKE & DIP MODE"
410 LOCATE 4, 20: PRINT "Arrow on sample along strike line": GOTO 470
420 IF mo = 3 GOTO 450
430 LOCATE 3, 20: PRINT "AZIMUTH =dip direction & DIP MODE"
440 LOCATE 4, 20: PRINT "Arrow on sample along direction of dip": GOTO 470
450 LOCATE 3, 20: PRINT "AZIMUTH =direction antiparallel to dip & DIP MODE"
460 LOCATE 4, 20: PRINT "Arrow on sample antiparallel to the direction of dip"
470 LOCATE 6, 10: INPUT "Should I print data (1/0) "; pr
480 IF (pr - 1) * pr <> 0 GOTO 470
490 LOCATE 8, 10: INPUT "Should I write results into file (1/0) "; WR
500 IF (WR - 1) * WR <> 0 GOTO 490

```

```

510 IF WR = 0 GOTO 600
520 LOCATE 10, 10: INPUT "Give me path for OUTPUT file (* - to repeat old path): "; pout$
522 IF pout$ = "*" THEN pout$ = pout1$ ELSE pout1$ = pout$
523 LOCATE 11, 10: INPUT "OUTPUT file name without extension? "; fileout$: fileout$ = pout$ + fileout$ + ".spn"
530 IF fileout$ = infile$ THEN LOCATE 12, 10: PRINT "Names of input and output file are the same ": GOTO 520
ELSE OPEN "A", 1, fileout$
540 IF pr = 1 THEN LPRINT "Calculation results located in file : "; fileout$
550 IF op = 2 GOTO 600
560 IF mo = 1 THEN WRITE #1, "Sample strike & dip mode": PRINT #1, "Sample Strike,dip"; " "; DECT$; " ";
INC$; " "; DECT$; "G"; " "; INC$; "G": GOTO 600
570 IF mo = 2 THEN WRITE #1, "Sample dip direction & dip mode"
580 IF mo = 3 THEN WRITE #1, "Sample Azimuth = direction antiparallel to dip & dip mode; Moleneaux conversion"
590 PRINT #1, "Sample Azimuth,dip"; " "; DECT$; " "; INC$; " "; DECT$; "G"; " "; INC$; "G"
600 IF op = 2 THEN IF EOF(2) GOTO 1170
610 ON ERROR GOTO 240
620 IF op = 2 THEN INPUT #2, SAM$, DAT$, TIM$, DEC, INC, INTEN, VOL: lin = lin + 1: GOTO 670
630 CLS : LOCATE 11, 10: PRINT "input X in "; DECT$; " ("; DECT$; "=X) to stop calculations": LOCATE 12, 16
640 IF mo = 1 THEN PRINT "(Sample Strike = G ) to repeat sample coordinates" ELSE PRINT "(Azimuth = G ) to
repeat sample coordinates"
650 IF op = 1 THEN INPUT "SAMPLE NAME :", SAM$
652 LOCATE 14, 10: PRINT DECT$; " = ": LOCATE 14, 20: INPUT DEC$: IF (DEC$ = "X" OR DEC$ = "x") THEN GOTO 1190
ELSE DEC = VAL(DEC$)
655 IF DEC$ <> "0" AND DEC = 0 THEN CLS : GOTO 630
660 LOCATE 15, 10: PRINT INC$; " = ": LOCATE 15, 20: INPUT INC
670 IF op = 2 AND lin > 1 GOTO 740
680 LOCATE 16, 10: IF mo = 1 THEN INPUT "Sample Strike = "; ST$ ELSE INPUT "Sample Azimuth = "; AZ$
690 IF mo = 1 THEN IF (ST$ <> "G" AND ST$ <> "g") THEN STRS = STR: STR = VAL(ST$) ELSE LOCATE 17, 10: PRINT
"Sample strike = "; STR; " Sample Dip = "; DIP: GOTO 720
695 IF ST$ <> "0" AND STR = 0 THEN STR = STRS: GOTO 680
700 IF (AZ$ <> "G" AND AZ$ <> "g") THEN AZ = VAL(AZ$) ELSE LOCATE 16, 10: PRINT "Sample Azimuth = "; AZ; "
Sample Dip = "; DIP: GOTO 720
710 LOCATE 17, 10: INPUT "Sample dip = "; DIP
720 IF op = 1 THEN IF pr = 1 THEN LPRINT SAM$
725 IF pr = 1 THEN IF mo = 1 THEN LPRINT USING "#####.###.###"; " sample strike = "; STR; " dip = "; DIP ELSE
LPRINT USING "#####.###.###"; " sample azimuth = "; AZ; " dip = "; DIP
730 IF op = 2 THEN PRINT "Sample dec inc decg incg ": IF pr = 1 THEN LPRINT "Sample dec inc decg incg "
740 IF mo = 1 THEN COSSTR = COS(PIF * STR): SINSTR = SIN(PIF * STR): ELSE COSAZ = COS(PIF * AZ): SINAZ =
SIN(PIF * AZ)
750 DEC1 = DEC: INC1 = INC
760 REM ' in next 2 lines Poles to planes are calculated
770 IF (SOP - 1) * (SOP - 2) = 0 THEN INC = 90 - INC
780 IF SOP = 1 THEN DEC = DEC - 90 ELSE IF SOP = 2 THEN DEC = DEC - 180
790 COSDIP = COS(PIF * DIP): SINDIP = SIN(PIF * DIP): SININC = SIN(PIF * INC): COSINC = COS(PIF * INC): COSDEC
= COS(PIF * DEC): SINDEC = SIN(PIF * DEC)
800 IF mo <> 1 GOTO 850
810 'strike mode
820 XG = COSSTR * COSINC * COSDEC - SINSTR * COSDIP * COSINC * SINDEC + SINSTR * SINDIP * SININC
830 YG = SINSTR * COSINC * COSDEC + COSSTR * COSDIP * COSINC * SINDEC - COSSTR * SINDIP * SININC
840 ZG = SINDIP * COSINC * SINDEC + COSDIP * SININC: GOTO 950
850 IF mo = 3 GOTO 910
860 'dip dir & dip mode
870 XG = COSAZ * COSDIP * COSINC * COSDEC - SINAZ * COSINC * SINDEC - COSAZ * SINDIP * SININC
880 YG = SINAZ * COSDIP * COSINC * COSDEC + COSAZ * COSINC * SINDEC - SINAZ * SINDIP * SININC
890 ZG = SINDIP * COSINC * COSDEC + COSDIP * SININC: GOTO 950

```

```

900 ' Moleneaux convension
910 XG = COSAZ * COSDIP * COSINC * COSDEC - SINAZ * COSINC * SINDEC + COSAZ * SINDIP * SININC
920 YG = SINAZ * COSDIP * COSINC * COSDEC + COSAZ * COSINC * SINDEC + SINAZ * SINDIP * SININC
930 ZG = -SINDIP * COSINC * COSDEC + COSDIP * SININC
940 'Angular parameters calculabions
950 ASIN = ATN(ZG / SQR(1 - ZG * ZG)): INCG = ASIN / PIF: IF YG = 0 THEN IF XG = 0 THEN DECG = 0: GOTO 980
960 IF XG = 0 THEN IF YG > 0 THEN DECG = 90 ELSE DECG = 270: GOTO 980
970 DECG = ATN(YG / XG) / PIF: IF XG < 0 THEN DECG = DECG + 180 ELSE IF YG < 0 THEN DECG = DECG + 360
980 INCG1 = INCG: IF (SOP - 1) * (SOP - 2) <> 0 GOTO 1030
990 'Recalculation Plane and line parameters for structural data
1000 IF SOP = 3 AND INCG1 < 0 THEN DECG = DECG + 180: INCG = -INCG: GOTO 1020'for lines
1010 INCG = 90 - ABS(INCG): IF SOP = 1 THEN IF INCG1 < 0 THEN DECG = DECG - 90 ELSE DECG = DECG + 90 ELSE IF
INCG > 0 THEN DECG = DECG + 180
1020 IF DECG < 0 THEN DECG = DECG + 360 ELSE IF DECG > 360 THEN DECG = DECG - 360
1030 'Printout for option 2
1040 IF op = 2 THEN PRINT USING "\          \####.## ###.## ####.## ###.## "; SAM$, DEC; INC; DECG; INCG:
IF pr = 1 THEN LPRINT USING "\          \####.## ###.## ####.## ###.## "; SAM$, DEC; INC; DECG; INCG
1045 IF op = 2 GOTO 1140
1050 'Printout for options 1 & 3
1060 LOCATE 19, 10: PRINT USING "#####.###&&###.###&&###.###&&###.###"; DECT$, " = "; DECI; " "; INC$, " = ";
INCI; " "; DECT$, "g = "; DECG; " "; INC$, "g = "; INCG
1070 IF pr = 1 THEN LPRINT USING "#####.###&&###.###&&###.###&&###.###"; DECT$, " = "; DECI; " "; INC$, " = ";
"; INCI; " "; DECT$, "g = "; DECG; " "; INC$, "g = "; INCG: LPRINT ""
1080 LOCATE 21, 10: PRINT "press any key to continue"
1090 IN$ = INKEY$: IF IN$ = "" GOTO 1090
1100 IF mo = 1 THEN STR1 = STR ELSE STR1 = AZ
1110 IF WR = 1 THEN PRINT #1, USING "\          \####.##,###.##,####.##,###.##,####.##,###.##"; SAM$, STR1;
DIP; DECI; INCI; DECG; INCG
1120 CLS : GOTO 630
1130 'Printout for option 2 - continued
1140 IF WR = 1 THEN WRITE #1, SAM$, DAT$, TIM$, DECG, INCG, INTEN, VOL:
1150 GOTO 600
1160 'closing a loop for direct calculations
1170 IF op = 2 THEN CLOSE #2: PRINT : PRINT "    press any key to continue "
1180 CON$ = INKEY$: IF CON$ = "" GOTO 1180
1190 IF WR = 1 THEN CLOSE #1
1200 CLS : GOTO 30
1210 CLS : GOTO 270
1220 CLS : LOCATE 7, 20: PRINT "Rotation of planes & lines"
1230 LOCATE 9, 10: PRINT "1 - planes - STRIKE & DIP"
1240 LOCATE 10, 10: PRINT "2 - planes - DIR of dip & DIP"
1250 LOCATE 11, 10: PRINT "3 - lines - TREND & PLUNGE"
1260 LOCATE 13, 10: INPUT "Choose option: ", SOP
1270 IF (SOP - 1) * (SOP - 2) * (SOP - 3) <> 0 GOTO 1260
1280 IF SOP = 3 THEN INC$ = "PLUNGE": DECT$ = "TREND" ELSE INC$ = "DIP": IF SOP = 1 THEN DECT$ = "STRIKE" ELSE
DECT$ = "DIPDIR"
1290 GOTO 270
1300 IF INKEY$ = "" GOTO 1300
1310 GOTO 10
1320 CLS
1330 END

```



```

440 PRINT : PRINT "Core Orientation Data, -- press numeric key for selection"
450 PRINT : PRINT "<1> set CDEC=90, CINC=0"
460 PRINT " (Above is convention for arrow due North and horizontal on core top)"
470 PRINT "<2> then enter CDEC, CINC in program"
480 PRINT
490 PRINT " Note mathematical convention, core axis inclination is complement of plunge!"
500 PRINT " Declination anticlockwise from due East !": PRINT
510 PRINT " SET POSITION <1>": PRINT : a$ = "1": REM INPUT A$
520 IF a$ = "1" THEN MO = 0: GOTO 550
530 IF a$ = "2" THEN MO = 1: GOTO 550
540 REM GOTO 510
550 IF MO = 0 THEN CD = 90: IC = 0: GOTO 570
560 INPUT "Core Declination, Core Inclination ="; CD, IC
570 CI = IC / pi: a2 = 0: LJ = 1: A1 = 0
580 REM now enter data, S1 to S6 for each specimen
590 ON qn GOSUB 1430, 1510, 1760
600 REM measurements are S(1) to S(M) where M=6 or 12
610 FOR j = 1 TO m
620 s(j) = 100 * s(j)
630 NEXT j
635 IF meth = 3 GOTO 690
640 a = .5: dof = 12
650 k1 = a * (s(1) + s(7))
660 k2 = a * (s(3) + s(11))
670 k3 = a * (s(5) + s(9))
680 k4 = a * (s(2) - s(4)): k5 = a * (s(6) - s(8)): k6 = a * (s(10) - s(12)): GOSUB 2580
690 GOSUB 940: GOSUB 1960: GOTO 700: REM calculate principal values and directions ...
700 IF prin = 1 THEN LPRINT DATES; " "; TIMES; " "; CN$; " Saved as "; FOUT$
710 IF prin = 1 THEN LPRINT "Core declination = "; CDEC; "Core inclination = "; CINC; "# of directions used = "; n
720 IF prin = 1 THEN LPRINT "Value Dec Inc R95 Magnitude St.dev."; U$
730 FOR i = 1 TO 3
740 IF prin = 1 THEN LPRINT USING X2$; B$(i); X1(i); Y1(i); V1(i); z1(i); V2(i)
750 IF i = 1 THEN PRINT "Saved as "; FOUT$
760 IF i = 1 THEN PRINT "Value Dec Inc R95 Magnitude St.Dev."; U$
770 PRINT USING x$; B$(i); X1(i); Y1(i); V1(i); z1(i); V2(i)
780 NEXT i
781 IF prin = 1 THEN
782 LPRINT "Anisotropy matrix :"
783 FOR i = 1 TO 3
784 LPRINT USING s$; aniz(i, 1); aniz(i, 2); aniz(i, 3)
785 NEXT i
786 END IF
787 IF qn = 2 THEN GOSUB 2600: REM calculation of residua
790 IF prin = 1 THEN LPRINT
800 PRINT : PRINT "Press any key to continue"
810 a$ = INKEY$: IF a$ = "" THEN GOTO 810
820 REM ...save data to disk in Stupavsky SI2 format
830 OPEN "0", #2, FOUT$
840 PRINT #2, DUMMY
850 PRINT #2, U$: PRINT #2, DUMMY: PRINT #2, DUMMY
860 FOR i = 1 TO 3
870 PRINT #2, X1(i)
880 PRINT #2, Y1(i)

```



```

890 PRINT #2, z1(i)
900 NEXT i
910 CLOSE #2: IF prin = 1 THEN LPRINT
920 CLS : GOTO 140: REM input more data
930 REM SUBROUTINE TO CALCULATE PRINCIPAL VALUES AND DIRECTIONS
940 P = -k1 - k2 - k3: Q = k1 * k2 + k1 * k3 + k2 * k3 - k4 * k4 - k5 * k5 - k6 * k6
950 R = k1 * k6 * k6 + k2 * k5 * k5 + k3 * k4 * k4 - k1 * k2 * k3 - 2 * k4 * k5 * k6
960 a = Q - P * P / 3: B = (2 * P * P * P / 27) + R - P * Q / 3
970 R = B / (2 * a * SQR(-a / 27))
980 AA = 1.5708 - ATN(R / SQR(1 - R * R))
990 AA = AA / 3: BB = 2 * SQR(-a / 3): RR = P / 3
1000 W1 = BB * COS(AA) - RR: W2 = BB * COS(AA + 2.0944) - RR: W3 = BB * COS(AA + 4.1888) - RR
1010 IF W1 > W2 AND W2 > W3 THEN A1 = W1: a2 = W2: A3 = W3: GOTO 1070
1020 IF W1 > W2 AND W2 < W3 THEN A1 = W1: a2 = W3: A3 = W2: GOTO 1070
1030 IF W2 > W1 AND W1 > W3 THEN A1 = W2: a2 = W1: A3 = W3: GOTO 1070
1040 IF W2 > W1 AND W1 < W3 THEN A1 = W2: a2 = W3: A3 = W1: GOTO 1070
1050 IF W3 > W1 AND W1 > W2 THEN A1 = W3: a2 = W1: A3 = W2: GOTO 1070
1060 IF W3 > W1 AND W1 < W2 THEN A1 = W3: a2 = W2: A3 = W1
1070 W(1) = A3: W(2) = a2: W(3) = A1
1080 FOR i = 1 TO 3
1090 B = 1E-16
1100 a = 0: A1 = 0: a2 = 0: R = k4 * k6 - k5 * (k2 - W(i))
1110 IF ABS(R) < B THEN 1140
1120 a = a + 1: A1 = (k4 * k5 - k6 * (k1 - W(i))) / R
1130 a2 = ((k1 - W(i)) * (k2 - W(i)) - k4 * k4) / R
1140 R = k4 * (k3 - W(i)) - k5 * k6
1150 IF ABS(R) < B THEN 1180
1160 a = a + 1: A1 = A1 + (k5 * k5 - (k1 - W(i)) * (k3 - W(i))) / R
1170 a2 = a2 + (k6 * (k1 - W(i)) - k4 * k5) / R
1180 R = (k2 - W(i)) * (k3 - W(i)) - k6 * k6
1190 IF ABS(R) < B THEN 1220
1200 a = a + 1: A1 = A1 + (k5 * k6 - k4 * (k3 - W(i))) / R
1210 a2 = a2 + (k4 * k6 - k5 * (k2 - W(i))) / R
1220 IF a = 0 THEN B = 100 * B: GOTO 1100
1230 A1 = A1 / a: a2 = a2 / a
1240 dec = ATN(A1): inc = ATN(a2 * COS(dec))
1250 a = COS(inc): A1 = a * COS(dec): a2 = a * SIN(dec): A3 = SIN(inc)
1260 x = A1 * COS(CI) + A3 * SIN(CI): z = A3 * COS(CI) - A1 * SIN(CI): IF ABS(z) = 1 THEN z = SGN(z) * 1.00001
1270 dec = CD - (90 * x / ABS(x)) + pi * ATN(a2 / x): inc = pi * ATN(z / SQR(ABS(1 - z * z)))
1280 IF LJ > 1 THEN 1370
1290 IF dec < 0 THEN dec = dec + 360
1300 IF dec > 360 THEN dec = dec - 360
1310 IF inc >= 0 THEN GOTO 1340
1320 inc = -inc: dec = dec + 180
1330 IF dec > 360 THEN LET dec = dec - 360
1340 X1(i) = dec: Y1(i) = inc: z1(i) = .01 * W(i)
1350 XM(i) = x: YM(i) = a2: ZM(i) = z: T(i) = 0: T1(i) = 0: T2(i) = 0
1360 IF LJ = 1 THEN GOTO 1400
1370 a = ABS(XM(i) * x + YM(i) * a2 + ZM(i) * z): IF ABS(a) = 1 THEN a = SGN(a) * 1.00001
1375 AA = 1.5708 - ATN(a / SQR(ABS(1 - a * a)))
1380 T(i) = T(i) + AA * AA: T1(i) = T1(i) + W(i): T2(i) = T2(i) + W(i) * W(i)
1390 REM LPRINT "i="; I; T(I); T1(I); T2(I)
1400 NEXT i
1410 RETURN

```

```

1420 END
1430 REM input data for one specimen manually
1440 CLS
1450 FOR i = 1 TO n
1460 PRINT " s("; i; ") = ": PRINT
1470 INPUT s(i): CLS
1480 NEXT i
1490 GOSUB 1800
1500 RETURN

```

```

1510 REM input data for one specimen from file
1520 PRINT "ACCESS raw input data on drive and path of format as: <C:\path\> "
1522 PRINT " INPUT '*' TO REPEAT PREVIOUS DESTINATION ": INPUT DR$
1525 IF DR$ = "*" THEN DR$ = DR1$: GOTO 1530
1527 DR1$ = DR$

```

```

1530 INPUT "Give input file name (= <5 characters>); FM$

```

```

1540 Fin$ = DR$ + TYP$ + FM$ + ".SPN"

```

```

1550 PRINT "Data will be from file "; Fin$

```

```

1555 inp$ = Fin$

```

```

1556 ON ERROR GOTO 1568

```

```

1560 OPEN Fin$ FOR INPUT AS #1: GOTO 1570

```

```

1568 PRINT "Incorrect path or file": RESUME 1520

```

```

1570 FOR i = 1 TO n

```

```

1580 INPUT #1, NA1$(i), DT1$(i), TM1$(i), decx(i), incx(i), intx(i), VOL

```

```

1590 xs(i) = intx(i) * COS(decx(i) / pi) * COS(incx(i) / pi): ys(i) = intx(i) * SIN(decx(i) / pi) * COS(incx(i)
/ pi): zs(i) = intx(i) * SIN(incx(i) / pi)

```

```

1610 PRINT USING "\          \ #####.## #####.## #####.##"; NA1$(i); xs(i); ys(i); zs(i)

```

```

1620 s(i) = intx(i)

```

```

1630 NEXT i

```

```

1640 CLOSE #1

```

```

1645 PRINT "press any key to continue"

```

```

1646 ans$ = INKEY$: IF ans$ = "" GOTO 1646

```

```

1650 CLS

```

```

1651 PRINT "Do you want to SUBTRACT any RESIDUAL vector from all data <Y/N> ?"

```

```

1652 INPUT subtr$: IF subtr$ = "Y" OR subtr$ = "y" THEN GOSUB 2100

```

```

1655 PRINT "Choose method of calculations of anisotropy matrix elements:"

```

```

1660 PRINT "intensity as component along field direction - 1"

```

```

1670 PRINT "Component along field direction calculated - 2"

```

```

1680 PRINT "Least - square method - 3"

```

```

1690 INPUT meth

```

```

1700 IF meth = 1 GOTO 1740

```

```

1710 s(1) = -xs(1): s(3) = -ys(3): s(5) = -zs(5): s(7) = -xs(7): s(9) = -zs(9): s(11) = -ys(11)

```

```

1720 fac = -1 / SQR(2): s(2) = fac * (xs(2) + ys(2)): s(4) = -fac * (xs(4) - ys(4)): s(6) = fac * (xs(6) +
zs(6))

```

```

1730 s(8) = fac * (xs(8) - zs(8)): s(10) = fac * (ys(10) + zs(10)): s(12) = fac * (ys(12) - zs(12))

```

```

1735 IF meth = 3 THEN GOSUB 2500

```

```

1740 GOSUB 1800

```

```

1750 RETURN

```

```

1760 REM ** input test measurements for an ellipsoid

```

```

1770 s(1) = .0003621: s(2) = 3.8368E-04: s(3) = 4.1942E-04: s(4) = .0004147: s(5) = 4.1065E-04: s(6) =
3.9953E-04: s(7) = 3.6379E-04: s(8) = 3.8064E-04: s(9) = 4.2582E-04: s(10) = 3.9818E-04: s(11) = 4.3459E-04:

```

```

s(12) = 4.4302E-04
1780 GOSUB 1800
1790 RETURN

1800 IF prin <> 1 THEN GOTO 1900
1810 IF qn = 2 THEN LPRINT "From "; inp$
1820 IF qn = 1 THEN LPRINT "Data entered from keyboard were: "
1830 IF qn = 3 THEN LPRINT "Test data for 12 direction measurement"
1840 IF meth = 1 THEN LPRINT "Intensity as component along field direction"
1850 IF meth = 2 THEN LPRINT "Component along field direction is calculated "
1855 IF meth = 3 THEN LPRINT "Least -square method"
1860 IF meth <> 3 THEN LPRINT USING s$; s(1); s(2); s(3); s(4); s(5); s(6)
1870 IF meth <> 3 THEN LPRINT USING s$; s(7); s(8); s(9); s(10); s(11); s(12)
1 8 8 0   R E M   " T E S T   D A T A   F O R   1 2   D I R E C T I O N S :
3.6210D-4,3.8368D-4,4.1942D-4,4.1470D-4,4.1065E-4,3.9953E-4,3.6379E-4,3.8064E-4,4.2582E-4,3.9818E-4,4.3459E-4,4
.4302E-4,
1900 RETURN

1910 REM          DEC    INC    R95    MAGNIT.  SDEV
1920 REM  MIN    191.35  4.68  12.8    3.5904E-4  8.545E-8
1930 REM  INT     95.40  51.73  12.8    3.9993E-4  9.129E-6
1940 REM  MAX    285.00  37.88   3.1    4.4922E-4  6.913E-6
1950 END

1960 LJ = 2
1970 k1 = s(1): k2 = s(3): k3 = s(5): k4 = s(2) - .5 * (k1 + k2)
1980 k5 = s(6) - .5 * (k1 + k3): k6 = s(10) - .5 * (k2 + k3): GOSUB 940
1990 k1 = s(7): k2 = s(11): k3 = s(9): k4 = .5 * (k1 + k2) - s(4)
2000 k5 = .5 * (k1 + k3) - s(8): k6 = .5 * (k2 + k3) - s(12): GOSUB 940
2010 GOSUB 2030
2020 RETURN

2030 a = 112 / LJ
2040 V1(1) = a * SQR(T(1)): V1(2) = a * SQR(T(2)): V1(3) = a * SQR(T(3))
2050 a = 1 / LJ: AA = a * a
2060 V2(1) = .01 * SQR(ABS(a * T2(1) - AA * T1(1) * T1(1))): V2(2) = .01 * SQR(ABS(a * T2(2) - AA * T1(2) *
T1(2))): V2(3) = .01 * SQR(ABS(a * T2(3) - AA * T1(3) * T1(3)))
2070 RETURN

2090 REM - subtraction of high coercive residual magnetization
2100 PRINT " input dec, inc and intensity of vector to be subtracted"
2110 INPUT "DEC = "; decr: INPUT "INC = "; INCr: INPUT "Intensity = "; INTr
2115 PRINT "Vector to be subtracted:": IF prin = 1 THEN LPRINT "Vector to be subtracted:"
2117 PRINT "  dec    inc    int ": IF prin = 1 THEN LPRINT "  dec    inc    int "
2120 PRINT USING " ###.## ###.## #####.## "; decr; INCr; INTr
2130 IF prin = 1 THEN LPRINT USING " ###.## ###.## #####.## "; decr; INCr; INTr
2140 xr = INTr * COS(decr / pi) * COS(INCr / pi): yr = INTr * SIN(decr / pi) * COS(INCr / pi): zr = INTr *
SIN(INCr / pi)
2145 REM IF prin = 1 THEN LPRINT " XYZ comp. of subtracted vector:": LPRINT xr, yr, zr
2150 PRINT " Save NEW remanent magnetization data ? <y/n> "
2160 INPUT sav$: IF sav$ <> "Y" AND sav$ <> "y" THEN GOTO 2190
2170 sav = 1: PRINT :
2171 PRINT "SAVE file in the path as: <C:\path\> "
2172 PRINT " INPUT '*' TO REPEAT PREVIOUS DESTINATION ": INPUT DR3$

```

(1)

) +

) =  
-04:

```

2173 IF DR3$ = "*" THEN DR3$ = DR4$: GOTO 2175
2174 DR4$ = DR3$
2175 INPUT "Give file name to save recalculated data(=<5 characters)"; savefile$
2176 savf$ = DR3$ + TYP$ + savefile$ + ".SPN"
2177 ON ERROR GOTO 2185
2180 OPEN savf$ FOR OUTPUT AS #3: inp$ = savf$: GOTO 2190
2185 PRINT "Incorrect path or file": RESUME 2171
2190 PRINT : PRINT "Recalculated data are saved in file "; savf$
2195 IF prin = 1 THEN LPRINT "Recalculated data are saved in file "; savf$
2200 FOR i = 1 TO 12
2210 xs(i) = xs(i) - xr: ys(i) = ys(i) - yr: zs(i) = zs(i) - zr
2220 xss = xs(i): yss = ys(i): zss = zs(i): GOSUB 2300
2230 PRINT USING FMT$; NA1$(i); DT1$(i); TM1$(i); decn; incn; intn; VOL
2235 IF prin = 1 THEN LPRINT USING FMT$; NA1$(i); DT1$(i); TM1$(i); decn; incn; intn; VOL
2240 IF sav = 1 THEN WRITE #3, NA1$(i), DT1$(i), TM1$(i), decn, incn, intn, VOL
2245 decx(i) = decn: incx(i) = incn: intx(i) = intn: s(i) = intx(i)
2250 NEXT i
2260 IF sav = 1 THEN CLOSE #3
2270 PRINT
2290 RETURN

```

```

2300 REM Calculation of dec, inc and intensity of corrected data
2310 sq = SQR(xss * xss + yss * yss)
2320 IF sq = 0 THEN decn = 0: inc = SGN(zss) * 90: intn = ABS(zss): RETURN
2325 intn = SQR(zss * zss + sq * sq): incn = ATN(zss / sq) * pi
2330 ds = .0001: sn = yss / sq: cs = xss / sq
2340 IF cs = 0 THEN cs = ds
2346 decn = ATN(ABS(sn / cs)) * pi
2348 IF sn > 0 AND cs < 0 THEN decn = 180 - decn
2350 IF sn < 0 AND cs < 0 THEN decn = 180 + decn
2352 IF sn < 0 AND cs > 0 THEN decn = 360 - decn
2355 RETURN

```

```

2500 REM Calculation of anisotropy matrix elements by least- square method
2510 m = 6: dof = 36
2520 k1 = 100 * (-xs(1) - xs(7) + fac * (xs(2) - xs(4) + xs(6) + xs(8))) / 4
2530 k2 = 100 * (-ys(3) - ys(11) + fac * (ys(2) + ys(4) + ys(10) + ys(12))) / 4
2540 k3 = 100 * (-zs(5) - zs(9) + fac * (zs(6) - zs(8) + zs(10) - zs(12))) / 4
2550 k4 = 100 * (-xs(3) - xs(11) - ys(1) - ys(7) + fac * (ys(2) - ys(4) + ys(6) + ys(8) + xs(2) + xs(4) +
xs(10) + xs(12))) / 8
2560 k5 = 100 * (-xs(5) - xs(9) - zs(1) - zs(7) + fac * (zs(2) - zs(4) + zs(6) + zs(8) + xs(6) - xs(8) + xs(10)
- xs(12))) / 8
2570 k6 = 100 * (-ys(5) - ys(9) - zs(3) - zs(11) + fac * (ys(6) - ys(8) + ys(10) - ys(12) + zs(2) + zs(4) +
zs(10) + zs(12))) / 8
2572 GOSUB 2580
2575 RETURN

```

```

2579 REM Anisotropy matrix
2580 aniz(1, 1) = k1 / 100: aniz(2, 2) = k2 / 100: aniz(3, 3) = k3 / 100
2585 aniz(1, 2) = k4 / 100: aniz(1, 3) = k5 / 100: aniz(2, 3) = k6 / 100
2590 aniz(2, 1) = k4 / 100: aniz(3, 1) = k5 / 100: aniz(3, 2) = k6 / 100
2595 RETURN

```

```

2600 REM Calculation of sums of residuum between experimental and calculated data

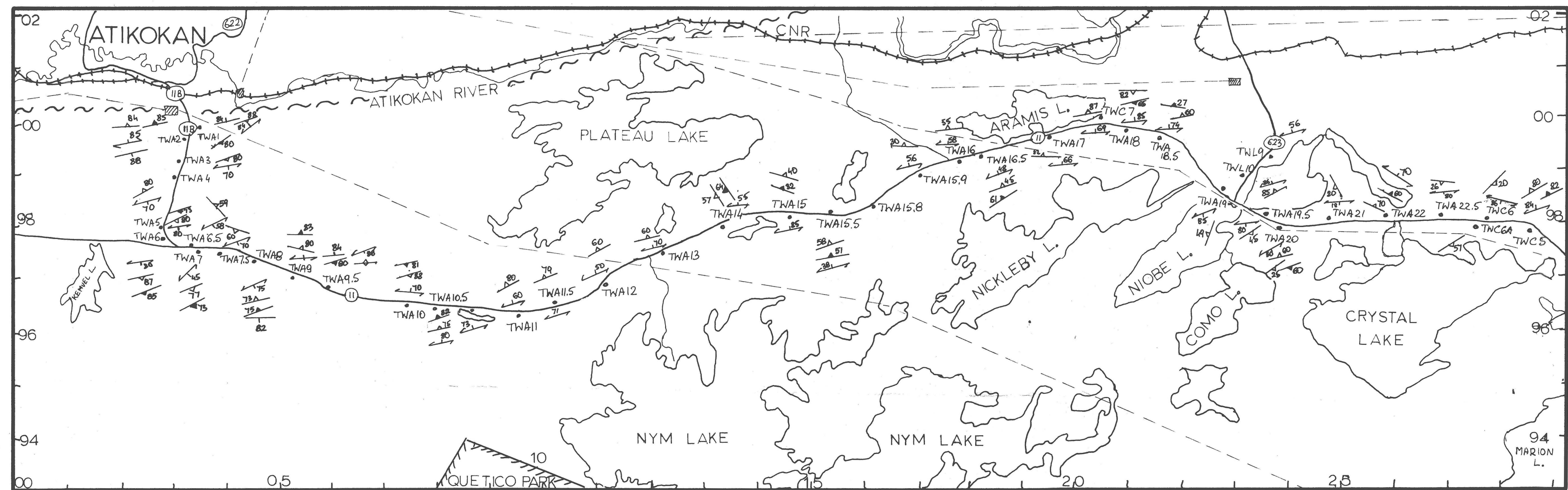
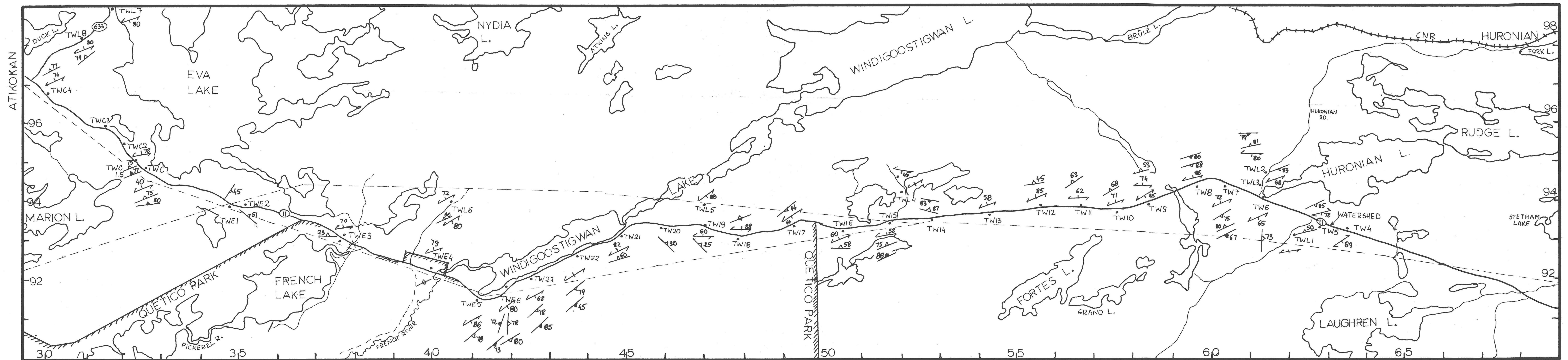
```

```

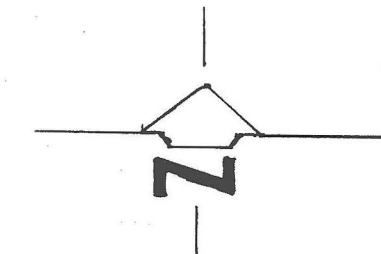
2601 FOR i = 1 TO 3
2602 FOR k = 1 TO 3
2603 e(i, k) = 0
2604 NEXT k
2605 NEXT i
2620 e(1, 1) = -1: e(1, 7) = -1: e(2, 3) = -1: e(2, 11) = -1: e(3, 5) = -1: e(3, 9) = -1
2630 e(1, 2) = fac: e(1, 4) = -fac: e(1, 6) = fac: e(1, 8) = fac
2640 e(2, 2) = fac: e(2, 4) = fac: e(2, 10) = fac: e(2, 12) = fac
2650 e(3, 6) = fac: e(3, 8) = -fac: e(3, 10) = fac: e(3, 12) = -fac
2660 FOR i = 1 TO 12
2670 REM IF prin = 1 THEN LPRINT USING "#.####"; e(1, i); e(2, i); e(3, i)
2680 NEXT i

2695 res2 = 0
2696 PRINT "      Measured magnetization  Calculated magnetization": PRINT "No      Dec   Inc   Int   Dec
Inc      Int      errX  errY   errZ"
2697 IF prin = 1 THEN LPRINT "      Measured magnetization  Calculated magnetization "
2698 IF prin = 1 THEN LPRINT "No      Dec   Inc   Int   Dec   Inc   Int   errX  errY   errZ"
2700 FOR i = 1 TO 12
2710 FOR j = 1 TO 3
2712 rc(j, i) = 0
2715 FOR k = 1 TO 3
2720 rc(j, i) = rc(j, i) + aniz(j, k) * e(k, i)
2721 NEXT k
2725 NEXT j
2726 res(1, i) = xs(i) - rc(1, i): res(2, i) = ys(i) - rc(2, i): res(3, i) = zs(i) - rc(3, i)
2727 FOR k = 1 TO 3
2728 res2 = res2 + res(k, i) * res(k, i)
2729 NEXT k
2737 REM PRINT USING s$; xs(i); rc(1, i); res(1, i): REM IF prin = 1 THEN LPRINT USING s$; xs(i); rc(1, i);
res(1, i)
2738 REM PRINT USING s$; ys(i); rc(2, i); res(2, i): REM IF prin = 1 THEN LPRINT USING s$; ys(i); rc(2, i);
res(2, i)
2739 REM PRINT USING s$; zs(i); rc(3, i); res(3, i): REM IF prin = 1 THEN LPRINT USING s$; zs(i); rc(3, i);
res(3, i)
2740 xss = rc(1, i): yss = rc(2, i): zss = rc(3, i): GOSUB 2300: dece(i) = decn: ince(i) = incn: inte(i) = intn
2750 PRINT USING " ## ####.## ###.## ####.## ####.## ###.## ####.## ####.## ###.## ###.## "; i; decx(i);
incx(i); intx(i); dece(i); ince(i); inte(i); res(1, i) * 100 / intx(i); res(2, i) * 100 / intx(i); res(3, i) *
100 / intx(i)
2760 IF prin = 1 THEN LPRINT USING " ## ####.## ###.## ####.## ####.## ###.## ####.## ####.## ###.## ###.##
"; i; decx(i); incx(i); intx(i); dece(i); ince(i); inte(i); res(1, i) * 100 / intx(i); res(2, i) * 100 /
intx(i); res(3, i) * 100 / intx(i)
)
2785 NEXT i
2786 gof = SQR(res2 / (dof - 6)): n1 = SQR(dof - 6) / dof: amean = (z1(1) + z1(2) + z1(3)) / 3: ares = z1(3) -
z1(1): ares = gof * 100 / ares: gof = gof * 100 / amean
2787 PRINT USING "Residual sum of squares: " + s$; res2: IF prin = 1 THEN LPRINT USING "Residual sum of
squares: " + s$; res2
2788 PRINT USING "Goodness of fit (%): ####.## ###.##"; gof; gof * n1: IF prin = 1 THEN LPRINT USING "Goodness
of fit: ####.## ###.##"; gof; gof * n1
2789 PRINT USING "Resolution of anisotropy (%): ####.## ###.##"; ares; ares * n1: IF prin = 1 THEN LPRINT USING
"Resolution of anisotropy: ####.## ###.##"; ares; ares * n1
2890 RETURN

```



- LEGEND:
- - stations
  - S<sub>1</sub> tectonic } foliation
  - ▲ AMS } foliation
  - ▲ AARM } foliation
  - S<sub>0</sub> bedding
  - ⊖ HIGHWAYS
  - +++ RAILWAY
  - POWER LINES
  - ~ QUETICO FAULT



TOMASZ WERNER - M.SC. THESIS  
LAKEHEAD UNIVERSITY

ATIKOKAN-HURONIAN LAKE AREA  
- TECTONIC & MAGNETIC FABRICS

SHEET NO. 1	NTS: 52B/12, 52B/11, 52B/10
- FOLIATIONS	SCALE: 1:50,000